Vitaly Gitis and
Gadi Rothenberg

Ceramic Membranes

Also published by one of the Authors:

Rothenberg, G.

Catalysis

Concepts and Green Applications

2008
Print ISBN: 978-3-527-31824-7

Vitaly Gitis and
Gadi Rothenberg

Ceramic Membranes

New Opportunities and Practical Applications

WILEY-VCH
Verlag GmbH & Co. KGaA

Authors

Vitaly Gitis
Ben-Gurion University of Negev
Unit Environmental Engineering
84105 Beer-Sheva
Israel

Gadi Rothenberg
Van't Hoff Institute for Molecular
Sciences / Univ.of Amsterdam
Science Park 904
1090 XH Amsterdam
Netherlands

Cover: created on the basis of an illustration by Itamar Daube. Used with permission.

All books published by **Wiley-VCH** are carefully produced. Nevertheless, authors, editors, and publisher do not warrant the information contained in these books, including this book, to be free of errors. Readers are advised to keep in mind that statements, data, illustrations, procedural details or other items may inadvertently be inaccurate.

Library of Congress Card No.: applied for

British Library Cataloguing-in-Publication Data
A catalogue record for this book is available from the British Library.

Bibliographic information published by the Deutsche Nationalbibliothek
The Deutsche Nationalbibliothek lists this publication in the Deutsche Nationalbibliografie; detailed bibliographic data are available on the Internet at <http://dnb.d-nb.de>.

© 2016 Wiley-VCH Verlag GmbH & Co. KGaA, Boschstr. 12, 69469 Weinheim, Germany

All rights reserved (including those of translation into other languages). No part of this book may be reproduced in any form – by photoprinting, microfilm, or any other means – nor transmitted or translated into a machine language without written permission from the publishers. Registered names, trademarks, etc. used in this book, even when not specifically marked as such, are not to be considered unprotected by law.

Print ISBN: 978-3-527-33493-3
ePDF ISBN: 978-3-527-69657-4
ePub ISBN: 978-3-527-69658-1
Mobi ISBN: 978-3-527-69656-7
oBook ISBN: 978-3-527-69655-0

Printed on acid-free paper

To our wives, Diana and Live, and our children,
Abigail, Ariel, Avital, Daniel and Emil,
who wondered what we did all this time.

Contents

Preface *XI*

1 The Basics *1*
1.1 General Introduction and Historical Perspective *1*
1.2 The Basics of Membrane Separation *4*
1.3 Membrane Separation Processes *8*
1.4 The Morphology of Membranes *11*
1.5 Membrane Modules *15*
1.6 Fouling and Cleaning *18*
1.6.1 Fouling *18*
1.6.2 Cleaning *20*
1.7 Ceramic versus Polymer Membranes *22*
1.8 Raw Materials for Ceramic Membranes *25*
1.8.1 Alumina *26*
1.8.2 Silica *27*
1.8.3 Titania *28*
1.8.4 Zirconia *29*
1.8.5 Zeolites *30*
1.9 Preparation of Ceramic Membranes *32*
1.9.1 Support Your Local Membrane *32*
1.9.1.1 Forming the Initial Slurry *34*
1.9.1.2 Mixing and Pugging *39*
1.9.1.3 Shaping the Slurry *41*
1.9.2 Drying and Thermolysis *42*
1.9.3 Sintering *45*
1.9.3.1 Sintering Variables *50*
1.9.4 Finishing *53*
1.10 Intermediate and Top Layers *54*
1.10.1 Preparing the Intermediate Layers *56*
1.10.2 Fundamentals of Chemical Vapour Deposition *58*
1.10.3 Sol–Gel Coating *66*
1.10.4 Zeolite Coating *69*

1.11 Industrial Applications of Ceramic Membranes *73*
1.12 Further Reading *74*
References *79*

2 Fundamentals of Membrane Separation *91*
2.1 A Short Introduction to Mass Transfer Phenomena *91*
2.2 Fick's Law *96*
2.3 The Mass Diffusivity D_{AB} *99*
2.3.1 Diffusion in Gases *99*
2.3.2 Diffusion in Liquids *103*
2.3.3 Diffusion in Solids *105*
2.4 Integral and Differential Expressions of Mass Balance Equation *107*
2.5 Convective Mass Transfer *111*
2.5.1 Momentum and Mass Diffusivity Profiles *113*
2.6 Fluxes of Liquids through Porous Membranes *115*
2.6.1 The Flux of Pure Solutes *115*
2.6.2 The Flux of Mixtures *117*
2.6.2.1 The Concentration Polarization Model *118*
2.6.2.2 The Resistance-in-Series Model *122*
2.6.2.3 The Pore Blocking Model *123*
2.7 Fluxes of Gases through Porous Membranes *124*
2.7.1 Knudsen Diffusion *125*
2.7.2 Surface Diffusion *128*
2.7.3 Capillary Condensation *131*
2.7.4 Molecular Sieving *133*
2.7.5 Transport of Gases through Ceramic Membranes with Several Simultaneous Processes *134*
2.7.5.1 The Parallel Transport Model *134*
2.7.5.2 The Resistance-in-Series Model *138*
2.8 Fluxes through Non-porous Membranes *138*
References *143*

3 Characterization of Ceramic Membranes *149*
3.1 Introduction *149*
3.2 Pore Size and Pore Size Distribution *150*
3.2.1 Permeability *153*
3.2.2 The Gas–Liquid Displacement Bubble Point Technique *156*
3.2.3 Liquid–Liquid Displacement *158*
3.2.4 Mercury Porosimetry *159*
3.2.5 Gas Adsorption–Desorption *160*
3.2.6 Gas–Liquid Permporometry *161*
3.2.7 Solid–Liquid Thermoporometry *162*
3.2.8 Nuclear Magnetic Resonance *164*
3.2.9 Solute Rejection Tests *165*
3.2.9.1 Solid Solutes *168*

3.2.9.2 Ions and Dissolved Organics *169*
3.2.9.3 Spiking Tests *169*
3.3 Visualization of Membrane Surfaces *171*
3.3.1 Optical Microscopy *172*
3.3.2 Confocal Scanning Laser Microscopy *173*
3.3.3 Scanning Electron Microscopy *174*
3.3.4 Transmission Electron Microscopy *176*
3.3.5 Atomic Force Microscopy *178*
3.4 Chemical Methods for Membrane Characterization *181*
3.4.1 Backscattered Radiation *182*
3.4.2 Vibrational Spectroscopy *185*
3.5 Physical Parameters of Ceramic Membranes *189*
3.5.1 Membrane Porosity and Pore Tortuosity *190*
3.5.2 Mechanical Strength Tests *192*
3.5.3 Hydrophobicity of Ceramic Membranes *196*
3.5.4 Charge of Ceramic Membranes *197*
3.6 Conclusions *201*
References *206*

4 Applications *217*
4.1 Classical Applications of Ceramic Membranes *217*
4.2 Gas Separation with Ceramic Membranes *221*
4.2.1 Sustainable Reduction of CO_2 Emissions with Ceramic Membranes *225*
4.2.1.1 CO_2 Capture from Flue Gases *226*
4.2.2 Hydrogen Purification *232*
4.2.3 Fuel Cell Applications: The Real Hydrogen Economy *239*
4.2.3.1 Dense Ceramic Membranes for Fuel Cell Applications *244*
4.2.3.2 Oxygen Separation by Dense Mixed Ionic–Electronic Conducting Membranes *249*
4.3 Ceramic Membrane Reactors *250*
4.3.1 Membrane Reactor Types and Their Applications *250*
4.3.2 The Inert Membrane Reactor *250*
4.3.3 The Catalytic Membrane Reactor *254*
4.3.4 Composite Infiltrated Ceramic Membranes *259*
4.3.5 Membrane Reactors Using Dense Ceramic Membranes *264*
4.4 Liquid Separation and Purification *265*
4.4.1 Water Treatment *266*
4.4.2 Surface Water Treatment with Ceramic Membranes *268*
4.4.3 Low-Cost Ceramic Filters *271*
4.4.4 Treating Additional Pollutants *274*
4.4.5 Membrane Distillation *275*
4.4.6 Pervaporation *280*
4.5 Cleaning of Wastewater with Ceramic Membranes *286*
4.5.1 Membrane Bioreactors *286*

4.5.2 Oil–Water Separation *291*
4.5.2.1 Applications in Oil Recovery *291*
4.5.2.2 Applications in Bilge Water Treatment *295*
4.6 Ceramic Membranes in Food Applications *297*
4.6.1 The Dairy Industry *298*
4.6.1.1 Cheese Production *300*
4.6.1.2 Whey Separation *303*
4.6.1.3 Brine Disinfection *304*
4.6.1.4 Pathogen Removal *304*
4.6.2 Mineral Water and Juice *307*
4.6.2.1 Orange Juice *308*
4.6.2.2 Apple Juice *310*
4.6.3 Fermented Food Industry *314*
4.6.3.1 Beer and Ceramic Membranes *315*
4.6.3.2 Winemaking and Ceramic Membranes *321*
References *330*

5 Economics *355*
5.1 Introduction *355*
5.2 A Layman Scientist's Guide to Project Appraisal: SWOT, PEST and LCA *357*
5.2.1 SWOT Analysis *358*
5.2.1.1 Identifying, Matching and Converting *359*
5.2.2 PEST Analysis *359*
5.2.3 Life Cycle Assessment *360*
5.3 Economic Considerations in the Manufacturing and Application of Ceramic Membranes *362*
5.3.1 Case Study 1: Atech Innovations GmbH (Germany) *362*
5.3.2 Case Study 2: LiqTech A/S (Denmark) *365*
5.3.3 Case Study 3: Metawater Co. (Japan) *368*
5.3.4 Case Study 4: Pretreatment of Petrochemical Wastewater in Mahshahr, Iran *370*
5.3.5 Case Study 5: Techno-Economic Analysis of CO_2 Capture from Flue Gases (France) *373*
5.4 Discussion *376*
5.4.1 Market Size and the Adversity to Change *378*
5.4.2 Specific Product Demands Dictated by Application *379*
5.4.3 Detailed Technical Know-How *380*
5.5 Outlook *381*
5.5.1 Persistent Market Entry Barriers *381*
5.5.2 Global Changes and New Opportunities *381*
References *385*

Index *389*

Preface

This textbook tells the story of ceramic membranes. Ceramics are making a comeback as hi-tech materials, and the membranes are used in many processes, from uranium purification to orange juice finishing. Moreover, they can help us address urgent environmental issues air pollution and shortage of clean drinking water. It is definitely the time to study them.

The book is divided into five thematic chapters. Chapter 1 gives a general introduction to the membrane field and then covers the making of ceramic membranes. The physics of flow models and mass transfer through membranes are discussed in Chapter 2. Chapter 3 deals with membrane characterization, from the most common methods to the state-of-the-art. We then move to applications in Chapter 4, containing a range of industrial sectors, including chemicals, food and beverages and fuel cells. Finally, Chapter 5 looks at ceramic membranes from a different viewpoint: We examine the economics of membrane manufacturing and predict, on the basis of case studies, the future market for ceramic membrane technologies.

We wrote this book for both researchers and students. Thus, each chapter includes detailed references, as well as exercises. To help you master the membrane jargon, key terms are printed *in italics* and defined the first time they appear in the text. The book contains over 1000 references, whereof >90% are original papers in peer-reviewed journals. We cite reviews when introducing a subject, and articles when discussing specific topics (plus some patents in the industrial examples). Chapter 1 also contains a "Further Reading" list of books on related specialized subjects.

We thank our families for their patience and support during the past 3 years, and our colleagues Vittorio Boffa, Hessel Castricum, David Dubbeldam, Andre ten Elshof, Giovanni Catania, David Farrusseng, Slava Freger, Freek Kapteijn, Chiho Kojima, Erik Kossin, Daniel Sereth Larsen, Marc Pera-Titus, Ehsan Salehi, Jesus Santamaría, Lev Tsapovski, Ning Yan and Gennady Ziskind for their help and advice. V.G. thanks Rabbi Daniel Lewenstein for his support and encouragement. We also thank Itamar Daube for drawing the cover picture and Wiley-VCH editors Waltraud Wüst and Gudrun Walter for their encouraging and professional attitude.

January 2016

Vitaly Gitis — *Beer-Sheva, Israel*
Gadi Rothenberg — *Amsterdam, The Netherlands*

1
The Basics

1.1
General Introduction and Historical Perspective

This chapter covers the basic definitions, main features and engineering and design of ceramic membranes. We give a brief history of the development of ceramic membranes, define key terms in membrane science, outline the popular separation processes (ultrafiltration (UF), nanofiltration (NF), pervaporation and gas separation) and explain the main module designs (plate-and-frame, spiral-wound, tubular, honeycomb and hollow fibres). The historical overview shows how membranes started, when the big breakthrough occurred, where membranes are now and how the near future will look like. The actual making of ceramic membranes is in itself an interesting story, and a good part of the chapter is devoted to the synthesis of various layers of the membrane. We give an overview of the main methods and materials used for preparing such membranes and characterizing them, as well as their key advantages and limitations. The discussion covers both isotropic and anisotropic membranes, prepared from a range of materials (zirconia, titania, alumina, hafnia, tin oxide, mixed oxides, zeolite membranes, silica, hybrid organic–ceramic membranes and metallo-organic frameworks). We analyse in detail the formation of support layer and list some rules of thumb collected by many researchers in numerous trials. A key aspect here is the gradual transition from the support layer through the intermediate layers and ultimately to the top layer. The development of top layer is reviewed through the basics of chemical vapour deposition (CVD), sol–gel technology and zeolite modifications. The chapter concludes with a list of books for further reading, qualitative and quantitative exercises and references.

A membrane is a semipermeable active or passive barrier that permits the passage of one or more components in the initial mix and limits the passage of others. Although Graham in 1848 used a sort of membrane in the development of diffusion law, and although the first membranes were synthesized more than a century ago, the development and implementation of membranes really turned into a scientific discipline in the second half of the twentieth century.

Ceramic Membranes: New Opportunities and Practical Applications, First Edition. Vitaly Gitis and Gadi Rothenberg.
© 2016 Wiley-VCH Verlag GmbH & Co. KGaA. Published 2016 by Wiley-VCH Verlag GmbH & Co. KGaA.

Today's membranes, with their modest energy demands and small footprint, have become even more attractive and are often compared favourably with conventional separation processes such as distillation, adsorption, absorption, extraction and crystallization. There are many books on the development, characterization and implementation of polymer membranes. Ceramic membranes are much less in the focus, and this book will hopefully rectify this a little, by shedding light on this important subfield of membrane science.

By the layman's definition, ceramics are materials made of pottery (*κέραμοζ* in Greek) that is then hardened by heat. A more scientific definition (from the *Ceramic Tile Institute of America*) describes ceramic material as an inorganic, non-metallic solid prepared by the action of heat and subsequent cooling [1]. This definition explores an older Sanskrit meaning of the Greek *keramos* – to be burned (unlike glass that is amorphous, ceramics are crystalline materials). Ceramics are compounds of metallic and non-metallic elements such as aluminium and oxygen (Al_2O_3), zirconium and oxygen (ZrO_2) or silicon and carbon (SiC). These compounds occur naturally in clays and other minerals and are processed in supported forms. With such available ingredients, simple recipes and long-term robustness, no wonder that archaeologists have found man-made ceramics that date back to at least 24,000 BC [2]. The durability of ceramic artefacts has given them prominence in archaeology [3]. Ceramics were one of the remarkable keystones that marked the transition from Stone to Bronze Age when humans first started using man-made tools instead of sharpened stones. In this sense, ceramics are the oldest of three large classes of solid materials (ceramics, metals and polymers) on the main development route of industrial products. The first ceramics, found in former Czechoslovakia, were made of animal fat and bone mixed with bone ash and clays [4]. The initial mix was hardened at kilns dug in the ground at temperatures between 500 and 800 °C. We do not know how these ceramics were then used. The first use of ceramics as containers for holding and storing grains and other food dates back to 9000 BC. Heating the sand that contained calcium oxide combined with soda resulted in a coloured glaze on ceramic containers in Upper Egypt about 8000 BC [5]. One of the earliest civilizations, the Sumerians who lived in Southern Mesopotamia (modern Iraq) more than 5000 years ago, wrote on ceramic stone plaques. The ceramic amphora, which was invented in Greece, became a standard for the transport and storage of liquids (mostly wine and olive oil) in the Roman Empire. The need to purify the water transported in air-open aqueducts [6] expanded the use of ceramics in the Empire. Figure 1.1 shows one of the first ceramic filters, which dates back to Israel Iron Age II – 800 BC (an artefact from the Israeli National Museum).

So ceramics have been with us for thousands of years, but ceramic technology has really developed only in the last century. Today's ceramics are no longer just dinnerware, bricks and toilets. Technical ceramics are used in space shuttles, engines, artificial bones and teeth, computers and other electronic devices and of course membranes. The first modern industrial application of ceramic membranes was in the separation of U-238 and U-235 isotopes for making nuclear



Figure 1.1 One of the first ceramic filters dated back to the second Iron Age, circa 800 BC. A clay vessel that is probably used for serving beer. (https://www.pinterest.com/pearsonaf/pottery-of-the-past/.)

weapons and fuels in the 1940s and 1950s [7]. This separation was performed at high temperatures by forcing highly corrosive UF_6 through semipermeable membranes. The only membrane materials that could withstand such harsh environments were oxides such as Al_2O_3, TiO_2 and ZrO_2. Many aspects of that work, carried out by the Western Bloc during the Second World War (the so-called *Manhattan Project*), are still classified [8]. The only information on these comes from several patents filed in the 1970s. Trials using the same membranes in purification of liquids met with limited success, mainly due to low separation efficiency and low flux. The idea of dividing a membrane into a skin and a porous substructure, proposed by Loeb and Sourirajan [9] in 1962 for polymer membranes, boosted the development of a new generation of ceramic membranes. It appeared that ceramic membranes could also be made in a number of layers like onions. In this new anisotropic membrane, the skin layer determines the separation and the support layer gives the mechanical strength and uninterrupted flux. Technical questions on fusion of layers made from different materials were significantly facilitated by Burggraaf and Cot [10] who developed in the 1980s a concept and procedures for intermediate membrane layers. This opened the door to applications in food and beverage industries [11,12], gas separation [13,14] and biotechnology [15], albeit in small installations.

In the past two decades, ceramic membranes have become a valuable component of fuel cells and play a central part in the hydrogen economy. Full-scale installations for water and wastewater purification started in Japan in 1998, and have recently started spreading to Europe and the United States. The separation of uranium isotopes, that started more than half a century ago, reached its maximum in the 1970s when nuclear energy was considered a valuable replacement of fossil fuels. However, after the Chernobyl disaster in 1986, reassessment of true amount of

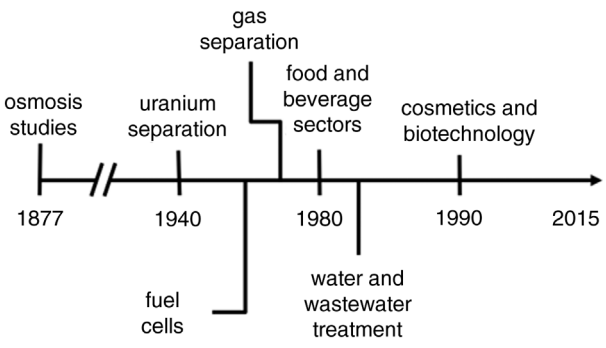


Figure 1.2 A timeline of ceramic membrane applications.

fossil fuels available, and development of more cost-effective uranium enrichment techniques such as centrifuge and laser, the use of ceramic membranes for uranium enrichment halted. Companies such as Atech Innovations, Orelis, Veolia Water, Hyflux, Kubota, TAMI Industries, Inoceramic GmbH, Metawater, Mitsui, Meidensha, Jiangsu Jiuwu, Pervatech and Ceraver [16,17] [acquired by Alcoa in 1986, then Societe des Ceramiques Techniques as USFilter in 1992, and (since April 2002) Pall Corporation] now advance ceramic membranes in new fields such as the water and wastewater treatment, food and beverages, chemical, pharmaceutical, electronic, petrochemical and energy sectors. Figure 1.2 sketches a brief of ceramic membrane history and their entry into various industrial sectors.

Today, ceramic membranes are established in modern separation techniques. As we will show in this book, in the future ceramic membranes with their clear advantages in chemical and thermal stability, longer lifetime, higher flux and higher recoveries will be employed in more applications. This is supported by recent reports on large-scale piloting with ceramic membranes and several full-scale installations. Here we will introduce the main developments in ceramic membranes, starting with a brief introduction into the general field of membranes that will help us to discuss technical details of membrane preparation and operation.

1.2 The Basics of Membrane Separation

Here we give a very brief introduction to the general membrane field emphasizing the difference between ceramic and other membranes, where appropriate. For readers wishing to delve deeper into the principles of membrane separations, there are several books that give a good introduction to the subject [16–18]. Other books with a special emphasis on the ceramic membranes are also briefly discussed in the 'Further Reading' section at the end of this chapter (Section 1.10).

Ceramic membranes, as any other membranes, are used for separating suspensions, aerosols and mixtures. They leave particles, organic molecules, dissolved salts or even gases and liquids on one side and transfer purified gases and liquids to the other. Thus, the ceramic membrane is a semipermeable barrier that separates purified and concentrated streams out of a mixture. Figure 1.3 depicts the essentials of membrane separation where the initial feed is separated into *permeate* and *retentate* streams. If the separation is performed for purification purposes, the permeate stream is the final product and the retentate stream is the by-product. If the separation is performed to concentrate a component in the mixture, the retentate stream is the product and the permeate is the by-product.

Mathematically, we express the above definition as the feed flow that approaches the membrane splits into permeate and retentate flows:

$$Q_f = Q_r + Q_p \tag{1.1}$$

where Q_f, Q_r and Q_p are the feed, the retentate and the permeate flows.

The efficiency of separation is evaluated using two parameters: the quantity of purified gas–liquid on the permeate side and the degree of purification. With different membrane areas and measurement periods, the quantity is unified by the transmembrane flux defined as the volume of gas–liquid passing through a unit of membrane area per a period of time:

$$J = \frac{Q_p}{A_m} \tag{1.2}$$

where J is the volume flux, Q_p is the flow of the fluid that passes through a membrane, and A_m is the membrane surface area. Fluxes in liquid–liquid separations are typically reported in litres per square metre of the membrane surface per hour (l/(m^2 h)) or gallons per square foot per day (gallons/(ft^2 day)). Fluxes in

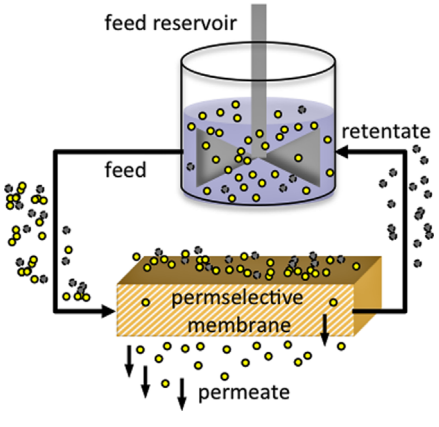


Figure 1.3 The basic membrane separation set-up showing the feed tank, the permselective membrane and the feed, permeate and retentate flows.

gas and vapour separation are reported in cubic centimetres of gas per second per square centimetre of membrane area ($cm^3/(cm^2\ s)$). Transmembrane pressure and temperature significantly change gas fluxes and reported gas flux values assume standard conditions of 0 °C and 1 atm. The volume flux J can be converted into mass flux or molar flux by using the density and the molecular weight of the feed, respectively. Some processes, for example DNA or protein purification, require high separation efficiency [19]. In others, the membranes must provide a predetermined flux (e.g. in dialysis or controlled drug release). Membranes used in controlled drug delivery need to provide a certain flux of a drug from a reservoir to the body. The ratio of permeate to the feed flux/flow is called the recovery ratio, RR, and defined as

$$\mathrm{RR} = \frac{Q_\mathrm{p}}{Q_\mathrm{f}} \tag{1.3}$$

A fluid passes through a membrane by the shortest path. Intuitively, the fluid should be forced through a membrane perpendicularly to its surface following this general concept of *dead-end filtration*. The concept of filtration perpendicular to the filter surface was developed for granular filters in France in the middle of the eighteenth century. An additional tangential or a *cross-flow filtration* (CFF), also known as *tangential flow filtration* (TFF), was developed in the middle of the twentieth century. In this mode, a fluid flows in parallel to the membrane surface. A pressure difference across the membrane drives the fluid through the membrane. Figure 1.4 shows the dead-end and cross-flow filtration modes.

The *transmembrane pressure* (TMP) in dead-end filtration is calculated as

$$\mathrm{TMP} = P_\mathrm{f} - P_\mathrm{p} \tag{1.4}$$

The TMP in cross-flow filtration is an average between the pressure on permeate and retentate sides:

$$\mathrm{TMP} = \frac{1}{2}(P_\mathrm{f} + P_\mathrm{r}) - P_\mathrm{p} \tag{1.5}$$

Here P_f, P_r and P_p are the feed, retentate and permeate pressures, respectively. In a single-stage installation, the permeate pipe is open to the air and, therefore, P_p

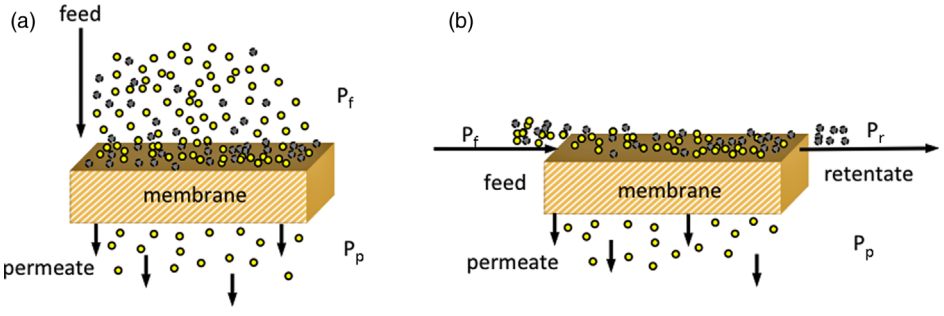


Figure 1.4 Schematics of dead-end (a) and cross-flow (b) filtration modes.

equals 1 bar. The TMP thus is the additional pressure (above the atmospheric pressure) needed to pass a fluid through a membrane. Dead-end filtration is more suitable for treating dilute suspensions. Conversely, cross-flow filtration is used for more concentrated suspensions when the deposits are swept away from the membrane surface by the shear stress that is exerted by the flow.

A fluid passes through the membrane overcoming its resistance. This resistance has two components: the intrinsic resistance of the membrane itself, and the resistance of materials accumulated within the membrane during the filtration operation:

$$R_t = R_m + R_o \tag{1.6}$$

where R_m, R_o and R_t are the membrane resistance, the operational resistance and the total resistance, respectively. The increase in the total resistance is the result of changes in the operational resistance when the membrane resistance remains constant.

A flux J (Eq. (1.2)) through the membrane system is related to the TMP (Eq. (1.4)) through the total resistance R_t (see Eq. (1.6)) as

$$J = \frac{\mathrm{TMP}}{R_t \mu} \tag{1.7}$$

where μ is the viscosity of the fluid at a given temperature. A ratio of flux to TMP for a given membrane depends on the total membrane resistance and the viscosity but not on the operational parameters. The *membrane permeability M* (Eq. (1.8)) is independent of the applied pressure and permits the comparison of the performances of different membranes operating under various conditions:

$$M = \frac{J}{\mathrm{TMP}} \tag{1.8}$$

A permeability coefficient through a gas separation membrane takes into account the membrane thickness:

$$P^* = \frac{J \Delta l}{\Delta P} \tag{1.9}$$

Here P^* is the permeance through a membrane of thickness Δl and ΔP is the partial pressure difference of a gas across the membrane. A transmembrane gas flux J depends on the membrane thickness but does not depend on fluid viscosity as in Eq. (1.7).

The degree of purification or the membrane selectivity is often evaluated using its retention ratio R or the separation factor α. In dilute solutions, it is more convenient to report the selectivity by R assuming that the solute is partially retained by the membrane when the solvent passes freely through the membrane:

$$R = 1 - \frac{C_p}{C_f} \tag{1.10}$$

where C_p and C_f are the concentrations of the separable compound in the permeate and in the feed, respectively. The retention ratio is dimensionless and

does not depend on the units in which concentration is expressed. Its value ranges from 0 for a free penetration up to 1 for complete retention. The membrane selectivity in separation of gases and organic liquids, α_{AB}, is expressed by the ratio of pure gas permeabilities for the individual components A and B:

$$\alpha_{AB} = \frac{P_A}{P_B} \tag{1.11}$$

Permeation through membranes occurs in two stages. A sorption of gas molecules onto and into membrane surface is followed by the diffusion of a gas through the membrane. Thus, the permeability P can be expressed as a multiplication of a thermodynamic component K related to sorption and kinetic component related to diffusion D:

$$\alpha_{AB} = \frac{P_A}{P_B} = \left(\frac{K_A}{K_B}\right)\left(\frac{D_A}{D_B}\right) \tag{1.12}$$

In this equation, the diffusion coefficients D_A and D_B reflect mobilities of individual molecules in the membrane material, while the gas sorption coefficients K_A and K_B (cm^3 of component in cm^3 of membrane) express the number of molecules A and B adsorbed or dissolved in the membrane material. The K_A/K_B ratio can be viewed as the sorption or solubility selectivity of gases A and B [18]. As defined in Eqs. (1.11) and (1.12), α_{AB} is the ideal coefficient that does not account for mutual interactions of gases as they pass through a membrane. In binary mixtures with significant concentrations of A and B, the coefficient is calculated as the molar retention ratio, α_{AB}:

$$\alpha_{AB} = \frac{y_A/y_B}{x_A/x_B} \tag{1.13}$$

where [y_A, y_B] are concentrations of gases A and B in the permeate, and [x_A, x_B] are their concentrations in the feed.

The selectivity is always >= 1. If the concentration of A in the permeate is higher than the concentration of B, the separation is denoted as α_{AB}. If the concentration of B in the permeate is higher than that of A, the separation is denoted as α_{BA}. If $\alpha_{AB} = \alpha_{BA}$, no separation is achieved [16].

1.3 Membrane Separation Processes

Membrane separation is a field that embraces many processes. These are subdivided by the origin of the applied driving force, phases of feed and permeate and pore size. The division by the driving force describes the origin of the force needed to transfer the fluid from the feed to the permeate side. Pressure, temperature, concentration or electrical potential are the driving forces available. Table 1.1 lists some common membrane processes, separation phases, driving forces, sizes of retained compounds and their types.

Table 1.1 Common membrane separation processes.

Membrane process	Feed phase – permeate phase	Driving force	Size of retained compounds	Type of retained compounds
Microfiltration (MF)	L → L	ΔP	0.1–100 μm	Bacteria, fine solids
Ultrafiltration (UF)	L → L	ΔP	5 nm to 100 μm	Viruses, total suspended solids, natural organic matter
Nanofiltration (NF)	L → L	ΔP	1 nm to 100 μm	Inorganics, sugars, dyes, surfactants
Reverse osmosis (RO)	L → L	ΔP	0.1 nm to 100 μm	Salts, metal ions, minerals
Gas separation	G → G	ΔP	0.5 nm to 100 μm	Gases
Vapour permeation	G → G	ΔP	0.5 nm to 100 μm	Liquids
Pervaporation	L → G	ΔP	0.5 nm to 100 μm	Liquids
Electrodialysis	L → L	$\Delta\Phi$		Ions
Dialysis	L → L	ΔC		
Membrane distillation	L → L	ΔT		Liquids

Note: G and L stand for gas and liquid phases, respectively, ΔP is the pressure difference, $\Delta\Phi$ is the electrical potential difference, ΔC is the concentration difference and ΔT is the temperature difference.

Except for membrane distillation (see Section 4.4.5) that uses a temperature difference as the driving force, ceramic membrane separations use pressure. The level of applied pressure varies as a function of size of solutes separated by a membrane. For the same flux J, small pores require high pressure and offer a retention of small solutes. A relation between pore size, solute size, flux and applied pressure resulted in an additional subclassification of pressure-driven membrane processes mostly applicable in particle–liquid separation. Particles in liquids can be quite big and reach the maximum size of 100 μm. Membranes are generally not applied for the retention of particles larger than 100 μm. These separations are typically done using either sedimentation or filtration. Membranes separate particles using pressure as the driving force and micro-, ultra-, nano- and subnanopores incorporated in microfiltration (MF), ultrafiltration, nanofiltration and reverse osmosis (RO) membranes. Table 1.1 details proper implementation of pressure-driven membranes in particle–liquid separation. *Reverse osmosis* and *nanofiltration* are processes used for separating solute and solvent components on the nanoscale. Water desalination is the most famous example of RO technology. The separation is so sensitive that while water molecules with a radius of 1.3 Å diffuse through the membrane, electrolytes and organic solutes with several hydrophilic groups cannot pass. Nanofiltration is similar to RO, and uses the same principles. The pores of NF membranes are slightly larger than in RO membranes and they can separate multivalent ions.

Two main advantages of NF over RO membranes are the lower operational costs due to a lower required TMP and a wider choice of membrane materials. Both processes are commercially performed with polymer membranes, where the dense polymer layer needed for separation of monovalent ions can be synthesized from cellulose acetate (CA) or polyamide (PA). Similarly, NF membranes are made from cellulose acetate blends or polyamide composites but can also be synthesized from more stable polymers such as polysulfone or polypiperazine. Ceramic NF membranes are prepared from alumina, titania, hafnia, silica–zirconia and zeolites, although higher cost and lower mechanical strength are currently limiting their wide commercialization.

Ultrafiltration and *microfiltration* are another popular subclass of membrane separation processes. Although RO, NF, UF and MF processes are all pressure-driven, a significant difference in the pore size determines different applications and features of these membranes. The UF/MF membranes are used in the food and beverage industries, in water and wastewater purification, in pharmacology and in medicine. A typical size of separable colloidal particles and high-molecular-weight solutes ranges from single nanometre to micrometres, so UF/MF membranes cannot be used in desalination. On the positive side, the bigger pore size means that a much lower TMP is needed to achieve a reasonable flux. Polymeric MF/UF membranes are synthesized from polyacrylonitrile (PAN), polysulfone (PS), polyethersulfone (PES) and polyvinylidene fluoride (PVDF). These polymers are more mechanically, thermally and chemically stable than cellulose acetate and polyamide and the resulting UF/MF membranes are employed under harsh conditions. There is no clear distinction between UF and MF (basically, the same particles can be retained by both membranes with the same applied TMP and with higher separation efficiency of UF membranes). The recent trend is therefore to use more UF membranes with a smaller pore size and a wider range of separated materials. Ceramic UF membranes synthesized from alumina, titania and zirconia are used in separations performed at high temperatures or with non-aqueous solvents such as benzene or toluene.

Gas separation, pervaporation and membrane distillation membranes deal with small molecules. The separation of gas molecules on the basis of their size requires small pores that can be described as low NF pores. The subdivision into MF, UF or NF membranes is therefore not applicable here and it is not implemented. Unsurprisingly, gas separation is performed with gas separation membranes. The basic role in the implementation of a certain type of membranes is rather simple – a preset degree of purification is to be achieved at a lowest possible cost. Larger membrane pores produce less resistance to the transmembrane flow and demand less pump energy. Thus, the membrane operational costs increase in the order MF → UF → NF → RO but so does the retention. This subdivision is somewhat arbitrary and the same membrane may be described as UF, MF or NF (although RO membranes are rarely mixed with others). We will get back to definitions and methods of detection of membrane pores in Chapter 3.

1.4
The Morphology of Membranes

From a morphological point of view, membranes are divided into two large groups. *Porous membranes* transport the solutes in a continuous fluid phase through the voids within the membrane structure. *Dense membranes* transport solutes by dissolution and diffusion across the membrane. Most ceramic membranes are porous. The examples of non-porous ones include Pd membranes for hydrogen separation and mixed (electronic, ionic) conducting oxides for oxygen separation [20]. Both porous and dense membranes can be prepared from polymers, ceramics, paper, glass and metals. The polymer membranes are also called 'organic' ones, while ceramic, glass and metal membranes are called 'inorganic'. Polymer membranes are synthesized from different polymers, including cellulose, polyacrylonitrile, polyamide, polysulfone, polyethersulfone, polycarbonate, polyethylene, polypropylene and polyvinylidene fluoride. In addition, many polymers are grafted, custom-tailored, blended or used in a form of copolymers [21,22]. These modifications are made to increase the flux and retention of certain compounds or to avoid the flux drop due to accumulation of compounds on the membrane surface. Metal membranes are manufactured from palladium, nickel, silver, zirconium and their alloys, while ceramic membranes are made from metal oxides (alumina, titanium, zirconia), silica, zeolites and other mixed oxides.

There are various membrane preparation techniques, each with its own pros and cons. Typically, polymer membranes are prepared by phase inversion [9], track etching [23] and stretching [24]. Inorganic membranes are prepared by calcination and sintering and coated using sol–gel processes, chemical vapour deposition or hydrothermal methods. A detailed discussion on preparation techniques of ceramic membranes is given in Section 1.9.

The morphology of ceramic membranes is closely related to the membranes' pores. Pore size and size distribution, structure and tortuosity, interconnectivity and density (i.e. the number of pores per unit area) are the physical parameters that affect flux and separation efficiency. Membrane pore sizes are subdivided into *macropores* (diameter >50 nm), *mesopores* (between 50 and 2 nm) and *micropores* (<2 nm). The International Union of Pure and Applied Chemistry (IUPAC) also distinguishes between *supermicropores* (<2 nm) and *ultramicropores* (<0.7 nm) [25]. Pore size distribution indicates the presence of pores of different sizes within the membrane. Pore density is described by the *porosity* – the membrane surface or the membrane volume occupied by pores versus the total membrane surface or volume, respectively. Detailed definition of pore densities and their definitions are given in Chapter 3. Less porous structures are stronger, but also more resistant to flow, so the optimal porosity is a trade-off between the stability and the flux. There is no one-to-one relation between the porosity and the separation efficiency. After the initial packing of particles, the colloidal or polymer soils are heated at high temperatures. The sintering that occurs during the heating results in changes in porosity and pore size. Yet, the higher packing density of smaller initial grains, that is a low initial porosity,

embeds more uniform distribution of grains during the sintering and will result in denser membranes with smaller pores [26].

Membrane structures are divided according to the type of their pores. Membranes with finger-like pores are called *isotropic* (having symmetrical pores going from one to another membrane side with the same width). Membranes with sponge-like pores are called *anisotropic* (having asymmetrical pores, see Figure 1.5).

The synthesis of membranes with symmetric pores is relatively simple, and symmetric nitrocellulose MF and UF membranes were successfully prepared in Germany a century ago [27]. These membranes were later commercialized by Sartorius and used by the German army during the Second World War for bacteriological water quality tests in cities where the water supply system was destroyed. A symmetric membrane has a rigid void structure with randomly distributed interconnected pores. Such a membrane acts as a molecular sieve, retaining solutes that are larger than its pore size and transferring those having similar or smaller dimensions. The pore size itself, however, can vary significantly from 100 μm all the way down to 3–5 Å. It can be so small that these membranes are sometimes described as non-porous [17]. The transition through such pores is by diffusion, driven by either concentration or electrical potential gradient. Porous membranes can be electrically charged when the pore walls carry either a positive charge (anion exchange membranes) or a negative one (cation exchange membranes). The main problem of symmetric membranes is their inherent high resistance to the flow due to the pore width uniformity. Moreover, the selectivity of symmetric membranes is determined already at the skin membrane part and does not change through the pore.

In 1962, Loeb and Sourirajan solved the problem of unnecessary resistance to the flow, inventing asymmetric polymeric membranes [9]. Here, the separation is determined by the upper membrane layer, and the mechanical strength and support are provided by the lower layers. The upper separation layer has the smallest pores within the membrane structure, while the supporting system has larger

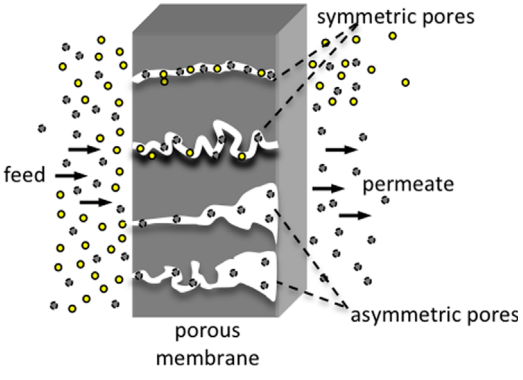


Figure 1.5 Symmetric and asymmetric membrane pores.

pores with lower hydraulic resistance to the permeate flow. The surface and support layers can be prepared simultaneously or sequentially. The membrane can be *homogeneous*, that is made from one material, or a *composite* made from different materials. In the latter case, the pore size and structures are conveniently determined by each constituent. Most ceramic membranes are asymmetric composites made from four or even five different layers. The composite structure of ceramic membranes is depicted in Figure 1.6, together with a cross-sectional scanning electron micrograph of a γ-alumina thin top layer of small pore sizes on top of an α-alumina support layer with gradually increasing pores towards the permeate side.

The membrane support layer D, often called simply 'the support', has to provide the maximum mechanical strength at the minimum membrane resistance. The support is therefore often over 1 mm thick and macroporous. Such thick supports are very stable but are also resistant to transmembrane flow. An intrinsic deficiency of membrane supports is their high average pore size, high surface roughness and high void defect density. The ideal membrane support layer should be strong, homogeneous, stable and possess minimum flow resistance but not the separation ability [29]. It must also be chemically compatible with the intermediate and filtration layers, and mechanically and thermally stable.

The intermediate layers B and C must provide good chemical and thermal stability, and must have a narrow pore size distribution and a smooth homogeneous surface. While the former is a general requirement for the entire ceramic membrane, the smooth surface relates to the main function of intermediate layers. It is almost impossible to coat the separation layer A on top of the support layer D with macroporous voids. Therefore, the intermediate layers B and C are used to gradually decrease the pore size of the support, thus preventing the penetration of the very fine particles used for the formation of top layer. Typical intermediate layers are thick enough to increase the mechanical strength of a ceramic membrane. The thickness of a single intermediate layer is usually a few

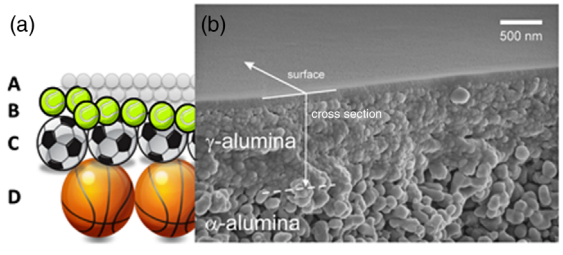


Figure 1.6 (a) Pictorial representation of an asymmetric composite ceramic membrane that consists of a nanofiltration-modified separation layer of 50 nm depth with pores less than 2 nm wide (A), an ultrafiltration layer of 100–500 nm depth with 10 nm pores (B), a 1–10 μm microfiltration intermediate layer with pores 100–200 nm wide (C) and a porous support of 1–1.5 mm width (D). (b) Scanning electron micrograph of a cross section of a ceramic composite membrane: γ-alumina on top of an α-alumina support [28].

hundred micrometres. Pore widths are in a mesoporous range of 2–50 nm in diameter. The number of intermediate layers varies, depending upon the difference in grain sizes between layers A and D, and the intended membrane use. Membranes for water and wastewater treatment might possess a support and maybe one intermediate layer. Gas separation membranes will contain four to five layers with macropores in the support and ultramicropores in the top layer. Generally, the bigger the difference in the pore widths between the support and the top layer, the higher the number of layers. An insufficient number of intermediate layers will result in penetration of small particles into the next-layer pores, leading to an increase of flow resistance and low mechanical stability of the sintered membranes [20].

The actual separation is performed in the top layer A. This layer is typically coated last on top of an existing membrane from different materials. It is responsible for the separation and therefore contains the smallest pores in the membrane structure. Note that this layer is not responsible for the mechanical strength of the membrane and thus it is relatively thin. A typical thickness of the separation layer is between 10 and 20 µm, and the intermediate and support layer are of 1–2 mm in total. Similar to layers B and C, the top layer A should be chemically and thermally stable and must possess a narrow pore size distribution and a smooth homogeneous surface. Importantly, the top layer may not have any large pores – even a few macropores will render the membrane useless as the entire flux will be directed through those pores. In fact, a good top layer should also compensate for any structural defects of the intermediate layers.

Together, this multilayer configuration provides the membrane its separation and flux properties. Every membrane layer is functional and purposeful, yet the total number of membrane layers varies depending upon the separation processes. For a precise separation such as gas separation or water desalination, the membrane will contain all A + B + C + D layers. Conversely, the concentration of proteins in food and dairy industries or sterilization of beverages does not require the microporous separation and can be performed with layers C and D only. Table 1.2 shows the link between a number of layers in a ceramic membrane and its designated separation process [30].

Table 1.2 The layer structure of composite ceramic membranes.

Separation process	Number of layers	Average pore size
Microfiltration (MF)	1	5 µm
	2	0.25 µm
Ultrafiltration (UF)	3	100 nm
Nanofiltration (NF)	4	2 nm
Reverse osmosis (RO), gas separation, pervaporation, vapour permeation	5	10 Å

Source: After Bonekamp [30].

Layer A is sintered; layers B, C and D are produced by sequential calcination at high temperatures making the manufacturing of ceramic membranes a complicated procedure. Layer A is often produced by CVD or by sol–gel techniques [31] and requires a high variability to suit the separation needs.

1.5 Membrane Modules

Laboratory-scale ceramic membranes are typically produced in a plain form, often as small discs suitable for cylindrical benchscale filtration units. This geometry reduces production expenses and makes further examination of the membrane surface easier. Small solid ceramic discs are also fun to play with. Typical available membrane surface ranges from a few to a few dozen square centimetres. Practical, real-life industrial membrane applications require hundreds or even thousands of square metres of membrane surface, raising the question of packing density. The *membrane packing density* is defined as the total membrane surface available per a module volume. Each module needs space and the packing density is an expression of membrane footprint. Commercial membranes are produced in plate or tubular form. The membranes are packaged in modules that represent the 'smallest discrete separation unit in a membrane system' [32]. Each module contains at least several square metres of the membrane surface potted or sealed into an assembly. Modules are assembled in larger production units, also called *skids*, *racks* or *trains*. A production unit shares feed, retentate and filtrate valves, and allows the isolation of single modules. Plate membranes are assembled in plate-and-frame and spiral-wound modules, and tubular membranes are assembled in tubular and hollow fibre modules. Plate-and-frame and spiral-wound modules are often employed in cross-flow mode (see Figure 1.4). Tubular and hollow fibres are often used in dead-end and semi-dead end installations. Plate ceramic membranes cannot be bent, and therefore relevant ceramic membrane skid geometries are plate-and-frame, tubular (also called honeycomb) and hollow fibres.

The development of membrane modules started soon after the membranes entered large-scale industrial processes. *Plate-and-frame modules* developed in the 1960s are probably the oldest configurations used in commercial applications [33]. The design of modules was inspired by the filtration technology and is similar to a simple filter press. A module consists of multiple flat sheet units packed together as a multilayered sandwich. Each unit includes a support plate, a flat membrane sheet and feed and permeate spacers. A flat sheet placed on the permeate spacer is bent over the support plate, forming an envelope open to the feed from both sides. The edges of the membrane are sealed to the support. Many of these units, called cassettes, are stacked in parallel to form the module. Figure 1.7 shows an example of industrial tubular membranes made of alumina, the essence of the module. The feed fills the entire empty volume and is either released through a central permeate channel as the permeate or collected at the

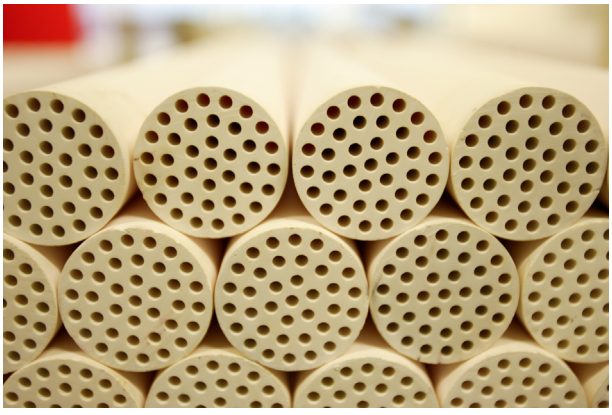


Figure 1.7 Stacks of tubular alumina membranes after the sintering stage. (Photo courtesy of Atech Innovations GmbH.)

exit as the retentate. Two main advantages of plate-and-frame modules are the ease of cleaning and replacement of defective membranes and the ability to handle viscous feeds. A low packing density is the main disadvantage of plate-and-frame modules. The packing density of plate-and-frame modules can be increased with alumina multichannel monolithic elements [34] or by stacking many membrane sheets together [35].

The packing density of flat sheets was increased in *spiral-wound modules* invented at the end of 1960s [36,37], a few years after the plate-and-frame modules. The module is arranged exactly as you would expect – several pairs of membrane sheets are placed back-to-back and then wound up. The edges of each pair of sheets are sealed to each other on three sides. On the fourth side, they are attached to a central perforated permeate channel of a pressure vessel. The sheets in a pair are separated by a fabric spacer that allows a permeate flow. A single spiral-wound module may consist of up to 20 pairs of sheets, each separated by a plastic mesh called a *feed spacer*. Viewed from the side, the path of a fluid on either feed or permeate side looks like an Archimedean spiral. The feed is usually pumped into the space outside the envelope through the feed spacers. Similarly, the permeate flows through a permeate spacer to the permeate channel. The advantages of the spiral-wound module are the high packing density and relatively low manufacturing cost. Its disadvantages are the difficulties in cleaning and repair of damaged membranes.

A parallel approach for increasing the packing density is to synthesize narrow hollow tubes, each only a few millimetres in diameter [38]. Although the diameter of each hollow fibre is small, a bundle of fibres packed inside a pressure vessel will have several square metres in total membrane surface. A typical commercial hollow fibre module consists of a few hundred to several thousand fibres. The fibres are often glued with a resin on the end that is far from the

pump, so the feed must pass through the membrane. In this case, the hollow-fibre module works in a dead-end mode, having only two streams: one for the feed and one for the permeate. The retentate is held inside the fibres and released only during washing. If the feed can go through the membrane and be released as the retentate, the membrane works in a cross-flow mode. The modules are typically mounted vertically (although the option of a horizontal mounting does exist). If the skin membrane layer A (Figure 1.6) is synthesized near the lumen part of the fibre (the inside), the separation is performed in *inside-out mode*. If the skin layer is on the outer part of the fibre, the separation is performed in *outside-in mode*. The advantages of a hollow-fibre module include high packing density, a relative ease of cleaning and replacement/shutting down of single fibres and low dead volumes. Reported packing densities calculated as surface area to volume ratios are 30–250 m^2/m^3 for tubes, 130–500 m^2/m^3 for plate and frame and up to 9000 m^2/m^3 for hollow fibres [39]. The main disadvantage is the fragility of single fibres.

Hollow tubes can be small in diameter and thus fragile, or larger and more robust. Originally, *tubular modules* consisted of several single tubes with large inside diameters between 0.3 and 2.5 cm [40]. The wall thickness of a single element was about 2 mm. The tubes are bundled together similarly to hollow fibres and placed inside a plastic or stainless steel vessel to form a cartridge. These tubular membranes can have either circular or elliptic cross sections. Such membranes are usually cast in place within a support tube made of fibreglass, ceramic, plastic or stainless steel. Higher mechanical strength and relative ease of cleaning and replacement of single tubes are the advantages of tubular modules. The tubes are also less prone to clogging than fibres and spirals [41]. Low packing density, high capital cost and high dead end volume are the main disadvantages. A high internal hold-up volume of each tube allows creating turbulent flow regimes with intensive pumping and indeed tubular membranes are used in feeds with high solid content. Although there are some suppliers that still produce those elements, majority of them have switched to *multichannel* or *honeycomb* configurations. The channels of millimetres have become a part of one large element. The elements were produced commercially by SCT-Exekia and Orelis and called Membralox® and Kerasep® membrane modules, respectively. Further development of the elements changed the cylindrical shape of the channels for non-cylindrical flower-like geometries [42]. These elements with cross-sectional diameters of 10 or 25 mm and excellent packing density were developed by Metawater (Japan) and Tami Industries (France). The total dimensions of a single element can be up to 0.2 m in diameter and 1.5 m in length, and their total available membrane area is above 10 m^2. The typical membrane element size cannot be increased any further due to limited hydraulic resistance of top layer and a chance for peeling off the top layer. Table 1.3 compares the relative advantages of each configuration, emphasizing the exploitation advantages of each module.

Here the *hold-up volume* is defined as the volume of the fluid retained inside the filter during the filtration process. An additional parameter significant in the

Table 1.3 Advantages and disadvantages of tubular and plate-and-frame modules.

	Hollow fibre	Plate-and-frame	Tubular
Cost/area	Low	High	Low
Membrane replacement cost	Moderate	Low	Moderate/low
Flux (l/(m^2 h))	Good	Low	Low
Packing density (m^2/m^3)	Excellent	Good/fair	Good
Hold-up volume	Low	Medium	Medium
Cleaning in place	Good	Fair/poor	Fair/poor

Source: Modified after Ref. [43].

selection of a membrane module is the feed channel height. Selecting the correct height can prevent channel blockage. A rule of thumb in the industry is that the channel height should be at least 10 times larger than the diameter of the largest particle that can ever enter the channel. That ratio increases up to 25 : 1 in spiral-wound modules [44]. Companies resort to the lowest possible ratio to prevent intensive pumping. Larger pump capacities are needed in filtration with modules with high channel heights.

The above analysis of relative advantages and disadvantages of different modules has been known to membrane manufacturers for a long time. Still, companies use all types of modules when the exact design is a proprietary of the membrane manufacturer. For example, Asahi Kasei (Japan), GE Healthcare (United Kingdom) and inge AG (Germany) use hollow fibres. Pall Corporation (USA), Sartorius (Germany), GE Healthcare (UK) and Microdyn-Nadire (Germany) use plate-and-frame modules. Pall Corporation (USA), NovaSep Process (France), Tami Industries (France) and IBMEM (Germany) are using tubular modules. Koch membrane systems (USA) uses all types of modules.

1.6 Fouling and Cleaning

1.6.1 Fouling

A membrane module can be operated in either constant flux or constant pressure mode. In a constant flux mode, the flux through the membrane remains constant, but the TMP rises as the operation continues. Conversely, in a constant pressure mode, the pressure remains constant, but the flux decreases. In both cases, we understand that the main operational parameters change during the operation and membrane performance deteriorates. This happens because of fouling, defined as 'The process resulting in loss of performance of a membrane

due to the deposition of suspended or dissolved substances on its external surfaces, at its pore openings, or within its pores' [45]. The deterioration is so severe that the membrane operation must be stopped periodically for cleaning. Both fouling and cleaning are two integral parts of the membrane operation that now can be properly described as a sequence of four stages: normal operation – fouling – cleaning – integrity test. Many books and thousands of research papers have been written on fouling and cleaning. Here we provide only a brief overview. Readers who are especially interested in fouling are referred to 'Fundamentals of fouling' by Field [46], 'Fouling and cleaning of ultrafiltration membranes: a review' by Shi *et al.* [47] or 'Membrane chemical cleaning: from art to science' by Liu *et al.* [48].

The loss of membrane performance can be due to two separate phenomena, but only one of them is called fouling. The other is the pre-concentration of solutes near the membrane surface due to a preferential passage of a solvent through the membrane. These solutes, however, are located near the membrane surface but not attached to the membrane in any way. They reduce the solvent activity and the flow. This is known as *concentration–polarization*, a natural phenomenon that can be mitigated by TMP and flux. Conversely, fouling is a phenomenon of attachment of solutes to the membrane surface that reduces the available membrane surface or blocks membrane pores. Two other forms of fouling are *cake formation* and *gel formation*. A 'cake' is formed when the fouling layers are built up on each other. In this case, the main fouling cause is the solute–solute attachment. In a case of the extreme concentration–polarization, certain macromolecules such as proteins can form a gel layer near the membrane surface.

Fouling is subdivided into four categories – inorganic, colloidal, organic and biofouling [49]. *Inorganic fouling* or *scaling* is caused by the accumulation of inorganic precipitates on membrane surface or within pore structure. Precipitates are formed when the concentration of chemical species exceeds their solubility limit. For example, if a reverse osmosis plant is operated at 0.75 recovery ratio (RR), the concentration of sparingly soluble salts in the retentate will be four times larger than their concentration in the feed. Some salts such as $CaSO_4$, $CaCO_3$ and silica are only slightly soluble and that pre-concentration level could be enough to cause scaling. Other salts such as CaF_2, $BaSO_4$ and $SrSO_4$ have a scaling potential and their concentration should be carefully inspected not to exceed the solubility limits. The inorganic fouling due to concentration polarization in MF and UF membranes is much less common, but can occur due to chemical interactions between ions and other fouling materials, such as organic polymers.

Colloidal fouling can occur with different kinds of particles. Algae, bacteria and certain natural organic matters fall in the size range of particle and colloids. However, they are different from inert particles and colloids such as silts and clays. In most cases, particles and colloids do not really foul the membrane. This is because the flux decline caused by their accumulation on the membrane surface is largely reversible by hydraulic cleaning measures such as backwash and air scrubbing. A

rare case of irreversible fouling by particles and colloids happens when they are small relative to the membrane's pores. Such particles and colloids can enter and get trapped within the pores. Removing these by hydraulic cleaning is difficult.

Organic fouling is caused by organic solutes with molecular weights ranging between few thousands and 1 million Da. For example, proteins present the main challenge in biopurification and food industry. The fouling is caused by complex solute–solvent–membrane interactions such as electrostatic, lyophilic/lyophobic, steric and covalent bonding effects. Many factors can affect organic fouling: the properties of the feed constituents such as size, hydrophobicity, charge density and isoelectric point; the properties of the membrane (hydrophobicity, charge density, surface roughness and porosity) and the properties of the solution phase, such as pH, ionic strength, and concentration of metals. Other factors of importance are the hydrodynamics of the membrane system (characterized by the solution flux) and surface shear.

Microbial fouling is a result of formation of biofilms on membrane surfaces. Once bacteria attach to the membrane, they start to multiply and produce extracellular polymeric substances (EPS) to form a viscous, slimy, hydrated gel. The EPS typically consists of heteropolysaccharides which have a high negative charge density. This gel structure protects bacterial cells from both hydraulic shearing and chemical attacks of biocides such as chlorine.

In gas separations, membrane fouling has often been neglected, mainly because feeds are protected by upstream filtration and are therefore relatively clean. The remaining foulants can damage the membrane or the seals but cannot cause fouling. There are a few reports on the organic fouling in vapour permeation [50]. We will discuss some typical fouling models in detail in Chapter 2.

1.6.2 Cleaning

Membrane cleaning can be defined as 'a process whereby material is relieved of a substance that is not an integral part of that material' [51]. An efficient cleaning should leave the membrane physically, chemically and microbiologically clean. The cleaned membrane should display adequate flux and separation efficiency, close to the features of a virgin (pristine) membrane. Cleaning of membranes is performed by physical and chemical methods, and really depends on the type of fouling. In general, physical cleaning is preferred over chemical cleaning, for two reasons. First, a physical cleaning is faster and cheaper. Second, the chance to damage a membrane by an adequate physical cleaning is much lower. However, despite all these advantages, chemical cleaning is an integral part of many membrane operations. The main reason is that not all foulants can be removed by physical cleaning. Ideally, after cleaning, the membrane surface should contain no foulants. Without dismantling the module after each cleaning, the degree of cleaning is assessed by the flux ratios through virgin and cleaned membranes. If the flux after physical cleaning is as high as the flux through a virgin membrane, the fouling is considered reversible and no chemical cleaning is needed. That

said, some foulants will deposit on the membrane surface irreversibly and their cleaning will require chemicals. A fouling that can be cured by physical cleaning is called *reversible fouling*, while one that requires a chemical intervention is called *irreversible fouling*. Figure 1.8 schematically depicts the TMP development over time in reversible and irreversible fouling.

Physical cleaning of ceramic membranes can be done by relaxation, flushing, mechanical scouring and electrical cleaning. Membrane relaxation (i.e. discontinuous operation) allows reversibly attached foulants to diffuse away from the membrane surface under the influence of a concentration gradient [52]. Flushing the membrane surface (surface wash) or membrane pores if they exist (backwash) is done with a slight overpressure, forcing the fluid to move from the permeate side to the feed side. Similarly, air scouring is employed to enhance foulant removal, especially at a relatively high TMP values. Different methods such as air backwash, air sparging and air scrubbling are employed to inject the air into the module. This is done either intermittently or continuously through either the retentate side or the permeate side of the membrane.

Chemical cleaning is done following the *similia similibus curantur* or 'like cures like' principle. In general, there are six groups of cleaning chemicals (acids, caustic, oxidants, chelating agents, surfactants and enzymes), and each group is used for treating different foulants. Caustic agents such as NaOH, for example, are typically used for cleaning membranes fouled by organic and microbial foulants by hydrolysis and solubilization. Acids such as citric acid ($HOOCCH_2C(COOH)(OH)CH_2COOH$) and nitric acid ($HNO_3$) are used primarily for

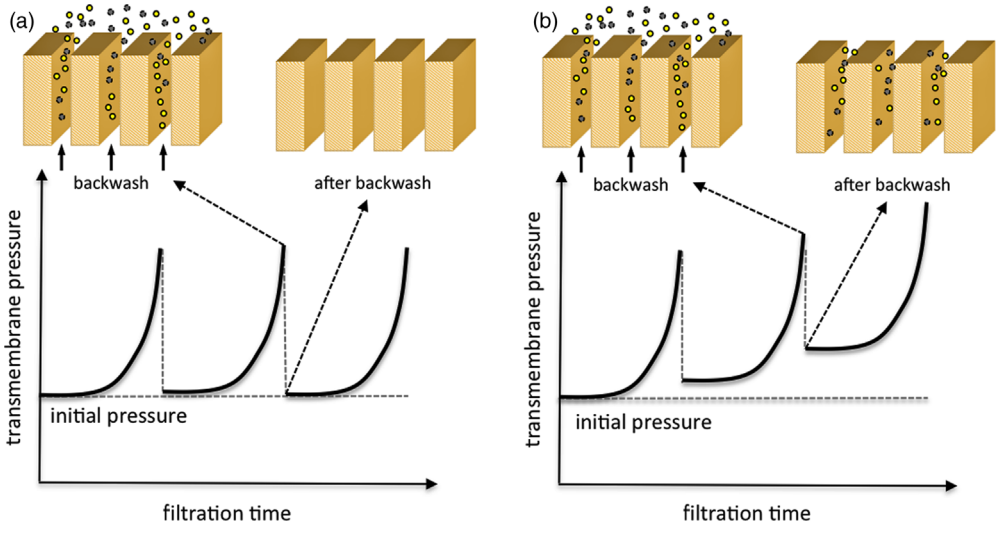


Figure 1.8 Development of reversible fouling (a) and irreversible fouling (b) in UF membranes working under a constant flux regime.

removing scales and metal oxides from fouling layers. Oxidants such as chlorine, HOCl and H_2O_2 partially decompose the foulant, forming more soluble compounds that contain ketone, aldehyde and carboxylic functional groups. Chelating agents such as ethylenediaminetetraacetic acid (EDTA) lock and remove divalent cations, thus significantly reducing the strength of a fouling layer [53]. Surfactants solubilize the foulants to dislocate them from the membrane surface and to enclose them in micelles [54]. Finally, enzymes are especially useful in cleaning membranes fouled by proteins when both a complete cleaning and the integrity of the cleaned membrane are important.

A chemical cleaning process has six stages: (i) dissolution and reaction of the cleaning agents, (ii) transport of these agents to the membrane surface, (iii) penetration through the fouled layers, (iv) cleaning reactions, (v) transporting the reaction products back to the interface, and (vi) transporting the products back to the bulk solution. The entire process can be done without dismantling the membrane module, simply by introducing the cleaning agents through the feed or the permeate openings. This kind of chemical cleaning mode is called *cleaning-in-place* (CIP) and it is run as long as it can successfully revamp the membrane to its initial flux level. When a more specific cleaning is needed, the module is dismantled from a rack and treated by *cleaning-out-of-place* (COP). Both CIP and COP can be performed by a combination of chemical and physical cleaning methods, depending on the fouling problem at hand [54].

Both physical and chemical cleaning processes can affect the membrane in different ways, including altering its integrity [55,56]. Therefore, the checking of membrane integrity after each cleaning is now a standard part of any membrane operation. There are several different methods for doing this. We will discuss these methods in detail in Chapter 3.

1.7 Ceramic versus Polymer Membranes

Although ceramic membranes have been known for centuries while polymer ones are relative newcomers, the latter are dominating the market. There are three good reasons for this, namely money, money and money (typically, ceramic membranes cost three to five times as much as polymer ones). Rough estimates are considering the material cost of US\$2000/m^2 of ceramic membrane versus US\$400/m^2 of a polymer one [57]. Accounting for higher fluxes and longer lifetimes of ceramic membranes, the difference becomes less dramatic: \$60 versus \$20 per unit of permeate volume, but still significant. Polymer membranes are much cheaper than ceramic ones and are therefore preferred in new installations. Ceramic membranes require more expensive starting materials, their fabrication process is complex and consists of multiple stages and their packing density in each membrane module is low. All that said, ceramic membranes also have many advantages and unique features that are helping them gradually enter the industrial market. The question of cost that is now central to the future of ceramic membranes is gradually being

resolved by industrial R&D. Historically, the same happened with polymer membranes. Some 50 years ago polymer membranes were so expensive that they were predicted to be used in laboratory installations only. A prediction made in 1949 says that *For the purpose of thermodynamic demonstrations, it is accepted that films exist, that are selective to one given component. In practice, it has been possible to prepare only a few of the membranes postulated in theory* [58]. Some 30 years ago, using RO polymer membranes was a more expensive option for desalination and new installations used the distillation process. Now polymer membranes are not the only option for the new RO desalination plants, and old plants are being revamped to use the membranes. Polymer membranes have put out of business other filtration technologies with a stable growth rate of 6–7% per year. All this time, membrane manufacturers improved their membranes in a strong competition for ever-growing markets. As a result of last 30 years of development, water flux has doubled and the salt passage has dropped sevenfold [17]. In the two decades from 1980 to 1999, the cost of RO membrane operation has dropped by over 80% [59].

We believe that the same will happen with ceramic membranes. A growing consensus regarding the positive features of ceramic membranes currently results in a massive piloting in the last decade for several full-scale installations in water and wastewater sector (mainly in Japan, with two new installations in the United States). Ceramic membranes are an established technology in food and beverage industry, and play an integral part in reshaping the energy strategy through the hydrogen economy and fuel cells. Tailor-made ceramic membranes serve as ultimate solutions in several gas separation processes and gradually enter the water and wastewater treatment market. Due to their robustness, ceramic membranes are one of the fastest developing membrane applications for the treatment of liquid wastes. The ability to perform CIP at high temperatures with any chemical cleaning agents, or to apply steam sterilization for sanitizing membrane plants is unique feature of ceramic membranes. Several companies such as SCT (Societe des Ceramique Techniques), thereafter Alcoa and now Pall Corp. (USA), Atech Innovations GmbH (Germany), LiquiTech (Denmark), CeraMem (now Corning, USA), TAMI Industries (France), Rhodia Orelis (NovaSep/Orelis, France), Filtrox (Switzerland) and Jiangsu Jiuwu Hitech Co. (China) realized the potential of ceramic membranes and currently offer full-time installations. Soon other companies will join. Applications of ceramic membranes constantly increase by field, by the total number of the installed plants and by the sales. Current sales of ceramic membrane modules are estimated between $650–$850 million with a forecast CAGR of 10–15% a year [42]. We believe that in a decade, numbers and relations between polymer and ceramic membranes will become irrelevant. We therefore give here the current price ratios, as this is the data available, yet realizing that the price will not determine the future of ceramic membranes. A detailed discussion of the economics of ceramic membrane manufacturing and application is given in Chapter 5.

The main advantages of ceramic membranes over polymer ones are their higher flux and longer lifetime. Reported fluxes of up to 360 l/(m^2 h) through ceramic membranes are on average double that of polymer membranes [60].

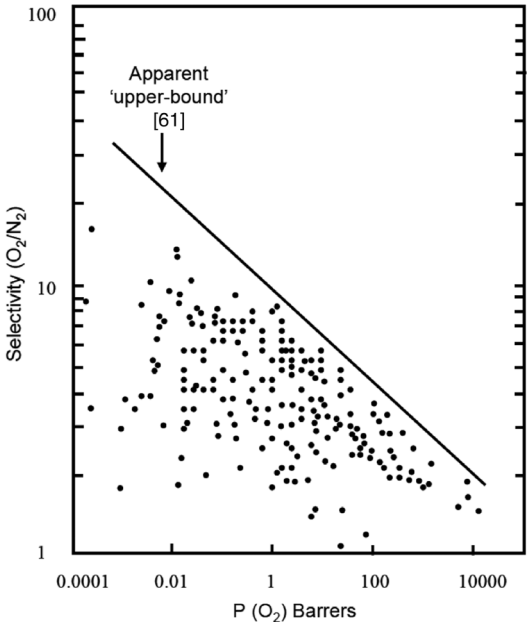


Figure 1.9 A typical Robeson diagram, showing a plot of the O_2/N_2 upper limit selectivity–permeability trade-off [61]. The dots denote the data points of various polymer membranes investigated and the line is the upper limit of selectivity/permeability. The oxygen permeability is expressed in Barrers (1 Barrer = 10^{-10} cm^3 (STP) cm/(cm^2 s cmHg)).

Moreover, unlike polymer membranes which show deteriorated selectivity at higher flux, the selectivity of ceramic membranes does not change as a function of TMP. One of more powerful examples is the so-called *Robeson diagram* for polymer and ceramic membranes shown in Figure 1.9. The analysis in the paper clearly shows that in O_2/N_2 gas separation, the combined (flux + separation) efficiency of ceramic membranes is far above the efficiency of polymer ones.

However, the higher flux is accomplished by application of membranes with bigger pores or operation at higher TMPs. In the latter case, the average permeability of 1.3 ± 0.1 and 0.87 ± 0.08 l/(h m^2 Pa) through ceramic and polymer membranes, respectively, are almost equal [57]. The average 15–20 years lifespan of ceramic membranes is roughly double than the 7–10 years of current polymeric membranes [57]. Curiously, this fact actually creates problems for ceramic membrane manufacturers. In comparison to polymeric membranes, ceramic membranes are mechanically, thermally and chemically stable. Uhlhorn *et al.* [62] also mentioned long-term durability of ceramic membranes, although the polymer membranes had also improved tremendously since their report. Table 1.4 compares the advantages and disadvantages of ceramic membranes and lists some applications where these advantages are important. Below, we survey the raw materials used for making ceramic membranes. In the next section, we explain and discuss the fabrication

Table 1.4 Advantages, limitations and current applications of ceramic membranes.[a)]

Advantages	Disadvantages	Current status	Applications
Thermal stability (>200 °C)	Low hydrothermal stability of composite membranes with a silica top layer. Complicated sealing at high temperatures	Surface modification to improve hydrothermal stability	Reactions at high temperature, pervaporation, gas separation
Resistance to organic solvents	Expensive source materials, complex processing; relatively high capital installation costs		Separation of organic liquids and oils, wastewater treatment
Chemical stability over a wide pH range	Difficult sealing and module construction		Chemical cleaning, separation at extreme pH, recovery of acids/bases
Long-time operational stability, no ageing, potentially lower life cycle cost	Low packing density		Small-scale applications
Mechanical stability under large pressure gradients	Brittleness incurs special configurations and supporting systems		Operation at high flux (up to 500 l/(m^2 h)), backwashing at high flux
High structural integrity	Relatively high installation and modification costs in case of defects	Depends on the separation process	
Uniform pore size distribution	Difficulty to achieve high selectivity on a large scale		Precise size-based separations in pharma and bio applications
(Electro)catalytic and electrochemical activity easily realizable	Low permeability of high-selectivity (dense) membranes at medium temperatures		Solid oxide and other dense electrolyte fuel cells

a) The advantages of ceramic membranes depend strongly on the type of ceramics used in their preparation.

of different layers (Section 1.4) in ceramic membranes. Indeed, improving the price/performance ratio of ceramic membranes depends on both the raw materials and the production process.

1.8 Raw Materials for Ceramic Membranes

Ceramic membranes can be made from many materials. A strict definition of ceramics as inorganic non-metallic material prescribes the use of metal oxides or zeolites, and indeed alumina and silica are among the most common membrane

precursors [10]. The limited stability of these membranes and the ongoing optimization led to the use of more stable (but also more expensive) titania and zirconia. Recent reports on membranes made of tin and hafnium oxides or mixtures of different oxides show that the search continues. Meanwhile, the definition of ceramic membranes has broadened. Today, a composite ceramic membrane is defined as a membrane that has at least one of its layers made of a ceramic material. This definition includes inorganic membranes on a metal or glass support [63], as well as hybrid ones with an organic-templated top layer [57]. Here we describe several typical materials used in the preparation of ceramic membranes, and explain their inherent advantages and drawbacks. A detailed description of the different membrane synthesis procedures is given in Chapter 2.

1.8.1 Alumina

The most known material associated with the ceramic membrane is aluminium oxide (alumina, Al_2O_3) [64]. Alumina is abundant, has good chemical and thermal stability, relatively good strength and thermal and electrical insulation properties. It has several allotropes, including the α- and γ-alumina, the two forms used in the preparation of ceramic membranes. The internal crystal structure of α-alumina is a hexagonal close-packed array of O^{2-} anions. The Al^{3+} cations fill two-thirds of the octahedral interstices and form close-packed planes inserted between the oxygen layers. Each Al^{3+} centre is octahedral. The structure of γ-alumina is often described as a defect cubic spinel, with vacancies on part of the cation positions. Each γ-alumina unit cell contains 32 oxide and 64/3 aluminium ions to fulfil stoichiometry. The aluminium ions occupy both octahedral and tetrahedral positions, but the relative partial occupancy in each position is still a matter of dispute, since the structure in practice is highly complex [65]. Alumina ceramic membranes are usually made by sintering α-alumina and γ-alumina powders at high temperatures (>1300 °C). Figure 1.10 depicts the stability of various forms of alumina as a function of temperature [1,66].

The main source of aluminium in nature is the ore bauxite (named after the French village *Les Baux*, where its high aluminium content was discovered in the 1820s). Bauxite is a mixture of gibbsite $Al(OH)_3$, boehmite γ-AlO(OH), diaspore α-AlO(OH) minerals, two iron oxides, kaolinite clay and small amounts of TiO_2. Heating the ore results in a formation of all allotropic forms such as α-, γ-, δ-, η-, θ-, and χ-alumina. However, sintering above 1000 °C transforms all these forms to α-Al_2O_3, which is the most thermodynamically stable allotrope. The melting point of α-Al_2O_3 is about 2047 °C, but the impurities and alloying elements will melt at significantly lower temperatures. Typical pore sizes of α-alumina membranes are dozens to hundreds of nanometres, making them suitable as support layers for composite membranes. Subsequently, γ-alumina, which has much smaller pores (down to single nanometre), is coated on these using sol–gel methods. The coating step is followed by firing (calcination) at 500 °C to avoid the gamma-

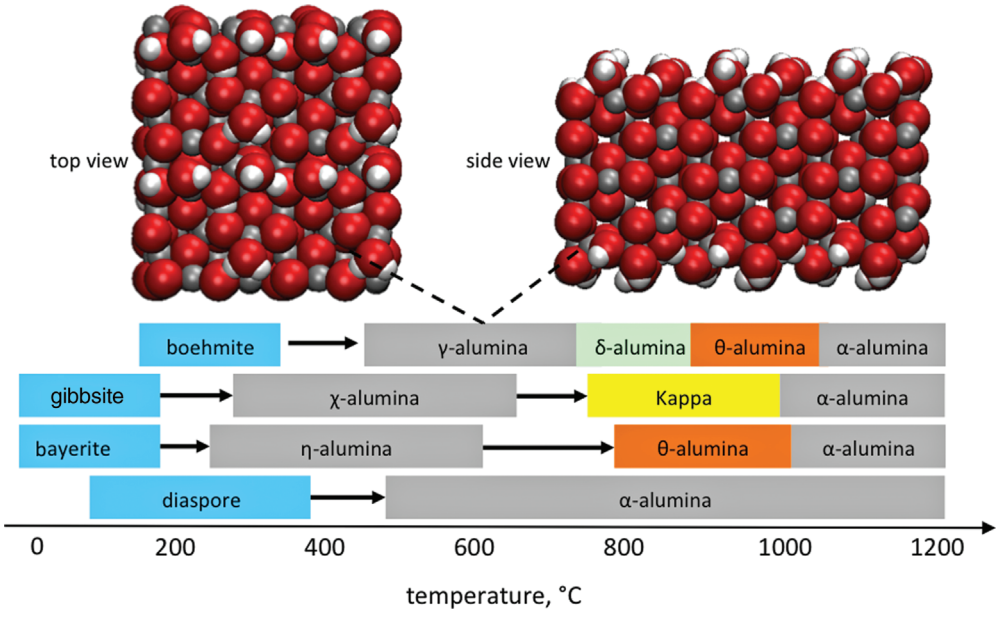


Figure 1.10 Simulated structures of a repeating γ-alumina unit cell (front and side view; simulation courtesy of Dr. Manuel Louwerse) and a diagram showing the phase transitions of alumina at different temperatures starting from different mineral ores. (Data redrawn from Ref. [1].)

to-alpha transition. This protocol was developed in the 1980s by the groups of Burggraaf, at the University of Twente, and Cot, at University of Montpellier [10]. The aluminium metal powder is subdivided into first-grade (A1–A5) that contains at least 99% of pure aluminium powder and second-grade that contains between 80 and 95% α-Al_2O_3. Ceramic membranes are usually prepared from the second-grade powder that is cheaper but also contains many impurities. These hamper the sintering, resulting in weakened membranes that can crack at relatively low stress values.

1.8.2 Silica

Silicon dioxide (SiO_2, commonly referred to as silica, from the Latin *silex*) is another inorganic material often used in ceramic membranes. Silica has a tetrahedral structure where each Si atom is surrounded by four oxygen atoms. A part of the Si electron density is transferred to its neighbouring oxygen atoms that in turn share their electronegativity with their neighbour silicon atoms in a polymeric structure that has SiO_2 as its net chemical formula. This endless network of covalently bonded 'SiO_4' units gives rise to a large number of different amorphous and crystallized forms, including mineral quartz, cristobalite and tridymite. The lengths of the Si—O bonds fluctuate around 1.6 Å, and the Si—O—Si

angles vary between 140° in α-tridymite and up to 180° in β-tridymite [67]. Similarly, the Si—O—Si flexibility and almost free rotation of the bond around the axis give to amorphous silica (no long-range order) its unique properties often used in preparation of thin (down to 30 nm) coating layers used for molecular sieving applications. This coating is done by CVD and sol–gel methods. The CVD results in a formation of ultra-micropores (less than 0.7 nm) that have superior separation properties but low fluxes. A sol–gel coating typically produces super-micropores (between 0.7 and 2.0 nm) that are less selective but permit higher fluxes. Some authors claim that pores of sizes 3–4 Å can be achieved by the sol–gel method [29]. Silica is the only available truly microporous material that can be employed in molecular sieving. The sol–gel membranes are much easier to prepare, but their low reproducibility precludes many industrial applications.

Silica-coated membranes are highly popular in a variety of separation processes, from gas separation [68] to water desalination [69]. The major drawback of amorphous silica is its hydrothermal instability. Typical lifetimes of silica-based microporous membranes are just a few days at moderate temperatures (<100 °C) [31]. Humidity and heat, even under mild conditions of 200 °C [60], cause a substantial shrinkage of pore volume due to physisorption of water molecules on the surface silanol Si—OH groups followed by a reaction with nearby siloxane Si—O—Si bonds. Scission of these bonds releases silica 'molecules' (small oligomers) that migrate to small pores, recondense there and block them. The low hydrolytic stability of siloxane sets a natural limit to use of pure inorganic silica membranes, restricting full applications to water-free atmospheres only. Currently, on industrial scale, the silica-coated membranes are mainly used in gas separations. Interestingly, the water sensitivity problem can be solved using *hybrid silica*, a combination of SiO_2 and organic linkers, invented by Castricum *et al.* [70].

1.8.3 Titania

Titanium dioxide (titania, TiO_2) is another popular material used for coating ceramic membranes, sought after for its excellent chemical resistance at both acidic and alkali pH. Titania occurs in nature mainly in a form of ilmenite, a $FeO{\cdot}TiO_2$ ore that contains between 15 and 40% of iron, and rutile that contains up to 15% iron and other impurities (and therefore 85% TiO_2). The other main impurities are magnesium and manganese. Two of the three crystalline forms of titania, anatase and brookite, are metastable and convert into the stable rutile form upon heating. The rutile form is the only one used commercially. Its crystalline structure has a tetragonal unit cell, wherein each Ti^{4+} cation is surrounded by an octahedron of six oxide ions. These O^{2-} anions are in turn surrounded by titanium cations in a trigonal planar coordination. The TiO_6 octahedra are linked by their edges, form chains parallel to the *z*-axis. The structure of ilmenite is a hexagonal close-packed anion lattice. Here, Fe and Ti

cations occupy two-thirds of the available octahedral interstices in a way that cation–oxygen octahedra share edges in a honeycomb arrangement in one plane and octahedral faces between adjacent planes [71]. Titania particles and colloids are widely used in paints and varnishes as well as in paper and plastics, thanks to two features – white pigmentation and photocatalysis under ultraviolet (UV) light. Chemical companies use the photocatalytic feature of TiO_2 to either degrade organic pollutants or to perform transformation of organic compounds in gas and liquid phases. The melting point of rutile TiO_2 is about 1800 °C.

In ceramic membranes, titania can be applied as both self-standing and coating layers. The self-standing titania membranes are produced as tubes of nanometric diameter and micrometric length. These are obtained from titania nanoparticles either by synthesis of titanium alkoxide compounds under alkali conditions or by a direct hydrothermal attack on TiO_2 nanoparticles under alkali conditions. In the latter case, the nanotubes are made of pure anatase that shows a greater photocatalytic activity than rutile [72]. The prepared titanium nanofibres, rods and surfaces fall under the definition of membranes mainly because these structures are porous and a fluid can pass through them. Conversely, the self-standing titania membranes suffer from poor structural stability [73]. They cannot be assembled into a module. When they are used, for example in catalytic reactions, they are suspended as particles in the reactor.

The coating of supports with a titania layer is mainly performed via the sol–gel method, similar to silica coating. Ti-based organometallic precursors are hydrolyzed in the presence of excess water and dip coated or spin coated on the support surface, followed by firing at relatively low temperatures. A transition from amorphous titania to anatase occurs at 300–400 °C, and from anatase to rutile between 400 and 600 °C. The anatase-to-rutile phase transformation is generally undesirable [72] due to a brittle structure and low photocatalytic activity of rutile TiO_2. Sol–gel coating is usually done using either amorphous titania or anatase titania having smaller pore sizes than the rutile. The resulting membranes have pore sizes below 2 nm. Other methods include a direct deposition of titania from an aqueous solution of titanium tetrafluoride on an α-alumina support [74] or photografting and photopolymerisation of a blend that contains photocatalyst particles and suitable polymers [75]. Part of these methods, including the physical deposition of TiO_2 particles entrapped within the pores of a UF membranes, intend to ensure the presence of TiO_2 particles on the membrane surface rather than forming a solid separation layer. Research and implementation of titania-encapsulated membranes mainly use the photocatalytic feature of TiO_2 for catalysis [76].

1.8.4 Zirconia

Zirconium dioxide (zirconia, ZrO_2) is one of the most popular ceramic coating materials. This popularity reflects its chemical stability, especially in alkali solutions [3]. Zirconia occurs in nature mainly as baddeleyite, a rather rare ore that

comes in a variety of monoclinic prismatic crystal forms. Baddeleyite is a refractory mineral that melts at 2700 °C. Hafnium is a substituting impurity and may be present in quantities ranging from 0.1% to several percent. Zirconia exists in three crystalline forms – monoclinic, tetragonal and cubic. Unlike titania, which features six-coordinate Ti in all phases, monoclinic zirconia consists of seven-coordinate Zr centres (this difference is attributed to the larger size of Zr ions). The transition from one crystalline form to another is triggered by heating, where the higher cubic symmetry forms at temperatures above 2370 °C. A transition from a monoclinic to tetragonal zirconia occurs at 1173 °C, so zirconia membranes can crack after sintering at high temperatures. This cracking, which is a known problem of zirconia membranes, is due to a large volume change (about 9%) in the transition from tetragonal to monoclinic phases. To avoid it, zirconia used in coating top layers is fired at 500–600 °C, or doped with yttria (Y_2O_3) in its cubic polymorph, which increases its thermal stability. The thermal stability of zirconias can also be improved by adding 12–13 mol% CaO, 8–9 mol% Y_2O_3 and Sc_2O_3 or 8–12 mol% of other rare-earth oxides (Yb_2O_3, Dy_2O_3, Gd_2O_3, Nd_2O_3, Sm_2O_3) [8]. Yttria-substituted zirconia is currently the state of the art in solid electrolyte membrane materials for high-temperature fuel cells (see details in Chapter 4).

1.8.5 Zeolites

Another common membrane material group is the crystalline-hydrated aluminosilicate minerals called *zeolites*. These crystalline materials are made of tetrahedral cations of Al and/or Si surrounded by four oxide anions. The units are linked to each other by sharing the oxygen ions in a three-dimensional polyhedral (cubes), hexagonal prisms or cubo–octahedral arrangements. These superstructures contain intracrystalline channels or interconnected voids and can be extended infinitely. The channels are partially filled with water that can be removed by heating (hence the name ζέω, meaning 'to boil' and λίθοζ, 'stone'). The negative charges of the AlO_4 tetrahedra (SiO_4 is neutral) are counterbalanced by mobile cations (e.g. Na^+, K^+, Mg^{2+} or Ca^{2+}) from nearby channels. Chemically, zeolites can be represented by an empirical formula $M_{2/n}O{\cdot}Al_2O_3{\cdot}aSiO_2{\cdot}bH_2O$ where a is between 2 and 200, b is the water trapped in voids and n is the valence of the metal cation M [77].

Zeolites were discovered in 1756, and for the first 200 years were used mainly in adsorbent applications. Some zeolites possess exceptional chemical and thermal stability, in addition to their catalytic activity and natural nanometric pore dimensions [78]. Starting from the mid-twentieth century, zeolites were synthesized in several industrial laboratories. Today, over 200 different families of zeolite frameworks are known [79]. These new compounds are used in numerous technological processes, including catalysis, adsorption, ion exchange and, of course, separation. That said, only a few zeolites and zeolite-like structures are useful in membrane separations (here we shall focus only on the applications of

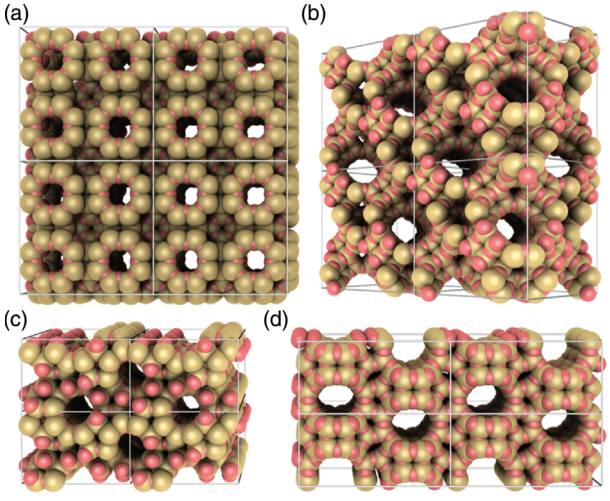


Figure 1.11 Three-dimensional simulations of four different zeolite structures (courtesy of Dr. David Dubbeldam): (a) Linde Type A (LTA). (b) Faujasite (FAU). (c) Zeolite SOCONY Mobil 5 (ZSM-5, MFI). (d) Zeolite beta (BEA).

zeolites as ceramic membrane components). Four of the most popular ones are Linde Type A (zeolite A, eight-ring pores of 0.30–0.45 nm), ZSM-5 (10-ring pores of 0.45–0.60 nm), zeolite Y (faujasite, 12-ring pores of 0.6–0.8 nm) and zeolite beta (see structures in Figure 1.11).

Zeolite membranes can be prepared as self-standing materials, as well as top layers for composite membranes. A recent trend is growing zeolite crystals during the synthesis of polymer membranes for a formation of metal-organic frameworks (MOFs) with tunable separation properties and permeability [80]. The self-standing zeolite crystals are typically first grown on a support such as Teflon that is removed after the synthesis. Membranes of this type are of interest in model studies of an ideal zeolite layer, but their practical applications are limited. This is because growing zeolite layers larger than few square centimetres is difficult, and the fragility of the structures prevents their industrial implementation. Usually, zeolite membranes are used as the top layers in a composite arrangement. They are prepared by crystallization followed by a substantial growth on the support. The crystallization is done on the surface and/or in pores without seeds for nucleation (the so-called *in situ* nucleation), or with seeds deposited on the support or in the vapour phase. This method gives structures that are reasonably defect-free (and the defects, even when they exist, are not much larger than the zeolite pores), so the only transport of fluids occurs through the zeolite pores. The inherent deficiency of zeolite membranes is the main transport mechanism. Compounds pass through pores by adsorption, making it difficult to maintain a steady-state operation as the zeolite becomes saturated with adsorbate. That said, the retention by adsorption can also be viewed as advantageous, as large-pore zeolites can combine high permeate fluxes with high

selectivity. Thermal stability up to 400–500 °C and resistance to organic solvents are additional advantages of zeolites over polymer membranes with same pore widths, facilitating their implementation. Zeolite membranes are often used in gas separation and catalytic membrane reactors at elevated temperatures. More details on these applications are given in Chapter 4.

1.9 Preparation of Ceramic Membranes

There are numerous methods for preparing ceramic membranes. These include structural leaching or sublimation of one component of a mixture, slipcasting, tape casting, extrusion, pressing, pyrolysis, sintering of suspensions that contain ceramic powders and various additives, sol–gel synthesis, hydrothermal treatment, anodic oxidation and chemical vapour deposition. This variety reflects the different raw materials that often dictate the method of choice. In many cases, different membrane layers are prepared from various materials using methods suitable for that specific material. The support layer is often made of α-alumina by extrusion, slipcasting or tape casting. This gives a ceramic membrane support with micrometre-size pores and millimetre-depth thickness. Then, intermediate layers are typically prepared from γ-alumina by dip coating the support layer followed by calcination. The number of intermediate layers depends on the grain size of the initial slurry and the degree of separation required (the intermediate layer is 300–400 μm thick and contains nanometric pores). Above these, the top layer, which determines the membrane's separation abilities, can be made from many materials using different methods. These include sol–gel synthesis of silica, titania and zirconia, chemical vapour deposition of silica, pyrolysis of carbon, SiC or Si_3N_4, hydrothermal treatment of zeolites such as NaA and NaY, anodic oxidation of amorphous alumina and structural leaching of silica. In the following sections, we will outline the main methods of preparing ceramic membrane supports. Further discussion on the preparation of composite membranes for specific applications is given in Section 1.10.

1.9.1 Support Your Local Membrane

A membrane support has two seemingly controversial functions. It must make the membrane stronger without interrupting the transmembrane flow. The two are sometimes incompatible, because thick supports are stronger, but also more flow-resistant. Therefore, the support must be sufficiently thick, but also porous. The typical thickness of a membrane support is 1–2 mm and its typical pore size is on the order of micrometres. Support layers were mainly investigated back in the 1990s, and the current shortlist of widely used supports contains ceramics, ceramic composites and stainless steel. One of the main demands from supports

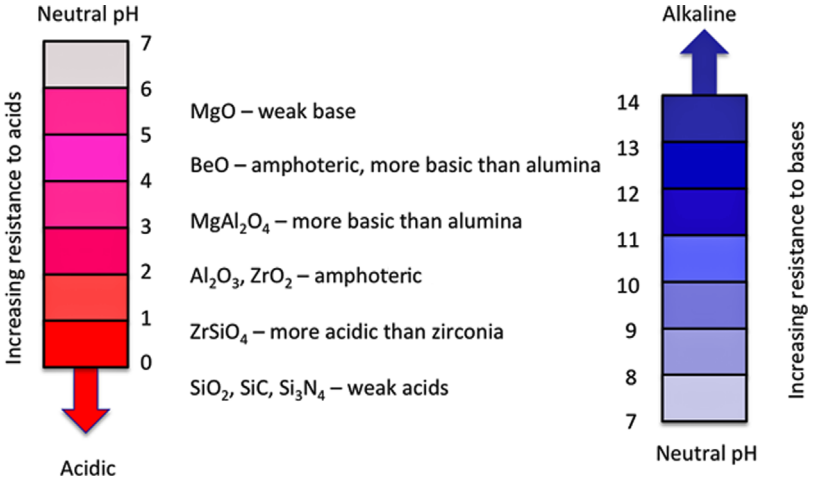


Figure 1.12 Relative resistance of various ceramic materials to acids and bases. (Drawn after Ref. [85].)

is good chemical and thermal stability. Alumina and silica are considered more thermally stable [82,83], whereas anatase titania and zirconia have a limited thermal stability due to their relatively low phase transition temperature [84]. Figure 1.12 shows the relative resistance of various ceramic materials to acids and bases.

Generally, the more acidic a ceramic is, the greater is its resistance towards acids, and vice versa with bases. If the ceramic material is more base resistant, it is more prone to acidic attacks. For example, silica, which is slightly acidic, has poor alkaline resistance. The chemical resistance may vary between allotropes. For example, α-alumina is very stable against strong acids and bases, but γ-alumina decomposes at $pH \leq 4$ and $pH \geq 9$ [86]. Titania and zirconia are considered very chemically resistant membrane materials, and yet enjoy only a limited success in manufacturing due to a highly sensitive (and therefore costly) synthesis procedure [87].

The majority of supports are prepared from α-alumina, which is cheap, commercially available, chemically inert, durable and withstands high pressures and temperatures [88]. Its two main disadvantages are its wide pore size distribution and the tortuosity of synthesized supports. As defect-free coating is not possible on surfaces with the average roughness of 1 μm and higher [30], α-alumina supports must be covered by intermediate layers that smooth the surface. Often, these intermediate layers are prepared from γ-alumina. They are less inert and increase the flow resistance, negating the advantages of α-Al_2O_3 support. Nevertheless, α-alumina is preferred over supports made from TiO_2, ZrO_2, CeO_2, because the latter give higher flow resistance and might crack at high pressures. Stainless steel supports have some mechanical and manufacturing advantages, but they are even rougher than ceramic ones, and have a low compatibility with

coating ceramic layers. Their high thermal expansion coefficient can promote cracking at sintering or problems with adhesion of layers of the sintered support.

Ceramic supports are prepared by several sequential steps. The first is the formation and mixing of the initial slurry that consists of powder grains, solvent and chemical additives. At the second stage, the slurry is shaped by dry pressing, extrusion of ceramic paste or slipcasting or tape casting into the desired shape. These are typically disks, tubes, hollow fibres and honeycomb monoliths (see Section 1.4). Dehydration to evaporate water and drying at low temperatures to decompose volatile organics is the third stage of preparation. At the fourth stage, the consolidated slurry called the *green body* (GB) is sintered at high temperatures. Finally, the support is cooled and polished. Figure 1.13 shows the five stages in the preparation of a ceramic support. Details and highlights of each stage in the preparation are discussed below.

1.9.1.1 Forming the Initial Slurry

The formation of a ceramic slurry starts from a powder of inorganic particles such as Al_2O_3. Other oxides such as TiO_2 and ZrO_2 can also be used, although their small sintered pores often cause a large flow resistance. The conventional method for preparing an α-alumina powder from bauxite by hydrothermal attack with NaOH was invented by Karl Josef Bayer in 1892 [89]. This method is highly efficient and the final powder contains 99.4–99.9% pure alumina. The remaining impurities, mostly SiO_2 and Fe_2O_3, precipitate during sintering, thus increasing cavities within the ceramic construct and reducing its mechanical strength. The concentration of impurities can be reduced below 0.1% or even 0.01% using a modified Bayer process, but that has additional stages (and increased costs) [89]. Alumina powders can differ in their grain size, shape and size distribution. The differences in size and shape have more influence on the permeability and the mechanical strength of the sintered support [30]. Since a wide grain size distribution will result in undesirable large pore size distribution, the slurry is preferably made from monodispersed particles. When such a powder is not available or

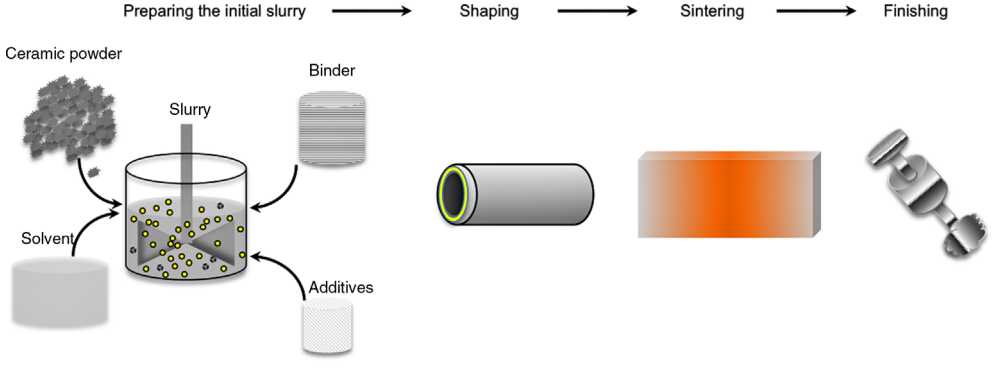


Figure 1.13 The five stages in the preparation of a ceramic membrane support layer.

prohibitively expensive, the fraction of particles with largest diameters is removed by sedimentation or by centrifuging. Small grains decrease the support's porosity and fluid permeability but increase the mechanical strength of the final sintered membranes. Several equations suggest the same empirical correlation between the tensile strength of a support σ_t and a grain size d_g in the form $\sigma_t \sim 1/\sqrt{d_g}$ [29]. A correlation between the pore size d_p and grain size d_g varies between 2 : 5 and 2 : 3. Thus, if the mean grain diameter is 1 μm, the pores will typically have a mean diameter of 400–660 nm [8]. This ratio, however, is influenced strongly by the shape of the grains [90]. Grains of 1–2 μm are the largest that can still ensure the formation of hard and dense membranes (using larger grains gives low-density macroparticle membranes). The 0.5 μm grains are the lower limit of the grain size, ensuring that the support permeability will be at least 10 times higher than that of the top layer.

Dense packing of particles in the initial slurry increases mechanical strength and decreases membrane permeability. A paste with higher density is less likely to shrink during sintering. The *packing density* is defined as a dimensionless ratio of particle fraction to the total slurry. An ordered packing with equal spherical particles can reach a packing density value of 0.74. The densest packing is achieved by an ordered (crystalline) stack of particles in parallel hexagonal layers forming the so-called Barlow packing (the highest coordination number of 12, theoretically predicted by Newton in 1694) at density $\rho = \pi/\sqrt{18} \approx 0.74$ [91]. Here the *coordination number* of a central particle is defined as the number of its nearest neighbours. Usual packing densities range between 0.58 (cubic packing type, coordination number 6) and 0.62 (orthorhombic packing type, coordination number 8). In ceramic supports, packing densities typically range 0.3–0.7 based on dry solid loading.

> Ancient sellers sold dry grains (such as barley, oats and wheat) by volume and not by weight. And why did it matter? They increased their profit by an old trick. Pouring grains into a container with a stick inserted inside and slowly removing the stick can result in loose packing density of 0.55, increasing the seller's profit by approximately 10% [91].

Packing densities higher than 0.74 can be achieved by preparing the initial slurry from a powder that intentionally contains more than one grain size [74]. Figure 1.14 illustrates how, in this approach, the small grains fill the voids between the large ones, 'glueing' the large particles together without increasing the overall slurry volume.

The optimal size ratio determined through studies of various large/small grain arrangements is 0.155, wherein the small particle touches three neighbouring large particles (coordination number 3) [92,93]. There is no similar simple rule regarding the quantity ratio of large/small grains. Li reported that exceeding the optimal quantity of small particles forces large grains apart and no longer improves packing density [26]. In our experience [75], the dual-size grain approach has a small negative effect on the flux and a significant positive effect

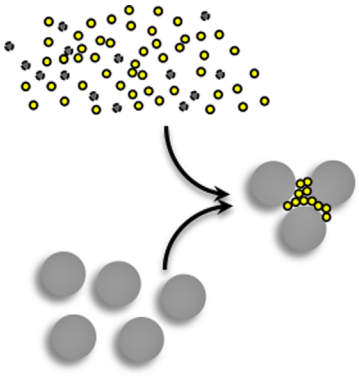


Figure 1.14 The increased packing density of slurry that intentionally contains particles of two different sizes.

on the mechanical strength. Adding 1 wt% of 13 nm particles into a powder of 0.85–1.0 μm α-Al_2O_3 increases the mechanical strength by 16% and decreases the flux by 3% only, and adding 3 wt% increases the mechanical strength by 44% and decreases the flux by 6% [75].

The powder should be equally dispersed in a liquid before it can be consolidated into the so-called *green body* (sometimes also called a *green cast*; this term refers to an unfinished membrane before sintering that has its final form but not the ceramic properties, just like unripe fruit). A solvent is added to suspend the ceramic powder and dissolve additives and binders that form the initial slurry. The solvent should evaporate with no traces during the heating stage resulting in the formation of the GB. Water is the cheapest solvent. Using water, however, significantly increases evaporation time and may result in agglomeration due to hydrogen bonding [94]. Organic solvents such as toluene [95] and ethanol [96] dry faster than water, yielding GBs with a high density. The advantage of another popular non-aqueous solvent, trichloroethane, is its non-flammability, although it is also a VOC with adverse environmental effects [97].

The initial slurry of a powder and a solvent is milled or ultrasonically dispersed for uniformity. The exact homogenizing process depends on the viscosity of the slip, the time span allocated for the process, and the quantity of additives. During the homogenizing, grains constantly bump into each other. This bumping should not result in agglomeration. If the grains are already clustered, the homogenization should promote deagglomeration. Adding a deflocculant (sometimes also called a dispersant) increases the electrostatic repulsion or the steric hindrance of two particles in aqueous and non-aqueous suspensions, respectively, thus preventing agglomeration. Deflocculants coat ceramic particles and prevent a direct contact between them. The positive influence of a deflocculant increases as the size of powder particles decreases. Popular deflocculants for aqueous suspensions are relatively inexpensive soda ash, polyacrylates [94] and sodium silicates [95]. The advantage of polyacrylates is their relatively low

molecular weight that affects the stability and rheology of aqueous slurries. Polyethyleneimines [96], menhaden fish oil, phosphate ester and glyceryl trioleate [10] are popular dispersants for non-aqueous mixtures. Li lists 27 dispersants for use in organic solvents, mostly fatty acids and esters [26]. There is an optimum in the concentration of the dispersant in the slurry. For example, Sarraf and Havrda [98] report an optimal 0.5 wt% of a dispersant to stabilize the alpha alumina (α-Al_2O_3) slurry.

Solvent evaporation during the drying should not affect the plasticity nor the mechanical resistance of the GB. Binders and plasticizers are added to maintain GB shapes before drying, and to prevent cracking at sintering. These are typically long-chain polymers with a backbone of covalently bonded carbon–carbon linkages with different side chains. They either physically wet the powder grains or chemically adsorb organic functional groups on the grain surfaces [99]. A good binder should strengthen the GB, improve lubrication, be inexpensive, non-toxic and decompose completely at 300–500 °C leaving no ashes. Onoda [100] indicated three possible locations of binder in GBs that are redrawn here in Figure 1.15. Poor wettability (Figure 1.15a) results in no glue between grains. Too viscous a binder completely covers the grains (Figure 1.15c) preventing the attracting interactions between near grains that are crucial at the end of drying and beginning of thermolysis. A wetting (pendular) state (Figure 1.15b) where the binder is located at the neck intercept (a junction of few grains) is the desirable one, promoting formation of particle clusters linked by 'liquid necks' [101]. Thanks to the repulsion between near clusters, the pore structure remains open and the pores become smoother and rounder. The exact structure depends on the binder used and its quantity, particle size and shape and the number of particle interactions.

In a sense, the perfect binder is 'the last line of defence' that decomposes later than any other additive, leaving voids that change their form and dimensions during sintering [102]. The open voids are the membrane pores in the final support structure. Pore sizes can be governed by the molecular weight of binder molecules [103] and the pore density by the binder concentration. The optimal concentration should be as low as needed to prevent cracking, and at the same time reduce pore size distribution (a narrow pore size distribution is more valuable in separation). Adding more than 10 wt% binder increases the pore size distribution [104], promotes particle agglomeration in the slurry and results in the formation of closed pores [105]. But burning out green bodies that contain more than 10 wt% binder is more difficult. Many polymers can be used as binders. Examples

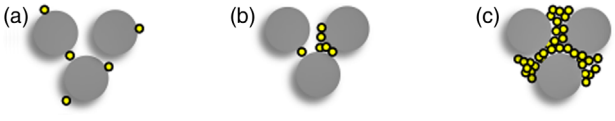


Figure 1.15 Location of a binder between slurry grains: non-wetting liquid (a), good wetting, perfect binder position (b) and viscous liquid (c). (Drawn after Ref. [90].)

of non-aqueous suspensions include polyvinyl butyral (PVB) [97], polyvinyl acetate (PVAc), poly(propylene carbonate) (PPC), poly(butyl methacrylate) (PBMA) and poly(methyl methacrylate) (PMMA). For aqueous suspensions, the commonly used binders are poly(ethylene oxide) (PEO)/poly(ethylene glycol) (PEG), starch [106], polyvinyl alcohol (PVA) and cellulose ethers (methyl cellulose, hydroxyethyl cellulose) [107]. Long-chain linear polymers in aqueous solutions ensure binder solubility. However, adding a binder is not the only method for creating porosity during sintering. The idea of sacrificing molecules or particles for the generation of voids can be realized with the addition of sawdust, coal, spongy polymers such as cellular plastic, latex [108] or foamed polyurethane [109].

Plasticizers are low-molecular-weight polymers that are typically added with the binder to the initial slurry. A plasticizer penetrates into the binder, improving its distribution in the slurry. This softens the binder, increasing flexibility and lowering the glass transition temperature [99]. The plasticizer also lubricates, allowing a slide movement of neighbour binder molecules, thus increasing the flexibility of green body and reducing cracking [110]. Adding a plasticizer might increase the surface area, the pore volume and the pore diameter of the final ceramic membrane [111]. Plasticizers are more common in tape casting where the flexibility of the tape is important. Popular plasticizers in aqueous suspensions are ethylene glycols and glycerol [112]. Polyethylene glycols [113] and dibutyl-*o*-phthalates [94] are often used in non-aqueous suspensions.

Lubricants are sometimes used in addition to the plasticizers to help withdraw green bodies from their moulds during slipcasting [114]. Wax emulsions [95] and ammonium stearates [115] are often used in aqueous suspensions, while stearic acids are used in non-aqueous suspensions.

The addition of dispersants plus mechanical stirring can give foam that can cause cracks or abnormal pores in the green body and/or later in the membrane. Antifoam agents may either prevent or destroy the foam by forming a monomolecular hydrophobic layer over the slurry surface and reducing the surface tension [116]. Interestingly, sometimes the foaming itself is used as for producing highly porous ceramics with very large pores (50 µm to 5 mm) [117].

Magnesium oxide (MgO) or yttrium oxide (Y_2O_3) are sometimes added as a material that will melt before the matrix phase in liquid-phase sintering, or to obtain dense membranes with low pore size distribution in solid-state sintering. The former is used to help sinter materials such as Si_3N_4, WC and SiC. According to Dörre and Hübner [118], MgO prevents the discontinuous growth of the grains as the pore will become part of the grain, the diffusion distance between the grains will significantly increase and the pore will not shrink. Other relatively rare additives that impart specific ceramic membrane properties promote porosity, water retention and antistatic properties or act as fungicides/bactericides [26]. Figure 1.16 summarizes different studies and shows the percentage of each ingredient in the initial slurry [119]. The majority of green bodies were prepared with 60–80 wt% ceramic powder, 20–40 wt% water and 0–20 wt% organics (mainly binder or plasticizer). Table 1.5 summarizes and clarifies main functions of each additive in the initial slurry.

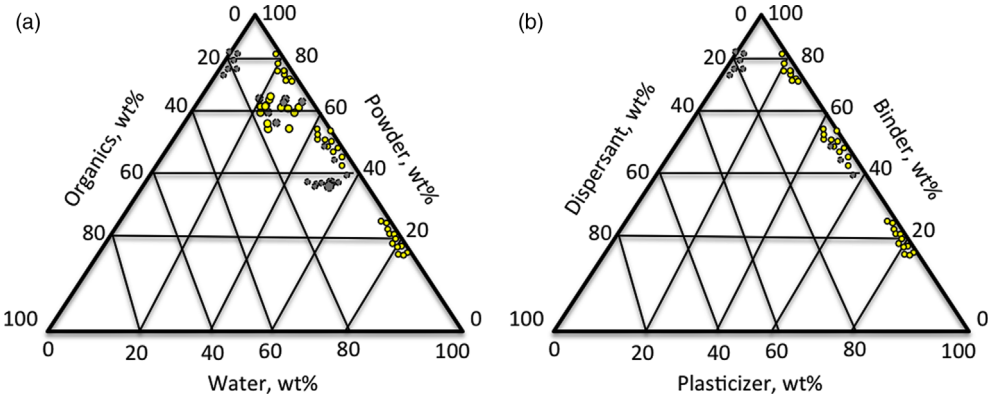


Figure 1.16 Ceramic slurry content [119]. (a) The diagram presents wt% of solvent, organics and ceramic powder in ceramic slurry summon from different studies. (b) The diagram presents the wt% of organic content (binder, plasticizer and dispersant).

1.9.1.2 **Mixing and Pugging**

Using the right grains and additives is important, but composition is not the whole story. The order on which the ingredients are added, mixed and pugged is essential to prevent voids that might lead to membrane cracking at later stages. Here (unfortunately) there are no hard-and-fast rules. Obtaining a good homogeneous paste is an empirical process, closer to art than to science. Indeed, in our research for this book, we were amused to learn that practically all

Table 1.5 A summary of the functions of additives in ceramic processing.

Additive	Function
Common	
Solvent	Suspends the ceramic powder and dissolves additives and binders that form the initial slurry
Deflocculant/dispersant	Increases the electrostatic repulsion or the steric hindrance of grains in aqueous and non-aqueous suspensions, respectively, and prevents aggregation
Binder	Maintains green body features and prevents cracking at sintering
Less common	
Plasticizer	Penetrates into the binder to structurally expand it and improve its distribution in the slurry
Antifoam	Prevents or destroys foam
Lubricant	Helps in releasing the green body from its mold
Chelating agent[a)]	Inactivates undesirable ions
Fungicide/bactericide[a)]	Stabilizes against degradation with ageing

a) From Ref. [120].

companies that make ceramic membranes have a few experienced employees who are the only ones who can determine the correct conditions for the paste. Typical protocols start from a dissolution of a known quantity of a dispersant in a certain volume of solvent by stirring or by rolling [26]. The percentage of grains added at the next stage depends on grain size and the ability of the dispersant to keep the final mixture deagglomerated – more grains can be added when an efficient dispersant is used. If several grain types are used, they are mixed first. Adjustments to the solid loading are often a question of experience. Organic additives are added after the grains starting from a most hygroscopic one [90]. Usually it is first plasticizer and then binder. The slurry is then well mixed, and the mixing efficiency depends on the viscosity, amount of deflocculants and time [90]. Insufficient mixing results in the formation of aggregates and cracking at later stages. Table 1.6 compares the three popular mixing techniques.

During the mixing, the slurry can trap air bubbles that must then be removed, usually by partial vacuum and a gentle stirring. Air bubbles can lead to cracking at the sintering step.

In tape casting and slipcasting, the paste is shaped quickly to avoid premature drying and ageing that can result in phase separation, formation of agglomerates and cracking at sintering. In extrusion, the order of addition can change and organic additives sometimes are added before a solvent [90]. The quantity of added solvent is optimized empirically. Too little solvent will not give good extrusion. Too much solvent will result in soft suspensions unsuitable for shaping. Adding a solvent gives a viscous slurry that is kneaded into a plastic consistency. This is called *pugging* and is done for a short period with high intensity. The resulting paste is aged for several days prior to extrusion.

Table 1.6 Slurry mixing techniques.

	Description	Mixing time (h)	Advantages	Disadvantages
Ball milling	A rotating container that hosts the slurry mixed by inert parts (e.g. metal balls) moving inside it	6 [121], 12 [122], 20 [123], 24 [124], 48 [125]	Applicable on large scale and at different stages, cheap	Noisy, long mixing time
Ultrasonic milling	The sonication results in high- and low-pressure cycles, promoting cavitation	0.25 [126], 0.16 [127]	Very short mixing time, high homogeneity	Very strong – can break the grains, harmful noise
Magnetic stirring	A rotating magnetic field turns a bar that quickly mixes the slurry	24 [128–130]	No noise, immersed magnets are inert and easily cleaned	Inapplicable on large scale, used in non-viscous suspensions only

1.9.1.3 Shaping the Slurry

Now the paste is ready to be shaped into one of four membrane geometries. The choice between plates, tubes, hollow fibres and honeycomb monoliths will determine if the slurry will be shaped by dry pressing, extrusion or slip/tape casting. Dry pressing is done in a special press. Typical pressures exceed 100 MPa and give a dense layer approximately 0.5 mm thick. This method is limited by the size of the press and is often used in fundamental research for optimizing ceramic membranes. Typically, one studies the effects of particle size, binder quantity, applied pressure and sintering temperature on pore size distribution of ceramic supports [129–131]. Small discs, a few centimetres in diameter, are the most common membranes made by dry pressing.

Extrusion is done by forcing the paste through a small opening (an extruder) with the help of an endless screw (in industry) or a piston (in the laboratory). The speed of extrusion and extrusion pressure vary and should ensure the formation of homogeneous tubes [90]. Typical extrusion rates range between 10 and 60 rpm of a screw barrel [132], at 10–15 bar. To avoid paste separation and excessive drying of the solvent, the extrusion is performed at room temperature and high partial pressure of the solvent (up to 80% relative humidity [132]). The geometry of extrusion nozzle (number of channels and their diameter) may vary and result in the generation of mono- and multichannel tubes. Tubular geometries are suitable for large industrial installations. Extrusion in ceramic membranes is similar to spinning in polymer ones, except for the presence of coagulation bath and one-step process in the latter [26].

Tape casting and *slipcasting* are used for preparing flat membranes and discs. Figure 1.17 depicts a tape casting process (the so-called *doctor blade*) for large-scale fabrication of ceramic supports and multilayered structures.

The paste is poured into a reservoir behind a casting knife and cast onto a stationary or moving surface passing through a blade [119]. In laboratory applications, the surface is fixed and the doctor blade moves at a controlled speed to ensure the uniform thickness of the tape. This gives tapes of up to 0.5 m width, 2 m length and 1–2 mm thickness [90]. Industrial ceramic supports are based on the moving surface, such as endless stainless steel, glass coated with silicon oil or polymer film belt (e.g. polyethylene) and a fixed doctor blade. The thickness of the slurry is controlled by adjusting the gap between the blade and the surface. Other important parameters include the reservoir depth, paste viscosity and carrier speed [26]. The usual casting speed is 0.1–1.5 m/min, depending upon the surface length, drying time and tape thickness. The typical thickness is a few millimetres, although membranes a few micrometres thick were also reported. The length can reach 40 m [90]. The tape is then dried by passing through a tunnel, peeled from the moving surface and rolled for storage. Supports prepared by tape casting are usually smoother, with fewer defects. Tape casting is a favourable method for preparing multilayer membrane structures where the intermediate and top layers are easily coated on a flat support.

Slipcasting is much simpler. Here, neither a doctor blade nor a moving tape is used. Instead, the slurry is poured directly into porous moulds of a desired

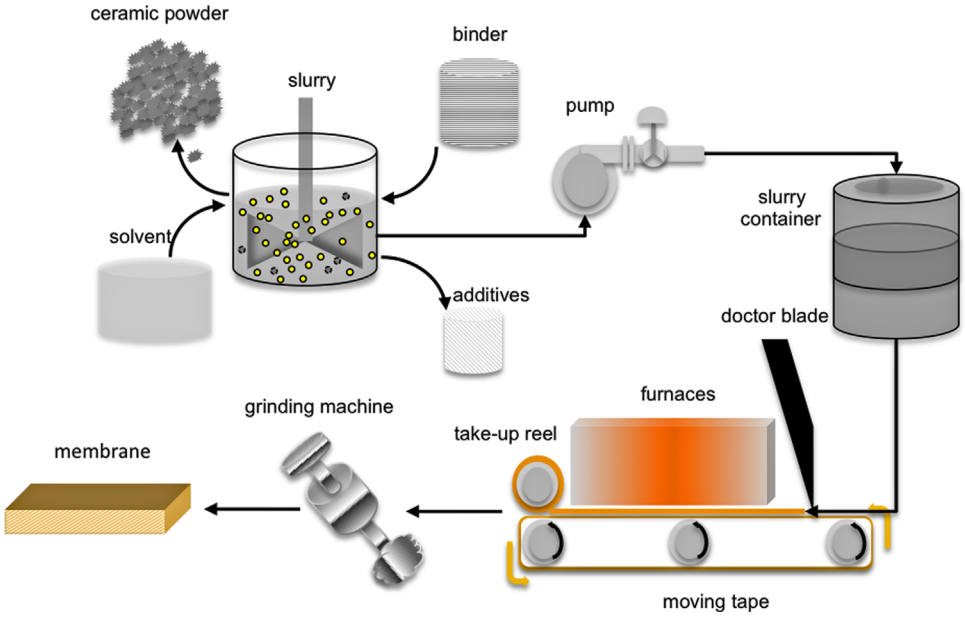


Figure 1.17 A tape casting process for large-scale fabrication of ceramic supports and multi-layered structures.

shape. The paste is sucked into the mould by a capillary action and fills all available space within the mould structure. The depth of penetration of a paste into the mould structure increases with time. Figure 1.18 shows that the shape of the final membrane is limited only by the mold shape. The disadvantage of slipcasting is the large number of intermediate steps, including pouring the slurry into a mould and peeling a green body when the desired shape is achieved. In addition, the casting time is usually long and the membrane thickness is usually high and more difficult to control.

1.9.2 Drying and Thermolysis

Drying, thermolysis and sintering are the three stages of heating that give the membrane its final properties. All three procedures are performed at different temperatures and with various heating ramps, as can be seen in Figure 1.19.

Drying is the initial heating stage that evaporates the solvent while keeping the grain network in order. It can be done at room temperature or at elevated temperatures. Drying at room temperature requires no energy for heating but takes significant time (up to few days). Industrial membrane producers usually dry at higher temperatures. The drying should remove the solvent, and yet keep organic additives, such as binders and plasticizers, in the bulk. These will be

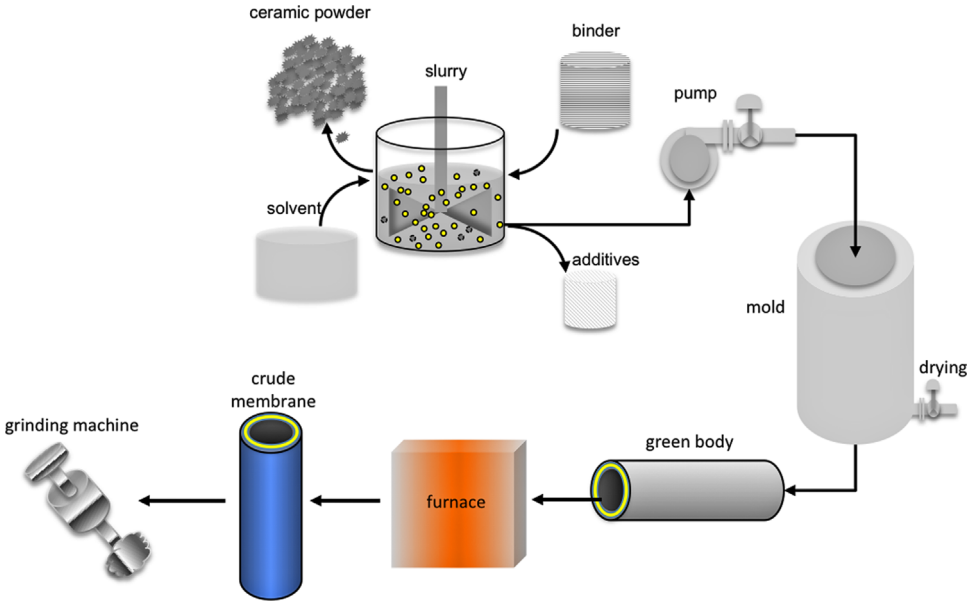


Figure 1.18 Various stages of ceramic membrane preparation by slipcasting.

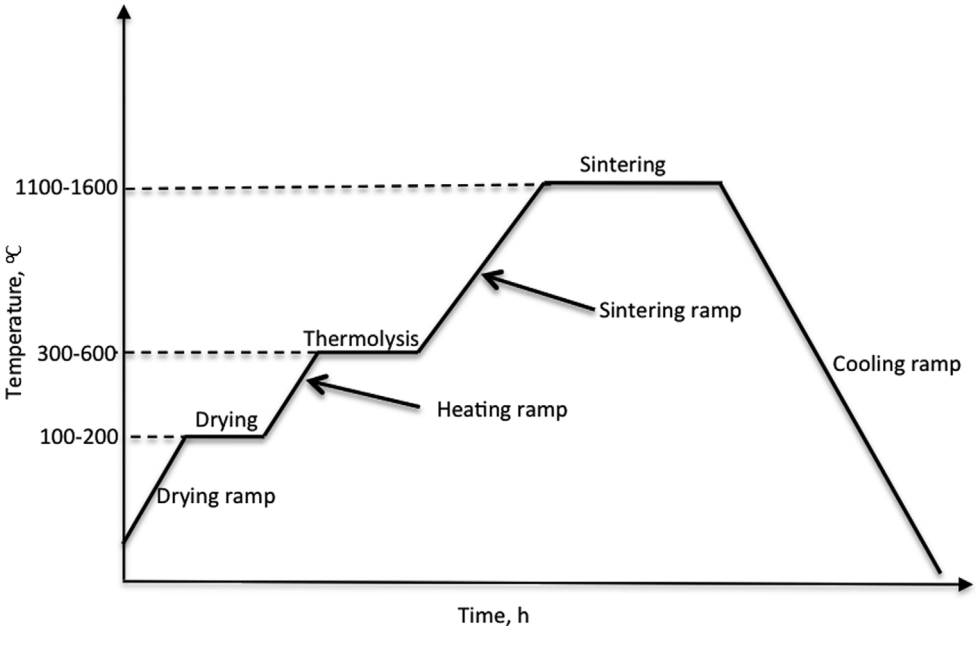


Figure 1.19 The three stages of heating – drying, thermolysis, sintering – in the preparation of ceramic membranes from the green body.

evaporated at the thermolysis stage, when no significant changes in the grain spatial arrangement are expected.

Concurrently, grains are moving closer to each other until they come into direct contact. The ceramic body shrinks to what will become the final membrane structure. At the membrane–air interface, the solvent changes its form from a flat to a meniscus, minimizing the liquid–vapour contact area. The evaporation rate decreases since evaporation from a curved interface is lower than that from a flat surface. The first falling rate period continues until the solvent maintains its continuity. When the solvent becomes disconnected (slurry saturation less than 10%) and remains only at the 'necks' between grains, the second falling rate period begins [99]. The solvent attached to the grains (e.g. by hydrogen bonds if the solvent is water) is removed by decomposition at higher temperatures rather than by evaporation from the slurry surface. During the second falling rate period, the slurry can be heated as no additional shrinkage is expected. The heating only results in a weight loss [90]. At the end of the drying, the slurry obtains its initial shape including the pores. The resulting green body has the desired shape, but it is still weak. At this stage, the process is still reversible, and immersing the green body into the solvent will dissipate it back into the initial slurry.

Now we are ready to eliminate binders and plasticizers by thermolysis (degradation at high temperatures). Note that thermolysis has been identified as a separate stage only lately [26]. Previous reports describe thermolysis as a part of the firing or sintering stage [90]. The exact binder elimination is a complex process that combines chemical and mass transfer phenomena. It was and still is a subject of many fundamental and practical studies. Due to its complexity, the thermolysis scheme (temperature–time–heating rate–atmosphere) is based on one of two extreme hypothetical practices. One uses a slow heating ramp (the increase of heating temperature from drying to thermolysis), low temperature at heating plateau (the heating at the constant temperature) and a long heating period. The other is rapidly passing from drying to thermolysis that is performed at high temperatures for short time periods to achieve the maximum weight loss rate. The latter is determined using thermogravimetric analysis (TGA). The difference can be as significant as between 1 and 20 °C/min, 300 and 600 °C, hours and days [133,134]. Both approaches aim at complete removal of binders and plasticizers by decomposition into volatile organic compounds (VOCs) and carbon residues. Many mechanisms can initiate this decomposition, although thermal and oxygen-induced degradations are the most common ones [135]. The diffusion rate is higher in gases than in liquids and therefore keeping the interstitial pores open will likely result in uniform heating, fast decomposition and removal of VOCs with no residues. Still, the proper heating rate should balance between massive gas production and diffusion during the binder degradation. Sometimes this is impossible, and the thermolysis generates involatile carbon and bubbles that cause cracking at the sintering stage.

Thermolysis of thermoplastic binders can lead to bubble formation, while that of thermoset binders can cause cracks in the final membrane [134]. Polyvinyl

butyral [97], polyvinyl alcohol and polyvinyl acetate are eliminated by side group elimination (a scission of the pendant groups attached along the polymer chain backbone [99]). PPC, PBMA and PMMA are decomposed by depolymerization, giving monomeric volatile products. PEOs and PEGs are decomposed by random scission, producing a spectrum of molecular fragments [99]. Side group elimination and random scission, as well as the thermolysis of cellulose ethers (e.g. methyl cellulose and hydroxyethyl cellulose [107]), often incurs side reactions such as cyclization and cross-linking [136]. This gives highly branched, non-aromatic carbon residues that are involatile at elevated temperatures (up to 1000 °C) under oxygen-deficient conditions. These carbons stay inside the green body, and removal requires an oxidative atmosphere. The organic weight loss passes through regions of rapid elimination of 70–80 wt% at 200–350 °C and final weight loss (20–30%) of carbon residues due to the oxidation (basically, burning under air).

The formation of non-volatile compounds is more likely at higher binder concentrations, and these are linked to the shaping method used. Dry pressing and slipcasting require less plasticity and, therefore, use less binder (up to 10 wt%). Tape casting (3–17 wt% binder) and extrusion (7–20 wt% binder) are built on a continuous paste. These high concentrations are likely to leave the interstitial volume full with binder, even after drying. The VOCs must exit through pores completely filled with binder, unlike the quick escape of VOCs through open pores at low binder concentrations. Moreover, the moving heating front will not be planar, resulting in different heating regimes for different green bodies. The formation of non-volatile carbon residues over a broad temperature range is more likely. This uneven heating can lead to bubbles when local temperatures exceed the boiling point of the solvents and plasticizers yet remain under the binder's boiling point.

The thermolysis of green bodies with high binder content is problematic, and must be avoided. One simple solution is using less binder. Keeping the ratio of binder to particle volume below 0.08–0.15 will leave the pores open [137]. Alternatively, you can use more plasticizers that will evaporate at low temperatures, thus leaving interstitial pores open to the fast escape of VOCs, combining this with low-viscosity binders and high volatile diffusivity (which generally depends on molecular weight). You can also limit the formation of non-volatile carbon by making lighter green bodies. This can be done by using larger powder grains. Finally, minimizing the diffusion path by reducing the thickness of the green body may also help.

1.9.3 Sintering

We now approach the most important stage in the formation of ceramic membranes. Sintering is, in fact, one of the oldest technologies used by man to produce dishware, storage cans and iron tools. It is also the last process step where the microstructure of the final ceramic can be changed. The word 'sinter' comes

from the Middle High German *Sinter* and is similar to the English 'cinder'. Technically, sintering is a process that uses thermal energy to produce consolidated materials from ceramic or metal powders. There are two consolidation types: *General consolidation* gives a dense polycrystalline solid (also called a *compact*). Conversely, *local consolidation* affects only a limited number of grains. Among the four categories of sintering (solid-state, liquid-phase, viscous sintering and vitrification), we will focus only on *solid-state sintering*, the most commonly applied method in membrane preparation. The solid-state pressure-less conventional sintering (we will call it simply sintering) is the heating of a green body to a temperature that is between 0.5 and 0.9 of the melting point of the grains in the absence of a liquid [26]. This sintering is different from liquid-phase and viscous sintering that are done in the presence of 3 and ~25% of liquid, respectively,[1] and from glass vitrification which is performed at or above the softening temperature [138]. It is also performed without additional pressure, unlike pressure sintering that uses hot pressing. Solid-state sintering is the most attractive sintering method for making ceramic membranes, because it is effective, simple and cheap.

Kinetically, sintering is often divided into initial, intermediate and final stages. This division is arbitrary. Each stage is described by a simplified model, such as a two-particle model at the initial stage, the channel pore model at the intermediate stage and the isolated pore model at the final stage. According to the two-particle model, at the initial sintering stage, two neighbour grains develop a solid neck between them and become a new united cluster. This happens as soon as the heating temperature gives atoms, ions and atomic clusters within a grain some degree of mobility. Actually, some mobility exists at any temperature above absolute zero. However, there is a difference between an elementary jump process of an atom between two neighbour sites and the succession of steps that lead to a macroscopic diffusion. An elementary atomic jump takes $\sim 10^{-13}$ s [139] and it is much quicker than the mean residence time of an atom on a lattice site. This elementary jump is chaotic and cannot be described in terms of diffusion. Generally, nine consecutive moves in one direction are considered as a meaningful movement of atoms that result in their relocation. Atoms will hop from one to a nearby vacant site if vacancies (point defects) are available,[2] or will detach from a grain for a further attachment due to Brownian motion. The latter mechanism is called evaporation/condensation, and is different from diffusion, which occurs entirely within a discrete grain.

The consolidation of two grains during sintering covers three types of diffusion that differ in the start and end points of their path. If the start and end points and all vacant sites are on the grain surface, the diffusion is called a *surface diffusion*. If the start and end points are on the grain surface, but the vacant

1) The high percentage of liquid at viscous sintering results in the full densification of a compact in the grain–liquid mixture. The liquid-phase sintering is also called a transient sintering as the liquid is present only at the initial stages of sintering and disappears at advanced stages, so the densification is completed in the solid state.
2) The number of vacancies increases exponentially with an increase in the temperature.

sites are within the grain volume, the diffusion is called a *lattice diffusion*. Compressive stresses on the grain boundary were suggested as an alternative mechanism for the atom ordered movement, although they are still marked as lattice diffusion [140]. If atoms move from the grain volume to its surface, it is called a *plastic deformation* (in this case it is also irreversible). The latter is considered unimportant in pressure-less sintering [140].

Practically, sintering can be viewed as a rearrangement of atoms on surface grains. In all three diffusion types, the number of vacancies increases exponentially at higher temperatures. Other factors that influence the diffusion are the partial pressure, the impurity and the type of the diffusion path. The vacancy diffusion flux depends on sintering temperature and diffusion path (surface or lattice). Similarly, the impurity diffusion path will depend on the quantity and type of the impurity. The overall sintering rate will depend on the slower diffusing ion, due to both diffusion rate and availability of defects. In α-alumina, the sintering rate is determined by the aluminium while oxygen rapidly diffuses on grain surface [118]. Some studies also distinguish between surface and lattice diffusion on the grain and on the intercept of two grains [138] to forecast the speed of neck formation. Figure 1.20 shows the various atom transport mechanisms during the three sintering stages.

According to Ashby, at each moment there is only one dominant transport mechanism [141]. Although the so-called *Ashby diagrams* vary in terms of green body materials and sintering conditions, the general trend is that after a preliminary adhesion, the initial stage of sintering is mostly influenced by the grain boundary diffusion. If the sintering is done at the same temperature, the grain boundary diffusion is followed by surface diffusion. Conversely, if the sintering temperature is raised at intermediate and final stages, lattice diffusion will dominate. Many Ashby diagrams also predict the kinetics of neck growth as the function of the grain diameter. This prediction is based on previous laboratory

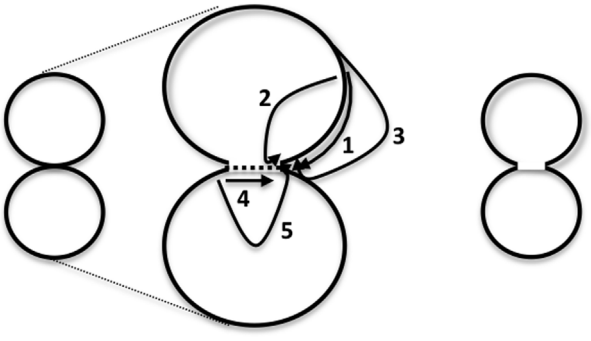


Figure 1.20 Three stages in sintering: (i) the initial neck contact; (ii) the subsequent growth; (iii) the final form formation. 1: surface diffusion; 2: lattice diffusion from the grain surface; 3: vapour transport; 4: grain boundary diffusion; 5: lattice diffusion from the grain boundary. (Drawn after Ref. [26].)

measurements and on *Herring's scaling law* that predicts the kinetics of diffusion as a function of the dominant diffusion mechanism. The relation is given by

$$\frac{t_2}{t_1} = \left(\frac{R_2}{R_1}\right)^m, \tag{1.14}$$

where R_2 and R_1 are sizes of powder grains with t_2 and t_1 sintering time periods, and m is an integer that corresponds to a transport mechanism ($m = 2$ evaporation/condensation; $m = 3$ lattice diffusion; and $m = 4$ surface diffusion[3]). According to this law, the transport by diffusion is much faster than by evaporation/condensation, and sintering of fine particles is much faster than of large ones.

An increased movement of atoms results in more frequent collisions. The driving force for sintering comes from the excess free energy that exists in powder compacts due to the annihilation of the solid–vapour interface. The enthalpy of the entire system decreases as the energy required for forming new solid–solid bonds at the neck between two grains is lower than the energy released at the annihilation of solid–vapour interface. A necessary condition for sintering is that the gain of the elimination will be larger than the loss of the generation. The formation of a neck decreases irregularities on grain surfaces, reshaping them into perfect spheres but not necessarily shrinking or compacting the entire matrix. The densification at this stage is small, around 2–3%. A considerable densification (up to 90% relative density) occurs at the intermediate stage. At the end of the intermediate stage, the compact contains only irregular isolated pores. These pores contribute up to 7% relative density and they are eliminated at the final stage. As a rule of thumb, the initial stage is said to continue until the distance between two opposite points on the concave neck curvature will reach 0.3 of a grain diameter.

At the *intermediate stage*, the neck continues to grow and evolve into a 3D structure of solid particles and continuous channel-like pores. This evolution can take two pathways: In the first, a grain or a cluster of two grains can grow as a separate unit when the surface diffusion and vapour transport lead to the rounding of particles and growth of necks. The migration of grain boundaries leads to increased grain and pore sizes, the latter due to pore coalescence. This process is called *coarsening*. It increases the diffusion path for atomic transport, thus reducing the sintering rate. The final compact will have an increased porosity along with lowered density. In the second pathway, clusters can evolve into 3D structures by developing necks with other grains by a process called *densification* immediately at the beginning of the intermediate stage. The dense membrane will have fewer open pores. As the intermediate stage occurs at high temperatures, there is no direct evidence of the exact evolution path. The exact pathway is discussed in a frame of one of two main theories. According to the first [142], the intermediate stage begins from coarsening that is a necessary step towards the densification. The theory is built on the Ashby diagram that states that the grain boundary diffusion is the ultimate initial stage. Following the

3) $m = 1$ corresponds to viscous flow in metals.

diagram, the sintering at constant temperature will lead to coarsening, but will not consolidate the compact [138]. Raising the temperature will lead to consolidation, shortening the required sintering time.

Alternatively, the second theory proposes that grain growth and densification are two parallel processes that are linearly related to each other [143], both eventually resulting in a compact. The two processes are necessary for the continuous densification during sintering. One weakness of this view is that experimental observations show unequal grain growth. While one assumes that all grains are grown by a simple and invariable increase of the grain size with time, the experiments report a quick formation of some exceptionally large grains in the matrix of fine grains with a very slow growth rate. The formation of the abnormal grains is explained by Ostwald ripening that postulates that in the event of uneven distribution of grains, there is a critical grain radii $r*$. Grains with radii larger than $r*$ will grow and those with radii smaller than $r*$ will dissolve, 'feeding' the large particles with atoms and cluster building blocks. Such a bimodal grain size distribution is opposite to the unimodal distribution required for linking grain growth and densification. At the end of the intermediate stage, the channel-like pores break down into separated voids [138] that are eliminated at the *final stage* [26]. This stage, however, is not relevant to the ceramic membranes field and will not be discussed here. Figure 1.21 shows the sintering of a ceramic membrane showing the development stages of the final membrane structure.

The exact outcome of sintering is not known *a priori*, and the process is usually based on trial and error. However, certain variables have a proven effect on the final membrane. We divide these into two groups: green body parameters and operational variables. The first group includes, in addition to the grain size, shape and size distribution, the degree of agglomeration, the mixing of the slurry, the starting porosity, the chemical composition of the powder compact, the degree of homogeneity (presence of impurities) and the binder amount. These parameters will also determine the coarsening/densification competition at the intermediate sintering stage. The second group (operational variables) in

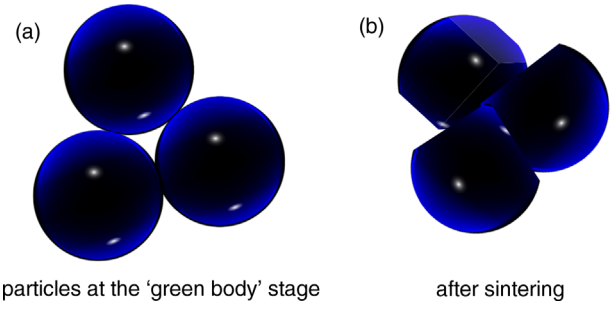


Figure 1.21 Development of a final membrane structure (b) from a green body (a) during sintering of a ceramic membrane.

pressure-less sintering includes temperature and time. We will describe the influence of some of these parameters in the next section, together with a few tested and proven recipes for sintering ceramic membranes.

1.9.3.1 Sintering Variables

Temperature is one of the most influential parameters. Historically, the lack of programmable furnaces has limited the flexibility in sintering. Today, however, any sintering temperature can be set, and any sintering regime programmed. The flexibility in controlling these two features gives endless variations of the sintering protocol. Here we describe general experimental observations regarding the temperature and the sintering regime (exact sintering protocols are often kept as a trade secret by manufacturers).

As a rule of thumb, the sintering temperature is set at 0.5–0.9 of the melting temperature (see above). This offers a wide range of sintering temperatures between 250 and 1700 °C. Table 1.7 gives the sintering temperatures of selected ceramics.

The exact sintering temperature depends on many factors, including the required target density and porosity, the presence of impurities, the sintering time and the intended service temperature. Short sintering times require high temperature and better furnaces, and the sintering temperature should be well above the service temperature. In general, sintering at high temperatures promotes densification and depresses coarsening but also increases the production cost. Sintering of α-alumina at 1550 and 1800 °C results in the formation of membranes with 4 and 2 μm average roughness (R_a), respectively [30]. A dense membrane has smaller grains and reduced porosity. This often results in superior mechanical strength and low transmembrane flux. Lowering the sintering temperature will generate membranes with high porosity and low mechanical strength. Since the ideal membrane should have both a high mechanical strength and a high flux, the sintering temperature must be optimized. This optimization, however, is not that simple. Using mid-sintering temperatures might result in the formation of a bimodal pore size distribution with a fraction of large pores. The presence of a transient stage has been reported in studies on the influence

Table 1.7 Recommended sintering temperatures of several ceramics.

Ceramic	Sintering temperature (°C)
Alumina porcelain	~1250
Quartz porcelain	~1300
Steatite	~1300
Cordierite	1250–1350
Aluminium oxide	1100–1600
Recrystallized silicon carbide	2300–2500
Sintered silicon carbide	~1900

of sintering temperature on pore size distribution in aluminium oxides [144]. A monomodal pore size distribution at 1000–1200 °C changes to a bimodal pore size distribution with a fraction of large pores at 1300–1400 °C and pore shrinkage at 1500–1600 °C. Microcracks were formed at temperatures of 1700 °C and above due to proximity of a melting point of aluminium oxide. The mechanical strength constantly increases in the entire sintering range until temperatures above 1700 °C, where the membrane loses its ceramic properties.

Many protocols recommend sintering with a gradual increase of temperature. This saves time and promotes densification instead of coarsening. The sintering temperature is usually increased by a constant increment over time, called the *sintering rate*. The final compact is cooled back to the room temperature with a certain *cooling rate*. Sintering and cooling rates are measured in degrees per minute, and can acquire values between 0.1 and 1000 °C/min. Typical heating rates are 2–15 °C/min. Steep sintering rates promote the formation of dense membranes due to a short time spent at low temperatures. The concept of fast sintering (also known as *fast-firing*) arose from adjustments to the sintering rate targeting the maximal densification at minimal coarsening [145]. In line with the rate-controlled approach, the green body is heated quickly to the sintering temperature, held at the constant sintering temperature plateau for a certain time period to allow consolidation and then cooled down with a certain cooling rate. A short processing time and reduced energy consumption are two economic benefits of steep sintering and cooling rates. The risk is the possibility of cracking of the final compact by a thermal shock caused by a fast temperature change. Slow sintering rate (the so-called *isothermal-stage sintering*) prevents the formation of temperature gradients that can lead to cracking and breaking, or to a differential densification (a formation of an outer dense layer with large internal voids). It is done by heating the green body for many hours up to the final sintering temperature and immediate cooling thereafter. This minimizes the holding time at the sintering temperature, giving membranes with high porosity (albeit with a lower mechanical strength). Definitions of high and low sintering rates are subjective, however, and depend on the grains used. According to Rahaman [138], very high and very low sintering rates result in coarsening, while intermediate sintering rate favour densification. The cooling rate should be sufficiently high to save process time and reduce energy consumption, yet low enough to prevent thermal shock and breaking of already formed compact.

Regardless of whether you want dense or porous membranes, you must leave a certain degree of effective porosity to produce a transmembrane flux. The holding time is thus important. In general, long holding times result in significant densification and the entire process might enter the final sintering stage where transmembrane pores gradually disappear. Short holding times may result in the transition from coarsening to densification and in a production of large pores. The mechanical strength of the entire membrane will then be lower.

Grain size and grain size distribution also influence sintering. Basically, small grains give denser membranes. Current research focuses on the properties of ceramics made of nanosized grains. These studies are motivated by the

expectation that many ceramic properties will vary significantly with nanometric grains. However, the production of unisized nanosized powders is expensive, and benefits of such a membrane are moot. We will therefore focus on the typical micrometric grain sizes and their distribution. As already discussed, typical grains are of the sizes between 0.5 and 1.0 μm. This grain size is considered optimal for sintering a membrane of sufficient mechanical strength and low resistance. The ratio of the grain to the pore sizes was established before, and with the grains in the 0.5–1.0 μm range, the expected pores will be between 0.16 and 0.50 μm. These pores can be stable during sintering or may collapse to give the final compact with no pores. Note that the outcome of the sintering depends mainly on the initial sintering stage and is in general independent of the grain size. The only correlation reported by Chaim *et al.* [146] is that once the pore size exceeds the grain size, the pore elimination time is proportional to the fourth order of pore diameter. In practical terms, such pores cannot be eliminated.

Sintering protocols vary from one study to another, and, as already explained, industrial protocols are often kept as trade secrets. Therefore, we present here some of detailed sintering protocols found in the literature. Table 1.8 summarizes some known sintering protocols divided into drying, heating, sintering and cooling stages.

Table 1.8 Sintering protocols.

Raw materials	Drying and heating	Sintering	Cooling
Alumina (Alcoa Chemicals), magnesia (Merck), native potato starch (Portugal); TRECOMEX AET (Sweden), polyacrylic acid [106]	1 °C/min up to 500 °C; hold for 1 h at 200, 300 and 1000 °C	1600 °C for 2 h	
Alumina (Martinswerke); Zircosil 5, PVA [131]	20 °C/min to 1000 °C; rate of 5 °C/min up to sintering temperature	1200–1500 °C; 1 h soaking after sintering	
$La(NO_3)_3$, $SrCO_3$, $Co(NO_3)_2{\cdot}6H_2O$, Fe_2O_3, ZrO_2, isopropanol [147]	5 °C/h in 150–400 °C range; 60 °C/h to sintering temperature	1200 °C for 5–10 h	
$Ce_{0.8}Gd_{0.2}O_{2-x}$ (Rhodia), $(Co(NO_3)_2–6H_2O$, (Fluka), ethanol (Fluka) [148]	120 °C for 2 h; 1 °C/min to 450 °C; 3 °C/min to sintering temperature	900–1400 °C for 2 h	5 °C/min
Alumina, titanium tetraisopropoxide (Aldrich), zirconium *n*-propoxide (Alfa), PVA, HPC [84]	100 °C/h to sintering temperature	500–1000 °C for 30 h	100 °C/h
Kaolin, quartz, calcium carbonate, sodium carbonate, boric acid and sodium metasilicate [149]	20 °C for 24 h; 100 °C for 12 h; 250 °C for 24 h; 2 °C/min to sintering temperature	850–1000 °C for 5 h	5 °C/min

1.9.4 Finishing

No matter how precisely we follow the manufacturing protocol, a ceramic membrane will never come out perfect. It could be a result of uneven drying or sintering, different shrinkage, gravity effects and a million other random factors. Membranes with major deviations in the form of cracks, curved surfaces, uneven support covering or cavities will be discarded. Figure 1.22 displays common failures in the preparation of membrane supports.

Conversely, minor deviations in the form of curved or rough ceramic surfaces can be fixed mechanically if the deviation from the linear average membrane thickness does not exceed 2%. Otherwise, the membrane is discarded. The definition of a bearable defect that can be fixed allowing further use of the membrane is unique for ceramic membranes. Polymer membranes have deviations of less than 1% that are regarded as their integral feature. If deviations exceed this value, the membranes are simply discarded with no attempts to prepare them for future use (unlike ceramic membranes). Similarly, metallic membranes are routinely machined to 25 μm tolerance with no difficulty or significant costs.

Finishing of ceramic membranes can be done by *grinding*, *lapping* and *polishing*. Grinding is a machining process, a subset of cutting that uses a grinding wheel as the cutting tool. Here, machining is a controlled alteration of a surface of a sintered membrane to achieve a desired degree of uniformity. Grinding is also implemented to alter membrane dimensions and shape, usually when the optimization of membrane preparation steps does not bring the desirable results. It is basically a very precise cutting technology that can reach single-micrometre

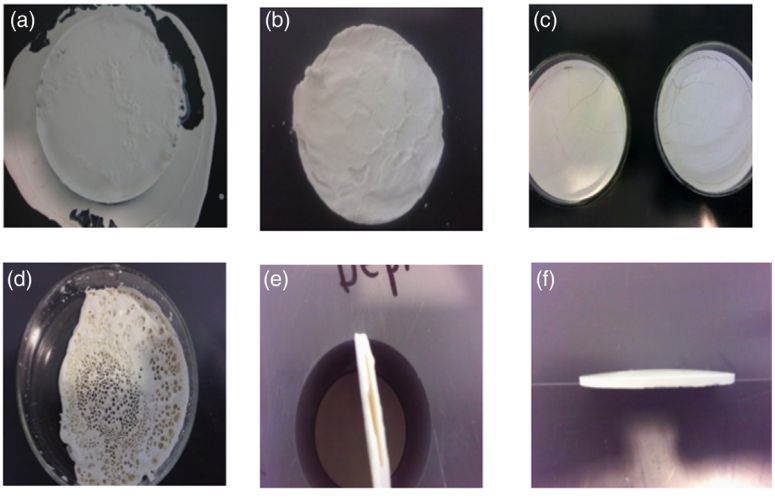


Figure 1.22 Examples of failures in preparation of α-Al_2O_3 support membranes due to insufficient dispersant (a), high binder concentration (b), wrong drying regime (c and d), gypsum drying (e) and wrong sintering protocol (f). (Photographs by L. Tsapovsky.)

resolution. The preciseness of grinding is viewed different from cutting that is considered a macroscopic process. Abrasive grits (hard particles with sharp edges such as polycrystalline diamond (PCD) or cubic boron nitride CBN) are located on the edge of the grinding wheel that rotates at high speed. The geometry of surface grinding is variable and includes horizontal/vertical spindle, cylindrical grinding, internal grinding, centreless grinding and form (or plunge) grinding [150].

Lapping and polishing are finishing processes in which ceramic and abrasive surfaces slide parallel to each other. In this case, the finishing action is due to the presence of an abrasive pressed towards the membrane surface with either hand or a machine. *Coarse lapping* is performed with abrasives such as aluminium oxide, jeweller's rouge, optician's rouge, emery, silicon carbide or diamond, and can result in surfaces that bring the deviation down to 20 μm. The relative movement of the two surfaces removes material from both. *Gentle lapping* is performed with softer materials such as diamond or sand paper that are often wetted for easy sanding. Very intense and precise hand polishing may result in deviation of <1 μm. Lapping and polishing result in membranes with uniform thickness and decreased tortuosity of the membrane surface. The processes can also be used to fit the membrane to the required size of the support. This operation is often used in laboratory preparation of new membranes. The polished membranes are cleaned by ultrasonic rinsing in ethanol or by flushing water to clean the polished powder that can block the pores. In general, machining is considered as crude and expensive. Riedel and Chen [150] estimated the machining cost as 60–80% of the total manufacturing cost.

1.10 Intermediate and Top Layers

After all the hard work, many trials and a bit of luck, we have our first ceramic membrane. But is our membrane ready for industrial applications? Not really. At the moment we have a *membrane support*, a one-layered structure that is used in laboratory research and some low-cost industrial applications. For all other large industrial applications, the performance of membrane support is not sufficiently attractive to move from other separation technologies into ceramics. The performance of ceramic membranes should, therefore, be significantly improved in both separation efficiency and transmembrane flux. The ideal approach is to increase both the selectivity and the flux. As this is not possible, a wishful approach is to increase the flux without affecting selectivity or to increase the selectivity without affecting the flux. Is it possible? The answer is not that obvious. Although many industrial applications are built on sieving, improvements based on surface modifications are possible. The modification can target the membrane pore size compression that will definitely affect the selectivity. But this comes at the cost of a lower transmembrane flux. The other route is coating the membrane with molecules that give the membrane new and improved

features. Basically, both pore shrinkage and coating are processed through the attachment of additional layers to the membrane support, and the main difference between the two is in the retention mechanism. Whereas pore shrinkage aims at retaining molecules by physical restriction, coating can additionally adsorb desired molecules by designated end groups in the coating layer.

All ceramic membranes are modified to improve their performance. In many applications, only one type of ceramic material is suitable for the separation, such as dense perovskites for oxygen transport in fuel cells. Separations based on molecular sieving enjoy the possibility to choose from many ceramic membranes (as well as polymer and metallic ones). Those are room-temperature hydrogen and carbon dioxide separations, pervaporation, water and wastewater treatment, juice, beer and wine clarification and milk and cheese production. These applications are discussed in detail in Chapter 4. The implementation of dense membranes occurs through solution–diffusion and therefore requires a close match between the membrane material and the transferred compound. Convection is the driving force through porous membranes, and size restriction is the main separation mechanism. Many of the latter applications require a molecular sieving, that is a precise separation between two compounds with close dimensions, on the size base. The sieving mechanism requires a membrane with unified small size pores and minimal pore size distribution. Gas separations are usually performed with 0.3–0.4 nm pore size membranes. Liquid separation can be performed with 20–30 nm pores.

Homogeneous ceramic membranes with pore sizes >1 μm can be used in microfiltration of liquids. All other applications require modifications by the addition of several intermediate layers and a top membrane layer. These modifications can be specific, targeting a single industrial application. Alternatively, they can be general, producing generic membranes suitable for many applications. Gas permeation membranes are not suitable in liquid applications due to their small pores and low flux. Similarly, liquid permeation membranes cannot separate gases, although they exhibit infinite fluxes.

Ultrafiltration ceramic membranes are formed from two- or three-layered structures. Typical pore sizes in UF membranes are between 2 and 50 nm; this structure can be obtained by sintering. Nanofiltration and gas and vapour separations are performed with microporous membranes with pore sizes between 0.7 and 2 nm. The pores can be obtained by either formation of a separate layer of nanoparticles or by a controlled development of the intrinsic structure of ceramic materials. The top layers can be prepared from ceramic oxide nanoparticles by a coating of these on the membrane intermediate layer. They can also be made by growing membrane materials such as zeolite crystals or by graphitization at high temperatures of organic carbons [42]. Ceramic oxide particles are incorporated on top of intermediate layers by different processes. The processes can be subdivided into physical vapour deposition (PVD), chemical vapour deposition, electrolytic deposition, sol–gel formation and hydrothermal treatment of zeolites.

PVD methods include thermal evaporation, physical sputtering, cathodic arc deposition and pulsed laser deposition. The reason why PVD techniques form a

separate category is that the film grows from a condensation of single atoms. In CVD techniques, molecular species react at the surface to form a film layer. The electrolytic deposition uses electrolyte where the atoms that form the film are present in as positively charged metal cations. Sol–gel is a general name for the process that converts a colloidal or polymeric 'solution' (sol) of silica, titania and zirconia to a gelatinous substance (gel). Here we will focus on three major modification methods, namely CVD, sol–gel and zeolite modifications. Both CVD and sol–gel can produce amorphous films with similar characteristics. The sol–gel route seems to offer more flexibility for tailoring the porosity and composition of separating layer. However, the final porosity depends drastically on various parameters and thus the reproducibility of sol–gel layers is challenging.

1.10.1 Preparing the Intermediate Layers

Our main message here is that the intermediate membrane layers cannot be prepared the same way as the support layer. A membrane structure can be sintered once and once only. This limits the choices of methods for forming intermediate layers. The most suitable method is called *dip coating* or *withdrawal coating*. Here the support layer is dipped into a ceramic dispersion and subsequently fired after withdrawal. Pressure filtration of a suspension through the support is an additional method to initiate the formation of intermediate layers, although this is limited to membranes with flat geometries.

The support layer has micrometre-sized pores and millimetre-depth thickness. It is suitable for separating compounds substantially larger than those typically affiliated with membrane processes. Examples of separable materials include bacteria and protozoa, coal dust, blood cells, milled flour and paint pigments. These are all micrometre-sized particles. Few applications require the separation of these materials by membranes. The application spectrum of ceramic membranes can be enlarged if the membrane pore size is reduced. As we saw above, the support layer is tuned by subsequent coating of intermediate and top layers. The number of intermediate layers may differ between one and three, depending on the pore size difference between the support and separation layers. A larger difference requires more layers. In each consecutive layer, the pore size decreases until at the very fine separation it drops from micrometres to single nanometre. This can be seen as the intentional compression of the pore size, but it is not the case. There is an empirical correlation between the pore size and the grain size (see Section 1.9.3). If the average grain size is 1 μm, then the mean pore width is between 400 and 660 nm. The grain size in the intermediate layer cannot be much smaller than the pore width. The first intermediate layer is expected to form from particles with 300–400 nm mean size, yielding a layer with 100–150 nm pores. Thus, the next layer will start with grains of 70–100 nm and yield pores of 30–40 nm. The third and final layer is likely to form from grains of 25–35 nm size and produce pores of 8–10 nm width. This pore size is sufficient for a smooth coating of separation layer that will contain 2–3 nm or

even 0.2–0.3 nm pores. The purpose of an intermediate layer is to successfully coat the membrane with a unified layer that will leave no uncovered places where the previous layer can be seen. This approach was proven effective in recent reports on defect-free surfaces obtained by the deposition of three intermediate γ-alumina layers. The layers were prepared by dip coating of boehmite AlOOH sols with 630, 200 and 40 nm particles. The top layer was made of silica [151,152] and silica–alumina [153]. One clear drawback of this approach is that making the interlayers is labour-intensive and time-consuming.

The thickness of the coating layer should be larger than the roughness of the support, so that it covers the support completely. With an estimated maximum roughness (R_{max}) of 20–30 μm, a 30–40 μm thickness of the first intermediate layer is required [30]. This requirement will be reduced from layer to layer as each consecutive layer will be smoother. The average roughness (R_{av}) of the last intermediate layer should be below 1 μm as it is not possible to coat defect-free on support with an average roughness larger than 1 μm. In practice, the thickness of each layer is kept as low as possible to ensure a complete covering on the one hand and to avoid adding unnecessary membrane resistance on the other. A typical thickness of a coating layer is 100–1000 times the pore diameter [30]. This suggests that producing layers with smaller pores will at the same time reduce the thickness of each consecutive layer. For example, a typical thickness of a silica separation layer having pores of 2–3 nm is 200–300 nm [30]. The added membrane thickness of up to 0.1 mm can improve the mechanical strength, but thick intermediate layers lead to a higher resistance from the interlayers and reduce transmembrane flux.

Intermediate layers are built of ceramic particles. The coating particles should be chemically compatible with the support material to ensure a proper adhesion. Typically, the intermediate layers are made of same particles as the particles used in the preparation of the support, namely γ-Al_2O_3, SiO_2, TiO_2, ZrO_2 or their mixtures. This ensures not only decreased thickness and well-controlled pore size but also good thermal and chemical stability. Contrary to the support layer, the prepared suspension should remain stable during the coating process. Any aggregates or significant sedimentation can affect the drying process and result in non-uniform coating of the substrate. Hence, the average dry content of the suspension is approximately an order of magnitude lower than in preparation of substrate (3–5% for the intermediate layer versus 70% for the substrate).

When the support is withdrawn from a suspension, the dense dispersion layer of a defined thickness should not delaminate from it. Practically, this means that the support is wetted by the dispersion liquid. A consolidated coating is achieved after drying and calcination. Several intermediate layers can be obtained by the same routine, usually with a calcination step between each two consecutive coatings and by adapting the coating conditions.

An initial dispersion is either made of colloidal particles such as alumina or zirconia powders or prepared *in situ* from boehmite and titania sols using organometallic precursors. These particles are mixed in a polar solvent such as water or in an organic solvent such as ethanol or methanol. The suspension

should attach itself to the support so that it remains intact after being withdrawn from the suspension. There are two possible modes for this: *capillary colloidal filtration* and *film coating*. Capillary colloidal filtration occurs when the dry substrate contacts the suspension and the pore surface is wetted by the dispersion liquid. There are few research papers on the topic of intermediate layers. From what is available, Bayati *et al.* [154] found that decreasing the boehmite–titania content from 5 to 3 wt% results in the elimination of cracks and formation of more uniform intermediate layers on the support surface.

Any interactions between the support and the coating material should not lead to decreased permeability or defects in the membrane system such as microcracks. The thermal expansion behaviour of the coating should be comparable with that of the support. If the chemical compositions of support and filtration layers are sufficiently different, the intermediate layers need to buffer thermal expansion coefficients of various layers to minimize the number of defects formed during drying and calcination.

A membrane that has support and intermediate layers is suitable for MF and UF liquid separation processes, but not for those processes that require thermal, chemical and mechanical robustness. Such applications require a further coating of the ceramic membranes by a top layer. There are many methods for making such coatings. Here we will describe the two main ones: chemical vapour deposition and sol–gel. A zeolite coating is a different topic that is unique to zeolite-type structures.

1.10.2 Fundamentals of Chemical Vapour Deposition

Chemical vapour deposition is defined as a condensation of precursor compounds onto membrane support surface. Carrier gases such as hydrogen, nitrogen or argon deliver volatile precursor compounds such as metal halides, carbonyls or alkoxides into the reaction chamber [155]. The gas mixture in the reaction chamber flows over a membrane surface heated to a temperature needed to execute a chemical reaction such as oxidation, hydrolysis, thermal decomposition or compound formation. These reactions can occur in the vapour phase over a heated surface or by adsorption of reaction intermediates on the membrane followed by a surface reaction. This single-step operation gives a solid deposit layer. Heating can have a form of membrane heating, thermal radiation and photoradiation heating. Historically, the first experiments were run in the vapour phase using oxidation under atmospheric pressure and were named atmospheric pressure chemical vapour deposition (APCVD) or simply CVD. The deposition temperature ranges from 600 to 1500 °C depending on the reaction system. For many compounds, however, the heating temperature was high and CVD was considered an energy-intensive operation that can also damage the membrane surface. Further experiments aimed at reducing heating temperature by implementing plasma-assisted chemical vapour deposition (PACVD) or plasma-enhanced chemical vapour deposition (PECVD) [156]. PACVD and PECVD require temperatures below 500 °C and

sometimes as low as ambient temperatures. This is because electrical discharges in the gaseous phase are used for initiating the chemical reaction rather than thermal energy. Both methods give coating layers with high selectivity and a narrow pore size distribution. The deposition at low temperatures in PACVD and PECVD is suitable for temperature-sensitive compounds. The thickness of deposition layer is largely determined by the deposition time [157]. That said, the plasma bombardment of membrane surface can damage both the membrane and the coating film. In general, the efficiency of PACVD and PECVD depends strongly on the radio frequency, gas pressure, reagent flow rate and reactor geometry.

Photochemical vapour deposition (PCVD) uses high-energy photons that interact with the precursors either in the gas phase or on the growth surface. It is usually done with UV radiation due to the higher energy input and the absorption bands of simple organic precursors (that are often located in the UV range). It can also be performed at low or even ambient temperature and target a specific deposition area. PCVD enjoys the freedom of film thickness control due to the independency of bulk and membrane temperatures. However, it is limited to the precursor compounds that absorb photons and response in a predictable manner, with no or minimum side reactions and by-products.

In atomic layer deposition (ALD) the precursors are introduced to the reaction chamber such that they reach the saturated adsorption level on the membrane surface. The deposition is due to a sequence of adsorption–chemical reactions steps. Here, the introduction of the precursors is controlled by an inert gas purge. This removes any excess precursor molecules and by-products from the reaction chamber preventing gas-phase reactions [158]. ALD has a superior control over the coating layer thickness due to a controlled step coverage. It is typically carried out at 250–300 °C, below the thermal decomposition threshold of most precursors. This thermal regime minimizes bulk reactions and avoids side reactions.

There are additional options such as laser chemical vapour deposition (LCVD), low-pressure chemical vapour deposition (LPCVD), metal–organic chemical vapour deposition (MOCVD) and chemical vapour infiltration (CVI). All together, the CVD processes form a family of chemical deposition processes with a common ground: Precursors are brought into reaction chamber in a vapour phase and turned into thin solid film on membrane surface after a chemical reaction of vapour-phase precursors. The reaction occurs either in the gas phase or on the membrane surface.

Due to the variety of precursors and possible gas-phase and surface reactions, CVD processes are extremely complex. Figure 1.23 presents an overall reaction scheme that includes both mass transfer and chemical reaction steps.

A classical CVD includes seven stages [158]:

1) Evaporation and transport of precursors into the reactor chamber
2) Gas-phase reaction of precursors in the reaction zone to produce reactive intermediates:

$$A_g \rightarrow B_g + C_g \tag{1.15}$$

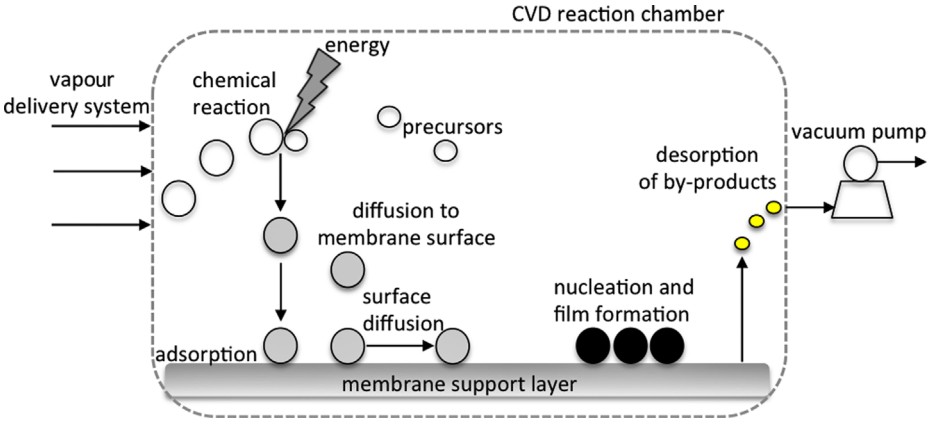


Figure 1.23 Precursor transport and reaction processes in CVD.

3) Diffusional transport of the intermediates to the membrane surface
4) Adsorption of the intermediates on the surface

$$B_g \rightarrow S_s \tag{1.16}$$

5) Surface diffusion to growth sites, nucleation and surface chemical reactions that form the deposition film:

$$S_s + S_s \rightarrow S_2 \tag{1.17}$$

$$S_2 + S_s \rightarrow S_3 \tag{1.18}$$

$$S_3 + S_s \rightarrow S_4 \tag{1.19}$$

6) Desorption of by-products from the membrane surface and transport away of by-products from the membrane and from the bulk
7) Forced expel of by-products and carrier gases from the reaction chamber.

In the list above, A is a precursor compound, B is the reaction intermediate and S is an adsorbed B that contacts with other intermediates on the membrane surface. In parallel schemes, B can react and form oligomers in the gas phase. Thus, the oligomers land on the membrane surface and coalesce to form a porous network [159]. Some CVD processes might not have bulk reactions. In others, the film is already formed in the bulk and just lands as is on the membrane surface.

The formation of dense membranes requires that the vapour reactions be depressed and the film formation occur on the membrane surface only. This mode of film formation requires a smooth membrane surface, and is appropriate for growing films on mesoporous supports with 2–10 nm pores. The membrane pore size and structure here depend on the size and shape of precursors, as well as on the heating and drying conditions. The precursors are either decomposed in the vapour or land on the membrane support unconverted for further reactions. Growing a layer on the membrane support with pores larger than

10 nm requires a more sophisticated approach. The initial small nucleation centres are typically created in the bulk and land on the membrane support in the form of small clusters. The clusters are then grown on the support to form a film. Parallel heterogeneous reactions are needed to close the interparticle voids [159]. Growing a layer on the support with large pores results in a coating of not only the membrane surface but also the internal pore surface.

In traditional thermal CVD, the film growth rate is determined by the temperature of the membrane surface, the operating pressure of the CVD reaction chamber and the composition and chemistry of the gas phase. Figure 1.24 shows the dependence of the film growth on the temperature.

The plot in Figure 1.24 is divided into three regions. At low reactor temperatures, the film growth rate is controlled by the kinetic of chemical reactions. It increases exponentially with temperature, following an Arrhenius relation:

$$\text{Growth rate} \approx e^{E_A/RT}, \tag{1.20}$$

where E_A is the activation energy, R is the gas constant and T is the temperature. The film thickness here is controlled by the reaction temperature and the contact time. A uniform film thickness can be achieved by thorough temperature control over the membrane surface [158].

An increase in the reaction chamber temperature shifts the control to the diffusion of reacted intermediate species to the membrane surface. The overall film growth rate becomes diffusion controlled under the assumption that there is a boundary layer of passive precursors and counter-diffusing by-products near the membrane surface. Similarly, overheating of the membrane surface results in a massive desorption of intermediate species from the membrane surface before they react and become a part of a solid film. The film growth rate is controlled by the desorption rate and is usually lower than in the previous two regions.

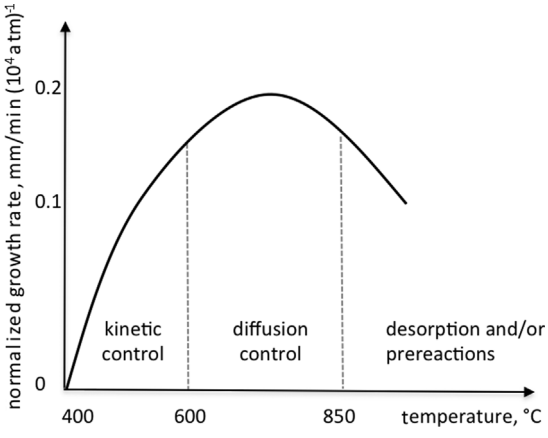


Figure 1.24 The dependence of the film growth on temperature. (Concept based on Ref. [160].

The relative importance of each region is determined not only by the temperature but also by the pressure inside the chamber. Under APCVD, the gas-phase reactions are important and contribute to the formation of a significant boundary layer. The growth of a deposition film is controlled by both gas-phase reactions and diffusion through the boundary film. In low-pressure CVD (LPCVD), as the pressure falls below 1000 Pa, gas-phase reactions become less important. When the pressure is below 100 Pa, the reactions occur exclusively on the membrane surface. At very low pressures of 0.001 Pa, there is no mass transfer and the layer growth is controlled by the gas and substrate temperatures [158].

Many compounds can serve as CVD precursors. The following are the main requirements from these precursors [158]:

1) *Reactivity and thermal stability*. The precursor needs to react in a certain temperature window to give the desired intermediate. Not all precursors are volatile at ambient temperature, and some must be heated in a carrier before entering the reaction chamber. This can cause decomposition, generating particles that might contaminate the coating film [161]. Reactions at the membrane surface are especially vulnerable. A typical reaction at the membrane surface occurs at several hundred degrees, and yet the precursor should react at the membrane surface only. The precursor, therefore, should be reactive just in this narrow temperature range.
2) *Reasonable volatility at moderate evaporation temperatures, preferably well below the temperature of their thermal decomposition*. Some precursors are solids or liquids at room temperature, and boil/sublime at elevated temperatures. The volatility is affected by intermolecular forces such as van der Waals interactions, π-stacking and hydrogen bonds, and it increases with temperature.
3) *Thermal stability at evaporation temperatures*. Differential scanning calorimetry (DSC) is commonly used for determining the thermal stability of precursors by measuring the difference in heat flux between a precursor and a reference material as a function of temperature.
4) *High chemical purity*. A rather extreme example provided in Ref. [158] shows that the unintentional presence of 1 ppm of metal impurity makes a semiconductor unacceptable for most device applications. Carbon impurities might result in the thermal decomposition of either precursor or already formed film.
5) *Absence of or minimal side reactions and by-products*.
6) *Good adsorption* of reaction intermediates on the membrane surface.
7) *Long shelf life* under ambient conditions. The precursor should also be stable under misuse or a spilling accident to avoid massive losses at industrial conditions.
8) *Absence of or low toxicity* and no hazard risk. A low toxicity minimizes the expenses for storage and precautions during film formation. The environment-friendly precursors should preferably be recyclable.

9) Competitive cost/performance ratio.

CVD is used in many industrial applications, including glass coating, silicon semiconductors, compound semiconductors, high-speed electronic devices, diode lasers and solar cells. According to a 2011 estimate, each of these has an annual turnover exceeding $3 billion [162]. Industrial applications use a variety of precursors, including low-k silan-based precursors such as $SiH(Me)_3$, $Si(Me)_4$, and $Si(Me)_2(OMe)_2$, high k precursors such as $Ta(OEt)_5$, $Al(Me)_3$, $HfCl_4$, $Hf(OtBu)_4$, C_8H_{18}, C_6H_{14}, SiO_2 and SiN precursors such as Si_2Cl_6, $Si(OMe)_4$, $SiCl_4$, $GeCl_4$ and metal and nitride precursors such as $TiCl_4$, TaF_5, $TaCl_5$, $Ru(EtCp)_2$, and $W(CO)_6$.

In the ceramic membrane industry, CVD is considered a high-tech application that is relatively costly and difficult to scale up [157]. It is implemented when other options such as sol–gel are inapplicable or when the top layer should combine a very efficient precise separation with a high flux. Two of most popular implementations of CVD are coating of ceramic membranes with TiO_2 using PACVD and MOCVD [163], and silica membranes for hydrogen separation [155]. The latter application gains more interest due to its potential industrial use. The specific interest in inorganic membranes for that application is due to the possibility to create a thin yet defect-free top layer that will combine a high separation with high flux. This separation can be performed at elevated temperatures and under extreme chemical conditions.

In view of the thermostability demand, several silica precursors were used. These are SiH_4, $SiCl_4$, tetraethoxysilane (TEOS) and tetramethoxysilane (TMOS). These precursors react with an oxidizing agent, typically oxygen, water vapours or ozone. The reactants land on the support that can be either Vycor glass or alumina. Both materials are compatible with silica precursors and reactants. The initial work was reported on Vycor glass due to its small pores and intrinsic high uptake of hydrogen out of H_2–N_2 mixture. However, the limited permeance due to narrow pores in the glass shifted the attention towards the α-alumina and to γ-alumina coated on top of α-alumina despite their relatively large pore sizes between 110 and 180 nm [164]. In addition to a higher flux, alumina membranes are also cheaper and mechanically stronger than Vycor glass ones [155].

The CVD precursors form reactive intermediates in the vapour phase due to one of the following five reactions:

Oxidation

$$SiH_4(g) + O_2(g) \rightarrow SiO_2(s) + 2H_2(g) \uparrow \tag{1.21}$$

$$Si(OC_2H_5)_4 + 6O_2 \rightarrow SiO_2 + 10H_2O + 8CO_2 + \text{by-product mixtures} \tag{1.22}$$

Reduction

$$SiCl_4(g) + CH_4 \rightarrow SiC(s) + 4HCl(g) \uparrow \tag{1.23}$$

Nitridation

$$3SiCl_4(g) + 4NH_3(g) \rightarrow Si_3N_4(s) + 12HCl(g) \uparrow \quad (1.24)$$

Hydrolysis

$$SiCl_4(g) + 2H_2O \rightarrow SiO_2 + 4HCl \quad (1.25)$$

Or else they are thermally decomposed (pyrolized) on the membrane support:

$$SiH_4(g) \rightarrow Si(s) + 2H_2(g) \uparrow \quad (1.26)$$

The first examples of using CVD for coating ceramic membranes with silica compounds were reported 40 years ago. Most of the initial work was performed in vapour phase using oxidation under atmospheric pressure CVD (APCVD). For example, the group of Gavalas used the oxidation of SiH_4 on the Vycor glass tubes with 4 nm pore sizes [165]. The reaction was run for 15 min until the pores were plugged. The H_2–N_2 separation factor was as high as 3000 and H_2 permeance was 1.4×10^{-8} mol/(m^2 s Pa). These membranes, however, were not thermally stable at temperatures above 873 K and underwent 'densification', which is one of the most unpleasant surprises that accompany silicon coating ever since. The densification is attributed to a significant shrinkage of membrane pores in exposure to moisture. This shrinkage results in loss of up to 50% permeability during first 12 h of operation [166,167], preventing the industrial application of such membranes. Today, one of the central aspects in silica membrane studies is the development of silica-coated membranes that are stable at high temperatures in the presence of moisture. Several approaches were taken, including the incorporation of methyl groups into the silica microstructure [168], steam calcination [169] and Ni doping [170].

Vapour-phase reactions at elevated temperatures typically give high film growth rates of 200–300 nm/min. With typical film thickness of 0.5–1.0 μm, the entire top layer can be built in several minutes, although the usual step coverage is uneven. Such a 'bread-loafing' effect is often seen on the electron microscopy microfilms where SiO_2 loafs are separated by voids that are detrimental to both the separation and the permeation. One way of solving this problem is by using another precursor. Another way is by forming SiO_2 films on the membrane surface by thermal decomposition of precursors. A first attempt was done by Okubo and Inoue [171] who thermally decomposed tetraethoxysilane (TEOS) on a membrane surface heated up to 473 K. The experiment was also performed on a Vycor glass membrane, this time with 2 nm pores, and resulted in more efficient separation of helium and ozone. The He–O_3 separation factor however increased from 3 to 6 and was not considered a significant improvement in terms of gas separation. The second approach is realized via Eley–Rideal or Langmuir–Hinshelwood mechanism. In the former, a precursor A is adsorbed on the support surface and reacts with another precursor B that is in a gas phase. The growth rate is regulated by the covering of the support with molecules of A.

In the latter, molecules of both A and B are adsorbed on the support and react on the surface. The maximum growth rate is obtained when the support is covered equally [172].

Whether a reaction will run in the bulk or on the membrane surface is not only a question of precursors. The reactor geometry is also a factor. In one-side geometry, all reactants are introduced into the reaction chamber from the same side of the membrane surface. In counter-diffusion geometry, the precursors and oxidizers are supplied from the opposite side of the membrane surface. They counter-diffuse through the membrane and react inside or near membrane pores. Figure 1.25 shows the two types of CVD reactor configurations. The one-sided geometry is suitable for reactions in the vapour phase followed by chemisorption on the membrane support, and pyrolysis of precursors on the support. In hollow fibres and honeycomb geometries, pore plugging is avoided by sealing the permeate exits. This gives a relatively thick silica film.

Conversely, the counter-diffusion geometry yields a thin SiO_2 layer either on the membrane surface or within the pores. Several parameters influence the preferable location and the deposition rate: the molecular weight of a precursor, the membrane pore size and pore size distribution and the partial pressures of precursor and reactant [173]. The deposition rate slows down with time as the precursors and reactants diffuse not only through membrane pores but also through a previously deposited layer. Note that deposition inside the pores results in a pore narrowing and plugging. This plugging stops the reaction in a pore as the precursor and the reactant cannot meet [159].

In both one-sided and counter-diffusion geometries, precursors and reactants are introduced simultaneously. The reaction is fast, especially at temperatures above 600 °C, and the limited control over the reaction rate creates a concentration gradient along the support surface. Alternatively, one can run the reaction in a one-sided geometry, where either the precursors or the reactants are supplied in oversaturation and the reaction proceeds until the concentration of the second compound drops to zero [174]. Then only the second compound is supplied to complete one reaction cycle. This introduction mode minimizes the

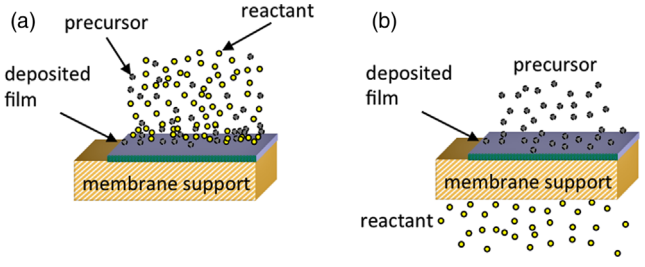


Figure 1.25 Schematic diagrams of precursor and reactant transport and reaction in one-sided (a) and counter-diffusion (b) processes in CVD. In the counter-diffusion geometry, the size of a precursor might restrict its entrance into the pores, limiting the reaction to the outer part of the membrane support.

homogeneous particle formation limiting the reaction just to SiO_2 formation [159]. The film formation rate is slow as several reaction cycles are necessary to build a sufficiently thick coating layer.

There are many more studies on the formation and performance of silica-coated ceramic-based membranes [155]. Recent improvements raised the permeance to 10^{-7} mol/(m^2 s Pa) and the H_2/N_2 selectivity to ~1000. This range is already of a commercial interest. Still the silica-coated ceramic-based membranes suffer from low hydrothermal stability. The CVD operation is still considered more expensive than sol–gel process, although the produced membranes possess a superior coverage [155]. One of the recent advances is the preparation of silica layers in non-oxide systems such as Si—C, Si—N, Si—C—N and Si—B—C—N. The latter approach resulted in a formed SiBCN-based layer with pores sizes of 0.6, 2.7 and 6 nm, and layer thickness of 1.75 mm [175]. The layer can withstand high temperatures and is therefore of interest for industrial applications. The silica stability in humid environments is increased by doping the membranes with alumina, zirconia or titania [176].

1.10.3 Sol–Gel Coating

In the sol–gel process, a colloidal or polymeric suspension is converted into a gelatinous network. The sol is a colloidal suspension of solid particles in a liquid, and gel is a porous solid 3D net. Colloids in a sol are metallic or metalloid elements surrounded by various ligands. The ligands do not include another metal or metalloid atom. For example, common colloids for aluminium oxide are inorganic salts such as $Al(NO_3)_3$ and metal alkoxide such as $Al(OC_4H_9)_3$. Silica gels are often made of tetraethoxysilane ($Si(OC_2H_5)_4$, abbreviated as TEOS) or tetramethoxysilane (TMOS). Metal alkoxides are metallo-organic compounds with a general formula $M(OR)_n$, where M is Si, Sn, Ti, Zr, Al, Mo, W and Ce and alkoxide OR is OC_nH_{2n+1}. The reactivity of these precursors falls on an order of $Si(OR)_4 \ll Sn(OR)_4 = Ti(OR)_4 < Zr(OR)_4 = Ce(OR)_4$ [177].

The sol–gel technology for coating ceramic membranes was first reported in the mid-1980s. Previously, ceramic membranes with pore sizes larger than 50 nm were used in coarse separation, competing with other separation technologies. The new layered structure of ceramic membranes opened new research opportunities. The pore sizes first narrowed towards 2–10 nm, yielding membranes that were suitable for liquid filtration. Since the 1990s, sol–gel-coated membranes have been considered a valid gas separation technology. This separation requires membranes with pores smaller than 1 nm. New horizons were set in the mid-1990s when tailor-made syntheses allowed controlled pore size and porosity, hydrophilic/hydrophobic membranes, catalytic activity and ionic conduction.

One striking example is the separation of nitrogen and oxygen based on their kinetic diameters. These two gases are nearly identical (kinetic diameters of 3.64 and 3.46 Å and molecular weights of 28 and 32 g/mol, respectively). Nevertheless, a properly designed ceramic membrane can separate them using

solution–diffusion and molecular sieving mechanisms. Another example is the generation of dense ceramic ion-conducting membranes for solid oxide fuel cells. These applications and other applications of membranes prepared using sol–gel technology are discussed in detail in Chapter 4. Here we will cover only the basics of the sol–gel operation and discuss the advantages and possible uses of this technology. Readers interested in more details of the fundamental sol–gel process should consult Ref. [178].

The sol–gel process is basically a sequence of chemical reactions starting from the dissolution of the precursor in polar or non-polar solvent such as water or organics. Depending on the chosen solvent, the reaction proceeds through either the gelation of separate colloids or the formation of polymer net. Water directs the sol–gel to the colloidal route. Alcohol as a solvent favours the polymer route. In the case of silicon alkoxide, the use of a base catalyst leads to the colloidal route, while adding an acid catalyst leads to open polymeric species [179]. Upon dissolution, the precursors are hydrolyzed as shown in Eq. (1.27), forming a colloidal sol that contains particles of sizes between 0.01 and 0.1 μm or linear organic–colloidal polymers.

$$\text{M-OR} + \text{H}_2\text{O} \rightarrow \text{M-OH} + \text{R-OH} \tag{1.27}$$

The stability of colloids in the sol is maintained by electrostatic repulsion of charged particles or by steric interactions of surface-active or polymer substances. Here, R represents an alkyl group C_nH_{2n+1}, M—OR is the alkoxide and R—OH is the alcohol. The reaction replaces the alkoxide group OR with hydroxyl group OH. Depending on the amount of water and catalyst present, hydrolysis may go to completion (so that all of the OR groups are replaced by OH), or stop while the metal is only partially hydrolyzed $M(OR)(OH)_n$. The stability of colloidal sol is interrupted by changing its pH value so that two hydrolyzed colloids react with each other in an alcohol (alcoholysis) and water (hydrolysis) condensation reaction, resulting in the formation of a 3D gel laying on the membrane surface:

$$\text{M-OR} + \text{M-OH} \rightarrow \text{M-O-M} + \text{R-OH} \tag{1.28}$$

or

$$\text{M-OH} + \text{OH-M} \rightarrow \text{M-O-M} + \text{H}_2\text{O} \tag{1.29}$$

Polymers in the sol are intentionally unstable and form condensate spontaneously. The condensation reaction and self-polymerization produce metal–oxo-metal bonds and liberate small by-product molecules such as ethanol. Unlike the polymer gels, the formation of colloidal gels is reversible. Alcoholysis and hydrolysis are catalyzed by mineral acids, ammonia, acetic acid, KOH, amines, KF, HF and various oxides [180]. This colloidal route provides a possibility for forming both linear and cross-linked polymers. The degree of polymerization depends on the water:alkoxide ratio, as well as on the catalyst concentration.

Subsequently, the wet gel is transformed into a xerogel by removing the water in a series of heating steps. The water (or alcohol) is first evaporated at

100–200 °C. This process is similar to the initial stage of drying described earlier. Evaporation first occurs from the sol–gel surface, followed by solvent diffusion to the surface. The evaporation rate is high and uneven. One reason for this is that the interplay with the capillary forces results in a faster release of the solvent from larger pores, forming unintended U-shapes. Quick drying may cause cracking and even peeling off of the entire layer. Therefore, drying is done gradually, with 0.15–2.0 °C/min heating ramp targeting a temperature slightly above 100 °C for water and below 200 °C for organic solvents. This gradual regime also helps in minimizing the aggregation of particles in the sol, which results in unevenly distributed pores, high pore volume and low mechanical strength of the entire film. A good microporous membrane requires individual grains of 10 nm or less. The grains should be kept separated until the calcination stage. Ultimately, the separation is driven by strong electrostatic repulsions of colloids in a sol, or significant steric hindrance that prevents the formation of aggregates at the stage of gel formation. Dense microporous membranes are obtained from uniform grains that ensure the highest packing density of 0.74 (see Section 1.9) and low porosity of $\varepsilon < 0.3$ [181].

In classical sol–gel applications, the porous bulk oxides are simply made by drying and calcination of separate gels in aqueous or organic solvents. But the formation of a multilayer ceramic membrane requires that the sol–gel layer be placed on top of a porous membrane support. The coating is performed in the form of dip coating or spin coating. Both methods use an already existing gel. This differs from liquid- and gas-phase impregnation, where the coating is done by the reacting several precursors, either on the surface, nearby or inside the membrane support. In dip coating, a porous support is dipped into a gel solution for few seconds. The coating film is formed by the capillary suction of the sol dispersant by the support pores. This is a slow process, and the thickness of the coating layer depends on suspension viscosity and dipping time. Conversely, film coating is fast and the viscosity of the suspension is high.

The final step in the formation of a top layer is the calcination, performed at 200–600 °C. This step (if done above 350 °C) yields a pure inorganic membrane. Any physically adsorbed water, residual organic solvents, hydroxides, nitrates or sulfates are decomposed. As in sintering, a continuous heating results in the formation of necks between the particles (calcining below 350 °C is used in the synthesis of hybrid membranes, yet leaves residual organics in the gel) [182]. The necks broaden, forming a 3D dense final metal oxide [183]. Figure 1.26 summarizes the various steps of the sol–gel routes.

The choice between the colloidal and polymer route depends on the intended membrane application. Through the colloidal route, the final net will be a series of interconnected colloids. These will be at a distance from each other and the final structure will be crystalline and mesoporous, containing pores in sizes of 2–10 nm at least. This pore size range is suitable for intermediate membrane layers and for liquid filtration. Conversely, gas separation membranes should have pores smaller than 1 nm and linear species with limited branching. These layers are produced by the polymeric route. The branched structure of the

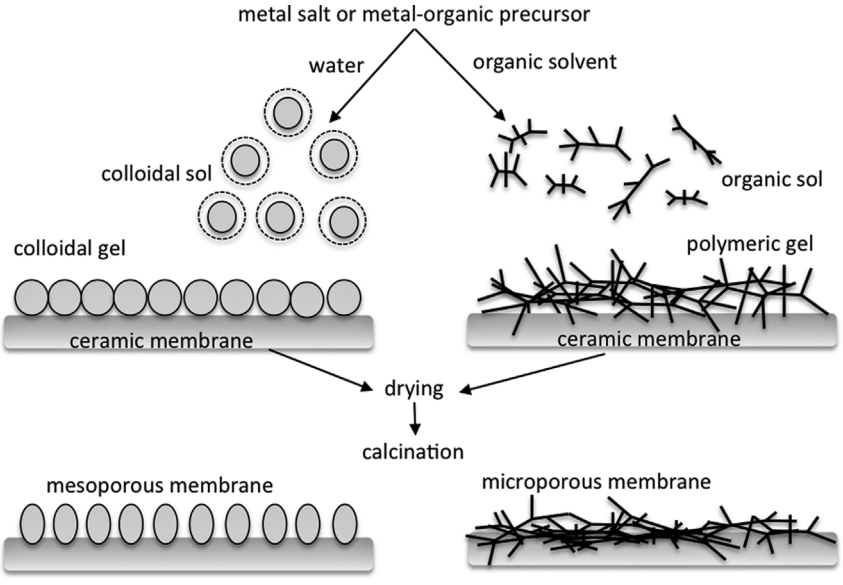


Figure 1.26 Diagram of colloidal and polymer routes in the preparation of sol–gel-coated ceramic membranes.

polymer intermediates is partially destroyed during calcination. This gives an amorphous microporous net with pores in an order of the spaces inside polymer chains that are considerably smaller than interpolymer distances.

1.10.4
Zeolite Coating

Zeolites are a special class of ceramic compounds that contain a uniform system of channels with a 0.3–2 nm diameter. That pore size is close to the size of single molecules and therefore zeolites are good molecular sieves. The separation requires uniformity in pore size and indeed zeolites possess a narrow pore size distribution. There are three options for zeolite membrane filtration: Zeolites can be used as self-standing membranes or coated on top of ceramic supports. An intermediate option is embedding zeolite crystals into a dense polymer membrane. All three options are used, although coating is the most popular. Self-standing zeolites are grown on a support such as mercury or Teflon that is easily separated from the zeolite crystal when the growth is complete. Such zeolites are interesting for modelling transport studies, but not for practical applications. This is because growing zeolite layers larger than few square centimetres is difficult, and the fragility of large zeolite structures prevents their industrial implementation. A proper zeolite type governs the membrane selectivity, and the content of embedded zeolite determines membrane permeability. At the moment however, the method suffers from technical difficulties in the formation of large

defect-free membrane surfaces. The inherent problem of embedded zeolites is the general zeolite selection mechanism. The preferable absorption might with time clog zeolite pores and discard the entire membrane. There is no regeneration option for zeolite–organic frameworks.

Conversely, zeolites coated on top of ceramic supports present many important advantages over sol–gel and CVD methods. Zeolites are crystals with a crystalline structure that determines the pore dimensions and uptake selectivity. Their crystallinity reduces the chances of inconsistency, layer breach or abnormal pores. The zeolite layer is thin yet strong.

There is an additional large group of materials that are not zeolites *per se*, but possess pores of the same size range. These are 'zeolite-like materials' or zeotypes, such as silicalites, aluminophosphates (AlPO) and silicoaluminophosphates (SAPO). The variety of zeotype structures increases the chance of finding a perfect separation layer with the right pore size, shape and density. There are more than 300 structures with pores in the range of 0.3–2 nm to choose from. Each structure contains pores of one size. The size is determined by the ring structure. Theoretical calculations showed that zeolites with 4, 6, 8, 10 or 12 oxygen anions in one ring have the maximum pore openings of 0.26, 0.34, 0.42, 0.63, and 0.74 nm, respectively [184].

The chemical composition (and therefore the properties) of a coated zeolite is changeable. Its Si/Al ratio determines the membrane hydrophilicity and the metal exchange capacity. Hydrophilic zeolites have a low Si/Al ratio. They can be used for separating organic–aqueous mixtures by selective uptake of water. The most successful (and currently, the only industrial) zeolite membrane separates water from water–organic mixtures [185]. This application is called *pervaporation* (for details on this and other membrane applications, see Chapter 4). Zeolites with a high silica level such as silicalite-1 are hydrophobic and can serve for a selective uptake of organics out of the same mixture. When a solution contains a cation different from that of the zeolite, the latter can serve as an ion exchanger. One of the known features of NaA zeolites is their capacity to release Na^+ cations, accumulating Ca^{++} and Mg^{++} from water. This operation is called *water softening* and it is efficient in reducing water hardness. NaA zeolites are typically arranged in a bed and can be easily regenerated when all sodium ions are replaced by the calcium and magnesium ions.

Several zeolites are used in chemistry and petrochemistry as catalysts. Thus, zeolite membranes can combine separation with catalytic activity (for details on such combined applications and zeolite membrane reactors, see Chapter 4). Zeolites can selectively uptake and transfer other than H_2 or O_2 molecules in dense high-temperature catalytic reactions. For example, a zeolite membrane was used for separating isooctene from hexadecene at temperatures >25 °C. Under optimal pressure of 15 bars and temperature higher than 70 °C, using a catalytic zeolite reactor allowed increasing the yield of C_8 target fraction and depressing the further undesirable conversion to C_{12} and C_{16} fractions [186].

The zeolites are coated on top of different ceramic supports, including alumina, titanium dioxide, zirconia and mullite. Coating is performed by crystallization

followed by a substantial growth of the initial crystals on the membrane support. The crystallization goes via one of the following four routes [187]: (i) The nuclei can be generated in a bulk and attracted to the membrane support by collision or diffusion. (ii) They can be attached to the substrate surface before the crystallization. (iii) The nuclei-formed compounds can be transported to the substrate surface for the *in situ* generation of the initial nuclei (the so-called *in situ* nucleation). (iv) A dry gel that contains potential nucleus can be placed on the substrate surface and activated by vapour or steam (the so-called dry gel conversion method). Either route can occur on the support surface or within the pores.

The use of prenucleated seeds as the nucleation bases (route (i)) separates the stages of crystal nucleation and growth. Here, the initial step is the forming of a colloidal suspension that contains zeolite crystals smaller than 1 μm [188]. Then, the preformed zeolite crystals are attached to the support using dip coating, filtering, electrostatic attraction or rubbing. Dip coating is a simple process, but it needs to be repeated several times for a proper coverage of the support surface. It can be improved by modifying the surface charges of the support with a cationic electrolyte or by electrophoretic deposition [189]. For example, silicalite-1 seeds are negatively charged and a coating of a support surface with a positively charged polydiallyldimethylammonium (PDDA) chloride increases the electrostatic attraction [190].

Filtering can increase the surface coverage without electrostatic effects [191,192]. The secondary growth is performed at concentrations lower than those needed for the nucleation, formation of new nucleation centres is unlikely and the zeolite layer forms by growing of preformed crystal seeds. A more strict control over the formation and growth of zeolite crystals prevents the crystallization of undesired zeolite phases and the dissolution of support [193]. The additional advantage of the seeding is the possibility to control the crystal orientation. A passage of molecules through the membrane is possible only when interconnected zeolite channels are turned perpendicular to the support surface. For example, MFI zeolites have straight, sinusoidal and elliptic pores, and an unfavourable direction of the straight pores might result in low or no transmembrane flow. Usually, the initial orientation achieved during seeding remains after the calcination step [80].

Another method for attaching the zeolite powder to the support surface is by rubbing it with a small brush, followed by hydrothermal attack (route (ii)). This results in a partial dissolution of the zeolites and leaching of Si and Al ions. The dissolved ions serve as additional nucleation bases that encourage crystallization of zeolites, giving a continuous defect-free zeolite layer. The penetration of dissolved Al and Si ions into the support enhances the integrity of the entire construct and the mechanical strength of the separation layer. At a later stage, one can remove the zeolite powder from the support surface, as this gives a more homogeneous layer [194]. If the initial zeolite seeds are not removed, the zeolite layer grows preferentially in a close vicinity of the initial nucleus. The disadvantage of this process is its low reproducibility.

The *in situ* nucleation (route (iii)) often results in defect-free zeolite separation layer. Any defects are not much larger than the zeolite pores, so the transport of

fluids occurs only through the zeolite pores. The *in situ* nucleation is performed by covering a support with a gel that contains hydrated silica and alumina and organic template to form a zeolite structure. Typical zeolite supports are α-alumina and sintered stainless steel with pore sizes between 0.1 and 10 μm. Another option is coating on an α-alumina support that is itself coated with a γ-alumina intermediate layer. Using the intermediate layer enables the synthesis of membranes with 5 nm pores [195]. Other supports are seldom used, as this changes the mechanism of nucleation. For instance, the support itself may undergo dissolution in the synthesis gel and change its composition or provide nucleation sites with new elements [193].

Basically, the *in situ* nucleation route is a modified sol–gel process performed under controlled hydrothermal conditions, using crystalline zeolites instead of amorphous silica. The controlled conditions include temperature that can be between 90 °C (zeolite A) and 180 °C (silicalite A) and time that can range from hours to days [196]. Formation of a separation zeolite layer starts from the immersion of the support in a synthesis gel with a composition similar to that reported in the synthesis of self-standing crystals. The synthesis gel is prepared from a silica source (e.g. TEOS, sodium silicate or fumed silica), an aluminium source (e.g. sodium aluminate, aluminium sulfate or alumina), a mineralizing agent (e.g. NaOH, NaF or KOH) and a templating agent such as tetrapropylammonium hydroxide (TPAOH) or tetrapropylammonium bromide (TPABr) [197,198]. Using high concentrations of silicon and aluminium increases the chances of a defect-free layer.

The support is dipped into the gel solution in an autoclave, and the gel is crystallized under pressure at elevated temperatures for several days, and then calcined. For example, Matsukata and Kikuchi [184] performed calcination at 500 °C using a 0.1 °C/min heating rate in the temperature range between 100 and 500 °C. The number of synthesis cycles depends on the particular zeolite and intended depth of the coating layer. Vroon and coworkers [199] used two consecutive hydrothermal treatments at different temperatures of 371 and 459 K to prepare an MFI membrane on α-alumina support. One cycle was not enough for connecting the individual zeolite grains. Three cycles gave a thick layer that cracked after the template was removed. Technical difficulties in *in situ* nucleation arise at the nucleation stage [196]. Loose control over crystallization results in generation of zeolite layers with undesirable microstructure [200]. A better control over nucleation and crystal growth is obtained by acid treatment, deposition of metals and metal oxides, mechanical polishing, adsorption of surfactant molecules or seeding [200]. The forming of a zeolite layer by *in situ* nucleation is a question of trial and error, and depends on gel compositions, synthesis times, methods for wetting the support and even the rotation of autoclave [188].

The dry gel conversion method (route (iv)) uses a dry aluminosilicate gel (the so-called *parent gel*) [201,202] and different solvents such as ethylene glycol [203], ethylenediamine and triethylamine [204]. The gel is deposited on top of a membrane support and converted into a zeolite layer by vapour or steam. In this case, the vapour phase contains organic compounds that are needed for the formation of the initial crystals. The layer formation is performed in autoclaves.

For example, Cheng *et al.* [205] reported a formation of a uniform zeolite layer with $\alpha(CO_2/N_2)$ of 55 by covering the surface of alumina support with seeds of zeolite and then with aluminosilicate gel. The layer was exposed to water vapour in an autoclave for several days. In steam-assisted crystallization, the steam contains the solvent that prevents homogeneous nucleation and reduces the consumption of binders and other organic additives [206].

The problem of zeolite membranes is their transport mechanism. Materials pass through the pores by adsorption, making it difficult to maintain a steady state as the zeolite becomes saturated with adsorbate. That said, retention by adsorption can also be advantageous, as large-pore zeolites can combine high permeate fluxes with high selectivity. Thermal stability up to 400–500 °C and resistance to organic solvents are additional advantages of zeolites over polymer membranes with same pore widths, facilitating their implementation. Zeolite membranes are often used in gas separation and catalytic membrane reactors at elevated temperatures. More details on these applications are given in Chapter 4. Several companies such as GFT Membrane Systems GmbH (Germany), Mitsui Engineering & Shipbuilding Corp. (Japan) and Sulzer Chemtech Allschwil Ltd. (Switzerland) offer full-scale installation of zeolite ceramic membranes. Laboratory experiments develop new zeolite synthesis strategies such as dynamic hydrothermal process [207], microwave heating [208], pre-aging of support material in the synthesis gel [209] and pore-plugging method [210]. There is now an extensive knowledge on the synthesis procedures and formation mechanisms (nucleation and growth) of zeolite layers. The future of zeolite membrane layers is probably in the development and implementation of new zeolite materials and combination of zeolites and polymers in mixed matrix membranes (MMMs).

1.11
Industrial Applications of Ceramic Membranes

Finally, after lots of hard work, many trials and a bit of luck, you have made your first ceramic membrane. It might not be perfect, but surely good for something. We only have to understand how this membrane separates mixtures and what are its features. These subjects are covered in Chapters 2 and 3, respectively. Then, we can offer our membrane to one of the relevant industrial sectors: the food and beverages, biotechnology, chemicals, pharmaceuticals and recovery and recycling (see the summary in Table 1.9).

In general, ceramic membranes are applied in those areas where they can compete with polymer membranes in performance and economics, as well as in specific cases that require their unique features. In the latter, they compete with other separation technologies but not with other membranes. The advantages of ceramic membranes include a wide range of possibilities for physical and chemical cleaning, a high resistance to harsh operating conditions and superior mechanical, thermal and chemical stability. Ceramic membranes are a dynamically developing field. New applications include industrial wastewater

Table 1.9 Applications of ceramic membranes in liquid-phase separations.

Area	Membrane type	Application examples
Food and beverage industry	MF and UF	Concentration of milk, concentration of protein, clarification of fruit juice, clarification of beer and wine, removal of microorganisms at fermentation
Biotechnology and pharmaceutical industry	MF and UF	Microorganism separation and cell debris filtration, plasma separation
Chemical and industrial applications	MF and UF	Oil–water separation, purification of used oil, removal of precipitated heavy metals and solids
Recovery and recycling	UF and NF	Drinking water and wastewater treatment

treatment (including the retention of heavy metals and synthetic dyes [211–213]), separation of asphaltene from crude oil [214] and the separation and concentration of organic solvents such as ethanol and hexane [215–217]. The classical applications are in the food and beverage industry, in gas separation (especially O_2/N_2 separation), in the reduction of CO_2 in power plants and, of course, in high-temperature fuel cells. All these applications and more are discussed in detail in Chapter 4. The corresponding economic considerations are outlined in Chapter 5.

1.12 Further Reading

There are many books about membranes, if fewer about ceramic ones. Here is a selection of further reading. All of the books listed below were in print and commercially available in January 2016.

Basic Principles of Membrane Technology by Mulder [16] is a clear and well-written graduate-level textbook. It gives an excellent introduction to many aspects of membrane technology. A clear, concise and yet comprehensive coverage at the sufficient depth level makes the book valuable for both membrane experts and students. Unfortunately, it is outdated (the last edition of the book was printed in 1996, 20 years ago). The membrane field has expanded tremendously since then and in many places the text needs updating with new ideas and discoveries.

Membrane Technology and Applications by Baker [17] is a more updated introductory level book on the basics of the membrane technology. It gives a comprehensive overview of membrane-based separation processes. Although the book starts with a series of general chapters on membrane preparation, transport theory, membrane modules and concentration polarization phenomenon, it

places much emphasis on the application fields, with numerous examples and much practical advice.

Encyclopedia of Membrane Science and Technology, edited by Hoek and Tarabara [218], and *Advanced Membrane Technology and Applications*, edited by Li *et al.* [18], are two large collective volumes that serve as references for various aspects of membrane principles, operations, materials, processes and applications. These books are written by invited groups of experts and cover numerous aspects of synthetic membranes at the fundamental as well as practical levels. Both books can be viewed as a reference guide in a branched membrane field but not as introductory books. Their relatively high price implies that they are more suitable for institute or corporate libraries.

Inorganic Membranes , by Burggraaf [219], and *Fundamentals of Inorganic Membrane Science and Technology*, edited by Burggraaf and Cot [10], are two excellent books on the basics and applications of ceramic membranes, although both were published almost 20 years ago. They give good and clear introduction to many aspects of ceramic membranes. The fabrication, characterization, transport theory and applications of porous and dense ceramic membranes are covered in detail.

Several other books on inorganic membranes detail applications of inorganic membranes in different fields. The emerging field of inorganic membrane reactors has been discussed in the book *Inorganic Membranes for Separation and Reaction* published in 1996 by Hsieh [85]. Several books on different aspects of uses of ceramic membranes had been published since then. *Recent Advances in Gas Separation by Microporous Ceramic Membranes*, edited by Kanellopoulos [220], and *Ceramic Membranes for Separation and Reaction*, published by Li [26] discuss the gas separation with inorganic membranes. *Catalytic Membranes and Membrane Reactors* by Sánchez Marcano and Tsotsis [221], *Nonporous Inorganic Membranes: For Chemical Processing* by Sammells and Mundschau [222], *Membrane Technology: In the Chemical Industry* by Nunes and Peinemann [223], and *Inorganic Membranes: Synthesis, Characterization and Applications* edited by Mallada and Menendez [60] discuss aspects of implementation of ceramic membranes in chemical industry. *Inorganic Membrane Reactors: Fundamentals and Applications* by Tan and Li discusses advances in inorganic membrane reactors with extensive coverage of ceramic, silica and zeolite reactors [224].

Exercises

1.1. Draw a three-layered ceramic membrane and list and explain the depth range and pore size of each layer.

1.2. A ceramic membrane was used in the direct purification of organic waste of a pharmaceutical factory. Suggest the most likely type of fouling, as well as a

cleaning procedure that aims at restoring the initial flux. How would your answer change if a polymer membrane was used instead of a ceramic one?

1.3. Calculate the volume flux, in l/(m^2 h), through a 0.5 m^2 of α-alumina membrane. The total flux is 20 cm^3/s and the membrane works at 0.85 recovery ratio. What assumption do you have to make? Is the flux you found high or low? Explain your answer.

1.4. Which ceramic membrane would you choose for separating water from a water–benzene mixture? Give at least two advantages of the membrane of your choice compared to other ceramic or polymer membranes.

1.5. You are in charge of optimization of α-alumina membrane supports. Currently, the membrane is 2 mm thick, has a mechanical strength at break of 30 MPa and the volume flux of 40 l/(m^2 h). Your task is to increase the flux, while keeping the mechanical strength. Discuss the anticipated change in membrane properties as a function of

- grain size of the initial powder,
- amount of plasticizer,
- sintering temperature, and
- drying/heating/cooling rate.

1.6. Explain the difference between a retention ratio and molar retention ratio, and how it affects the transmembrane flux. A manufacturer offers you two alumina-based membranes for separating organic mixtures. Membrane (i) has a retention ratio of 0.1 and a transmembrane flux of 150 l/(m^2 h). Membrane (ii) has a molar retention ratio of 0.1 and transmembrane flux of 50 l/(m^2 h). Which one do you prefer?

1.7. You and your colleague discuss different membrane supports. You claim that α-alumina is a well-known and generally accepted material that your factory uses for 50 years. Your colleague says that it is out of mode and the entire membrane field revolves around titanium dioxide. Is your colleague correct? How would you convince them to continue using alumina supports?

1.8. A support layer has a nitrogen flux of 0.02 cm^3/(cm^2 s cmHg). Calculate the flux in l/(m^2 h)) and in gallons/(ft^2 day).

1.9. Your site manager is considering changing several separation processes into membrane-based ones. What type of membrane would you recommend for:

- Desalination of sea water
- Separation of bacteria from surface water
- Isolation of ethanol from a fermentation broth
- Separation of CO_2 from flue gas

1.10. Figure 1.27 depicts two sintering protocols for membranes A and B. Assume that the green body of both membranes was made of exactly the

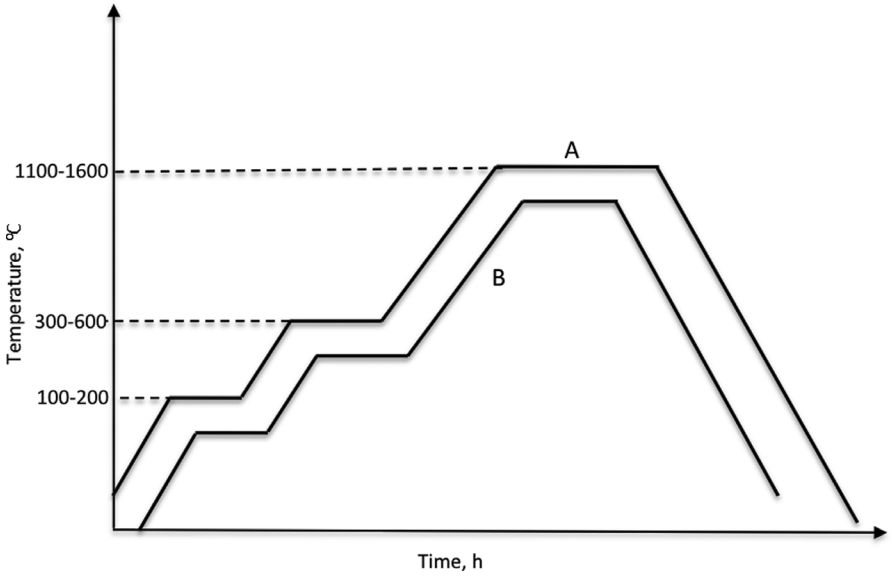


Figure 1.27 Stages of heating, thermolysis and sintering in the preparation of ceramic membranes A and B.

same materials and the only difference between two membranes is in the sintering protocol. Describe the anticipated difference in flux, retention ratio and mechanical strength of sintered A and B.

1.11. Search the Internet and find the structures of zeolites A and Y. Assume that there are two ceramic membranes where each of these zeolites is coated on top of γ-alumina. Based on the structure of both zeolites, explain the difference in the retention ratio and transmembrane flux of these membranes.

1.12. List the main foulant of ceramic membranes used in

- cheese production,
- orange juice clarification,
- surface water treatment,
- wastewater treatment, and
- gas separation

What type of cleaning protocol would you use in each case? Explain your answer.

1.13. List three separation processes where ceramic membranes can successfully compete with polymer ones. How can you maximize the advantages of ceramic membranes in each case?

1.14. A ceramic membrane is used for purifying surface water for drinking. The average transmembrane flow is $2\,m^3/h$, with a 0.95 recovery ratio. The

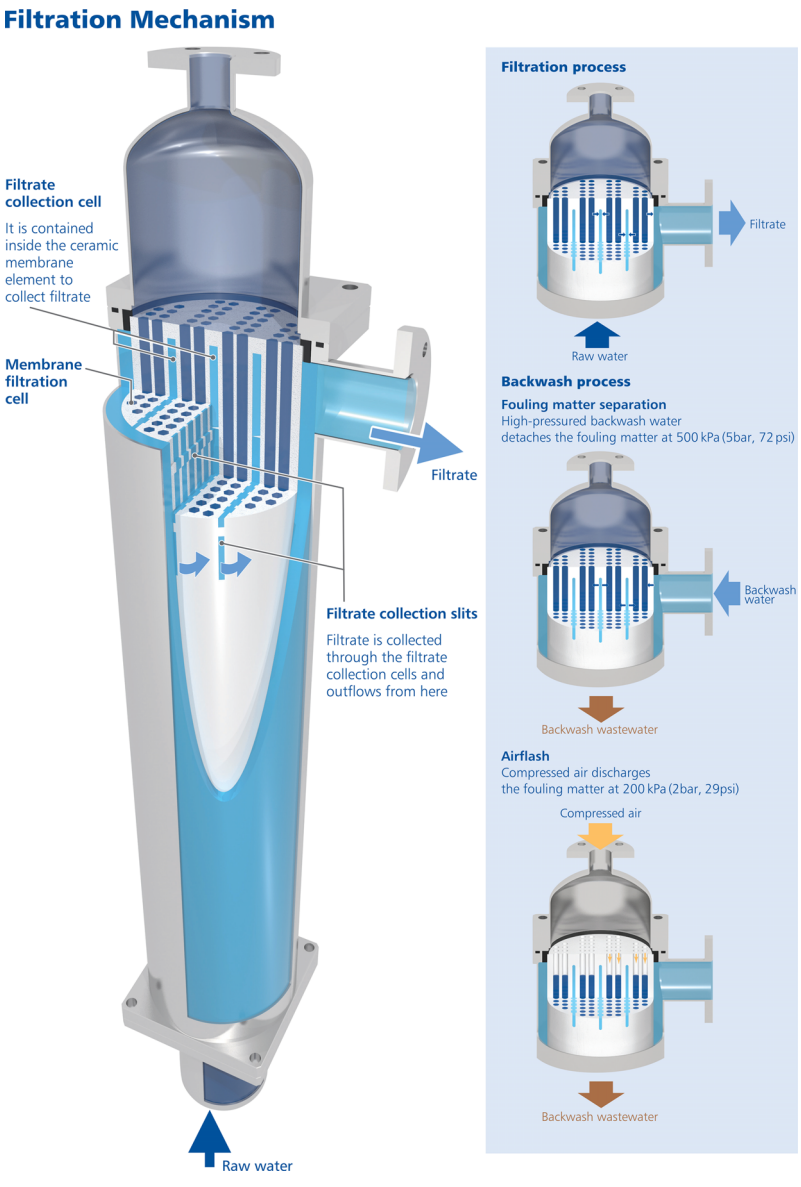


Figure 1.28 Schematic showing the filtration and backwash processes in a Metawater ceramic membrane element. (Image courtesy of Metawater Co., Japan.)

membrane is physically backwashed daily for 1 h (see Figure 1.28). Due to severe fouling, the site manager switches to two daily backwash cycles. How will this affect the recovery ratio? (You may assume that the recovery ratio is influenced only by the permeate losses due to hydraulic backwashes.)

References

1 Liu, D.M. (1996) *Porous Ceramic Materials: Fabrication, Characterization, Applications*, Trans Tech Publications Ltd., Zurich.
2 Owoeye, F.T., Olokode, O.S., Aiyedun, P.O., Balogun, H.O. and Anyanwu, B.U. (2012) Preparation and characterization of ceramic microfiltration membrane for water treatment. *The Pacific Journal of Science and Technology*, **13**, 28–38.
3 Harari, Y.N. (2012) *From Animals into Gods: A Brief History of Humankind*, CreateSpace, Charleston.
4 Fahlman, B.D. (2011) *Materials Chemistry*, Springer, Dordrecht.
5 Johnson, RL. (2011) Ceramics in the classroom. Available at http://depts.washington.edu/matseed/mse_resources/Webpage/Ceramics/ceramics.htm (updated 18/7/2015).
6 Harris, R. (2003) *Pompeii*, Random House Paperbacks, New York.
7 Gillot, J. (1991) The developing use of inorganic membranes: a historical perspective, in *Inorganic Membranes: Synthesis, Characteristics and Application* (ed. R.R. Bhave), Chapman & Hall, New York, pp. 1–9.
8 Bhave, R.R. (1991) *Inorganic Membranes: Synthesis, Characteristics, and Applications*, Van Nostrand-Reinhold, New York.
9 Loeb, S. and Sourirajan, S. (1962) Sea water demineralization by means of an osmotic membrane. *Advances in Chemistry Series*, **38**, 117–132.
10 Burggraaf, A.J. and Cot, L. (1996) *Fundamentals of Inorganic Membrane Science and Technology*, Elsevier, Amsterdam, The Netherlands.
11 Vanderhorst, H.C. and Hanemaaijer, J.H. (1990) Cross-flow microfiltration in the food industry: state of the art. *Desalination*, **77** (1–3), 235–258.
12 Bolduan, P. and Latz, M. (2000) Ceramic membranes and their application in food and beverage processing. *Filtration+Separation*, **37** (3), 36–38.
13 de Vos, R.M. and Verweij, H. (1998) High-selectivity, high-flux silica membranes for gas separation. *Science*, **279** (5357), 1710–1711.
14 Aaron, D. and Tsouris, C. (2005) Separation of CO_2 from flue gas: a review. *Separation Science and Technology*, **40** (1–3), 321–348.
15 Shackleton, R. (1987) The application of ceramic membranes to the biological industries. *Journal of Chemical Technology and Biotechnology*, **37** (1), 67–69.
16 Mulder, M. (1996) *Basic Principles of Membrane Technology*, Kluwer, Dordrecht.
17 Baker, R. (2004) *Membrane Technology and Applications*, 2nd edn, John Wiley & Sons, Inc., Chichester.
18 Li, N.N., Fane, A.G., Ho, W.S.W. and Matsuura, T. (2011) *Advanced Membrane Technology and Applications*, John Wiley & Sons, Inc., Hoboken, NJ.
19 Arkhangelsky, E., Sefi, Y., Hajaj, B., Rothenberg, G. and Gitis, V. (2011) Kinetics and mechanism of plasmid DNA penetration through nanopores. *Journal of Membrane Science*, **371** (1–2), 45–51.
20 Burgraaf, A.J. (1996) Important characteristics of inorganic membranes, in *Fundamentals of Inorganic Membrane Science and Technology* (eds A.J. Burgraaf and L. Cot), Elsevier, Amsterdam.
21 Freger, V., Gilron, J. and Belfer, S. (2002) TFC polyamide membranes modified by grafting of hydrophilic polymers: an FT-IR/AFM/TEM study. *Journal of Membrane Science*, **209** (1), 283–292.
22 Herzberg, M., Sweity, A., Brami, M., Kaufman, Y., Freger, V., Oron, G. *et al.* (2011) Surface properties and reduced biofouling of graft-copolymers that possess oppositely charged groups. *Biomacromolecules*, **12** (4), 1169–1177.
23 Apel, P. (2001) Track etching technique in membrane technology. *Radiation Measurements*, **34** (1–6), 559–566.
24 Riscanu, D., Favis, B.D., Feng, C.Y. and Matsuura, T. (2004) Thin-film membranes derived from co-continuous polymer blends: preparation and performance. *Polymer*, **45** (16), 5597–5609.
25 Rouquerol, J., Avnir, D., Fairbridge, C.W., Everett, D.H., Haynes, J.H.,

Pernicone, N. *et al.* (1994) Recommendations for the characterization of porous solids. *Pure and Applied Chemistry*, **66** (8), 1739–1758.

26 Li, K. (2007) *Ceramic Membranes for Separation and Reaction*, John Wiley & Sons, Inc., Chichester.

27 Zsigmondy, R. and Bachmann, W. (1918) Über neue Filter. *Zeitschrift fur Anorganische und Allgemeine Chemie*, **103**, 119–128.

28 Gaikwad, A.V., Boffa, V., ten Elshof, J.E. and Rothenberg, G. (2008) Cat-in-a-cup: facile separation of large homogeneous catalysts. *Angewandte Chemie, International Edition*, **47** (29), 5407–5410.

29 Biesheuvel, P.M. and Verweij, H. (1999) Design of ceramic membrane supports: permeability, tensile strength and stress. *Journal of Membrane Science*, **156** (1), 141–152.

30 Bonekamp, B.C. (1996) Preparation of asymmetric ceramic membrane supports by dip-coating, in *Fundamentals of Inorganic Membrane Science and Technology* (eds A.J. Burggraaf and L. Cot), Elsevier, Amsterdam.

31 Sah, A., Castricum, H.L., Bliek, A., Blank, D.H.A. and ten Elshof, J.E. (2004) Hydrophobic modification of gamma-alumina membranes with organochlorosilanes. *Journal of Membrane Science*, **243** (1–2), 125–132.

32 EPA (2001) Low-pressure membrane filtration for pathogen removal: application, implementation, and regulatory issues. US Environmental Protection Agency Office of Water 2001, EPA 815-C-01-001.

33 Stern, S.A., Sinclair, T.F., Gareis, P.J., Vahldieck, N.P. and Mohr, P.E. (1965) Helium recovery by permeation. *Industrial and Engineering Chemistry*, **57**, 49–60.

34 Hsieh, H.P., Bhave, R.R. and Fleming, H.L. (1988) Microporous alumina membranes. *Journal of Membrane Science*, **39** (3), 221–241.

35 Dyer, P.N., Richards, R.E., Russek, S.L. and Taylor, D.M. (2000) Ion transport membrane technology for oxygen separation and syngas production. *Solid State Ionics*, **134** (1–2), 21–33.

36 Bray, T.D. (inventor) (1968) Reverse osmosis purification apparatus. U.S. Patent US3,417,870 (Gulf General Atomic Inc., assignee).

37 Westmoreland, J.C. (inventor) (1968) Spiral wrapped reverse osmosis membrane cell. US Patent US3,367,504 (Gulf General Atomic Inc., assignee).

38 Mahon, H.I. (inventor) (1966) Permeability separatory apparatus, permeability separatory membrane element, method of making the same and process utilizing the same. US Patent US3,228,876 (Dow Chemical Co., assignee).

39 Liu, S.M. and Gavalas, G.R. (2005) Oxygen selective ceramic hollow fiber membranes. *Journal of Membrane Science*, **246** (1), 103–108.

40 Charcosset, C. (2012) *Membrane Processes in Biotechnology and Pharmaceutics*, Elsevier, Amsterdam.

41 EPA (2003) Membrane filtration guidance manual. US Environmental Protection Agency, Contract No. EPA 815-D-03-008.

42 Pierre, A. and Christian, G. (2008) Current status and prospects for ceramic membrane applications, in *Handbook of Membrane Separations*, CRC, Boca Raton, FL, pp. 139–179.

43 Porter, M.C. (1990) Ultrafiltration, in *Handbook of Industrial Membrane Technology* (ed. M.C.E. Porter), Noyes Publications, Westwood, CA.

44 Lipnizki, F. and Dupuy, A. (2013) Food industry applications, in *Encyclopedia of Membrane Science and Technology*, John Wiley & Sons, Inc., Hoboken, NJ.

45 McNaught, A.D. and Wilkinson, A. (eds) (1997) *International Union for Pure and Applied Chemistry: Compendium of Chemical Terminology*, 2nd edn (the *Gold Book*), Blackwell Scientific Publications, Oxford.

46 Field, R. (2010) Fundamentals of fouling, in *Membrane Technology, Volume 4: Membranes for Water Treatment* (eds K.V. Peinemann and S. Pereira Nunes), Wiley-VCH Verlag GmbH, Weinheim.

47 Shi, X., Tal, G., Hankins, N.P. and Gitis, V. (2014) Fouling and cleaning of ultrafiltration membranes: a review.

Journal of Water Process Engineering, **1** (0), 121–138.

48 Liu, C., Caothien, S., Hayes, J., Caothuy, T., Otoyo, T. and Ogawa, T. (2006) Membrane chemical cleaning: from art to science. Pall Corporation, New York. Available at http://www.pall.com/pdfs/Water-Treatment/mtcpaper.pdf (updated 18/7/2015).

49 Scott, K. (1995) *Handbook of Industrial Membranes*, Elsevier, Amsterdam.

50 Faibish, R.S. and Cohen, Y. (2001) Fouling-resistant ceramic-supported polymer membranes for ultrafiltration of oil-in-water microemulsions. *Journal of Membrane Science*, **185** (2), 129–143.

51 Tragardh, G. (1989) Membrane cleaning. *Desalination*, **71** (3), 325–335.

52 Le-Clech, P., Chen, V. and Fane, T.A.G. (2006) Fouling in membrane bioreactors used in wastewater treatment. *Journal of Membrane Science*, **284** (1–2), 17–53.

53 Hong, S.K. and Elimelech, M. (1997) Chemical and physical aspects of natural organic matter (NOM) fouling of nanofiltration membranes. *Journal of Membrane Science*, **132** (2), 159–181.

54 Naim, R., Levitsky, I. and Gitis, V. (2012) Surfactant cleaning of UF membranes fouled by proteins. *Separation and Purification Technology*, **94**, 39–43.

55 Levitsky, I., Duek, A., Arkhangelsky, E., Pinchev, D., Kadoshian, T., Shetrit, H. *et al.* (2011) Understanding the oxidative cleaning of UF membranes. *Journal of Membrane Science*, **377** (1–2), 206–213.

56 Arkhangelsky, E., Kuzmenko, D. and Gitis, V. (2007) Impact of chemical cleaning on properties and functioning of polyethersulfone membranes. *Journal of Membrane Science*, **305** (1–2), 176–184.

57 Yacou, C., Wang, D., Motuzas, J., Zhang, X., Smart, S. and Diniz da Costa, J.C. (2013) Thin-film ceramic membranes, in *Encyclopedia of Membrane Science and Technology*, John Wiley & Sons, Inc., Hoboken, NJ.

58 Schwob, Y. (1949) *Sur l'hémiperméabilité à l'eau des membranes de cellulose régénérée*. E. Privat, Toulouse, France.

59 Furukawa, D.H. (1999) New developments in desalination, in *Providing Safe Drinking Water in Small Systems: Technology, Operations, and Economics* (eds J.A. Cotruvo, G.F. Craun and N. Hearne), CRC Press, Boca Raton, FL, pp. 257–263.

60 Mallada, R. and Menéndez, M. (2008) *Inorganic Membranes: Synthesis, Characterization and Applications*, Elsevier, Amsterdam.

61 Robeson, L.M. (1991) Correlation of separation factor versus permeability for polymeric membranes. *Journal of Membrane Science*, **62** (2), 165–185.

62 Uhlhorn, R.J.R., Zaspalis, V.T., Keizer, K. and Burggraaf, A.J. (1992) Synthesis of ceramic membranes. 2. Modification of alumina thin-films: reservoir method. *Journal of Materials Science*, **27** (2), 538–552.

63 Kucera, J. (2013) Membrane materials and module development: historical perspective, in *Encyclopedia of Membrane Science and Technology* (eds E.V. Hoek and V.V. Tarabara), John Wiley & Sons, Inc., Hoboken, NJ.

64 Charpin, J., Bergez, P., Valin, F., Barnier, H., Maurel, A. and Martiner, J.M. (1987) Inorganic membranes: preparation, characterization, specific applications. *Material Science Monograph*, **38**, 2211–2235.

65 Louwerse, M.J. and Rothenberg, G. (2013) Modeling catalyst preparation: the structure of impregnated–dried copper chloride on γ-alumina at low loadings. *ACS Catalysis*, **3** (7), 1545–1554.

66 Wefers, K. and Bell, G.M. (1972) Oxides and hydroxides of aluminum. Alcoa Research Laboratories. Available at https://www.alcoa.com/global/en/innovation/papers_patents/pdf/TP19_Wefers.pdf.

67 Holleman, A.F., Wiberg, E. and Wiberg, N. (2001) *Holleman–Wiberg's Inorganic Chemistry*, Academic Press, San Diego, CA.

68 de Vos, R.M. and Verweij, H. (1998) Improved performance of silica membranes for gas separation. *Journal of Membrane Science*, **143** (1–2), 37–51.

69 Xu, R., Wang, J.H., Kanezashi, M., Yoshioka, T. and Tsuru, T. (2013) Reverse osmosis performance of organosilica membranes and comparison

with the pervaporation and gas permeation properties. *AIChE Journal*, **59** (4), 1298–1307.

70 Castricum, H.L., Kreiter, R., van Veen, H.M., Blank, D.H.A., Vente, J.F. and ten Elshof, J.E. (2008) High-performance hybrid pervaporation membranes with superior hydrothermal and acid stability. *Journal of Membrane Science*, **324** (1–2), 111–118.

71 Baerlocher, C. and McCusker, L.B. (2001) Database of zeolite structures. Available at http://www.iza-structure.org/databases/ (cited and updated 9/08/2013).

72 Zakersalehi, A., Choi, H., Andersen, J. and Dionysiou, D.D. (2013) Photocatalytic ceramic membranes, in *Encyclopedia of Membrane Science and Technology* (eds E.M.V. Hoek and V.V. Tarabara) John Wiley & Sons, Inc., Hoboken, NJ.

73 Nair, P., Mizukami, F., Okubo, T., Nair, J., Keizer, K. and Burggraaf, A.J. (1997) High-temperature catalyst supports and ceramics membranes: metastability and particle packing. *AIChE Journal*, **43** (11), 2710–2714.

74 Kritikaki, A. and Tsetsekou, A. (2009) Fabrication of porous alumina ceramics from powder mixtures with sol–gel derived nanometer alumina: effect of mixing method. *Journal of the European Ceramic Society*, **29** (9), 1603–1611.

75 Tsapovski, L. (2013) *Ceramic Catalytic Membranes for Tertiary Wastewater Treatment*, Ben Gurion University of the Negev.

76 Phonthammachai, N., Gulari, E., Jamieson, A.M. and Wongkasemjit, S. (2006) Photocatalytic membrane of a novel high surface area TiO_2 synthesized from titanium triisopropanolamine precursor. *Applied Organometallic Chemistry*, **20** (8), 499–504.

77 Kulprathipanja, S. (2010) *Zeolites in Industrial Separation and Catalysis*, Wiley-VCH Verlag GmbH, Weinheim.

78 Siebdrath, N., Ziskind, G. and Gitis, V. (2012) Cleaning secondary effluents with organoclays and activated carbon. *Journal of Chemical Technology and Biotechnology*, **87** (1), 51–57.

79 Baerlocher, C., McCusker, L.B. and Olson, D.H. (2007) *Atlas of Zeolite Framework Types*, Elsevier, Amsterdam.

80 Lai, Z.P., Bonilla, G., Diaz, I., Nery, J.G., Sujaoti, K., Amat, M.A. *et al.* (2003) Microstructural optimization of a zeolite membrane for organic vapor separation. *Science*, **300** (5618), 456–460.

81 Komolikov, Y.I. and Blaginina, L.A. (2002) Technology of ceramic micro and ultrafiltration membranes (review). *Refractories and Industrial Ceramics*, **43** (5–6), 181–187.

82 Lin, Y.S., Chang, C.H. and Gopalan, R. (1994) Improvement of thermal stability of porous nanostructured ceramic membranes. *Industrial and Engineering Chemistry Research*, **33** (4), 860–870.

83 Delange, R.S.A., Keizer, K. and Burggraaf, A.J. (1995) Aging and stability of microporous sol–gel-modified ceramic membranes. *Industrial and Engineering Chemistry Research*, **34** (11), 3838–3847.

84 Chang, C.H., Gopalan, R. and Lin, Y.S. (1994) A comparative study on thermal and hydrothermal stability of alumina, titania and zirconia membranes. *Journal of Membrane Science*, **91** (1–2), 27–45.

85 Hsieh, H.P. (1996) *Inorganic Membranes for Separation and Reaction*, Elsevier, Amsterdam.

86 Sekulic, J., Luiten, M.W.J., ten Elshof, J.E., Benes, N.E. and Keizer, K. (2002) Microporous silica and doped silica membrane for alcohol dehydration by pervaporation. *Desalination*, **148** (1–3), 19–23.

87 Van Gestel, T., Vandecasteele, C., Buekenhoudt, A., Dotremont, C., Luyten, J., Leysen, R. *et al.* (2002) Alumina and titania multilayer membranes for nanofiltration: preparation, characterization and chemical stability. *Journal of Membrane Science*, **207** (1), 73–89.

88 Chang, Y., Ling, Z.Y., Liu, Y.S., Hu, X. and Li, Y. (2012) A simple method for fabrication of highly ordered porous alpha-alumina ceramic membranes. *Journal of Materials Chemistry*, **22** (15), 7445–7448.

89 Byrappa, K. and Yoshimura, M. (2001) *Handbook of Hydrothermal Technology:*

A Technology for Crystal Growth and Materials Processing, Noyes Publications, Norwich.

90 Larbot, A. (1996) Ceramic processing techniques of support systems for membranes synthesis, in *Fundamentals of Inorganic Membrane Science and Technology* (eds A.J. Burggraaf and L. Cot), Elsevier, Amsterdam.

91 Aste, T. (2005) Variations around disordered close packings. *Journal of Physics: Condensed Matter*, **17**, S2361–S2390.

92 Bideau, D. and Troadec, J.P. (1984) Compacity and mean coordination number of dense packings of hard disks. *Journal of Physics C: Solid State Physics*, **17** (28), L731–L740.

93 Visscher, W.M. and Bolsterl, M. (1972) Random packing of equal and unequal spheres in 2 and 3 dimensions. *Nature*, **239** (5374), 504–507.

94 Zhang, Y.H., Qin, C.W. and Binner, J. (2006) Processing multi-channel alumina membranes by tape casting latex-based suspensions. *Ceramics International*, **32** (7), 811–818.

95 Shanefield, D.J. (1996) *Organic Additives and Ceramic Processing, Second Edition: With Applications in Powder Metallurgy, Ink, and Paint*, Kluwer Academic Publishers, Dordrecht.

96 Shan, M., Mao, X.J., Zhang, J. and Wang, S.W. (2009) Electrophoretic shaping of sub-micron alumina in ethanol. *Ceramics International*, **35** (5), 1855–1861.

97 Das, N., Bandyopadhyay, S., Chattopadhyay, D. and Maiti, H.S. (1996) Tape-cast ceramic membranes for microfiltration application. *Journal of Materials Science*, **31** (19), 5221–5225.

98 Sarraf, H. and Havrda, J. (2007) Rheological behavior of concentrated alumina suspension: effect of electrosteric stabilization. *Ceramics-Silikaty*, **51** (3), 147–152.

99 Lewis, J.A. (1997) Binder removal from ceramics. *Annual Review of Materials Science*, **27**, 147–173.

100 Onoda, G.Y. (1976) Theoretical strength of dried green bodies with organic binders. *Journal of the American Ceramic Society*, **59** (5–6), 236–239.

101 Bayliss, R.W. (1986) *The Sintering, Microstructural Analysis and Mechanical Properties of Two Beta MgSiAlON Ceramics*. Department of Physics, University of Warwick.

102 Lindqvist, K. and Liden, E. (1997) Preparation of alumina membranes by tape casting and dip coating. *Journal of the European Ceramic Society*, **17** (2–3), 359–366.

103 Das, N. and Maiti, H.S. (1998) Formation of pore structure in tape-cast alumina membranes: effects of binder content and firing temperature. *Journal of Membrane Science*, **140** (2), 205–212.

104 Yang, W.P., Shyu, S.S., Lee, E.S. and Chao, A.C. (1996) Effects of PVA content and calcination temperature on the properties of PVA/boehmite composite film. *Materials Chemistry and Physics*, **45** (2), 108–113.

105 Pierre, A.C. (1997) Porous sol–gel ceramics. *Ceramics International*, **23** (3), 229–238.

106 Lyckfeldt, O. and Ferreira, J.M.F. (1998) Processing of porous ceramics by 'starch consolidation'. *Journal of the European Ceramic Society*, **18** (2), 131–140.

107 Kristoffersson, A., Roncari, E. and Galassi, C. (1998) Comparison of different binders for water-based tape casting of alumina. *Journal of the European Ceramic Society*, **18** (14), 2123–2131.

108 Zhang, Y.G. and Binner, J. (2002) Tape casting aqueous alumina suspensions containing a latex binder. *Journal of Materials Science*, **37** (9), 1831–1837.

109 Saggiowoyansky, J., Scott, C.E. and Minnear, W.P. (1992) Processing of porous ceramics. *American Ceramic Society Bulletin*, **71** (11), 1674–1682.

110 Othman, M.R. and Mukhtar, H. (2000) Review on development of ceramic membrane from sol–gel route: parameters affecting characteristics of the membrane. *International Islamic University Malaysia Engineering Journal*, **1** (2), 29–34.

111 Lambert, C.K. and Gonzalez, R.D. (1999) Effect of binder addition on the properties of unsupported gamma-Al_2O_3 membranes. *Materials Letters*, **38** (2), 145–149.

112 Hutchison, R.B., Curryhyde, H.E. and Raper, J.A. (1994) Preparation of composite ceramic membrane from titania powders. *Powder Technology*, **81** (3), 249–257.

113 Lin, B., Zhang, S.Q., Zhang, L.C., Bi, L., Ding, H.P., Liu, X.Q. *et al.* (2008) Prontonic ceramic membrane fuel cells with layered $GdBaCO_2O_5$+x cathode prepared by gel-casting and suspension spray. *Journal of Power Sources*, **177** (2), 330–333.

114 Ding, X.B., Fan, Y.Q. and Xu, N.P. (2006) A new route for the fabrication of TiO_2 ultrafiltration membranes with suspension derived from a wet chemical synthesis. *Journal of Membrane Science*, **270** (1–2), 179–186.

115 Wang, Y.H., Zhang, Y., Liu, X.Q. and Meng, G.Y. (2007) Sol-coated preparation and characterization of macroporous alpha-Al_2O_3 membrane support. *Journal of Sol-Gel Science and Technology*, **41** (3), 267–275.

116 Kim, D.J., Park, I.S., Choi, H.J., Lee, D.Y. and Han, J.S. (2004) Aqueous-based alumina tape casting for 3-dimensional forming. *Key Engineering Materials*, **264–268**, 173–176.

117 Sepulveda, P. and Binner, J.G.P. (1999) Processing of cellular ceramics by foaming and *in situ* polymerisation of organic monomers. *Journal of the European Ceramic Society*, **19** (12), 2059–2066.

118 Dörre, E. and Hübner, H. (1984) *Alumina: Processing, Properties, and Applications*, Springer, Berlin.

119 Hotza, D. and Greil, P. (1995) Aqueous tape casting of ceramic powders. *Materials Science and Engineering A*, **202** (1–2), 206–217.

120 Pincus, A.G. and Shipley, L.E. (1969) The role of organic binders in ceramic processing. *Ceramic Industry*, **92** (4), 106–109.

121 Barmala, M., Moheb, A. and Emadi, R. (2009) Applying Taguchi method for optimization of the synthesis condition of nano-porous alumina membrane by slip casting method. *Journal of Alloys and Compounds*, **485** (1–2), 778–782.

122 Li, N., Wen, Z.Y., Liu, Y., Xu, X.G., Lin, J. and Gu, Z.H. (2009) Preparation of Na-beta-alumina film by tape casting process. *Journal of the European Ceramic Society*, **29** (14), 3031–3037.

123 Leenaars, A.F.M. and Burggraaf, A.J. (1985) The preparation and characterization of alumina membranes with ultrafine pores. 2. The formation of supported membranes. *Journal of Colloid and Interface Science*, **105** (1), 27–40.

124 Nishio, H., Sato, M. and Watanabe, K. (inventors) (1993) Method of producing ceramic sintered body having dense ceramic membrane. US Patent US5,250,242A (Nkk Corporation, assignee).

125 Wu, Z., Wang, B. and Li, K. (2010) A novel dual-layer ceramic hollow fibre membrane reactor for methane conversion. *Journal of Membrane Science*, **352** (1–2), 63–70.

126 Steenkamp, G.C., Keizer, K., Neomagus, H.W.J.P. and Krieg, H.M. (2002) Copper (II) removal from polluted water with alumina/chitosan composite membranes. *Journal of Membrane Science*, **197** (1–2), 147–156.

127 Qiu, M., Feng, J., Fan, Y. and Xu, N. (2009) Pore evolution model of ceramic membrane during constrained sintering. *Journal of Materials Science*, **44** (3), 689–699.

128 Jedidi, I., Khemakhem, S., Saïdi, S., Larbot, A., Elloumi-Ammar, N., Fourati, A. *et al.* (2011) Preparation of a new ceramic microfiltration membrane from mineral coal fly ash: application to the treatment of the textile dying effluents. *Powder Technology*, **208** (2), 427–432.

129 Xia, C.R. and Liu, M.L. (2001) A simple and cost-effective approach to fabrication of dense ceramic membranes on porous substrates. *Journal of the American Ceramic Society*, **84** (8), 1903–1905.

130 Bouzerara, F., Harabi, A., Achour, S. and Larbot, A. (2006) Porous ceramic supports for membranes prepared from kaolin and doloma mixtures. *Journal of the European Ceramic Society*, **26** (9), 1663–1671.

131 Falamaki, C., Afarani, M.S. and Aghaie, A. (2004) Initial sintering stage pore growth mechanism applied to the manufacture of ceramic membrane

supports. *Journal of the European Ceramic Society*, **24** (8), 2285–2292.
132 Aranzabal, A., Iturbe, D., Romero-Sáez, M., González-Marcos, M.P., González-Velasco, J.R. and González-Marcos, J.A. (2010) Optimization of process parameters on the extrusion of honeycomb shaped monolith of H-ZSM-5 zeolite. *Chemical Engineering Journal*, **162** (1), 415–423.
133 Isobe, T., Kameshima, Y., Nakajima, A., Okada, K. and Hotta, Y. (2006) Extrusion method using nylon 66 fibers for the preparation of porous alumina ceramics with oriented pores. *Journal of the European Ceramic Society*, **26** (12), 2213–2217.
134 Dong, C. (1990) *Binder Removal in Ceramics: Department of Materials Science and Engineering*, Massachusetts Institute of Technology.
135 Schnabel, W. (1981) *Polymer Degradation: Principles and Practical Applications*, Hanser International, Munich.
136 Higgins, R.J. (1989) The chemistry of carbon retention during non-oxidative binder removal from ceramic greenware. Ph.D. thesis, Department of Materials Science and Engineering, Massachusetts Institute of Technology.
137 Onoda, G.Y. and Hench, L.L. (1978) *Ceramic Processing before Firing*, Wiley-Interscience, New York.
138 Rahaman, N. (2007) *Sintering of Ceramics*, CRC Press, Boca Raton, FL.
139 Mehrer, H. (2007) *Diffusion in Solids: Fundamentals, Methods, Materials, Diffusion-Controlled Processes*, Springer, Berlin.
140 Kang, S.J.L. (2005) *Sintering: Densification, Grain Growth and Microstructure*, Elsevier, Amsterdam.
141 Ashby, M.F. (1972) A first report on deformation-mechanism maps. *Acta Metallurgica*, **20** (7), 887–897.
142 Shi, J.L., Deguchi, Y. and Sakabe, Y. (2005) Relation between grain growth, densification and surface diffusion in solid state sintering: a direct observation. *Journal of Materials Science*, **40** (21), 5711–5719.
143 Shi, J.L. (1999) Relations between coarsening and densification and mass transport path in solid-state sintering of ceramics: model analysis. *Journal of Materials Research*, **14** (4), 1378–1388.
144 Levanen, E. and Mantyla, T. (2002) Effect of sintering temperature on functional properties of alumina membranes. *Journal of the European Ceramic Society*, **22** (5), 613–623.
145 Brook, R.J. (1985) Processing technology for high-performance ceramics. *Materials Science and Engineering*, **71** (1–2), 305–312.
146 Chaim, R., Levin, M., Shlayer, A. and Estournes, C. (2008) Sintering and densification of nanocrystalline ceramic oxide powders: a review. *Advances in Applied Ceramics*, **107** (3), 159–169.
147 Balachandran, U., Dusek, J.T., Mieville, R.L., Poeppel, R.B., Kleefisch, M.S., Pei, S. *et al.* (1995) Dense ceramic membranes for partial oxidation of methane to syngas. *Applied Catalysis A: General*, **133** (1), 19–29.
148 Kleinlogel, C. and Gauckler, L.J. (2000) Sintering and properties of nanosized ceria solid solutions. *Solid State Ionics*, **135** (1–4), 567–573.
149 Nandi, B.K., Uppaluri, R. and Purkait, M.K. (2008) Preparation and characterization of low cost ceramic membranes for micro-filtration applications. *Applied Clay Science*, **42** (1–2), 102–110.
150 Riedel, R. and Chen, I.W. (2008) *Ceramics Science and Technology, Volume 1, Structures*, Wiley-VCH Verlag GmbH, Weinheim.
151 Gu, Y.F. and Oyama, S.T. (2007) Ultrathin, hydrogen-selective silica membranes deposited on alumina-graded structures prepared from size-controlled boehmite sols. *Journal of Membrane Science*, **306** (1–2), 216–227.
152 Gu, Y.F. and Oyama, S.T. (2007) High molecular permeance in a poreless ceramic membrane. *Advanced Materials*, **19** (12), 1636–1640.
153 Gu, Y.F., Hacarlioglu, P. and Oyama, S.T. (2008) Hydrothermally stable silica–alumina composite membranes for hydrogen separation. *Journal of Membrane Science*, **310** (1–2), 28–37.
154 Bayati, B., Bayat, Y., Charchi, N., Ejtemaei, M., Babaluo, A.A., Haghighi, M.

et al. (2013) Preparation of crack-free nanocomposite ceramic membrane intermediate layers on alumina tubular supports. *Separation Science and Technology*, **48** (13), 1930–1940.

155 Khatib, S.J. and Oyama, S.T. (2013) Silica membranes for hydrogen separation prepared by chemical vapor deposition (CVD). *Separation and Purification Technology*, **111**, 20–42.

156 Galuszka, J. and Giddings, T. (2011) Silica membranes: preparation by chemical vapour deposition and characteristics, in *Membranes for Membrane Reactors: Preparation, Optimization and Selection*, John Wiley & Sons, Inc., Chichester.

157 Yacou, C., Wang, D., Motuzas, J., Zhang, X., Smart, S. and da Costa, J.C.D. (2013) Thin-film ceramic membranes. *Encyclopedia of Membrane Science and Technology*, John Wiley & Sons, Inc., Hoboken, NJ.

158 Jones, A.C. and O'Brien, P. (1997) *CVD of Compound Semiconductors: Precursor Synthesis, Development and Applications*, Wiley-VCH Verlag GmbH, Weinheim.

159 Khatib, S.J., Oyama, S.T., de Souza, K. and Noronha, F.B. (2011) Review of silica membranes for hydrogen separation prepared by chemical vapor deposition, in *Inorganic Polymeric and Composite Membranes, Volume 14: Structure, Function and Other Correlations*, Elsevier, Amsterdam.

160 Leys, M.R. (1987) Metal organic vapour phase epitaxy. *Chemtronics*, **2** (4), 155–164.

161 Malik, M.A. and O'Brien, P. (1997) Basic chemistry of CVD and ALD precursors, in *CVD of Compound Semiconductors: Precursor Synthesis, Development and Applications*, Wiley-VCH Verlag GmbH, Weinheim.

162 Leese, A.B. and Mills, A.R. (1997) Commercial aspects of CVD, in *CVD of Compound Semiconductors: Precursor Synthesis, Development and Applications*, Wiley-VCH Verlag GmbH, Weinheim.

163 Puma, G.L., Bono, A., Krishnaiah, D. and Collin, J.G. (2008) Preparation of titanium dioxide photocatalyst loaded onto activated carbon support using chemical vapor deposition: a review paper. *Journal of Hazardous Materials*, **157** (2–3), 209–219.

164 Sea, B.K., Soewito, E., Watanabe, M., Kusakabe, K., Morooka, S. and Kim, S.S. (1998) Hydrogen recovery from a H2–H2O–HBr mixture utilizing silica-based membranes at elevated temperatures. 1. Preparation of H2O- and H2-selective membranes. *Industrial & Chemical Engineering Research*, **37**, 2502–2508.

165 Gavalas, G.R., Megiris, C.E. and Nam, S.W. (1989) Deposition of H_2-permselective SiO_2 films. *Chemical Engineering Science*, **44** (9), 1829–1835.

166 Wu, J.C.S., Sabol, H., Smith, G.W., Flowers, D.L. and Liu, P.K.T. (1994) Characterization of hydrogen-permselective microporous ceramic membranes. *Journal of Membrane Science*, **96** (3), 275–287.

167 Sea, B.K., Kusakabe, K. and Morooka, S. (1998) Hydrogen recovery from a H_2–H_2O–HBr mixture utilizing silica-based membranes at elevated temperatures. 2. Calculation of exergy losses in H_2 separation using inorganic membranes. *Industrial and Engineering Chemistry Research*, **37** (6), 2509–2515.

168 de Vos, R.M., Maier, W.F. and Verweij, H. (1999) Hydrophobic silica membranes for gas separation. *Journal of Membrane Science*, **158** (1–2), 277–288.

169 Gu, Y., Hacarlioglu, P. and Oyama, S.T. (2008) Hydrothermally stable silica–alumina composite membranes for hydrogen separation. *Journal of Membrane Science*, **310** (1–2), 28–37.

170 Kanezashi, M. and Asaeda, M. (2006) Hydrogen permeation characteristics and stability of Ni-doped silica membranes insteam at high temperature. **271** (1–2), 86–93.

171 Okubo, T. and Inoue, H. (1989) Introduction of specific gas selectivity to porous-glass membranes by treatment with tetraethoxysilane. *Journal of Membrane Science*, **42** (1–2), 109–117.

172 Lin, Y.S. and Burggraaf, A.J. (1992) CVD of solid oxides in porous substrates for ceramic membrane modification. *Aiche Journal*, **38** (3), 445–454.

173 Labropoulos, A.I., Romanos, G.E., Karanikolos, G.N., Katsaros, F.K., Kakizis,

N.K. and Kanellopoulos, N.K. (2009) Comparative study of the rate and locality of silica deposition during the CVD treatment of porous membranes with TEOS and TMOS. *Microporous and Mesoporous Materials*, **120**, 177–185.

174 Kim, S. and Gavalas, G.R. (1995) Preparation of H_2 permselective silica membranes by alternating reactant vapor deposition. *Industrial & Engineering Chemistry Research*, **34** (1), 168–176.

175 Voelger, K.W., Hauser, R., Kroke, E., Riedel, R., Ikuhara, Y.H. and Iwamoto, Y. (2006) Synthesis and characterization of novel non-oxide sol–gel derived mesoporous amorphous Si–C–N membranes. *Journal of the Ceramic Society of Japan*, **114** (1330), 567–570.

176 Morooka, S. and Kusakabe, K. (1999) Microporous inorganic membranes for gas separation. *MRS Bulletin*, **24** (3), 25–29.

177 Novak, B.M. (1993) Hybrid nanocomposite materials: between inorganic glasses and organic polymers. *Advanced Materials*, **5** (6), 422–433.

178 Sakka, S. (2005) *Handbook of Sol–Gel Science and Technology. 1. Sol–Gel Processing*, Kluwer Academic Publishers.

179 Bonekamp, B.C., Kreoter, R. and Vente, J.F. (2008) Sol–gel approaches in the synthesis of membrane materials for nanofiltration and pervaporation, in *Sol-Gel Methods for Materials Processing: Focusing on Materials for Pollution Control, Water Purification, and Soil Remediation*, Nato Science for Peace and Security Series C: Environmental Security (eds P. Innocenzi, Y.L. Zub and V.G. Kessler), Springer, pp. 47–65.

180 Voronkov, M.G., Mileshkevich, V.P. and Yuzhelevskii, Y.A. (1978) *Siloxane Bond: Physical Properties and Chemical Transformations*, Studies in Soviet Science, Springer, New York.

181 Guizard, C., Ayral, A., Barboiu, M. and Julbe, A. Sol–gel processed membranes, in *Handbook of Sol-Gel Science and Technology: Processing, Characterization and Applications*, Kluwer Academic Publishers, Dordrecht.

182 Guizard, C. (1996) Sol-gel chemistry and its application to porous membrane processing. *Fundamentals of Inorganic Membrane Science and Technology*, Elsevier, Amsterdam.

183 Riedel, R., Ionescu, E. and Chen, I.W. (2008) Modern trends in advanced ceramics. *Ceramics Science and Technology. Vol. 1: Structures*, Wiley-VCH Verlag GmbH, Weinheim.

184 Matsukata, M. and Kikuchi, E. (1997) Zeolitic membranes: synthesis, properties, and prospects. *Bulletin of the Chemical Society of Japan*, **70** (10), 2341–2356.

185 Morigami, Y., Kondo, M., Abe, J., Kita, H. and Okamoto, K. (2001) The first large-scale pervaporation plant using tubular-type module with zeolite NaA membrane. *Separation and Purification Technology*, **25** (1–3), 251–260.

186 Piera, E., Tellez, C., Coronas, J., Menendez, M. and SaIntamaria, J. (2001) Use of zeolite membrane reactors for selectivity enhancement: application to the liquid-phase oligomerization of i-butene. *Catalysis Today*, **67** (1–3), 127–138.

187 Myatt, G.J., Budd, P.M., Price, C. and Carr, S.W. (1992) Synthesis of a zeolite NaA membrane. *Journal of Materials Chemistry*, **2** (10), 1103–1104.

188 Fedosov, D.A., Smirnov, A.V., Knyazeva, E.E. and Ivanova, I.I. (2011) Zeolite membranes: synthesis, properties, and application. *Petroleum Chemistry*, **51** (8), 657–667.

189 Seike, T., Matsuda, M. and Miyake, M. (2002) Preparation of FAU type zeolite membranes by electrophoretic deposition and their separation properties. *Journal of Materials Chemistry*, **12** (2), 366–368.

190 Navascues, N., Tellez, C. and Coronas, J. (2008) Synthesis and adsorption properties of hollow silicalite-1 spheres. *Microporous and Mesoporous Materials*, **112** (1–3), 561–572.

191 Algieri, C., Bernardo, P., Barbieri, G. and Drioli, E. (2009) A novel seeding procedure for preparing tubular NaY zeolite membranes. *Microporous and Mesoporous Materials*, **119** (1–3), 129–136.

192 Pera-Titus, M., Llorens, J., Cunill, F., Mallada, R. and Santamaria, J. (2005)

Preparation of zeolite NaA membranes on the inner side of tubular supports by means of a controlled seeding technique. *Catalysis Today*, **104** (2–4), 281–287.

193 Coronas, J. and Santamaria, J. (1999) Separations using zeolite membranes. *Separation and Purification Methods*, **28** (2), 127–177.

194 Wang, Z., Ge, Q., Shao, J. and Yan, Y. (2009) High performance zeolite LTA pervaporation membranes on ceramic hollow fibers by dipcoating–wiping seed deposition. *Journal of the American Chemical Society*, **131** (20), 6910–6911.

195 Jia, M.D., Chen, B.S., Noble, R.D. and Falconer, J.L. (1994) Ceramic–zeolite composite membranes and their application for separation of vapor/gas mixtures. *Journal of Membrane Science*, **90** (1–2), 1–10.

196 Tellez, C. and Menendez, M. (2011) Zeolite membrane reactors. *Membranes for Membrane Reactors: Preparation, Optimization and Selection*, John Wiley & Sons, Inc., Chichester.

197 Au, L.T.Y., Mui, W.Y., Lau, P.S., Ariso, C.T. and Yeung, K.L. (2001) Engineering the shape of zeolite crystal grain in MFI membranes and their effects on the gas permeation properties. *Microporous and Mesoporous Materials*, **47** (2–3), 203–216.

198 Burkett, S.L. and Davis, M.E. (1995) Mechanisms of structure direction in the synthesis of pure-silica zeolites. 1. Synthesis OF TPA/SI-ZSM-5. *Chemistry of Materials*, **7** (5), 920–928.

199 Burggraaf, A.J., Vroon, Z., Keizer, K. and Verweij, H. (1998) Permeation of single gases in thin zeolite MFI membranes. *Journal of Membrane Science*, **144** (1–2), 77–86.

200 Chau, J.L.H., Tellez, C., Yeung, K.L. and Ho, K.C. (2000) The role of surface chemistry in zeolite membrane formation. *Journal of Membrane Science*, **164** (1–2), 257–275.

201 Xu, W.Y., Dong, J.X., Li, J.P., Li, J.Q. and Wu, F. (1990) A novel method for the preparation of zeolite ZSM-5. *Journal of the Chemical Society, Chemical Communications*, (10), 755–756.

202 Matsukata, M., Nishiyama, N. and Ueyama, K. (1994) Zeolitic membrane synthesized on a porous alumina support. *Journal of the Chemical Society, Chemical Communications*, (3), 339–340.

203 Bibby, D.M. and Dale, M.P. (1985) Synthesis of silica-sodalite from non-aqueous systems. *Nature*, **317** (6033), 157–158.

204 Xu, W., Dong, J. and Li, J. (1990) Simultaneous crystallization of two dissimilar zeolites from the system ethylenediamine-Na_2O-Al_2O_3-SiO_2-H_2O-triethylamine. *Journal of the Chemical Society, Chemical Communications*, (2), 131–132.

205 Cheng, Z.L., Gao, E.Q. and Wan, H.L. (2004) Novel synthesis of FAU-type zeolite membrane with high performance. *Chemical Communications*, (15), 1718–1719.

206 Alfaro, S., Arruebo, M., Coronas, J., Menendez, M. and Santamaria, J. (2001) Preparation of MFI type tubular membranes by steam-assisted crystallization. *Microporous and Mesoporous Materials*, **50** (2–3), 195–200.

207 Aoki, K., Kusakabe, K. and Morooka, S. (2000) Separation of gases with an A-type zeolite membrane. *Industrial and Engineering Chemistry Research*, **39** (7), 2245–2251.

208 Xu, X.C., Yang, W.S., Liu, J. and Lin, L.W. (2000) Synthesis of a high-permeance NaA zeolite membrane by microwave heating. *Advanced Materials*, **12** (3), 195–198.

209 Yan, Y.G., Chaudhuri, S.R. and Sarkar, A. (1996) Synthesis of oriented zeolite molecular sieve films with controlled morphologies. *Chemistry of Materials*, **8** (2), 473–479.

210 Miachon, S., Ciavarella, P., van Dyk, L., Kumakiri, I., Fiaty, K., Schuurman, Y. *et al.* (2007) Nanocomposite MFI-alumina membranes via pore-plugging synthesis: specific transport and separation properties. *Journal of Membrane Science*, **298** (1–2), 71–79.

211 Finley, J. (2005) Ceramic membranes: a robust filtration alternative. *Filtration+Separation*, **42** (9), 34–37.

212 Cheryan, M. (1998) *Ultrafiltration and Microfiltration Handbook*, CRC Press, Boca Raton, FL.

213 Sondhi, R., Bhave, R. and Jung, G. (2003) Applications and benefits of ceramic membranes. *Membrane Technology*, **2003** (11), 5–8.
214 Guizard, C., Rambault, D., Urhing, D., Dufour, J. and Cot, L. (1993) *Deasphalting of a Long Residue Using Ultrafiltration Inorganic Membranes*. Worcester Polytechnic Institute, Worcester, MA, pp. 345–354.
215 Marchetti, P., Solomon, M.F.J., Szekely, G. and Livingston, A.G. (2014) Molecular separation with organic solvent nanofiltration: a critical review. *Chemical Reviews*, **114** (21), 10735–10806.
216 Tsuru, T., Miyawaki, M., Kondo, H., Yoshioka, T. and Asaeda, M. (2003) Inorganic porous membranes for nanofiltration of nonaqueous solutions. *Separation and Purification Technology*, **32** (1–3), 105–109.
217 Tsuru, T., Narita, M., Shinagawa, R. and Yoshioka, T. (2008) Nanoporous titania membranes for permeation and filtration of organic solutions. *Desalination*, **233** (1–3), 1–9.
218 Hoek, E.V. and Tarabara, V.V. (eds) (2013) *Encyclopedia of Membrane Science and Technology*, John Wiley & Sons, Inc., Hoboken, NJ.
219 Burggraaf, A.J. (1992) *Inorganic Membranes*, Trans Tech Publications Ltd., Pfaffikon, Zürich.
220 Kanellopoulos, N. (2000) *Recent Advances in Gas Separation by Microporous Ceramic Membranes*, 1st edn, Elsevier, Amsterdam.
221 Sánchez Marcano, J.G. and Tsotsis, T.T. (2004) *Catalytic Membranes and Membrane Reactors*, Wiley-VCH Verlag GmbH, Weinheim.
222 Sammells, A.F. and Mundschau, M.V. (2006) *Nonporous Inorganic Membranes: For Chemical Processing*, Wiley-VCH Verlag GmbH, Weinheim.
223 Nunes, S.P. and Peinemann, K.V. (2001) *Membrane Technology: In the Chemical Industry*, Wiley-VCH Verlag GmbH, Weinheim.
224 Tan, X. and Li, K. (2015) *Inorganic Membrane Reactors: Fundamentals and Applications*, John Wiley & Sons, Inc., Hoboken, NJ.

2
Fundamentals of Membrane Separation

2.1
A Short Introduction to Mass Transfer Phenomena

Now that we have our first membrane, we will try to understand how it separates compounds from mixtures. This is not as simple as it sounds, and requires a basic knowledge of mass transfer phenomena. As understanding mass transfer is crucial for understanding how membranes work, we give here a short introduction (based on our undergraduate course 'Principles of mass transfer for biotechnology' at Ben-Gurion University). If you are already well versed in mass transfer of liquids and gases, you may skip to Section 2.3.3.

Mass transfer is analogous to membrane separation. It is defined as the movement of one component in a mixture relative to another. Similarly, we can define membrane separation as the relative movement of one (or more) component(s) in the initial mix and the limitations posed on the passage of others. This is why describing membrane separation in terms of mass transfer makes sense.

In the following, we will define fluxes and concentrations, and describe diffusion and convection in gases, liquids and solids. We will then determine diffusional mass transfer in a simple case without chemical reactions. Convective mass transfer will be discussed in a frame of filtration modules, outlining the calculations of mass transfer coefficients based on the key parameters used in evaluating separation systems (the Sherwood, Peclet and Schmidt numbers). Calculations of transmembrane flux will embrace simple pore flow models (Hagen–Poiseuille and Carman–Kozeny equations), advanced concentration polarization (CP) (including gel polarization) models and resistance-in-series (including the Hermia approach) models. Diffusion of gases will differentiate between *Knudsen diffusion*, *surface diffusion*, *capillary condensation* and *molecular sieving*. Aggregate approaches include the parallel transport and resistance-in-series models. These are the most important models for describing permeation through porous membranes. A brief description of gas transport through dense membrane is important for understanding how fuel cells work. We recommend that you familiarize yourself with the basic terms and theories, as we will use those throughout the book.

Ceramic Membranes: New Opportunities and Practical Applications, First Edition. Vitaly Gitis and Gadi Rothenberg.
© 2016 Wiley-VCH Verlag GmbH & Co. KGaA. Published 2016 by Wiley-VCH Verlag GmbH & Co. KGaA.

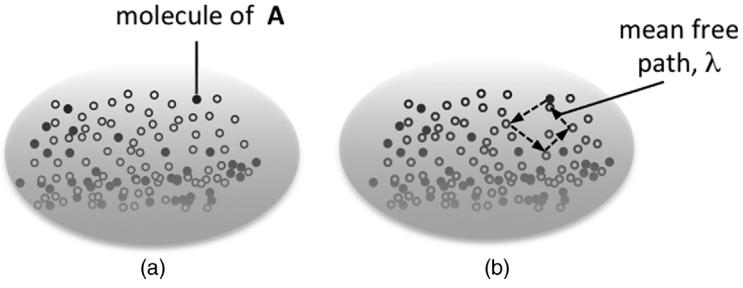


Figure 2.1 Elemental volume that contains a mixture of molecules including molecule A (a) and schematic of the mean free path (b). The mean free path is calculated as the average path of a molecule A between collisions ($\lambda = (1/N)\sum_{i=1}^{N} \lambda_i$, where N is the number of collisions and λ_i is the length of path between collisions).

Mass transfer involves a mixture of at least two components. It differs from heat transfer, which can be carried out by a single medium (such as air or water at different temperatures). The presence of two components allows us to define a concentration – a relative amount of a substance in a unit volume. Let us consider a unit volume that contains a mixture of only two types of molecules: A and B, a so-called binary mixture. For simplicity, we shall assume throughout the chapter that in any given volume there are more molecules of B than A. Figure 2.1a presents molecules of A in a unit volume of a bulk V.

Each molecule of A has a given mass. The *mass concentration* of A in the bulk (ρ_A) is defined as the total mass of molecules A, in kg, per unit volume V in m^3. The mass concentration of B is defined in the same way. You may be more familiar with another term for mass concentration – the *density*, denoted for species A and B as partial densities ρ_A and ρ_B, respectively. The density of the entire mixture will be a sum of partial densities, or

$$\rho = \rho_A + \rho_B \tag{2.1}$$

A relative amount of A in the mixture is called a *mass fraction* m_A, defined as

$$m_A = \frac{\rho_A}{\rho} = \frac{\text{mass of species A}}{\text{mass of mixture}} \tag{2.2}$$

so that

$$m_A + m_B = \frac{\rho_A}{\rho} + \frac{\rho_B}{\rho} = 1 \tag{2.3}$$

When describing chemical reactions, the mass concentration is replaced by the *mole concentration* c_A, defined as the number of moles of A present in the unit volume V. The mole concentration c_A and the partial density ρ_A are related through M_A, the molecular weight of species A.

$$c_A = \frac{\rho_A}{M_A} \tag{2.4}$$

Similarly to Eq. (2.1), the mole concentration of the mixture c is defined as the total number of moles for all species per unit volume:

$$c = c_A + c_B \tag{2.5}$$

The *mole fraction* x_A is the number of moles of A per mole of mixture:

$$x_A = \frac{c_A}{c} = \frac{\text{moles of A}}{\text{moles of mixture}} \tag{2.6}$$

Similarly to the mass fraction, it follows that the sum of mole fractions is

$$x_A + x_B = \frac{c_A}{c} + \frac{c_B}{c} = 1 \tag{2.7}$$

Both mass and mole fractions will always have values between 0 and 1:

$$0 \le x_A \le 1, \qquad 0 \le m_A \le 1 \tag{2.8}$$

Many gaseous mixtures behave approximately as *ideal gases*, that is hypothetical gases whose molecules bounce off each other and the walls of their containers with perfect elasticity, zero size and zero intermolecular forces. Such mixtures obey the ideal gas equation of state:

$$PV = nRT \tag{2.9}$$

where P is the total pressure (Pa), V is the gas volume (m^3), T is the absolute temperature (K), R is the universal gas constant (see Example 2.1) and n is the number of moles of gas. By definition, the mole concentration c is the number of moles in the unit volume, or in terms of Eq. (2.9),

$$c = \frac{n}{V} = \frac{P}{RT} \tag{2.10}$$

Thus, the mole fraction of A (Eq. (2.6)) in gases can be calculated as

$$\frac{c_A}{c} = \frac{P_A/RT}{P/RT} = \frac{P_A}{P} \tag{2.11}$$

This equation states that in ideal gases the mole fraction of A can be calculated by the ratio of partial pressure P_A to the total pressure P. The latter is simply the sum of partial pressures of gases A and B following Dalton's law:

$$P = P_A + P_B \tag{2.12}$$

Here is an example that illustrates the usefulness of Eq. (2.10).

Working Example 2.1

Determine the mole concentration of air at 25 °C and 1 atm.

Solution

Repeated experiments show that at 0 °C (273 K) and 1 atm (1.013×10^5 Pa), one mole of gas ($n = 1$) occupies a volume of 22.4 l. Using this experimental value, the gas constant is

$$R = \frac{PV}{nT} = \frac{(1.013 \times 10^5 \text{ Pa})(0.0224 \text{ m}^3)}{(1 \text{ mol})(273 \text{ K})} = 8.314 \text{ Pa m}^3/(\text{mol K}) \tag{2.13}$$

The volume of air at 25 °C or 298 K is different from that at 0 °C:

$$V = \frac{nRT}{P} = \frac{(1 \text{ mol})(8.314 \text{ Pa m}^3/(\text{mol K}))(298 \text{ K})}{1.013 \times 10^5 \text{ Pa}} = 0.0245 \text{ m}^3 \tag{2.14}$$

And if 1 mol occupies 0.0245 m^3, the number of moles per 1 m^3 is

$$c = \frac{1 \text{ mol}}{0.0245 \text{ m}^3} = 40.9 \text{ mol/m}^3 \tag{2.15}$$

Membrane separation is a dynamic phenomenon, with species moving with different velocities at various directions. Hence, we need a species-average velocity. We will define here the mass-average velocity (although in the same way we can define the mole-average velocity). This *mass-average velocity* is defined through a *mass flux J* as a sum of mass fluxes of all species,

$$\vec{J} = \sum_i \vec{J}_i \tag{2.16}$$

where each mass flux of a species i here is defined as a product of partial density p_i multiplied by its velocity v_i:

$$\vec{J} = \rho_i v_i \tag{2.17}$$

Thus, Eq. (2.16) can be rewritten as

$$\rho\vec{v} = \sum\nolimits_i \rho_i \vec{v}_i \tag{2.18}$$

and the mass-average velocity can be defined as

$$\vec{v} = \frac{\sum_i \rho_i \vec{v}_i}{\rho} = \frac{\sum_i \rho_i \vec{v}_i}{\sum_i \rho_i} \tag{2.19}$$

Here v_i is the absolute velocity of species i relative to a fixed axis. Note that v_i can differ from v, meaning that a single species can move in a different direction and at a different speed than the entire mixture. This distinction is important in mass transfer. Although in general molecules of A are moving with v_A and molecules of B with v_B, we will assume here that the amount of A in the mixture is less than 0.1%. Thus, the mixture is practically B and therefore, for all practical purposes, $v = v_B$. We will neglect the influence of A on the mixture and assume

that molecules of A are moving in B (strictly speaking, A moves in the mixture [A + B] that forms the bulk, but we will ignore this). While the entire bulk is moving with an average velocity, a single species can have its own velocity and direction. A sovereign random movement of a species in the bulk is called *diffusion*. A directed movement is called *convection*. In our A + B mixture, the diffusive movement of A may differ from the bulk movement of B.

The following example illustrates the difference between convection and diffusion: Imagine a tubular module that is used for purifying orange juice. To filter the orange juice we separate the juice–pulp suspension in a cross-flow mode. Concurrently, gravity causes some of the pulp to leave the bulk and approach the tube wall. The pulp concentration near the tube wall increases compared with that in the bulk. After some time, the concentration of pulp in the suspension will decrease, as part of the pulp will foul the tube wall. That action, a deliberate expression of pulp independence not provoked by the convection flow, is the diffusion (for more details and a diagram of the orange juice process, see the applications section in Chapter 4). The diffusion velocity $(v_A - v)$ is the difference between the velocity v_A of species A and the mass-average velocity v. Similarly, the diffusional mass flux, j_A, is determined as the product of the partial density p_A and the diffusion velocity $(v_A - v)$, or

$$\vec{j}_A = \rho_A(\vec{v}_A - \vec{v}) \tag{2.20}$$

Opening brackets and implementing the definition of mass flux from Eq. (2.17), we see that

$$\vec{j}_A = \rho_A(\vec{v}_A - \vec{v}) = \rho_A\vec{v}_A - \rho_A\vec{v} = \vec{J}_A - \rho_A\vec{v} \tag{2.21}$$

Rearranging Eq. (2.21) gives

$$\vec{J}_A = \underbrace{\rho_A\vec{v}}_{\text{convection}} + \underbrace{\vec{j}_A}_{\text{diffusion}} \tag{2.22}$$

The mass flux of species A includes the convection term $p_A v$ and the diffusion term j_A.

Here is another example: Imagine that you take your morning coffee with milk and sugar. Normally, you would add sugar to the cup with a spoon and mix it. But what if you do not mix the sugar? Would it spread evenly in the cup? The answer is yes. The difference is in time and in the effort, or in the energy requirement. Mixing is a convectional operation that saves time but requires energy. If you do not mix the sugar, and just leave it to spread in the coffee by diffusion, this will take more time, but requires no energy. Strictly speaking, stirring with a spoon triggers a turbulent diffusion, so mixing in that case is a combination of convection and diffusion [1]. Thus, convection transfers mass quickly, while diffusion is a slow method that saves energy. 'To mix or not to mix' is not the question. Both methods will sweeten your coffee. The real question here is whether you like your coffee hot, or not.[1)]

1) As the coffee is cooling down, the sugar solubility also changes. So if you decide to drink your coffee cold, it will probably taste less sweet.

One important clarification of diffusion fluxes comes from a combination of Eqs. (2.16) and (2.22):

$$\vec{J} = \sum_i \vec{J}_i = \sum_i \rho_i \vec{v} + \sum_i \vec{j}_i = \rho \vec{v} + \sum_i \vec{j}_i = \vec{J} + \sum_i \vec{j}_i \tag{2.23}$$

Hence,

$$\sum_i \vec{j}_i = 0 \tag{2.24}$$

Thus, the diffusional mass fluxes must add up to zero, as they are defined relative to the mean mass flux.

2.2 Fick's Law

Until now we only described mixtures in which the bulk and separate species are moving. Such systems can sometimes be simplified and the diffusional flux can be viewed as negligible relative to the convectional flux. We will discuss that point in Section 2.5. But what happens when the entire bulk B is at rest, and the only mass transfer is the diffusional movement of A? Then we should calculate the diffusional flux carefully to account properly for the expected mass transfer. There are many examples of such systems in real life. Consider a pond which contains viruses, bacteria and protozoa. The concentration of microorganisms in the water will decrease constantly due to their diffusional movement to the pond's borders. Similarly, if the surface water is exposed to the dry air stream, its vapour pressure might be high enough to produce a significant diffusion of vapour into the air stream (this is also how perfumes and fragrances spread off the skin). Other examples include reverse osmosis (the small ions in the bulk move towards a membrane and then through the membrane by a diffusional mass transfer) and gas separation (which is based on diffusion of certain ions through tiny pores in the membrane structure). In all these examples, species diffuse from high-concentration areas to low-concentration areas. This tendency to equalize concentrations in each and every unit volume not separated by barriers is a basic natural law that was shown experimentally by Parrott in 1815. Four decades later, and still before any quantitative experiments had been performed, Fick suggested that the diffusional flux should be proportional to the concentration difference between two points, offering the following empirical relationship:

$$j_A = -D_{AB} \nabla \rho_A \tag{2.25}$$

This equation, known as *Fick's first law of diffusion*, states that the diffusional flux of species A moving inside the bulk of B is proportional to the concentration difference of A within a unit volume with a diffusion coefficient D_{AB}. The minus sign denotes that the flux is from high to low concentrations.

Working Example 2.2

Prove that despite the fact that Fick's equation has a negative nominator, the diffusional flux is always positive.

Solution

Let us consider two possibilities – the diffusion along the *z*-axis and the diffusion towards zero. In both cases, the diffusion occurs only along the *z*-axis, so Fick's law can be written as

$$j_A = -D_{AB}\frac{d\rho_A}{dz} \tag{2.26}$$

In the first case, the concentration of A at point z_1 is higher than its concentration at point z_2,

$$p_{A,z_1} > p_{A,z_2}$$

Thus, applying Fick's equation we get

$$j_A = -D_{AB}\frac{d\rho_A}{dz} = -D_{AB}\frac{\rho_{A,z_1} - \rho_{A,z_2}}{z_1 - z_2} \tag{2.27}$$

But here z_1 is smaller than z_2, so the difference $(z_1 - z_2)$ will be negative and the entire expression will be positive.

In the second case, the concentration of A at point z_1 is lower than its concentration at point z_2,

$$p_{A,z_1} < p_{A,z_2}$$

Applying Fick's law gives

$$-j_A = -D_{AB}\frac{d\rho_A}{dz} = -D_{AB}\frac{\rho_{A,z_2} - \rho_{A,z_1}}{z_2 - z_1} \tag{2.28}$$

The flux direction is opposite to the axis direction, so the negative flux is equal to a negative expression, so once again the flux is positive.

There are many derivations of Fick's law. Taking the definition of mass fraction m_A from Eq. (2.2) and rearranging it to express explicitly the p_A, we can withdraw the overall density from the gradient obtaining Eq. (2.25) in the form

$$j_A = -\rho D_{AB}\nabla m_A \tag{2.29}$$

that can be expressed as

$$\text{Flux} = -\begin{pmatrix}\text{overall}\\ \text{density}\end{pmatrix}\begin{pmatrix}\text{diffusion}\\ \text{coefficient}\end{pmatrix}\begin{pmatrix}\text{concentration}\\ \text{gradient}\end{pmatrix}$$

We can write a similar expression for the mole fraction,

$$j_A = -cD_{AB}\nabla x_A \tag{2.30}$$

The D_{AB} diffusion coefficient value does not change between Eqs. (2.29) and (2.30), or between mass and molar diffusion expressions. Moreover, in binary diffusion[2] its value for A diffusing through B is equal to that for B diffusing through A:

$$D_{AB} = D_{BA} \tag{2.31}$$

Early experiments of molecular diffusion could not verify Fick's law [2]. Steffan (1872) and Maxwell (1877) then hypothesized that whenever the diffusional transport occurs, it brings also a convective movement due to density differences. To prove this point, the equation for diffusional transport (Eq. (2.20)) was combined with Eq. (2.26) in the form

$$-D_{AB}\frac{d\rho_A}{dz} = \rho_A(v_A - v) \tag{2.32}$$

where for a case of a binary system (e.g. two immiscible gases A and B) the system flux can be expressed as

$$\rho v = \rho_A v_A + \rho_B v_B \tag{2.33}$$

The average mass velocity in that case will be

$$v = \frac{\rho_A v_A + \rho_B v_B}{\rho} \tag{2.34}$$

Substituting Eq. (2.34) into Eq. (2.32) gives

$$-D_{AB}\frac{d\rho_A}{dz} = \rho_A v_A - \rho_A\frac{\rho_A v_A + \rho_B v_B}{\rho} \tag{2.35}$$

Introducing the definition of mass fraction m_A from Eq. (2.2) and mass fluxes J_A and J_B from Eq. (2.17), we can rearrange Eq. (2.35) as

$$-D_{AB}\frac{d\rho_A}{dz} = J_A - m_A(J_A + J_B) \tag{2.36}$$

or

$$J_A = -D_{AB}\frac{d\rho_A}{dz} + m_A(J_A + J_B) \tag{2.37}$$

The mass flux J_A of a binary system at rest is a sum of diffusional ($-D_{AB}(d\rho_A/dz)$) and convectional ($m_A(J_A + J_B)$) fluxes relative to a fixed spatial coordinate system. A similar expression for a molar flux is

$$N_A = -D_{AB}\frac{dc_A}{dz} + x_A(N_A + N_B) \tag{2.38}$$

2) Actually, Fick's law is strictly valid only for binary mixtures. It was later approximated for multicomponent mixtures. For this, the diffusion coefficient was redefined.

Here and in Eq. (2.37), $x_A(N_A + N_B)$ expresses the possibility of movement of A due to the movement of B, for example when diffusing B molecules collide with molecules of A or block their diffusional pathways.

2.3 The Mass Diffusivity D_{AB}

Although we saw already the diffusion coefficient in several expressions of Fick's law, we still did not define it properly. To start with, we will define its dimensions using any of the above equations. For example, from Eq. (2.26) we can see that

$$D_{AB} = \frac{-j_A}{(d\rho_A/dz)} = \left[\frac{M}{L^2T}\frac{1}{(M/L^3)(1/L)}\right] = \left[\frac{L^2}{T}\right] \tag{2.39}$$

Here the diffusion coefficient is expressed as area [L^2] over time [T] (m^2/s in SI units). These units are identical to the *kinematic diffusivity* ν (also called the momentum diffusivity). Diffusion coefficients depend upon composition of the mixture, temperature and pressure. It is easier to diffuse through empty space, and therefore a higher diffusion will be observed in low-density gases and dilute liquids. Diffusion coefficients in gases are on average higher than those in liquids, and both are higher than those in solids. The average diffusion coefficients in gases at room temperature are about $10^{-5}\,m^2/s$. For liquids, the coefficient is only about 10^{-9} to $10^{-11}\,m^2/s$, and for solids between 10^{-14} and $10^{-20}\,m^2/s$. Generally, the diffusion coefficient decreases with size of diffusing A, so larger particles have smaller coefficients. It also increases with temperature. In the following subsections, we will describe the basic approaches and common equations for calculating diffusion coefficients in gases, liquids and solids.

2.3.1 Diffusion in Gases

Descriptions of diffusion coefficients in textbooks on mass transfer always start from gases, continue with liquids and sometimes touch solids [2–5]. There are two good reasons for this: First, in gases the diffusion is very important and can significantly influence mass transfer. Second, because it is important, the theory of gas diffusion is well developed and contains many interesting aspects that are indirectly implemented in calculations of diffusion coefficients in liquids and solids. Here we will describe the diffusion in all three phases distinguishing between transport of A through the membrane in gases and liquids, and the formation of ceramic membranes by diffusion of A in solids.

Diffusion in gases is typically assessed through the ideal gas assumptions and the diffusion of A through its isotope A^* [2]. The self-diffusing coefficient in 3D motion of A is then defined as

$$D_{AA^*} = \frac{1}{3}\lambda\nu \tag{2.40}$$

where λ is the mean free path of species A (see Figure 2.1b) and v is the mean velocity of species A with respect to the molar average velocity, which can be approximated using Maxwell's equilibrium formulae [6].

The D^*_{AA} for self-diffusion is equal to

$$D_{AA^*} = \frac{(k_B/\pi)^{3/2}}{\sigma_A^2}\left(\frac{N_{AV}}{M_A}\right)^{1/2}\frac{T^{3/2}}{P} \tag{2.41}$$

where M_A is the molecular weight of A (g/mol), N_A is Avogadro's number (6.02×10^{23} molecules/mol), P is the system pressure (atm), T is the absolute temperature (K), k_B is Boltzmann's constant ($1.38\times10^{-23}\,m^2\,kg/(s^2\,K)$) and σ_A is the cross-sectional diameter of A. Based on the simple model for self-diffusion, the diffusion coefficient varies as $T^{3/2}$ and $1/P$.

More accurate results are obtained when Eq. (2.41) is modified to take into account two central facts: (i) molecules are not really hard spheres and (ii) the molecular sizes of A and B are different. A modified formula using results from the Chapman–Enskog theory [7] reads

$$D_{AB} = \frac{(1.8583\times10^{-7})T^{3/2}}{P\sigma_{AB}^2\Omega_D}\sqrt{\frac{1}{M_A}+\frac{1}{M_B}} \tag{2.42}$$

Here σ_{AB}, in Å, is the collision diameter calculated as

$$\sigma_{AB} = \frac{\sigma_A+\sigma_B}{2} \tag{2.43}$$

and Ω_D is the collision integral based on the Lennard-Jones potential. Its value is found as a function of k_BT/ε_{AB}, where ε_{AB} (J) is the effective potential well depth required to separate A and B from each other:

$$\varepsilon_{AB} = \sqrt{\varepsilon_A\varepsilon_B} \tag{2.44}$$

Figure 2.2 shows σ_{AB} and ε_{AB} in a Lennard-Jones potential diagram.

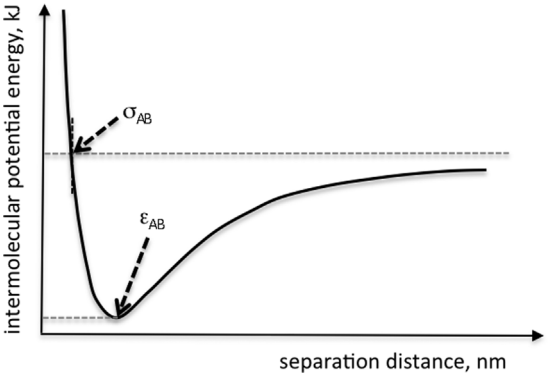


Figure 2.2 Lennard-Jones potential.

Although Eq. (2.42) indicates that the diffusivity is independent of mixture concentrations, the gas density affects the accuracy of the calculations [8]. The reported average error is within ±8%.

In Eqs. (2.41) and (2.42), we assumed that there is an infinite space for molecules to interact with each other. In reality, the molecules are confined within a volume and interact with the boundaries as often as they interact with each other. This is especially relevant for gases diffusing through pores in ceramic membranes. Equations for the diffusion in infinite space are based on the *free mean path* λ described as the average length of path between two consecutive collisions of A and B. The mean free path λ in low-density gases is approximately $10d$, where d is an approximate molecular diameter. But when the pore width is smaller than λ, and the gas density is low, the gas molecules will interact with pore walls more frequently than with each other. That phenomenon is known as *Knudsen diffusion*. Here, A bumps into the pore wall because the distance to the wall is smaller than that to a nearest molecule. The relative importance of Knudsen diffusion is evaluated through another dimensionless number, unsurprisingly called the *Knudsen number*, or *Kn*.

$$Kn = \frac{\lambda}{d_p} \tag{2.45}$$

As a rule of thumb, if $Kn \gg 1$, the Knudsen diffusion is important. This diffusion is considered the dominant transport mechanism in pores of 2–50 nm size, covering the important microporous and mesoporous ranges [9]. Knudsen diffusion is not limited to gases. It can also occur in liquids, but usually the average mean free path in liquids is too short ($\sim 1d$), so the diffusion in liquids is described by hindered diffusion models.

The diffusion coefficient for Knudsen diffusion, D_{Kn}, is calculated by replacing the mean free path λ by the pore diameter d_p (m) [10]. This gives

$$D_{Kn} = 194 d_p \sqrt{\frac{T}{M_A}} \tag{2.46}$$

A comparison between D_{Kn} in Eq. (2.46) and D_{AB} in Eq. (2.42) shows that Knudsen diffusion is independent of the absolute pressure P and presence of species B in the mixture. It is also less sensitive to temperature. We will discuss the practical implications of these dependences in Section 2.7.

For very simple cases, one may think that it is either Knudsen diffusion or infinite diffusion. In fact, in membrane processes both diffusions are often relevant. With a typical pore size distribution of 1–100 nm, we can assume that A molecules will diffuse through confined and infinite pores simultaneously. A well-known method for calculating the total diffusion coefficient is using an analogy with Ohm's law, where the current through a conductor between two points is inversely proportional to the resistance. In the case of a parallel circuit, the total resistance R_{total} is calculated as a sum of inverses of resistances R_1 and R_2. We can describe similarly the parallel diffusion through confined and infinite pores,

$$\frac{1}{D_{total}} = \frac{1}{D_{AB}} + \frac{1}{D_{Kn}} \tag{2.47}$$

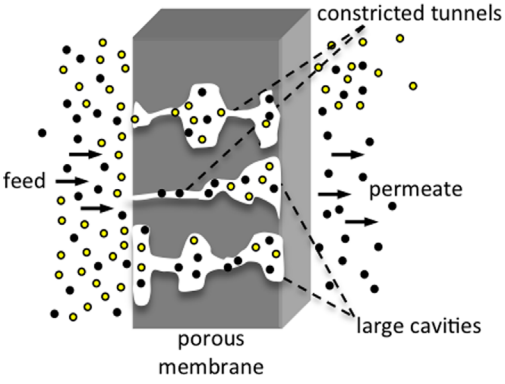


Figure 2.3 Idealized schematic cross section of ceramic membrane that comprises large cavities and constricted windows.

where D_{total} is the total diffusion coefficient. The assumption of parallel diffusion is based on ideal cylindrical pores that cross the membrane. Reality is often less nice. Membrane pores are twisted and interconnected, so that the path of A through the membrane is tortuous. Figure 2.3 depicts one hypothetical model of a pore structure in ceramic membranes [11].

If the pore size is larger than the size of the molecule [2], we can calculate D_{total} through the effective porosity ε:

$$D'_{\text{total}} = \varepsilon^2 D_{\text{total}} \tag{2.48}$$

In the unique case where the pore and the molecule are equal, the jump of a molecule through the constricted window requires some activation energy. The theory of entropic selectivity for advanced gas separation membranes was developed by Koros and co-workers [11–13]. It is based on the Van't Hoff and Arrhenius expression for the temperature variation of the rate constant for a chemical reaction, which since 1920s was adapted for calculating diffusion coefficients as

$$D'_{\text{total}} = D_{\text{total}} \exp\left(\frac{-E_{\text{D}}}{RT}\right) \tag{2.49}$$

or

$$\ln(D'_{\text{total}}) = -\frac{E_{\text{D}}}{R}\frac{1}{T} + \ln(D_{\text{total}}) \tag{2.50}$$

where E_{D} (J/mol) is the energy of activation needed for a diffusive jump between two neighbouring cavities (depending on D_{p} and the size of the penetrating molecule) and D_{total} is the temperature-independent pre-exponential term calculated as [14]

$$D_{\text{total}} = e\lambda^2 \frac{k_{\text{B}} T}{h} \exp\left(\frac{S_{\text{D}}}{R}\right) \tag{2.51}$$

where λ is the average diffusive jump length, S_D is the activation entropy of diffusion and h is Planck's constant. The assumption that the activation energy plays an important role in the diffusion of two gas molecules came from observing the separation of O_2/N_2. Both of these gases have sphero-cylindrical molecules with similar dimensions: 4.07×3.09 Å in N_2 and 3.65×2.68 Å in O_2. Yet oxygen penetrated freely through the pores while nitrogen was restricted. Singh and Koros suggested that the reason is the entropic selectivity of diffusion, S_D [11].

2.3.2 Diffusion in Liquids

Gases are much more dilute than liquids. Their molecules are separated from each other and collide sporadically. In liquids, molecules are always in contact with their neighbours and exert forces on each other continuously. From a macroscopic point of view, those forces relate to viscosity, a measure of a fluid's resistance to flow. The kinetic theory of gases does not hold for liquids. Instead, calculation of diffusion coefficient in liquids is based on empirical theories, for example the hydrodynamic theory. This describes the diffusion as a trade-off between viscous and diffusional forces, where the viscous forces F_A are usually assumed to be proportional to an average velocity v_A via the friction coefficient f, as $F_A = f v_A$. This friction coefficient is given by Stokes' relation for the drag on a sphere,

$$f = 6\pi\mu_B R_A \left(\frac{1 + 2\mu_B/\beta R_A}{1 + 3\mu_B/\beta R_A} \right) \tag{2.52}$$

where R_A is the effective hydrodynamic radius of A, μ_B is the dynamic viscosity of the bulk and β is a coefficient of sliding friction for a friction force proportional to v_A. This model contains two approximations. The first is that Stokes' law applies here although it describes a movement of spheres at Reynolds numbers below 1. The second is that there are no external forces acting on the moving molecule such as electric field acting on ions. An immediate outcome of the second assumption is that molecules of A are moving due to diffusion that mathematically can be described by Brownian motion,

$$D_{AB} = k_B T \frac{v_A}{F_A} \tag{2.53}$$

Substituting Eq. (2.53) into the expression for friction forces gives [15]

$$D_{AB} = \frac{k_B T}{6\pi\mu_B R_A} \left(\frac{1 + 3\mu_B/\beta R_A}{1 + 2\mu_B/\beta R_A} \right) \tag{2.54}$$

There are some complications in applying this equation in practice, namely in the determination of β. It was therefore suggested to consider two extreme situations: small solutes and large solutes. If the molecules of A are smaller than 5–10 Å [16], there is a complete slip of B at the surface of A meaning that the

layer of B next to A moves with the same velocity as far away of it. As a result, $\beta \to 0$ and the diffusion coefficient for small molecules becomes

$$D_{AB} = \frac{k_B T}{4\pi\mu_B R_A} \tag{2.55}$$

Conversely, large A particles will incur no-slip conditions (no movement of B near the surface of A). Thus, $\beta \to \infty$ and the diffusion coefficient becomes

$$D_{AB} = \frac{k_B T}{6\pi\mu_B R_A} \tag{2.56}$$

Calculations of D_{AB} in Eqs. (2.55) and (2.56) require the effective hydrodynamic radius of A, R_A. In the case of large particles, A can be viewed as a sphere with well-defined borders and applying Eq. (2.56) is usually successful. Small molecules, however, are often non-spherical and the link between R_A and M_A is weak. The R_A is roughly proportional to the cube root of the molecular weight [16]. An accurate calculation of D_{AB} in that case is crucial, as it would show whether the diffusion contribution is important [17]. Several empirical equations based on Eq. (2.55) were developed for such cases. One fairly successful and widely accepted expression is the *Wilke–Chang equation* [18],

$$D_{AB} = 7.4 \times 10^{-8} \frac{\sqrt{\Phi_B M_B} T}{\mu_B V_A^{0.6}} \tag{2.57}$$

where V_A is the molar volume of the solute at normal boiling point and Φ_B is the so-called 'association parameter' for solvent B ($\Phi_B = 2.6$ in water).

Until now we described D_{AB} for free liquids, in order to understand the basics of diffusion in liquids. The diffusion through membrane pores will once again be influenced by the pore size, and is therefore considered 'hindered diffusion', also known as *Renkin diffusion* [2], where D_{Ap} is related to D_{AB} through

$$D_{Ap} = D_{AB} F_1(\varphi) F_2(\varphi) \tag{2.58}$$

Here $F_1(\varphi)$ and $F_2(\varphi)$ are two correction factors that are functions of φ, which is a dimensionless parameter that relates the pore diameter d_p to the effective hydrodynamic radius R_A via $\varphi = 2R_A/d_p$. The correction factor F_1 is a simple geometric comparison of cross-section areas, accounting for steric hindrance:

$$F_1(\varphi) = \frac{\text{flux area available to solute}}{\text{total flux area}} = \frac{\pi(d_p - 2R_A)^2}{\pi d_p^2} = (1-\varphi)^2 \tag{2.59}$$

Similarly, the correction factor F_2 accounts for a hydrodynamic hindrance and is valid in the $0 < \varphi < 0.6$ interval [19],

$$F_2(\varphi) = 1 - 2.104\varphi + 2.09\varphi^3 - 0.95\varphi^5 \tag{2.60}$$

Many other empirical and theoretical equations that relate diffusion through pore and φ were developed [20]. However, they all share the same common

assumptions [1] such as

$$F(\varphi) \approx \begin{cases} 1 & \text{for} \quad \varphi < 0.001 \\ 0.6 & \text{for} \quad \varphi = 0.1 \\ 0 & \text{for} \quad \varphi \to 1 \end{cases} \tag{2.61}$$

Note that these equations apply when $0 < \varphi < 1$, because if $\varphi > 1$ the solute is too large to enter the pore. In typical low-pressure membranes with an average pore size of 10 nm and hydrodynamic radius of 2 nm, the diffusivity is reduced to 10% of diffusivity in the free liquid.

2.3.3 Diffusion in Solids

For a long time, scientists believed in the old Latin expression *corpora non agunt nisi soluta* (bodies do not move unless they are in solution). The first experiments that clearly showed that diffusion can actually occur in solids were performed by Roberts-Austen in 1896 [21], some 70 years after Parrot first reported on diffusion of gases. Figure 2.4 shows the most common mechanisms for diffusion in solids. The diffusion of atoms through solids during sintering of ceramic membranes was discussed earlier in Chapter 1. Here we will expand the discussion on vacancy diffusion and outline other diffusion types that occur during sintering, including interstitial and direct exchange diffusion. Readers interested in a detailed treatment of diffusion in solids should consult the books of Mehrer [22] and Kou [23].

Diffusion through solids can be described rigorously and simply, because the crystal lattice prescribes the positions and migration paths of diffusing atoms. In that sense, the diffusion in solids differs from gases with their

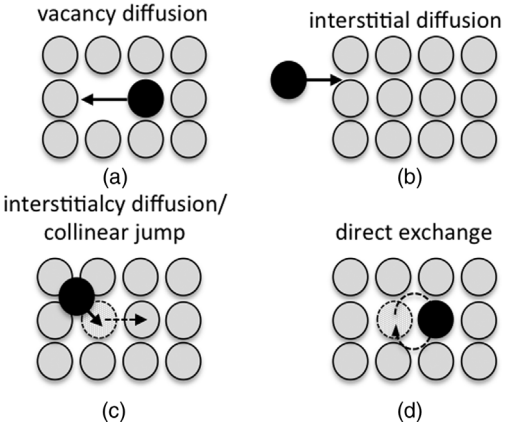


Figure 2.4 Schematic illustration of diffusion in solids: vacancy diffusion (a), interstitial diffusion (b), interstitialcy diffusion/collinear jump (c) and diffusion by direct exchange (d).

random distributions and liquids that are neither really randomly nor really orderly organized [22]. In solids, with the exception of vacancy diffusion, all diffusion mechanisms require negotiating a 'bargain' between the lattice atoms. The *vacancy diffusion* occurs through point defects in the membrane structure, when an atom on a normal site jumps into an adjacent unoccupied site (a vacancy). This is currently viewed as the dominant mechanism for the solid diffusion of matrix atoms. The concept of point defects was introduced by Frenkel [24,25] who suggested that under finite temperature atoms 'evaporate' from their normal lattice sites, leaving behind lattice vacancies that could propagate the movement of atoms within a solid structure. Such defects are known as *Frenkel defects*. Frenkel's theory contains two interesting assumptions: The first is that point defects can travel along the membrane structure, acting as 'vehicles for diffusion'. The second is that the concentration of point defects increases at high temperatures [22]. The presence of Frenkel defects induces a macroscopic diffusion of atoms through the membrane by a series of jumps into other vacant sites.

Interstitial diffusion occurs when an interstitial atom jumps to the neighbouring interstitial site of the host lattice. Such atoms are often smaller than those on the normal lattice positions and form an interstitial solid solution. Examples in ceramic membranes include H, C, N and O atoms. The diffusing atoms tend to migrate from areas of high concentration to ones of low concentration. A jump occurs when an atom's accumulated thermal energy overcomes the energy barrier set by the Arrhenius equation. When only the jumping atoms are involved, we speak of a *direct interstitial mechanism*. The lattice atoms remain in place, and no lattice defects are required. Because of this, the diffusing coefficients for atoms migrating in this way are fairly high. For the unidirectional diffusion of interstitials in a simple cubic crystal, the diffusion coefficient D_{As} is estimated as

$$D_{\mathrm{As}} = \frac{1}{6}\Gamma\lambda^2 \tag{2.62}$$

where Γ is the jump rate and λ is the jump length (analogous to the mean free path in gases) [22].

When the interstitial atom is roughly the same size as the lattice atoms, an extra atom located between lattice sites can act as the diffusion vehicle. This extra atom displaces a lattice atom from its normal location, and occupies its site. Concurrently, the 'pushed' atom at the interstitial position in turn displaces a neighbour lattice atom. This is a collective mechanism where at least two atoms are moving simultaneously. It is also known as the *indirect interstitial mechanism*, a sort of relay race where the diffusing atom is constantly replaced by its neighbour. In collinear jumps, the atom on the normal lattice site is pushed in the same direction as that of the diffusing atom. In non-collinear jumps, the directions of pushed and diffusing atoms differ. This mechanism can be neglected in thermal diffusion, as it has much higher barriers compared with the vacancy diffusion, but it is important in radiation-induced diffusion [22].

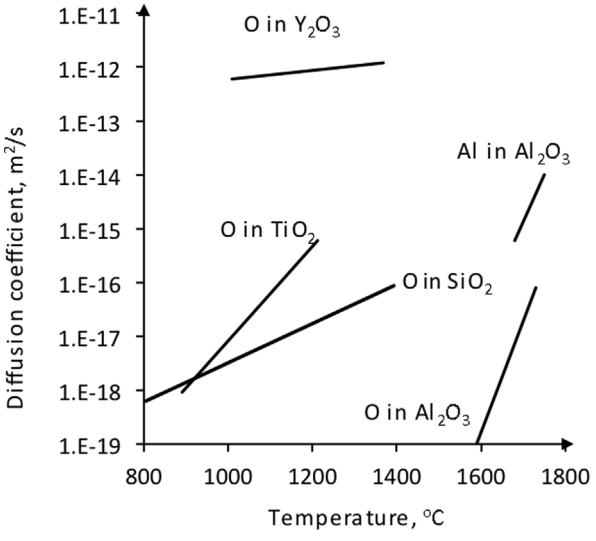


Figure 2.5 Diffusion coefficients in single and polycrystalline ceramics. (From Ref. [28], with permission.)

Another example of a collective diffusion that involves a simultaneous movement of two lattice atoms is the direct exchange of two neighbouring atoms. The probability of such an exchange in a close-packed lattice is low, as it requires large distortions in the lattice to physically replace the atoms and high activation energy to break bonds with neighbours. This energy comes from the thermal energy of atomic vibrations,

$$D_{\mathrm{As}} = B^* k_{\mathrm{B}} T \tag{2.63}$$

where B^* is the self-diffusion mobility [26]. The interest in direct exchange was renewed recently as it can explain some effects observed near phase transitions. The *ring diffusion* mechanism, wherein at least three atoms exchange places in a rotational motion, is considered unlikely (especially after the discovery of the Kirkendall effect [27], which shows that even similar atoms in a lattice will diffuse at different rates).

Figure 2.5 presents the experimental data for diffusion in several crystalline oxides.

2.4 Integral and Differential Expressions of Mass Balance Equation

Until now we regarded the diffusion as the only possibility for the change of concentration of A within a given membrane volume. This is not strictly true. We now use one of the most basic laws of conservation that states that mass can be neither created nor destroyed. In this simple way, we can account for changes of A within

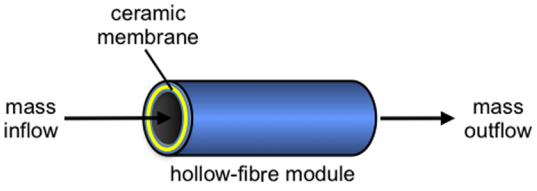


Figure 2.6 A hollow-fibre membrane module with a single input and output.

a system by a so-called macroscopic mass balance approach. To do so, we must control the membrane's module input and output, as shown in Figure 2.6.

Looking at Figure 2.6 we can formulate the most basic principle of mass conservation – possible changes in concentration of A at the entrance to and the exit from a membrane module are due to the accumulation of A within the module plus any chemical reaction that can produce or consume A:

$$\left\{\begin{array}{c}\text{rate}\\ \text{of mass}\\ \text{inflow}\end{array}\right\} - \left\{\begin{array}{c}\text{rate}\\ \text{of mass}\\ \text{outflow}\end{array}\right\} = \left\{\begin{array}{c}\text{rate}\\ \text{of mass}\\ \text{accumulation}\end{array}\right\} - \left\{\begin{array}{c}\text{rate}\\ \text{of chemical}\\ \text{production}\end{array}\right\} \tag{2.64}$$

Here the rate of mass inflow through an element dS of the cross section can be expressed as

$$\left\{\begin{array}{c}\text{rate}\\ \text{of mass}\\ \text{inflow at d}S\end{array}\right\} = \rho_{\mathrm{A,in}} v_{\mathrm{A,in}}\, \mathrm{d}S \tag{2.65}$$

and the rate of mass outflow can be expressed as

$$\left\{\begin{array}{c}\text{rate}\\ \text{of mass}\\ \text{outflow at d}S\end{array}\right\} = \rho_{\mathrm{A,out}} v_{\mathrm{A,out}}\, \mathrm{d}S \tag{2.66}$$

where dS is an element of a surface through which A enters or exits the membrane module. Note that the actual surface through which A enters and exits the membrane module can be different, so we are better off expressing the total inflow/outflow in terms of mass, rather than concentration. Any accumulation of A occurs inside the membrane module, and is therefore expressed by units of volume V:

$$\left\{\begin{array}{c}\text{rate}\\ \text{of mass}\\ \text{accumulation}\end{array}\right\} = \frac{\partial}{\partial t}\iiint \rho_{\mathrm{A}}\, \mathrm{d}V \tag{2.67}$$

Incorporating Eqs. (2.64)–(2.67) into a single equation and ignoring for now the possibility of the chemical reaction within a module, we derive the mass conservation law in the integral form that reads

$$\iint \rho_{\mathrm{A}}\, \mathrm{d}S = \frac{\partial}{\partial t}\iiint \rho_{\mathrm{A}}\, \mathrm{d}V \tag{2.68}$$

This integral might look daunting, but in fact it is fairly simple. The changes in concentration of A as it passes through a membrane module are due to its accumulation. That macroscopic approach to the mass balance takes the membrane module as a 'black box' having no interest in the internal processes. While in process engineering this approach can be useful, it might not be the best option for predicting internal processes. A more useful and very popular approach defines a certain volume within the module and applies the same mass balance on it. This volume is called the *control volume*, probably because historically it was the volume that one could control. Now it is a region of space in which the conditions of mass, energy and momentum conservation are valid. Most textbooks on mass transfer draw the control volume as a cube with three couples of parallel surfaces (called *control surfaces*). The reason for choosing a cube is that we are more familiar with Cartesian coordinates than with spherical or cylindrical ones. For a hollow fibre (see Figure 2.6), the control volume will lie just inside the geometrical dimensions of the module and will have cylindrical coordinates.

Basically, the microscopic approach accounting for the next rate of mass efflux, accumulation and reaction within the control volume is similar to Eq. (2.68):

$$\nabla J_{\mathrm{A}} + \frac{\partial \rho_{\mathrm{A}}}{\partial t} - r_{\mathrm{A}} = 0 \tag{2.69}$$

or, using partial derivatives and cylindrical coordinates,

$$\left[\frac{1}{r}\frac{\partial}{\partial r}(rJ_{\mathrm{A},r}) + \frac{1}{r}\frac{\partial J_{\mathrm{A},\theta}}{\partial \theta} + \frac{\partial J_{\mathrm{A},z}}{\partial z}\right] + \frac{\partial \rho_{\mathrm{A}}}{\partial t} - r_{\mathrm{A}} = 0 \tag{2.70}$$

Here the only unknown term is r_{A}, which is the rate of the chemical reaction that produces A within the control volume. The minus sign in front of r_{A} denotes that A has been produced, while the plus sign in front of the accumulation means that A is accumulated within the membrane volume.

Deriving the microscopic mass balance equation is beyond the scope of this book (for an excellent rigorous explanation, see Ref. [2]). Instead, we will describe several special forms of Eq. (2.69), which are useful for understanding the transfer of A within membrane modules. Here we will use several approximations (each following approximation already includes all the previous ones).

If there is no homogeneous reaction that occurs uniformly within the given membrane module, $r_{\mathrm{A}} = 0$ and Eq. (2.69) becomes

$$\nabla J_{\mathrm{A}} + \frac{\partial \rho_{\mathrm{A}}}{\partial t} = 0 \tag{2.71}$$

If the diffusion coefficient does not change within the membrane module, Eq. (2.71) becomes

$$\nabla(\rho_{\mathrm{A}} v) + \frac{\partial \rho_{\mathrm{A}}}{\partial t} - D_{\mathrm{AB}} \nabla^2 \rho_{\mathrm{A}} = 0 \tag{2.72}$$

To derive Eq. (2.72), we used the definition of flux from Eq. (2.22) and Fick's first law of diffusion denoted in Eq. (2.25). If the density of the bulk can be assumed

constant ($\nabla\rho = 0$), Eq. (2.72) can be written as

$$v\nabla\rho_A + \frac{\partial\rho_A}{\partial t} - D_{AB}\nabla^2\rho_A = 0 \tag{2.73}$$

In addition, if there is no fluid motion ($v = 0$) and A is transferred by the diffusion only, Eq. (2.73) reduces to

$$\frac{\partial\rho_A}{\partial t} = D_{AB}\nabla^2\rho_A \tag{2.74}$$

Equation (2.74) is also called *Fick's second law of diffusion* and predicts how diffusion will change the concentration of A with time. The assumption of no fluid motion restricts its applicability to diffusion in solids and stationary liquids. An additional case where the Fick's second law is applicable is binary mixtures of gases and liquids undergoing counterdiffusion, that is when the fluxes of A and B are equal in magnitude but in opposite directions [2].

Equation (2.74) can be simplified further under the assumption of a *steady-state* condition. At steady state, the concentrations remain constant, $\partial\rho_A/\partial t = 0$ and the equation reduces to

$$D_{AB}\nabla^2\rho_A = 0 \tag{2.75}$$

This is the simplest form of the mass balance equation that is relatively easily transformed into Fick's first law of diffusion (Eq. (2.25)) by marking the first unknown integration constant j_A. If no steady-state condition can be assumed, we can solve Fick's second law of diffusion only by assuming that at time zero $p_A(z, 0) = p_{A0}$ for all z.

Working Example 2.3

Find an expression for a diffusional flux of hydrogen through flat-sheet ceramic membrane.

Solution

Consider a flow parallel to the membrane surface as shown in Figure 2.6. Although the transport of the feed gas is parallel to the x-axis, the transfer of hydrogen molecules occurs only along the z-axis. Then, assuming that the steady-state condition applies, Eq. (2.75) for one-dimensional diffusion can be written as

$$-D_{AB}\frac{d^2\rho_A}{dz^2} = 0 \tag{2.76}$$

After two integrations assuming a linear flow, the general integral form of Eq. (2.76) is

$$D_{AB}\rho_A = C_1 z + C_2 \tag{2.77}$$

where C_1 and C_2 are two undefined constants. To define them we will apply two first-type boundary conditions

$$\text{at} \quad z = 0 \quad p_A = p_{A1} \tag{2.78}$$

$$\text{at} \quad z = \delta \quad p_A = p_{A2} \tag{2.79}$$

A separate substitution of the boundary conditions into Eq. (2.77) gives

$$\rho_A = \frac{\rho_{A2} - \rho_{A1}}{L} z + \rho_{A1} \tag{2.80}$$

Now, using Fick's first law of diffusion (Eq. (2.25)), we can then determine the diffusional flux through the membrane as

$$j_A = -D_{AB} \frac{\partial \rho_A}{\partial z} = D_{AB} \frac{\rho_{A1} - \rho_{A2}}{L} = D_{AB} \frac{\Delta \rho_A}{L} \tag{2.81}$$

This basically says that H_2 diffuses through the membrane of thickness δ with a flux that is proportional to the concentration difference $\Delta\rho_A$. The diffusion occurs when the concentration in the feed is higher than that in the permeate, that is when $p_{A1} > p_{A2}$ (note that we changed the variables in Eq. (2.81) to obtain a positive expression).

2.5 Convective Mass Transfer

Defining convection as the movement of a fluid due to an external force (such as gravity), we still focus on A molecules. The convection mass transfer problem appears when the concentration of A changes *during the transfer*. In such cases, we must understand what is the nature of change and what is the average concentration of A that will be transferred. We will restrict our discussion to steady-state situations (no change in time) and systems of one or two dimensions. But what causes this change in the concentration of A during the transfer? It is the difference in concentration of A at two points along its diffusion path that causes a 'rush' towards a low concentration point? When and how does that happen? There are three scenarios: (i) the release or accumulation of A from the surface, (ii) a chemical reaction or aggregation that results in more/less A in the bulk and (iii) passage of A between two relatively immiscible moving fluids (in all these situations we assume that the system remains monophasic at all times).

Several textbooks on mass transfer discuss problems that arise in the passage of A to/from a surface, indicating that the concentration on the surface $\rho_{A,s}$ is different from the concentration in the bulk $\rho_{A,\infty}$ [4,15]. Under steady-state conditions, the concentrations $\rho_{A,s}$ and $\rho_{A,\infty}$ should equalize soon after the diffusion starts. That does not happen because a conventional flow brings new 'chunks' of a moving fluid with $\rho_{A,\infty}$ and because A molecules on the surface undergo changes (physisorption, chemisorption, reaction and/or extraction). The implications of these changes are beyond the scope of this book (what happens on the

surface stays on the surface). The implications of these changes are beyond the scope of this book. It is a steady consumption/generation of A at the final destination of the diffusional path that keeps the concentration of A constantly lower than the concentration in the diffusional departing point. In other words, despite the diffusion, the concentrations of A in the bulk and on the surface remain constant.

Thus, we can calculate the mass flux of A due to diffusion as

$$J_A = K_c \Delta\rho_A \tag{2.82}$$

Here J_A is the mass flux of species A, measured relative to fixed spatial coordinates, $\Delta\rho_A$ is the concentration difference and K_c (m/s) is the convective mass transfer coefficient. To find a similarity between Eqs. (2.81) and (2.82) for the molecular diffusion, we can substitute K_c by a diffusional mass coefficient D_{AB}/L. This substitution is valid only when A is transferred by diffusion. In many cases, the transfer is a complex mix of diffusion and convection, and K_c therefore can be viewed as a more general term. But calculating this K_c is no mean task. In convective mass transfer the diffusional path is less known and depends on surface geometry, surface composition, the fluid composition, velocity, and physical properties. In many problems, K_c is linked to the geometry of the surface and its size. That type of problem is usually two-dimensional when the feed fluid travels along the X-axis and A diffuses along the Z-axis (see Figure 2.7). When both the convection and the diffusion are along the same axis, the relative importance of diffusion is assessed through the Peclet number, defined as

$$Pe = \frac{\text{convection factor}}{\text{diffusion factor}} = \frac{Lv_\infty}{D_{AB}} \tag{2.83}$$

where L is the membrane thickness of flat-sheet membrane in the direction of flow and v_∞ is the free-stream fluid velocity. If $Pe \ll 1$, the convection can be neglected. If $Pe \gg 1$, the diffusion can be neglected. When the convection is

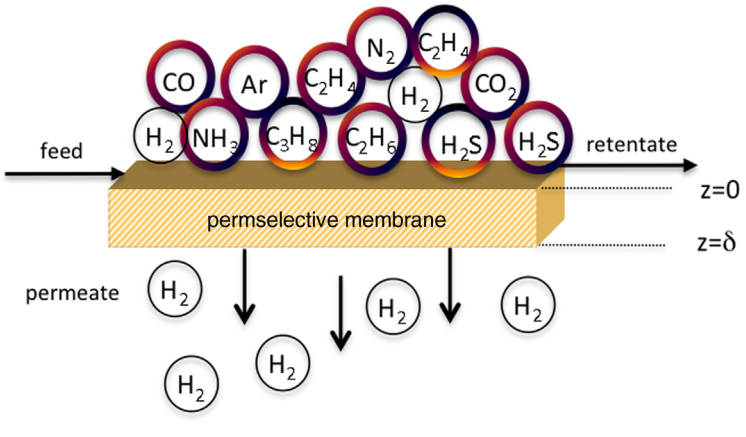


Figure 2.7 Diffusion of gases through a permselective ceramic membrane.

along the X-axis and diffusion is along the Z-axis, we arrive at the classical two-dimensional convection mass transfer problem.

2.5.1 Momentum and Mass Diffusivity Profiles

Previously, we defined the diffusional mass transfer phenomena as the situation where the concentration of A is small enough so that it does not influence the bulk properties of B. This applies also to the convective mass transfer and to calculations of K_c. All the calculations consider only the cases where the concentration of A is small. For example, when water molecules evaporate from a reservoir into air at room temperature, the air specific humidity (the capacity to hold water vapour) is 15 g of water per kg of air. That is a relatively minor amount and diffusing water molecules have a minor influence on the bulk properties of the air. Conversely, when the evaporation is at boiling temperature, the specific humidity rises to 762 g/kg. That is a high mass transfer rate that results from a very active boundary layer. This so-called Couette flow problem is solved first for impermeable walls with the same geometry and flow conditions. The low mass transfer rate coefficients K_c are then correlated for high mass transfer rates [29,30].

Solving a transfer problem for a simplified situation and then implying that the solution fits in a more complicated situation is a common approach in convective mass transport. Diffusion of momentum and heat are one-variable problems and in that respect are simpler than mass transfer cases. Many of these problems were solved before, and if the surface geometry and flow conditions in these problems match those of mass transfer problems, analytical solutions for momentum or heat diffusion are reassigned to mass transfer. The similarity in flow conditions is assessed through momentum, mass and thermal diffusivity using dimensionless numbers such as the *Lewis number*, *Le*, that links thermal and mass diffusivities, and the *Schmidt number*, *Sc*, that suggests a relation between momentum and mass diffusivities:

$$Le = \frac{\text{thermal diffusivity}}{\text{mass diffusivity}} = \frac{k}{\rho C_p D_{AB}} \tag{2.84}$$

$$Sc = \frac{\text{momentum diffusivity}}{\text{mass diffusivity}} = \frac{\mu}{\rho D_{AB}} \tag{2.85}$$

In these equations, C_p is the molecular heat capacity, k is thermal conductivity, ρ is the fluid density and μ is the viscosity. The similarity between these diffusivities is often exemplified by concentration and velocity profiles for a fluid flowing past a solid surface. Figure 2.8 shows a development of a velocity profile near a stationary surface. The velocity profiles follow the no-slip condition at a stationary wall. The layer of fluid adjacent to the wall has the same velocity as the wall itself (the wall is stationary, so the relative velocity in the layer is zero). A layer next to the stationary layer has some velocity, which due to a friction is smaller than the average velocity in the bulk. This build-up of retarded layers continues,

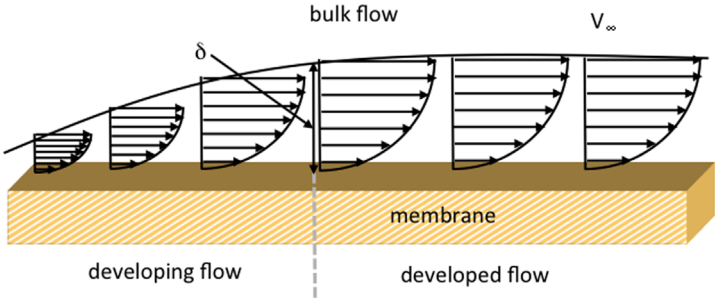


Figure 2.8 Development of the momentum boundary layer drawn in a form of streamlines (line-drawn tangents to the velocity vector at each point in a flow field).

until at a certain distance δ from the surface the velocity equals the bulk velocity, v_∞. Such an imaginary view on the development of velocity profile from a surface into a bulk illustrates the presence of a *boundary layer*, a concept introduced by Prandtl in 1904 [31]. According to Prandtl's hypothesis, there is a thin layer near the surface with no significant changes in pressure across it. The Navier–Stokes equation is thus simplified to include only velocity gradients and can be solved analytically.

The flow regime in the boundary layer is considered laminar. This concept of ordered or chaotic flow pattern in a response to a flow situation was introduced by Stokes and popularized by Reynolds. The famous *Reynolds number*, *Re*, differentiates between laminar, transient and turbulent flow regimes (Eq. (2.86) and Figure 2.9).

$$Re = \frac{vL\rho}{\mu} \tag{2.86}$$

Here v is the relative velocity of the object under consideration, L is the characteristic linear dimension in a direction of the movement (such as travelled length of the fluid or hydraulic diameter), μ is the dynamic viscosity of the fluid and ρ is its density. The laminar flow over a surface is characterized by a developing velocity profile. In a turbulent flow, the velocity is constant for all but the boundary layer.

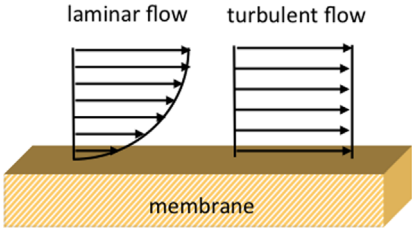


Figure 2.9 Laminar (left) and turbulent (right) flow regimes.

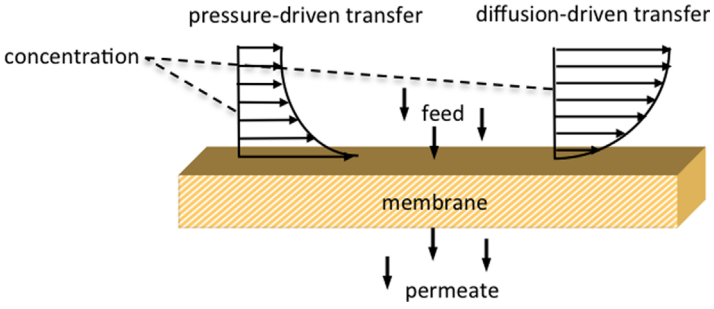


Figure 2.10 Concentration profiles near a membrane surface for a pressure-driven (left) and a diffusion-driven (right) transfer.

The boundary layer approach was so successful that it was implemented for visualizing concentration profiles, despite the fact that concentration is a scalar with no vector component. Figure 2.10 shows different types of concentration boundary layers near a stationary wall. The thickness of a boundary layer increases as a fluid flows downstream until it reaches a constant asymptotic value. This differentiates between the boundary layer and the bulk (where the concentration of A is constant). There are two typical concentration profiles. In *pressure-driven processes*, the convective flow towards the membrane results in higher concentrations of A near the membrane surface. In *diffusion-driven processes*, the concentration near the membrane is lower than that in the bulk for diffusion to occur. Comparing the transport through the boundary layer with transport through the membrane, we see that in pressure-driven processes (MF, UF, NF, RO) the transport through the boundary layer is faster. Conversely, in diffusion-driven processes (gas separation, pervaporation, dialysis, electrodialysis), the transport through the membrane is faster.

2.6
Fluxes of Liquids through Porous Membranes

2.6.1
The Flux of Pure Solutes

The transport of A through a porous membrane is described by two variables – the concentration of A at any point in the bulk and the transmembrane flux. This seems simple, yet there is no single model that can predict both values and how they change. In this section, we will explain some simple modelling approaches that form the basis of membrane terminology and common concepts. We will refer to these concepts in Chapter 3 describing methods for pore size detection and in Chapter 4 when we deal with practical applications of ceramic membranes. Fundamental studies on transport phenomena in membranes can be found elsewhere [32,33].

Porous ceramic membranes are typically MF and UF membranes that have pores in sizes between 2 nm and 10 μm. The flux through the membranes is convective and could be marked as J_{A+B}, a flux of the entire mixture. However, we use the standard denomination J instead. The liquid flux is displayed in units of volume per unit area per unit time such as litres per square meter per hour (LMH) or gallons per square foot per day (GFD). There are two basic concepts in the transport through porous membranes. The membrane is viewed as a series of cylindrical pores or the packed medium that has transferable tortuous routes. The respective Hagen–Poiseuille and Carman–Kozeny equations are simple yet helpful and useful for determining which structural parameters are important and how the membrane performance can be improved. For example, one of the main methods for determining pore sizes is based on the liquid permeance through a membrane. An average pore diameter is then calculated based on Hagen–Poiseuille and Carman–Kozeny equations (Section 3.2.1).

Darcy offered the first and the most basic equation describing filtration through packed media,

$$J = \frac{k}{\mu}\frac{\Delta P}{L} \tag{2.87}$$

where J is the permeate flux ($m^3/(m^2\ s)$), k is the intrinsic permeability of the medium (m^2), μ is the liquid dynamic viscosity (Pa s), ΔP is the pressure difference on both sides of a medium (Pa) and L is the length over which the pressure drop occurs (m). Darcy's law states that the transmembrane flux is proportional to the driving force, that is the pressure difference ΔP across the membrane of thickness L, and inversely proportional to the fluid viscosity μ. Further models give more details on k, yet still keeping the dependence of flux on ΔP, L and μ. The medium permeability k is used for comparing performances of various membranes.

Similarly, the *Hagen–Poiseuille equation* describes the membrane as the media that possess ideal pores. The pores are cylindrical, uniformly distributed and evenly sized, parallel to each other and perpendicular to the membrane surface. Such ideal pores do not interact with A and do not prevent the passage of B. The volume flux through these pores is then described by

$$J = \frac{\varepsilon d_p^2}{32\mu}\frac{\Delta P}{\Delta x} \tag{2.88}$$

where d_p is the pore diameter (in case of pore size distribution, the mean pore diameter), μ is the fluid viscosity, Δx is the pore length (that here equals the membrane thickness) and ε is the surface porosity of the membrane. Figure 2.11 shows schematically the pore parameters.

Later, Carman and Kozeny [34,35] simplified the membrane in this concept down to liquid-transportable voids between well-packed spheres. The flux through the porous structure then becomes

$$J = \frac{\varepsilon^3}{\Phi_s \mu S(1-\varepsilon^2)}\frac{\Delta P}{\Delta x} \tag{2.89}$$

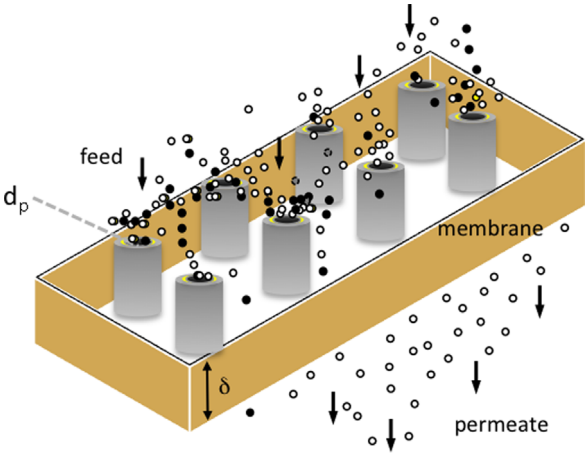


Figure 2.11 Schematic side view of a membrane with ideal cylindrical pores, uniformly distributed and evenly sized, parallel to each other and perpendicular to the membrane surface. These pores form the basis of the Hagen–Poiseuille flux equation.

where S is the total surface membrane pore area (m), Φ_s is the sphericity of grains in the packed bed and ε is the porosity. In reality, ideal pores and ideal spheres are rare. According to the original Kozeny theory, sphericity is a value between 0 and 1 that expresses how close the main form of grains in the construct is to perfect spheres. Values suggested by Kozeny are 0.5 for circle cross sections, 0.562 for squares, 0.592 for equilateral triangles and 0.66 for thin slots. Carman, however, claimed that the value of 0.2 gives the best fit with experimental results [35].

2.6.2 The Flux of Mixtures

Previous models viewed the feed as a homogeneous fluid. In these models, the flux of the fluid through the membrane depends mainly on the membrane parameters such as pore diameter, grain sphericity, membrane thickness, total surface membrane pore area and porosity. Accordingly, operational variables include a pressure drop and the liquid dynamic viscosity. The membrane resistance is low and consequently the pure solvent flux is high. Fluxes higher than 500 l/(m^2 h bar) for MF and 200–500 l/(m^2 h bar) for UF are normal. In separation of A + B mixtures, the flux is much lower and also deteriorates with time. The deterioration can be so severe that the flux could drop to 5% of its initial value. These pure liquid models are therefore useful for evaluating fluxes of pure solutes and the initial flux of mixtures. Other models are needed to describe when a mixture of A + B passes through a membrane. The free passage of B through the membrane leads to a different mixture in the permeate with low concentrations of A. Thus, the concentration of A at the feed side constantly

increases as part of B in the mixture becomes constantly smaller. Depending on the flow conditions, as well as on the nature of A and its concentration, A can

- pass through the membrane along with B,
- remain near the membrane feed side or diffuse back to the bulk (polarization), or
- become attached to the membrane surface or within membrane pores (fouling).

Here we will discuss briefly the second and third options in terms of concentration polarization, resistance-in-series and pore blocking models.

2.6.2.1 The Concentration Polarization Model

The free passage of B through the membrane increases the concentration of A near the feed side. A build-up of concentration difference will generate a diffusive flow of A back to the bulk that after a certain period will reach a steady state with constant convective and diffusive mass fluxes to and from the membrane, respectively. Simultaneously, the flux through the membrane in systems operated in constant-pressure mode deteriorates. This is due to the formation of a secondary layer of A that decreases the driving force for the bulk transfer, and can be attributed either to concentration polarization or to fouling. When the deterioration is accompanied by the increase in concentration of A in the permeate (since many membranes only give a certain retention percentage), the concentration polarization is the most likely cause, and we will focus our attention on this aspect.

The first model accounting for the deteriorating flux in UF membranes was the gel polarization model [36]. Here, the membrane permeation rate is limited by the presence of a gel layer deposited on the surface. The layer increases the effective membrane thickness and reduces its hydraulic permeability. According to Field *et al.* [37], there exists a certain *critical flux*, J_{crit}, above which the permeability of the membrane is independent of the applied TMP. This is due to the formation of a thick secondary or gel layer. If that is correct, the bulk flow through the membrane can be calculated on the basis of the membrane-retained species A. The species experience two processes – convection towards the membrane and diffusion back to the bulk. At its simplest interpretation, the flux J_A brought to the membrane surface by convection is equal to the diffusive flux back. This is a variation of Eq. (2.73) with the assumptions of *steady state* and *unidimensionality*, where J_A is integrated once in limits between J_A in the bulk and 0 on the surface:

$$\rho_A J_A - D_{AB} \frac{d\rho_A}{dx} = 0 \tag{2.90}$$

Variable separation and integration gives

$$J_A x \Big|_0^{\delta} = D_{AB} \ln \rho_A \Big|_{\rho_{A,\infty}}^{\rho_{A,s}} \tag{2.91}$$

or

$$J_A = \frac{D_{AB}}{\delta} \ln \frac{\rho_{A,s}}{\rho_{A,\infty}} \tag{2.92}$$

Here δ is the thickness of the boundary layer over which the concentration of the solute varies. The quotient D_{AB}/δ is the diffusional mass transfer coefficient K_c described earlier, and is also known as the concentration polarization mass transfer coefficient. Equation (2.92) describes the flux near an impermeable membrane and gives a little information about the permeate flux. To gain more information, we need a mass balance equation that includes the flux on the permeate side:

$$\rho_A J_A - D_{AB} \frac{d\rho_A}{dx} = \rho_{A,p} J_A \tag{2.93}$$

where $\rho_{A,p}$ is the concentration of A in the permeate. The concentration polarization model is visualized in Figure 2.12.

The solution of Eq. (2.93) differs only slightly from that of Eq. (2.92) because $\rho_{A,p}$ is assumed to be constant,

$$J_A = \frac{D_{AB}}{\delta} \ln \left(\frac{\rho_{A,s} - \rho_{A,p}}{\rho_{A,\infty} - \rho_{A,p}} \right) \tag{2.94}$$

or

$$\frac{\rho_{A,s} - \rho_{A,p}}{\rho_{A,\infty} - \rho_{A,p}} = \exp \left(\frac{J_A \delta}{D_{AB}} \right) \tag{2.95}$$

The above discussion may seem fundamental, yet these equations have important practical applications. CP depends on two factors – flow parameters such as J and $\rho_{A,p}$, and hydrodynamics (D_{AB} and δ), and it can be mitigated. It is severe in MF and UF both because J is high and D_{AB} is low. The average D_{AB} values of retained macromolecules are estimated as 10^{-10} to 10^{-11} m^2/s. The effect of CP is less severe

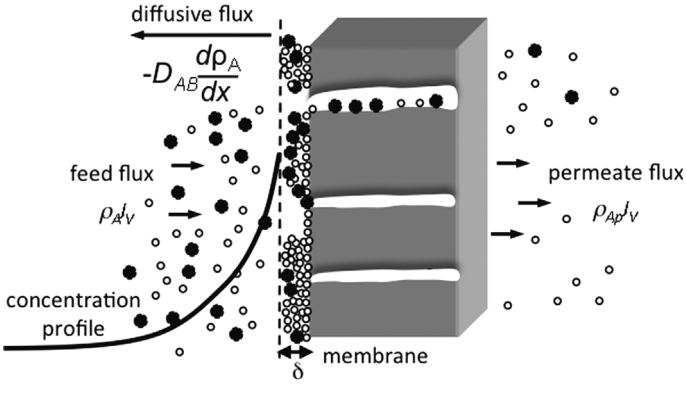


Figure 2.12 Schematic representation of feed, permeate and diffusion fluxes in the concentration polarization model near a porous membrane surface.

in RO membranes because J_V is lower and the average D_{AB} of small solutes is in the order of 10^{-9} m^2/s. In gas separation and pervaporation, CP is negligible [38].

CP does not exist when $\rho_{A,s}/\rho_{A,\infty} \leq 1$ and becomes increasingly bothersome when $\rho_{A,s}/\rho_{A,\infty} \gg 1$. Thus, increasing cross-flow velocity to decrease δ or heating the water to increase D_{AB} can decrease the CP influence. The latter method is problematic, however, due to a higher energy demand and expected higher flux J that will in parallel increase $\rho_{A,s}$. Alternatively, one can use short modules where the developing flow regime with lower L will be more significant. In RO membranes, the CP influence is decreased by using spacers – porous structures that where separate two membranes and induce local turbulent streams.

Sometimes the CP mass transfer coefficient K_c is found through the *Sherwood number*, *Sh*, that represents the ratio between convective and diffusion factors,

$$Sh = \frac{\text{convection transport}}{\text{diffusion transport}} = \frac{K_c d_H}{D_{AB}} \tag{2.96}$$

Here d_H is the hydraulic diameter calculated as four times the cross section available for flow divided by wetted perimeter of the channel [38]. It equals $\pi d/4$ for cylindrical pores and d for tubes and circular cross sections [39]. For slits of width a and height b, we get

$$d_H = 4\frac{ab}{2(a+b)} \tag{2.97}$$

that transforms into $d_H = 2b$ when $a \gg b$ [38]. When the information about pore size is unavailable, Rene and Lalande [40] propose using $16/Re$ for a laminar flow regime and

$$d_H = 0.046\left(\frac{1}{1-\psi}\right)^{4.8} Re^{-0.2} \tag{2.98}$$

for a turbulent one. Here ψ is the 'equivalent roughness parameter' ($\psi = 0$ for smooth surfaces).

Several dozen correlations for laminar and turbulent flows were proposed [41]. Here we present a few of the most widely used ones [38].

For laminar flow conditions ($Re < 1800$):

$$\text{(Grober)} \quad Sh = 0.664 Re^{0.5} Sc^{0.33} \left(\frac{d_H}{L}\right)^{0.5} \tag{2.99}$$

$$\text{(Graetz}-\text{Leveque)} \quad Sh = 1.86 Re^{0.33} Sc^{0.33} \left(\frac{d_H}{L}\right)^{0.33} \tag{2.100}$$

For turbulent flow conditions ($Re > 2000$–4000):

$$\text{(Chilton}-\text{Colburn)} \quad Sc < 1, \quad Sh = 0.023 Re^{0.8} Sc^{0.33} \tag{2.101}$$

$$\text{(Deissler)} \quad 1 \leq Sc \leq 1000, \quad Sh = 0.023 Re^{0.875} Sc^{0.25} \tag{2.102}$$

The example below shows how such models are used for predicting the flux through a porous membrane.

Working Example 2.4

Membralox® GP membranes (Pall Exekia, France) are used for concentrating proteins out of milk at room temperature. In the process, the typical protein concentrations in the bulk, near the membrane surface and in the permeate are 33, 200 and 5 g/l, respectively. The milk density is 1030 kg/m^3, its dynamic viscosity is 10^{-3} kg/(m s) and diffusivity of proteins is 10^{-10} m^2/s. Based on these data, calculate the expected flux for a 1.5 m hollow-fibre membrane module containing 1000 capillaries, each 0.9 mm in diameter, given that the cross-flow rate in the module is 45 l/min (if you are interested in more details on the milk separation process, see the applications section in Chapter 4).

Solution

We will have to find a K_c from *Sh*, and for that we will calculate *Re* and *Sc* first. The cross-flow velocity is

$$v = \frac{Q}{[(\pi d^2)/4]n} = \frac{45 \times 10^{-3}\,[\mathrm{m^3/min}]}{[\pi(9 \times 10^{-4}\,[\mathrm{m}])^2/4] \times 1000} = 70.7\,\left[\mathrm{m/min}\right]$$

$$= 1.18\,\left[\mathrm{m/s}\right] \tag{2.103}$$

and therefore the Reynolds number is

$$Re = \frac{vd\rho}{\mu} = \frac{1.18\,[\mathrm{m/s}] \times 9 \times 10^{-4}\,[\mathrm{m}] \times 1030\,[\mathrm{kg/m^3}]}{10^{-3}\,[\mathrm{kg/(m\ s)}]} = 1093 \tag{2.104}$$

and the Schmidt number is

$$Sc = \frac{\mu}{\rho D_{AB}} = \frac{10^{-3}\,[\mathrm{kg/(m\ s)}]}{1030\,[\mathrm{kg/m^3}] \times 10^{-10}\,[\mathrm{m^2/s}]} = 9708 \tag{2.105}$$

The calculated *Re* value indicates a laminar flow regime and we can use Eq. (2.100) to calculate the Sherwood number:

$$Sh = 1.86 Re^{0.33} Sc^{0.33} \left(\frac{d_H}{L}\right)^{0.33}$$

$$= 1.86 \times 1093^{0.33} \times 9708^{0.33} \left(\frac{9 \times 10^{-4}\,[\mathrm{m}]}{1.5\,[\mathrm{m}]}\right)^{0.33} = 33.48 \tag{2.106}$$

and now, using the definition in Eq. (2.96),

$$K_c = \frac{Sh\, D_{AB}}{d_H} = \frac{33.48 \times 10^{-10}\,[\mathrm{m^2/s}]}{9 \times 10^{-4}\,[\mathrm{m}]} = 3.72 \times 10^{-6}\,\left[\mathrm{m/s}\right] = 13.4\,\left[\mathrm{l/(m^2\ h)}\right] \tag{2.107}$$

And finally using Eq. (2.94), we can obtain the flux *J*:

$$J = K_c \ln\left(\frac{\rho_{A,s} - \rho_{A,p}}{\rho_{A,\infty} - \rho_{A,p}}\right) = 13.4 \ln\left(\frac{200 - 5}{33 - 5}\right) = 26\left[\frac{L}{\mathrm{m^2 \bullet h}}\right] \tag{2.108}$$

2.6.2.2 The Resistance-in-Series Model

Previously, we described fouling and concentration polarization as two independent phenomena. This is not strictly true. Fouling can result from CP when a solute A near the membrane interacts with membrane surface. The interactions depend on both A and the membrane, and can lead to fouling via adsorption, cake formation and pore plugging (see Figure 2.13).

All these mechanisms have at least one thing in common: They reduce the convective flux J_A by separating A from the bulk. According to Eq. (1.6), this flux reduction can be expressed through resistances to the transmembrane flux. Equation (1.5) shows that the total membrane resistance R_t can be divided into membrane intrinsic resistance R_m and operational resistance R_o. The operational resistances are not mutually exclusive and the flux definition can be further detailed to include adsorption resistance R_a, cake formation resistance R_c and pore blocking resistance R_p as in

$$J = \frac{\mathrm{TMP} - \Delta\pi}{\mu(R_m + R_a + R_c + R_p)} \tag{2.109}$$

where $\Delta\pi$ is the osmotic pressure difference across the membrane. Alternatively, operational resistances can be divided into internal and external, or reversible and irreversible, or backwashable and backwash-resistant ones [42].

In the ideal case, the total resistance equals R_m only. The adsorption resistance R_a takes place both on the outer surface and in the pores. It is due to hydrophobic interactions, polar interactions and charge transfers, and begins as soon as the membrane comes in contact with the feed solution. Similarly, pore blocking is mainly attributed to colloidal fouling when the colloids penetrate into the membrane, increasing the contribution of R_p. The cake resistance R_c is a cumulative term for CP, gel polarization and cake formation. Its main contributors are the possible transition of CP into a gel layer when the flux exceeds the critical

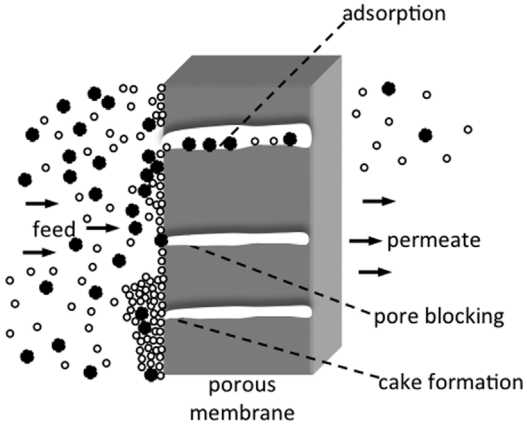


Figure 2.13 Fouling by adsorption, pore blocking and cake formation in convective transport of A through pressure-driven porous ceramic membrane.

flux J_{crit} value and the inability to evaluate to what extent the cake interacts with the membrane surface.

There are two interesting approaches for assessing the influence of each of these fouling mechanisms on the flux drop. The first is evaluating the relative importance of each fouling mechanism by running experiments under various conditions. For example, the intrinsic membrane resistance can be found by filtering pure water, where no fouling is expected. Similarly, reversible forms of fouling such as pore blocking are determined by backwashing of the membrane followed by flux measurements, while irreversible ones are determined by chemical cleaning followed by the flux measurements. The resistances have $[L^{-1}]$ dimensions and typical values of $10^{11}\ m^{-1}$ in advanced wastewater treatment [43]. Resistance values can grow exponentially with filtration time.

The second approach assesses the relative importance of each fouling mechanism by fitting the flux drop, assuming that the flux–time plot follows a power law. Resistances increase with time and a timely assessment can prevent or minimize their negative impact. This approach was suggested by Hermia [44] and further developed by Field *et al.* [37]. It is mostly valid for colloidal particles, under the assumption that such particles can block the pores, thus causing internal fouling.

2.6.2.3 The Pore Blocking Model

According to Hermia [44], the fouling for all types of constant-pressure filtrations can be expressed as

$$\frac{d^2t}{dV^2} = K_0\left(\frac{dt}{dV}\right)^n \tag{2.110}$$

where V is the volume of accumulated filtrate per unit of filter area, t is the filtration time and K_0 is a kinetic constant. The values of n, type of fouling and its definition are provided in Table 2.1.

The implementation of Eq. (2.110) in practice was suggested by Field *et al.* [37] in a form of definition of $dV/dt = J$. The substitution of the definition into the equation gives

$$\frac{d^2t}{dV^2} = \frac{d}{dV}\left(\frac{dt}{dV}\right) = \frac{d}{dV}\left[d(1/J)\right] = -\frac{1}{J^2}\frac{dJ}{dt}\frac{dt}{dV} = -\frac{1}{J^3}\frac{dJ}{dt} \tag{2.111}$$

Table 2.1 Fouling mechanisms and their definitions as provided by Hermia [44].

Fouling type		Value of *n*
Complete blocking	Every retained particle acts to block a pore	2
Intermediate blocking	Particles will probably block the pores	3/2
Internal pore plugging	Adsorption of particles inside the pores that narrows their width	1
Cake formation	Does not block the pores	0

and then

$$-\frac{1}{J^3}\frac{\mathrm{d}J}{\mathrm{d}t} = K_0\left(\frac{1}{J}\right)^n \tag{2.112}$$

Thus, the flux drop due to complete blocking is

$$J = J_0 \exp(-K_0 t) \tag{2.113}$$

And due to other mechanisms

$$J = J_0 a(-K_0 t)^{-n} \tag{2.114}$$

where a is equal to 2/3, 1/2 and 1/3 and n is equal to 2/5, 1/3 and 1/4 for intermediate pore blocking, internal pore blocking and cake formation, respectively. Another form of dependence, based on classic filtration equations, describes cake filtration as

$$J = \frac{J_0}{(1 + K_0 t)^n} \tag{2.115}$$

This differs from Eq. (2.109) by defining a constant initial membrane intrinsic resistance R_m. The cake resistance R_c can also be evaluated through the specific cake resistance, r_c, as

$$R_\mathrm{c} = L_\mathrm{c} r_\mathrm{c} \tag{2.116}$$

where L_c is the cake thickness. The specific cake resistance is often expressed by the Carman–Kozeny relationship

$$r_\mathrm{c} = 180\frac{(1-\varepsilon)^2}{d_\mathrm{s}^2 \varepsilon^3} \tag{2.117}$$

where d_s is the hydrodynamic diameter of A and ε is the porosity of the cake layer defined in Eq. (1.12). The thickness of the cake then becomes

$$L_\mathrm{c} = \frac{m_\mathrm{s}}{\rho_\mathrm{s}(1-\varepsilon)A} \tag{2.118}$$

where m_s is the mass of the cake, ρ_s is the density of the solute and A is the membrane area. The effective thickness of the cake layer is in the order of several micrometres and depends on operating condition and filtration time [45]. Figure 2.14 depicts the determination of two fouling mechanisms – complete pore blocking and cake formation based on the above approach [46].

2.7 Fluxes of Gases through Porous Membranes

Generally speaking, the same equations for pure solutes described in Section 2.6.1 apply also for pure gas fluxes. However, gas separation membranes usually have much smaller pores < 1 nm. In this range, the gases diffuse through the membrane. The diffusion occurs from high to low partial pressure and therefore requires pressure on the feed side of the membrane. There are four different

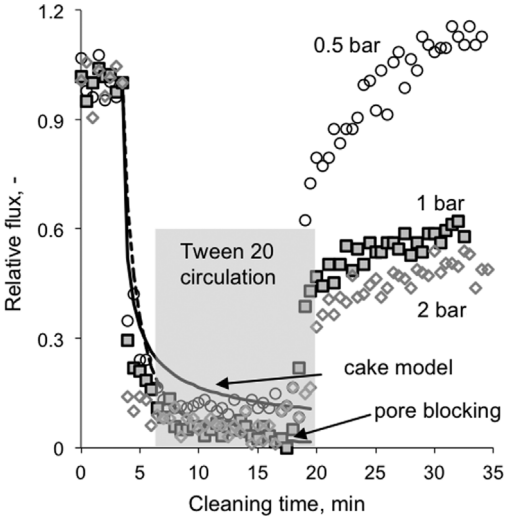


Figure 2.14 The recognition of pore blocking and cake formation in transmembrane flux drop through PES-30 plugged with Tween 20 micelles [46].

idealized gas transport mechanisms: *Knudsen diffusion*, *surface diffusion*, *capillary condensation* and *molecular sieving* [47]. Figure 2.15 shows the various transport mechanisms in porous membranes.

2.7.1 Knudsen Diffusion

Knudsen diffusion occurs when the pore size is larger than the molecule size but smaller than the mean free path of a molecule. On average, a diffusing molecule must collide with the pore wall many more times than with other molecules. Both A and B pass through the pore, but the flux of B is significantly higher. A is larger than B and on average will bump into the pore walls more times than B. In each molecule–wall collision, molecules lose momentum to the wall. Therefore, more collisions decrease the absolute velocity of A through the membrane. Gases will permeate through a membrane in proportion to their molecular velocity and, hence, in inverse proportion to the square root of their molecular weight.

According to Liepmann [48], Knudsen diffusion becomes important when $K_n > 100$, is larger than 100. According to Ho Bum Park, Kn should be larger than 5 [49]. Following Thornton *et al.* [50], Knudsen diffusion is important when $Kn > 1$. A borderline $Kn \sim 1$ is called the intermediate region between Knudsen diffusion and viscous flow. According to Li [51], Knudsen diffusion becomes important in microporous and mesoporous pores of 2–50 nm sizes. Following Keizer *et al.* [52], for nuclear fuel separation pore sizes have to be

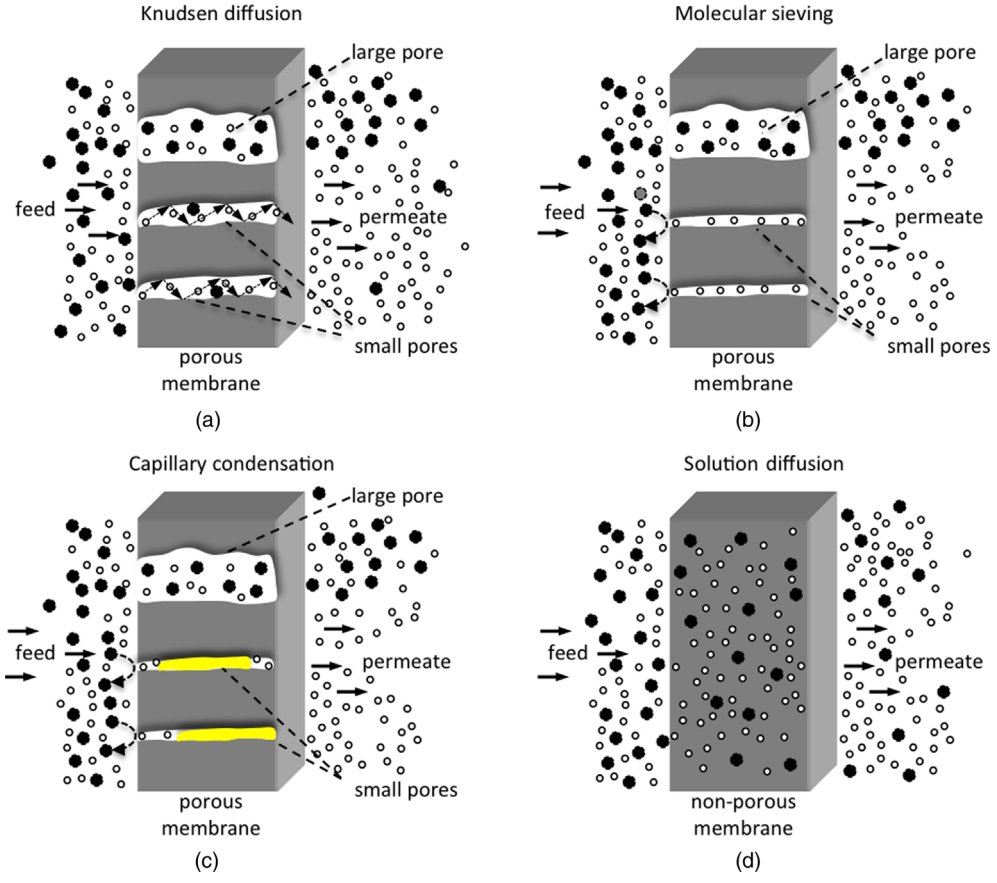


Figure 2.15 Transport mechanisms in gas separation through ceramic membrane: Knudsen diffusion (a), molecular sieving (b), capillary condensation (c) and solution diffusion (d).

between 2–200. The upper limit of 50 nm is applicable under standard conditions (100 kPa and 20 °C). Both definitions relate the Knudsen diffusion with the pore size and not with the membrane material. This explains how under standard conditions polymer membranes are equally applicable for gas separation and will be used when the temperature of the gas mixture is below 60 °C. Ceramic membranes will be used in mixtures under high pressure (up to 10 MPa) and temperature (up to 200 °C), as well as for separating radioactive and corrosive mixtures.

The most famous use of Knudsen diffusion was in the separation of gaseous uranium U-238 and U-235 isotopes for nuclear fuels in the so-called Manhattan Project in the 1940s and 1950s [53]. Natural uranium contains 0.7% of the U-235 isotope. The remaining 99.3% is mostly U-238 which does not contribute

Table 2.2 Values of separation factor α in separation of some typical gas mixtures by Knudsen diffusion.[a)]

Gas mixture	α
$U_{235}F_6/U_{238}F_6$	1.0036
O_2/N_2	0.94
CO_2/CH_4	0.60
CO_2/N_2	0.80
H_2/CH_4	2.83
He/CH_4	2.00
H_2/N_2	3.74
H_2/C_3H_8	4.69
H_2/C_6H_{12}	6.48

a) Data from Ref. [52].

directly to the fission process (though it does so indirectly by forming fissile isotopes of plutonium). Effective uranium enrichment should result in 3–5% U-235 in the fuel. The efficiency of separation was not very high, as can be seen from the values of the separation factor α shown in Table 2.2, and therefore today uranium enrichment is performed by centrifuging. Table 2.2 provides the theoretical separation factors calculated from

$$\alpha_{A/B} = \sqrt{\frac{MW_B}{MW_A}} \tag{2.119}$$

where MW_B and MW_A are the respective molecular weights of B and A [54].

From this table, we see that Knudsen diffusion is not a commercially attractive gas separation mechanism for a variety of gases except hydrogen. The large separation factors of the latter are due to its small size.

Note that the above values of α are somewhat higher than those obtained in commercial applications. A possible explanation offered by Keizer *et al.* [55] points to experimental conditions such as the applied pressure. The reported α of 3.74 in H_2/N_2 separation was achieved only when the P_i/P_p ratio of feed to permeate pressure approached zero. Any increase in the ratio towards unity, that is the equalization of pressures on both sides of the membrane, decreased selectivity. No separation was observed at $P_i = P_p$ due to the back-diffusion. The authors suggested that back-diffusion can be prevented when the pressure ratio is smaller than 0.1, meaning that the pressure on the feed side should be at least 10 times that on the permeate side. Still, despite the back-diffusion and need for a high feed pressure, Knudsen diffusion might be attractive due to the high transmembrane fluxes and the possibility for applying commercial ceramic membranes in harsh chemical and thermal environments.

2.7.2 Surface Diffusion

Gas separation by Knudsen diffusion is limited to gas mixtures with a large difference in their molecular masses. All other cases rely on other separation mechanisms such as *surface diffusion*. Surface diffusion occurs when at least one component in the feed adsorbs preferentially on the membrane surface. The transport of adsorbing gas through membrane pores is a sequence of four stages (Figure 2.16):

1) Diffusion of adsorbing molecules through the feed bulk to the vicinity of the membrane surface.
2) Reversible sorption of the molecules to the membrane surface.
3) Transport of the adsorbed molecules through the membrane pores by surface diffusion.
4) Desorption of the molecules from the membrane surface to the permeate bulk.

Surface diffusion can be important and even dominating if the surface area is high and the concentration of adsorbed molecules on the surface is high. For typical operation condition, the diffusion of gas molecules through the membrane is slow compared with their diffusion in the bulk on either side of a membrane [56]. This implies that both bulk diffusion and surface adsorption are faster than porous diffusion. That scenario is called *Fickian diffusion* and is considered 'normal'. Conversely, in *non-Fickian diffusion* the diffusion through pores is faster than that through the bulk.

The preferential adsorption depends on three groups of factors – the gas mixture, the nature of the membrane surface and the operational conditions. The first reflects primarily the adsorption capacity of the molecules, their molecular

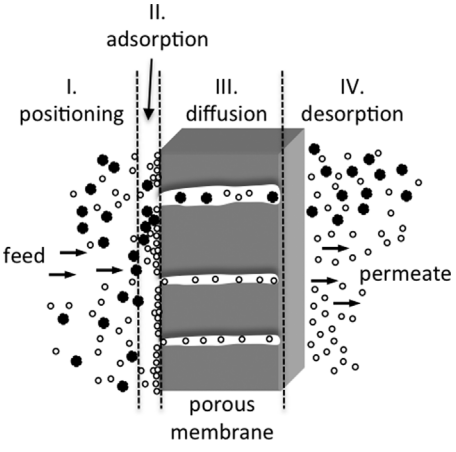


Figure 2.16 A sketch of molecular transport through a membrane by surface diffusion. (I) Positioning of adsorbing molecule against membrane surface; (II) adsorption of the molecule on the membrane surface; (III) diffusion of the adsorbed molecule through membrane pores; (IV) desorption of the molecule on the permeate side of the membrane.

weight and dimensions. Similarly, the membrane surface can be described by its physico-chemical parameters and by the membrane pore width. The operational conditions include pressure, temperature and flow direction.

The adsorption capacity of different molecules differs from surface to surface and from molecule to molecule. For example, in the diffusion of methane, ethane and ethylene in activated carbon at 20 °C and pressure below 0.2 atm, the contribution of surface diffusion to the total flux ranges between 40 and 80% [57]. For propane diffusion in silica gel at <75 °C and low pressures, the contribution of surface diffusion is over 40% [58]. A 40% contribution of surface diffusion to the total flux was also reported in the diffusion of CO_2 in alumina [59]. The influence of the molecular weight is complicated. In general, if light molecules are the adsorbing ones, they will move faster increasing the separation. However, if the heavy molecules are the adsorbing ones, they can quickly diffuse ('glitch') along membrane pore walls selectively, increasing their velocities and reducing the separation efficiency [60].

The influence of the membrane surface is specific and not obvious. There are reports that the surface modification of γ-alumina membranes with magnesia results in lower separation of CO_2 from N_2 despite an increase in adsorption [61]. Other reports suggest modifications of membrane surfaces as an efficient means to separate hydrogen from carbon compounds (CO_2, CO, CH_4) by silica membranes supported on porous alumina [62], silica on glass [63], or γ-alumina coated on α-alumina [64]. One can also adjust the pore size or exclude non-adsorbing species from membrane pores [65].

The effect of the pressure is clear – at any time if a pressure gradient exists one of the gases will adsorb preferentially. The applied gradient, however, should be small, because a large gradient increases adsorption but decreases mobility. Uhlhorn *et al.* [61] reported a decrease in the H_2/N_2 separation by γ-alumina membranes from 9 to 5 when the pressure was increased from 50 to 200 kPa. Keizer *et al.* [55] found a similar influence of the temperature in a separation of CO_2/N_2 with an increase in the mixture temperature from 240 to 360 K. A meaningful surface diffusion occurs at sufficiently low temperature and low partial pressure of adsorbed molecules. According to Uhlhorn *et al.*, the pores should be smaller than 3 nm and the temperature should be below 300 K. Keizer *et al.* [52] suggest temperatures below 373 K and pressures between 0 and 100 kPa as the effective range for the surface diffusion. Similarly, Park assumes that surface diffusion becomes negligible at temperatures higher than 400 °C [49]. At higher pressures and temperatures, the contribution of surface diffusion to the gas separation is small. We found several possible explanations to the reported tendencies. The first, offered by Burggraaf and Cot [60], is that the enhanced adsorption results in a fast surface diffusion of one of the gases, thereby reducing the separation factor. The second, offered later by Uhlhorn and Burggraaf [66], is that in general enhanced adsorption results in lower mobility of all gases due to the saturation of the adsorbent. The third, offered by Keizer *et al.* [52], is that the increase in pressure and temperature affects physical adsorption, that is by definition not very selective for a specific gas, and therefore does not increase the separation efficiency.

There are three central models that describe possible mechanisms of surface diffusion:

The *hydrodynamic model* – the adsorbed gas is viewed as a liquid film (condensed gas) that 'glides' along the membrane pore under the influence of a pressure gradient [67].

The *hopping model* – molecules can hop over the surface. The surface flux is calculated by the mean hopping distance and the velocity, with which the molecules leave the site [68].

The *random walk model* – molecules travel by a succession of random steps between vacant sites in the pore, guided by the difference in adsorbed phase concentration of the diffusing species towards the permeate [69].

Note that the worthiness of different models is a moot point. Burggraaf reported that the random walk model is most frequently used [52,66], while Lito *et al.* [70] claim that 'the hopping model is most frequently adopted for representing surface diffusion in micropores'.

Knudsen diffusion and surface diffusion are not mutually exclusive, and evaluating the relative contribution of each one of them in the gas transport through micropores is hard. In Figure 2.17, we summarize the effects of pore size, pressure and temperature on surface and gaseous phase fluxes.

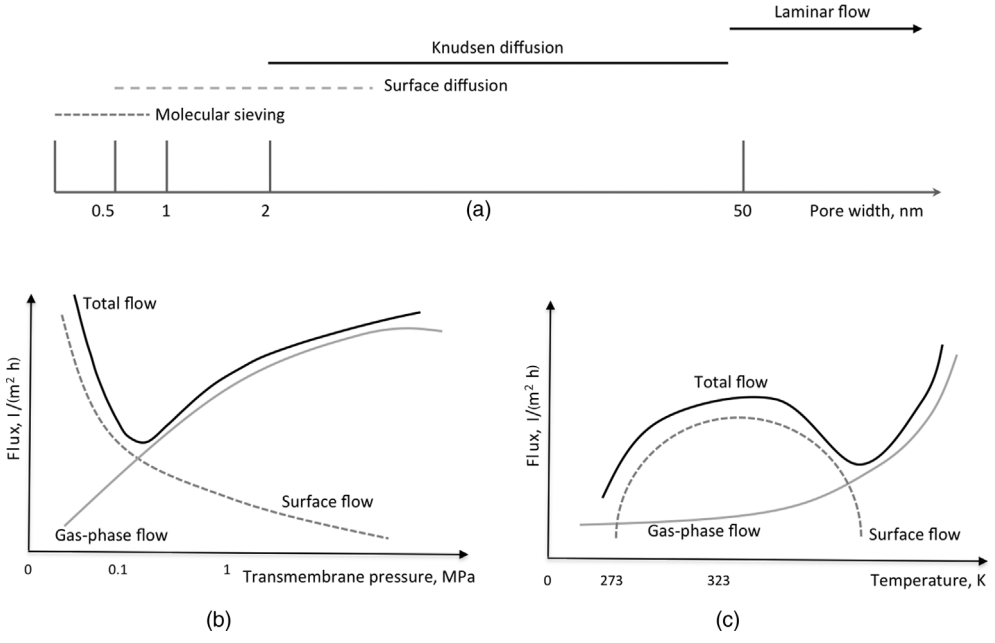


Figure 2.17 Effects of pore width (a), pressure (b) and temperature (c) on Knudsen diffusion and surface diffusion. In (b) and (c), a dashed grey line represents the flow that results from surface diffusion, a solid grey line is the flow in the gas phase and the black line is the total flow through a microporous ceramic membrane. All drawings are sketches and are not to scale. The effect of pressure is an interpretation of a figure drawn in Ref. [71].

The question of the pore size will be discussed separately but as a first attempt we estimate that when the pores of the membrane are roughly the same size as the gas molecule's diameter, molecular sieving will be the main separation mechanism. Regarding the appropriate pore size range, we estimate that it is between 0.1 and 1.0 nm (when the pore width is smaller than the molecular diameter, there is no diffusion). If the gas is strongly adsorbed on the membrane pores, surface diffusion will occur. Occurs when the pore is larger than the molecular diameter but smaller than the Knudsen diffusion range (1–3 nm) [72]. For pores that are large relative to the molecular size of the permeating gases, Knudsen diffusion is the mechanism that controls the transport rate (2–50 nm). A laminar flow will be the main transport mechanism at pores larger than 50 nm. At this range, no separation will occur.

There is no transmembrane flow without a pressure gradient. The effect of the gradient on the surface diffusion is more pronounced below 100 kPa. At higher pressures, the adsorption of adsorbing gas increases but its mobility decreases. Efficient Knudsen diffusion is achieved when the pressure on the feed side is at least 10 times that on the permeate side.

The diffusion of non-adsorbing gases increases monotonically with temperature. There is a minimum flux that is often observed at low temperatures [70]. We attribute this to a superposition of low surface diffusion at temperatures higher than 373 K, and moderate increase in the gas flow diffusion. Within the range of 273–373 K, we assume that the peak of surface diffusion is at 323 K. At lower temperatures, the diffusivity of adsorbed molecules increases even though the surface coverage is low. At higher temperatures, the desorption becomes more pronounced than the adsorption. Moreover, the mobility of adsorbed molecules decreases. At higher temperatures, the gaseous diffusion prevails due to the exponential increase of diffusion through micropores. The exponential increase is explained by the Arrhenius-like expression of the diffusion coefficient as expressed in Eq. (2.49).

2.7.3 Capillary Condensation

By definition, capillary condensation is the 'process by which multilayer adsorption from the vapour into a porous medium proceeds to the point at which pore spaces become filled with condensed liquid from the vapour' [73]. A reversible adsorption keeps a dynamic equilibrium between sorption and desorption. The pressure can shift the equilibrium towards increased sorption, so as the pressure increases, the number of free sites decreases. At a certain pressure, all free sites within the membrane structure are occupied by the adsorbing molecules. This is followed by multilayer adsorption. Adsorbing molecules form a film on the pore walls. In case of a condensable gas, the film is a sort of liquid phase. According to Lee and Hwang [74], this liquid film may block the pores. We can distinguish two cases here: In the first, adsorption occurs across the entire pore surface, so the pressure in the 'condensing pore' is higher than that in other pores. The

condensation occurs selectively in some pores due to the pore size distribution. Capillary condensation occurs at 0.5–0.8 of the saturation pressure. In this mechanism, the pore is not clogged. The presence of liquid condensed film might selectively increase the transport of large vapour molecules. For example, the transport of propene after condensation became higher than the transport of nitrogen. In a gas phase, nitrogen transport by Knudsen diffusion was 1.2 times faster than the transport of propene. After condensation, the transport of propene constantly increased. At 0.42 propene saturation pressure, it moved through the membrane twice as quickly as the smaller N_2 [52].

In the second case, a continuous increase in the applied pressure results in the formation of a liquid drop. This drop interconnects both sides of the pore and clogs it. It has a meniscus with a curved surface on both the feed and the permeate liquid–vapour interfaces [74]. The condensation in pores occurs below the saturation vapour pressure of a pure liquid, because of the formation of the meniscus. Another parameter that influences the condensation pressure is the pore width. Condensation in smaller pores occurs at lower pressure than in larger ones. The condensate travels from the feed to the permeate by hydrostatic pressure difference across the meniscus or by capillary suction pressure in unfilled pores [75]. A detailed analysis of various scenarios of the condensate flow under capillary suction is published by Uhlhorn *et al.* [76]. The transmembrane flux, however, drops as the pressure difference is small and the liquid flux is in general lower than the vapour flux Figure 2.18 shows the transmembrane flux as the function of relative pressure. We see that at low pressure (region I) the transmembrane pressure is low and so is the gaseous flux. Increasing the partial pressure results in capillary condensation and the transport of the condensed molecules along the membrane walls. Further increase results in massive condensation and pore blocking. The flux of condensed molecules in the liquid phase (region III) is lower than that of the molecules in the gas phase.

The achievable separation can be very high as the condensing gas blocks the entrance of the molecules of the non-condensed gas into the pores [76]. For example, the separation factor α in separation of C_3H_4 from N_2 is 7.1 [77]. Condensation increases this value to 13.0 due to the blocking of membrane pores for N_2 transport and a low solubility of N_2 in liquid C_3H_4 liquid. Thus, for good separation by the capillary condensation, the molecules of the non-condensing gas should not dissolve (or dissolve only a little) in the condensed component. Even higher separation efficiency of up to 1000 at SO_2 partial pressure of 0.75 was found in separation of H_2/SO_2 mixture. The separation factor α value drops below 5 if the capillary condensation disappears [52]. Other interesting and valuable examples of separation due to capillary condensation include the separation of water from hydrocarbons, alcohols or solvents such as acetone or DMF at about 100 °C [78].

The influence of the pore size here is the same as in the previous cases. Capillary condensation occurs in pores slightly larger than molecular sieves (2–10 nm). Small pores increase the selectivity but decrease the flux. For example, a decrease of the pore size to below 2 nm results in increase of the separation factor to >60 [79]. The applicability of capillary condensation is limited by

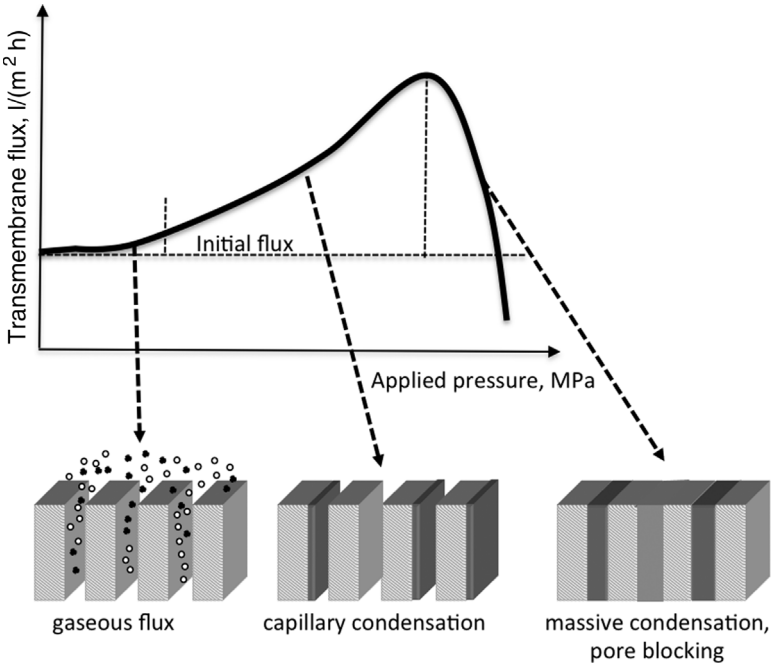


Figure 2.18 Effect of applied pressure on transmembrane flux in transfer of condensable molecules. The three regions on the figure correspond to gaseous flux (left), capillary condensation (middle) and massive condensation (right). The massive condensation usually results in pore blocking. (Drawn after Ref. [76].)

the presence of a condensable gas, temperature below the critical temperature and a pressure of at least half the saturation pressure.

2.7.4
Molecular Sieving

Molecular sieving separates gas molecules using membrane pores that have roughly same size as the molecules themselves. Keizer *et al.* [52] suggested that the upper limit of pore diameter for molecular sieving should not exceed three times the molecular diameter, with strong interactions between the diffusing molecule and the pore wall. Typical pore sizes for molecular sieving are <2 nm, though it is extremely difficult to characterize the pores quantitatively. Relatively large molecules of B cannot enter the pores at all, increasing infinitely the A/B separation factor. The permeability here will depend on diffusion rate of A. In practical examples, many of these separations consider a mixture of hydrogen and another gas (see Table 2.3).

The transport rate in micropores increases with temperature. Typical activation energy values are less than 10 kJ/mol, which is lower than that for dense membranes. Optimal separations are achieved at elevated temperatures (100–300 °C).

Table 2.3 Values of separation factor α in separation of some typical gas mixtures by molecular sieving.[a)]

Gas mixture	α
H_2/C_3H_6	160
H_2/CH_4	200
CO_2/CH_4	600
H_2/N_2	2000
H_2/CH_4	56
O_2/N_2	7
He/N_2	21
He/O_2	3

a) Data from Refs. [52,80,81].

The common molecular sieves are porous aluminosilicates (zeolites) and carbon solids. Molecular sieving is a simple yet effective mechanism based on the differences in the molecular sizes of gases. Hydrogen separation is the classical example, but there are good possibilities also for separating other gases.

2.7.5 Transport of Gases through Ceramic Membranes with Several Simultaneous Processes

Gas transport through porous ceramic membranes is due to the above-discussed mechanisms of size exclusion, Knudsen diffusion, surface diffusion and capillary condensation. Usually, the dominating mechanism depends on several factors such as pore size and pore size distribution, the size ratio between pore and permeating molecule, operating temperature and pressure, and affinity and condensability of penetrating molecules. The mechanisms are not mutually exclusive and gas transport depends on several transition mechanisms that occur simultaneously. There are two common types of 'combination models': The transport of gas molecules that travel through different pores, each by a different mechanism, is explained by the *parallel transport model*. Similarly, the transport of molecules that consequently travel in pores of different diameters is described by the *resistance-in-series transport model*. In this section, we will outline these two models in some detail.

2.7.5.1 The Parallel Transport Model

The parallel transport model views the total flux as a superposition of contributions from molecules that travel through various pores. Each pore has its constant size that goes throughout the entire membrane from the feed to the permeate. No pore-to-pore transition occurs. In this case, the membrane permeability is the sum of permeabilities due to above-described mechanisms:

$$F_{\text{total}} = F_{\text{KN}} + F_{\text{LF}} + F_{\text{MS}} + F_{\text{CC}} \tag{2.120}$$

where the total permeability F_{total} is the sum of permeabilities due to Knudsen diffusion F_{KN}, laminar flow F_{LF}, molecular sieving F_{MS} and capillary condensation F_{CC}. In each pore size range, different selectivity mechanisms dominate, and therefore expressions for the total permeability are divided into three pore size ranges. According to Keizer *et al.* [52], those are the areas that correspond to $2 < d_p < 50$ nm, $d_p < 2$ nm and $d_p = 0$ nm. The most interesting is the pore segment between 2 and 50 nm where laminar flow, Knudsen diffusion and surface diffusion can take place. The expression of F_{total} due to these mechanisms had been found in publications of Burggraaf and Keizer [78], Uhlhorn *et al.* [76], Hsieh [82] and others [55,61], given as

$$F_{total} = \frac{4}{3}\frac{\sqrt{2}}{\sqrt{\pi}}\left(\frac{\varepsilon}{\beta}\right)\frac{1}{\sqrt{RTM_A}}r_p + \left(\frac{\varepsilon}{\beta}\right)\frac{P}{8\mu RT}r_p^2 + \left(\frac{\varepsilon}{\beta}\right)\frac{2D_s}{A_0 N_{AV}}\frac{dx_s}{dP}\frac{1}{r_p} \qquad (2.121)$$

where F_{total} is the total permeability (mol/(m^2 s Pa)), ε is the membrane porosity, β is the pore tortuosity (typical values between 2 and 10), M_A is the molecular mass, R is the gas constant (8.31 J/(mol K)), T is the absolute temperature (K), P is the TMP (Pa), μ is the gas viscosity (Pa/s), D_s is the surface diffusion coefficient of adsorbed gases (m^2/s), A_0 is the surface area occupied by one molecule (m^2), N_{AV} is Avogadro's number, x_s is the fraction of occupied sites (by adsorption) on the membrane surface in relation to a monolayer and r_p is the membrane pore radius [78].

The first term on the right-hand side represents the Knudsen diffusion, the second term is the laminar flow contribution and the third is the surface diffusion. Molecular sieving is the simplest mechanism based on the difference in the molecular sizes of gases. If the molecules that we want to separate are roughly of the same diameter, their separation can be based on the difference in adsorbability and condensability. Knudsen diffusion effectively separates molecules with a significant molecular weight difference, such as the separation of hydrogen from a mixture. When the pore diameter is larger than the mean free path of molecules, gases passes through membranes by laminar and turbulent flows. Although the flux in these flows is very high, the separation is low. Thus, laminar and turbulent flows are not really desirable separation options.

Surface diffusion, Knudsen diffusion and laminar flow all depend on the pore size. Dependences are different, and plotting either one as a function of pore size is problematic. However, the options are not mutually exclusive and their superposition can provide a prediction of the main transport mechanism depending on the pore size. Figure 2.19 displays a plot of all three transfer mechanisms and their superposition, in a pore size range between 0.01 and 4 nm.

Surface diffusion is important for pore sizes <1 nm. These are too small for Knudsen diffusion or laminar flow. The contribution of the surface diffusion increases as the pores narrow. It also increases with an increase in the surface diffusion coefficient D_s and the fraction adsorbed on the surface as a function of TMP. The graph declines exponentially towards zero due to a reciprocal dependence of the permeability on the pore radius. The 1 nm value, however, is less important and might change with a substitution of different constants into

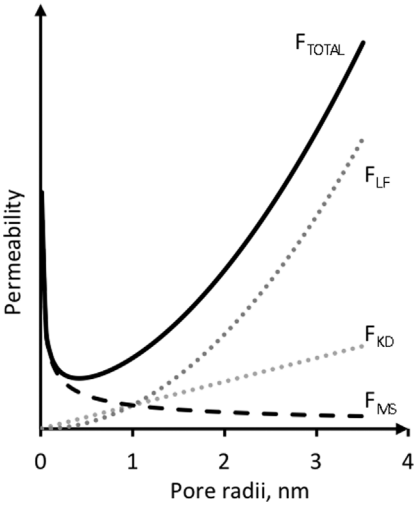


Figure 2.19 Gas permeability as a function of pore radius. Here F_{total} is the total permeability, F_{KN} is the permeability due to Knudsen diffusion, F_{LF} is the permeability of laminar flow and F_{MS} is the permeability due to the molecular sieving. Permeability values are calculated from Eq. (2.121). For simplicity, all variables in the equation except the pore size are assumed to be equal to unity.

Eq. (2.121). A more accurate prediction provided by Burggraaf and Keizer gives a range between 1 and 3 nm [78]. At values higher than 1 nm, laminar flow has the highest influence on the permeability, and already above 4 nm becomes the single most important factor influencing the separation. Note that the classical gas separation theory predicts that laminar and turbulent flows are important at values higher than 50 nm, while Burggraaf and Keizer provide a range between 5 and 50 nm. The surface diffusion can be important even in cases where the pore size changes. For example, Figure 2.20 depicts a membrane structure that contains pores of constant and varying diameters.

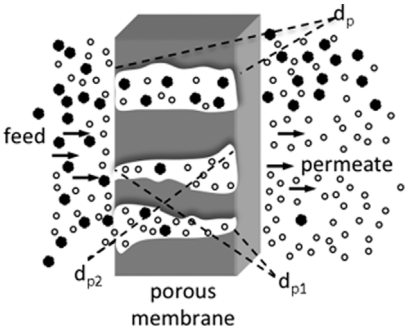


Figure 2.20 Schematic models for a porous ceramic membrane with constant d_p (top) and varying from d_{p1} to d_{p2} (bottom) pores.

In pores of 1–2 nm, surface diffusion competes with Knudsen diffusion. The exact contribution of either depends on the membrane material and gas molecules in the mixture. Keizer *et al.* [52] suggest that surface diffusion is two to three times slower than gas diffusion and therefore contributes less to the total transport in the case where the pores are large enough for both diffusions to occur. Park, on the contrary, suggests that surface diffusion is two to four times faster than Knudsen diffusion [49]. The competition between two types of diffusion might result in no separation at all. This happens when the faster diffusion of one gas in a mixture due to one of the diffusion mechanisms is counterbalanced by a faster diffusion of the other component by the second diffusion. Keizer *et al.* describe a CO_2/CH_4 separation by micro- and mesoporous membranes. Average ratios for surface to Knudsen diffusion coefficients D_S/D_{KN} are 0.3–0.4, and when the pore sizes are bigger than 1–2 nm the competition between surface and gas diffusions might result in no separation at all.

For example, surface diffusion of CO_2 on alumina is faster than the surface diffusion of CH_4. This means that the separation factor α in separating CO_2 and CH_4 by surface diffusion is >1. Table 2.2 shows that the α for CO_2/CH_4 separation by Knudsen diffusion is 0.6. This means that CO_2/CH_4 can be separated in micropores, but not in mesopores. In the latter, surface and Knudsen diffusions neutralize each other. The same is true when separating hydrocarbons including C_2H_6, C_3H_6 or *i*-butane from low-mass molecules [52]. In pores of about 1–2 nm, the faster surface diffusion of larger molecules is counterbalanced by the faster Knudsen diffusion of lighter ones. There is, however, one exception: Surface diffusion of hydrogen can be twice as fast as its gas diffusion. Moreover, Knudsen diffusion of H_2 is faster than that for any other gas. A combination of two can result in high total separations of hydrogen from other gases. For example, a H_2-to-N_2 transport ratio of 9 : 1 was reported [52]. In summary, the surface diffusion seems to be important for enhancing the separation in small pores and becomes less influential in 1–2 nm pores. The exception is the separation of hydrogen. Table 2.4 details the main gas transport regimes and their selectivity based on the pore size in the membrane.

Table 2.4 The main gas transport regimes in ceramic membranes.

Transport mechanism	Pore diameter (nm)	Selectivity[a)]
Turbulent flow	>50	–
Laminar flow	>20	–
Knudsen diffusion	2–50	$\sqrt{M_2/M_1}$, $M_1 < M_2$
Surface diffusion	1–3	+
Capillary condensation	2–10	++
Molecular sieving	0–2	++
Solution diffusion	0	+++

a) Here – denotes poor selectivity, while +, ++ and +++ denote good, very good and excellent selectivity, respectively.

2.7.5.2 The Resistance-in-Series Model

The resistance-in-series transport model assumes that the pore size might change as a molecule passes through. As a result of the change, the molecules face various pore resistances that control the rate of diffusion. For this scenario, the total permeability is inversely proportional to the total resistance:

$$R_{\text{total}} = \frac{l}{F_{\text{total}}} = \frac{l}{F_{\text{KN}}} + \frac{l}{F_{\text{LF}}} + \frac{l}{F_{\text{MS}}} + \frac{l}{F_{\text{CC}}} \tag{2.122}$$

The difference between parallel and resistance-in-series transport models was discussed in detail by Gilron and Soffer [83]. The expression of F_{total} following these mechanisms was developed by Henis and Tripodi [84] and Lopez *et al.* [85] as

$$R_{\text{total}} = \frac{l}{F_{\text{total}}} = \frac{l}{F_{\text{LF}}} + \frac{d_{\text{p}}}{F_{\text{MS}} x_{\text{K}} + F_{\text{KN}}(1 - x_{\text{K}})\beta} \tag{2.123}$$

where l is the total pore length, d_{p} is the pore width, x_{K} is the pore fraction where molecular sieving dominates, $(1 - x_{\text{K}})$ is the pore fraction where Knudsen diffusion dominates and β is the pore tortuosity.

The effect of the pore size on the gas separation is not obvious. While it is clear that the pore size should be below 50 nm, surface modifications aimed at reducing the pore diameter might not hit the target. The separation mechanism depends on the gases' properties including adsorbability and condensability. A size-based separation strategy applies when the difference in molecular weights of gases in the mixture is significant. Even then, the separation efficiency is not high. Separation factors of 2–5 based on Knudsen diffusion can be increased to 10–20 by surface diffusion. Capillary condensation might result in separation factors of 7–500 for water–alcohol and H_2–SO_2 mixtures separated by modified alumina and carbon membranes. According to Burggraaf and Keizer [78], separations in membranes with pores smaller than 2 nm are due to capillary condensations rather than molecular sieving.

2.8 Fluxes through Non-porous Membranes

The separation of gases by porous membranes is fast and affordable, yet not always efficient. Efficient separation requires a major difference between the gases in the feed. This can be based on molecular weight, adsorption or condensability of A and B. If the gases are similar, porous membranes are less useful. Examples include oxygen/nitrogen and hexane/heptane.

The situation is different when dealing with dense membranes. By definition, dense membranes contain no pores. Ultramicroporous membranes contain pores less than 0.7 nm, so practically the pore size difference between these porous membranes and dense membranes is minor. The main difference is in the transport mechanism. Whereas porous membranes transfer molecules, dense

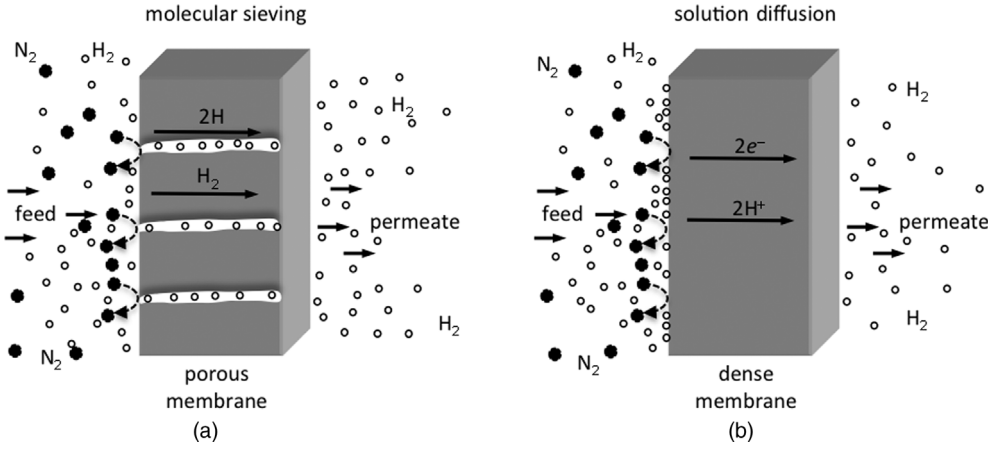


Figure 2.21 Permeation of hydrogen through a porous ceramic membrane (a) and a dense one (b). The H_2 can permeate as neutral atoms (a) and as protons (b). The diffusion of electrons is parallel to the protons to maintain the electroneutrality and zero net current.

membranes transfer ions. Figure 2.21 shows schematically the separation of H_2 from a H_2/N_2 mixture by porous and dense ceramic membranes.

The ion-transfer mechanism is specific for certain ceramics such as perovskites or fluorites and ions of oxygen or hydrogen. Dense membranes are mostly impermeable to all other gases, giving extremely high selectivity towards oxygen or hydrogen. This transport becomes significant above 600 °C [52] and might be due to a pressure or electrical potential gradient. Good permeability was reported in experiments with perovskites that possess high electronic conductivity. Keizer *et al.* [52] suggest that the diffusion in non-porous membranes is more strongly activated than in microporous systems, and that is the difference between molecular sieving in porous membrane and diffusion through solid membranes.

The transport of gases through a dense membrane has six stages:

1) Diffusion of adsorbing molecules through the feed bulk close to the membrane surface.
2) Reversible sorption of the molecules on the surface.
3) Dissociation of the adsorbed gas into ions.
4) Diffusion of the ions (and electrons) through the membrane.
5) Recombination of the ions and electrons on the permeate side.
6) Desorption of gas molecules from the surface to the permeate bulk.

The process is similar to the Knudsen diffusion we discussed in Section 2.7.2, with the added stages of dissociation and recombination. The similarity is in the discussion of the rate-determining step. The assumption is that in both cases Fickian diffusion mode prevails. In Fickian diffusion, bulk diffusion is much faster than the diffusion through a membrane. Thus, the penetration through a dense membrane is governed by the membrane diffusion and the gas dissolution/recombination on the feed/permeate side of the membrane. The processes of

dissolution and recombination are often seen as *chemical reactions* as they involve the conversion of a gas into ionic species and back to a gas. For example, the conversion of oxygen is described as

$$\frac{1}{2}O_2 + V_a^{\infty} + 2e^- \rightarrow O_0^0 \tag{2.124}$$

and its recombination on the permeate side with the production of molecular oxygen as

$$O_0^0 \rightarrow \frac{1}{2}O_2 + V_a^{\infty} + 2e^- \tag{2.125}$$

The diffusion is possible because the dissociation of the gas into diffusing atoms creates a large concentration gradient across the membrane. The lower concentration of ions will always be on the permeate side when ions recombined with electrons leave into the bulk. Hence, the diffusion will always be from the feed side to the permeate side. We already discussed earlier in this chapter the possible pathways for diffusion in solids. The vacancy diffusion is considered the most important mechanism. Dense ceramic membranes made of perovskites are often intentionally doped with oxygen-deficient materials to increase the number of ion vacancies (defects). More defects result in a higher flux.

Expressions for the diffusional flux have to consider two streams: ions and electrons. Hydrogen penetrates as protons and therefore electrons travel parallel to the protons' flux. Oxygen penetrates as oxide anions when electrons diffuse in a direction opposite to the diffusion of oxygen. The diffusional flux expressions of charged species through a membrane are derived from Fick's law (e.g. Eq. (2.25)), where the diffusion coefficient D_{AB} is replaced with the ionic/electronic conductivity σ and the concentration gradient c_A with the electrochemical potential η_A. Similarly, the electrochemical potential is replaced by chemical and electrical potentials and a mixed ionic/electronic conductivity is a superposition of intercorrelated fluxes of oxygen ions and electron charge carriers (electrons and/or holes). This superposition is accurate in ionic media where chemical and electrical potentials act simultaneously. Under steady-state conditions [86,87], the oxygen diffusional flux is expressed as

$$J_{O_2} = \frac{1}{(4F)^2 L}\int_{\mu_{1s}}^{\mu_{2s}} \frac{\sigma_{ion}\sigma_{el}}{\sigma_{ion}+\sigma_{el}}\,d\mu \tag{2.126}$$

where J_{O_2} is the permeation flux density of molecular oxygen, L is the membrane thickness of a flat-sheet membrane in the direction of the flow, σ_{ion} and σ_{el} are the partial ionic and electronic conductivities, respectively, and μ_{1s} and μ_{2s} are the values of oxygen chemical potential μ at the membrane surface on permeate and feed sides, respectively.

Electronic conductivity is typically higher than ionic conductivity. Using the relationship $d\mu = dRT \ln P_{O_2}$ and assuming no divergence in fluxes, we can modify Eq. (2.126) into

$$J_{O_2} = -\frac{RT}{16F^2 L}\int_{\ln P'_{O_2}}^{\ln P''_{O_2}} \frac{\sigma_{ion}\sigma_{el}}{\sigma_{ion}+\sigma_{el}}\,d\ln P_{O_2} \tag{2.127}$$

where P''_{O_2} and P'_{O_2} are the oxygen partial pressures maintained at the gas phase boundaries. Here F is the Faraday constant, R is the gas constant and T is the absolute temperature.

The *Wagner equation* is valid for mixed conductors such as perovskites and can be written for hydrogen in a similar form as [88]

$$J_{H_2} = -\frac{RT}{4F^2L}\int_{\ln P'_{H_2}}^{\ln P''_{H_2}} \frac{\sigma_{ion}\sigma_{el}}{\sigma_{ion}+\sigma_{el}} \mathrm{d}\ln P_{H_2} \tag{2.128}$$

According to Wagner's theory, the permeation flux is proportional to partial gas concentrations in feed and permeate, membrane thickness L, and ionic and electronic conductivities ($\sigma_{ion}\sigma_{el}/(\sigma_{ion}+\sigma_{el})$). Among these, the partial gas concentration in the feed is constant, and in the permeate is close to zero. The reduction of membrane thickness is limited by a need for a mechanically stable membrane and by the presence of a characteristic membrane thickness value L_c [51]. Below L_c, the influence of membrane thickness on the flux becomes marginal as the surface exchange kinetics become rate limiting. The increase in the permeate flux is therefore often linked to high ionic and electronic conductivities. An increase in the conductivity depends on the design of the separation membrane and on the material used. In the conventional membrane concept, the membrane element is a self-supported single-phase material that conducts both electrons and oxygen ions. This pertains to perovskites and fluorites that can transfer both ions and electrons.

Other dense ceramic conducting materials are not easy to find, but electrons can also be transferred through an external circuit. Using a sandwich-like design, a dense membrane is placed between two porous materials that act as mixed ionic/electronic conducting electrodes. The porous materials (but not the membrane) are permeable to both ions and electrons. The dense membrane allows a selective transfer of oxygen ions, while the electrons flow through an external circuit (see Figure 2.22). The second approach allows a precise control over the oxygen flux by

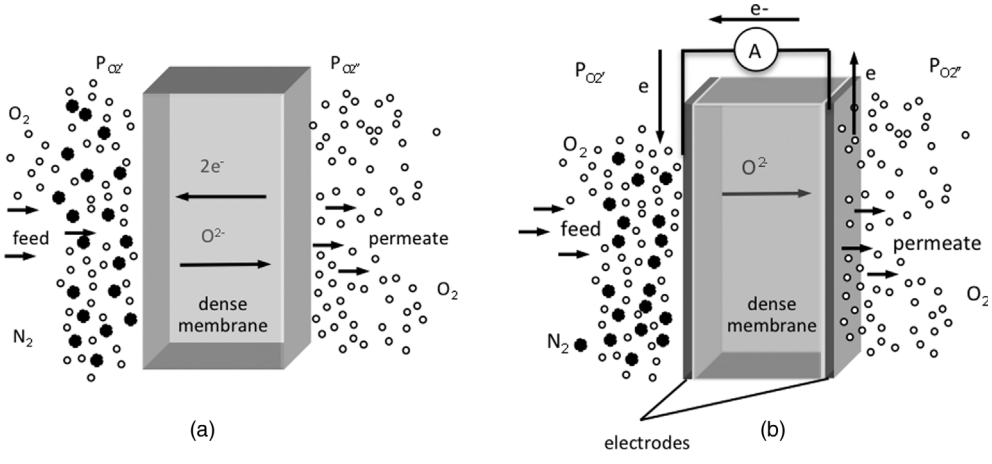


Figure 2.22 Permeation of oxygen through a self-supported single-phase dense ceramic membrane (a) and a solid electrolyte cell (so-called oxygen pump) (b).

adjusting the current flowing between electrodes [89]. Two-phase composites are more flexible in design of their microstructure including grain size and distribution in the porous phase. Fabrication and operation of mixed conducting membranes is simpler than oxygen pumps due to the absence of an external circuit. The use of perovskites and fluorites is therefore a cheaper option. We will discuss the applications of such membranes in solid oxide fuel cells in more detail in Chapter 4.

Exercises

2.1. Using Working Example 2.1, determine the mole concentration of air at 0, 50 and 75 °C (at 1 atm pressure in all cases).

2.2. Plot a graph that describes the change in the mole concentration of air as a function of temperature.

2.3. Calculate the volume occupied by 200 g of butane (C_4H_{10}) at standard conditions.

2.4. The most important gaseous mixture we know is air. It has the following composition:

Gas	Molecular weight	Mass fraction of the 'dry' portion of the atmosphere
N_2	28.016	0.7552
O_2	32	0.2315
Ar	39.444	0.012 89
CO_2	44	0.000 035

Determine the mass and mole concentrations p and c of each of the four main components of air. What does this tell you about projects aiming at extracting CO_2 from the atmosphere?

2.5. Using Working Example 2.3, develop an equation for the mass transfer by implementing a second-type boundary condition that says that the flux through a membrane boundary is constant, that is

$$n_A|_{z=\delta} = -D_{AB}\frac{d\rho_A}{dz}|_{z=\delta} = \text{const}$$

2.6. A typical flue gas contains 15 vol.% CO_2, 5 vol.% O_2, 70 vol.% N_2 and 10 vol.% H_2O. In a first approximation, the primary retention of CO_2 from flue gas is its separation from nitrogen. This can be done using membrane technology. The molecular weight, critical temperature, critical pressure and kinetic diameter for CO_2 are 44 g/mol, 304 K, 72.9 atm and 3.3 Å, respectively. The corresponding values for N_2 are 28 g/mol, 126 K, 34 atm and 3.64 Å, respectively.

- Choose an appropriate membrane technology: should it be nitrogen selective or CO_2 selective?

- Examine the parameters of both gases and suggest an appropriate separation technology. Which parameter is your choice based on? Explain your answer.
- Which type of membrane would be most suitable for this operation? Explain your answer.

2.7. Calculate the diffusion coefficient D_{AB} of carbon dioxide in air using the Chapman–Enskog equation (Eq. (2.42)). You may assume that the air is at room temperature (20 °C) and ambient pressure (1 atm $\sim 10^5$ Pa). The collision diameters and ε_A/k_B of CO_2 are 3.996 Å and 190 K, respectively, and those of air are 3.617 Å and 97 K, respectively. The collision integral Ω_D can be found from the following table:

k_BT/ε	Ω_D	k_BT/ε	Ω_D	k_BT/ε	Ω_D
0.3	2.662	1.0	1.439	1.7	1.128
0.4	2.318	1.1	1.375	1.8	1.116
0.5	2.066	1.2	1.32	1.9	1.094
0.6	1.877	1.3	1.273	2.0	1.075
0.7	1.729	1.4	1.233	2.1	1.057
0.8	1.612	1.5	1.198	2.2	1.041
0.9	1.517	1.6	1.167	2.3	1.026

References

1 Schwarzenbach, R.P., Gschwend, P.M. and Imboden, D.M. (2005) *Environmental Organic Chemistry*, John Wiley & Sons, Inc., Hoboken, NJ.
2 Welty, J.R., Wicks, C.E., Wilson, R.E. and Rorrer, G. (2001) *Fundamentals of Momentum, Heat, and Mass Transfer*, 4th edn, John Wiley & Sons, Inc., Hoboken, NJ.
3 Bird, R.B., Stewart, W.E. and Lightfoot, E.N. (2007) *Transport Phenomena*, John Wiley & Sons, Inc., Hoboken, NJ.
4 Crank, J. (1979) *The Mathematics of Diffusion*, Oxford University Press, New York.
5 Bergman, T.L. and Incropera, F.P. (2011) *Fundamentals of Heat and Mass Transfer*, John Wiley & Sons, Inc., Hoboken, NJ.
6 Tien, C.L. and Lienhard, J.H. (1979) *Statistical Thermodynamics*, CRC Press, Boca Raton, FL.
7 Hirschfelder, J.O., Curtiss, C.F. and Bird, R.B. (1954) *Molecular Theory of Gases and Liquids*, John Wiley & Sons, Inc., New York.
8 Poling, B., Prausnitz, J. and O'Connell, J. (2000) *The Properties of Gases and Liquids*, McGraw-Hill, New York.
9 Malek, K. and Coppens, M.O. (2003) Knudsen self- and Fickian diffusion in rough nanoporous media. *Journal of Chemical Physics*, **119** (5), 2801–2811.
10 Hines, A.L. and Maddox, R.N. (1985) *Mass Transfer: Fundamentals and Applications*, Prentice Hall, Upper Saddle River, NJ.
11 Singh, A. and Koros, W.J. (1996) Significance of entropic selectivity for advanced gas separation membranes. *Industrial & Engineering Chemistry Research*, **35** (4), 1231–1234.
12 Singh-Ghosal, A. and Koros, W.J. (2000) Air separation properties of flat sheet homogeneous pyrolytic carbon

membranes. *Journal of Membrane Science*, **174** (2), 177–188.
13 Steel, K.M. and Koros, W.J. (2003) Investigation of porosity of carbon materials and related effects on gas separation properties. *Carbon*, **41** (2), 253–266.
14 Crank, J. and Park, G.S. (1968) *Diffusion in Polymers*, Academic Press, London.
15 Lienhard, J.H., IV and Lienhard, J.H., V (2013) *A Heat Transfer Textbook*, Courier Corporation, North Chelmsford, MA.
16 Baker, R. (2012) *Membrane Technology and Applications*, John Wiley & Sons, Ltd, Chichester.
17 Asraf-Snir, M. and Gitis, V. (2011) Tracer studies with fluorescent-dyed microorganisms – a new method for determination of residence time in chlorination reactors. *Chemical Engineering Journal*, **166** (2), 579–585.
18 Wilke, C.R. and Chang, P. (1955) Correlation of diffusion coefficients in dilute solutions. *AIChE Journal*, **1** (2), 264–270.
19 Renkin, E.M. (1954) Filtration, diffusion, and molecular sieving through porous cellulose membranes. *The Journal of General Physiology*, **38** (2), 225–243.
20 Quinn, J.A., Anderson, J.L., Ho, W.S. and Petzny, W.J. (1972) Model pores of molecular dimension – preparation and characterization of track-etched membranes. *Biophysical Journal*, **12** (8), 990–1007.
21 Roberts-Austen, W.C. (1896) On the diffusion of metals. *Science*, **III** (75), 827–829.
22 Mehrer, H. (2007) *Diffusion in Solids: Fundamentals, Methods, Materials, Diffusion-Controlled Processes*, Springer, Berlin.
23 Kou, S. (1996) *Transport Phenomena and Materials Processing*, John Wiley & Sons, Inc., Hoboken, NJ.
24 Frenkel, J. (1926) Zur Theorie der Elastizitätsgrenze und der Festigkeit kristallinischer Körper. *Zeitschrift für Physik*, **37** (7–8), 572–609.
25 Aaron, D. and Tsouris, C. (2005) Separation of CO_2 from flue gas: a review. *Separation Science and Technology*, **40** (1–3), 321–348.
26 Callister, W.D. and Rethwisch, D.G. (2012) *Fundamentals of Materials Science and Engineering: An Integrated Approach*, John Wiley & Sons, Inc., Hoboken, NJ.
27 Smigelskas, A.D. and Kirkendall, E.O. (1947) Zinc diffusion in alpha brass. *Transactions of the AIME*, **171**, 130–142.
28 Kingery, W.D., Bowen, H.K. and Uhlmann, D.R. (1976) *Introduction to Ceramics*, John Wiley & Sons, Inc., New York.
29 Mills, A.F. (2001) *Mass Transfer*, Prentice Hall, Upper Saddle River, NJ.
30 Lienhard, J.H. (2011) *A Heat Transfer Textbook*, Dover Publications.
31 Prandtl, L. (1904) Über Flüssigkeitsbewegung bei sehr kleiner Reibung. *III Internationale Mathematik Kongress*, **1** (1), 484–491.
32 Lakshminarayanaiah, N. (1965) Transport phenomena in artificial membranes. *Chemical Reviews*, **65** (5), 491–565.
33 Lakshminarayanaiah, N. (1969) *Transport Phenomena in Membranes*, Academic Press, New York.
34 Kozeny, J. (1927) Ueber kapillare Leitung des Wassers im Boden. *Sitzungsberichte der Akademie der Wissenschaften*, **136**, 271–306.
35 Carman, P.C. (1937) Fluid flow through a granular bed. *Transactions of the Institution of Chemical Engineers*, **15**, 150–166.
36 Blatt, W.F., Dravid, A., Michaels, A.S. and Nelsen, L. (1970) Solute polarization and cake formation in membrane ultrafiltration: causes, consequences, and control techniques, in *Membrane Science and Technology* (ed. J. Flynn), Plenum Press, New York.
37 Field, R.W., Wu, D., Howell, J.A. and Gupta, B.B. (1995) Critical flux concept for microfiltration fouling. *Journal of Membrane Science*, **100** (3), 259–272.
38 Mulder, M. (1996) *Basic Principles of Membrane Technology*, Kluwer Academic Publishers, Dordrecht.
39 Eykamp, W. (1995) Microfiltration and ultrafiltration, in *Membrane Science and Technology* (eds D.N. Richard and S.A. Stern), Elsevier, Amsterdam, pp. 1–43.
40 Rene, F. and Lalande, M. (1991) Momentum and mass transfer during

ultrafiltration of dextran with tubular mineral membranes in turbulent flow regime. *Journal of Membrane Science*, **56** (1), 29–48.
41 Vandenberg, G.B., Racz, I.G. and Smolders, C.A. (1989) Mass transfer coefficients in cross-flow ultrafiltration. *Journal of Membrane Science*, **47** (1–2), 25–51.
42 Diez, V., Ezquerra, D., Cabezas, J.L., Garcia, A. and Ramos, C. (2014) A modified method for evaluation of critical flux, fouling rate and *in situ* determination of resistance and compressibility in MBR under different fouling conditions. *Journal of Membrane Science*, **453**, 1–11.
43 Arkhangelsky, E., Lerch, A., Uhl, W. and Gitis, V. (2011) Organic fouling and floc transport in capillaries. *Separation and Purification Technology*, **80** (3), 482–489.
44 Hermia, J. (1982) Constant pressure blocking filtration laws – application to power-law non-Newtonian fluids. *Transactions of the Institution of Chemical Engineers*, **60** (3), 183–187.
45 Naim, R., Epsztein, R., Felder, A., Heyer, M., Heijnen, M. and Gitis, V. (2014) Rethinking the role of in-line coagulation in tertiary membrane filtration of municipal effluents. *Separation and Purification Technology*, **125**, 11–20.
46 Naim, R., Levitsky, I. and Gitis, V. (2012) Surfactant cleaning of UF membranes fouled by proteins. *Separation and Purification Technology*, **94**, 39–43.
47 Cussler, E.L. (1997) *Diffusion: Mass Transfer in Fluid Systems*, Cambridge University Press, New York.
48 Liepmann, H.W. (1961) Gas kinetics and gas dynamics of orifice flow. *Journal of Fluid Mechanics*, **10**, 65–79.
49 Park, H.B. (2013) Gas separation membranes, in *Encyclopedia of Membrane Science and Technology* (eds E.M.V. Hoek and V.V. Tarabara), John Wiley & Sons, Inc., Hoboken, NJ.
50 Thornton, A.W., Hill, J.M. and Hill, A.J. (2010) Modelling gas separation in porous membranes, in *Membrane Gas Separation*, John Wiley & Sons, Ltd, Chichester, pp. 85–109.
51 Li, K. (2007) *Ceramic Membranes for Separation and Reaction*, John Wiley & Sons, Ltd, Chichester.
52 Keizer, K., Uhlhorn, R. and Burggraaf, T.J. (1995) Gas separation using inorganic membranes, in *Membrane Science and Technology* (eds R.D. Noble and S.A. Stern), Elsevier, Amsterdam, pp. 553–588.
53 Gillot, J. (1991) The developing use of inorganic membranes: a historical perspective, in *Inorganic Membranes: Synthesis, Characteristics and Application* (ed. R.R. Bhave), Chapman & Hall, New York, pp. 1–9.
54 Isobe, T., Shimizu, M., Matsushita, S. and Nakajima, A. (2013) Preparation and gas permeability of the surface-modified porous Al_2O_3 ceramic filter for CO_2 gas separation. *Journal of Asian Ceramic Societies*, **1** (1), 65–70.
55 Keizer, K., Uhlhorn, R.J.R., Vanvuren, R.J. and Burggraaf, A.J. (1988) Gas separation mechanisms in microporous modified gamma-Al_2O_3 membranes. *Journal of Membrane Science*, **39** (3), 285–300.
56 Abdel-Jawad, M.M., Gopalakrishnan, S., Duke, M.C., Macrossan, M.N., Smith Schneider, P. and Diniz da Costa, J.C. (2007) Flowfields on feed and permeate sides of tubular molecular sieving silica (MSS) membranes. *Journal of Membrane Science*, **299** (1–2), 229–235.
57 Costa, E., Calleja, G. and Domingo, F. (1985) Adsorption of gaseous hydrocarbons on activated carbon – characteristic kinetic curve. *AIChE Journal*, **31** (6), 982–991.
58 Yang, R.T. (1997) *Gas Separation by Adsorption Processes*, Imperial College Press, London.
59 Rivarola, J.B. and Smith, J.M. (1964) Surface diffusion of carbon dioxide on alumina. *Industrial & Engineering Chemistry Fundamentals*, **3** (4), 308–313.
60 Burggraaf, A.J. and Cot, L. (1996) *Fundamentals of Inorganic Membrane Science and Technology*, Elsevier, Amsterdam.
61 Uhlhorn, R.J.R., Keizer, K. and Burggraaf, A.J. (1989) Gas and surface diffusion in modified gamma-alumina systems. *Journal of Membrane Science*, **46** (2–3), 225–241.

62 Lee, D., Zhang, L., Oyama, S.T., Niu, S. and Saraf, R.F. (2004) Synthesis, characterization, and gas permeation properties of a hydrogen permeable silica membrane supported on porous alumina. *Journal of Membrane Science*, **231** (1–2), 117–126.

63 Lee, D. and Oyama, S.T. (2002) Gas permeation characteristics of a hydrogen selective supported silica membrane. *Journal of Membrane Science*, **210** (2), 291–306.

64 Kim, Y.S., Kusakabe, K., Morooka, S. and Yang, S.M. (2001) Preparation of microporous silica membranes for gas separation. *Korean Journal of Chemical Engineering*, **18** (1), 106–112.

65 Rao, M.B. and Sircar, S. (1993) Nanoporous carbon membranes for separation of gas mixtures by selective surface flow. *Journal of Membrane Science*, **85** (3), 253–264.

66 Uhlhorn, R.J.R. and Burggraaf, A.J. (1991) Gas separations with inorganic membranes, in *Inorganic Membranes: Synthesis, Characteristics and Applications*, Chapman & Hall, New York, pp. 155–176.

67 Gilliland, E., Baddour, R.F. and Russel, J.L. (1958) Rates of flow through microporous solids. *AIChE Journal*, **4**, 90–96.

68 Weaver, J.A. and Metzner, A.B. (1966) The surface transport of adsorbed molecules. *AIChE Journal*, **12**, 665–671.

69 Okazaki, M., Tamon, H. and Toel, R. (1981) Interpretation of surface flow phenomenon of adsorbed gases by hopping model. *AIChE Journal*, **27** (2), 262–270.

70 Lito, P.F., Cardoso, S.P., Rodrigues, A.E. and Silva, C.M. (2014) Kinetic modeling of pure and multicomponent gas permeation through microporous membranes: diffusion mechanisms and influence of isotherm type. *Separation & Purification Reviews*, **44** (4), 283–307.

71 Shindo, Y., Hakuta, T., Yoshitome, H. and Inoue, H. (1984) Separation of gases by means of a porous glass membrane at high temperatures. *Journal of Chemical Engineering of Japan*, **17** (6), 650–652.

72 Bhave, R.R. (1991) *Inorganic Membranes: Synthesis, Characteristics, and Applications*, Van Nostrand Reinhold, New York.

73 Schramm, L.L. (1993) *The Language of Colloid and Interface Science: A Dictionary of Terms*, ACS Professional Reference Books, American Chemical Society, Washington, DC.

74 Lee, K.H. and Hwang, S.T. (1986) The transport of condensable vapors through a microporous Vycor glass membrane. *Journal of Colloid and Interface Science*, **110** (2), 544–555.

75 Burggraaf, A.J. (1996) Transport and separation properties of membranes with gases and vapours, in *Fundamentals of Inorganic Membrane Science and Technology* (eds A.J. Burggraaf and L. Cot), Elsevier, Amsterdam, pp. 331–433.

76 Uhlhorn, R.J.R., Keizer, K. and Burggraaf, A.J. (1992) Gas transport and separation with ceramic membranes. Part I. Multilayer diffusion and capillary condensation. *Journal of Membrane Science*, **66** (2–3), 259–269.

77 Tamon, H., Kyotani, S., Wada, H., Okazaki, M. and Toei, R. (1981) Surface flow phenomenon of adsorbed gases on activated alumina. *Journal of Chemical Engineering of Japan*, **14** (2), 136–141.

78 Burggraaf, A.J. and Keizer, K. (1991) Ceramic membranes, in *Concise Encyclopedia of Advanced Ceramic Materials* (ed. R.J. Brook), Pergamon Press, Oxford, pp. 62–67.

79 Asaeda, M. and Du, L.D. (1986) Separation of alcohol/water gaseous mixtures by a thin ceramic membrane. *Journal of Chemical Engineering of Japan*, **19** (1), 72–77.

80 van den Bergh, J., Zhu, W., Gascon, J., Moulijn, J.A. and Kapteijn, F. (2008) Separation and permeation characteristics of a DD3R zeolite membrane. *Journal of Membrane Science*, **316** (1–2), 35–45.

81 Okubo, T. and Inoue, H. (1989) Introduction of specific gas selectivity to porous glass membranes by treatment with tetraethoxysilane. *Journal of Membrane Science*, **42** (1), 109–117.

82 Hsieh, H.P. (1996) *Inorganic Membranes for Separation and Reaction*, Elsevier, Amsterdam.

83 Gilron, J. and Soffer, A. (2002) Knudsen diffusion in microporous carbon membranes with molecular sieving character. *Journal of Membrane Science*, **209** (2), 339–352.

84 Henis, J.M.S. and Tripodi, M.K. (1981) Composite hollow fiber membranes for gas separation – the resistance model approach. *Journal of Membrane Science*, **8** (3), 233–246.

85 Lopez, J.L., Matson, S.L., Marchese, J. and Quinn, J.A. (1986) Diffusion through composite membranes – a two-dimensional analysis. *Journal of Membrane Science*, **27** (3), 301–325.

86 Bouwmeester, H.J.M. and Burggraaf, A.J. (1996) Dense ceramic membranes for oxygen separation, in *Fundamentals of Inorganic Membrane Science and Technology*, Elsevier, Amsterdam.

87 Kharton, V.V., Naumovich, E.N. and Nikolaev, A.V. (1996) Materials of high-temperature electrochemical oxygen membranes. *Journal of Membrane Science*, **111** (2), 149–157.

88 Pierre, A. and Christian, G. (2008) Current status and prospects for ceramic membrane applications, in *Handbook of Membrane Separations*, CRC Press, Boca Raton, FL, pp. 139–179. p.

89 Christian, G. and Adam, S. (2015) Ceramic membranes technology: current applications and future development, in *Handbook of Membrane Separations: Chemical, Pharmaceutical, Food and Biotechnological Applications*, CRC Press, Boca Raton, FL, pp. 215–258.

3
Characterization of Ceramic Membranes

3.1
Introduction

Membrane characterization is a well-documented (and rather technical) subject. The two most significant aspects of any membrane are the pore network and the physicochemical properties of the membrane surface. A membrane's pore network structure determines how the solutes will pass through, while the membrane surface determines the uptake of these solutes and potential for fouling. Many membranes are asymmetric, so a complete set of information about each membrane layer is very important. Membrane characterization is often subdivided into three parts: the information needed for industrial operation, comparison of pilot and industrial needs and information gathered for research. The last set is the most comprehensive one and is subdivided into data provided by the membrane manufacturer, the data obtained from previous studies and the information collected during a current investigation. When the industry needs to confirm that the membrane has not changed from batch to batch and the pilot manager wants to compare different membranes by well-accepted features, researchers can look for a link between the membrane's fabrication process, morphology and performance.

One can also subdivide membrane characterization into physical and chemical aspects. Roughly speaking, the physical characteristics of a membrane describe its morphology, pore structure, mechanical strength and charge [1]. All these are essential for the day-to-day operation. Conversely, chemical characteristics describe membrane surface layer and its composition, and are more relevant for predicting a membrane's behaviour under different feeds and explaining why the membrane works well (or not). Physical characteristics typically cover the entire membrane structure from feed to permeate. Chemical features help us study the complexity of the membrane surface and several micrometres into the membrane depth. As we saw already in Chapter 1, this top layer is considered the most important for membrane behaviour.

Ceramic Membranes: New Opportunities and Practical Applications, First Edition. Vitaly Gitis and Gadi Rothenberg.
© 2016 Wiley-VCH Verlag GmbH & Co. KGaA. Published 2016 by Wiley-VCH Verlag GmbH & Co. KGaA.

In this chapter, we focus on the key methods and processes for characterization of ceramic membranes. For simplicity and clarity, we divide the methods into five sections:

- Methods for detection of pore size and pore size distribution, including permeability, the bubble point, liquid–liquid displacement (LLD), mercury porosimetry, gas adsorption–desorption, gas–liquid permporometry, solid–liquid thermoporometry, nuclear magnetic resonance (NMR) and solute transport tests.
- Microscopy methods for membrane surface images, including optical microscopy, confocal scanning laser microscopy (CSLM), scanning electron microscopy (SEM), transmission electron microscopy (TEM) and atomic force microscopy (AFM).
- Chemical methods, including backscattered radiation and vibrational spectroscopy such as X-ray diffraction (XRD), energy-dispersive X-ray spectroscopy (EDS or EDX), X-ray photoelectron spectroscopy (XPS), Rutherford backscattering spectrometry (RBS), Fourier transform infrared spectroscopy (FTIR) and Raman spectroscopy.
- Physical methods for characterizing membrane porosity, pore tortuosity, surface roughness and mechanical strength.
- Other methods often used for characterizing membrane hydrophilicity and surface charge, such as contact angle and streaming potential.

Note that rather than compiling a comprehensive review of all the techniques available for characterizing membranes, we will focus on these most useful methods, in line with the hands-on approach of this book.

3.2 Pore Size and Pore Size Distribution

Membranes are selective barriers that provide a good flux *and* a good separation between feed components. Both flux and separation depend upon the main transport mechanism. High-pressure membranes are dense and transfer feed components by diffusion. Low-pressure membranes are porous and transfer feed components by advection. We focus mainly on porous microfiltration (MF) and ultrafiltration (UF) as only these membranes have pores. Here the pore size determines which particles or molecules are retained and which will pass through the membrane. The exact membrane material is less important for this aspect, as the separation efficiency is correlated with the pore size. Dense membranes have no pores and their performance is determined by the chemistry of their surfaces. The characterization of a dense membrane might require a proof of absence of the pores. This is usually achieved by the measurements of permeation and rejection of solutes such as ions and soluble organics. These methods are described in Sections 3.2.1 and 3.2.9.2, respectively.

The pores in low-pressure membranes should be large enough to ensure a good flux and yet small enough to provide a good separation, often between two

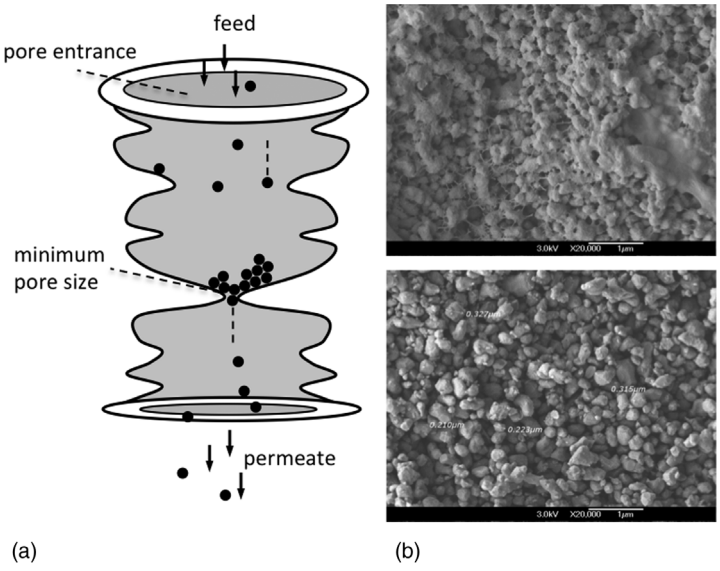


Figure 3.1 Cartoon of a membrane cross section showing the wide pore entrance with a narrowing in the pore (a) and scanning electron micrographs of ceramic membranes (b). The micrographs were taken on a JEOL HR-SEM JSM 7400F; samples were coated with 10 nm gold prior to imaging.

different phases. Here, 'large' and 'small' are the definitions of pore diameter or, more precisely, the pore width. This width is defined as the distance between two opposite walls of the pore [2].

There are over 10 different groups of methods for the detection of pore size and pore size distribution. Here, we focus on the more traditional and widely accepted methods that are or could be implemented for the characterization of pores in ceramic membranes. This variety suggests that there is no single optimal method, and with good reason: Membrane pores are typically complex structures with multiple features, such as 'throats' and constrictions (see Figure 3.1).

Part of the complexity of pore size determination stems from the variety of membrane pore sizes. Different membranes possess pores between subnanometre and up to 200 µm. Even within a single membrane, the range of pore sizes can be as large as one order of magnitude [3]. No single method can cover the entire pore range. Most of the methods fail to properly describe the most interesting nanometric pores. Pores are embedded inside membrane constructs, so porous systems are often interconnected networks. In real-life membranes, the pores always differ in size, giving a range rather than a single value. The result of the measurement even depends on the sequence in which the pores are accessed [4]. Pore can change during normal membrane operation. Even the

exact pore size and pore size distribution defined in a pristine membrane become fouled and its pore size depends on the degree of internal fouling. The pores might also change after membrane cleaning and even after the pore size test. Note that fouling and cleaning apply chiefly to liquid filtration – pores in gas separation membranes typically remain unchanged. Despite all these limitations, the pore size and size distribution are the most important features of a ceramic membrane.

There are several groups of pore size tests:

- Pressure-based tests relate the permeation of a liquid or a gas through the membrane to its pore size, or check for the liquid displacement by a gas or by another liquid using the so-called bubble point method [5]. These include permeability tests, gas–liquid displacement, liquid–liquid displacement and mercury porosimetry.
- Tests based on the assumption that the pores are gradually covered with a monolayer of gas molecules adsorbed in pores such as gas adsorption–desorption.
- Tests based on a phase change from gas to liquid or from liquid to solid. These use the gradual blockage of pores to a free transfer of a gas or a liquid as a function of partial pressure or temperature. Gas–liquid permporometry and solid–liquid permporometry fall in this category.
- Tests based on a different behaviour of adsorbed versus bulk molecules, such as nuclear magnetic resonance.
- Marker-based tests, performed by tracing passive markers that are either natural or are spiked periodically into the membrane feed. These include turbidity particles, ions, organic molecules, metal nanoparticles and microorganisms.

Below we describe the principles, advantages and disadvantages of pore size tests with emphasis on their sensitivity, reliability and feasibility for various types of membranes. The sensitivity is the ability to detect the full range of pores in the membrane matrix and include only transmembrane pores. This means that dead-end pores (which cannot transfer anything through the membrane) should be excluded. As we discussed in Chapter 1, pore sizes are subdivided into *macropores* (diameter >50 nm), *mesopores* (2–50 nm) and *micropores* (<2 nm) [6]. Pore distributions and fractions thereof are typically referred to by d_n, where d is the diameter and n is the percentage of pores up to this diameter. Thus, d_{50} is the median pore diameter, d_{90} is the diameter that is larger than that of 90% of the pores in the membrane matrix and d_{100} is the diameter of the biggest pore. In other words, a membrane has absolute retention of any particle with a diameter larger than d_{100}. Figure 3.2 shows a typical pore size distribution in low-pressure membrane. Note that the above definition does not characterize the membrane or the pores of the membrane. It only describes the size of the particles or molecules retained by it.

The two remaining parameters, reliability and feasibility, pertain to the application of the membrane in various situations. Reliability reflects the repeatability of the results and the linearity in the test response to the signal stimuli. The

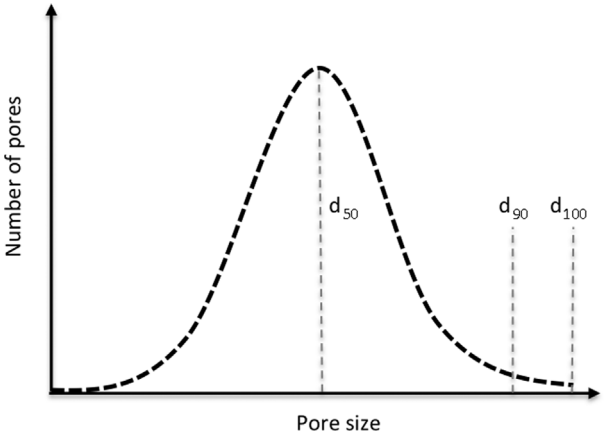


Figure 3.2 Pore size distribution for a typical low-pressure membrane.

feasibility reflects the performance of the membrane in various application scenarios (low pressure, high pressure, immersions and so forth).

3.2.1 Permeability

Permeability is second only to visualization as a simple yet comprehensive test of membrane features and abilities. It measures the flux of a fluid through a membrane. In the simplest configuration, a piece of a membrane is fixed in a bench scale apparatus and the permeate flux is measured volumetrically or gravimetrically over time. In industrial applications, the flux is measured routinely using flowmeters. The initial flux through a virgin membrane gives information about the pore size distribution, pore size and connectivity. Similarly, the transmembrane flux can indicate if the pores are conductive and a fluid comes out of a membrane on permeate side, or whether the pores are dead-end ones and the membrane should be discarded. If an experiment is continued over time and the flux starts to gradually decrease, we can obtain a first sign and information about possible fouling. And finally, after a cleaning, the measurement of the flux indicates how well the membrane was cleaned. This is done by simply comparing the flux through the membrane after the cleaning with that flowing through a virgin membrane.

Permeation tests measure the permeability of a pure liquid or gas through the membrane using simplification of the pore to obtain its average radius. The test is purposefully performed prior to operation to avoid bias due to fouling or compaction. This latter phenomenon is related to polymer membranes. In liquid permeability tests, membrane pores are simplified either into channels connecting the feed and permeate sides or into liquid-transportable voids between well-packed spheres. The former corresponds to the Hagen–Poiseuille equation and the latter

to the Carman–Kozeny equation. Typically, the total gas permeation rate through ceramic membranes is approximated as a sum of Poiseuille flow and Knudsen diffusion in porous medium [7]. The accuracy of liquid and gas permeability tests depends largely on the similarity between the approximation and the real pore tortuosity (Section 3.5). Large fluctuations between pores also affect the results [8].

According to the Hagen–Poiseuille equation, the average pore radius of a membrane pore r_p (m) is equal to

$$r_p = \sqrt[4]{\frac{\Delta Q}{\Delta P}\frac{8\mu\delta}{n\pi}} \tag{3.1}$$

where ΔQ is the change in the flow of a liquid (m^3/s), ΔP is the transmembrane pressure (Pa), μ is the liquid viscosity (Pa s), δ is the pore length that is equal to the membrane thickness (m) and n is the number of pores per unit area. This equation is constructed under the assumption that all pores are cylindrical, straight, identical, parallel to each other, perpendicular to the membrane surface and cross the membrane from the feed to the permeate. Basically, it describes an ideal pore that is seldom found in real membrane structures. It can help in comparing different membranes. The empirical coefficients δ and n are helpful to account for more complex pore geometries [9].

According to the Carman–Kozeny equation, the average pore radius of a membrane pore r_p (m) is equal to

$$r_p = \sqrt{\frac{J}{\Delta P}\frac{8\mu\delta\tau}{\varepsilon\pi}} \tag{3.2}$$

where J is the permeation flux of a liquid ($m^3/(m^2\ s)$), ΔP is the transmembrane pressure (Pa), μ is the liquid dynamic viscosity (Pa s), δ is the pore length that is equal to the membrane thickness (m), τ is the tortuosity (–) and ε is the porosity (–). This equation contains two correlation factors – tortuosity and porosity – that allow fitting almost any set of permeability data to a pore radius. An independent evaluation of these factors prior to permeability experiments greatly enhances the validity of the results [10]. Both equations suggest a relation between the permeability and the transmembrane pressure (TMP). This relation can be used to establish the average pore radius considering the ideal stimuli response of the flux to TMP, or the pore size distribution considering that liquid confined in small pores will be pressed out at increased TMP.

The same principle is realized in the gas permeability test. The average pore size r_p (m) received after certain approximations [10] is given by Eq. (3.3):

$$r_p = \frac{16\mu}{3}\left(\frac{K_p}{K_k}\right)\sqrt{\frac{8RT}{\pi M}} \tag{3.3}$$

where K_p and K_k are the permeability coefficients of gas transport according to the Poiseuille viscous and Knudsen diffusion flow mechanisms ($mol/(mm^2\ Pa\ s)$), M is the molecular weight (g/mol), μ is the gas viscosity (Pa s), R is the gas constant (8.3174 m^3 Pa/(mol K)) and T is the absolute temperature (K). The measurements

are done with inert gas at different pressures [10]. Using this method, Al_2O_3 and yttria-stabilized zirconia showed pore sizes between 10 and 100 μm [11]. A pore size distribution can be obtained by the addition of standard normal distribution and log-normal distribution functions to the equation [12]. Gas permeation tests were also used to obtain the effective porosity (ε/L_p) defined as the ration of porosity and the effective pore length [13]. Note that the effective porosity takes into account the tortuosity τ of membrane pores.

Gas permeation tests are often performed on dense ceramic membranes made of solid oxides to check structural integrity. Integral membranes will have a high permeability for one compound only. For example, solid oxide fuel cells (SOFCs) transfer only oxide anions O^{2-} (see Chapter 4 for more details) but no gases. Mixed conducting membranes typically transfer only oxygen or hydrogen. The tests are performed for different time periods needed to set and maintain a constant partial pressure on both sides of the membrane. To ensure the membrane integrity at elevated temperatures, another inert gas is added. This gas is added to the feed side, and any traces of it in permeate suggest that the membrane integrity had been compromised. For example, in oxygen permeation tests, air or nitrogen is used as an inert gas and the presence of nitrogen in permeate indicates that the membrane is not intact [10]. This air or nitrogen is also used for adjusting the oxygen partial pressure. The tests are typically run in an oxygen permeation apparatus with small piece of a membrane where the oxygen concentration in permeate and retentate are continuously measured with an oxygen meter. Trace amounts of nitrogen can be detected by a gas chromatograph. The oxygen flux is calculated using Eq. (3.4):

$$J_{O_2} = \frac{1}{G}\frac{V_t C_{O_2}}{A_t} \tag{3.4}$$

where V_t is the volumetric flow rate of the effluent stream (m^3/s), C_{O_2} is the oxygen concentration (M/m^3) and A_t is the membrane area (m^2) [10]. G is the dimensionless factor that corrects for the effect of non-axial diffusion [14].

Hydrogen permeation tests are somewhat similar to the oxygen permeation tests except that in hydrogen tests, the water vapour must be considered. In proton exchange membrane fuel cells (see also the examples in Chapter 4), water vapour is the actual source of hydrogen and the test might display incorrect results or even damage the membrane by a dry hydrogen stream. Hydrogen permeation tests are therefore run in a wet environment where the conditions on both sides of a membrane are well defined [10]. For example, the H_2 permeation flux can be calculated from the rate of water produced at the permeate side of a membrane where H_2 reacted with O_2 to produce water. In this case, the hydrogen flux is calculated using Eq. (3.5):

$$J_{H_2} = \frac{P_0}{RT}F_s\frac{\Delta RH}{A_t} \tag{3.5}$$

where F_s is the total flow rate of the sweep gas stream (mol/m^3), ΔRH is the difference in the relative humidity between the outlet and the inlet of the sweep

gas, A_t is the membrane area (m^2), P_0 is the saturated vapour pressure (Pa) and T is the air temperature (K) [15]. Hydrogen permeation tests are often done at 300–350 °C, as this is the temperature of reformate streams. Higher permeation rates at increased temperatures help detect the hydrogen concentration in the permeate. Another approach to ensure the absence of leaks is to perform the test at different fluxes. A stable partial pressure/concentration of the permeable gas proves that the permeation is driven by diffusion mechanisms and not through abnormal pores.

3.2.2
The Gas–Liquid Displacement Bubble Point Technique

Permeability measures the flux at various pressures. The oldest and the simplest pressure-based variant is the *bubble point test* [16]. This test is based on blowing a liquid out of membrane pores with a gas. Actually, this test does not even require flux measurements [5]. The one and only data point needed for the bubble point measurement is the pressure applied at the moment when the first gas bubble appears on the permeate side. Figure 3.3 shows a membrane cross section with different membrane pores and a graph of the gas flow rate as a function of TMP [5].

The bubble point test starts when a wetting liquid spontaneously fills the pores. This happens because the surface free energy of the liquid–membrane interface is lower than that of the air–membrane interface; the filling is thus accompanied by a decrease in free energy. The spontaneous wetting requires a match between the membrane hydrophilicity and the wetting liquid. Hydrophilic membranes are filled

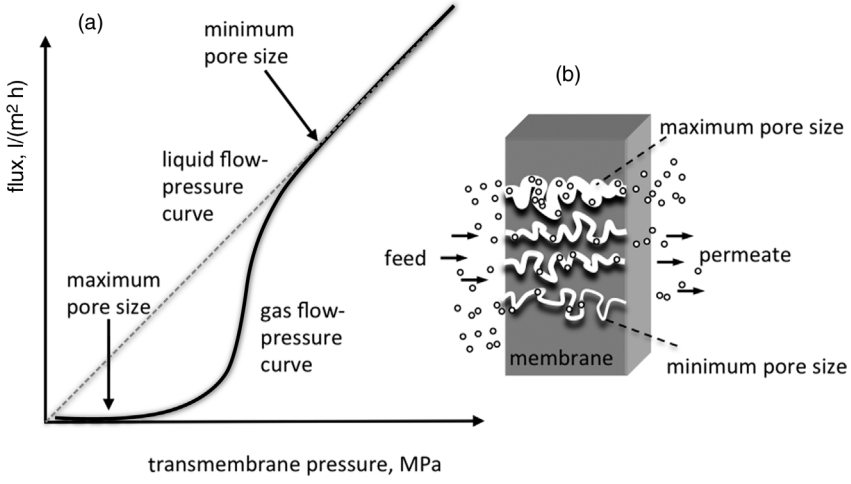


Figure 3.3 Theoretical flow-pressure curve for the bubble point test/progressive displacement test (a) and cartoon of a bubble point test (b).

with water, while hydrophobic membranes are filled with alcohol–water mixtures [17]. The liquid is held by capillary forces and cannot leak out spontaneously. Then, by applying external pressure, a gradual removal of the wetting liquid from membrane pores occurs. First, all pores are filled with liquid and the gas flow through the membrane is zero. The first pore that will empty due to the increasing gas pressure is the one with the largest diameter. The pressure that overcomes the capillary pressure is related to the capillary (the pore) size and can be given by the Laplace equation, derived from a balance of static forces on the meniscus in a capillary tube [18]:

$$P_{\mathrm{bp}} = \frac{4\sigma \cos\theta}{D_{\mathrm{p}}} \tag{3.6}$$

where P_{bp} is the differential inert gas pressure on the wetting liquid in the pore (kPa), σ is the surface tension at the gas–liquid interface (dyn/cm), θ is the contact angle of the wetting liquid with the membrane (°), and D_{p} is the pore diameter (μm).

Typically, the pore size is evaluated under the assumption that the membrane is absolutely hydrophilic (θ is 0°) and the water is blown out of membrane pores by air at 25 °C (σ is 72 dyn/cm). This yields a simple relation:

$$D_{\mathrm{p}} = \frac{288}{P_{\mathrm{bp}}} \tag{3.7}$$

The method was developed further to account for pore size distribution [19]. A gradual increase of the pressure above the threshold value will displace the liquid from smaller and smaller pores and increase the gas flow rate. The recorded gas flow rate is placed as a function of applied pressure in the famous S-shaped pore size distribution curve (Figure 3.3). Here, dashed and solid lines indicate the relation between the applied pressure and airflow of dry and wetted liquids, respectively. The first air bubble represents the largest pore emptied at the bubble point pressure. When the gas flow through the wet membrane is equal to the flow through a dry membrane, it means that the smallest pore is detected. Using the Laplace equation, one can estimate pore diameters at each applied pressure data point.

The bubble point test is a well-known simple method for determining the pore sizes in MF and UF membranes. But it is not perfect. The time needed for the gas to fully displace the liquid from the pores at each applied pressure causes the method to overestimate the smallest pore sizes. The result depends on the liquid used, as well as on the rate of pressure increase and the pore lengths. Unfortunately, as is the case for most of methods for measuring pore size distribution, the method is not standardized. This makes comparing results more difficult. Moreover, the assumed absolute hydrophilicity of the membrane lowers the diameters of detected pores. Figure 3.4 shows the test pressure versus the equivalent pore diameter for several typical membrane polymers. The evaluation of 3 μm with a bubble point is easy and for all membranes it is achieved with less than 1 bar transmembrane pressure. A higher pressure is required for detecting

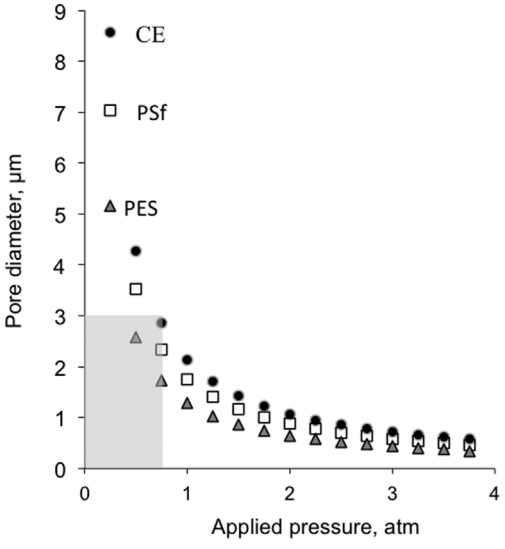


Figure 3.4 A relationship between test pressure and equivalent pore diameter in membranes made of cellulose acetate (CE), polysulfone (PSf) and polyethersulfone (PES). The typical contact angles are 42.5° for CE [20], 52.4° for PSf [21] and 63.4° for PES [21]. The contact angle of 92.9° for PVDF [22] results in negative pore values (not plotted on this graph).

smaller pores. This detection pressure often exceeds the upper pressure limit allowed by the membrane manufacturer.

3.2.3 Liquid–Liquid Displacement

Liquid–liquid displacement, also known as *bi-liquid permporometry*, is similar to the gas flow bubble point test (Section 3.2.2). The method was introduced in 1933 by Erbe and further developed by Capannelli *et al.* [23]. The only difference between LLD and bubble point test is in the use of two immiscible liquids. The liquids should have a small difference in their surface tension [24]. The membrane is saturated under vacuum with the wetting solvent and thereafter the second solvent is pressurized gradually from the feed side [25]. After reaching the threshold pressure, the liquid flow is recorded and plotted against applied pressure. The pore sizes and their distribution are then calculated using the Hagen–Poiseulle equation (Eq. (3.1)).

The biggest advantage of LLD is the significant reduction in relative pressure needed to blow the liquid from the pores. For example, the air pressure required to blow out water from a pore size of 10 nm is as high as 29 bars (assuming a surface water tension of 72.3×10^{-3} N/m and a 0° contact angle) (Eq. (3.6))). Using liquid displacement, Gekas and Zhang [26] were able to characterize the entire pore size distribution in UF membranes with pressure below 8 bars. A

second important advantage is that the wetting liquid is displaced only from interconnected pores. The drawback is that the LLD set-up is rather complex and a possible pressure build-up can change the pore size and interfere with the measurements [27].

3.2.4 Mercury Porosimetry

One of the variations of bubble point and liquid displacement techniques is *mercury intrusion porosimetry* (MIP). This method is based on gradual filling of pores in a pre-vacuumed dry membrane by mercury using an increasing mercury pressure [28]. The measurements are run in a special sample cup penetrometer with small membrane pieces. First, the membrane is immersed into mercury (a non-wetting liquid), and the initial mercury volume is determined. During the measurement, the mercury fills the pores under increasing pressure, and at each pressure point the total mercury volume is registered. When the mercury volume in the penetrometer remains unchanged, the depletion from a capillary stem reservoir connected to the sample cup can be accurately measured. Figure 3.5 depicts a mercury porosimetry set-up and a theoretical curve of cumulative volume of mercury as a function of the applied pressure.

The pore size is recalculated from the pressure data using the Laplace equation (Eq. (3.6)), and the measurement continues until the further pressure increase does not change the mercury volume inside the reservoir. Subsequently, the percentage of total pore volume is plotted against the pore diameter, giving information on the average pore size and pore size distribution [29]. Additional data are obtained from a subsequent extraction experiment by reducing the pressure. This method is quick (typically takes <30 min) and can be used for

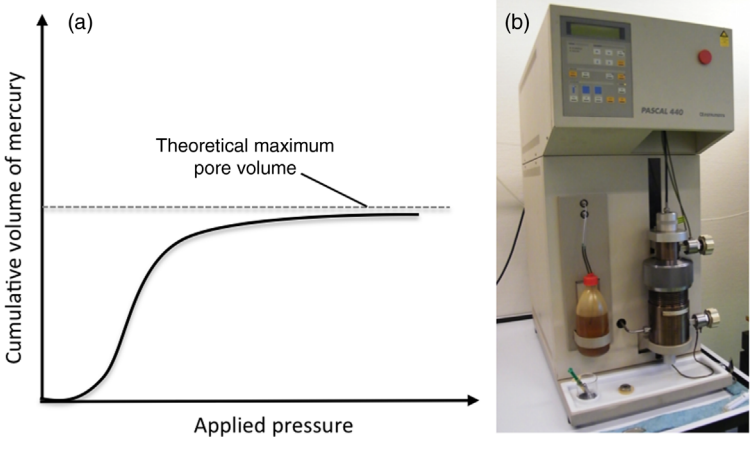


Figure 3.5 Theoretical curve of cumulative volume of mercury versus applied pressure (a) and photo of a mercury porosimetry measurement set-up (b).

determining the total pore volume or porosity, the skeletal and apparent density and, uniquely, the specific membrane surface area.

Mercury porosimetry, however, does have limitations. Usually, pores are not cylindrical and the technique measures the largest entrance towards a pore but not the actual inner pore size [30]. A correction in a form of a morphological constant is thus needed [10]. Moreover, only pore sizes between 3.5 nm and 500 μm can be investigated. A 425 bar pressure is needed to detect a 3.5 nm pore size (a 485 dyn/cm surface tension and 140° contact angle of mercury with α-alumina are reported by most researchers) [31]. The high pressure needed to fill the small pores with mercury changes the membrane structure and opens dead-end pores that would be unavailable under normal operating conditions. This test is performed under dry conditions, and the membrane can undergo compaction that changes or even collapses pores. Some mercury always remains entrapped in pores, so the membranes cannot be used further after the analysis is completed [32]. Finally, both the mercury itself and the apparatus are expensive, and many laboratories avoid using mercury for safety reasons.

3.2.5
Gas Adsorption–Desorption

Gas adsorption–desorption employs the Brunauer–Emmett–Teller (BET) method for determining pore size, pore size distribution and surface area of ceramic membranes. In this method, the membrane is exposed to a flow of gas molecules that adsorb in the pores. Different gases can be used, most commonly N_2, argon or CO_2. The amount adsorbed depends on the membrane and the pressure. Both physical and chemical adsorption can occur, but the former is more important since it applies to all gases and surfaces. Such physical adsorption, or *physisorption*, is relatively weak (typical adsorption energies are 20–40 kJ/mol). The amount of adsorbed gas at constant pressure increases at lower temperatures, so most experiments are done at low temperatures (e.g. 77 K at 1 atm as the boiling point for pure nitrogen). The experiment starts at low pressures when the gas molecules will be adsorbed in big pores. A gradual increase in partial gas pressure will result in adsorption in smaller and smaller pores until all pores are filled. At each pressure point, the volume of adsorbed gas is measured, giving the same type of the curve described in Section 3.2.3 (where the pore diameter is plotted against pore relative fraction). The result is fitted to the BET isotherm that provides the total number of adsorbed molecules filling the primary monolayer. The total pore area is calculated from the known area per gas molecule, and the pore radius is determined from the ratio of total pore volume to the total pore area [10]:

$$r_p = -\frac{4.15 \times 10^{-10}}{\log(P/P_0)} + 3.54 \times 10^{-10}\left(-\frac{5}{2.303\log(P/P_0)}\right)^{0.333} \tag{3.8}$$

where P and P_0 are the applied pressure and the saturation pressure (Pa), respectively.

Gradually reducing the pressure then strips the adsorbed molecules from the surface, and once again the total gas volume can be measured. The adsorption and stripping curves show a hysteresis, which is attributed to capillary cracks (molecules remain in these cracks due to lower vapour over the concave meniscus formed by the condensed liquid in the pores) [33]. Both curves are useful in evaluating membrane surface areas, pore volumes and pore size distributions. The main drawback of this technique is that it also includes dead-end pores, which do not participate in transport [34].

3.2.6
Gas–Liquid Permporometry

Permporometry, developed by Eyraud *et al.* [35] as gas–liquid permporometry and improved to gas–vapour permporometry by Mey-Marom and Katz [36], is a combination of permeability and pore measurement or porometry, that is the measurement of permeability of a gas through pores. Mixtures of immiscible gases at the same pressure are blown through the membrane from both sides (see Figure 3.6). Each mixture contains a condensable gas with a low condensation point (e.g. CCl_4, methanol, ethanol or cyclohexane [37]) and an inert gas with a suitable vapour pressure and a high evaporation rate (e.g. N_2). When the feed side of the membrane is flushed with a mixture of N_2 and a condensable gas and the permeate side is flushed with a mixture of N_2, O_2 and the condensable gas, a diffusive transport of O_2 occurs [8]. The only thing that prevents the transport is the capillary condensation of the condensable gas that clogs the pores [10].

The test is performed in two stages. At the first clogging stage, the flushing of a dry membrane is performed with the condensable gas at its partial saturation. The diffusion of the inert gas will continue in pores with partial pressure below the saturation of the condensable gas and will stop in pores where partial pressure is higher than partial saturation pressure. In these pores, the gas condensates and the gas flow through the liquid halts. This first stage of the measurement is performed using a gradually increasing pressure that causes a gradual blockage of the pores. At the second stage (the stripping stage), the relative pressure of the

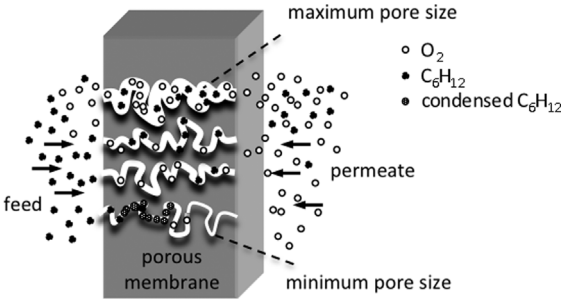


Figure 3.6 Principles of the permporometry method.

condensed gas is reduced stepwise. The reduction gradually evaporates the condensed gas, first from the large pores and then from the small pores, and increases the transmembrane diffusion of O_2. Pore size distribution is usually measured at the second stage. The relative concentration of oxygen on the opposite side of the membrane is recorded with a gas chromatograph or with an oxygen electrode. Then, the relation between the radius capillary (in fact, the pore radii) and a change in the vapour pressure is calculated using Kelvin's equation [38]:

$$\ln \frac{P}{P_0} = -\frac{2\gamma \cos \varnothing V_m}{r_K RT} \tag{3.9}$$

where P and P_0 are the actual and the saturated vapour pressures of the condensable gas (Pa), γ is the gas–solid interfacial tension (J/m^2), θ is the contact angle (°), V_m is the molar volume of the condensable gas (m^3/mol), R is the gas constant (8.3174 m^3 Pa/(mol K)), T is the temperature (K) and r_K is the Kelvin radius (m). The latter is related to the real pore width d_p (m) via Eq. (3.10):

$$d_p = 2(r_K + t) \tag{3.10}$$

In this equation, t is the thickness of the t-layer [39] adsorbed on the inner surface of the pores at low initial pressure (m). Under most conditions, t values vary between 0.3 and 0.5 nm [36,40]. Setting the initial relative pressure to 1 and linking the pressure decrease to the size of unblocked pores gives the relative pore size distribution. All other parameters in Eq. (3.9) are approximated as constants. This method was used by Cao *et al.* for measurements of pore sizes in γ-alumina membranes [8]. They found a pore size range between 2 and 10 nm.

The biggest advantage of gas–liquid permporometry compared to other gas adsorption–desorption methods is that it measures only the interconnected 'active' membrane pores. These are the pores that are responsible for the actual transport. In addition, the test does not use a high external pressure and therefore does not require a high mechanical stability of tested membranes. This test can detect *mesopores* in a size range between 2 and 90 nm where the Kelvin equation is valid. The measurement itself, however, is complex, mainly due to the difficulty of maintaining equivalent pressure on both sides of the membrane. It is also time-consuming and therefore often done at desorption stage, when the thermodynamic equilibrium at each partial pressure value is achieved faster than at the adsorption.

3.2.7
Solid–Liquid Thermoporometry

Both permporometry and thermoporometry are based on a continuous clogging of pores with a substance that undergoes a gradual phase change. Permporometry uses condensation of gases by changing their partial pressure. Thermoporometry uses solidification of liquids (usually water) by changing its temperature. In both cases, the clogging happens gradually and depends on the pore size. The

exothermic liquid/solid phase change (freezing) results in a decreased transient heat flow that can be sensed by a differential scanning calorimeter (DSC). The measurements can also be performed when a wetting liquid is first frozen inside the pores at low temperatures [41]. A gradual slow melting occurs below the bulk melting point and can be detected by measuring the quantity of mobile liquid using nuclear magnetic resonance cryoporometry (NMRC) [42] or by measuring the amplitude of neutron scattering from the imbibed crystalline or liquid-phase cryoporometry [43]. The difference between the bulk and pore freezing/melting points is called the *solidification temperature depression*. It is linked to the pore size via Gibbs–Thomson equation [44]:

$$\Delta T_{\mathrm{m}} = T_{\mathrm{m}}^{\infty} - T_{\mathrm{m}}\left(d_{\mathrm{p}}\right) = \frac{4\sigma_{\mathrm{cl}} T_{\mathrm{m}}^{\infty}}{d_{\mathrm{p}} \Delta H_{\mathrm{f}} \rho_{\mathrm{s}}} \tag{3.11}$$

where ΔT_{m} is the solidification temperature depression, T_{m}^{∞} is the normal melting point of bulk liquid, $T_{\mathrm{m}}(d_{\mathrm{p}})$ is the melting point of crystals of diameter d_{p}, σ_{cl} is the surface energy at the crystalline–liquid interface, ΔH_{f} is the bulk enthalpy of fusion per gram of material and ρ_{s} is the density of the crystal.

The depression of the phase equilibrium between solid, gas and liquid phases in highly dispersed systems was first described by Kubelka and Munk [45]. Thus, whereas in the bulk the freezing of water occurs at 0 °C, temperatures between 0 and −40 °C are needed to freeze the water in membrane pores. Brun *et al.* [30] explained this large temperature gap by pointing on the need for formation of a critical nucleus having a minimal size. The critical size of cylindrical pores was found directly proportional to the confined liquid temperature for both cases of solidification:

$$r_{\mathrm{p0}}(\mathrm{nm}) = \left(-\frac{64.67}{\Delta T_{\mathrm{s}}}\right) + 0.57 \tag{3.12}$$

and melting [30]

$$r_{\mathrm{p}}(\mathrm{nm}) = \left(-\frac{32.33}{\Delta T}\right) + 0.68 \tag{3.13}$$

where

$$\Delta T = T - T_0 \tag{3.14}$$

Here T_0 (°C) is the normal-phase transition temperature of the liquid and T (°C) is the temperature where the phase transition in membrane pores is actually observed. The difference in expressions between the solidification and the melting is due to the different curvatures of the interfaces at the time of phase transition. In spherically shaped pores, there is no difference in the shape and the same solid → liquid and liquid → solid expression applies [30].

Inside fine pores the crystal mean size is equal to the pore diameter minus the thickness of a *t*-layer. The presence of a 0.8 nm (for water) *t*-layer that does not undergo a phase change was later explained by the high Gibbs free energy of the boundary liquid [46,47].

If the exact temperature gap ΔT is unknown, the use of differential scanning calorimetry helps to relate the ΔT to the heat released or required during solidification (Eqs. (3.15) and (3.16)) [30]:

$$Q = -5.56 \times 10^{-2} \Delta T^2 - 7.43 \Delta T - 332 \tag{3.15}$$

and melting

$$Q = -0.155 \Delta T^2 - 11.39 \Delta T - 332 \tag{3.16}$$

In these equations, Q (J/g) is the energy released or adsorbed per gram of a membrane. Changes in Q over time are therefore related to the changes in the pore volume and to the approximate pore radius [10].

Solid–liquid thermoporometry can determine pores in a fairly wide range, between 1.5 and 150 nm [30]. The results are in a good agreement with other methods such as gas adsorption–desorption [48]. Measurements are relatively simple if a differential scanning calorimeter is available. The results received during several runs on the same membrane showed high repeatability [48]. However, it is less popular than mercury porosimetry and gas adsorption–desorption. The effect of specific interactions between the freezing liquid and the membrane is largely unknown and may lead to misinterpretation of calorimetric signals [49]. The method's accuracy also suffers from a possible deformation of the pore structure during solidification and the inclusion of dead-end pores in the pore size distribution. Moreover, it measures cavity sizes rather than inlet sizes [37].

3.2.8
Nuclear Magnetic Resonance

Another method that has recently been adapted for pore size determination is NMR. The basic principle here is that the portion of pore fluid near a pore wall undergoes spin–lattice (T1) and spin–spin (T2) relaxation in a magnetic field at a faster rate than the bulk fluid. This, coupled with the fast diffusional exchange of fluid between regions within a pore, yields a unique average relaxation time constant for each different geometrical environment (i.e. pore size) within a porous material. This relaxation time constant is dependent on the ratio of surface fluid to non-surface (bulk) fluid in the pore, which is a measure of the pore hydraulic radius.

From the two-fraction fast-exchange model, the measured T1 can be related to the pore hydraulic radius by

$$\frac{1}{T_1} = \alpha + \frac{\beta}{r_\mathrm{p}} \tag{3.17}$$

where α is the reciprocal spin–lattice relaxation of the bulk fluid and β is the surface interaction parameter determined for partially saturated samples with different fluid contents.

A saturated porous medium, such as a membrane, should relax as a combination of its different geometrical regions, that is pores. Pore size distributions can be determined via NMR relaxation experiments if the observed relaxation curve can be deconvoluted into its component parts and if the relationship between pore size and relaxation time constants can be determined. The NMR measurements must be calibrated using a known pore population material. Nevertheless, no specific pore geometry has to be assumed. The maximum size of the membrane samples to be analysed by this experimental method is limited by the homogeneity of the magnetic field [2].

Note that while this method is very accurate, and can even detect *mesopores*, it is complicated and requires very expensive equipment.

3.2.9
Solute Rejection Tests

Solute rejection tests are considered today the state of the art in the determination of membrane pore sizes, mainly due to two reasons. First, industrial applications are less interested in pore size distribution but demand knowledge of the diameter of the biggest pore d_{100}. That is the size of the smallest solute that will be rejected under given operational conditions with 100% efficiency. If the absolute retention is not feasible, then 90% retention pore size value is practised. A proven degree of retention of a solute of interest is then direct and indisputable, no assumption and further calculations are needed. Other tests provide membrane pore dimensions that can later be translated into retention levels. Solute rejection tests can also be applied for the detection of retention degree of a solute of interest. The second advantage of tracking membrane rejection is that it can be applied at any time during the membrane operation. Other tests are applied periodically and require a stop of membrane operation. Most of the tests require dismantling of the membrane module, as well as complex instrumentation. Conversely, solute rejection tests supply information continuously and on-site, and with proper recording can indicate when and how the membrane pore changes. The test itself is well known to the personnel at the operation site and requires no special training.

Solute rejection tests are performed uniformly. The solute is injected or added to the feed site of the membrane and tracked on the permeate side. Operational conditions are the same as during a normal operation as the retention degree should display the real situation. The only test variable is the solute itself and its concentration. The choice of the solute depends on the tested membrane, required results, test frequency, test sensitivity and the availability of the solute and testing equipment. A large arsenal of solutes include gases such as oxygen and nitrogen, liquids such as organic acids, polysaccharides, polyethylene glycols, ions such as Na^{+}, Mg^{2+}, Ca^{2+}, dyes (including soluble fluorescent dyes) and colloidal particles, bacteria and viruses. Less sensitive tests are applied constantly with solutes available in the feed. More sensitive tests are applied periodically by spiking a concentrated tracer into the feed stream and tracking its traces in the

filtrate/permeate. Spiking tests with viruses and bacteria are applied industrially; the use of soluble dyes, gold, silver and ferric nanoparticles, powdered activated carbon (PAC) and organic molecules is reported [50,51].

The degree of retention is calculated as

$$R = 1 - C_p/C_f \tag{3.18}$$

where C_p and C_f are the concentration of a solute in the permeate and in the feed, respectively. The concentration units are not provided intentionally, as they may vary. In salt rejection tests, C_p and C_f are replaced by K_p (mS/m) and K_f (mS/m), solution conductivities in the permeate and the feed, respectively.

If the retention degree is substantially higher than 0.9, it is often expressed as log removal values (LRV) [52]:

$$\text{LRV} = \log_{10} C_p/C_f \tag{3.19}$$

The passage of 0.01 and 0.001 tracers corresponds to 2 and 3 LRVs, respectively. When 100% retention is not achievable under normal test conditions, the 90% retention is reported. A widely accepted molecular weight cut-off (MWCO) value is nominally defined as the molecular weight of a neutral solute that is rejected to 90%. Typical solutes include dextran or poly(ethyleneglycol) (PEG). The rejection of a number of probe molecules is then plotted versus MW on a log scale. Subsequently, the MWCO is determined by the interpolation of 90% rejection with the curve. Figure 3.7 depicts the MWCO test.

The tests are typically performed with low solute concentrations of 200–1000 mg/l to minimize the influence of solute–solute interactions. Experiments are run simultaneously with a number of solutes and their feed and permeate

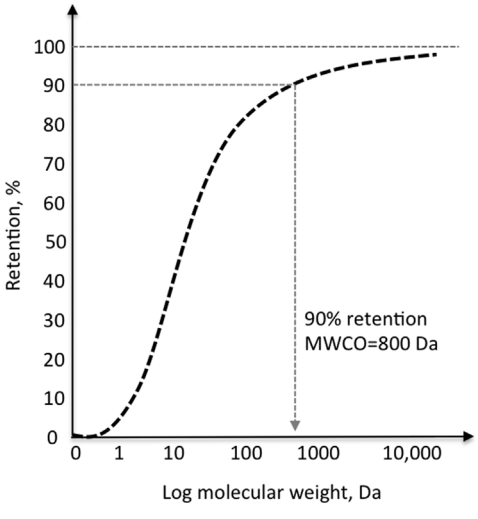


Figure 3.7 Plot showing the retention percentage for a membrane with a molecular cut-off of 800 Da. Note that the MWCO in this case corresponds to 90% retention.

concentrations are determined in a single run using gel permeation chromatography (GPC). The MWCO value is transferred to the pore radius using one of the approximations such as

$$r_p(\text{nm}) = 0.055(\text{MW})^{0.46} \quad (3.20)\ [53]$$

$$r_p(\text{nm}) = 0.33(\text{MW})^{0.46} \quad (3.21)\ [54]$$

$$r_p(\text{nm}) = 0.078(\text{MW})^{0.33} \quad (3.22)\ [55]$$

where MW is expressed in Da. Pore size distribution is often accepted from the solute transport results [56]. The MWCO is often accepted as the characteristic of the membrane pore size, but in fact it only reflects the retention of a certain model compound.

The solute rejection tests are considered indirect tests as they forecast the pore size from the rejection. Direct tests measure the pore itself. Despite their popularity, solute rejection tests are not perfect. One cannot define membrane separation characteristics by a single parameter such as the molecular weight of a solute. Other parameters that influence the retention are the shape and the flexibility of the solute, its interaction with the membrane and possible fouling [57]. Cut-off values defined in different ways under different test conditions (pressure, concentration and type of solute, test cell geometry) provide different results. Figure 3.8 shows an example of pore size distribution in membranes with sharp and diffuse cut-offs. The difference reflects the test conditions (measurements performed with different solutes such as protein (albumin), polysaccharide (dextran) or polyethyleneglycol [57]).

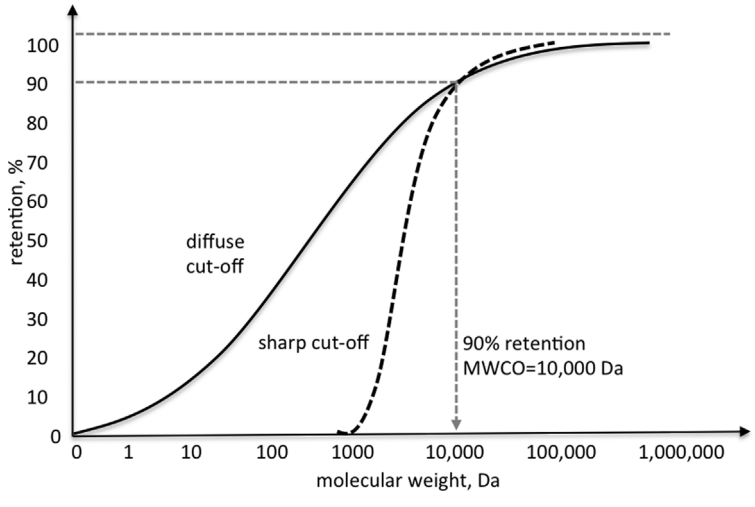


Figure 3.8 Rejection characteristics of a membrane with a 'sharp' cut-off compared with those of a 'diffuse' cut-off.

3.2.9.1 Solid Solutes

Retention of solutes by porous membranes can be estimated by solids, liquids and gases typically found in the feed or intentionally added to it. The choice of the solute largely depends on the membrane porosity and the required test sensitivity. For example, the common way for reporting the pore size in UF membranes is by detecting its MWCO. However, knowing the critical retention size or the LRV of a solute of interest could serve better than MWCO. The same principle applied to MF membrane would lead to an opposite conclusion as typical pore sizes in MF membrane are higher than the PEG line of available molecules [51]. Here we examine the most popular solute rejection tests, dividing these into tests with solid particles, organic molecules ions and tracers.

Inert solid particles can be used for determining the critical membrane pore size or LRV. The test itself is easy but requires dedicated equipment. However, the results pertain to one special preset value. This test is mainly performed in water and wastewater treatment where the preset value of 1 μm corresponds to the retention of oocysts of *Cryptosporidium parvum* [58].

Another common method is based on turbidity, the scattering of visible light that passes through a suspension. Turbidity is usually measured with a laser or laser diode light source at 660 ± 30 nm, estimating the amount of light scattering particles >700 nm. Except for highly diluted suspensions, the number of particles correlates with the turbidity, so higher turbidity levels mean more particles. Thus, an increase in turbidity level in the filtrate/permeate indicates a breach [59]. The concentration of penetrating particles in a certain narrow size range can be known exactly if a particle counter is used instead of a turbidimeter. A dedicated particle counter can even count and monitor particles with different sizes in the feed and filtrate [60]. Although detection starts at 500 nm particles, stable and repeatable results are obtained for particles in the range of 1–100 μm. The advantages of tracking the turbidity particles include the ability to track the integrity of all pressure-based membranes, a widespread use and a continuous monitoring of the filtrate quality. That said, the turbidimeters are not sensitive enough below one LRV [52]. This is simply because the minimum feed turbidity level of 0.5 NTU is seldom met [61]. However, a significant concentration of bacteria can be observed in water having less than 0.1 NTU turbidity [62].

The sensitivity of the method can be increased if the turbidimeters are replaced with particle counters having a minimum detection level of 1 particle/ml [59]. That concentration is very sensitive to minor water quality changes. However, it requires an individual monitoring of each module with a dedicated sensor. Panglisch *et al.* [63] estimated that detection of one broken capillary in 22 m^2 membrane area is possible if the feed particle concentration is higher than 7000 particles/ml. Total tracked membrane areas of 18 and 385 m^2 per a single particle counter were obtained experimentally in two independent studies with the same feed concentration of 200 000 particles/ml [64,65]. These measurements were done at least every 15 min during filtration. The disadvantages are that calibrating the particle counters in the field is difficult, repeatability of measurements

is low and readings observed at the beginning and at the end of measurements are less trustworthy [66]. Moreover, the particle counters can yield false-positive results, for example counting air bubbles trapped after air backwashing, or when two or more particles passing through the sensor simultaneously. The counters are more expensive than turbidimeters and their sensitivity is constantly counterbalanced by the treatment plants that use a minimal number of counters for the maximum membrane surface [67].

3.2.9.2 Ions and Dissolved Organics

Solute rejection tests can also be performed with ions or organic molecules measuring conductivity or TOC profiling. Tests with dissolved substances are practiced in NF and RO membranes that have pores substantially smaller than those detectable with colloidal particles (Figure 3.4). The idea is that NF and RO membranes will retain ions and NOM almost completely, so the passage of salts or organics is possible only when the membrane is damaged [68]. Any suspected integrity breach, however, will be small and will not be reliably tracked at permeate end of the entire module. Thus, the membrane integrity is tested with a long sample tube inserted into the permeate port and used to withdraw samples. Various points along the length of the permeate tube are monitored, and the conductivity/TOC is profiled along the length of the permeate tube [52]. The TOC monitoring is based on acidification of organic matter by a chemical/UV oxidation step to pH 2. At this pH all organic carbon is converted into CO_2, and a deduction of the inorganic carbon value from the total carbon gives the TOC value [69]. The tests are often combined with permeability tests as, for example, is recommended for FILMTEC membranes [67]. Online analysis of electrical conductivity is routinely used for monitoring RO membrane integrity for the integrated membrane system (IMS) of the N.V. PWN Water Supply Company [70]. The tests are performed with a synthetic test solution (NaCl in RO, $MgSO_4$ and $CaCl_2$ in NF) at $25 \pm 1\,^{\circ}C$ and $pH = 8$ [71]. These tests require at least one order of concentration magnitude difference between the feed and the permeate.

Conductivity and TOC tests have their limitations. Continuous membrane operation results in higher concentration of impurities near the membrane surface, followed by their increased passage through the membrane due to concentration–polarization effect. Thus, a significant increase in the concentration of impurities in permeate can easily be interpreted as an integrity breach, while in fact it is a false alarm.

3.2.9.3 Spiking Tests

Particle monitoring, conductivity and TOC profiling are continuous pore size and pore size distribution tests that produce subjective data. The absence of sufficient initial concentrations limits the sensitivity of LRV determination with continuous integrity tests.

All this brought the idea of using concentrated spikes of a specific impurity in the feed following its detection in permeate. In general, every compound can be

spiked and then tracked. However, stringent health regulations put constraints on possible tracers. The current list of possible tracers includes soluble dyes such as FD&C Red Dye #40 or Rhodamine WT [52], powdered activated carbon (PAC) particles [70], gold, silver [74] and magnetic nanoparticles [75] and native and dyed bacteriophages [76,77]. Figure 3.9 displays a range of highly monodispersed gold nanoparticles that can be used for both pore size distribution and integrity tests [51].

The unifying line of tracers is the ability of the membrane to nearly completely reject the tracer when intact. If a membrane cannot pass the threshold of at least 2 LRV retention, a high concentration of a tracer in the permeate indicates either a membrane defect or a seal defect. Many tracers are based on light adsorption or fluorescence to facilitate detection.

The technique includes the injection of a stable solution of nanoscale probes into the feed stream, followed by tracking their traces in the filtrate/permeate. When spiking is performed with a concentrated suspension, the samples in the permeate are diluted, as the penetration of the tracer through the membrane takes time [78]. A full picture is obtained when many samples are collected over a period that is at least two to three times longer than the hydraulic residence time τ (min). This is defined as $\tau = V/Q$, where V (m^3) is the membrane inner volume and Q (m^3/min) is the transmembrane flux. A collection of the full range of samples gives a degree

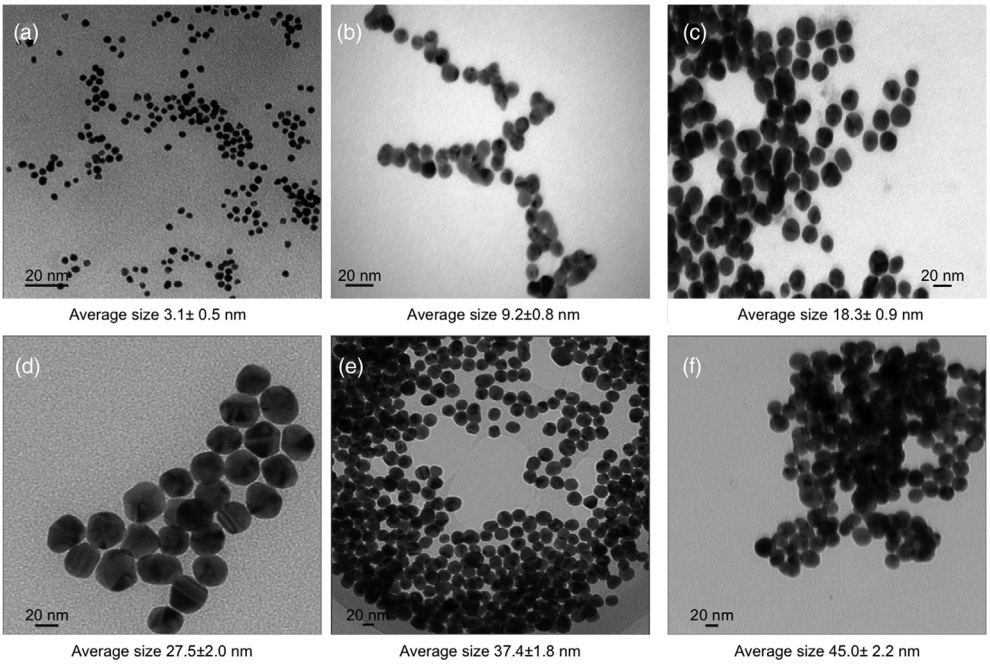


Figure 3.9 High-resolution transmission electron micrographs of gold nanoparticle suspensions. (Reproduced with permission from Ref. [51]. Copyright 2012, Elsevier Limited.)

of retention as the ratio of total tracer mass in the feed and in the permeate:

$$\text{Tracer passage} = M_p/M_f \tag{3.23}$$

where M_f and M_p are the total number or mass of the tracer in the feed and in the permeate, respectively. M_p can be calculated from

$$M_p = \sum\nolimits_i (C_i \Delta t_i) Q \tag{3.24}$$

where C_i (particle/m^3, mg/m^3) is the concentration in the collected probe, Δt_i (min) is the collection time period of individual samples and Q is the flow rate [79].

The spiking tests were developed under the assumption that the size rejection is the dominant retention mechanism. Thus, the dimensions of rejected compounds are related to the dimensions of membrane pores. The tests assume that the tracers are rejected by the membrane pore but not adsorbed to the membrane surface, and that removing larger tracers is easier. The simplicity of the main assumption also embeds the main weakness of the test: Experiments must be done with homological compound series of different dimensions. Thus, the experiments are performed with tracking non-ionic linear polymers, such as polyethylene glycols (PEGs) [80], dextrans [81,82], lithium dodecylsulfates [83] or charged organic particles [84]. We recently showed that the main test assumption is problematic and the inherent flexibility of the organic molecules is confusing. In fact, we could even measure a penetration of molecules that were nominally 300 times larger than the pore size [85].

3.3 Visualization of Membrane Surfaces

Membranes are complex structures and there is no single method that provides a complete set of data for describing a membrane. Nevertheless, scientists need simple and reliable methods that can provide at least partial information that is clear and unambiguous. Here lies the advantage of visualization methods. They are simple to run, and some do not need any special sample preparation. The results are intuitively obvious and easily interpreted.

We will describe here the most popular and often implemented microscopy methods, including optical microscopy, confocal scanning laser microscopy, scanning electron microscopy, transmission electron microscopy and atomic force microscopy. All these methods are applied in visualization of membrane surfaces. Classical optical microscopy is often used in fouling studies [86] and studies of membrane defects [58], including the stages of slurry and green body. Scanning laser microscopy is used in biofouling studies and studies of morphology of transparent (mainly polymer) membranes. High-resolution SEM, TEM and AFM are used in studies of membrane morphology, including pore size and pore size distribution. Coupling microscopy with other detection methods provides additional information. For example, coupling SEM with energy-dispersive

X-ray spectroscopy (EDS or EDX) gives an elemental map of membrane surface that combines topographical information with elemental analysis. Atomic force microscopy provides 3D pictures of membrane surface along with attraction/repulsion forces acting on the membrane surface. AFM is also often used to detect the roughness/tortuosity of membrane surfaces.

As in all other methods, microscopy has its drawbacks and limitations. High-resolution set-ups are expensive. Measurements are time-consuming and require trained personnel. Moreover, high resolutions are applied to small membrane pieces and the significant membrane surface heterogeneity can be missed or undermined. Also, microscopy does not really give reliable information about membrane pores. Despite this, microscopic determination of membrane pore size is highly popular in characterization of ceramic membranes [87].

3.3.1 Optical Microscopy

Optical microscopy uses light transmitted through the membrane or reflected from its surface. The reflected light forms an image that is magnified by lenses. Recent developments, such as phase-contrast microscopy, use the dependence of the coherent scattering of the light on the position and microstructure of the source area. Confocal microscopy eliminates the disturbing background scattering from the sample surface. The use of fluorescent confocal microscopy significantly amplifies the signal and opens a variety of new methods suited for 3D characterization of membrane surfaces [88].

The advantages of light microscopy are its relative ease of operation and affordability. The membrane can be analysed in wet and dry states as the sample is not exposed to vacuum during imaging. However, the resolution of optical microscopes is poor and only objects larger than 1 μm are detectable. That is much bigger than the membrane pores and therefore the implementation of optical microscopes is limited to observation of presence/absence of large defects on the membrane surface, the uniformity of coating layer and the heterogeneity of fouling. Optical microscopy was used for the examination of 300 kDa, 0.1 and 0.45 μm ceramic membranes and the results were compared with the information obtained from high-resolution microscopes [89]. An optical microscope was used for inspection of absence of visible pinholes or cracks in ceramic hollow fibres used for coating of graphene oxide [90].

Optical microscopes are routinely used in bulk examination of powder compacts. The packing density of grains and the thickness of the support layer are observed at different stages of membrane preparation. Generally, grains are observable if their refractive index is at least slightly different from the index of dispersant and/or binder. This method can detect defects in the membrane structure already at the initial slurry stage. The defects are subdivided into short-range defects, which are spatially confined within a short region of less than 1 mm, and long-range defects, which extend much further and may affect the entire compact [91]. Figure 3.10 shows the main defects that can be seen using optical microscopy.

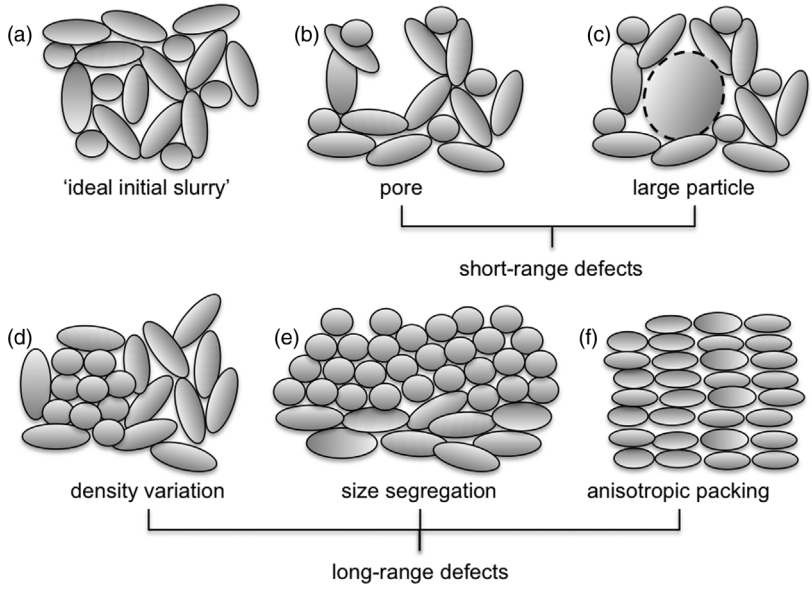


Figure 3.10 Schematic representation of an 'ideal initial slurry' (a) and various defects observable by light microscopy. Short-range defects include pores (b) and large particles (c); long-range ones include density variation (d), size segregation (e) and anisotropic packing (f).

3.3.2
Confocal Scanning Laser Microscopy

Confocal scanning laser microscopy (CSLM or LSCM) is a technique that gives high-resolution 3D optical images with depth selectivity using an optical microscope. The key feature of confocal microscopy is the ability to acquire in-focus images from selected depths, a process known as optical sectioning [92]. The difference between a typical optical microscope and a confocal one lies in the presence of a non-transparent specimen with a small pinhole. The specimen is located between the light beam and the sample. Light beams pass only through the pinhole. Passing light is then focused by the objective lens to a small spot at the image plane. This spot is located on a certain depth of a sample. The returning light passes through another aperture with a pinhole, so only the light coming from a focal point of the specimen passes to the detector. In the original apparatus invented by Minsky [93], the beam passed through sample and was collected by a detector on the other side. Modern microscopes use returning light, which is why the majority of probes used today are either naturally fluorescent or are chemically dyed in fluorescent dyes. Any light coming from above and below the focus plane will not be in focus and will be rejected by an opaque material that surrounds the pinhole.

Confocal microscopy can be used in determining the morphology of ceramic supports. Snyder *et al.* [94] used CSLM to obtain a 3D membrane representation

of zeolite membranes. Dying the liquid to be inserted into a sample before the imaging generates a coloured picture where grains are dark (as they contain no liquid) and holes are bright (because they are filled with fluorescent dye). Regions packed with fine particles appear moderately bright. The brightness level depends on the grain size and packing density. Typically, the clear focus region is about 3 μm, with an optical resolution of 0.2 μm, giving a clear 3D picture of the membrane support [91]. In addition to the fluorescent mode, CSLM can be used in the transmission mode as a simple optical microscope and in the reflection mode without fluorescence if support grains reflect light. The latter can be used to obtain an opposite to the fluorescent picture when grains reflecting light are seen as bright spots and pores are 'black holes.' If the membrane can be penetrated by the laser beam to a certain depth, there is a possibility to obtain a 3D map of inside membrane without slicing. Charcosset and Bernengo reported the depth profiling of a cellulose acetate membrane using CSLM in the reflection mode [95].

Applications of confocal microscopy are naturally limited by the resolution in both the focal x–y plane and optical axes x–z and y–z. The method is useful for detecting macroporous structure of membrane supports and their porosity. It can also be used for detecting different organic molecules such as proteins that foul a membrane, or the spatial arrangement of fluorescent foulants during operation.

Fluorescence, both natural and chemically induced [72,96], is often used for characterizing fouling layers in MBR membranes [97,98]. It cannot, however, give details on the morphology of layered membrane structures that contain not only support but also intermediate and top layers. For this, one must use high-resolution techniques such as SEM, TEM and AFM.

3.3.3 Scanning Electron Microscopy

Scanning electron microscopy uses a high-energy fine beam of electrons directed towards the membrane surface. Electrons have much shorter wavelengths than visible light photons and therefore give more detailed micrographs (a typical electron microscope provides between 10 000× and 500 000× magnification, compared to 250× for an optical one). The electrons interact with atoms in the membrane, producing response signals from the surface. These signals include secondary, transmitted and backscattered electrons, characteristic X-ray and light [99]. Membranes are typically characterized by secondary electrons emitted from the membrane surface, collected by a secondary collector and then converted to voltage and amplified. The result is thousands of white/black spots which form a 2D picture with various light intensities that can easily be interpreted as the membrane structure (Figure 3.11).

SEM with a typical resolution of 5 nm is routinely used to scan the membrane surface. The scan is further used to characterize the morphology of ceramic membranes, for example pore geometry, pore size, pore size distribution and surface porosity [89]. The lateral resolution of a typical SEM is 5–20 nm, enough

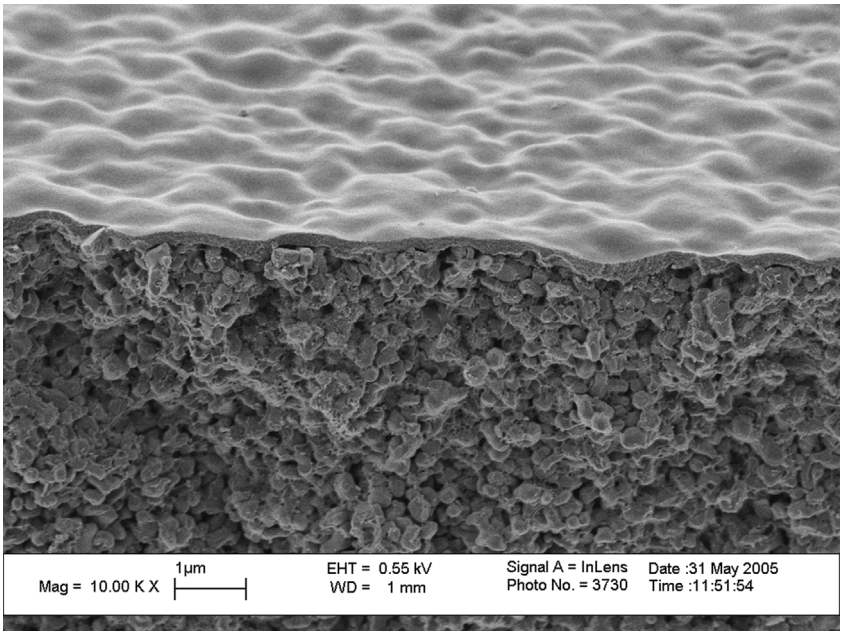


Figure 3.11 SEM micrograph of a cross section of a silica top layer coated directly on an α-alumina support. (Image taken by Dr. Vittorio Boffa and Dr. Andre ten Elshof, reproduced with permission.)

for determining the fine morphology of MF membranes. For example, SEM was used to analyse the integrity, pore size, porosity and structural density of low-cost clay-based MF membranes for solid–liquid separation [100–102]. The resolution can be increased to 1–5 nm using either environmental or field emission scanning electron microscopy (ESEM and FESEM, respectively), thus inspecting pores in UF membranes. Using a cold cathode instead of a thermoionic source results in low accelerating voltage and requires less metallization, which is important in the case of fragile membrane structures or when the clarity of the picture is important [103]. The depth resolution of scanning electron imaging is 1–10 nm and it is increased to 10–1000 nm using backscattered electrons [104]. SEM images also provide information on sample topography and chemical composition of the sample (Section 3.4.1). Figure 3.12 shows a cross section of a layered ceramic membrane. Notice, comparing with the image in Figure 3.11, how the presence of the intermediate mesoporous layer smoothes the top layer!

SEM is operated under vacuum to minimize interference with particles out of sample surface. The membrane is first dried and then coated with a thin layer of conducting material, typically 10–20 nm of gold. Carbon, platinum and palladium are other popular coating materials. The coating warrants the emission of secondary electrons and prevents local heating and charging. Both drying and coating might change the membrane structure giving a picture that differs from the initial sample [89]. In addition, the 2D pictures give the information about

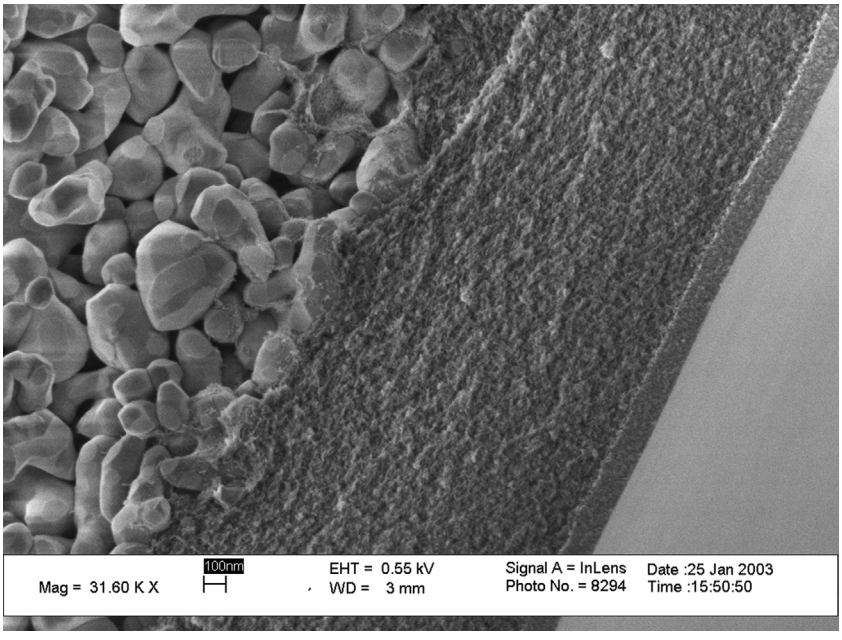


Figure 3.12 SEM micrograph of a cross section of a titania top layer coated on a γ-alumina intermediate layer that is in turn coated on an α-alumina support. (Image taken by Dr. Jelena Sekulic and Dr. Andre ten Elshof, reproduced with permission.)

the pore entrances but not about the pore constrictions, so the actual pore size that will determine the retention cannot be measured. Usually the pore size of a coated membrane surface is underestimated [105,106]. Using ESEM or cryoelectron microscopy does not require either drying or coating and can provide a more realistic picture of the membrane surface.

3.3.4
Transmission Electron Microscopy

Transmission electron microscopy uses a beam of electrons transmitted through the membrane surface. Unlike in SEM and fluorescent CSLM, the image is formed from electrons that pass through a sample in the beam direction. Electrons scattered perpendicular to the microscope axis and reflected back to the direction of electron gun are later displayed as black spots on a computer-reconstructed 2D image of a membrane. Conversely, those electrons that pass through the membrane are displayed as light spots on the image. Thousands of white/black spots give a 2D picture with various light intensities that is interpreted as the membrane structure. Figure 3.13 shows some TEM pictures of various membranes.

The system is based on a film or doped YAG screen-coupled charge-coupled device CCD camera [107]. TEM, therefore, provides interesting options of scanning through the membrane for studying its morphology. High-resolution TEM

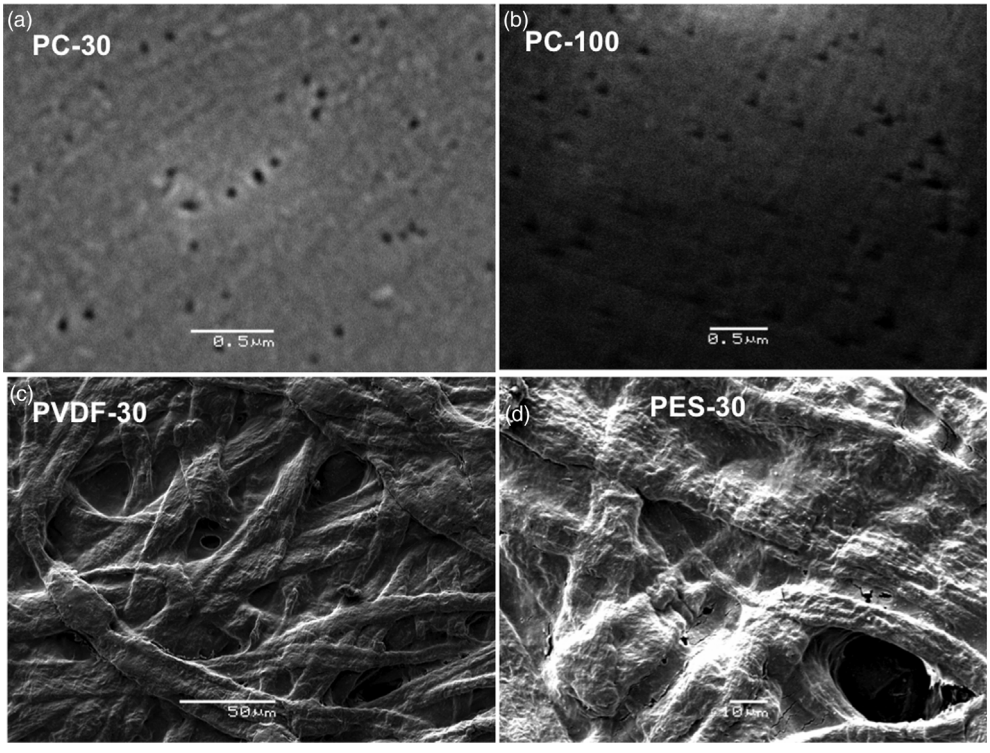


Figure 3.13 Transmission electron micrographs of PC-30, PC-100, PVDF-30 and PES-30 membranes. The graph in part (d) shows a large 20 μm hole in the upper membrane layer. (Reproduced with permission from Ref. [74]. Copyright 2012, Elsevier Limited.)

images allow the direct observation of nano-objects such as nanoparticles or nanotubes. However, the maximum thickness of a sample is about 100 nm. Thicker specimens must be sliced using an ultramicrotome to thin cross sections that are then mounted on a standard TEM grid [25]. In addition, contrast between regions of interest requires difference in electron density between porous and non-porous regions. Often the difference is too small and is enhanced by staining the membrane with heavy metal salts such as osmium or uranium [108,109]. Despite these limitations, TEM is a very popular technique for characterizing subatomic dimensions in ceramic membranes. The maximum resolution is 0.3–0.5 nm [110]. TEM is also useful in characterizing layered structures providing information on the inner structure of particles and differences in chemical structure as image contrasts [111].

TEM was used for the analysis of uniformity of nanoporous Fe_2O_3 coating on the porous alumina–zirconia–titania ceramic membranes [112]. De Vos and Verweij [113] used TEM to illustrate a multilayered structure of ceramic membrane that consisted of α-alumina support, γ-alumina intermediate layers and a

silica top layer. The micrograph clearly showed that the thin (less than 30 nm) silica layer was deposited on top of γ-alumina layer. TEM was also used to obtain the microscopic structure of zeolite membranes [114]. Despite many technical difficulties in sample preparation, TEM micrographs provided vital information on crystal structure of zeolite and presence of defects. TEM was also used for clarifying the charge-selective properties of macroporous composite inorganic membranes modified with nanoparticles of hydrated ZiO_2 [115].

The method has the same constraints as SEM regarding the drying, and therefore a possible change in the pore structure. Membranes are typically much thicker than the limiting 100 nm thickness of a scanned specimen. Thus, the main use of TEM in ceramic membranes is in characterizing unsupported coating layers or striped layers. Preparing thin specimens is difficult, time-consuming and might lead to artefacts in the resulting image [116]. Slicing ceramic membranes for TEM imaging requires embedding of the dry membrane in a resin. The influence of the resin on the membrane structure is unclear [117]. The porosity evaluated with TEM analysis might be smaller than in reality [118]. Despite the high resolution, even TEM cannot characterize microporous membranes with mean pore size below 2 nm [119].

3.3.5
Atomic Force Microscopy

Atomic force microscopy belongs to *scanning probe microscopy* (SPM) group of methods. SPMs are not optical microscopes. The common base of SPM methods is the use of mechanical or electromagnetic interactions between the membrane and a sharp tip that virtually touches the membrane surface [120]. This tip is sensitive enough to keep a constant distance between a cantilever and the membrane surface. Fluctuations in the cantilever movement along its sliding over membrane surface are recorded by a computer and transferred into a 3D picture that depicts the topography of the membrane surface [121]. SPM methods can also translate other characteristics of the membrane surface such as viscoelasticity, optical and magnetic properties, conductivity and chemical forces [25].

Atomic force microscopy is the most popular version of SPM, in which a sharp tip is brought to a close vicinity of the membrane surface [122]. Depending on the scanning mode, the distance might range between a mechanical contact to few nanometres [123]. In the closest contact mode, the tip is less than 1 nm from the surface and it responds to very short-range Born repulsive force. An AFM image is a collection of vertical positions of the moving tip required to keep the tip-membrane signal constant, and in a simplest way the AFM measures 3D surface topography of the scanned membrane sample.

AFM can also provide information about a membrane's physical, magnetic and chemical properties. One popular implementation of AFM is the measurement of 'force curves' as a function of distance between an AFM probe and the membrane surface. The measurements are performed using a standard AFM tip or colloid particle glued to the end of a cantilever instead of the tip. This particle is

modified to contain different functional groups suspicious as potential fouling agents [124]. It can also be an actual protein or bacteria [125]. The force curves point to the fouling tendency of a membrane surface with laboratory experiments without pilot or full-scale investigations. AFM can also be used for measurements of electrical properties of the membrane surface [126] and in the examination of membrane swelling [110].

In general, AFM is a highly sensitive technique and can provide the images on the angstrom to single nanometre scale [127]. This is both an advantage and a disadvantage. When nanometre-sized pores can be sensed, AFM can hardly be applied for screening. The biggest AFM pattern is $150 \times 150\,\mu m$, which is not enough for a statistically significant measurement. At such a high resolution, the quality of the image is limited by the curvature of the scanning tip, and using a wrong tip or scanning mode can give wrong results [10]. Although the AFM tip is very sharp, often less than 100 nm in diameter, its dimensions are finite and pores significantly smaller than the tip size will not be sensed. Moreover, the surface roughness may render the images difficult to interpret. Despite these limitations, AFM is widely used today for characterizing membrane surface morphology of MF, RO and gas separation membranes [128–130].

The main advantage of AFM over SEM and TEM is that no special preparation of the sample is needed. Whereas SEM/TEM require drying and gold coating of the sample, AFM samples can be used *as is*, often even at ambient condition. Although AFM pictures the membrane surface and not the pore itself, it is widely used for determining pore size, surface porosity, pore density and pore size distribution [131–133]. Practically identical pore sizes found by AFM, hydraulic permeability [105] and more conventional SEM were reported [128]. It is known that both SEM and AFM underestimate the pore dimensions [134], so it is probably safe to claim the same for the hydraulic permeability pore size determination. Some AFM pictures can even be taken on wet or immersed membranes. In comparison to SEM/TEM, this aspect does simplify the visualization and makes it economically affordable. Where SEM and TEM display a 2D picture, AFM adds a third dimension, the 'hills and valleys' of the membrane surface. These features make AFM a popular choice for visualizing membrane surfaces. Figure 3.14 shows AFM images of a ceramic membrane before and after cleaning.

As we can see, the AFM analysis gives a 3D map that can be used to detect the surface roughness. This roughness is basically the deviation of a real surface from its ideal form in the z-direction. The second term that defines roughness is the frequency – how often the real surface deviates from its ideal form. We will define roughness as high-frequency short-amplitude deviations of membrane surface from its ideal form. The surface roughness can significantly affect the membrane fouling [135], coating and biofilm formation [136]. For example, Hoek *et al.* concluded that colloidal particles will preferentially deposit in the valleys of a rough membrane [137]. The pores are usually located in valleys. Roughness impacts the hydrodynamics near membrane surfaces promoting concentration, polarization and fouling [3]. SEM and SPM are two methods that can be used for detecting membrane roughness. SEM, however, provides 2D

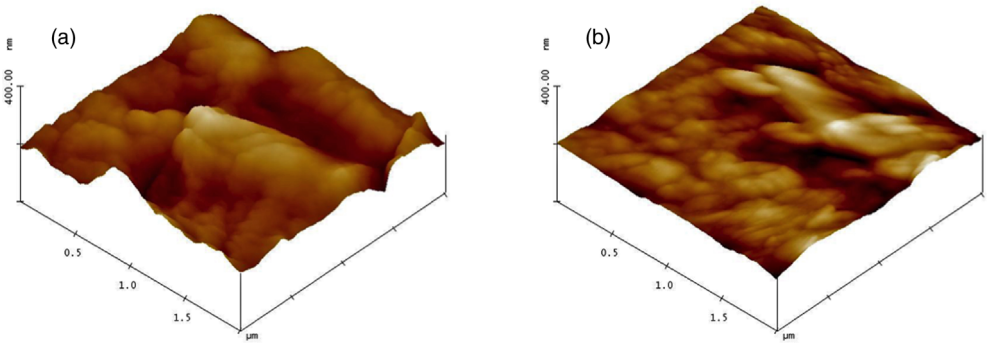


Figure 3.14 Three-dimensional AFM images of a fouled (a) and cleaned (b) UF membrane. The membrane was fouled during wastewater treatment of secondary effluent from Beer Sheva wastewater treatment plant at Sede Teiman and cleaned using a sodium hydroxide solution.

projections in which some information is inevitably lost [25]. Contact AFM mode is generally used in measurements of ceramic membranes [138].

The roughness is a quantitative parameter that is not an intrinsic property of the membrane surface itself. Its magnitude depends on the technique used. AFM can provide several statistical parameters that can characterize the roughness of membrane surface. The first and the most widely implemented is the average roughness, defined as the average absolute deviation of height from the mean height:

$$R_{\text{av}} = \frac{1}{N}\sum_i |Z_i(x)| \tag{3.25}$$

where Z_i is the height value for a particular point on the image (nm) and N is the total number of peaks within the image. Another useful parameter is the root mean square (rms) roughness defined as the standard deviation of the heights for all pixels in the image from the arithmetic mean:

$$\text{rms} = \sqrt{\frac{\sum_i (Z_i - Z_{\text{av}})^2}{N}} \tag{3.26}$$

where Z_{av} is the mean height of all pixels in the image (nm) and N is the total number of pixels within the image. This parameter, however, cannot differ between a profile and an inverted profile (when a valley turns into a hill, and vice versa). The skewness parameter rsk (Eq. (3.27), where N is the number of discrete points in the profile) measures the asymmetry of the profile about the mean line [139]. A positive value indicates that the surface has more 'peaks' than 'valleys.'

$$\text{rsk} = \frac{\sum_i Z_i{}^3(x)}{N\text{rms}^3} \tag{3.27}$$

Additional parameters include the *surface area difference*, defined as the increase in the surface area over the projected area due to the roughness; the *peak count*,

defined as the number of peaks in the scanned area; and the *maximum roughness depth* R_{max}, defined as the largest single roughness depth within the evaluation area [25]. Each parameter provides partial information on missing important parts such as the presence and the amplitude of periodical patterns on the membrane surface. More comprehensive information can be obtained by spectral analysis tools such as fast Fourier Transform (FFT) or a related power spectral density (PSD) [25]. The latter, defined as the roughness power per unit spatial frequency, can be generated using a built-in software in 1D and 2D yielding 1D spectrum or 2D spectral map [139].

Smoother surfaces reduce membrane fouling, improve permeability and prevent a preferred deposition. This holds for all types of membranes. For example, the flux of oily emulsion wastewater through a smooth ceramic membrane is higher than through a rough one [140]. In ceramic membranes, the roughness, its measurements and the reduction are extremely important at the stage of membrane formation. A high roughness of the support layer will be transferred to the top separation layer [141].

One of the main goals in the incorporation of intermediate layers is to reduce layer roughness. The support layer has a typical maximum roughness depth R_{max} of 20–30 μm, which means that the thickness of the first intermediate layer should be at least 30–40 μm (see Chapter 1) [142]. Thick coating layers increase the membrane total resistance and reduce the flux. It is therefore desirable to make the intermediate layers thin and smooth. This is a gradual process that should provide the average roughness R_{av} of the upper intermediate layer below 1 μm as it is not possible to coat defect-free on support with an average roughness higher than 1 μm. Thus, the top layer might have a reduced roughness in nanometric range. For example, coating alumina–zirconia–titania ceramic membranes with 4–6 nm iron oxide nanoparticles resulted in a decreasing 130 nm roughness after the coating [132]. Grafting of hydrophilic membranes with hydrophobic groups the rms to about 30 nm [143].

3.4
Chemical Methods for Membrane Characterization

A better understanding of membrane properties and functioning can be achieved by a chemical analysis of the membrane structure. The methods differ in resolution, sensitivity, dimension of the probed region and specificity to different atoms [25]. There are methods for detecting the elemental composition of a membrane's surface and bulk. Other methods measure how these elements are bonded. Among methods for the elemental analysis, there are methods that are able to detect the major (>5%), minor (0.1–5%) and trace levels of elements. The latter are out of the scope of our book, and generally require highly selective, sensitive and precise techniques such as particle-induced X-ray emission (PIXE) or nuclear reaction analysis (NRA).

Significant information about ceramic membranes is obtained when the elemental analysis of the membrane surface is coupled with its lateral distribution. That is usually done by methods based on backscattered radiation. A high-energy beam of electrons directed towards a membrane interacts with membrane's atoms and generates various types of scattered or secondary radiation in the form of particles and electromagnetic waves [139]. That is a large piece of information about the elements in the membrane structure, their concentration and positions, a sort of 'elemental map' of the surface. Energy-dispersive X-ray spectroscopy (EDS or EDX) usually comes as an integral part of most scanning and transmission electron microscopes. This method is accepted and widely used, and will be detailed below. Information on other, less common methods such as PIXE, NRA, XRF, electron energy loss spectroscopy (EELS) and X-ray spectroscopy can be found elsewhere [139,144].

3.4.1
Backscattered Radiation

Figure 3.15 presents a general scheme of surface layer characterization. Here a well-defined probe introduces a local disturbance in the membrane. In the following relaxation process, elements on the membrane surface emit signals. Each signal characterizes a specific element. The location of the element is linked back to the disturbed region, and the signal intensity is indicative of the element content.

One well-known approach for characterizing ceramic membrane surfaces is by combining scanning electron microscopy with X-ray detection. The SEM/EDX combination uses the electron beam generated by the electron gun within SEM

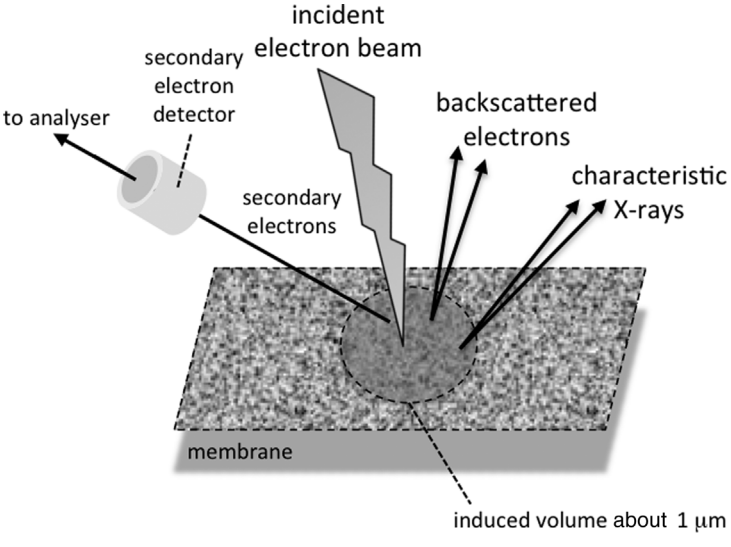


Figure 3.15 A general scheme of surface characterization.

to collect information about the X-ray scattering using EDX. A focused electron beam hits the surface and penetrates into the membrane. The beam is generated by an electron gun and focused by two magnetic lenses, so it hits the membrane surface in a very small spot of 3–10 nm diameter. Due to the highly concentrated energy, the electrons penetrate into the membrane. The penetration depth is usually as large as the optical field of view, roughly 1 µm. Some of the electrons are scattered back (so-called backscattered electrons) and provide information about mean atomic numbers of scattering atoms. Secondary electrons are released from the membrane surface close to the spot where the primary electrons enter, giving information on the topography. X-rays generated when a primary electron hits an atom with sufficient energy provide information about the atomic composition [139]. Each element generates a different specific spectrum. The majority of elements down to B (atomic number 5) can be detected, although the intensity of an atomic band increases with the atomic number and therefore the X-ray backscattered techniques are more sensitive to heavy elements [25]. EDS and EDX are energy-dispersive spectroscopies, meaning that they collect data from a wide spectral range simultaneously. The X-ray spectrum is usually displayed as a function of energy in the form of a continuous signal with superimposed characteristic elemental lines. Each line in the spectrum corresponds to a specific element. Elements with increasing atomic numbers display lines at higher energies. Figure 3.16 displays a typical SEM micrograph and an X-ray spectrum of a fouled membrane.

Measurements are performed in vacuum to avoid scattering from the bulk and absorption of electrons. SEM/EDX provides an elemental map of a surface that combines topographical information from an electron detector combined with elemental analysis from the X-ray detector. Although the chemical compounds

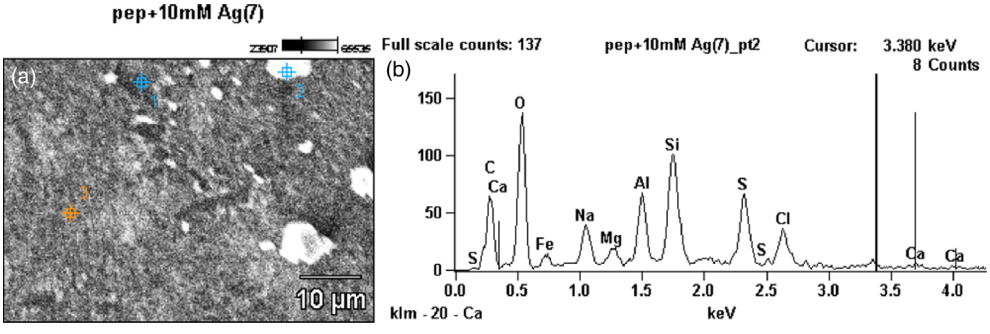


Figure 3.16 SEM micrograph of a fouled PES-50 hollow fibre (a) and the XPS spectra analysis of the fouling layer (b). The XPS was performed at Ilse Katz Institute for Nanoscale Science and Technology (Ben Gurion University of the Negev) with Thermo Fisher ESCALAB 250 spectrometer at vacuum pressure of 2×10^{-12} bar. The samples were irradiated with monochromatic Al Kα (1486.6 eV) X-rays. Survey spectra were recorded with pass energy of 150 eV and high-energy resolution measurements were performed with pass energy of 20 eV. The core level binding energies of the different peaks were normalized by setting the binding energy for the C1s at 284.8 eV.

cannot be identified directly, they can be deduced from the elemental composition. Due to its high resolution, the SEM/EDX technique is useful for detecting the chemically different or fouled regions within the membrane.

Another useful technique based on backscattering of electrons is called X-ray photoelectron spectroscopy. The kinetic energy of electrons depends on the energy of the source, usually not less than 1500 eV. The mean free path of the electrons in the membrane structure is therefore in the nanometre range and XPS is considered a surface technique (it can probe a few atom layers into the surface). The energy of photoelectrons is uniquely related to their binding energy within the atoms [25]. The intensity of binding energy is proportional to the content of a certain element within the membrane and therefore to its relative concentration. A unique feature of XPS is a shift of the bands in high-resolution spectra. This shift allows a differentiation of oxidation states of elements within the structure such as metal Al and Al_2O_3. This feature and the above-mentioned small probing depth make XPS uniquely suitable for chemical analysis of membrane surfaces.

X-ray scattering is a very powerful method for studying membrane surfaces. Many studies of SEM/EDX however reported the same deficiency – The number of surface atoms that might diffract electron beams and display a scattered X-ray spectrum is relatively low compared to their number in the bulk. Many laboratory X-ray generators are unable to provide sufficiently strong signals. SEM/EDX studies are therefore often reduced to 'favourable' surfaces that contained elements with high atomic numbers. The beam of electrons however might not only be scattered by atoms on the membrane surface but also diffracted by membrane structure if it is crystalline [145].

The experiment shows that a crystalline fracture diffracts X-ray wavelengths and the diffraction angle is determined by the crystalline structure. In parallel, William Lawrence Bragg and his father Sir William Henry Bragg [146], who were jointly awarded the Nobel Prize in 1915, showed that when the conditions of Braggs' law (Eq. (3.28)) are met, the crystalline structure produces intense peaks of reflected radiation (known as Bragg peaks):

$$n\lambda = 2d \sin\theta \tag{3.28}$$

where n (–) is an integer, λ (nm) is the wavelength of the incident wave, d (nm) is the spacing between planes in the atomic lattice and θ is the angle between the incident ray and the membrane surface. The reflection occurs when the distance between crystalline planes is proportional to $2d \sin \theta$. In the simplest case, an irradiation screening of a membrane sample at different angles gives in a pattern with well-defined peaks at certain 2θ values. Comparing the observed patterns of reflected radiation of known and unknown crystalline structures helps determine form of the basic minerals that compose it (e.g. tetragonal, cubic or rhombohedral).

X-ray diffraction is a powerful and rapid (less than 20 min) technique for identifying changes in membrane structures. The X-rays scattered from the membrane surface interfere with each other such that the intensity distribution of scattered X-rays is determined by the wavelength and by the atomic

arrangement of the membrane structure. Diffraction patterns are especially sensitive to the long-range order of crystalline structure [147]. The atomic level of a membrane can be determined from the diffraction pattern, although XRD is more suitable for tracking changes in the membrane structure. For example, Tan and Li tracked the changes in the membrane exposed to a methane-coupling environment [148]. Brown *et al.* [149] evidenced a slow development of a crystalline phase with increasing sintering temperature. In most cases, the XRD provides an exact determination of minerals or crystalline phases. That precise determination initiated another use of XRD in ceramic membranes. The membranes deposit the particles present in the air of an industrial workplace, such as quartz dust, silica and lead sulfide, for their further analysis by XRD [150]. The samples require minimal preparation and the interpretation of the XRD data is relatively straightforward. XRD is non-intrusive and non-destructive and has a particular advantage in characterization of fragile structures [37]. Its main disadvantages are that a clear detection requires an access to a standard reference file, the analysis requires hundreds of milligrams of material and the detection in mixed materials is limited to the presence of at least 2 mass% of each ingredient [151]. Mulder has also pointed out the difficulty in discriminating between crystalline and amorphous scattering in small crystallites [57].

Rutherford backscattering spectrometry (RBS) is a technique based on scattering of high-energy ions rather than electrons. These ions penetrate into the membrane to about 1 μm depth, losing their energy mostly by being scattered by the electrons within the membrane. A small fraction of ions is scattered directly by the atomic nuclei. The collisions of ion and nuclei are often elastic and the ion of nucleus is 'bounced' within the membrane structure by electrostatic repulsion. This elastic nucleus–nucleus collision is called *Rutherford scattering* [139]. The central concept of RBS is the measurement of statistical probability of scattering and energy loss. In an elastic collision, the energy of the ion immediately after scattering is related to the energy just prior to scattering. Thus, the number of ions scattered into a detector viewing a small angle interval is related by a scattering probability to the number of incident ions. In this way the backscattering of ions gives information about the presence of a single atom of interest within the membrane structure.

3.4.2
Vibrational Spectroscopy

Methods based on the backscattering of electrons and ions can provide valuable information regarding the physical state and molecular composition of ceramic membranes. Some advanced techniques, such as XPS, even allow differentiating the oxidation states of the elements. Yet these techniques give no direct information on the exact chemical bonding of elements on a membrane surface. In contrast, vibrational spectroscopy takes advantage of the inherent resonant vibrations within the molecules, giving reasonably accurate data on chemical bonding. Here, Raman and

infrared (IR) techniques are the most often used techniques for characterizing membranes, because they are sensitive to chemical interactions on surfaces.

Infrared spectroscopy measures the absorption of infrared light by chemical bonds on the membrane surface at each wavelength. In the simplest interpretation called 'dispersive spectroscopy', a monochromatic light is directed towards the membrane surface to measure how much of light is absorbed. This operation is repeated many times at different wavelengths until finally the general picture of how much light was absorbed at each wavelength is received. In the more modern (and nowadays common) Fourier transform infrared spectroscopy, a polychromatic beam is directed towards the membrane surface. The amount of the beam absorbed by a membrane is recorded. At the next step, the beam is modified to contain different frequencies. Once again, the membrane surface is hit with a polychromatic beam and how much of the light is absorbed by the surface is recorded. The beam light is modified by a moving mirror located within the instrument. This mirror periodically blocks certain wavelengths due to wave interference. The interference is a result of an arrangement of mirrors called a *Michelson interferometer*. The light wave passes through the mirrors before being released to the membrane surface. That operation is then repeated many times until the full set of data is obtained. The data from all records are intercept to analyse how much light was absorbed at each wavelength using an algorithm called the Fourier transformation [152].

On the membrane surface, vibrating molecules absorb specific wavelengths that match the transition energy of a vibrating bond. The vibration frequency should be similar to the IR wave frequency (the latter is inversely proportional to the wavelength) to give a resonance. Absorption occurs at resonant frequencies that are characteristic of the absorbing molecules. The energies are determined by the shape of molecular potential energy surfaces, mass of elements and vibration types. Only molecules and bonds with a dipole moment are considered 'IR active' [153].

'Inverse spectroscopy' instruments had been tried with a limited success since the late 1960s. The major disadvantage of infrared spectroscopy was its low sensitivity compared to high-vacuum spectroscopic techniques. A recent modification in the form of inverse Fourier transformation and internal reflection–absorption spectroscopy has markedly improved the sensitivity and applicability of infrared spectroscopy in membrane surface analysis. *Internal total reflection* is a technique where an infrared wave is confined in a space with high reflection indices on the space edges. At each edge, the wave is reflected back to the confined space making a transient wave that travels along the membrane surface. After numerous reflections, the beam leaves the space. Figure 3.17 depicts a set-up used to sense and detect chemical bonds on the ceramic membrane surface.

When the wave strikes the internal edge close to the membrane surface at an angle greater than the so-called critical angle [154], some energy passes inside the membrane in the form of evanescent waves. The physical explanation for the presence of the evanescent waves is that the radiation field cannot be discontinuous at a boundary. The waves can penetrate into a membrane to a depth

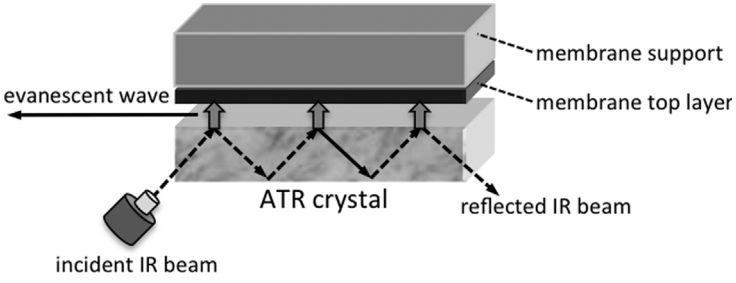


Figure 3.17 Schematic of an ATR-FTIR set-up.

of 0.5–2 μm until they are reflected and leave the membrane. A detector placed on the edge of a membrane sample collects the data about absorbed and transmitted IR wavelengths. The reflection at the membrane surface is due to a crystal called internal reflection element that is externally attached to the membrane surface. Typical crystals are made of germanium, KRS-5 (thallium–bromide–iodide) and zinc selenide. This method, called *attenuated total reflection Fourier transform infrared spectroscopy* (ATR-FTIR), is often used for detecting complex asymmetric molecules on membrane surfaces. In addition to giving useful information regarding the chemical bonds on the surface, ATR-FTIR enables a direct examination of wet membranes with fouling layers without long preparation or drying. ATR-FTIR is best applied for characterizing dense and smooth surfaces, because roughness and high porosity decrease the contact between the crystal and the membrane surface.

The first FTIR spectrometers were developed for the far-infrared range of 15 μm to 1 mm due to a need for good optical performance related to the wavelength of the used light. Current ATR-FTIR mainly uses the mid-IR range, with wavelengths between 2 and 8 μm that correspond to wavenumbers 2000–4000 cm^{-1}. This range is suitable for detecting chemical bonds, including O—H, C—O, C—C, C—S, RC—O—CR, and aromatic systems [22]. In this way, ATR-FTIR was used to characterize a polydimethylsiloxane (PDMS) layer coated on ZrO_2/Al_2O_3 porous ceramic support [155], the structure of ferroxane (iron)-derived ceramics [156], the effect of ceramic addition in ionoconductor gels [157], the cleaning efficiency of a ceramic membrane fouled by a 3.5 wt% whey protein concentrate suspension [158] and microbiological fouling in membrane bioreactors [159]. The penetration depth is additional field of studies covered by ATR-FTIR. With extreme changes of critical angle, the penetration depth can reach 5 μm, and that is enough to studying differences in the fouling layer both on the membrane surface and within its depth [160]. For example, depth profiling of bovine serum albumin (BSA) in MF and UF membranes showed that whereas in MF membranes the BSA fouling occurred on the surface and pore entrances [161], in UF membrane UF fouling was inside the pores [162]. Other applications of ATR-FTIR in membrane studies include measurement of

polymer swelling, partitioning and diffusivity of solutes. These, however, pertain mostly to polymer membranes [163,164].

The second popular technique is *Raman spectroscopy*. The Raman effect is the inelastic scattering of photons by nuclei of molecules on membrane surface.

Although all molecules have vibrations and rotations, not all are Raman active. Two basic selection rules apply: First, intense Raman scattering occurs from molecules that exhibit symmetric vibrations. This is opposite to IR where the light absorption is due to asymmetric vibrations. Second, centrosymmetric molecules do not provide a band in IR and Raman spectroscopy. This means that IR and Raman spectroscopy are complementary methods that provide information about the presence of asymmetric and symmetric molecules, respectively. For example, molecules such as CO_2 and C_2H_4 with inverse centre of symmetries will be observable in Raman spectra. H_2O with its large dipole moment will provide strong IR signals but will be invisible in Raman spectra. Raman spectroscopy can therefore be used for studying biofilms on ceramic membranes.

Classical Raman spectroscopy is not particularly sensitive to surfaces and may give signals from adsorbed gases and vapour molecules. For example, CO_2 are observed at 2200 cm^{-1} shift and pyridine provides a distinct shift at 1030 cm^{-1}. Several modifications are applicable in the characterization of membrane surfaces. Fourier transform Raman spectroscopy, FT-Raman, can determine the overall chemical structure of a membrane but not an asymmetric structure of a porous membrane matrix [165–167]. Micro-Raman is a combination of a spectrometer with a microscope that allows a 3D mapping of a membrane. It is sensitive to small contents of molecules as the signal is collected from a small specific area [168,169]. Surface-enhanced Raman spectroscopy (SERS), discovered in 1974, provides a very strong (10^3–10^6) amplification of a scattered signal that allows the detection of single molecules [170]. Although the mechanism of the observed amplification is still under discussion, there is a consensus that the effect arises because the incoming light is concentrated in 'plasmonic hotspots' (nanoscale clefts, gaps and fissures). Even unconventional imaging devices such as near-field scanning optical microscopes are limited to 30 nm. Yet this effect was theoretically predicted and shown in practice [171]. Currently, ceramic membranes are mainly used as a substrate for the studies of the effect of magnitude of the electric near-field on SERS enhancement factor. For that, the pores in the alumina membrane were coated with gold and silver [172].

There are several characteristics that make Raman spectroscopy very useful for ceramic membrane analysis. Raman is molecular-specific, non-destructive, non-invasive technique with high spatial and spectral resolution. Current Raman spectroscopes are small and portable, with a few instrument variables, minimal spectral manipulation and simple data interpretation. Taking a good-quality Raman spectrum in micro-Raman spectroscopy is fast (a few minutes). In addition, Raman spectroscopy can examine aqueous solutions, sample inside glass containers and samples without any preparation [173]. It can analyse a wide range of materials including organics and inorganics and their mixtures. Raman spectroscopy can differentiate between polymorphic

forms of mineral species, for example between rutile and anatase forms of TiO_2, and provide physical structure and qualitative analysis of minerals simultaneously.

Raman spectroscopy can distinguish between calcination and sintering. For example, a transition from anatase to rutile forms of TiO_2 occurs at 600 °C and detection of anatase suggests that TiO_2 is in the top layer calcinated on a support. The presence of rutile would therefore suggest that the membrane support includes TiO_2. Some of crystalline transformations occur as a function of both temperature and applied pressure. Confocal Raman spectroscopy is sensitive enough to spot where exactly ferroelastic domain transformations in ceria-stabilized zirconia occur [174]. Perovskites are often characterized by Raman spectroscopy due to the presence of distinct peaks at 800–150 cm^{-1} Raman shifts. These minerals have the general structure $\mathbf{AB}O_3$, and are used as membranes in fuel cell applications (we will discuss them in detail in Chapter 4). The structure can be divided into a covalent-bonded lattice formed of $\mathbf{B}O_6$ octahedra with shared oxygen atoms and **A**-cation lattice. Raman spectroscopy allows a separate tracking after changes in both lattices. Low Raman shift wavelengths of 100–250 cm^{-1} correspond to cations and 250–800 cm^{-1} are due to stretching vibrations of octahedron [175]. If **A** is Ba, Sr and Ca and **B** is Zr, Ce and Ti, the perovskite belongs to a family of high-temperature protonic conductors. In addition, the **B**-site must be doped with trivalent cations such as lanthanides or rare earth elements to form oxide ion vacancies. Raman spectroscopy is routinely used for the characterization of carbon-based nanomaterials such as nanotubes, fullerenes and graphene. The materials are symmetric and therefore provide distinct Raman bands useful for the differentiation of allotropic forms [176].

However, Raman spectroscopy has its own limitations. Some elements display high fluorescence or phosphorescence signals where a molecule after emitting a photon returns to the same energy level. Moreover, the method is not quantitative because the intensity of scattering is proportional to the electric dipole–electric dipole polarizability change of the analysed sample and its spatial orientation.

3.5
Physical Parameters of Ceramic Membranes

The manufacturing of ceramic membranes is largely an empirical process that might result in noticeable fluctuations of membrane characteristics. Even membranes with the same permeability, pore size and pore size distribution might differ significantly in morphology, mechanical properties and charge. These characteristics might also change as a result of fouling and chemical cleaning. Although the physical parameters of ceramics are bulky, they can provide a valuable insight into daily membrane operation and behaviour.

3.5.1 Membrane Porosity and Pore Tortuosity

Ceramic membranes are formed from particles suspended in a mixture of solvent, binder and dispersant (see Chapter 1). The slurry is dried to remove these liquids and to form a 'green body' with a certain shape such as plate, tube, honeycomb or hollow fibre. This green body is later thermolized and sintered, giving the final membrane. During all these stages, the particles are statistically distributed in the shape in a way that contains the particles themselves and the voids between them. Dimensions of the voids significantly exceed the characteristic scale of molecular dimensions or structural fluctuations [25]. Many variables along the process cause fluctuation in the voids, their location and uniformity. Therefore, the porosity cannot be predicted simply from the grain diameter and the preparation process.

Not all ceramic membranes are porous. Cerias, perovskites and doped zirconia are examples of dense membranes (see Chapter 4 for a discussion of dense membranes and their applications). Porous membranes consist of 'islands' of ceramic materials isolated by voids. The voids are much smaller than the islands and can be described as channels inside a membrane. On the membrane surface, these channels are seen as pores and with time the same pores spread over the entire channel. Pores can have different forms and shapes, as shown in Figure 3.18. The simplest is the symmetric pore that goes through the entire membrane. The pore is very popular in approximations and in reality can be seen in one-layered support structures of alumina. Asymmetric structures can be made of the same alumina as well as of zirconia, titania and composite ceramic–ceramic and ceramic–metal compacts. The multilayered structure is characterized by different pore sizes in various layers. It is obtained when the support and top layers are made from various materials. For example, a classical ceramic membrane made of α-alumina in support layer, γ-alumina in intermediate layer and silica or titania in top layer will display the cross section of a multilayered structure. In each layer there is a relation between particle diameter, pore diameter and packing symmetry (coordination number). However, the relation changes as a result of drying and sintering, so at the end a nicely structured network will contain

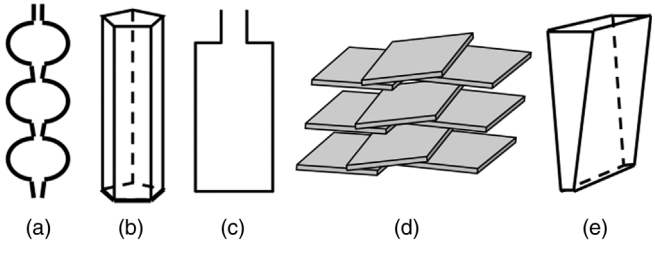


Figure 3.18 Pores may vary in size, shape and connectivity. (a) Channel/cage structures. (b) Polygonal capillaries. (c) 'Ink bottle' pores. (d) Laminae. (e) Slit pores.

isolated, dead-end, tortuous, rough, constricted and conical pores. The porosity detects all but isolated pores giving only very vague approximation of the real porous structure within ceramic membrane. For example, dead-end pores do not contribute to transport but do contribute to porosity.

There are two main definitions of porosity. Both definitions are nice and simple, although they have limitations where real membranes are concerned. The *surface porosity* of a membrane is defined as

$$\varepsilon_s = \frac{A_p}{A_T} \tag{3.29}$$

where A_p and A_T are the porous and the total membrane surface area (m^2), respectively. For symmetrical pores, the $A_p = n\pi r_p^2$, where n is the number of pores for a given membrane area and r_p is the pore radius. Surface porosity is often used in calculation of permeability giving an important separation between pores and solids on the membrane surface. In reality, the surface porosity and the porosity defined in Eq. (3.30) can deviate to a large extent, as the pore structure even within the top layer can be significantly different from the membrane surface [3].

The second definition of *membrane porosity* is given by

$$\varepsilon = \frac{V_v}{V_v + V_s} = \frac{V_v}{V_T} \tag{3.30}$$

where V_v is the volume of the void space (m^3), V_s is the volume of solids (m^3) and V_T is the total sample volume (m^3). In the simplest case, the porosity is seen as the weight difference of a membrane in the wet and dry states divided by the density of a liquid that fills the membrane pores and by the volume of the membrane in the wet state. This porosity vary between $\varepsilon = 0.2$ and $\varepsilon = 0.6$, although the majority of ceramic membranes will have $0.3 < \varepsilon < 0.4$. Once again, this value has more symbolic than practical importance as the actual porosity of a multilayered membrane largely correlates with the support layer's large pores.

Pores are rarely symmetric, constricted or conical. The majority of pores are tortuous (i.e. twisted, having many turns). This tortuosity is simply defined as

$$\tau = L/C \tag{3.31}$$

where L is the pore length and C is the distance between pore ends.

In another definition, the tortuosity is taken as the ratio of transport rates through perfectly straight and tortuous rate of the same pore size and membrane thickness. Tortuosity values are always higher than unity, and in porous membranes typical values of tortuosity are between 1.5 and 5 [177]. Note that while in theory porosity and tortuosity are independent, in practice they are related. Both porosity and tortuosity are considered complementary parts that should describe all morphological features of the membrane [3]. They are used as a correlation factor in calculations of the main pore diameter based on, for example, the Poiseulle equation. The permeability coefficient L in the definition of permeation flux by Darcy equation contains information about porosity and tortuosity [178].

3.5.2 Mechanical Strength Tests

Mechanical strength tests are performed to determine the extent to which a membrane remains intact after a stress. For example, membranes in fuel cells or in oxygen separation used to reduce CO_2 emissions (oxyfuel combustion, see Chapter 4 for details) are constantly exposed to temperatures of 800–900 °C and large pressure gradients of 4–5 MPa. These severe conditions induce high mechanical stresses during the operation and the start-up/shutdown stages. The mechanical tests are performed to ensure the long-time reliability of ceramic membranes at operational conditions. These tests are run when visual examinations and leak tests show that the membrane is intact under optimal conditions such as ambient temperature and pressure. After that the stress and temperature are gradually increased up to the point where the membrane fails due to fracturing or cracking. The membrane can be tested from the inside and from the outside depending on its geometry and the intended operation mode. Test methods are used in conjunction with a plan that outlines any special conditions or operational requirements. The pass/fail criteria are established by a series of experiments designed to identify the failure threshold. Note, however, that testing is often influenced by the operator's technique, equipment variability, raw material selection and membrane geometry [179]. Even when conditions are standardized, the results are extremely sensitive to the presence of small flaws such as cracks, voids and inclusions. Flaws as small as 10–50 μm can reduce the strength of a ceramic structure to a fraction of its theoretical value. Such small flaws are hard to find. Moreover, membrane manufacturers rarely share test results.

Mechanical and mechanical/thermal stresses (mechanical stresses at elevated temperatures) are an integral part of membrane characterization. By definition, the stress is the force that acts on the unit area of a membrane:

$$\sigma = F_z/A \tag{3.32}$$

where σ (MPa) is the stress, F_z (N) is the applied force and A (m^2) is the cross-sectional area of the membrane sample perpendicular to the force vector. A membrane can be a subject of compressive, tensile, bending and shear stresses. If it is placed under a load that tends to compress or shorten it, the internal resistance to such a load is called a compressive stress. As a result of a stress, a membrane might change its dimensions. The change is called a compressive strain, defined as

$$E_{\text{strain}} = \frac{l_{\text{strain}} - l_0}{l_0} = \Delta l_{\text{strain}}/l_0 \tag{3.33}$$

where E_{strain} is the compressive strain, l_{strain} is the shrunk membrane length at the test and l_0 is the initial membrane length. A *tensile stress* is caused by a load that tends to elongate the membrane and it is always accompanied by a tensile strain. A *shear stress* is produced by a twisting or torsional action on a membrane. A *bending test* is caused by a load that bends a membrane and it is accompanied by a bending strain. Every stress leads to deformation in the

membrane structure that can be reversible (elastic) and irreversible (plastic, also called 'break stretching'). The upper limit of a membrane's elasticity is defined by Young's modulus, calculated as

$$E = \frac{\sigma}{E'_{\text{strain}}} = \frac{F_z/A}{\Delta l_{\text{strain}}/l_0} = \frac{F_z l_0}{A\Delta l} \tag{3.34}$$

where E (Pa) is Young's modulus of elasticity and E'_{strain} (−) is the ultimate elastic elongation defined as the largest separation between the gauge marks just before deformations become irreversible. High Young's moduli indicate that the elastic deformations under a given mechanical stress are small (i.e. the membrane is stiff). A low value indicates that the membrane has a higher degree of elasticity and is more likely to withstand harsh operational conditions.

Deformations can be tracked by applying a constantly increasing mechanical load and measurement of displacement by a sensor. Each test is performed with a separate device. Figure 3.19 shows a typical apparatus for measuring the tensile and compressive strengths of ceramic membranes.

Tensile/compressive strengths are tested on a membrane clamped between two holders. The low membrane holder is attached to a lower constant stage and the upper holder is attached to a strain–gauge-based force sensor. The upper holder moves with a constant velocity inducing tensile/compressive stresses. Dense membranes are tested for inelastic deformation at constant high temperature and constantly increasing mechanical load. The degree of shrinkage/elongation can be tracked and plotted as a function of the applied strength. Figure 3.20 shows a typical stress–strain curve where the area of elastic

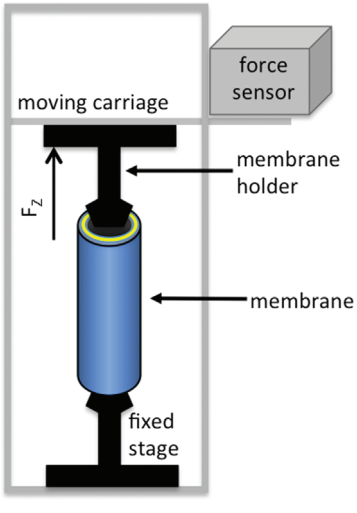


Figure 3.19 Schematic representation of apparatus for measuring tensile and compressive strengths of a ceramic membrane.

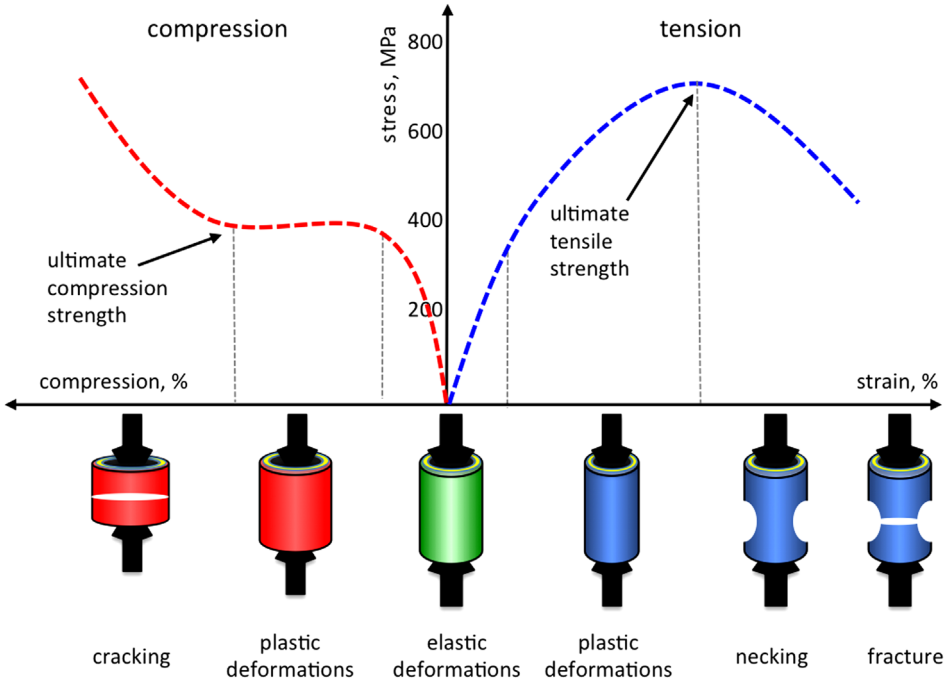


Figure 3.20 Typical stress–strain (right) and stress-compression (left) diagrams of ceramic membranes, together with the corresponding deformations (bottom).

deformations is found from the intercept of the tangential line within the region of elastic deformation (usually in the area of 0.5–1% tensile or creep strain), with a horizontal line drawn at the height of the tensile/creep strength at break.

The test can be done by compression or by elongation, yielding tensile strength and compression strength values. Elongation tests are less common due to problems with a fixture for brittle materials at elevated temperatures. In addition, ceramic membranes are typically brittle, and fracture at low elongations. Lee and Rainforth note that ceramic membranes have a high compression and low tensile strengths [180]. Often, the test continues until the membrane fractures/cracks, even when the membrane is long, into plastic deformations. The highest value of membrane strain just before the break is called the ultimate tensile/compression strength at tension/compression, respectively. According to Knudsen [181], this value depends on porosity, particle size and sintering temperature:

$$\sigma_T \approx d_p^{-c} \exp(-b\varepsilon) \tag{3.35}$$

where d_p is the particle diameter, b and c are powers and ε is the porosity. Here c is 0.5 and b varies between 4 and 7 [182]. Coble and Kingery [183] found a slight decrease in the tensile strength only at 1000 °C sintering temperature.

A *three-point bending test* is used to control the bending strength of a ceramic membrane. The test is performed on a membrane sample that is set on two supports. The sample always has a length-to-diameter ratio higher than 10 : 1. A measurable force is applied to the middle of a membrane and the bend stress is determined as in Eq. (3.32). The test continues until the sample fractures. The bending strength of a ceramic membrane correlates with the sintering temperature, and for hollow fibres it is calculated as

$$\sigma_{\mathrm{F}} = \frac{8F_{\mathrm{m}}L}{\pi D^3} \tag{3.36}$$

where F_{m} (Pa) is the force at which the membrane bends, L (m) is the length of the membrane between the supports and D (m) is the outer diameter of a hollow fibre [184].

The *Young modulus E* is defined here as

$$E = \frac{4L^3F_{\mathrm{m}}}{3\pi D^4 E_{\mathrm{strain}}} \tag{3.37}$$

where E is in Pa and E_{strain} (m) is the strain at the fracture. The bending test is relatively easy to perform and therefore it is widely used for the characterization of mechanical strength of ceramic membranes [185,186]. Sometimes bending tests are performed at elevated temperatures to find the mechanical failure under typical operational conditions [187]. The ultimate bending strength is usually lower at higher temperatures.

Another interesting and useful parameter is the *burst strength*, which reflects the ability of a membrane to resist rupture when pressure is applied in a controlled and repeatable manner to its interior space. This test is performed for hollow fibres that are placed outside of a deformable rubber membrane in a housing that serves as a protection wall [184]. A measurable pressure is applied on the rubber membrane. The value of the burst pressure depends on the sintering temperature and can be compared with the results of bending strength.

The *peel strength test* (also known as the 'Scotch tape test' [188]) can be used to evaluate the possibility of peeling off intermediate/top layers in a layered ceramic membrane. Here, a piece of Scotch tape is stuck onto the membrane surface and torn off rapidly. If the intermediate and top layers are sufficiently integrated into the membrane structure, they will not be torn together with the tape. This test is simple, quick and repeatable and correlates with burst strength. However, the results are sensitive to the peel angle and other experimental factors.

Other methods including the measurement of crack opening displacement [189], the compact tension method [190] and the scratch method [149] are less popular. Although the mechanical strength of ceramic membranes is an important issue, it attracts less interest nowadays. Research papers routinely report the results of mechanical strength tests on modified membranes, yet a recent thorough comparison of different methods is lacking. The last such reports were published in the 1990s [191].

3.5.3 Hydrophobicity of Ceramic Membranes

The affinity to water is a key feature of ceramic membranes. They can be water repelling (hydrophobic) or water absorbing (hydrophilic). For example, in membrane distillation and pervaporation (see Chapter 4 for more details), the membrane should be hydrophobic, because this will keep the pores free of a liquid and will facilitate the vapour transport. Conversely, in liquid filtration, hydrophilic membranes are preferable, as they will either increase water flux for the same TMP or allow reducing the applied pressure to maintain the same flux. Indeed, the affinity to water plays a major role in choosing membranes for applications in biotechnology, pharmaceuticals, dairy processes, food and beverage and chemical processes.

The common way for measuring membrane hydrophobicity is the *contact angle method*, which measures the surface wettability of ceramic membranes. When a drop of water falls on a membrane surface, we can think of two extreme situations: either the droplet will spread completely on the membrane surface or it will rest as a droplet without any significant contact with the surface. These are the cases of completely hydrophilic and hydrophobic surfaces. Usually, the membrane materials have some degree of hydrophilicity, so the droplet occupies some membrane surface. The contact angle is the angle at which a liquid interface meets the surface. It is measured by placing a water droplet on the surface and measuring the angle at the droplet edge. The contact angle varies between 0° for a completely hydrophilic and 180° for a completely hydrophobic surface. Physically, this angle reflects the mechanical equilibrium of a liquid drop under the action of three interfacial tensions:

$$\gamma_{MG} = \gamma_{ML} + \gamma_{LG} \cos\theta \tag{3.38}$$

where γ_{MG}, γ_{ML} and γ_{LG} (N/m) are the interfacial tensions between the membrane and the gas, the membrane and the liquid and the liquid and the gas. This definition, suggested by Thomas Young in 1805, is usually referred to as *Young's equation* [192]. The surface tension is an internal force that acts when two different phases (e.g. liquid and solid) are brought into contact to form an interface or a boundary. This force is due to the tendency of all materials to reduce their surface area in contact between phases. Surfaces with high surface tension values will make a droplet to spread resulting in contact angles of 90° and below. Surfaces with low surface tension will keep the droplet spherical and contact angle above 90°. Figure 3.21 shows the contact angle in hydrophilic and hydrophobic membranes.

The evaluation of surface wettability using Eq. (3.38) is mostly applicable for polymer membranes that are smoother than ceramic membrane surfaces. On rough surfaces such as ceramic membranes, the surface wettability is evaluated by a modification of Young's equation that includes roughness factor r_w:

$$\gamma_{LM} = \gamma_{SM} + \gamma_{LG} r_w \cos\theta \tag{3.39}$$

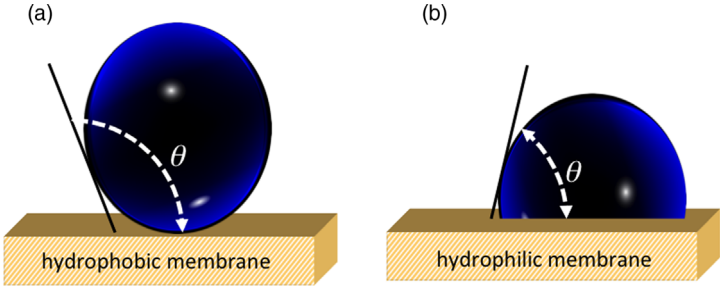


Figure 3.21 Contact angles of hydrophobic (a) and hydrophilic (b) ceramic membranes.

The roughness factor r_w is a ratio of areas of rough and smooth surfaces. As per definition, r_w is always larger than unity, because $r_w = 1$ means that the actual membrane area is absolutely smooth. According to Wenzel's Eq. (3.39), the roughness increases the interfacial tensions between the liquid and the membrane γ_{LM}, meaning that rough surfaces are more hydrophilic. Rough surfaces provide more possibilities for a contact between water droplet and surface, although in rough surfaces a droplet of water placed on the membrane surface has a range of contact angles and not just one. This is known as contact angle hysteresis. The range of the observed angles is usually determined by measurements of the advancing (maximum) and receding (minimum) angles [116]. The advancing angle corresponds to hydrophobic part and the receding angle to hydrophilic part of a membrane surface [193,194].

Measuring the contact angle between membrane and water is often done on a goniometer using the sessile drop method. A 20 µl drop of DI water or organic liquid is placed onto a dried membrane surface using a microsyringe and the air–water–surface contact angle is measured after 10 s. The advancing contact angle is measured by increasing the drop volume and the receding angle by decreasing the drop volume [195]. The contact angle of dry membrane is not necessarily the same as that of a wet one. In a captive bubble/drop method, a drop of air or liquid is attached from below to the downfacing surface of a membrane immersed in a liquid. If the liquid droplet is used, two liquids should be immiscible [194]. The *captive bubble method* is considered more reliable as the membrane is under normal operational conditions.

The contact angle method is simple, fast and widely used for characterizing membrane surfaces. Although the measurement is not very precise due to roughness of the surface, it is a standard relative index of hydrophilicity/hydrophobicity provided by membrane manufacturers. Ceramic membranes are considered hydrophilic with typical contact angles less than 30°.

3.5.4
Charge of Ceramic Membranes

Most solid surfaces immersed in an aqueous electrolyte solution are charged. The charge of mineral and metal oxides is due to the amphoteric behaviour of

surface hydroxyl groups [196,197]. Neutral membranes adsorb ions, usually anions, as well as surfactants, polyelectrolytes and charged macromolecules from the solution [198]. The zeolites are charged because their crystalline structure consists of $[SiO_4]^-$ and $[AlO_4]^-$ tetrahedral units that form a framework with small pores [199]. In addition to the membrane surface, the pores can also become charged. The charge affects the transmembrane flux and retention of solutes and therefore the surface charge is one of most basic features of a membrane. In practice, surface charge under operation is measured and not evaluated. The complexity of the measurement and evaluation is due to the presence of an electrical double layer (EDL) that covers the membrane surface with oppositely charged ions from the surrounding solution in two layers. The first layer is permanently attached and cannot be removed from an immersed membrane. The presence of the layer prevents a direct contact between a probe and the membrane surface. A second, diffuse layer cannot be removed but can be reshaped under the influence of an external force, so the measurement of an electric potential within the layer can indirectly indicate how the surface charge of a membrane and the electrolyte will affect the filtration process. Depending on the membrane and the measurement set-up, this value is called the *zeta potential* in static measurements and *streaming potential* in dynamic measurements. The surface charge of a membrane can also be characterized by impedance spectroscopy and membrane potential measurements. These methods can estimate the membrane charge both qualitatively and quantitatively.

An electrolyte pumped parallel near the membrane surface under constant pressure results in accumulation of ions from the diffuse EDL layer downstream. The ions diffuse back in the direction opposite to the direction of pumping. This electroosmotic flow generates a stable potential difference (the streaming potential) ζ (mV) [198]. According to the Helmholtz–Smoluchowski approximation of Poisson–Boltzmann equation, the streaming potential is equal to

$$\zeta = \frac{\Delta E}{\Delta P}\frac{\eta k}{\varepsilon_0 \varepsilon} \tag{3.40}$$

where ΔE is the potential difference across the membrane (mV), ΔP is the applied pressure (Pa), η is the dynamic viscosity of the electrolyte (Pa s), k is the specific conductivity of bulk electrolyte (1/(Ω m)), ε (−) is the dielectric permittivity of water and ε_0 ($C^2/(N\ m^2)$) is the permittivity of vacuum.

The streaming potential is determined as a slope of the potential versus pressure ($\Delta E/\Delta P$) and it should be zero at no applied pressure to ensure the absence of asymmetric potentials. Instead of constant pressure, the potential can be measured by applying a pressure pulse to one side of a membrane and measuring the instantaneous potential difference. However, this method is valid only when the potential difference is linearly dependent on the applied pressure [200].

In general, the surface membrane charge does not have to be equal to its pore charge. The presence of coated top layers, integral structure of a typical ceramic membrane and acquisition of a charge during the operation all lead to a possible difference in streaming potentials. This difference can be actually measured. In

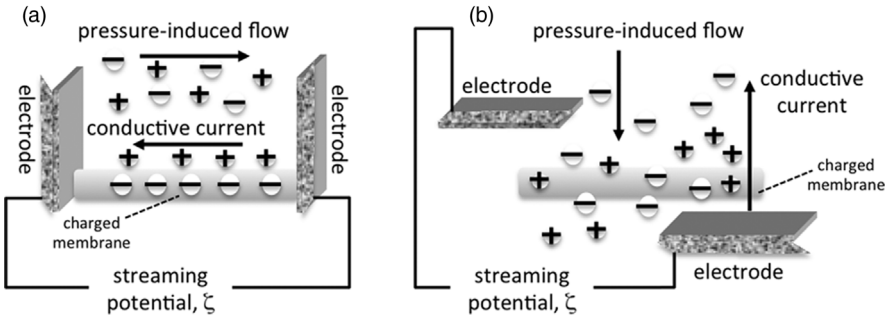


Figure 3.22 Typical set-ups for tangential (a) and transmembrane (b) streaming potential measurements.

measurements of surface potential, two electrodes are placed on the same side of a membrane and an electrolyte is pumped tangentially to the membrane surface. In transmembrane streaming potential, the electrodes are placed on the opposite feed and permeate sides, and an electrolyte is pumped through the membrane [196]. Figure 3.22 depicts set-ups used in measurements of tangential and transmembrane streaming potentials.

Besides the surface charge and the electrolyte, the streaming potential also depends on the solution pH. The surface charge changes due to protonation/deprotonation and/or dissociation of acidic/basic surface groups. More/less charged surfaces attract/retard more/less ions. Streaming potentials are usually measured over a pH range rather than for a single value. The range depends on the curiosity of a researcher and stability of electrode materials versus actual needs. In water and wastewater treatment, for example, the pH range is 6–9. A good compromise for streaming potential measurements is run between pH 3–11. The resulting curve depicts a change in streaming potential values as a function of pH. Figure 3.23 shows a typical streaming potential curve.

A streaming potential curve provides two values often used in membrane characterization. Typical streaming potential values are positive at low pH and negative at high pH. The curve therefore passes through an inflection point where the positive charge of membrane charged end groups is equal to the negative charge. This is the *point of zero charge* (pzc), sometimes also called the *isoelectric point* (iep). The second characteristic value is the streaming potential at relevant pH. For many applications, the important pH is alkaline and the streaming potential displays a constant value that is stable for the entire alkaline pH range. The stability is due to a full deprotonation of charged surface groups on the membrane surface. In theory, both values can be linked to the surface charge of the membrane. But in practice they are most often used as stand-alone parameters.

Electrochemical impedance spectroscopy (EIS) is performed on membranes immersed in an electrolyte of a known concentration. A small alternating current is applied externally on the electrolyte that moves according to the surface

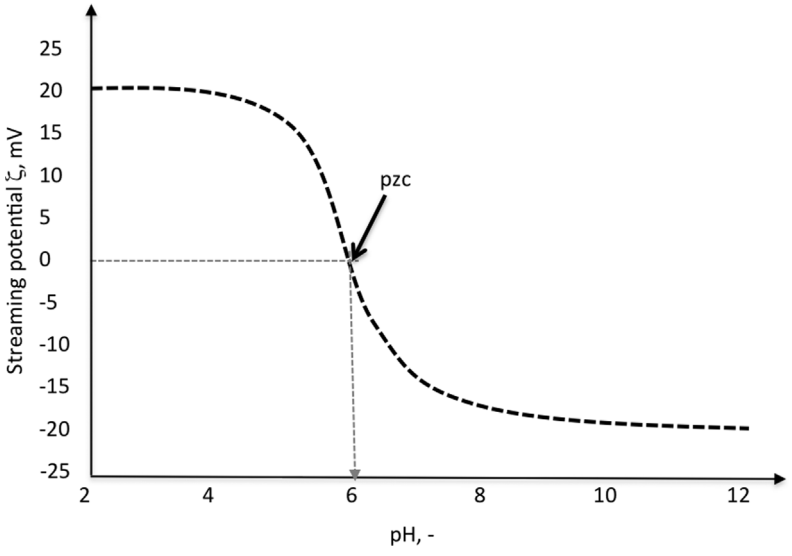


Figure 3.23 A typical streaming potential curve showing the regions of positive charge, electroneutrality and negative charge, where pzc denotes the point of zero charge.

charge of the membrane. This movement generates a surface potential difference that is recorded by electrodes located on two opposite sides of the membrane surface.

Another method mostly applicable to thin membranes such as NF and RO ones is the measurement of membrane potential. The membrane is positioned between two solutions of the same electrolyte with different concentrations. A solution with a higher salt concentration is in contact with the active side of the membrane and the solution with a lower salt concentration is in contact with the membrane support layer. Due to the salt gradient, a constant electroosmotic diffusion of ions or solvents creates a stable transmembrane potential that is measured by electrodes placed on opposite sides of the membrane. The diffusion of ions or the solvent depends on the pore charge, pore radius, the valence of electrolyte ions and the Donnan potential. The latter is related to uneven distribution of ions near semipermeable membranes when partial retention of anions/cations results in an enhanced penetration of other anions/cations. An enhanced penetration of anions/cations generates an electric potential across the membrane. This method, however, is less applicable to composite membranes where the top layer is very thin (15–100 nm) and the support layer is very thick (up to 2 mm). Apart from complications with retarded diffusion, the major impediment here is the large (and unknown *a priori*) resistance of a support layer [25].

The surface charge affects the membrane performance in several ways. Charged surfaces are more hydrophilic, and usually give a higher flux for a given TMP. That said, the combination of a high pore charge and a dilute solution might result in a significant pore clogging, reducing the flux. This happens when

the pore width is comparable with the thickness of the EDL expressed by Debye length $1/k$:

$$\frac{1}{k} = \frac{1}{e}\sqrt{\frac{\varepsilon_0 \epsilon k_B T}{\sum_i c z_i^2}} \tag{3.41}$$

where c (ions/m^3) is the concentration of the ion i, z (−) is the valence of the ion, e (C) is the elementary charge, k_B (J/K) is Boltzmann's constant and T (K) is the absolute temperature.

The electrostatic repulsion of oppositely charged ions results in more salt rejection by a charged membrane [201]. So the highest 50% rejection in an alumina-free silicate membrane was due to a strong electrostatic shielding of Na^+ ions by the monopolar surface [202]. Concurrently, the cationic adsorption onto negatively charged surfaces might enhance diffusion by establishing a charge gradient [203,204]. The equilibrium adsorption amount and the sorption kinetics of charged solutes are determined by the surface charge and its density, so charged surfaces experience more fouling by charged solutes.

3.6 Conclusions

Characterization of membrane surfaces is a varied field that can both predict and explain the obtained results. The most disputable, intriguing and non-resolved aspect is the characterization of the membrane pore size. The pore size and the other methods for bulk characterization of membranes, including charge, hydrophilicity, mechanical strength, flux and porosity, are the information usually provided by the membrane manufacturer. This information is needed for both daily operation and pilot studies initiated to choose a most suitable membrane for the application. Different applications require different membranes as will be explained and exemplified in Chapter 4. Chronologically, the bulk methods were developed and implemented before surface characterization, and most of them remain unchanged to date. Conversely, surface characterization methods are continuously changing and developing. These methods share a high spatial resolution and minimal probing depth to extensively characterize the membrane surface. Other methods such as Raman spectroscopy, time-of-flight secondary ion mass spectroscopy (TOF-SIMS) are currently on their way to become a part of the family. These methods are concisely described here and the interested readers might expend their knowledge by looking at textbook on each method and on papers that describe the implementation of the method in membrane investigation [205,206].

A third group is the methods that are currently emerging in membrane research but not yet fully implemented for the membrane characterization. At the moment, methods like electron energy loss spectroscopy (EELS) and X-ray microscopy are not sufficiently sensitive or do not have surface-sensitive

modifications. These methods are not described here, although we foresee that their importance will increase in the coming decade.

Exercises

3.1. The bubble point method determines pore sizes in low-pressure membranes.

- Consider two ceramic membranes with the same pore size distribution, one made from α-Al_2O_3 and the other from ZrO_2. Will these membranes show the same bubble point if the same wetting liquid is used in the measurement? Explain your answer.
- Figure 3.24 shows the pore size distribution of a ceramic membrane. What is the bubble point pressure of this membrane when wetted with water that is blown out of the membrane pores by air at 25 °C, given that its σ is 72 dyn/cm?
- What will the bubble point pressure be if the water is replaced with a liquid that has 10° contact angle with the membrane? You may assume that there is no change in the surface tension and in the pore size distribution.
- Typical differential inert gas pressure on the wetting liquid in the pore should not exceed 10 bars. Using the data in Table 3.1, decide and explain which liquid will help you to detect the smallest pore size. You may assume a 0° contact angle between the wetting liquid and the membrane.

3.2. You have three membranes, made from alumina, zirconia and titania, respectively. MWCO tests with polyethylene glycols (PEGs) and polyethylene oxides (PEOs) revealed the retention values shown in Table 3.2. Determine the MWCO value for each membrane.

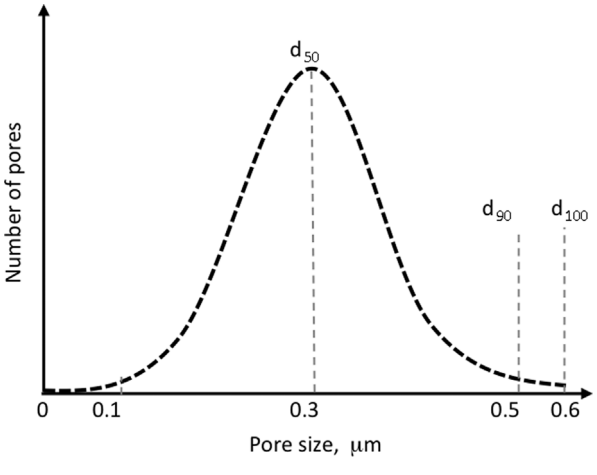


Figure 3.24 Pore size distribution as accepted after bubble point test.

Table 3.1 Surface tension of various liquids in dyn/cm against air.[a)]

Liquid	Temperature (°C)	Surface tension σ
Water	25	71.97
Water	50	67.91
Water	100	58.85
Ethanol	20	22.27
Ethanol (40%) + water	25	29.63
Ethanol (11.%) + water	25	46.03
Acetic acid	20	27.6
Methanol	20	22.6
Liquid nitrogen	−196	8.85
n-Hexane	20	18.4
Isopropanol	20	21.7

a) Data from Ref. [207].

Table 3.2 Retention data for three ceramic membranes.

PEG/PEO (kDa)	Al_2O_3 membrane Retention (%)	ZrO_2 membrane Retention (%)	TiO_2 membrane Retention (%)
0.3	0.2	0.1	3
0.6	5	0.3	7
1.0	15	1	12
1.5	23	1.8	20
2.0	42	3.1	30
3.0	59	6	60
10.0	67	28	90
20.0	79	41	93
35.0	92	60	96
50	94	75	99
100	97	86	100
300	99	89.5	100

3.3. Table 3.3 gives the contact angles for six different ceramic membranes using various wetting liquids. List the membranes in order of hydrophobicity (from most hydrophobic to most hydrophilic). Which applications would you suggest for the zeolite membrane? Explain your answer.

3.4. Table 3.4 details the results of measurement of the potential difference as a function of applied pressure. Measurements were conducted with Ag/AgCl reference electrodes and a high impedance digital multimeter in

Table 3.3 Contact angles for six different membranes.

Membrane	Wetting liquid	Contact angle (°)
Al_2O_3	Water	23
ZrO_2	Water	25
Perovskite	Water	32
TiO_2	Ethanol	45
SiO_2	Ethanol (40%) + water	18
SiO_2	Ethanol (11%) + water	24
Zeolite	Isopropanol	67

Table 3.4 Potential differences as a function of applied pressure.

ΔP (Pa)	ΔE, tangential streaming potential (mV)	ΔE, transmembrane streaming potential (mV)
10^4	9	5
2×10^4	19	9
4×10^4	38	18
6×10^4	61	32
8×10^4	79	39
10^5	98	51

the pH range of 3–10.5 (at pH > 10.5, the electrode is unstable, while at pH < 3, solution conductivity will be too large and will affect the measurement). The dynamic viscosity of the electrolyte η is 10^{-3} Pa s. The dielectric permittivity of water at 20 °C is 80.1. The permittivity of vacuum is 8.85×10^{-12} C^2/Nm^2. The specific conductivity of 10^{-3} M KCl electrolyte used in the experiments at 25 °C is 0.0147 1/Ωm.

Find the streaming potential on the membrane surface and inside the pores. What is the reason for the difference between the two values?

3.5. Draw a graph showing a cumulative volume of mercury as a function of the applied pressure for ceramic membranes with 2, 20 and 200 nm pores.

3.6. According to the Ferry–Renkin equation [208], the retention of a solute correlates with the solute size and pore width as

$$R = \begin{cases} 1 - 2\left(1 - \dfrac{a}{r_p}\right)^2 + \left(1 - \dfrac{a}{r_p}\right)^4, & \text{for } a/r_p \le 1 \\ 1, & \text{for } a/r_p > 1 \end{cases} \tag{3.42}$$

- Discuss what penetration mechanism the equation addresses and what are the main assumptions at its base.

Table 3.5 Permeation fluxes for two membranes at different pressures.

ΔP (Pa)	Membrane A Permeation flux ($m^3/(m^2\ s)$)	Membrane B Permeation flux ($m^3/(m^2\ s)$)
10^4	5	5
2×10^4	7	10
4×10^4	9	20
6×10^4	12	30
10^5	15	50

- Plot the degree of retention for the 2, 20 and 200 nm particles as a function of pore size. Find the d_{50}, d_{90} and d_{100} values for each particle. What are the practical limitations of this equation?

3.7. Calculate the surface porosity of ceramic membrane of 10 cm^2 size having 10^{12} pores per cm^2. You may assume that all the pores are cylindrical and the pore diameter is 20 nm.

3.8. The data in Table 3.5 were collected during permeation flux measurement through two UF membranes.

- Assuming that the membrane structure of liquid-transferable voids inside a well-packed structure (Carman–Kozeny equation) applies, plot the pore sizes that were found at each transmembrane pressure. The experiments were run with water at 25 °C. The water dynamic viscosity is 8.9×10^{-4} Pa s, the pore length is 2 mm, the pore tortuosity is 2 and the porosity is 0.4.
- Find and explain the difference between the two curves. Relate this difference to pore size and pore size distribution.

3.9. Verify the dimensions of Eq. (3.41).

3.10. Find the average roughness, the root mean square roughness and the skewness of α-Al_2O_3 and γ-Al_2O_3 membranes from the data presented in Table 3.6 that were obtained during AFM measurements.

3.11. Draw schematically the change in Debye length as a function of the ionic strength of a solution. The ionic strength is defined as

$$I = \frac{1}{2}\sum_{i=1}^{n} c_i z_i^2 \tag{3.43}$$

where c (ions/m^3) is the concentration of the ion i and z (–) is its valence.

3.12. Discuss the differences between scanning electron microscopy and transmission electron microscopy. Which type of electron microscopy would you use to detect the surface and the structure of ceramic and polymer membranes? Explain your answer.

Table 3.6 AFM measurements data for two alumina membranes.

Peak number	α-Al_2O_3 membrane Height value of a pixel (nm)	γ-Al_2O_3 membrane Height value of a pixel (nm)
1	13	5
2	26	7
3	3	3
4	14	12
5	28	25
6	99	17
7	56	8
8	10	15

References

1 Arkhangelsky, E., Kuzmenko, D., Gitis, N.V., Vinogradov, M., Kuiry, S. and Gitis, V. (2007) Hypochlorite cleaning causes degradation of polymer membranes. *Tribology Letters*, **28** (2), 109–116.

2 Burggraaf, A.J. and Cot, L. (1996) *Fundamentals of Inorganic Membrane Science and Technology*, Elsevier, Amsterdam.

3 Cuperus, F.P. and Smolders, C.A. (1991) Characterization of UF membranes: membrane characteristics and characterization techniques. *Advances in Colloid and Interface Science*, **34**, 135–173.

4 Klobes, P., Meyer, K. and Munro, R.G. (2006) *Porosity and Specific Surface Area Measurements for Solid Materials*, National Institute of Standards and Technology, Washington, DC.

5 Jakobs, E. and Koros, W.J. (1997) Ceramic membrane characterization via the bubble point technique. *Journal of Membrane Science*, **124** (2), 149–159.

6 Rouquerol, J., Avnir, D., Fairbridge, C.W., Everett, D.H., Haynes, J.H., Pernicone, N. *et al.* (1994) Recommendations for the characterization of porous solids. *Pure and Applied Chemistry*, **66** (8), 1739–1758.

7 Tan, X.Y., Liu, S.M. and Li, K. (2001) Preparation and characterization of inorganic hollow fiber membranes. *Journal of Membrane Science*, **188** (1), 87–95.

8 Cao, G.Z., Meijerink, J., Brinkman, H.W. and Burggraaf, A.J. (1993) Permporometry study on the size distribution of active pores in porous ceramic membranes. *Journal of Membrane Science*, **83** (2), 221–235.

9 Bason, S., Kaufman, Y. and Freger, V. (2010) Analysis of ion transport in nanofiltration using phenomenological coefficients and structural characteristics. *Journal of Physical Chemistry B*, **114** (10), 3510–3517.

10 Li, K. (2007) *Ceramic Membranes for Separation and Reaction*, John Wiley & Sons, Ltd, Chichester.

11 Liu, L.H., Tan, X.Y. and Liu, S.M. (2006) Yttria stabilized zirconia hollow fiber membranes. *Journal of the American Ceramic Society*, **89** (3), 1156–1159.

12 Kong, J.F. and Li, K. (2001) An improved gas permeation method for characterising and predicting the performance of microporous asymmetric hollow fibre membranes used in gas absorption. *Journal of Membrane Science*, **182** (1–2), 271–281.

13 Khayet, M. and Matsuura, T. (2004) Pervaporation and vacuum membrane distillation processes: modeling and

experiments. *AIChE Journal*, **50** (8), 1697–1712.
14 Tenelshof, J.E., Bouwmeester, H.J.M. and Verweij, H. (1995) Oxygen-transport through LA1-XSRXFEO3-delta membranes. 1. Permeation in air/He gradients. *Solid State Ionics*, **81** (1–2), 97–109.
15 Cheng, S.G., Gupta, V.K. and Lin, J.Y.S. (2005) Synthesis and hydrogen permeation properties of asymmetric proton-conducting ceramic membranes. *Solid State Ionics*, **176** (35–36), 2653–2662.
16 Bechhold, H. (1907) Kolloidstudien mit der Filtrations-methode. *Zeitschrift fur Physikalische Chemie*, **60**, 257–318.
17 Chisti, Y. (2007) Principles of membrane separation processes, in *Bioseparation and Bioprocessing: A Handbook* (ed. G. Subramanian), Wiley-VCH Verlag GmbH, Weinheim.
18 Meltzer, T.H. (1987) *Filtration in the Pharmaceutical Industry*, Marcel Dekker, New York, 1120 pp.
19 Nunes, S.P. and Peinemann, K.V. (1992) Ultrafiltration membranes from PVDF PMMA blends. *Journal of Membrane Science*, **73** (1), 25–35.
20 Kuzmenko, D., Arkhangelsky, E., Belfer, S., Freger, V. and Gitis, V. (2005) Chemical cleaning of UF membranes fouled by BSA. *Desalination*, **179** (1–3), 323–333.
21 Goren, U., Aharoni, A., Kummel, M., Messalem, R., Mukmenev, I., Brenner, A. *et al.* (2008) Role of membrane pore size in tertiary flocculation/adsorption/ ultrafiltration treatment of municipal wastewater. *Separation and Purification Technology*, **61** (2), 193–203.
22 Levitsky, I., Duek, A., Arkhangelsky, E., Pinchev, D., Kadoshian, T., Shetrit, H. *et al.* (2011) Understanding the oxidative cleaning of UF membranes. *Journal of Membrane Science*, **377** (1–2), 206–213.
23 Capannelli, G., Vigo, F. and Munari, S. (1983) Ultrafiltration membranes: characterization methods. *Journal of Membrane Science*, **15** (3), 289–313.
24 Nakao, S. (1994) Determination of pore-size and pore-size distribution: 3. Filtration membranes. *Journal of Membrane Science*, **96** (1–2), 131–165.
25 Bernstein, R., Kaufman, Y. and Freger, V. (2013) Membrane characterization. *Encyclopedia of Membrane Science and Technology*, John Wiley & Sons, Inc., Hoboken.
26 Gekas, V. and Zhang, W. (1989) Membrane characterization using porosimetry and contact-angle measurements: a comparison with experimental ultrafiltration results. *Process Biochemistry*, **24** (5), 159–166.
27 Lee, Y., Jeong, J., Youn, I.J. and Lee, W.H. (1997) Modified liquid displacement method for determination of pore size distribution in porous membranes. *Journal of Membrane Science*, **130** (1–2), 149–156.
28 Uchytil, P. (1994) Gas permeation in ceramic membranes. 1. Theory and testing of ceramic membranes. *Journal of Membrane Science*, **97**, 139–144.
29 Almandoz, M.C., Marchese, J., Pradanos, P., Palacio, L. and Hernandez, A. (2004) Preparation and characterization of non-supported microfiltration membranes from aluminosilicates. *Journal of Membrane Science*, **241** (1), 95–103.
30 Brun, M., Lallemand, A., Quinson, J.F. and Eyraud, C. (1977) New method for simultaneous determination of size and shape of pores: thermoporometry. *Thermochimica Acta*, **21** (1), 59–88.
31 Giesche, H. (2006) Mercury porosimetry: a general (practical) overview. *Particle and Particle Systems Characterization*, **23** (1), 9–19.
32 Hernandez, A., Calvo, J.I., Pradanos, P. and Tejerina, F. (1996) Pore size distributions in microporous membranes: a critical analysis of the bubble point extended method. *Journal of Membrane Science*, **112** (1), 1–12..
33 Allen, T. (1997) Particle size measurement. *Surface Area and Pore Size Determination*, vol. **2**, 5th edn, Chapman & Hall, London.
34 Burgraaf, A.J. (1996) Important characteristics of inorganic membranes, in *Fundamentals of Inorganic Membrane Science and Technology* (eds A.J. Burgraaf and L. Cot), Elsevier, Amsterdam.
35 Eyraud, C., Betemps, M., Quinson, J.F., Chatelut, F., Brun, M. and Rasneur, B.

(1984) Determination of the pore-size distribution of an ultrafilter by - gas-liquid permporometry measurement - comparison between flow porometry and condensate equilibrium porometry. *Bulletin De La Societe Chimique De France Partie I-Physicochimie Des Systemes Liquides Electrochimie Catalyse Genie Chimique*, (9–10), I237–I244.

36 Mey-Marom, A. and Katz, M.G. (1986) Measurement of active pore size distribution of microporous membranes: a new approach. *Journal of Membrane Science*, **27**, 119–130.

37 Julbe, A. and Ramsay, J.D.F. (1996) Methods for the characterization of porous structure in membrane materials, in *Fundamentals of Inorganic Membrane Science and Technology* (eds A.J. Burgraaf and L. Cot), Elsevier, Amsterdam.

38 Thomson, W. (1871) On the equilibrium of vapour at a curved surface of liquid. *Philosophical Magazine*, **42**, 448–452.

39 Sing, K.S.W., Everett, D.H. and Haul, R.A.W., Moscou, L. Pierotti, R.A., Rouquerol, J. *et al.* (1985) Reporting physisorption data for gas/solid systems with special reference to the determination of surface area and porosity (Recommendations 1984). *Pure and Applied Chemistry*, **57** (4), 603–619.

40 Katz, M.G. and Baruch, G. (1986) New insights into the structure of microporous membranes obtained using a new pore size evaluation method. *Desalination*, **58** (3), 199–211.

41 Bothun, G.D., Ni, Q. and Ilias, S. (2008) Solvent-dependent permeability in asymmetric ceramic membranes with tortuous or non-tortuous mesopores. *Journal of Membrane Science*, **325** (2), 982–988.

42 Mitchell, J., Webber, J.B.W. and Strange, J.H. (2008) Nuclear magnetic resonance cryoporometry. *Physics Reports*, **461** (1), 1–36.

43 Webber, J.B.W. and Dore, J.C. (2008) Neutron diffraction cryoporometry: a measurement technique for studying mesoporous materials and the phases of contained liquids and their crystalline forms. *Nuclear Instruments & Methods in Physics Research Section A: Accelerators Spectrometers Detectors and Associated Equipment*, **586** (2), 356–366.

44 Jackson, C.L. and McKenna, G.B. (1990) The melting behavior of organic materials confined in porous solids. *Journal of Chemical Physics*, **93** (12), 9002–9011.

45 Kubelka, P. and Munk, F. (1931) Ein Beitrag zur Optik der Farbanstriche. *Zeitschrift für technische Physik*, **12**, 593–601.

46 Thomson, J. (1860) On crystallization and liquefaction, as influenced by stresses tending to change form in the crystals. *Proceedings of the Royal Society of London*, **11**, 473–481.

47 Gibbs, J. (1961) *The Scientific Papers of J. Willward Gibbs*, Dover Publications, New York.

48 Cuperus, F.P., Bargeman, D. and Smolders, C.A. (1992) Critical points in the analysis of membrane pore structures by thermoporometry. *Journal of Membrane Science*, **66** (1), 45–53.

49 Landry, M.R. (2005) Thermoporometry by differential scanning calorimetry: experimental considerations and applications. *Thermochimica Acta*, **433** (1–2), 27–50.

50 Muhammad, N., Sinha, R., Krishnan, E.R. and Patterson, C.L. (2009) Ceramic filter for small system drinking water treatment: evaluation of membrane pore size and importance of integrity monitoring. *Journal of Environmental Engineering*, **135** (11), 1181–1191.

51 Arkhangelsky, E., Duek, A. and Gitis, V. (2012) Maximal pore size in UF membranes. *Journal of Membrane Science*, **394**, 89–97.

52 American Society for Testing and Materials (2010) *Standard Practice for Integrity Testing of Water Filtration Membrane Systems*, American Society for Testing and Materials, West Conshohocken, PA.

53 Ioan, C.E., Aberle, T. and Burchard, W. (2000) Structure properties of dextran. 2. Dilute solution. *Macromolecules*, **33** (15), 5730–5739.

54 Ren, J.Z., Li, Z.S. and Wong, F.S. (2006) A new method for the prediction of pore size distribution and MWCO of

ultrafiltration membranes. *Journal of Membrane Science*, **279** (1–2), 558–569.
55 Geankoplis, C.J. (2003) *Transport Processes and Separation Process Principles: Includes Unit Operations*, Prentice Hall, Upper Saddle River, NJ.
56 Mochizuki, S. and Zydney, A.L. (1992) Dextran transport through asymmetric ultrafiltration membranes: comparison with hydrodynamic models. *Journal of Membrane Science*, **68** (1–2), 21–41.
57 Mulder, M. (1996) *Basic Principles of Membrane Technology*, Kluwer Academic Publishers, Dordrecht.
58 Gitis, V. and Rothenberg, G. (2013) Membrane integrity monitoring. *Encyclopedia of Membrane Science and Technology*, John Wiley & Sons, Inc., Hoboken.
59 EPA (2003) Membrane Filtration Guidance Manual, United States Environmental Protection Agency, Contract No. EPA 815-D-03-008.
60 Colvin, C., Brauer, R., DiNatale, N. and Scribner, T. (2001) Comparing laser turbidimetry with conventional methods for monitoring MF and UF membrane integrity. AWWA Membrane Technology Conference Proceedings, March 4–7, San Antonio, TX.
61 Landsness, L.B. (2001) Accepting MF/UF technology: making a final cut. Proceedings of the American Water Works Association 2001 Membrane Technology Conference, San Antonio, TX.
62 Rajagopalan, N., Qi, S. and Pickowitz, J.P. (2001) Field evaluation of ceramic microfiltration membrane in drinking water application. Proceedings of the 2001 AWWA Membrane Technology Conference, San Antonio, TX.
63 Panglisch, S., Deinert, U., Dautzenberg, W., Kiepke, O. and Gimbel, R. (1998) Monitoring the integrity of capillary membranes by particle counters. *Desalination*, **119** (1–3), 65–72.
64 Adham, S.S., Jacangelo, J.G. and Laine, J.M. (1995) Low-pressure membranes: assessing integrity. *Journal American Water Works Association*, **87** (3), 62–75.
65 Glucina, K., Do-Quang, Z. and Laine, J.M. (1997) Assessment of particle counting method for hollow fiber membrane integrity. Workshop on Membranes in Drinking Water Production: Technical Innovations and Health Aspects, L'Aquila, Italy.
66 EPA (2001) Low-Pressure Membrane Filtration for Pathogen Removal: Application, Implementation, and Regulatory Issues. US EPA Office of Water, EPA 815-C-01-001.
67 Dow (2004) FILMTEC™ Reverse Osmosis Membranes Technical Manual, Dow Water Solutions.
68 Steigelmann, E.F. (inventor) (1980) Method for detecting membrane leakage patent. US Patent US4,188,817A (Standard Oil Company (Indiana), assignee).
69 Chapman, M. and Linton, W.K. (2000) Methods for Monitoring the Integrity of Reverse Osmosis and Nanofiltration Membrane Systems. United States Department of Interior and Bureau of Reclamation.
70 Kruithof, J.C., Kamp, P.C., Folmer, H.C., Nederlof, M.M. and van Hoof, S.C.J.M. (2001) Development of a membrane integrity monitoring strategy for the UF/RO Heemskerk drinking water treatment plant. *Water Science and Technology*, **1** (5–6), 261–271.
71 ASTM D4194-03 (2008) *Standard Test Methods for Operating Characteristics of Reverse Osmosis and Nanofiltration Devices*. American Society for Testing and Materials.
72 Gitis, V., Adin, A., Nasser, A., Gun, J. and Lev, O. (2002) Fluorescent dye labeled bacteriophages: a new tracer for the investigation of viral transport in porous media: 1. Introduction and characterization. *Water Research*, **36** (17), 4227–4234.
73 Gasser, G., Rona, M., Voloshenko, A., Shelkov, R., Tal, N., Pankratov, I. *et al.* (2010) Quantitative evaluation of tracers for quantification of wastewater contamination of potable water sources. *Environmental Science and Technology*, **44** (10), 3919–3925.

74 Duek, A., Arkhangelsky, E., Krush, R., Brenner, A. and Gitis, V. (2012) New and conventional pore size tests in virus-removing membranes. *Water Research*, **46** (8), 2505–2514.

75 Guo, H., Wyart, Y., Perot, J., Nauleau, F. and Moulin, P. (2010) Application of magnetic nanoparticles for UF membrane integrity monitoring at low-pressure operation. *Journal of Membrane Science*, **350** (1–2), 172–179.

76 Gitis, V., Haught, R.C., Clark, R.M., Gun, J. and Lev, O. (2006) Nanoscale probes for the evaluation of the integrity of ultrafiltration membranes. *Journal of Membrane Science*, **276** (1–2), 199–207.

77 Gitis, V., Haught, R.C., Clark, R.M., Gun, J. and Lev, O. (2006) Application of nanoscale probes for the evaluation of the integrity of ultrafiltration membranes. *Journal of Membrane Science*, **276** (1–2), 185–192.

78 Ziskind, G., Shmueli, H. and Gitis, V. (2011) An analytical solution of the convection–dispersion–reaction equation for a finite region with a pulse boundary condition. *Chemical Engineering Journal*, **167** (1), 403–408.

79 Levenspiel, O. (1999) *Chemical Reaction Engineering*, 3rd edn, John Wiley & Sons, Inc., New York.

80 Cleveland, C.T., Seacord, T.F. and Zander, A.K. (2002) Standardized membrane pore size characterization by polyethylene glycol rejection. *Journal of Environmental Engineering*, **128** (5), 399–407.

81 Mehta, A. and Zydney, A.L. (2006) Effect of membrane charge on flow and protein transport during ultrafiltration. *Biotechnology Progress*, **22** (2), 484–492.

82 Zydney, A.L. and Xenopoulos, A. (2007) Improving dextran tests for ultrafiltration membranes: effect of device format. *Journal of Membrane Science*, **291** (1–2), 180–190.

83 Issid, I., Lavergne, M. and Lemordant, D. (1992) Using micelles to determine the pore-size of UF membranes. *Journal of Membrane Science*, **74** (3), 279–287.

84 Lee, S., Park, G., Amy, G., Hong, S.K., Moon, S.H., Lee, D.H. *et al.* (2002) Determination of membrane pore size distribution using the fractional rejection of nonionic and charged macromolecules. *Journal of Membrane Science*, **201** (1–2), 191–201.

85 Arkhangelsky, E., Sefi, Y., Hajaj, B., Rothenberg, G. and Gitis, V. (2011) Kinetics and mechanism of plasmid DNA penetration through nanopores. *Journal of Membrane Science*, **371** (1–2), 45–51.

86 Wyart, Y., Georges, G., Deumie, C., Amra, C. and Moulin, P. (2008) Membrane characterization by optical methods: ellipsometry of the scattered field. *Journal of Membrane Science*, **318** (1–2), 145–153.

87 Jia, M.D., Peinemann, K.V. and Behling, R.D. (1993) Ceramic zeolite composite membranes: preparation, characterization and gas permeation. *Journal of Membrane Science*, **82** (1–2), 15–26.

88 Suoninen, E.J. (1997) Optical microscopy. *Surface Characterization: A User's Sourcebook*, Wiley-VCH Verlag GmbH, Weinheim.

89 Wyart, Y., Georges, G., Demie, C., Amra, C. and Moulin, P. (2008) Membrane characterization by microscopic methods: multiscale structure. *Journal of Membrane Science*, **315** (1–2), 82–92.

90 Huang, K., Liu, G., Lou, Y., Dong, Z., Shen, J. and Jin, W. (2014) A graphene oxide membrane with highly selective molecular separation of aqueous organic solution. *Angewandte Chemie, International Edition*, **53** (27), 6929–6932.

91 Riedel, R. and Chen, I.W. (2008) *Ceramics Science and Technology, Synthesis and Processing*, vol. **3**, Wiley-VCH Verlag GmbH, Weinheim.

92 Pawley, J. (2006) *Handbook of Biological Confocal Microscopy*, Springer, Berlin.

93 Minsky, M. (inventor) (1961) Microscopy apparatus patent. US Patent 3,013,467A (M. Minsky (assignee)).

94 Snyder, M.A., Vlachos, D.G. and Nikolakis, V. (2007) Quantitative analysis of membrane morphology, microstructure, and polycrystallinity via laser scanning confocal microscopy: application to NaX zeolite membranes. *Journal of Membrane Science*, **290** (1–2), 1–18.

95 Charcosset, C. and Bernengo, J.C. (2000) Comparison of microporous membrane morphologies using confocal scanning laser microscopy. *Journal of Membrane Science*, **168** (1–2), 53–62.

96 Asraf-Snir, M. and Gitis, V. (2011) Tracer studies with fluorescent-dyed microorganisms: a new method for determination of residence time in chlorination reactors. *Chemical Engineering Journal*, **166** (2), 579–585.

97 Herzberg, M. and Elimelech, M. (2007) Biofouling of reverse osmosis membranes: role of biofilm-enhanced osmotic pressure. *Journal of Membrane Science*, **295** (1–2), 11–20.

98 Sweity, A., Ying, W., Ali-Shtaye, M.S., Yang, F., Bick, A., Oron, G. *et al.* (2011) Relation between EPS adherence, viscoelastic properties, and MBR operation: biofouling study with QCM-D. *Water Research*, **45** (19), 6430–6440.

99 Avadhani, G.S. (2010) Techniques for characterization of nanomaterials. The Sixth International Conference on Mathematical Modeling and Computer Simulation of Material Technologies (MMT 2010), Ariel, Israel.

100 Anandkumar, J., Sahariah, B.P. and Dasgupta, S. (2014) Synthesize and characterization of clay based low-cost membrane for solid-liquid separation. *Recent Research in Science and Technology*, **6** (1), 14–17.

101 Nandi, B.K., Das, B., Uppaluri, R. and Purkait, M.K. (2010) Preparation and characterization of inexpensive submicron range inorganic microfiltration membranes. *Membrane Water Treatment*, **1** (2), 121–137.

102 Shafiei, K., Kazemimoghaddam, M., Mohammadi, T. and Pakdehi, S.G. (2015) An investigation on manufacturing of alumina microfiltration membranes. *Desalination and Water Treatment*, **53** (9), 2429–2436.

103 Gaikwad, A.V., Boffa, V., ten Elshof, J.E. and Rothenberg, G. (2008) Cat-in-a-cup: facile separation of large homogeneous catalysts. *Angewandte Chemie, International Edition*, **47** (29), 5407–5410.

104 Goldstein, J., Newbury, D.E., Joy, D.C., Lyman, C.E., Echlin, P., Lifshin, E. *et al.* (2003) *Scanning Electron Microscopy and X-Ray Microanalysis*, 3rd edn, Kluwer Academic Press, New York.

105 Bowen, W.R., Hilal, N., Lovitt, R.W. and Williams, P.M. (1996) Atomic force microscope studies of membranes: surface pore structures of cyclopore and anopore membranes. *Journal of Membrane Science*, **110** (2), 233–238.

106 Fritzsche, A.K., Arevalo, A.R., Connolly, A.F., Moore, M.D., Elings, V. and Wu, C.M. (1992) The structure and morphology of the skin of polyethersulfone ultrafiltration membranes: a comparative atomic force microscope and scanning electron microscope study. *Journal of Applied Polymer Science*, **45** (11), 1945–1956.

107 Williams, D.B. and Carter, C.B. (2009) *Transmission Electron Microscopy: A Textbook for Materials Science*, Springer Science + Business Media, New York.

108 Sheldon, J.M. (1991) The fine-structure of ultrafiltration membranes: 1. Clean membranes. *Journal of Membrane Science*, **62** (1), 75–86.

109 Wallheinke, K., Heckmann, W., Potschke, P. and Stutz, H. (1998) Localizing compatibilizers in immiscible blends by SEM. *Polymer Testing*, **17** (4), 247–255.

110 Freger, V., Bottino, A., Capannelli, G., Perry, M., Gitis, V. and Belfer, S. (2005) Characterization of novel acid-stable NF membranes before and after exposure to acid using ATR-FTIR, TEM and AFM. *Journal of Membrane Science*, **256** (1–2), 134–142.

111 Freger, V., Gilron, J. and Belfer, S. (2002) TFC polyamide membranes modified by grafting of hydrophilic polymers: an FT-IR/AFM/TEM study. *Journal of Membrane Science*, **209** (1), 283–292.

112 Karnik, B.S., Baumann, M.J., Corneal, L.M., Masten, S.J. and Davies, S.H. (2009) TEM characterization of iron-oxide-coated ceramic membranes. *Journal of Materials Science*, **44** (15), 4148–4154.

113 de Vos, R.M. and Verweij, H. (1998) Improved performance of silica membranes for gas separation. *Journal of Membrane Science*, **143** (1–2), 37–51.

114 Iwamoto, Y. and Kawamoto, H. (2009) Trends in research and development of nanoporous ceramic separation membranes: saving energy by applying the technology to the chemical synthesis process. *Science & Technology Trends: Quarterly Review*, **32**, 1–10.

115 Dzyazko, Y.S., Volfkovich, Y.M., Sosenkin, V.E., Nikolskaya, N.F. and Gomza, Y.P. (2014) Composite inorganic membranes containing nanoparticles of hydrated zirconium dioxide for electrodialytic separation. *Nanoscale Research Letters*, **9** (271), 1–12.

116 Li, N.N., Fane, A.G., Ho, W.S.W. and Matsuura, T. (2011) *Advanced Membrane Technology and Applications*, John Wiley & Sons, Inc., Hoboken.

117 Flegler, S.L., Heckman, J.W. and Klomparens, K.L. (1995) *Scanning and Transmission Electron Microscopy: An Introduction*, Oxford University Press, New York.

118 Bowen, W.R., Hilal, N., Lovitt, R.W. and Wright, C.J. (1999) Atomic force microscope studies of membrane surface. *Surface Chemistry and Electrochemistry of Membranes*, Marcel Dekker, New York.

119 Dullien, F.A.L. and Batra, V.K. (1970) Determination of structure of porous media. *Industrial and Engineering Chemistry*, **62** (10), 25–53.

120 Rugar, D. and Hansma, P. (1990) Atomic force microscopy. *Physics Today*, **43** (10), 23–30.

121 Sawyer, L., Grubb, D.T. and Meyers, G.F. (2008) *Polymer Microscopy*, Springer, New York.

122 Binnig, G., Quate, C.F. and Gerber, C. (1986) Atomic force microscope. *Physical Review Letters*, **56** (9), 930–933.

123 Paredes, J.I., Martinez-Alonso, A. and Tascon, J.M.D. (2003) Application of scanning tunneling and atomic force microscopies to the characterization of microporous and mesoporous materials. *Microporous and Mesoporous Materials*, **65** (2–3), 93–126.

124 Sweity, A., Ronen, Z. and Herzberg, M. (2014) Induced organic fouling with antiscalants in seawater desalination. *Desalination*, **352**, 158–165.

125 Bernstein, R., Belfer, S. and Freger, V. (2011) Bacterial attachment to RO membranes surface modified by concentration–polarization-enhanced graft polymerization. *Environmental Science and Technology*, **45** (14), 5973–5980.

126 Bowen, W.R., Doneva, T.A. and Stoton, J.A.G. (2002) The use of atomic force microscopy to quantify membrane surface electrical properties. *Colloid Surface A*, **201** (1–3), 73–83.

127 Enzel, P., Henderson, G.S., Ozin, G.A. and Bedard, R.L. (1995) Imaging the surfaces of nanoporous semiconductors by atomic-force microscopy. *Advanced Materials*, **7** (1), 64–68.

128 Bottino, A., Capannelli, G., Grosso, A., Monticelli, O., Cavalleri, O., Rolandi, R. *et al.* (1994) Surface characterization of ceramic membranes by atomic force microscopy. *Journal of Membrane Science*, **95** (3), 289–296.

129 Zeng, Z.Q., Xiao, X.Y., Gui, Z.L. and Li, L.T. (1997) AFM study on surface morphology of Al_2O_3–SiO_2–TiO_2 composite ceramic membranes. *Journal of Membrane Science*, **136** (1–2), 153–160.

130 Cortalezzi, M.M., Rose, J., Wells, G.F., Bottero, J.Y., Barron, A.R. and Wiesner, M.R. (2003) Ceramic membranes derived from ferroxane nanoparticles: a new route for the fabrication of iron oxide ultrafiltration membranes. *Journal of Membrane Science*, **227** (1–2), 207–217.

131 Hilal, N., Al-Khatib, L., Al-Zoubi, H. and Nigmatullin, R. (2005) Atomic force microscopy study of membranes modified by surface grafting of cationic polyelectrolyte. *Desalination*, **184** (1–3), 45–55.

132 Karnik, B.S., Baumann, M.J., Masten, S.J. and Davies, S.H. (2006) AFM and SEM characterization of iron oxide coated ceramic membranes. *Journal of Materials Science*, **41** (20), 6861–6870.

133 Deng, W., Yu, X., Sahimi, M. and Tsotsis, T.T. (2014) Highly permeable porous silicon carbide support tubes for the preparation of nanoporous inorganic membranes. *Journal of Membrane Science*, **451**, 192–204.

134 Bowen, W.R., Hilal, N., Lovitt, R.W. and Williams, P.M. (1996) Atomic force microscope studies of membranes: surface pore structures of diaflo ultrafiltration membranes. *Journal of Colloid and Interface Science*, **180** (2), 350–359.

135 Hendren, Z.D., Brant, J. and Wiesner, M.R. (2009) Surface modification of nanostructured ceramic membranes for direct contact membrane distillation. *Journal of Membrane Science*, **331** (1–2), 1–10.

136 Ciston, S., Lueptow, R.M. and Gray, K.A. (2008) Bacterial attachment on reactive ceramic ultrafiltration membranes. *Journal of Membrane Science*, **320** (1–2), 101–107.

137 Hoek, E.M.V., Bhattacharjee, S. and Elimelech, M. (2003) Effect of membrane surface roughness on colloid–membrane DLVO interactions. *Langmuir*, **19** (11), 4836–4847.

138 Kaupp, G. (2008) *Atomic Force Microscopy, Scanning Nearfield Optical Microscopy and Nanoscratching Application to Rough and Natural Surfaces*, Springer, Berlin.

139 Brune, D., Hellborg, R., Whitlow, H. and Hunderi, O. (2007) *Surface Characterization: A User's Sourcebook*, Wiley-VCH Verlag GmbH, Weinheim.

140 Zhong, Z., Xing, W. and Zhang, B. (2013) Fabrication of ceramic membranes with controllable surface roughness and their applications in oil/water separation. *Ceramics International*, **39** (4), 4355–4361.

141 Wei, W., Qin, G., Hu, H., You, L. and Chen, G. (2007) Preparation of supported carbon molecular sieve membrane from novolac phenol-formaldehyde resin. *Journal of Membrane Science*, **303** (1–2), 80–85.

142 Bonekamp, B.C. (1996) Preparation of asymmetric ceramic membrane supports by dip-coating, in *Fundamentals of Inorganic Membrane Science and Technology* (eds A.J. Burggraaf and L. Cot), Elsevier, Amsterdam.

143 Wei, C.C. and Li, K. (2009) Preparation and characterization of a robust and hydrophobic ceramic membrane via an improved surface grafting technique. *Industrial and Engineering Chemistry Research*, **48** (7), 3446–3452.

144 Hoppert, M. (2006) *Microscopic Techniques in Biotechnology*, Wiley-VCH Verlag GmbH, Weinheim.

145 Forman, P. (1969) The discovery of the diffraction of X-rays by crystals: a critique of the myths. *Archive for History of Exact Sciences*, **6**, 38–71.

146 Bragg, W.L. (1913) The diffraction of short electromagnetic waves by a crystal. *Proceedings of the Cambridge Philosophical Society*, **17**, 43–57.

147 He, B.B. (2009) *Two-Dimensional X-Ray Diffraction*, John Wiley & Sons, Inc., Hoboken.

148 Tan, X.Y. and Li, K. (2006) Oxidative coupling of methane in a perovskite hollow-fiber membrane reactor. *Industrial and Engineering Chemistry Research*, **45** (1), 142–149.

149 Brown, I.W.M., Wu, J.P. and Smith, G. (2012) Fabrication, structure and properties of nanostructured ceramic membranes, in *Ceramic Materials: Progress in Modern Ceramics* (ed. F. Shi), InTech., Rijeka, Croatia.

150 Leroux, J. and Powers, C.A. (1970) Direct X-ray diffraction quantitative analysis of quartz in industrial dust films deposited on silver membrane filters. *Occupational Health Review*, **21** (1), 26–34.

151 Dutrow, B.L. and Clark, C.M. (2013) Geochemical Instrumentation and Analysis. Available from http://serc.carleton.edu/research_education/geochemsheets/techniques/XRD.html (updated January 4, 2014).

152 Griffiths, P.R. and De Haseth, J.A. (2007) *Fourier Transform Infrared Spectrometry*, 2nd edn, John Wiley & Sons, Inc., Hoboken.

153 West, A.R. (2014) *Solid State Chemistry and Its Applications*, 2nd edn, John Wiley & Sons, Ltd, Chichester.

154 Messica, A., Greenstein, A. and Katzir, A. (1996) Theory of fiber-optic, evanescent-wave spectroscopy and sensors. *Applied Optics*, **35** (13), 2274–2284.

155 Xiangli, F., Chen, Y., Jin, W. and Xu, N. (2007) Polydimethylsiloxane (PDMS)/

ceramic composite membrane with high flux for pervaporation of ethanol–water mixtures. *Industrial & Engineering Chemistry Research*, **46** (7), 2224–2230.

156 Tsui, E.M., Cortalezzi, M.M. and Wiesner, M.R. (2007) Proton conductivity and methanol rejection by ceramic membranes derived from ferroxane and alumoxane precursors. *Journal of Membrane Science*, **306** (1–2), 8–15.

157 Romagnoli, P., Trombetta, M. and Licoccia, S. (2004) ATR–FTIR spectroscopic study of the effect of ceramic addition in novel ionoconductor gels for biomedical applications in space. *Journal of the European Ceramic Society*, **24**, 1153–1156.

158 Blanpain-Avet, P., Migdal, J.F. and Bénézech, T. (2009) Chemical cleaning of a tubular ceramic microfiltration membrane fouled with a whey protein concentrate suspension: characterization of hydraulic and chemical cleanliness. *Journal of Membrane Science*, **337** (1–2), 153–174.

159 Chang, I.S., Le Clech, P., Jefferson, B. and Judd, S. (2002) Membrane fouling in membrane bioreactors for wastewater treatment. *Journal of Environmental Engineering*, **128** (11), 1018–1029.

160 Chan, R. and Chen, V. (2004) Characterization of protein fouling on membranes: opportunities and challenges. *Journal of Membrane Science*, **242** (1–2), 169–188.

161 Kim, K.J., Fane, A.G., Nystrom, M. and Pihlajamaki, A. (1997) Chemical and electrical characterization of virgin and protein-fouled polycarbonate track-etched membranes by FTIR and streaming-potential measurements. *Journal of Membrane Science*, **134** (2), 199–208.

162 Pihlajamaki, A., Vaisanen, P. and Nystrom, M. (1998) Characterization of clean and fouled polymeric ultrafiltration membranes by Fourier transform IR spectroscopy-attenuated total reflection. *Colloids and Surfaces A: Physicochemical and Engineering Aspects*, **138** (2–3), 323–333.

163 Cahill, D.G., Freger, V. and Kwak, S.-Y. (2008) Microscopy and, microanalysis of reverse osmosis and nanofiltration membranes. *MRS Bulletin*, **33** (1), 27–32.

164 Yarwood, J., Sammon, C., Mura, C. and Pereira, M. (1999) Vibrational spectroscopic studies of the diffusion and perturbation of water in polymeric membranes. *Journal of Molecular Liquids*, **80** (2–3), 93–115.

165 Boccaccio, T., Bottino, A., Capannelli, G. and Piaggio, P. (2002) Characterization of PVDF membranes by vibrational spectroscopy. *Journal of Membrane Science*, **210** (2), 315–329.

166 Gruger, A., Regis, A., Schmatko, T. and Colomban, P. (2001) Nanostructure of Nafion (R) membranes at different states of hydration: an IR and Raman study. *Vibrational Spectroscopy*, **26** (2), 215–225.

167 Khulbe, K.C. and Matsuura, T. (2000) Characterization of synthetic membranes by Raman spectroscopy, electron spin resonance and atomic force microscopy: a review. *Polymer*, **41** (5), 1917–1935.

168 Pastorczak, M., Wiatrowski, A., Kozanecki, M., Lodzinski, A. and Ulanski, J. (2005) Confocal Raman microscopy in 3-dimensional shape and composition determination of heterogeneous systems. *Journal of Molecular Structure*, **744**, 997–1003.

169 Turrel, G. and Dhamelincourt, P. (1996) Micro-Raman spectroscopy. *Modern Techniques in Raman Spectroscopy*, John Wiley & Sons, Ltd, Chichester.

170 Moskovits, M. (2011) Imaging: spot the hotspot. *Nature*, **469** (7330), 307–308.

171 Cang, H., Labno, A., Lu, C.G., Yin, X.B., Liu, M., Gladden, C. *et al.* (2011) Probing the electromagnetic field of a 15-nanometre hotspot by single molecule imaging. *Nature*, **469** (7330), 385–388.

172 Robinson, P.D., Kassu, A., Sharma, A., Kukhtareva, T., Farley, C.W., Smith, C. *et al.* (2013) Surface-enhanced Raman spectroscopy scattering from gold-coated ceramic nanopore substrates: effect of nanopore size. *Journal of Nanophoton*, **7**, 073592

173 Smith, E. and Dent, G. (2004) *Modern Raman Spectroscopy – A Practical Approach*, John Wiley & Sons, Ltd, Chichester.

174 Bolon, A.M. and Gentleman, M.M. (2011) Raman spectroscopic observations of ferroelastic switching in ceria-stabilized zirconia. *Journal of the American Ceramic Society*, **94** (12), 4478–4482.

175 Colomban, P. and Slodczyk, A. (2009) Raman intensity: an important tool in the study of nanomaterials and nanostructures. *Acta Physica Polonica A*, **116** (1), 7–12.

176 Dresselhaus, M.S., Jorio, A., Hofmann, M., Dresselhaus, G. and Saito, R. (2010) Perspectives on carbon nanotubes and graphene Raman spectroscopy. *Nanoletters*, **10** (3), 751–758.

177 Cuperus, F.P., Bargeman, D. and Smolders, C.A. (1992) Permporometry: the determination of the size distribution of active pores in UF membranes. *Journal of Membrane Science*, **71** (1–2), 57–67.

178 Pierre, A. and Christian, G. (2008) Current status and prospects for ceramic membrane applications. *Handbook of Membrane Separations*, CRC, Boca Raton, FL, pp. 139–179.

179 Johnson, M. (1997) An evaluation of what factors effect burst test results using rigid porous packages. Rochester Institute of Technology.

180 Lee, W.E. and Rainforth, W.M. (1994) *Ceramic Microstructures: Property Control by Processing*, Chapman & Hall, London.

181 Knudsen, F.P. (1959) Dependence of mechanical strength of brittle polycrystalline specimens on porosity and grain size. *Journal of the American Ceramic Society*, **42**, 376–387.

182 Biesheuvel, P.M. (2000) Porous ceramic membranes: suspension processing, mechanical and transport properties, and application in the osmotic tensiometer. University of Twente.

183 Coble, R.L. and Kingery, W.D. (1956) Effect of porosity on physical properties of sintered alumina. *Journal of the American Ceramic Society*, **39**, 377–385.

184 Larbot, A. (1996) Ceramic processing techniques of support systems for membranes synthesis. *Fundamentals of Inorganic Membrane Science and Technology*, Elsevier, Amsterdam.

185 Liu, Y.T., Tan, X.Y. and Li, K. (2006) $SrCe_{0.95}Yb_{0.05}O_3$-alpha hollow-fiber membrane and its property in proton conduction. *AIChE Journal*, **52** (4), 1577–1585.

186 Liu, Y.T., Tan, X. and Li, K. (2006) $SrCe_{0.95}Yb_{0.05}O_3$-alpha (SCYb) hollow fibre membrane: preparation, characterization and performance. *Journal of Membrane Science*, **283** (1–2), 380–385.

187 Pecanac, G., Bause, T. and Malzbender, J. (2011) Ring-on-ring testing of thin, curved bi-layered materials. *Journal of the European Ceramic Society*, **31** (12), 2037–2042.

188 Krongelb, S. (1968) Environmental effects on chemically vapor-plated silicon dioxide. *Electrochemical Technology*, **6** (7–8), 251–256.

189 Withers, P.J. and Preuss, M. (2012) Fatigue and damage in structural materials studied by X-ray tomography, in *Annual Review of Materials Research* (ed. D.R. Clarke), Annual Reviews, Palo Alto, CA, pp. 81–103.

190 Sata, T. (1999) Preparation and mechanical properties of NaCl ceramics. *Journal of the Ceramic Society of Japan*, **107** (2), 166–173.

191 Ponton, C.B. and Rawlings, R.D. (1989) Vickers indentation fracture toughness test: Part 1. Review of literature and formulation of standardised indentation toughness equations. *Materials Science and Technology*, **5** (9), 865–872.

192 Young, T. (1805) An essay on the cohesion of fluids. *Philosophical Transactions of the Royal Society of London*, **95**, 65–87.

193 Zhang, W. and Hallstrom, B. (1991) Membrane characterization using the contact angle technique: I. Methodology of the captive bubble technique. *Desalination*, **79** (1), 1–12.

194 Zhang, W., Wahlgren, M. and Sivik, B. (1989) Membrane characterization by the contact-angle technique: 2. Characterization of UF-membranes and comparison between the captive bubble and sessile drop as methods to obtain water contact angles. *Desalination*, **72** (3), 263–273.

195 Wang, L.K., Chen, J.P., Hung, Y.-T. and Shammas, N.K. (2011) *Membrane and Desalination Technologies*, Humana Press, New York.

196 Herbig, R., Arki, P., Tomandl, G. and Braunig, R.E. (2003) Comparison of electrokinetic properties of ceramic powders and membranes. *Separation and Purification Technology*, **32** (1–3), 363–369.

197 Theodoly, O., Cascao-Pereira, L., Bergeron, V. and Radke, C.J. (2005) A combined streaming-potential optical reflectometer for studying adsorption at the water/solid surface. *Langmuir*, **21** (22), 10127–10139.

198 Elimelech, M., Chen, W.H. and Waypa, J.J. (1994) Measuring the zeta (electrokinetic) potential of reverse-osmosis membranes by a streaming potential analyzer. *Desalination*, **95** (3), 269–286.

199 Dyer, A. (1988) *An Introduction to Zeolite Molecular Sieves*, John Wiley & Sons, Ltd, Chichester.

200 Fievet, P., Szymczyk, A., Aoubiza, B. and Pagetti, J. (2000) Evaluation of three methods for the characterisation of the membrane–solution interface: streaming potential, membrane potential and electrolyte conductivity inside pores. *Journal of Membrane Science*, **168** (1–2), 87–100.

201 Pendergast, M.M. and Hoek, E.M.V. (2011) A review of water treatment membrane nanotechnologies. *Engineering and Environmental Science*, **4** (6), 1946–1971.

202 Duke, M.C., O'Brien-Abraham, J., Milne, N., Zhu, B., Lin, J.Y.S. and da Costa, J.C.D. (2009) Seawater desalination performance of MFI type membranes made by secondary growth. *Separation and Purification Technology*, **68** (3), 343–350.

203 Li, L.X., Dong, J.H. and Nenoff, T.M. (2007) Transport of water and alkali metal ions through MFI zeolite membranes during reverse osmosis. *Separation and Purification Technology*, **53** (1), 42–48.

204 Li, L.X., Dong, J.H., Nenoff, T.M. and Lee, R. (2004) Desalination by reverse osmosis using MFI zeolite membranes. *Journal of Membrane Science*, **243** (1–2), 401–404.

205 Vandenabeele, P. (2013) *Practical Raman Spectroscopy: An Introduction*. John Wiley & Sons, Inc., Hoboken.

206 Fearn, S. (2015) *An Introduction to Time-of-Flight Secondary Ion Mass Spectrometry (ToF-SIMS) and Its Application to Materials Science*, Morgan & Claypool Publishers.

207 Silbey, R.J., Alberty, R.A. and Bawendi, M.G. (2004) *Physical Chemistry*, 4th edn., John Wiley & Sons, Inc., Hoboken.

208 Prasad, N.K. (2012) *Downstream Process Technology: A New Horizon in Biotechnology*, Prentice-Hall, New Delhi.

4
Applications

4.1
Classical Applications of Ceramic Membranes

Ceramic membranes are used in a variety of fields. Many research and piloting efforts are devoted to expand the use of membranes to new and exciting applications, especially in those market segments that are currently 'occupied' by polymer membranes. Most of these new applications, however, are still under development. Details on the most recent advances can be found in conference proceedings, typically on separation using inorganic membranes [1,2], and in research papers. We will describe here a broad selection of applications, focusing on those industrial sectors where the advantages of using ceramic membranes *per se* are significant. In general, using ceramic membranes is beneficial in those applications that require harsh environmental conditions: extreme pH values, high temperatures or the presence of strong oxidants. The main disadvantage is the cost. Despite the fact that ceramic membranes were developed more than 60 years ago, they only entered the market in a small number of applications. The infrastructure for their production on a large scale remained relatively undeveloped. Production-related parameters such as the module geometry, fittings and cleaning procedures stayed in place for a long time. But this is changing. Several large companies have recently decided to proceed with ceramic membrane applications, addressing the auxiliary issues as they appear. Most of these examples happened in countries with strong governmental support for such developments. Previously, a typical technological development was research-based (so-called technology push), where the new materials and membranes were first developed by academic groups and then slowly adopted by the market. Each one of these technological developments took several years and sometimes decades. Today, there are many applications where there is already a set of available membranes ready to use. These applications are performed with a limited number of materials and with several commercial-scale membrane suppliers. The list of potential suppliers is provided in Table 4.1.

First installations are coming on stream, and economic evaluation with them. It turns out that in terms of capital expenses (CapEx) the new generation of

Ceramic Membranes: New Opportunities and Practical Applications, First Edition. Vitaly Gitis and Gadi Rothenberg.
© 2016 Wiley-VCH Verlag GmbH & Co. KGaA. Published 2016 by Wiley-VCH Verlag GmbH & Co. KGaA.

Table 4.1 Commercial-scale ceramic membrane suppliers.[a)]

Company	Membrane	Pore size	Shape	Core business
Atech Innovations	Al_2O_3 TiO_2	0.1–1.2 µm 5 kDa to 50 nm	Tube Multichannel	Food, beverages, liquid wastes
Orelis	Kleansep™ Al_2O_3/TiO_2 TiO_2/ZrO_2		Multichannel	
Veolia Water	CeraMem SiC Al_2O_3 TiO_2	5, 50, 200 nm 0.1, 0.2, 0.5 µm 0.01, 0.1 µm	Tube	Water treatment
Hyflux	InoCep® α-Al_2O_3	20, 40, 100, 200, 500, 800, 1400 nm	Hollow fibres	Water, wastewater, food, beverages
Kubota	FILCERA® Al_2O_3	0.1 µm		MBRs
TAMI Industries	INSIDE CéRAM	1.6, 2.5, 3.5, 4.6, 5.5, 6 mm		Water treatment
Inoceramic GmbH	Inopor Al_2O_3/TiO_2 Inopor Al_2O_3/SiO_2	350, 750 Da 600 Da	Tube Multichannel	Pervaporation
Pall Exekia	Membralox Al_2O_3/ZrO_2 Al_2O_3/Al_2O_3	20–100 nm 0.1–5 µm	Multichannel	Food
Metawater	Al_2O_3	0.1 µm	Multichannel	Water purification
Mitsui	NaA zeolites	Ultra-microporous	Tube Multichannel	Pervaporation
Meidensha	Al_2O_3	0.1 µm		MBR
Jiangsu Jiuwu	Al_2O_3, TiO_2, ZrO_2	5 kDa, 0.05–0.2 µm	Multichannel	Water treatment, bio-industry, beverages
Pervatech	HybSi			Dehydration
GEA Westfalia	Membraflow	5 nm to 1.4 µm	Hollow fibres	Wine industry
CTI (Salindres, France)	Zeolites, processed silicas (H_2) on alumina, TiO_2, ZrO_2, SiC, perovskites			Gas separation

a) Based on Ref. [3], with additions and modifications.

ceramic membranes is closing the gap on the polymer ones. Moreover, when taking into account the costs of pretreatment and post-treatment, membrane replacement and lifetime, power consumption and cleaning operations, it looks like ceramic membranes are on par or cheaper on operating expenses (OpEx) compared with polymer ones. With more industrial installations and more interest in solving auxiliary technical issues, we foresee a much closer match between ceramic and polymer membranes. In this chapter, we will focus on the application themselves, while in Chapter 5 we will discuss the economic implications.

Two types of ceramic membranes have been developed. The first type includes porous membranes for filtering in the MF and UF ranges that are now widely used in liquid separations. This is a mature separation technology in the food sector (mainly for cheesemaking), the beverage industry (milk, juice, beer and wine) and the pharmaceuticals, water and wastewater treatment sectors. Today's ceramic membranes are multilayer structures composed of macroporous inorganic materials that support a microporous coating layer that has non-deformable porosity. These ceramic membrane elements are embedded in stainless steel housing (the so-called module) that can contain one or several membrane elements.

The second type includes microporous (NF) and even dense ceramic membranes for gas separation. For many years, gas separation with ceramic membranes could not compete with conventional gas separation technologies such as cryogenic distillation, condensation and amine absorption. Ceramic membranes, with their relatively large pores (compared with what is needed for separating gases) and low packing density, had a tough time entering the industrial gas separation market. However, in many gas applications the polymer membranes were not in a better shape, and as ceramic membrane technology developed, they became a more viable option. Today, ceramic membranes are slowly yet steadily establishing a position in the gas separation market. The most prominent examples are the application of ceramic membranes as molecular sieves in CO_2 and hydrogen separation, and as oxygen and/or proton conductors [4]. The relevant technologies are CO_2 capture in power plants, high-temperature fuel cells and pervaporation. First trials had been performed, and pilots are running. Meanwhile, R&D departments are working on new materials and on technology modifications that will increase gas separation selectivity.

This chapter is therefore equally divided between the implementation of ceramic membranes in gas and liquid separations. Table 4.2 gives an overview of these plus some additional implementations of ceramic membranes in specific industrial sectors.

In some of these applications, membrane modules are used 'as is', with industry building a special set-up to fit the membrane demands and abilities. In other cases, the membranes are modified to fit the industry requirements. Although we will discuss here both types of applications, we are mainly interested in the latter. The reason is that once standard membrane modules are applied, industrial applications can grow by volume in a given sector. We will focus on three large-volume industrial applications where we feel that ceramic membranes have a strong growth potential. One of these areas is the treatment of waste liquids and gases. Efficient waste treatment is now a 'hot topic' in many countries, and ceramic membranes with their robustness enjoy fast growth in this market segment. Another area of application is the food and beverage sector, an established market where ceramic membranes with stable operation over long periods of time are gradually replacing polymer membranes. The third field is gas separation, where we foresee the development of ceramic membranes in new applications such as hydrogen production and (high-temperature) fuel cells. In total, the market for ceramic membrane technologies in gas and liquid separation in 2012

Table 4.2 Industrial applications of ceramic membranes arranged by sectors.

Industrial sector	Application
Chemical	• Separation of gases (H_2, CO_2, O_2) with porous and dense membranes • Fuel cells (especially SOFCs) • Membrane reactors • Concentration of polymer suspensions and metal hydroxide solutions • Separation of catalysts • Recovery of dyes and pigments • Treating of oil/water product emulsions • Purification and recycling of organic solvents
Biotechnology	• Biomass recycling in membrane bioreactors • Clarification of fermentation broth for the production of antibiotics and enzymes • Concentration, fractionation, isolation and sterilization of antibiotics, enzymes, proteins, amino acids and vitamins
Metals	• Recycling and disposal of degreasing and rinsing baths • Particle removal from ultrapure gases and ultrapure water in electronics • Recovery of heavy metals from mining wastewater • Cleaning of wastewater from grinding processes • Treatment of wastewater from glass and glass fibre production
Textiles/pulp and paper	• Separation, concentration and dewatering of biomass and algae • Disposal of fat emulsions • Separation of yeast
Food and beverages	• Clarification of juice, cider, beer and wine • Concentration of juice • Sterilization of milk and whey (separation of proteins) • Concentration of whey and milk proteins • Clarification of fermentation broths in the production of amino acids, organic acids and polyols
Recycling and environment	• Purification of drinking water • Municipal and industrial wastewater treatment • Organic content reduction • Oil/water separation • Recovery of pharmaceuticals and pesticides • Retention of microorganisms • Retention of heavy metals and radioactive isotopes • Recycling of water from swimming pools

has reached $540 million [3]. In the following sections, we will discuss in detail the various applications and outline the current position of ceramic membranes in these fields.

There are additional fields where ceramic membranes slowly evolved into an established technology. Pharma- and bio-industry are such examples, but these are beyond the scope of this book. Nevertheless, we feel that the current shift towards the use of ceramic membranes for such sensitive applications as drug preparation, protein separation or the purification of final products from reaction species, debris and unreacted chemicals is noteworthy.

4.2
Gas Separation with Ceramic Membranes

Membranes separate two phases or two materials in the same phase. Good examples of the former are the purification of drinking water or membrane reactors. The single-phase separation of liquid/liquid and gas/gas mixtures depends on a selective uptake of one sort of molecules, the difference in their diffusion or both. Some single-phase separations are due to a phase change inside the membrane. For example, *pervaporation* separates two liquids but only one of them changes a phase into a vapour that diffuses through the membrane. Such separation processes are driven by pressure, temperature or electrical potential gradient between the feed and permeate sides. Examples of industrial membrane gas separation processes include hydrogen recovery in petroleum refining, the separation of nitrogen and oxygen from air, and the separation and recovery of carbon dioxide from biogas and syngas. Other examples include the removal of oxygen to prevent flame and the dehumidification of natural gas. The main competing conventional processes for gas separation are pressure swing adsorption (PSA) and cryogenic distillation.

The foundation for gas separation was laid by Thomas Graham in 1833 when he published data on gas transport in one of the first issues of *Philosophical Magazine*. Twenty years later, Fick proposed a quantitative description of gas transport through boundary layers. In 1866, Graham made the next important step in understanding the permeation process. He proposed that permeation involves a solution-diffusion mechanism by which permeate molecules, first dissolved in the upstream face of the membrane, were then transported through it by the same process as that occurring in the diffusion of liquids. The first successful application of membrane gas separation systems came a century later, in 1969, when DuPont developed a commercial gas separation membrane module, Permasep [5]. That module separated hydrogen and helium from a gas mixture with hollow polyester fibres. Separation of hydrogen from ammonia purge gas streams was the next step in commercialization of membrane-based gas separation. It was established in 1977 by Monsanto, using polydimethylsiloxane (PDMS)-coated polysulfone hollow-fibre membranes [6]. In 1980, Permea launched the first industrial installation for capturing carbon dioxide from syngas and for the separation of hydrogen in petroleum refineries. Since then, the acceptance of membrane-based gas separation has grown, implemented by several companies including Cynara-NATCO, Separex-UOP, GMS, Generon, Praxair, Air Products, Dow Chemicals, Grace Membrane Systems and UBE [7]. Today, membranes are applied in a range of gas separation processes (see Table 4.3 for a partial list).

So what makes membrane gas separation so attractive to industry? It is a simple, scalable, economical and eco-friendly process. Membrane gas separation does not require large adsorption towers, absorption beds, cryogenic distillation or large compressors. It consumes less energy, because it does not require a phase change as in cryogenic separation. Moreover, it is a continuous process

Table 4.3 Applications of gas permeation membranes.[a)]

Recovered gas	Process or application
Hydrogen	Methanol synthesis
	Syngas refineries purge (H_2, C_nH_m)
	Petrochemical (H_2, N_2CH_4, CO)
	Syngas ratio adjustment
	Hydrogenation reactions
Carbon dioxide	Natural gas
	Elimination from fuel cell
	Hydrocarbon gases
	Control for food preservation and fermentation
	Landfill drainage gas (CO_2, CH_4, C_nH_m)
Hydrogen sulfide	Hydrocarbon gases
	Sour gas treatment
Carbon monoxide and hydrogen	Synthesis gas
Nitrogen	Preservation and inert blanketing
	Air separation (O_2, N_2)
Oxygen	Oxidation in chemical industry
	Air separation
	Combustion use
	Medical gases
Helium	Hydrocarbon gases
	Diving gas (He/N_2, O_2, air)
Water vapour	General gas dehydration
	Well head gas
	Air dehumidification
	Natural gas dehydration
Oxygen-enriched air	Use as combustion gas
Hydrocarbon/air	Pollution control
	HC recovery

a) Based on Ref. [8], with additional modifications.

with no intermittent cycles of pressure swing adsorption. But the key factor in the shift towards membrane-based gas separation is the possibility to achieve a high-flux superior separation by industrially available asymmetric membranes. Although in general the latter description applies equally to polymeric and ceramic membranes, the historical recourse points on the prevalence of polymer membranes. Most companies used the existing polymer materials and tailored separation properties by carefully choosing the conditions (pressure, temperature, feed concentration). The publication of the famous Robeson diagram in 1991 pointed on the upper limit of ability of polymer membranes to separate nitrogen and oxygen [9]. With their limited thermal and mechanical stability, polymer membranes show a general trade-off between the selectivity and permeability. Highly selective membranes have low permeability, and vice versa. Indeed, many polymer membranes had been tried, but seldom exceeded

Robeson's upper bound. The research since then centred on the modification of existing polymer membranes (cross-linking or combining polymers), synthesis of new membrane polymers (polyimides, polycarbonates) and introduction of new membrane materials such as carbon and ceramic membranes. Indeed, ceramic membranes were already used in enrichment of uranium hexafluoride during the *Manhattan Project* (see Section 1.1 for details) but the process was abandoned in 1950s. The past decade has seen a renewed interest in using ceramic membranes due to their superior chemical and thermal stability. Still, most of commercial large-scale gas separation is performed with polymer membranes. The ceramic membranes are in a stage of intensive development and pilot evaluation. The three main aspects that need to be addressed in such pilots are the following:

- Membrane fabrication process is refined to reduce defects in large-scale membranes.
- Membranes combine high flux with high selectivity.
- Thermal mechanical performance is improved.

Membrane gas separation is based on one of the separation mechanisms detailed in Chapter 2 and can be performed with either dense or porous ceramics. Typical dense membranes for gas separation are made of crystalline materials, such as perovskites or fluorites [10]. Conversely, porous membranes are typically made of amorphous silica, alumina or zeolites. Dense or non-porous membranes enjoy the uniform crystalline structure with well-defined pore sizes, but suffer from low transmembrane fluxes. An important feature of dense membranes is that they can separate even gases of similar sizes efficiently, as long as the solubility of the gas molecules in the membrane differs significantly. Porous ceramic membranes, on the contrary, provide high fluxes due to the presence of pores but often low selectivity [11]. The following classification for gas separation processes suggested by Keizer *et al.* [12] differentiates between processes at ambient and elevated temperatures performed with porous and dense membranes. According to this, the five types of gas separation procedures are:

1) Separation of gases at ambient temperature using high pressure. This separation uses mostly the difference in molecular weights (sizes) of gases and therefore is mainly applied for separation of hydrogen using molecular sieving in porous membranes. Examples include O_2/N_2, H_2/N_2, H_2/CO, H_2/CO_2, H_2/CH_4, H_2/C_3H_8, H_2/CH_3OH, H_2/C_4H_{10} and He/CH_4 mixtures. The separation depends strongly on the material type, pore size and pore size distribution. Gases can be separated based on the difference in their molecular weight, size, shape and affinity to the membrane material.
2) Separation of condensable gases at ambient temperature. Examples are CO_2/CH_4, CO/CO_2, H_2O/air, (C_3 and C_4)/(C_1 and C_2), removal of acid gases (HCl, H_2S, SO_2), ammonia or hydrocarbons/air [12].

3) Separation of condensable gases at higher temperatures (up to 300 °C), applied mainly for separating hydrocarbons.
4) Separation of H_2 or O_2 at temperatures up to 1000 °C with dense ceramic membranes. The separation is due to the solution-diffusion mechanism.
5) A combination of transport and reaction for separating special gas mixtures that cannot be treated using conventional separation protocols, such as air that contains NO_x.

This classification suggests a division into separation at ambient temperature (points 1 and 2) and at elevated temperatures (points 3–5). Separations at room temperature prevail. Points 1 and 2 suggest molecular sieving and capillary condensation mechanisms, respectively. As we explained above, both of these mechanisms are built on pores sizes similar to the molecular diameters of gases that one wishes to separate. The next generation of ceramic membranes should therefore possess unique properties of molecular sieving materials as well as a better transport function. Promising new concepts include the development of mixed matrix membranes in which the sieving properties of various materials are combined with the film-forming properties of polymers.

> The last decade can be marked as a fresh start for ceramic membranes in gas separation processes. Well-known advantages of high thermal and mechanical stability had finally turned the attention to the industrial gas separation with ceramic membranes. Still, the majority of studies were performed in universities and R&D departments and concerned the development of ceramic membrane as a product for a future presentation in the market. The research was driven by the need for a lot of fundamental knowledge. Good ceramic membranes as a product require several years of development, and it looks like these years are behind us. Industry is now more involved in R&D. The use of ceramic membranes for gas separation and reactor applications is very promising. We are in a stage where the market will decide if the new generation of ceramic membranes deserves the industrial implementation or the ceramic membranes will be send for a new round of laboratory experiments and fine tunings.

The above quote, which sounds very timely, actually comes from the introduction to 'Feasibility of the application of porous inorganic gas separation membranes in some large-scale chemical processes' published 20 years ago [13]. Many things have changed since. We have much more data on testing inorganic membranes under industrial conditions. We also have a clear technical and economical evaluation of applications of ceramic membranes in various applications. Despite this, examples of actual industrial implementations of ceramic membranes in gas separation are rare, so in most cases we will have to discuss examples of the potential use of ceramic membranes rather than referring to actual large-scale industrial examples.

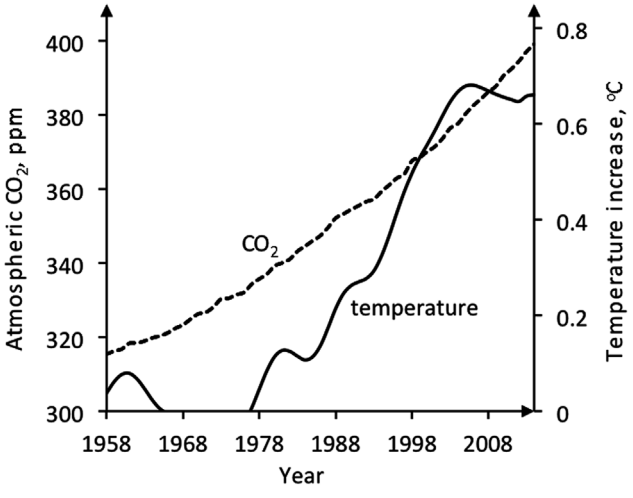


Figure 4.1 Average CO_2 concentrations in October during 1958–2014 measured at Mauna Loa, Hawaii, also known as the *Keeling curve*. The raw data are from Earth System Research Laboratory, Global Monitoring Division, http://www.esrl.noaa.gov/gmd/ccgg/trends/.

4.2.1
Sustainable Reduction of CO_2 Emissions with Ceramic Membranes

Global warming itself is a highly debated issue, and its possible causes are even more obscure [14,15]. However, there is no debate about the fact that CO_2 emissions have been rising continuously over the past decades. Figure 4.1 shows the famous 'Keeling curve', a plot of the change in CO_2 concentration in atmosphere of Mauna Loa, Hawaii [16]. The plot shows clearly the annual cycles of CO_2 concentrations, as well as a worrying fact: between 1958 and 2014 the concentration of atmospheric CO_2 increased from roughly 300 to 400 ppm. At the same time, the Earth temperature increased by 0.65 °C. There may be a link between the two phenomena in a form that doubling of carbon dioxide concentrations in the atmosphere as a direct result of burning fossil fuels can increase the Earth temperature by roughly a degree Celsius. Or maybe not. Along with other gases such as water vapour, methane, nitrous oxide and ozone, CO_2 can trap sun radiation and absorb and emit radiation within the thermal infrared range that would otherwise escape from Earth. This does not prove that anthropogenic (i.e. man-made) CO_2 emissions actually cause global warming. However, it is a cause for concern, because it may be that anthropogenic CO_2 emissions are affecting our environment. And as we have just one Earth to live on, we cannot take chances.

Carbon dioxide is probably the predominant greenhouse gas resulting from human activities. Other GHGs are water vapour, methane, nitrous oxide and ozone. There are international actions aimed at reducing the amounts of anthropogenic GHG emissions. These are worthy actions, not least because they

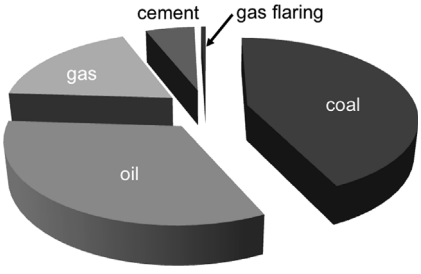


Figure 4.2 Relative contributions of different sources to carbon dioxide emissions in 2014. The raw data are from https://www.iea.org/publications/freepublications/publication/.

promote the debate and the thinking about human's ecological footprint. The *Kyoto Protocol* specifies the actions needed to decrease the CO_2 concentration in the atmosphere. Global CO_2 emissions in 2014 were 37 gigaton ($GtCO_2$). That value is already much higher than a prediction made just in 2007. The expected 49% increase in energy demand set intermittent points of 33.8 $GtCO_2$ in 2020 and 42.4 $GtCO_2$ in 2035 [17]. That level is long over already in 2014. Despite all other sources of energy, we still highly rely on fossil fuels and therefore the world energy-related CO_2 emissions are skyrocketing at the moment. The 92% CO_2 emissions are from fossil fuels and additional 8% from land use change (primarily deforestation). The land use change emission shows a decreasing trend from 2000. Other GHGs, such as CH_4 and N_2O, are produced from domestic livestock and rice cultivation. A breakdown of 2014 92% carbon dioxide emissions shows that coal accounted for 43%, oil for 33%, gas for 18%, cement for 5.5% and gas flaring for 0.5%. Figure 4.2 shows the relative contribution of each of these to the overall CO_2 pie [18].

The concentration of CO_2 in atmosphere could be reduced by its dedicated separation from a gas stream at several polluting areas. These include CO_2 capture from flue gases, purification of natural gas (gas sweetening), biogas upgrading, separation from gas stream formed during thermal enhanced oil recovery (see Section 4.5.2.1 for details) and CO_2 capture from other processes such as cement, iron and steelmaking industries. All operations differ in the initial gas mixture and require different membranes.

4.2.1.1 CO_2 Capture from Flue Gases

According to the Kyoto Protocol, the EU aims to reduce greenhouse emissions by an average 6–8% below 1990 level (the Kyoto countdown year) by the year 2015, and down to 40% by 2030. The central place in the new strategy is devoted to large CO_2 point sources: power plant flue streams, natural gas wells, fuel gas (syngas) and industrial plants, especially those involved in manufacturing iron, steel, cement and chemicals [19]. Each application involves different gas separations which impose distinct requirements and constraints. Globally, coal-based power is the largest source of electricity generation and also the highest source of CO_2 emission (~0.32–0.35 ton/MWh). Coal-based power plants account for

approximately 40% of global emissions and their relative contribution will remain high at least until 2035 [20]. Currently, the CO_2 is captured after the combustion by amine solvent absorbers (scrubbers using Rectisol® or Selexol™). The technology provides a high degree of CO_2 separation, but at a high cost of \$40–100/ton CO_2 captured. According to one estimate, the use of conventional technologies increases the energy requirements by 25–40% [21] or by \$0.06/kWh (a separate estimate by Electric Power Research Institute [22]). The additional drawbacks, highlighted in a paper by D'Alessandro *et al.* [23], are that any chemical employed to capture CO_2 will soon feel a short in supply and any chemical produced from CO_2 will rapidly saturate its need in a global market. The reduction in CO_2 emissions should be performed only with regenerable materials and preferably in a continuous manner. An additional drawback of current technologies is the location of CO_2 capturing devices. The current options are limited to post-combustion CO_2 capture when the heat is already turned into energy. A modern diversified approach to CO_2 capture can also be used in pre-combustion and oxy-fuel combustion schemes and decrease the energy penalty for capturing 90% of the CO_2 to 3.5%. There are several advanced technologies capable of providing the needed degree of CO_2 capture. These use ceramic membranes, advanced amine solvents, ionic liquids, metal-organic frameworks (MOFs), chemical looping and biofixation approaches [23]. The advantage of ceramic membranes over other technologies is in their maturity and applicability. The energy requirements of ceramic membranes are low, their efficiency in selective extraction of CO_2 from mixed gas streams is high and their configuration in the industrial plant is flexible relative to the conventional amine adsorber/desorber columns.

The CO_2 capturing strategy in power plants depends on the fossil fuel used (carbon or gas), and can be achieved at one of the three stages (see Figure 4.3): [24] using post-combustion technology, using pre-combustion technology or via the oxy-fuel combustion process. The target OpEx for the separation is less than \$10/ton captured CO_2.

The conventional *post-combustion technology* is applicable in any fossil fuel power plant. The CO_2 is stripped from the flue gas that is formed after a combustion reaction with air as the oxygen source, following the general equation

$$C_xH_y + (x + \tfrac{1}{4}y)O_2 + 3.76(x + \tfrac{1}{4}y)N_2 \rightarrow \tfrac{1}{2}yH_2O + xCO_2 + 3.76(x + \tfrac{1}{4}y)N_2 \tag{4.1}$$

A typical flue gas stream contains 15 vol.% CO_2, 5 vol.% O_2, 70 vol.% N_2, 10 vol.% H_2O and minor impurities including up to 0.01 vol.% of highly acidic SO_x (predominantly in coal) and NO_x [25]. Nitrogen is inert, but it is the main component of air and therefore a key factor in any gas separation that involves air. In fact, the retention of CO_2 from flue gas in post-combustion capture is primarily its separation from nitrogen. This is a difficult task, as the differences in properties between N_2 and CO_2 are relatively minor. The molecular weights of N_2 and CO_2 are 28 and 44 g/mol, and their kinetic diameters are 3.64 and 3.3 Å, respectively.

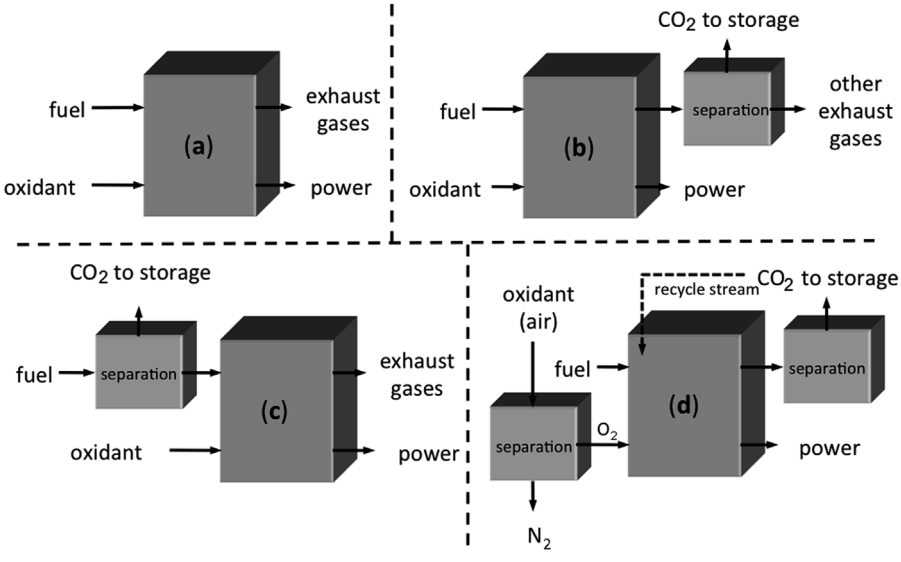


Figure 4.3 Schematic diagram of fossil fuel-based power generation (a), post-combustion CO_2 capture (b), pre-combustion CO_2 capture (c) and oxy-fuel combustion (d).

In this case, the primary separation is done using solution diffusion and molecular sieving [26]. Another challenge is the low CO_2 feed concentration and the ambient feed pressure. Several techniques to increase the feed CO_2 concentration included the use of O_2-enriched air that has 30–60 vol.% CO_2 [27] and the use of combustion air as a sweep for CO_2 permeate [28]. To achieve more than 90% CO_2 capture with selectivity between 100 and 200 in a single stage, liquid and polymer membranes were used. Long-time stability and performance of liquid membranes under real conditions [29,30] and a maximum CO_2/N_2 selectivity of 70–80 [31,32] bring a general conclusion that a desired separation cannot be achieved in one stage. Multistage membrane separation has been proposed as the key to achieve the desired CO_2 recovery [28]. This separation is often performed with polymer or carbon membranes. The latter, however, was found to be expensive with CapEX of \$100/ton CO_2 captured. That price was prohibitively high even to a traditional chemical adsorption on monoethanolamine (MEA) that costs \$59/ton CO_2 captured [33]. The OpEx can be lowered to \$15/ton CO_2 if the selectivity is reduced towards 50 [28].

In principle, the separation can be performed with either inorganic or organic membranes, and indeed many separations now are done with organic membranes. The fuel gas temperature, however, can vary between 50 and 1000 °C, depending on the location within the power plant [34]. Preferably, one should separate CO_2 without cooling it down, because this saves energy and lowers costs (plus it is better for the environment, which is the main impetus for separating the CO_2 in the first place) [35]. According to analysis published by Yang *et al.* [36], membrane technology saves energy and space. It is relatively easy to

Table 4.4 Challenges related to the application of membrane in *post-combustion* CO_2 separation.[a)]

Flue gas characteristics	Challenges related to membrane process	Potential solution	Membrane requirement
Low CO_2 concentration	Purification of large gas volumes	Scaling up of membrane units	High CO_2 selectivity and permeability, low cost
Low TMP	Low flux	Booster pumps	High CO_2 selectivity and permeability
Water vapour	Corrosion of pipeline during CO_2 transportation	Drying the flue gas	High CO_2/H_2O selectivity

a) Based on Ref. [19], with additional modifications.

scale-up and could be the future technology for CO_2 separation. There are, however, some challenges related to the membrane applications (see Table 4.4) that must be addressed before large-scale applications will be economically competitive (see also the discussion on economics and the case studies in Chapter 5).

In an alternative process, the *pre-combustion technology* removes CO_2 before combustion, just after the fossil fuel is converted to hydrogen. This process is usually implemented in natural gas power plants. The fuel (natural gas, which is mostly methane) reacts at high pressure and temperature to form the so-called synthesis gas (or syngas) mixture of $CO + H_2$.

$$H_2O + CH_4 \rightarrow 3H_2 + CO \tag{4.2}$$

Subsequently, the syngas reacts with water giving hydrogen and CO_2,

$$CO + H_2O \rightarrow H_2 + CO_2 \tag{4.3}$$

Choosing for pre-combustion separation of CO_2 offers two options – separating CO_2 from H_2 and separating H_2 from CO_2. These two options sound similar, and the end result is indeed similar, but the membranes are different: the first should be CO_2-selective and the second H_2-selective. The use of CO_2-selective membranes results in a pure H_2 stream in the retentate and a CO_2 stream in the permeate. The retentate stream can be directly used in the combustion turbine. Similarly, the permeate stream can be compressed for transportation and storage. The use of H_2-selective membrane changes permeate and retentate streams. H_2-selective membranes are operated at elevated temperature and have a potential for improving the thermal efficiency of the process by an integration with or using immediately downstream of the low-temperature shift reactor [37]. Water vapour that permeates along with H_2 leaves a dry CO_2 retentate stream. On the opposite side, CO_2-selective membranes are operable at ambient temperatures to allow CO_2 permeation and require much lower CapEx. Sequestering in this process is done at high pressure, lowering the energy cost of the CO_2 removal [38]. But the use of high temperatures and pressures requires ceramic membranes with high mechanical and thermal stability. Table 4.5 details some of the limitations posed in implementation of various membranes.

Table 4.5 Comparison of different H_2–CO_2 membranes.[a)]

Material	Temperature range (°C)	H_2 flux	H_2 selectivity	Transport mechanism
Dense polymer	<110	Low	Low	Solution diffusion
Porous carbon	150–550	Moderate	Low	Molecular sieving, surface diffusion
Microporous ceramics	200–600	High	Moderate	Molecular sieving
Dense ceramics	150–900	Moderate	High	Solution diffusion

a) Based on Ref. [19], with additions and modifications.

A single-stage membrane operation required to capture more than 90% CO_2 with 70–90% H_2 recovery must have H_2/CO_2 selectivity between 20 and 60 [37]. The highest H_2/CO_2 separation selectivity of more than 1000 is achieved with dense palladium membranes that are extremely selective to H_2 and almost impermeable to other gases. These membranes, however, are less stable in the presence of sulfur compounds, CO and unsaturated hydrocarbons. Pd membranes also undergo phase change below 571 K and 2 MPa that leads to boundary defects and H_2 embrittlement [39]. The membrane features are improved if Pd is alloyed with other metals such as Ag, Au, Cu and Ni. The hydrogen permeability, and thermal and chemical stability of alloys are better than those of dense Pd although the phase change remained an issue. Ceramic and zeolite membranes with their 10–100 H_2/CO_2 selectivity are also considered suitable candidates if the problem of the long-term stability under steam flow can be resolved. Polymeric membranes are cheaper, but they are limited to certain temperature regime and suffer from low H_2 flows and H_2/CO_2 selectivity. Nevertheless, the recent experiments with polybenzimidazole (PBI) H_2-selective membranes showed that 90% of CO_2 removal is achieved with \$39/ton CO_2 captured. This OpEx is lower than the OpEx of a Selexol absorption column [40]. The PBI is a thermostable polymer with a reported glass transition temperature of 420 °C.

The third option, *oxy-fuel combustion*, can be implemented in either coal-powered or natural gas power stations. This process uses pure oxygen to burn the fuel, instead of air. The nitrogen is excluded from the combustion process by a preliminary air separation step. In this case, the membranes can be implemented to separate O_2 from air. The absence of ballast N_2 (that is not needed for combusting the fuel yet reacts with oxygen at the combustion temperature) yields an input stream that contains up to 95% oxygen. The combustion exhaust stream contains typically 80–98% CO_2. The rest is water, which is removed from the stream by the condensation. Burning fuel with pure oxygen results in very high flame temperatures, higher than the desirable range. The oxygen content is therefore reduced with a pressurized CO_2-rich recirculating stream (see Figure 4.4). This closed loop is an example of a 'zero emission cycle', a concept advocated by government authorities and environmental protection agencies. Up to 75% of the carbon dioxide is returned back to the combustion process, thus

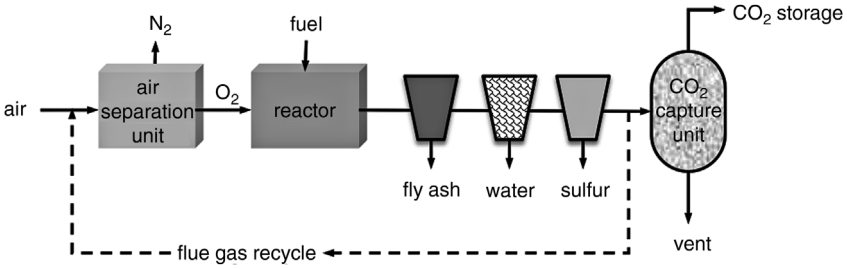


Figure 4.4 Simplified block diagram of the oxy-fuel combustion process.

significantly reducing the volume of released CO_2. Because the CO_2 stream is already concentrated, sequestering the CO_2 from it for the future storage or reaction is also easier.

The oxy-fuel combustion, however, requires significant redesign of turbines and is therefore not considered economical for existing plants. The significant energy demands in air separation unit are to be mitigated by no need for CO_2 capture [23]. Currently, there are no industrial installations that implement the oxy-fuel combustion option. The world's first pilot plant for oxy-fuel combustion was inaugurated in September 2008 by the European energy company Vattenfall, at Schwarze Pumpe in Germany. The largest coal-fired electrical generating station that will use oxy-fuel combustion generators, FutureGen 2.0, is now under construction in Morgan County, Illinois. Its estimated cost is US$1.65 billion (of which $1.0 billion is provided by US government). The project was first announced by President George W. Bush in 2003 and its construction started in 2014 after restructuring, cancelling, relocating and restarting. FutureGen 2.0 is a coal-fired electrical generating station that will capture and sequester most of its generated carbon dioxide. The CO_2 will then be piped into underground saline formations.

Ceramic membranes can potentially be implemented in all three combustion processes. They have a bigger advantage in pre-combustion and oxy-fuel combustion, because these technologies require high temperatures and pressures as a part of technological process. Each of the combustion processes requires the separation of different gases: CO_2/N_2 separation in the classical post-combustion, CO_2/H_2 in pre-combustion and O_2/N_2 in oxy-fuel combustion. The CO_2/N_2 separation is often done with microporous membranes made of carbon, silica or zeolites. Table 4.6 presents typical separation factors reported in the separation of carbon dioxide and nitrogen, as a function of membrane used.

Problems in the separations are due to the similar molecular sizes of CO_2, N_2, H_2 and water, all of which are present in the effluent stream. Typical industrial membranes lack the fine-tuning that can achieve a significantly better separation. The mechanisms of separation in ceramic membranes are typically based on molecular sieving and Knudsen diffusion [23] and might result in relatively low separation factors. For example, a typical H_2/CO_2 separation factor is 15. The

Table 4.6 Values of separation factor α in CO_2–N_2 separation [34].

Membrane	α	Reference
MgO/γ-alumina	1.1	Keizer *et al.* [41]
MgO/γ-alumina	1.0	Uhlhorn *et al.* [42]
Fe_2O_3/γ-alumina	1.68	Ma *et al.* [43]
Al_2O_3/γ-alumina	1.5	
CaO/γ-alumina	0.98	Cho *et al.* [44]
Silica/γ-alumina	1.4	
Silane/γ-alumina	1.7	Hyun *et al.* [45]
Pd/γ-alumina	0.79	Othman and Kim [46]

separation can be enhanced towards 40–50, yet the high selectivity is usually accompanied by a low permeability. Some of the new approaches for increasing the separation factor include the preparation of ultra-thin defect-free zeolite and silica membranes by ultrasound coating and chemical drafting. However, the silica used in coating has a limited stability against steam. As a result, the pore size can be altered and separation factor can suddenly drop. Another approach is to use dense ceramic membranes based on perovskite oxides (described in the next sections). The dense membranes, however, require operational temperatures of 600 °C and above.

An additional level of selectivity in ceramic membranes, especially in low-temperature/low-flux separations, can be provided by a hybrid membrane/chemical adsorption process. This strategy is based on covalent functionalization of pore walls. The modified membrane consists of α-alumina or zeolite support, coated with silica, alumina or zirconia and covered with a functional layer such as MgO that has a high chemical affinity to CO_2 [23]. A CO_2/N_2 selectivity as high as 120 at 350 °C has been reported [47]. The advantage of hybrid membranes is that they prevent oxygen contact with the adsorbent and therefore minimized degradation. Membranes consisting of metal-organic frameworks are another potential future development of CO_2 retention by ceramic membranes. $[Zn_4O(bdc)_3]$ and $[Zn(bim)_2]$ (ZIF-7, bim = benzimidazolate) coated on alumina supports exhibited an exceptional H_2/CO_2 separation ability [48,49].

4.2.2 Hydrogen Purification

Hydrogen is an important energy carrier, and its use and importance will increase in the coming years. Our society is using ever more energy. In the United States alone, energy consumption is expected to increase by 13% over the next two decades. Global consumption is expected to increase by 49% over the period from 2007 to 2035 [50], especially in developing countries that will become industrialized. Our energy sources and energy carriers are changing

continuously. Burning wood was the main energy source just 150 years ago. Today, mankind uses energy contributions from petroleum, coal, gas, hydro and nuclear sources. For the last 20 years, we are also using renewable energy sources, although much less in practice than what one would expect from the hype surrounding the subject. The slice of renewable energy depends strongly on the price of crude oil and natural gas. When the crude oil price is high, renewable energy schemes abound. When the price of crude oil drops (as is happening, for various reasons, at the time of the writing of this book), the trend of using fossil fuels as the main energy source returns. Updated forecasts show that 87% of the energy in the next five decades will continue to come from fossil fuels [51]. If we really want to reduce CO_2 emissions, we need globally a more comprehensive approach. The question is: Can hydrogen provide the answer, and what is needed for it to do so?

Hydrogen is the most abundant element in the universe, but there is no source of pure hydrogen on Earth. On the Earth's surface, most of the hydrogen is bonded to oxygen as water. In principle, pure hydrogen can be obtained from water by electrolysis. In practice, the energy cost of this process (50–80 kWh of electricity per kilogram of hydrogen produced) is still prohibitively high. Considering the current electricity prices of \$0.08/kWh, pure hydrogen would costs at least \$4 per kg. The current attempts to reduce the cost by using renewable energy (solar, wind, waves), or by biomass conversion, are still far from practical application. To become feasible, the hydrogen price should drop towards \$1.5 per kg [52]. Indeed, about 95% of hydrogen today is produced from fossil fuels [53]. The problem here is that at the end of the day, *hydrogen is just an energy carrier*, and many of the environmental effects of the fossil fuels are unchanged.

The commercial generation of hydrogen is performed by steam reforming of methane and petroleum feedstock such as naphtha at high temperature (700–1100 °C). It is a relatively simple, efficient, catalytic process that includes three steps. First, a hydrocarbon dissociates on the catalyst surface (typically a chromium/iron oxide) and reacts with steam to give CO and H_2 [52],

$$C_nH_m + nH_2O \rightarrow nCO + (n + m/2)H_2 \tag{4.4}$$

The addition of steam at low temperature (130 °C) continues the reaction and turns the formed carbon monoxide into either methane or carbon dioxide, depending on the hydrocarbon to steam ratio.

$$CO + 3H_2O \leftrightarrow CH_4 + H_2O \tag{4.5}$$

$$CO + H_2O \leftrightarrow CO_2 + H_2 \tag{4.6}$$

The overall reaction is strongly endothermic and heat must be supplied to the reformer, usually by burning part of the fuel (methane or naphtha). In the best-case scenario where 75–80% of methane is converted into CO and H_2, the dry basic composition of the syngas product is 75% H_2, 7% CH_4, 12% CO and 6% CO_2 [52].

The resulting hydrogen is not pure. It is a mixture of H_2, CH_4, CO and CO_2. Pure hydrogen can be obtained from this mixture by three separation methods. Those are adsorption of gas species other than hydrogen to produce pure hydrogen (PSA), cryogenic separation that provides multiple pure products including hydrogen and membrane separation. The PSA and cryogenic systems usually deliver highly pure hydrogen at relatively low operating costs (OpEx) compared with the membrane process. PSA shows better results in hydrogen production plants that utilize natural gas as the feedstock, which is often the best option based on cost and availability. The syngas produced from feedstocks with a high carbon to hydrogen ratio, such as heavy oils and coal, may be attractive for membrane separation. Although in large-scale separation plants the cost of hydrogen is dominated by the cost of feedstock, the investment required for hydrogen separation and purification is between 50 and 80% of the capital investment (CapEx) [52].

The first example of pure hydrogen recovery from a H_2/CO_2 mixture using a membrane system was reported by Mitchell over 180 years ago. The solution-diffusion theory of Graham published in 1866 was based on diffusional experiments with hydrogen [54]. DuPont developed the first commercial H_2 separation module Permasep in 1969. The first industrial application of membrane gas separation system was hydrogen separation from ammonia purge gas stream in mid-1970s [55]. This process used a so-called Prism separator, with PDMS-coated polysulfone hollow fibres. The design, developed by Permea (now Air Products and Chemicals), showed high H_2/N_2 membrane selectivity and was later extended to hydrogen recovery from H_2/CO and H_2/CH_4 product mixtures at power plants. Polymer membrane-based H_2 recovery with polysulfone and polyethersulfone (PES) hollow fibres or spiral-wound cellulose acetate and polyimide membranes is used today in a number of industrial applications due to its low CapEx and ease of operation. Examples include the MEDAL commercial polymeric membrane module [56] and China's trial hydrogen membrane recovery module at the Sinopec Zhenhai Refining Plant. A higher future spread of polymer membrane is less likely due to 'upper bound trade-off' drawn in 1991 by Robeson [9]. Studying the data from H_2/CO_2 separation experiments, Robeson concluded that there is a trade-off line that limits the possibilities of polymer membranes. Membrane permselectivity and permeation are inversely connected meaning that higher membrane selectivity can be obtained with smaller pores and hence lowered flux, and vice versa. Hydrogen permeates through polymer membranes by the solution-diffusion mechanism. Despite the high diffusion coefficient of H_2, the permeation is impeded by the low solubility of hydrogen in polymers. In addition, polymer membranes are severely degraded by CO gas even at low temperatures, and incur densification, ageing and plasticizing problems. The plasticizing is the swelling of the polymer matrix with gas molecules that can damage the membrane permanently. A parallel process used dense palladium and palladium alloys [57] several microns thick at relatively high temperatures. The hydrogen recovery by Pd is a unique process based on dissociation of hydrogen molecules into two H atoms on Pd surface. Other gases cannot dissociate to atoms at Pd surface, and therefore cannot penetrate into Pd lattice.

Theoretically, the penetration of H_2 through a Pd membrane can result in pure hydrogen in the permeate. Palladium membranes, however, suffer from poisoning by CO and by hydrocarbons starting from 0.5 ppm. On the upper end, oxygen concentrations above 50 ppm can lead to Pd-catalysed oxidation of hydrogen and generation of water. Water spots can lead to premature failure of metallic membranes. In addition, these Pd membranes are very costly, and are effective only at high temperatures (800 °C) [58].

There are two types of ceramic membranes suitable for hydrogen separation – porous membranes and dense ones. Dense ceramic membranes selectively transfer hydrogen ions at temperatures higher than 800 °C. They are made of perovskites, pyrochlores and acidic phosphates (see details below). Porous ceramic membranes separate hydrogen based upon selective adsorption and differences in diffusion coefficients. With the exception of helium (which is rather an academic one), hydrogen has the smallest molecular diameter (0.74 Å) *and* the smallest kinetic diameter (0.29 nm) of the different gases. This means that its diffusion rate is the highest. In the absence of solution selectivity or a reaction, a membrane separates by size exclusion: The small H_2 molecules in the feed mixture penetrate through the pores, while the larger CO, CO_2, O_2 and N_2 molecules are retained. The narrow pore size distribution is one of the advantages of ceramic membranes, especially zeolites. Polymer membranes typically have a much wider pore size distribution. Table 4.7 details five experimental cases of hydrogen separation with ceramic membranes.

Table 4.7 Hydrogen separation by porous ceramic membranes.[a)]

Membrane	Pore width (nm)	Temperature (°C)	Feed gas mixture	Permeance (mol/(m^2 s Pa))	Permselectivity
Al_2O_3 [59]	4	25	H_2/C_3H_8	6×10^{-5}	3.0
		250		4×10^{-5}	3.7
		475		3×10^{-5}	4.0
SiO_2 on Al_2O_3 [60]	100	25	H_2/C_3H_6	7×10^{-7}	14
		100		10×10^{-7}	62
		200		11×10^{-7}	156
SiO_2 on Al_2O_3 [61]	5	25	H_2/CH_4	1.8×10^{-8}	44
		250		5.4×10^{-8}	200
Silicate on ceramic disc [62]	45	20	H_2/N_2	2.3×10^{-7}	3.1
		20	H_2/n-C_4H_{10}	2.3×10^{-7}	146
		20	H_2/n-C_4H_{10}	2.0×10^{-7}	15
		20	H_2/i-C_4H_{10}	2.0×10^{-7}	55
SiO_2 on Al_2O_3 [63]	4	25	H_2/N_2	8.0×10^{-7}	6.7
		250	H_2/N_2	7.0×10^{-7}	11.3
		450	H_2/N_2	6.0×10^{-7}	19.1
		250	H_2/C_3H_8	1.0×10^{-7}	12.6
		450	H_2/C_3H_8	1.6×10^{-7}	20.2

a) Data from Ref. [64].

The table shows a small portion of the available data on H_2 separation by porous ceramic membranes. Nevertheless, it suffices for pointing out a typical tendency: although the flux through the membrane is high, the permselectivity is still too low. Manufacturing membranes with a uniform pore size that will, for example, exclude CO_2 from H_2/CO_2 feed mixture by size exclusion is very difficult, considering the narrow difference between their kinetic diameters (0.29 and 0.33 nm, respectively). The reported average separation factor of 15 in H_2/CO_2 separation is not sufficiently high to be attractive for industrial purposes, even if the separation is performed at room temperature. A sequence of separation stages is required to achieve desired hydrogen purity; however, the cost of the operation is high. The permselectivity increases at higher temperature; however, the porous ceramics can operate at temperatures up to 300 °C due to the instability of zeolites in H_2O atmospheres [65].

The permselectivity of porous ceramic membranes can be increased by exercising a tight control over the pore size. Typical γ-alumina membranes have a nominal pore size of 4 nm that is coarsened during operation due to the presence of steam. This pore size should be reduced towards 1 nm to achieve an effective Knudsen diffusion. Such a reduction can be accomplished by a sol–gel process, by the phase separation/leaching method or via chemical vapour deposition (CVD) in the case of silica and composite silica–zirconia. The modification typically gives a bimodal pore size distribution: Most of the pores are about 0.3 nm in diameter, but there are also several larger ones at 1–2 nm [65]. The membranes with 1–2 nm micropores exhibit H_2/N_2 selectivity of 42–87 and H_2/H_2O selectivity of 8–10 [66]. Unfortunately, silica is unstable in the presence of steam, and with time the selectivity of these membranes decreases because of pore coarsening.

Another approach uses gas separation by molecular sieving. This requires pore diameters of 0.3–0.4 nm, with no deficiencies and a narrow pore size distribution of 0.1 nm. Here, silica is often replaced by zeolites, but the measured permeation flux is very low, and the permselectivity is not very high either [67]. The temperature can be increased towards 300 °C, but this does not improve the permeation rate much. Moreover, high temperatures require more expensive gas-tight sealing, and scale-up can be a problem.

Unlike their porous counterparts, dense ceramics based on inorganic perovskite-type oxides do show a strong potential for future applications. The transport of hydrogen through dense ceramic membranes occurs in its ionic (proton) form, and indeed these membranes are sometimes called *proton conducting membranes*. In this process, hydrogen molecules first dissociate on the membrane surface to protons, H^+, and electrons, e^-. The protons then diffuse through the membrane, driven by a proton concentration gradient. Electrons move through the membrane by separate channels, recombining with the protons on the other side of the membrane (solid oxide fuel cells (SOFCs) operate on a similar principle; see later in this chapter). This recombination gives molecular hydrogen again, which detaches from the membrane surface on the

permeate side. Because the membranes are dense and only hydrogen dissociates on their surface, they are 100% selective to hydrogen. This is one case where ceramic membranes are clearly preferable over polymer ones [65].

Dense ceramic membranes with selective protonic conductivity are usually made of perovskite-type oxides. These are crystalline minerals with the general stoichiometric formula ABO_3, similar to the perovskite $CaTiO_3$ crystal structure. In these structures, A is a divalent ion such as Ca, Mg, Ba or Sr, and B is a tetravalent ion such as Ce or Zr. Simple perovskite-type minerals that possess proton conductance are barium cerate ($BaCeO_3$) and strontium cerate ($SrCeO_3$). Most cerates and zirconates, however, show a low conductivity at low temperatures. A reasonable conductivity in the range between 10^{-2} and 10^{-6} S/cm is seen at 800–900 °C. For improved proton conductivity at low temperatures, a small portion of either A or B is replaced by dopant elements to create oxygen deficiency represented by $A_{1-x}A'_xB_{1-y}B'_yO_{3-\delta}$, where A′ and B′ are dopant elements, x and y are fractions of dopants in A and B, respectively, and δ is the number of oxygen vacancies in the material formula [68]. Most often the doping is performed with trivalent ions such as yttrium (Y^{3+}) and ytterbium (Yb^{3+}) to obtain structures such as $SrCe_{0.95}Yb_{0.05}O_{3-\delta}$ (SCYb) and $BaCe_{0.8}Y_{0.2}O_{3-\delta}$ (BCY) [10]. The doping significantly increases the proton conductivity. For example, $BaCe_{0.95}Y_{0.05}O_{3-\delta}$ shows a proton conductivity of 1.27×10^{-2} S/cm at 800 °C in a H_2/H_2O atmosphere [69]. Perovskite oxides are also often used as dense membranes for solid oxide fuel cells (more details and examples are given later in this chapter).

Notwithstanding the advantages that doping brings to proton conductivity, the electronic conductivity remains low. However, it can be increased by incorporating separate electron conductors into the material. One way for doing this is by combining ceramic and metal phases into a biphasic composite. These 'cermet' materials feature both the high electronic conductivity of metals and the high proton activity of dense ceramics. One of the examples of cermet materials available on the market is CeramiCell®, a family of ceramic fuel cell components made of porous NiO–YSZ (nickel oxide yttria-stabilized zirconia) cermet made by CoorsTek (Golden, CO). However, these ceramic–metal frameworks are only partially stable in the presence of syngas components such as CO_2 and H_2O at high temperatures and easily react to form carbonates and oxides [70]. Most metals are embrittled by H_2, while the relatively inert ones such as platinum and gold are less compatible with ceramics due to a difference in thermal expansion coefficients. Thus, while using cermets for hydrogen separation remains an interesting option, alternative systems that can combine high proton conductivity, high electronic conductivity, and high thermochemical and thermomechanical stability are needed [65].

In summary, there are three options for hydrogen purification with ceramic membranes. Their pros and cons are summarized in Table 4.8. Currently, none of these options is used in industry, but this may change as the demand for purified hydrogen at a reasonable price increases. One possible solution is using ceramic/ceramic composites as an alternative to cermets, a concept introduced

Table 4.8 Options for hydrogen purification with ceramic membranes.[a)]

Membrane	Advantages	Drawbacks
Porous (zeolite)	High H_2 flux	Poor selectivity Low H_2 purity
Dense (doped perovskites)	High H_2 purity	Low H_2 flux Requires high temperature (800–900 °C) Insufficient electron conductivity
Dense composites (perovskite/Au or perovskite/Pt)	High H_2 flux High H_2 flux	Limited thermochemical and thermomechanical stability at high temperatures

a) Data from Ref. [65].

by Ceramatec, Inc. (Salt Lake City, UT). The advantages of this approach include thermomechanical and thermochemical stability (with ambient gases and the proton conducting perovskite) at testing conditions involving temperatures as high as 900 °C and pressures up to 5–10 atm [65].

The purified hydrogen can be used directly as transportation fuel in internal combustion engines, or in fuel cells to generate electricity. The technical feasibility of making a hydrogen-operated internal combustion engine was demonstrated already over 200 years ago by Francois Isaac de Rivaz [71]. Even that interim solution has some advantages over the gasoline-run internal combustion engine. The hydrogen engine efficiency is 38%, which is 8% higher than that of a gasoline-burning engine. Furthermore, using hydrogen as a combustion fuel solves the problems of air pollution, and no CO_2 is emitted from the engine (although CO_2 is probably emitted during the production of the pure hydrogen, this may be easier to contain and control). Today's direct fuel combustion for transportation and heating needs accounts for about two-thirds of the world's CO_2 emissions and air pollution [53]. If sustainable hydrogen were widely available, using it as a combustion fuel would therefore be an interesting alternative.

The future of hydrogen-burning engines, however, is unclear. Currently, the price of pure hydrogen moves between $2.5 and $4.0 per kg. To be economically viable, it should drop below $1.5 per kg. The purified hydrogen needs to be stored as liquid (at −253 °C) or as compressed gas (at 200 bar) to combine high energy density by weight and by volume. The energy density of hydrogen at ambient temperature and pressure is 0.003 kWh/l. At 200 bar, it becomes 0.5 kWh/l. Thick steel cylinders and compressors are needed, and stacks of the cylinders must be carried under or on top of vehicles. In addition, an adequate refuelling infrastructure is needed. Thus, in many practical respects, the hydrogen economy is much farther away than we would like. According to Elon Musk, the entrepreneurial CEO of Tesla Motors, companies are interested in manufacturing internal combustion hydrogen engine vehicles only because they are under pressure to show sustainability. 'Hydrogen is always labelled as "the fuel of the future", and always will be' [72].

4.2.3
Fuel Cell Applications: The Real Hydrogen Economy

Originally, the term 'hydrogen economy', coined by John Bockris in 1970, described a scenario of the direct burning of hydrogen in internal combustion engines. In our opinion, and based on the analysis given in the previous section, the real hydrogen economy will be the use of hydrogen in fuel cell devices to produce electricity. Here, hydrogen is a clean and convenient energy carrier that releases its energy as electricity in a highly efficient catalytic reaction with oxygen, producing water as the only by-product. Fuel cells are an attractive alternative to conventional combustion engines, because their theoretical (and practical) efficiency is much higher. A combustion engine's efficiency is limited by the thermodynamic constraints of the Carnot cycle [73]. Typical combustion engines are made of steel, and have a theoretical thermodynamic limit of 37%. In practice, the average efficiency of such engines is much lower, reaching about 18–20% [74,75]. Conversely, fuel cells convert the chemical energy that is stored in the chemical bonds of the fuel molecules directly into electrical energy, using an electrochemical catalytic process. Fuel cells typically operate under isothermal conditions, and can reach a theoretical efficiency of 82%. In practice, they reach about 40–60% efficiency [76]. The basic operation of the hydrogen fuel cell is simple and was demonstrated already in 1839 by William Grove [77]. It is the opposite of water electrolysis. In water electrolysis, an electric current is passed through the water, resulting in dissociation of water into hydrogen and oxygen. In a fuel cell, the recombination of hydrogen and oxygen produces an electric current. Figure 4.5 shows basic sketches of the electrolysis and recombination reactions.

Another way to view the fuel cell action is simply as an electrocatalytic combustion: hydrogen is burned in an electrochemical reaction, giving water, with a

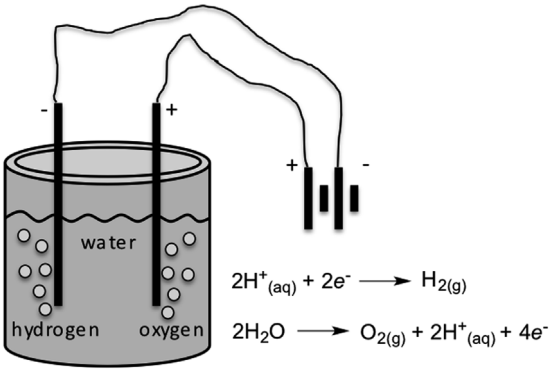


Figure 4.5 Electrolysis of water showing the anode and cathode reactions in an acidic environment.

theoretical electrochemical potential of 1.23 V. However, instead of generating heat, the fuel cell produces electrical energy.

$$H_2 + \tfrac{1}{2}O_2 \rightarrow H_2O \tag{4.7}$$

The practical significance of first electrolysis experiments was low, as the currents produced were very small. We can now say that it was because of the low contact areas between the gas, the electrode and the electrolyte, and because of the relatively large distance between the electrodes [78]. The first practical fuel cell was demonstrated in 1889 by Mond and Langer, who used industrial coal gas as the fuel and air as the oxidant [79]. They realized that increasing the surface area of the electrodes enhances the current. The use of expensive and unreliable fuel sources and Pt black electrodes, and the widespread use of internal combustion engines ended the commercialization of the project. The research continued in the laboratory, mainly due to economic issues, and many important advances were made. For example, the use of flat porous electrodes positioned at close distances allowed a penetration of electrolyte from one side and the gas from the other side, thus maximizing the contact between the electrode, the electrolyte and the gas. This promoted the catalytic dissociation of hydrogen molecules at the anode to protons and electrons:

$$H_2 \rightarrow 2H^+ + 2e^- \tag{4.8}$$

The protons then travel to the cathode and recombine there with oxygen and electrons to give water molecules.

$$2H^+ + \tfrac{1}{2}O_2 + 2e^- \rightarrow H_2O \tag{4.9}$$

To avoid 'short-circuiting' (an early reaction of protons with electrons or protons with oxygen), electrons are either extracted from the fuel cell and transported through an external circuit or transferred through separate channels. The cathode and the anode are isolated from each other by a membrane that is permeable to only one species. This membrane is literally sandwiched between the two electrodes. The electrochemical reaction at the interfaces between the membrane and the cathode/anode is facilitated by thin layer of catalyst. Platinum nanoparticles supported on high surface area carbon are usually used for this purpose. The combination of cathode, the anode, and the membrane is called a *membrane electrode assembly* (MEA). Fuel cells are divided into types based on their construction aspects and electrolyte/membrane types. In the case of proton diffusion, the membrane is called a *proton exchange membrane* (PEM), and the fuel cell is a proton exchange membrane fuel cell (PEMFC) [80]. Similarly, *molten carbonate fuel cells* (MCFCs) [81] use molten carbonate salts to transfer carbonate (CO_3^{2-}) anions, and SOFCs employ solid ceramic electrolytes to transfer oxide anions (O^{2-}) [82]. In this section, we will outline the function and application of PEMFCs and MCFCs, explaining the role of membranes. The SOFCs, which typically operate at a much higher temperature, are discussed in the following section. There are other types of fuel cells (e.g. the *phosphoric acid*

fuel cell [83] that also uses protons as charge carriers but with liquid H_3PO_4 instead of the polymer membrane as the electrolyte, and the *alkaline fuel cell* [84] that uses liquid KOH to transfer hydroxide (OH^-) anions), but these are less relevant to ceramic membranes, and thus beyond the scope of this book.

The PEMFCs were the first fuel cells commercialized by General Electric in 1950s, and used by NASA in the *Gemini* and *Apollo* space projects [85]. PEMFCs are often subdivided by the type of fuel they use into hydrogen PEMFCs and direct methanol fuel cells (DMFCs) [52]. The first PEMFCs used polymer membranes. Many PEMFCs used Nafion, a sulfonated tetrafluoroethylene PFSA-class fluoropolymer copolymer discovered in 1960s by Walther Grot of DuPont [86]. The considerable attention to Nafion, besides its unique ionic properties, is due to its excellent thermal and mechanical stability. Low-temperature PEMFCs typically have compact size and light weight. They do not emit pollutants such as NO_x and are suitable for automotive applications. The major drawback of polymeric PEMFCs is the temperature limitation inherently posed by using organic polymers. Typical electrocatalytic activity at 80 °C is low and therefore polymeric PEMFCs require relatively large amounts of noble metals such as Pt electrodes for H_2 dissociation. The Pt electrodes tend to be poisoned by CO, and getting CO-free hydrogen is costly and difficult. This problem must be solved, because *there is simply not enough platinum* to go around – we are already using 70% of the world platinum production for emission reduction in the automotive exhaust catalysts. If cars were to be powered by today's PEMFCs, we would need 10 times that. Research is moving forward in the area of metal-free PEMFC electrodes (the most promising materials are nitrogen-doped graphitic carbons) [87] but these are out of the scope of this book.

Another problem with polymer membrane-based PEMFCs is that their proton conductivity is poor due to inability of the polymer membranes to retain enough water at the operating temperatures. These unresolved technical issues plus the high costs inhibit the commercialization of polymer PEMFCs. But there are other possible membrane materials: metals and ceramics. Figure 4.6 links potential membrane materials with their operating temperature ranges.

PEMFCs can be built for operation at low temperatures using polymer membranes, at mid-range temperatures using metal membranes or at high temperatures using ceramic membranes. The operation of fuel cells at high temperatures does not require noble metal catalysts. Ni-based alloys at the anode and oxides

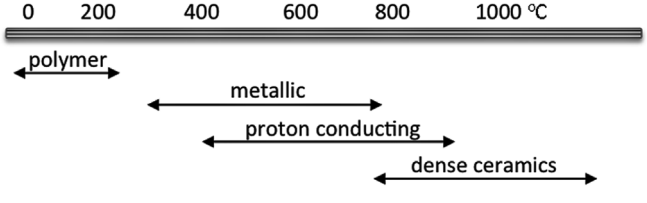


Figure 4.6 Thermal stability of various materials that can be used in fuel cells. Prepared based on reported membrane stability data.

at the cathode were used in mid-1960s, and since mid-1970s molten carbonate was used [85]. Due to high operating temperature, the water emerges as steam, so no water management is required at the cathode side. Instead, one needs to recover the heat generated by the steam [88]. Ceramic *proton conducting fuel cells* (PCFCs) are therefore much larger and more suitable for large-scale applications (e.g. in power plants). Their hydrogen feed does not have to be ultrapure, and the intrinsic rigidity of the ceramics gives a mechanical advantage: It allows a three-dimensional fuel cell structure, unlike polymer PEMFCs which are made mostly in two-dimensional planar form [89].

Another difference between PEMFCs and PCFCs is in the proton conducting mechanism. In PEMFCs, the protons are transported attached to water molecules, as hydronium ions (H_3O^+). The hydration is therefore important. Conversely, PCFCs operate in a dry environment. The protons are transported through the ceramic membrane without water [90]. This transport occurs via the so-called *Grotthuss mechanism* [91], through hydroxide defects produced by water incorporation into oxide ion vacancies generated in the crystal lattice upon extrinsic doping of tetravalent sites by trivalent ions, as shown in Eq. (4.10) using the Kröger–Vink notation,

$$H_2O + V_O^{\bullet\bullet} + O_O^0 \rightarrow 2OH_O^{\bullet} \tag{4.10}$$

The proton in a hydroxide defect, $OH_O^{\bullet}$, resides asymmetrically in an interstitial position near the oxide ion, resulting in high ionic conductivity with relatively low activation energy [92,93]. PCFC membranes typically have high proton conductivity, gas impermeability, high chemical and electrochemical stability, and adequate thermal and mechanical stability. Moreover, they should show resistance to harsh chemical and physical operating conditions, including strong acids, frequent dry–wet cycles, strong electrochemical oxidation at high potentials and water flooding at high current density [94].

The PCFCs and SOFCs made a special class of ceramic fuel cells. These were all-solid-state energy conversion devices that employ solid ceramic electrolytes. The main difference between the two types is at what side in the fuel cell the water is produced. In SOFCs (which are discussed in detail in the next section), the water is produced at the anode side. In PCFCs, a stream of protons and electrons is delivered to the cathode side to recombine with oxygen and produce water. Unlike SOFCs, which need very high temperatures, PCFCs can operate at intermediate temperatures, between 400 and 600 °C, due to a lower activation energy for the migration of dissolved protons. But PCFCs are sensitive to impurities in the gas feed, and require ultra-high-purity hydrogen (99.999% pure) with an estimated price of $5–6/kg. One of the reasons for such high purity is that CO, a common impurity in hydrogen gas, can poison the cells' electrodes, which are made of Pt and Pd. In PCFCs, the water is produced on the cathode side. Thanks to this, it does not dilute the fuel stream, nor constitute a danger of oxidizing the anode. The fuel utilization can therefore be in principle 100% and the theoretical overall efficiency at least 10% higher than that of SOFCs.

Traditional PCFC membranes are made of strontium or barium perovskite oxides that are proton conducting, such as $BaCeO_3$ or $SrCeO_3$. These minerals, however, suffer from significant chemical instability in the CO_2-rich environment due to the basicity of the alkaline earth cation. They react and form the carbonates $SrCO_3$ and $BaCO_3$, respectively, even in the presence of low CO_2 concentrations [90]. Barium zirconate, $BaZrO_3$, is more stable and has a higher bulk conductivity, but it also has the disadvantages of high sintering temperatures and grain boundary resistance [95]. The progress in PCFCs is therefore balanced between the lower grain boundary resistance and easier sintering of $BaCeO_3$, and higher grain interior conductivity and chemical stability of $BaZrO_3$. Recently, the perovskites were doped with Y^{3+}, Gd^{3+} or Nb^{3+} to increase their proton conductivity. PCFCs on doped perovskites yielded good performance with H_2 or NH_3 as fuels [96]. Recently, the sintering temperature in $BaZrO_3$ and related perovskites was reduced with the addition of ZnO and NiO [97,98]. Alternative non-perovskite PCFC materials are often silica-based, such as MCM-41, MCM-48, ZSM-5 and SBA-15. These are studied because of their proton conducting properties at ambient temperatures. The proton conductivity of such materials is around 10^{-6} S/cm, increasing with the dissociation of Si—OH groups or by a proton exchange with traces of water in the pores [94]. The Si—OH groups appear from the inner membrane surface.

Another type of ceramic-based fuel cell is the *molten carbonate fuel cell*. Instead of solid ceramic electrolytes, MCFCs use an electrolyte and alkali carbonate salt mixture. This mixture melts at the operational temperatures of 600–700 °C, forming a highly conductive medium that can transport carbonate (CO_3^{2-}) anions. The membrane is made of ceramic matrix of $LiAlO_2$. Due to the high operational temperature, Pt electrodes can be avoided. Instead, the anode is covered with Ni and the cathode with NiO. MCFCs are developed to work with a range of conventional as well as renewable fuels, including natural gas, coal and biogas. Like PCFCs, MCFCs have a large footprint. This, together with the need for continuous operation at high temperatures, makes them more suitable for large-scale stationary applications.

We believe that fuel cells will be an important new market segment for ceramic membranes that will increase substantially once the technology is adopted by consumers. Several companies worldwide offer both SOFCs and PCFCs for automotive applications and as domestic energy sources. Some car manufacturers develop their own fuel cell technology (General Motors, Toyota, Honda, Mazda). Others (DaimlerChrysler, Ford, Nissan, Hyundai, Fiat, Volkswagen) buy fuel cell stacks and systems from fuel cell developers such as Ballard Power Systems (Burnaby, Canada). Alset GmbH has developed hybrid fuel cells that can run on hydrogen or petrol. The first commercial hydrogen fuel cell car, the Toyota Mirai ('future' in Japanese), arrived in car dealerships in December 2014. The Mirai is a midsize four-door sedan powdered by a 113 kW (152 hp) fuel cell. It can drive for 650 km without refuelling. Refuelling takes between 3 and 5 min, similarly to a normal gasoline-powered engine. The current concept is to combine an electric motor with a fuel cell. At slow speeds in urban

conditions, the car runs as any electric car by using the energy stored in its battery. At higher speeds, the hydrogen fuel cell alone powers the car and charges the battery. Hydrogen is stored in two high-pressure tanks at 70 MPa.

In March 2015, China announced the production of the world's first hydrogen fuel cell-powered fixed rail electric tram [99]. The vehicle was developed by CSR Qingdao Sifang Company (CSR Sifang), a subsidiary of China South Rail Corporation. The tram is powered by Ballard Power Systems FCvelocity® fuel cell power modules. It is scheduled to run on 15 km assembly lines with a tank that can last for around 100 km.

The mass production of fuel cells has already reached the stage where companies diversify themselves to specific markets. Many had applied their efforts to the energy market, offering their PEMFCs as a clean, reliable and affordable alternative for power generators. Intelligent Energy (Loughborough, UK) markets PEM fuel cell stacks with air cooling. These cells use fans for both cooling and oxidant (air) supply. The stacks are available in 1 and 2.5 kW single-stack modules. They are suitable for stationary power, automotive and aerospace applications. Intelligent Energy had revenue of $75 million in 2012 and generated $13.4 million in profit. The company holds a recent contract to supply 100 MW across 10 000 Indian telecom towers aiming to convert the telecom towers from their current battery or diesel power to PEM fuel cells.

Bloom Energy (Sunnyvale, CA) offers solid oxide fuel cells built on low-cost materials and various renewable or fossil fuels. The company offers a number of power generators with base load output (net AC) of 50, 200 and 250 kW. Similarly, Doosan Fuel Cell (formerly ClearEdge Power, Inc. and Doosan Fuel Cell America located at South Windsor, CT) offers the Doosan PureCell® Model 400 that operates on natural gas and generates 440 kW of clean electricity and 1.7 million BTU/h of usable heat. The operating temperature is 160 °C. At this temperature, CO does not contaminate the fuel cell. Each unit costs $50 000 and has a lifespan of 10 years.

All these market advances are happening because the technology has now reached the stage where relatively cheap ceramics can be used instead of precious metals. PEMFCs, however, still require ultra-high-purity hydrogen for their operation. The cost of this pure hydrogen is prohibitive, and current markets rely heavily on government subsidies in one form or another.

4.2.3.1 Dense Ceramic Membranes for Fuel Cell Applications

One application where ceramic membranes are essential is solid oxide fuel cells. Here the choice must fall to ceramics simply because the operating temperatures (typically 700–1000 °C) are too high for organic polymers. SOFCs are attractive also because they are quiet, have no moving parts and can be designed for a variety of power generation applications [100]. They also emit far less pollutants (such as SO_x, NO_x and particulates) and give a high-grade thermal energy output compared with conventional power generation technologies.

Looking at Figure 4.7, we see that a typical solid oxide fuel cell contains four components: an anode, an electrolyte, a cathode and an external circuit [101].

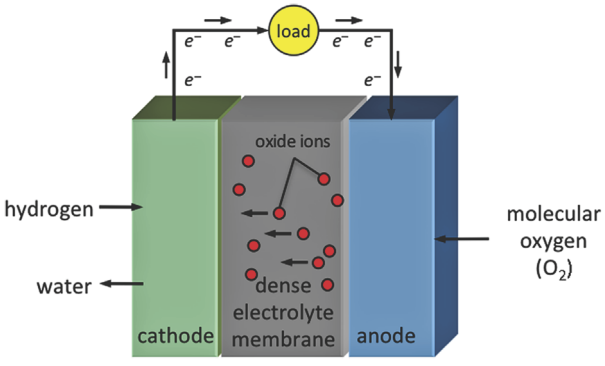


Figure 4.7 A simplified block diagram of a solid oxide fuel cell. The most common electrolyte used today is based on yttria-doped zirconia, Y_2O_3/ZrO_2, where the yttria concentration is typically 3–10 mol%.

The fuel (which can be hydrogen, methane, CO or any other chemical that can be oxidized) reacts with oxide ions at the anode, and the resulting electrons travel across the external circuit to the cathode, where they reduce oxygen to oxide (O^{2-}) ions. These ions close the cycle by diffusing through the solid electrolyte, which is essentially a dense (i.e. non-porous) ceramic membrane. Ideally, the dense membrane electrolyte is an ionic conductor and an electronic insulator (because if electrons can pass through the membrane, the cell will short and there will be no current travelling on the circuit). The fuel cell is therefore combining two chemical reactions: a reduction at the cathode and an oxidation at the anode. In most cases, the oxidant used in the cathode reaction is molecular oxygen, so the corresponding reaction is

$$\tfrac{1}{2}O_2 + 2e^- \rightarrow O^{2-} \tag{4.11}$$

at the anode, the oxide anions react with the fuel. If this is hydrogen, the stoichiometric reaction is

$$H_2 + O^{2-} \rightarrow H_2O + 2e^- \tag{4.12}$$

but high-temperature fuel cells are not limited to using hydrogen. At such temperatures, practically any fuel source will be oxidized. If methane, for example, is used as a fuel, it can either oxidize directly to CO_2 and water, giving 8 equiv of electrons (Eq. (4.13)), or, more likely, undergo steam reforming to syngas followed by CO oxidation (Eqs. (4.14) and (4.15)). Note that here the CO is oxidized electrochemically, meaning that it provides electrons and is released as CO_2, rather than remaining as a poison on the electrode (which is the bane of low-temperature PEMFCs).

$$CH_4 + 4O^{2-} \rightarrow CO_2 + 2H_2O + 8e^- \tag{4.13}$$

$$CH_4 + H_2O \rightarrow CO + 3H_2 \tag{4.14}$$

$$CO + O^{2-} \rightarrow CO_2 + 2e^- \tag{4.15}$$

Unlike the other applications where gas molecules travel through the membrane, here no molecules may go through. Several types of effective dense electrolyte membranes have been developed in the past decade, reaching a commercial technology level [100]. Designing such a membrane is much harder than it looks at first glance. This is because unlike in other applications, here the membrane must satisfy several tough constraints simultaneously: It must have high ionic conductivity (typically >0.1 S/cm), it must be completely non-porous, it must be chemically inert to the cell sealing materials and it must have a matching thermal expansion coefficient and good mechanical properties. The last two constraints, combined with the demand for low-cost materials, rule out many exotic solutions. SOFCs operate at very high temperatures and must run continuously for thousands of hours (typically 40 000–50 000 h, which is about 5 years). The oxide that meets best these conditions is zirconia (ZrO_2) which is often doped with yttria (Y_2O_3). Badwal and Ciacchi report that the 8 mol% doped mixed oxide, denoted as 8YSZ, shows the highest ionic conductivity with mechanical strength of about 150 MPa above 500 °C [102]. Reducing the dopant to 3 mol% strengthens the membrane (400 MPa at temperatures above 500 °C) but this comes at the expense of lower ionic conductivity and unstable and complex phases [103]. Incidentally, the fact that YSZ solid solutions are good conductors at high temperatures is not breaking news – it was already published by Nernst in 1899 [104].

Because of cost considerations and the problems associated with operation at high temperatures, much research is done to try and lower the operating temperature of SOFCs to more manageable ranges (a working regime of 600–800 °C is much easier to cope with than 1000 °C, and correspondingly less expensive materials can be used) [105]. The problem is that the ionic conductivity is highly correlated to temperature. For example, the ionic conductivity of 8YSZ reduces from 0.178 down to 0.052 S/cm when you lower the operating temperature from 1000 to 800 °C [103]. One way of solving this problem is using very thin electrolyte layers (prepared via coating or atomic layer deposition [106]). Another solution is switching over to a different composition or a different material. Alternative electrolytes with high ionic conductivity include doped cerias, doped Bi_2O_3, perovskites such as lanthanum strontium magnesium gallate (LSGM) and scandia-doped zirconia (Sc_2O_3/ZrO_2). The latter is interesting, as its stability, and thermal and mechanical properties are similar to those of Y_2O_3/ZrO_2, while its ionic conductivity at 800 °C is 0.109 S/cm, which is double that of 8YSZ at 800 °C [107,108]. Practically, however, Sc_2O_3 is too expensive for use in large-scale SOFC applications. Unlike rare earths and niobia, where the overall amount available is in fact ample yet is controlled by a few countries, scandium is distributed worldwide, but sparsely. It occurs in trace amounts in many minerals, and is found in (slightly) higher concentrations in some ores in Scandinavia and Madagascar. We will outline here some of the recent findings and materials. Readers interested in a more detailed review of intermediate-temperature fuel cells should consult the excellent overview recently published by Lo Faro and Aricò [109].

Ceramic Fuel Cells Limited (Victoria, Australia) has developed the Gennex™ fuel cell module that converts natural gas to electricity at optimum 60% electrical efficiency (1500 W electricity output). Several pilot installations include a historical building at Port Adelaide and the Smart Home, a fully functional house that is detached from the grid [110].

Economically, the most interesting application of SOFCs (including intermediate-temperature SOFCs) would be in the field of distributed generation of electrical energy, especially for small and medium stationary power requirements (50–100 kW scale). The main materials challenge lies in developing dense ceramic membranes that combine high-temperature stability (including resistance to fractures at large temperature changes) and high ion conductivity, or alternatively high ion conductivity at low and intermediate temperatures.

Working at lower temperatures will affect the electrochemical processes occurring at the electrode/electrolyte interface as well as the ion transport through the electrolyte itself. The key for solving this would be developing ceramic electrolytes that can give fast ionic transport at lower temperatures. Eric Wachsman's group at the University of Maryland has introduced several new electrolyte materials for intermediate-temperature fuel cells [111]. These include terbium and tungsten co-doped bismuth oxide electrolytes [112] that showed clear synergistic effects when using both dopants. Elsewhere, they reported the performance of Ni–Gd-doped ceria (GDC) anode-supported low-temperature SOFCs operating on a JP5 reformate gas at 550–650 °C, demonstrating the feasibility of such SOFCs for transportation applications. The tests were run for 500 h (about 3 weeks). This is impressively long for laboratory testing, but not conclusive enough for industrial purposes (for industrial applications, the cells would need to operate for years on end) [113,114].

The nickel- and gadolinium-doped cerias are part of a class of so-called mixed-ion conductors that deserve special attention because they opened the door to low-temperature SOFC possibilities. Cerium oxide, or ceria, has long been known as an effective oxygen exchange material and solid oxygen carrier for selective oxidation reactions [115]. Its fluorite lattice can be easily doped with different cations, and as long as the doping does not exceed 15–20% [116], the material will remain monophasic [117]. But the trade-off between ion conductivity and material stability at high temperatures remains a problem.

However, about 20 years ago, Zhu *et al.* reported that combining the traditional cation-doped ceria (e.g. yttria-doped ceria or samaria-doped ceria) with halides, hydroxides or nitrates increased the conductivity of the ceramic material at intermediate temperatures. Similar results were found when ceria was mixed with other rare earth oxides or even alumina. Unlike the monophasic doped ceria, these materials contain at least two phases and are commonly referred to as proton conducting salts and salt–oxide composites [118]. In this case, the enhancement in conductivity was explained as an ionic transport system which has at least one molten (liquid-like) state for the mobile ion species within a rigid lattice framework [119]. At the SOFC operating temperature, the salt would melt, giving a

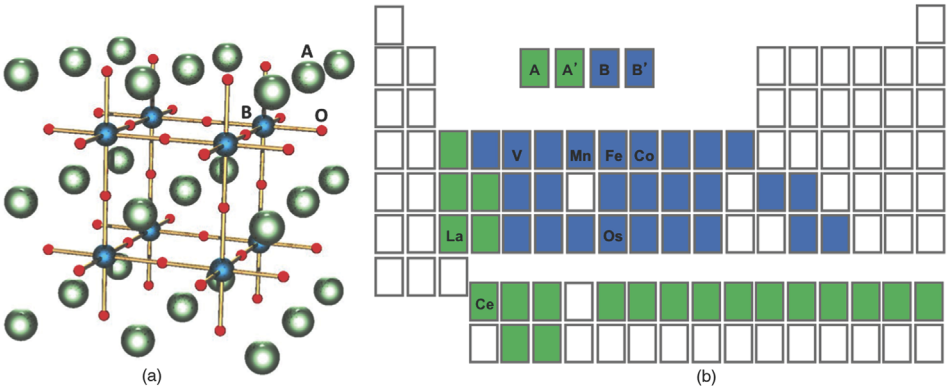


Figure 4.8 The perovskite crystal lattice (a) has the general formula ABO_3. Oxygen anions are shown in red, the larger ('A') cations are shown in green and the smaller ('B') cations in blue. Both A and B can be replaced with up to about 20% dopant A′ or B′, respectively, without forming a separate phase. This gives a variety of different possible perovskites $AA'BB'O_3$ (see the example shown by the periodic table (b), where the possible A′ and B′ dopants are shown when starting from [La, Ce] and [V, Mn, Os, Fe, Co]).

very high ion mobility. Conversely, the oxide would remain solid, providing the rigid lattice framework.

Perovskites are another class of attractive candidates as solid electrolytes for fuel cells, because they fill at least three of the key criteria: They are stable over a large range of temperatures, they allow ion conduction yet are relatively nonporous, and they can be easily made in medium and large quantities, for example using spray pyrolysis. What's more, the perovskite $AA'BB'O_3$ structure lends itself to easy doping (see Figure 4.8) [120], and typically up to 20% of the lattice ions can be replaced without causing phase separation [121]. The fact that they are wholly crystalline materials makes them also good candidates for modelling studies [122,123] and for *in silico* optimization using, for example, genetic algorithms [124,125]. One typical example, reported by Kato *et al.*, is a LaSrScAl compound. Its optimized formula, $La_{0.675}Sr_{0.325}Sc_{0.99}Al_{0.01}O_3$, shows the applicability and power of doping the $AA'BB'O_3$ structure [126]. Such materials lend themselves well to iterative modelling/experiment cycles [127].

The perovskite can accommodate a number of different cations with the constraints that ions of one, two, three, four and five valences will be accommodated in varying combinations if their sizes are in the range of 0.45–0.75 or 1.0–1.4 atomic units, and excluding the formation of compounds with hexavalent and heptavalent ions. Readers wishing to learn more about multiple ion substitution in perovskite lattices should consult the still highly relevant review authored by Roy in 1954 [128].

Incidentally, the same advantages of perovskites make them (with the right doping and coating) also interesting as high-temperature electrode materials [129–131]. Indeed, they are among the most popular cathode materials [119], but this subject is out of the scope of this book.

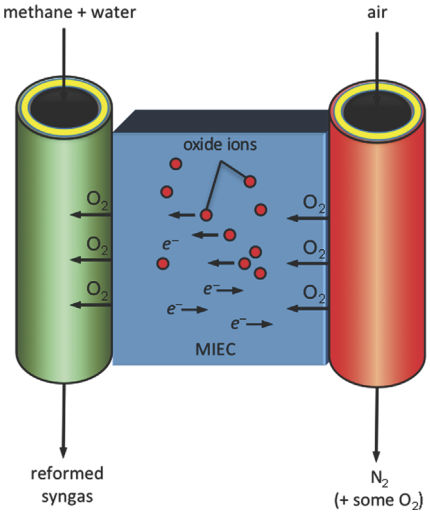


Figure 4.9 Cartoon showing the operating principle of the MIEC membrane, where the flux of electrons counterbalances that of the oxide ions.

4.2.3.2 Oxygen Separation by Dense Mixed Ionic–Electronic Conducting Membranes

Research into ionic conducting materials and membranes has been in progress for long time. The initial work was mainly focused on applications for solid oxide fuel cells and sensors. Interest in ion conducting membranes for separating oxygen from air arose in the 1980s when a number of new materials such as SrCoFeO and La(Co, Fe)O_3 were developed. These new materials, called *mixed ionic–electronic conducting membranes* (MIECs), can conduct the passage of both ions, but also electrons (see Figure 4.9) [132]. MIECs are attractive for gas separation, because the oxygen is transported through the membrane as ion rather than the conventional molecular diffusion [133]. This means that extremely high selectivity (theoretically up to 100%) can be achieved. The electronic conductivity plays an important role here, as it acts as an internal short circuit. This means that the mixed conducting membranes do not need electrodes nor an external circuit. If a MIEC membrane is placed under an oxygen chemical potential gradient, oxygen anions permeate from the high oxygen chemical potential side to the low oxygen chemical potential side while overall charge neutrality is maintained by a counterbalancing flux of electrons [134].

Unlike in a fuel cell, there is no need for an external circuit here. This makes building and operating MIEC membranes simpler. It also means that significant cost reduction can be expected and so these materials have attracted considerable interest [135]. In the past 10 years, efforts in efficient utilization of energy and reduction of emissions have indirectly stimulated research in mixed conducting membranes. One of the most important applications of mixed conducting membranes is high-purity oxygen production.

4.3
Ceramic Membrane Reactors

4.3.1
Membrane Reactor Types and Their Applications

Membrane reactors combine reaction and separation into one unit operation. They can be used to enhance reactant conversion and/or product yields by either introducing a reactant into the reaction zone or removing a product from it. Just like other chemical engineering tools for combined operation (e.g. reactive adsorption or reactive distillation), membrane reactors can help us overcome the constraints of thermodynamic equilibrium compared with simple batch or flow reactors. There are several recent and informative books and reviews about membrane reactors in general [136–139]. Here we will focus only on ceramic membrane reactors. We will first outline the key reactor configurations that are most relevant to ceramic membranes. Subsequently, we will examine several specific applications of such ceramic membrane reactors, ending the section with an outlook to their future use.

The concept of the membrane reactor itself is over 50 years old. As a very basic and general description, a membrane reactor combines a reaction unit (the reactor) and a separation unit (the membrane). The membrane is used to introduce a reactant into the reaction mixture in a controlled manner, remove a product or a by-product from it or both. Membranes can be used in combination with continuous stirred-tank reactors (CSTRs; see examples in Figure 4.10) or with plug-flow reactors (PFRs; see examples in Figure 4.11). The goal of the membrane reactor is increasing the reaction rate, product selectivity and/or yield.

The considerable developments in the manufacturing of ceramic membranes in the past two decades have made many improvements possible in membrane reactor technology. The feasible operation temperature of most porous ceramic membranes covers the 200–500 °C range, which means that they can be used for nearly all small-and-medium molecule work. Some of these membranes, and certainly most of the dense ceramics, operate best at 700–1000 °C, thus covering all the useful high-temperature range for industrial chemical processes.

4.3.2
The Inert Membrane Reactor

Following the classification introduced by Coronas and Santamaría [140], we will consider two main types of ceramic membrane reactors: the first is the *inert membrane reactor* (IMR), where the ceramic membrane is used for physical separation only. The simplest and most common application is the continuous removal of a reaction product. This is often done using a tubular membrane with a fixed bed of catalyst inside (see the example in Figure 4.11a). In this example of a catalytic dehydrogenation reaction, the hydrogen is removed from

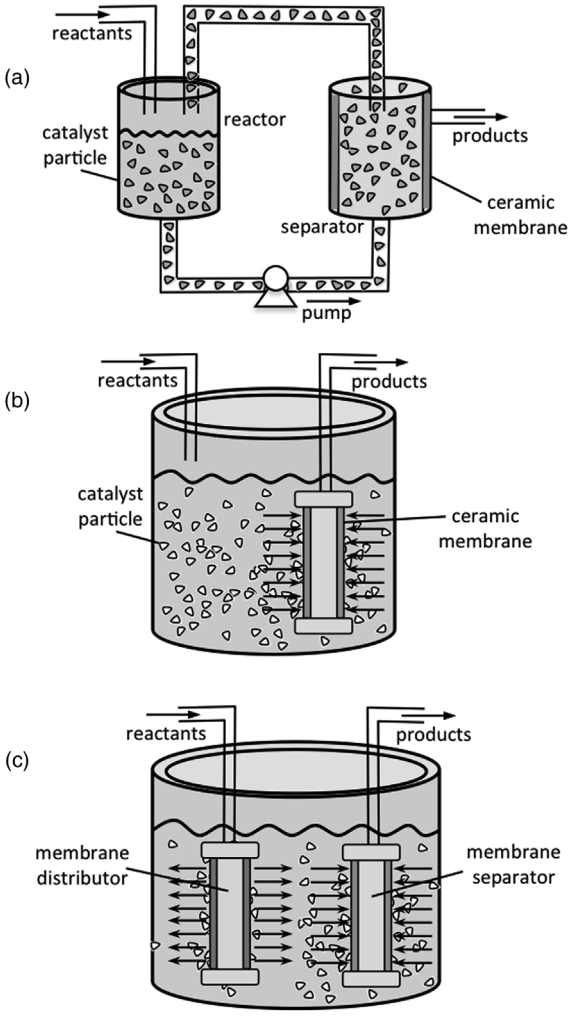


Figure 4.10 Three common examples of membrane reactor concepts using continuous stirred-tank reactors: a side stream membrane reactor (a), a submerged membrane reactor (b) and a dual-membrane reactor (c).

the mixture by diffusion through the microporous ceramic membrane, while the larger reactant and product molecules remain in the reactor [141]. This is a simple yet effective way to shift the equilibrium to the product side. In the case of dehydrogenation, which is most often endothermic [142], such a configuration can enable operation at a lower temperature. Another option is coupling the physical separation with a chemical reaction on the permeate side. In this way, one can shift the equilibrium further, and in some cases even change the thermodynamic balance. A common example is oxidative dehydrogenation [143], where the hydrogen by-product is reacted with oxygen to give water, resulting in

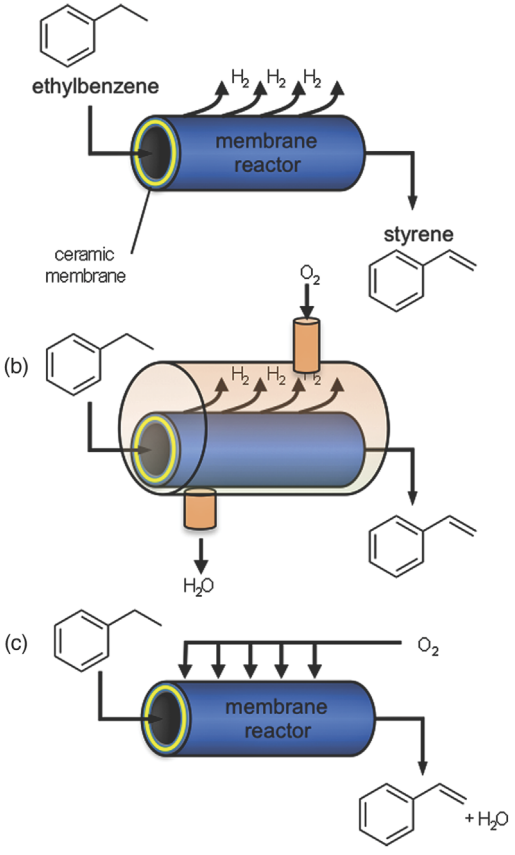


Figure 4.11 Plug-flow reactors with continuous product removal using an inert membrane reactor (a) and in combination with a chemical reaction on the permeate side (b). The same set-up can be used for introducing a reactant (c). (Diagrams redrawn after Ref. [140], with permission.)

a process that is overall exothermic (Figure 4.11b). The same type of set-up can be used for the gradual introduction of a reactant, for example in the controlled oxidation of hydrocarbons, where partial oxidation is desired or where a runaway reaction must be avoided (Figure 4.11c). Application examples include Vycor membranes (high-grade borosilicates) in the oxidative coupling of methane [144] and oxygen feeding in the oxidative dehydrogenation of propane [145,146] and butane [147].

An important family of ceramic membranes that has planted itself firmly in IMR applications is the *zeolite membranes*. Thanks to advances in their synthesis as supported layers in the last two decades, these molecular sieves are ideal for removing small product molecules such as H_2 or H_2O, increasing the conversion and the yield of dehydrogenation and dehydration reactions [148].

One such example is the use of a ZSM-5 membrane for continuous removal of water during the esterification of *i*-propanol with propionic acid (Figure 4.12a).

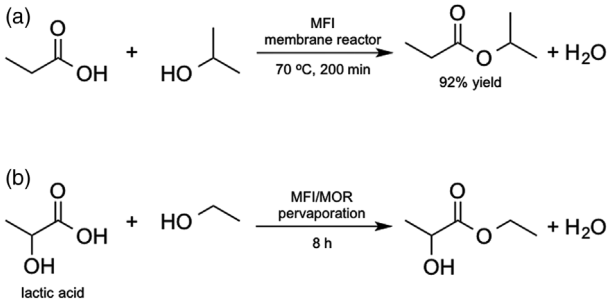


Figure 4.12 The syntheses of *iso*-propyl propanoate (a) and of ethyl lactate (b) are two examples where zeolite membranes can be used in an IMR configuration for removing the water by-product.

At t_∞, the membrane can increase the ester yield from 52 up to 92% [149]. This ZSM-5 membrane showed good acid stability (down to pH 1) but its low hydrophilicity (due to the high Si/Al ratio of 96) resulted in a flux that was too low for industrial applications. In another example, the esterification of lactic acid with ethanol to give ethyl lactate (Figure 4.12b) was enhanced by using hydrophilic ZSM-5 and MOR membranes in a pervaporation/vapour permeation IMR set-up. This shifted the equilibrium to the product side, giving nearly 100% conversion after 8 h.

Interestingly, even though hydrophilic membranes are the most used for dehydration applications, the hydrophobic all-silica DD3R membrane was reported by Kapteijn and co-workers to be excellent at water separation from organic solvents. Under pervaporation conditions, it removed water efficiently from ethanol, methanol and ethanol/methanol solutions [150]. This removal is attributed to molecular sieving, rather than adsorption (cf. the case with MOFs [151]): Water easily passes through the DDR structure, while the larger organic molecules are retained due to increasing diffusion hindrance.

The same group also published recently a detailed study on the dehydrogenation of isobutane, using a specially adapted DD3R zeolite membrane reactor in the presence of a commercial Cr_2O_3/Al_2O_3 catalyst [152]. The membrane itself was a commercial tubular DD3R zeolite membrane provided by NGK Insulators. Using pure isobutane as feed and nitrogen as the sweep gas (see Figure 4.13), the reaction was run at 440–500 °C. The authors then compared the results with control experiments in a conventional packed bed reactor. Here, combining the membrane reactor approach with the small pores of the zeolite offers a clear advantage: practically quantitative separation of hydrogen from isobutane by molecular sieving. At 500 °C, the membrane showed a 500 : 1 hydrogen/isobutane permselectivity, with a reasonable hydrogen permeance of about 4.5×10^{-8} mol/(m^2 s^1 Pa). The conversion values and the product (isobutene) yields exceeded the equilibrium values by as much as 50% when operating at low residence times. Thus, at 490 °C and using 0.13 kg_{feed}/(kg_{cat} h), the membrane reactor gave 41% isobutene, compared with the equilibrium yield of 28%. The higher yield was attributed to the selective removal of hydrogen from the reaction zone.

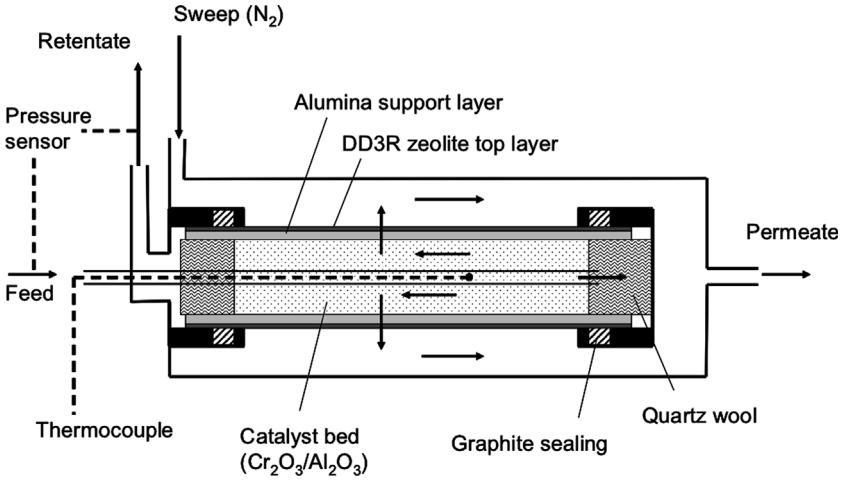


Figure 4.13 Schematic of the membrane reactor used for isobutane dehydrogenation. A ~1–2 μm thick zeolite layer is present on the outside of a 150 mm long γ-alumina tube. The outer diameter of the tube is 12 mm. The support consists of three layers of different pore sizes (0.2, 1 and 5 μm) and thicknesses (13, 70 and 1750 μm, respectively). The composite membrane was sealed in a stainless steel module using graphite O-rings, giving an effective tube length of 120 mm and a total of 0.0045 m^2 membrane area. The catalyst (pellets, 4.1 g, crushed and sieved to 0.7–1.0 mm) was commercial chromia–alumina (BASF Cr-0211-T) containing 18.0% Cr_2O_3, 0.25% ZrO_2 and about 82.0% Al_2O_3. (Reproduced from Ref. [152], with permission, © 2010 Elsevier B.V.)

Inert membrane reactors can also be used in batch and semi-batch modes (see Figure 4.10) for separating species based on their size and chemical affinity. One such example is the cat-in-a-cup concept developed in our laboratory, wherein a ceramic membrane is used for separating large homogeneous catalysts from the reaction solution. These porous membrane 'cups' are basically cylinders made of a thin nanoporous γ-alumina layer coated onto a macroporous α-alumina membrane (Figure 4.14a; a SEM image of this membrane is shown in Figure 1.6) [153]. They are capped at both ends with Teflon stoppers. The molecular weight cut-off of the γ-alumina layer is 1000 Da. Albeit this is heavier than many metal–ligand complexes used in homogeneous catalysis, it is well within the size range of dendrimers and oligomers. We attached a third-generation Fréchet-type 'dendrimer anchor' to a homogeneous complex (see Figure 4.14b). This created a dendritic catalyst that could be separated by nanofiltration in the membrane reactor cup [154].

4.3.3
The Catalytic Membrane Reactor

The second type of membrane reactor is the *catalytic membrane reactor* (CMR), where the membrane material itself functions as a catalyst (or becomes catalytically active during preparation by adding active precursors). In many ways, this is the

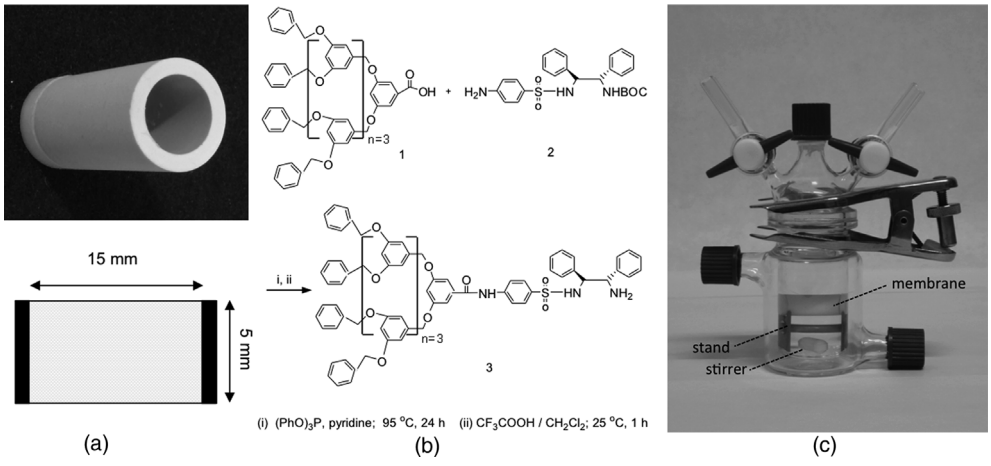


Figure 4.14 (a) Photo and schematic of the multilayered porous catalyst separation cup. The membrane has a pore diameter of 4 nm. (b) Attaching a Ru^{II} complex with (*S,S*)-*N*-arenesulfonyl-1,2-diphenylethylenediamine ligands to a third-generation Fréchet-type dendrimer scaffold creates a bulky catalyst that is easily filtered using an alumina membrane. (c) Photo of the inert membrane reactor used for demonstrating the 'cat-in-a-cup' concept.

more exciting option. Kapteijn and co-workers [155] outlined four main advantages for CMRs:

i) They can improve product selectivity by enabling a better control of the reactant contact time and thereby limiting the occurrence of unwanted consecutive reactions.
ii) They can reduce mass transfer limitations.
iii) They can shift the chemical equilibrium of the reaction by reducing the concentration of reagents and/or products that diffuse faster through the membrane (strictly speaking, this creates a continuous non-equilibrium situation or 'pseudo-equilibrium').
iv) They can increase operational safety when the membrane is used as an interfacial contactor, keeping certain reactants segregated and preventing the formation of flammable or explosive mixtures.

These advantages weigh against the increased cost and complexity (and therefore increased risk). We will discuss the economics side of these considerations in more detail in Chapter 5.

Following the classification of Julbe *et al.* [156], CMRs can be divided into three main types, depending on the interaction between the catalyst and the membrane. The catalyst can be supported on the membrane, integrated within the pores of the membrane or the membrane itself can be made of active catalyst material (Figure 4.15).

Of these three configurations, the first is also the simplest, because it is really just an inert membrane reactor with a catalyst (as particles or pellets) on one

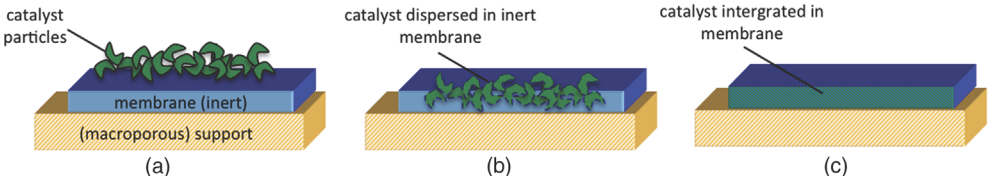


Figure 4.15 Cartoon showing the three main types of catalytic membrane configurations: a catalyst supported on an inert membrane (a), a catalyst dispersed in the pores of an inert membrane (b) and a membrane that in itself is made of a catalytically active material (c).

side of the membrane (Figure 4.15a). The membrane itself can be either dense or porous, and serves only as a separation layer. Things change when the catalyst is immobilized within the membrane pores (Figure 4.15b). Now, the catalysis and separation functionalities are in close proximity, and they influence each other. In classical reactors, the reactant conversion is often limited by the diffusion of reactants into the pores of the catalyst or catalyst carrier pellets. If the catalyst is inside the pores of the membrane, the combination of the open pore path and transmembrane pressure gives easier access of the reactants to the catalyst. Indeed, studies on catalytically active alumina membranes showed that the activity of such a 'membrane catalyst' can be an order of magnitude higher compared with regular catalyst pellets [157], provided that the reaction kinetics correspond to the membrane thickness and texture, and that there are enough active sites available in the membrane [158].

Incidentally, there is no requirement that the catalyst must be on the 'outside' of the membrane. You can also coat the catalyst particles themselves with a porous membrane coating, as in the example of the selective coating of pre-shaped Co/SiO_2 catalyst pellets by a HZSM-5 shell by Tsubaki and co-workers. In this example, the zeolite membrane coating enhances the selectivity for mid-sized *i*-paraffins and suppresses the formation of long-chain hydrocarbons in the Fischer–Tropsch process [159]. The product mixture was markedly different from that obtained using a physical mixture of H-ZSM-5 and Co/SiO_2. In another study, Nishiyama *et al.* succeeded in coating silicalite-1 on spherical Pt/TiO_2 particles, creating a silicalite/Pt/TiO_2 composite. The coated particles were then used for catalysing the hydrogenation of both linear and branched alkenes. In a mixture of 1-hexene and 3,3-dimethyl-1-butene, these catalysts gave hydrogenation selectivity of 12–20 at 50 °C and 18–30 at 100 °C, thanks to the selective permeation of 1-hexene through the zeolite membrane [160].

Another example where the catalytic particles are embedded inside the membrane matrix is the 'ship-in-a-bottle' concept, where the porous ceramic membrane surrounds the catalyst particles. The particles themselves do not have to be covalently bonded to the membrane – they can be just simply too large to get out of the pores. Wichner *et al.* demonstrated this concept in 2011 for gold and silver nanoparticles embedded in porous silica [161]. Under acidic sol–gel conditions, the surface charge of the silica correlates with the porosity. Charge-compensating cations are needed when the surface is negatively charged at pH >2–3.

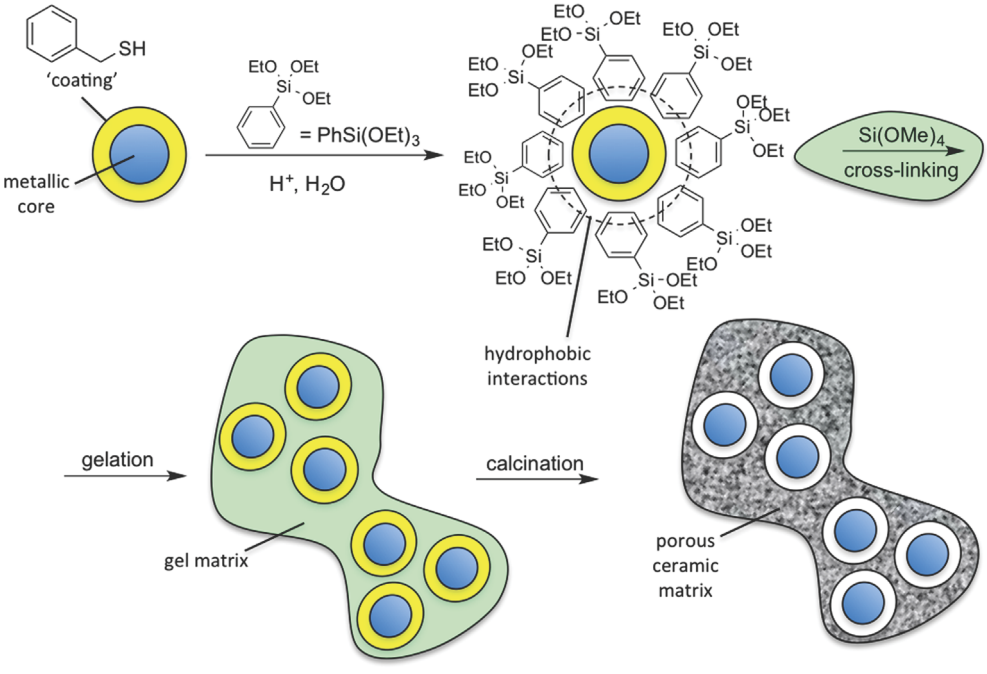


Figure 4.16 Cartoon showing the stepwise encapsulation of gold or silver catalyst nanoparticles in the silica porous membrane matrix. The calcination step burns out the organic shell surrounding each particle, creating a porous 'baby rattle' that enables the passage of small molecules to and from the catalyst, but prevents the gold/silver particles' diffusion and sintering.

These hydrated cations (e.g. H_3O^+) are the porogenic agents. At the isoelectric point (pH 1–3, depending on the composition), no porosity forms [162,163]. Therefore, two effects must be balanced: the ionic surface interactions of the sol–gel materials and the hydrophobic interactions between phenyl groups. Wichner *et al.* showed that the porosity can be tailored by controlling the synthesis pH.

The embedding of the catalytic gold or silver particles in the ceramic matrix was done by first capping them with phenylethylthiol that binds to the particles via the thiol group (see Figure 4.16). The other end of the capping agent can then form non-covalent weak bonds with a sol–gel precursor, phenyltriethoxysilane. Sol–gel polymerization with tetramethoxysilane and phenyltriethoxysilane is then carried out under acidic conditions. The resulting clear solutions are then treated with aqueous ammonia, increasing the pH of the mixture to the final target value, where condensation is accelerated [164]. Finally, the organic components (i.e. the capping agent of the NPs and the matrix phenyl groups) are removed by calcination. Interestingly, the as-made gels with the capped nanoparticles were dense, and only the calcined materials showed microporosity (324–514 m^2/g, depending on the particle loading).

The contact of the reactant with the catalyst surface is crucial in CMRs. Many catalytic reactions depend on surface reactions for their product selectivity, as the same type of reactions in the bulk would cause the formation of by-products. One such example is the selective oxidation of hydrocarbons, where the reactions in the bulk (in this case, the gas phase) are often free-radical processes that result in unwanted combustion of valuable reactants to CO_2 and water. The same principle of minimizing non-selective reactions in the bulk solution holds also for liquid/solid reactions, for example in the free-radical oxidation of ethyl lactate to ethyl pyruvate [165]. This problem can be tackled using the right kind of pores: microporous membranes, in which the Knudsen transport mechanism dominates, are typically favoured in biphasic systems such as gas/catalyst. Membranes with larger pores (10–25 nm) are preferable when three phases are involved (gas/liquid/catalyst), for example in the hydrogenation of nitrobenzene over platinum catalyst particles supported in the pores of γ-Al_2O_3 [166]. The classical applications of ceramic membranes supported with noble metal particles (typically Pt and Pd) are in hydrogenation and dehydrogenation reactions, using γ-Al_2O_3 [156], SiO_2 or TiO_2 [167] membranes. But there are also diverse examples of catalysts impregnated or dispersed in inert membrane supports, including the immobilization of Mn^{III}-salen complexes on modified silica membranes for the asymmetric epoxidation of styrene [168], iron oxide and manganese oxide nanoparticles on titania for water purification [169], NiO on alumina for catalytically removing particles, tars and ammonia from biomass gasification gas [170] and even enzymes such as carbonic anhydrase that was immobilized on titania for carbon capture and storage [171].

The third sort of ceramic membranes used in membrane reactor applications are the *inherently catalytic membranes* (Figure 4.15c). Here the ceramic membrane is responsible for both the catalysis and the separation, and in fact is the most important part of the reactor. Typical examples include inherently acidic porous materials such as alumina [157], titania [172], various zeolites such as zeolite Y [173] and H-ZSM-5 [174], or basic ones such as magnesia [175]. There are also borderline cases where the ceramic material and the catalytic function are so well integrated that the question of whether this is an inherently catalytic membrane or a supported catalyst is a moot point, as in the example of methane steam reforming over Pd-Ag/Al_2O_3 [176]. Several other ceramic materials can serve as dense 'catalytic membranes', especially in the case of oxygen exchange materials such as doped cerias [115] and perovskites [177], which can be used to 'sieve' hydrogen selectively from dehydrogenation reaction mixtures [178].

Catalytic membranes can also be combined in layers, as shown in an elegant example published by Itoh and co-workers [179]. They combined two different zeolites: an inactive silicalite-1 and a catalytically active ZSM-5. By making a ceramic membrane 'sandwich' of silicalite-1/ZSM-5/silicalite-1, Itoh's group created a separation/catalysis membrane that gave highly selective disproportionation of toluene at 400 °C (see Figure 4.17). The silicalite-1 layers on both sides of the ZSM-5 layer are non-reactive and similar in permeation property to the ZSM-5 layer. The researchers hypothesized that surface silicalite-1 layer will

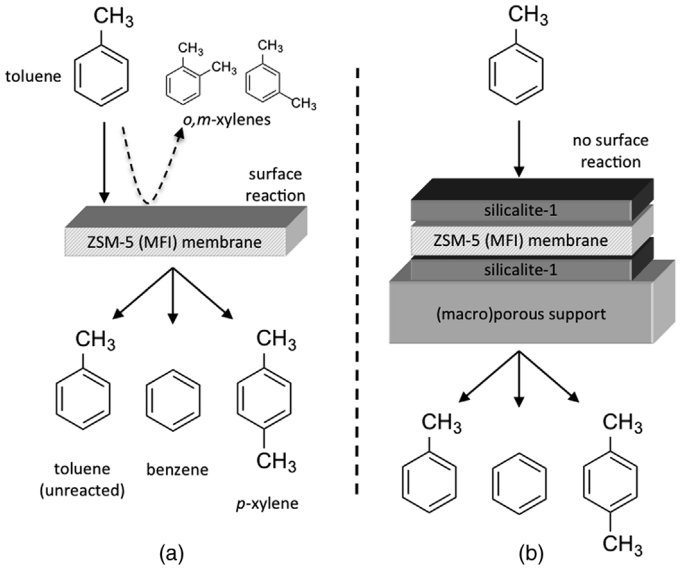


Figure 4.17 A membrane sandwich structure composed of two layers of silicalite-1 surrounding an active ZSM-5 layer (b) gives a much cleaner and more selective toluene disproportionation reaction compared with using only ZSM-5 (a). (Concept redrawn after Ref. [179], with permission.)

inhibit the surface reaction on the ZSM-5 layer. However, this should be compensated by the fact that silicalite-1 can bind better to the stainless support than ZSM-5. Consequently, the silicalite-1/ZSM-5/silicalite-1 sandwich should give high selectivity to *p*-xylene.

The membrane itself was prepared by hydrothermal synthesis, using a macroporous stainless steel filter (0.5 μm average pore size) as the support and characterized by SEM and X-ray diffraction. The results bore out the authors' hypothesis. The three-layer combination was by far the best one, giving nearly 97% selectivity to *p*-xylene (see Table 4.9).

4.3.4
Composite Infiltrated Ceramic Membranes

The examples shown in Figures 4.14 and 4.17 both relate to membranes prepared by layer deposition. This deposition of thin films on porous supports is a good way for obtaining high fluxes. But it also has disadvantages: First, it requires strict quality control and highly optimized synthesis protocols. This increases the cost of the membranes, creating a higher barrier for large-scale industrial applications. Second, these thin-layer membranes are often defect sensitive upon aging, and are less resistant to thermal and mechanical shocks. Overcoming these disadvantages requires simple and robust synthesis protocols. One interesting option is the synthesis of *porous infiltrated composite membranes*.

Table 4.9 Catalytic disproportionation of toluene using different zeolite configurations.[a)]

Membrane/catalyst configuration	Toluene feed rate (mol/s)	Time on stream (h)	Toluene conversion (%)	Xylene selectivity (%)		
				p-	*m-*	*o-*
Silicalite-1/ZSM-5/silicalite-1 membrane[b),c)]	1.20×10^{-8}	3	0.72	96.7	3.3	0
ZSM-5/silicalite-1 membrane[b),d)]	1.22×10^{-8}	3	0.86	86.0	8.8	5.2
ZSM-5 powder[b),e)]	1.88×10^{-8}	3	10.85	32.6	47.8	19.5
ZSM-5 powder[b),e)]	1.88×10^{-8}	5	4.23	31.9	47.5	20.6

a) Data from Ref. [179], reproduced with permission.
b) Reaction at 673 K and 0.1 MPa.
c) Weight of membrane 0.23 g.
d) Weight of membrane 0.14 g.
e) Catalyst 0.2 g.

Here, the membrane separation layer is deposited not only on the surface, but also *inside* the pores of a robust porous support (see Figure 4.18). This creates a composite material which can act as a separating barrier, but now with good thermochemical resistance and a lower sensitivity to defects [180]. Furthermore, in the case of catalytic membranes, using the porous infiltrated concept allows the deposition of a relatively large quantity of catalyst per weight of membrane material. This, plus the fact that the synthesis protocol is often simpler and less restrictive compared with thin-layer deposition, makes the porous infiltrated composite membranes good candidates for practical applications.

These composite membranes can be made using various methods. In one example, Wu *et al.* [181] used a combination of chemical vapour deposition and

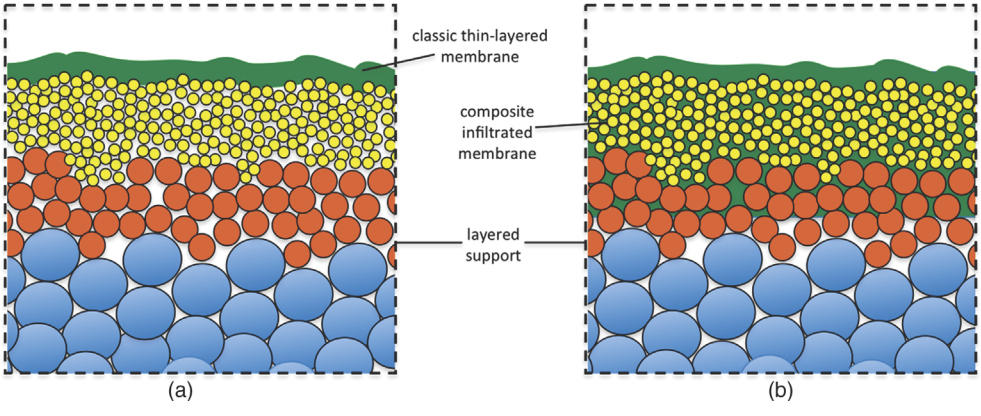


Figure 4.18 Cartoons of a typical thin-layer membrane (a) and a composite infiltrated membrane (b), both supported on a classic robust layered support.

infiltration (CVD/CVI) for preparing a silica/alumina composite membrane with high hydrogen permeation selectivity. They used 40 Å γ-alumina tubular membranes as the supports. The hydrogen permeance ranged from 0.028 to 17.6 $m^3/(m^2\ h\ atm)$, and the H_2/N_2 selectivity (the so-called *permeance ratio*) ranged between 12 and 72 at 600 °C. The selectivity to isobutane ranged from 40 to 240 at 300 °C and could be higher at a higher temperature. Diffusion through these modified membranes is attributed to two mechanisms: *hindrance diffusion* through micropores up to 5 Å and *Knudsen diffusion* through the larger pores [182].

Another simple and very effective way for preparing composite infiltrated ceramic membranes is the sol–gel technology (the key concepts of sol–gel synthesis are covered in several reviews [183–185], and the relevant aspects for membrane synthesis are discussed in Chapter 1). This highly versatile method is suitable for making a range of ceramic materials with controlled composition and porosity. In most cases, it is in fact used for making thin-layer membranes on top of a (macro)porous support [186–188]. However, it can also be used for making infiltrated composite membranes of both microporous and mesoporous ceramics. These can be either inert or inherently catalytic. Examples include silica, used in an IMR configuration as an oxygen distributor [141,189], and alumina, which was used in a CMR in combination with platinum [190]. The catalytic membranes can be synthesized directly as single or mixed oxides [191], or by dispersing/plating a catalytic metal precursor with the membrane precursor during the synthesis [192,193]. The membranes used as gas distributors are mainly mesoporous silica and alumina, prepared from colloidal silica [194] or boehmite sols [195], respectively. Interestingly, membranes operating in the viscous flow regime (i.e. macroporous ones) can be more efficient as oxygen distributors, because they have less back-diffusion [194].

Yet another approach for infiltrating one membrane material in the pores of a support is using *solvothermal synthesis*. This is a good method for depositing and infiltrating layers of zeolites on alumina, carbon or stainless steel [196]. The synthesis and application of zeolite membranes is a 'hot topic', which is covered in several recent reviews [148,155,197,198]. Many types of zeolites have been prepared as membranes, including ZSM-5 (MFI) [199], zeolite A (LTA) [200] and CHA (CHA, SAPO-34) [201]. Depending on the synthesis conditions (sol composition, reaction time, nature of the support and support pretreatment), one can obtain continuous zeolite polycrystalline layers of 2–50 μm thickness. In some cases, the sol itself can also soak into the pores of the support resulting in a composite infiltrated membrane. Owing to their specific adsorption and molecular sieving properties, zeolite membranes are used mainly for gas and vapour separations [196]. The Si : Al ratio in the zeolite framework is a key factor that influences the membrane properties in various ways. Zeolite membranes with low Si:Al ratios are hydrophilic and often used for water separation. Defects in these membranes can be sealed off by strongly adsorbed water molecules. However, membranes with higher Si : Al ratios have fewer defects and are therefore preferable (these membranes are also more stable) [149]. A detailed

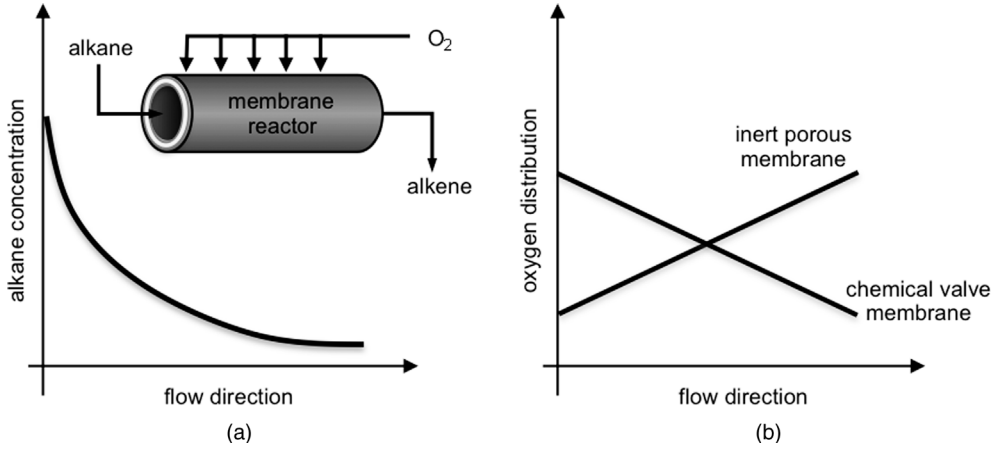


Figure 4.19 A typical plot of concentration of reactant (alkane) in a plug-flow membrane reactor with permeation of oxygen (a) and the distribution of oxygen when using a simple inert porous membrane and a 'chemical valve' membrane (b).

discussion of the applications of zeolite membranes in catalysis is given in the recent book chapter by van den Bergh *et al.* [155].

One very interesting application of composite infiltrated ceramic membranes is the *chemical valve concept* put forward by Farrusseng *et al*. Here, the CMR is used for creating a process environment that will influence the reactions in the CMR not only physically but also chemically. The researchers used a composite infiltrated ceramic membrane [202] (combining V_2O_5 and $AlPO_4$ crystallites in γ-Al_2O_3) for tuning oxygen concentrations along a plug-flow CMR. Figure 4.19a shows what typically happens in an alkane partial oxidation reaction that is run in a tubular porous membrane reactor where the membrane has a uniform thickness and is used for distributing oxygen to the reaction mixture. Typically, the alkane concentration decreases as the mixture flows through the reactor. The alkane is oxidized, and as oxygen is continuously introduced through the membrane's pores, the partial pressure of oxygen remains relatively constant and the alkane:oxygen ratio decreases. This is enhanced further by the influence of the pressure drop generated by the catalyst bed, which typically increases the O_2 permeation rate near the end of the reactor, due to the higher pressure gradient in that zone [203]. This change in the alkane:oxygen ratio along the reactor can cause problems for the catalytic reaction, because catalysts are typically optimized for a given reactant:reagent ratio, so changing the ratio can lower conversion and yields.

There are several ways to overcome this problem: The simplest, from a chemical engineering point of view, is co-feeding a part of the oxygen with the alkane into the reaction zone. But feeding more oxygen in the beginning of the reactor could also change the product selectivity. Alternatively, one can use a ceramic membrane of varying thickness, a sort of hollow cone shape, starting thin at the reactor entrance and increasing towards its exit [204]. This would increase the

oxygen diffusion times along the reactor by creating a larger physical diffusion barrier.

Farrusseng and co-workers proposed the chemical valve concept for regulating the oxygen flux in the reactor, by using a ceramic membrane whose permeability could be controlled by the redox properties of the gas phase [205]. They chose vanadia for this, utilizing the reversible redox switching between the V_2O_5 and V_2O_3 species. In the case of vanadia, the redox changes also alter the texture of the membrane, and can change the membrane permeance behaviour as shown in Figure 4.19b.

The redox-tunable membrane was prepared by depositing an organic solution of vanadium and phosphorous molecular precursors inside the pores of a commercial tubular γ-Al_2O_3 membrane. After calcining in air at 650 °C, the internal and intermediate layers of the asymmetric support were entirely filled with a combined ceramic material, containing V_2O_5 and $AlPO_4$ crystallites. The redox switching between V_2O_5 and V_2O_3 influenced the surface area, grain morphology, pore size distribution and pore volume. Changing these parameters resulted in permeance differences for the oxygen, showing that this ceramic membrane behaves like a chemical valve: its permeance is higher when it is reduced and lower when it is oxidized.

The last two decades have seen an explosion of research and development on process intensification, and membrane reactors were not neglected. One exciting application is the combination of ceramic membranes with/in microreactors, creating *ceramic membrane microreactors*. These can be designed in either IMR or CMR configurations. The combination of ceramic membranes and process miniaturization opens opportunities for cleaner, safer and more efficient chemical synthesis. One such example is the Knoevenagel condensation reaction reported by Yeung and co-workers, where the selective removal of the water by-product improved the conversion by 25% [206]. The reaction between benzaldehyde and ethyl cyanoacetate to produce ethyl-2-cyano-3-phenylacrylate (Figure 4.20) was catalysed by a CsNaX zeolite catalyst deposited onto stainless steel microchannel array reactors. Simultaneously, the water was selectively pervaporated across an LTA membrane [207]. All the water produced by the reaction was completely removed and the membrane was operating below its capacity [208]. This shows that the membrane reactor succeeded in removing both thermodynamic and mass transfer constraints (leaving only the kinetic limitation). Changing the catalyst to a more basic CsNaX–NH_2 increased the reaction rate further.

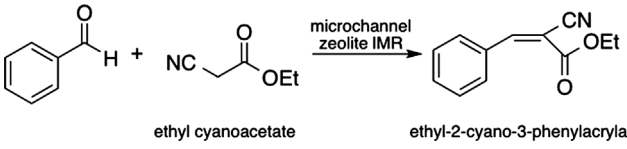


Figure 4.20 Knoevenagel condensation between benzaldehyde and ethyl cyanoacetate giving ethyl-2-cyano-3-phenylacrylate, a fine chemical intermediate.

Another successful application of ceramic membrane microreactors is the continuous selective oxidation of aniline by hydrogen peroxide on TS-1 nanoparticles in a multichannel membrane microreactor [209]. The multichannel plate was made by fabricating microchannels onto a porous stainless steel plate (SS 316L, nominal pore size 0.2 μm). This was done using electrical discharge micromachining. Thirty-five straight channels measuring 300 μm in width, 500 μm in depth and 25 mm in length were cut into a $25 \times 25 \times 1\,mm^3$ plate. The catalyst–membrane interface was then prepared by depositing a membrane layer at the back of the plate and coating the microchannels. Before depositing the ZSM-5 membrane, the back of the multichannel steel plate was first seeded with zeolite nanocrystals (100 nm, silicalite-1 seeds). Finally, the ZSM-5 membrane (25 μm) was grown on the seed layer. The same method could also be used for supporting layers of Sil-1 and VS-1 membranes [210]. The high surface area to volume ratio attained in the microreactor ($3000\,m^2/m^3$) enhanced the removal of the water by-product, slowing down catalyst deactivation.

4.3.5
Membrane Reactors Using Dense Ceramic Membranes

The above examples focus on IMRs and CMRs with porous membranes. However, membrane reactors can also operate using dense membranes. These processes need much higher temperatures, and so their membranes are exclusively ceramic. One typical example is the production of syngas from methane. This is one of the largest chemical processes worldwide, and is increasingly important with the shift towards natural gas and shale gas. The syngas product is then converted to fuels and chemicals via the Fischer–Tropsch synthesis or via methanol synthesis.

The main route from methane to syngas is by steam reforming, but this is a highly endothermic process which requires much energy. Alternatively, syngas can be produced by partial oxidation of methane with air. This is definitely exothermic, but it has its own disadvantages: First, the reaction can run away all the way to CO_2 and water. Second, most of the downstream processing cannot tolerate nitrogen and therefore pure oxygen is required (oxygen from air is the only viable oxidant at this gargantuan scale). Thus, the most significant cost associated with conventional partial oxidation of methane to syngas is that of the oxygen separation plant. Membrane reactors fitted with perovskite-type ceramic membranes enable syngas production from methane and air while avoiding the need for separation of the nitrogen either before or after the reaction, thereby reducing the CapEx of the process. The most active and selective catalysts for the partial oxidation of methane to syngas are Ni-based and noble metal-based ones (particularly Rh) supported on ceramic oxides [211]. For example, a $Sr_1Fe_{1-}CO_{0.5}O_x$ tubular membrane reactor enabled the separation of clean oxygen from air yielding methane conversion to syngas with over 99% efficiency in the presence of a reforming catalyst, at 850 °C for over 1000 h [212]. In another example, a $BaCo_{0.7}Fe_{0.2}Ta_{0.1}O_{3-x}$ tubular membrane reactor with a nickel-based catalyst

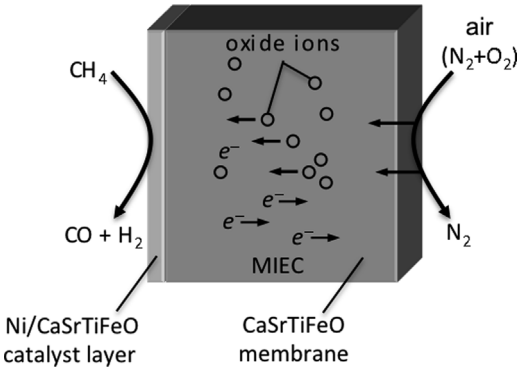


Figure 4.21 Methane conversion mechanism in a single-component ceramic membrane reactor.

enabled the separation of clean oxygen from air yielding methane conversion to syngas efficiency of over 99% at 900 °C for over 400 h without any fractures in the membrane [213].

The recent advances in the area of new mixed ionic conductors have also impact on IMRs and CMRs. These membranes have a high oxygen permeability, which should make them ideal for methane oxidation. But they also suffer from unwanted chemical reactions between the membrane and the catalyst under methane reforming conditions. The reaction between the catalyst and the mixed conductor decreases the oxygen permeation. This hampers oxygen transfer and increases coking at long times on stream. Different solutions have been proposed to this problem. One is using a single-component membrane reactor with a $Ca_{0.8}Sr_{0.2}Ti_{1-x}Fe_xO_{3-\delta}$ perovskite-type membrane. To prevent the chemical reaction between the catalyst and mixed conductor and carbon deposition (coking), the use of Ni catalysts supported on the perovskite type oxide, $Ni/Ca_{0.8}Sr_{0.2}Ti_{0.9}Fe_{0.1}O_{3-\delta}$, was examined (Figure 4.21). When this catalyst was applied in the partial oxidation of methane into syngas, it suppressed coking at 900 °C [214].

4.4
Liquid Separation and Purification

Ceramic membranes are used in several liquid clarification processes that can be grouped into two major applications – water and wastewater, and food. In both applications, ceramic membranes divide solids (bacteria, pulp, proteins) from water or liquids (milk, juice, beer, wine). Ceramic membranes can also separate liquids from liquids. This sort of operation is performed by membrane distillation and pervaporation, and is equally applicable in water treatment and liquid purification fields. For clarity, we will describe here the general process in each case first, followed by application examples.

4.4.1 Water Treatment

Long before people focused on water-borne diseases, some foulants in the water were already recognized and neutralized or purified. Boiling water and water-based drinks (such as beer, coffee and tea) was and still remains one of the safest methods for neutralizing water-soluble contaminants. Boiling is easily applied at the household level, and does not require fancy equipment. Another old home water purification method is the soaking of different substances such as pearl barley, onions, or wax [215]. Similarly, industrial water purification was performed by filtration through sand, soil, wool, bread crumbs or textiles. But even at the time of the Roman Empire, wealthy families kept their drinking water in closed ceramic containers, where it was purified through a ceramic filter at the bottom of the container.

The first ceramic filter in the modern era used to remove bacteria from drinking water is claimed to be implemented by Sir Henry Doulton in 1827. Indeed, the principles of filters have not changed much since. The only difference in the past two centuries is that the filter and the pores inside it are now much thinner and finer. Both of these differences affect the flux through the ceramic filter and its application in retention of small particles. Whereas historically ceramic filters were used for retaining millimetre-sized grains of sand and silt, today's ceramic membranes target single-nanometre viruses and protein molecules. This change from millimetres to nanometres is symbolized also in the name. *Ceramic filters* have become *ceramic membranes* somewhere in the 1970s.

Ceramic membranes are used in water purification alongside polymer ones. At first, the market was completely dominated by polymer membranes and ceramic membrane advocates had a hard time gaining a market share. They applied two marketing strategies: The first was competing with polymer membranes in traditional applications. The second was scouting for and inventing new applications where ceramic membranes might have an advantage. The first strategy became noticeable during the last decade, although the background for it has been in preparation for the last 40 years. When more demanding water regulations first came out, the developed world was using granular sand and anthracite filtration of surface water. Polymer membranes were tried as an alternative, and their use spread massively, especially after the Milwaukee outbreak of *Cryptosporidium parvum* in 1993. This outbreak had serious consequences: 400 000 were infected, and over 100 died. The indirect costs of the outbreak to US economy were almost $100 million [216], not including the potential loss of trust in public water systems following such outbreaks.

The popularity of polymer membranes was such that at the beginning of the twenty-first century practically all new surface water treatment installations used them, whereas ceramic membranes served in some small-sized industrial projects in the pharmaceuticals, chemicals, and food and beverage sectors. But at the same time when the entire world was starting to embrace polymer membranes as a relatively cheap option for water treatment, the Japanese government took a

strategic decision to develop and implement ceramic membranes. The strategy was backed up by a massive government funding needed to develop a more expensive alternative. Today, ceramic membranes are mechanically, chemically and thermally stable. They are bio-inert and their application is scalable. Economically, they are a serious alternative to polymer membranes. Current price estimates are that although CapEx in implementation of ceramic membranes is double that for polymer ones, the excellent membrane characteristics and the advantage of keeping functionality without maintenance for typically 8–10 years lower the OpEx considerably. All in all, ceramic membranes are cheaper in the long run (about 10 years) than polymer membranes as a water treatment alternative. The fact that ceramic membranes achieve such close competitiveness even without significant market volumes suggests that when they will enter one of the major markets they will become even more affordable.

The new application opportunities for ceramic membranes are mainly in those market segments that were previously occupied by other filtration options. Here we will describe three of these (although other options are emerging). The first opportunity is using ceramic membranes for treating separate water sources of rural and isolated communities. Typically, the larger water treatment plants are staffed by a qualified workforce that can deal with the technical challenges and operational problems of polymer membranes. Rural communities with less than 10 000 people require low-cost robust packaged filtration solutions, without any chemical pretreatment and with minimal post-filtration chemical disinfection [217]. Recent module developments that led to the invention and application of hollow-fibre ceramic membrane modules made drinking water treatment by ceramic filtration cost-effective. The reported flux of 150 LMH (l/(m^2 h)) is considered attractive not only for ceramic membranes, but also compared with polymer membrane separations. The retention level, however, is somewhat tricky. Usually, high fluxes imply the retention of large impurities, but not of small ones.

The second opportunity is the development of low-cost filters. Industrial membrane installations require very large capital investments, which may not be available in developing countries. At the same time, the water situation in these countries often demands the filtration today. One possible solution is teaching the local population to build and implement low-cost filters on the community level. Admittedly, the water quality will not be the same, and the quality control will be below best management practices (BMPs). But this short-term solution will ensure that people will avoid many life-threatening diseases.

The third important opportunity is in the applications of membrane distillation and pervaporation, especially for desalination of seawater and brackish water. Brackish water is more saline than freshwater, yet less saline than seawater. Although the principles have been well established for years, industrial applications lagged behind due to a significant cost gap compared with desalination with polymer membranes. In the last decade, there is a renewed interest in distillation as a green alternative to reverse-osmosis desalination. It turns out that unlike the latter, membrane distillation can be partially powered

by solar energy, waste heat, geothermal energy or other alternative energy sources.

In the following sections, we will expand each of these three opportunities in detail, referring to specific examples.

4.4.2 Surface Water Treatment with Ceramic Membranes

Most of us take drinking water for granted, but pure water is actually an extremely rare resource. It is typically available in large quantities in countries with a high quality of life, such as Norway, Switzerland, Germany, New Zealand, Sweden and the United Kingdom. The tap water quality is in fact correlated with a country's quality of life, as measured by the UN Human Development Index. This does not imply direct causality, as the index is a weighted average of life expectancy, education and gross domestic product (each weighs 33%). The quality of tap water does not feature in it. Yet it is thought provoking that the countries that routinely top the list are those with ample resources of fresh and clean water.

In many other countries, there is not enough water, or even when there is water it is highly polluted or overused. Other water sources are used for recreational purposes, remediation and support of other forms of life. Untreated water is not safe to drink, and many countries suffer from a shortage of pure water, and insufficient quality monitoring and analysis. Worldwide, more than 800 million people drink unsafe water that has a higher potential of water-borne diseases (diseases of chemical or microbiological origin spread by water). The most common and highly dangerous are the diseases spread by bacteria. Examples of water-borne bacteria with a devastating effect on human health are *Clostridium botulinum*, *Campylobacter jejuni*, *Vibrio cholerae*, *Mycobacterium marinum*, *Shigella dysenteriae*, *Legionella pneumophila* and *Salmonella typhi*. Every water treatment system is required to effectively remove all these bacteria. The required treatment levels are so high that they are reported in log removal values (LRVs) defined in Eq. (3.8). However, in total the variety of bacterial parasites is too large and new microbial threats appear frequently. Water authorities are unable to track down every possible germ and the treatment efficiency is reported in the retention of indicative microorganisms. The ultimate indicative microorganism is *Escherichia coli*. A high concentration of *E. coli* or the presence of diarrheagenic *E. coli* is an indicator of polluted water.

In the last 20–30 years when ceramic membranes were started to be considered a match to polymer ones for community water treatment, their efficiency was checked in a number of studies. A complete retention of *E. coli* and 1.5–2.5 LRV retention of mesophilic bacteria were reported by Bodzek and Konieczny [218]. Simonis and Basson [219] reported LRVs of 5.5, 4.2 and 3.6 in lithium aluminium silicate ceramic membrane retention of *E. coli*, *Enterococcus faecalis*, and *Bacillus cereus*, respectively. Six LRV retention of *E. coli* was achieved with low-cost ceramic membranes made of kaolin and quartz [220].

The efficient removal of microbiological threat using ceramic membranes was extended to protozoa such as *C. parvum* and *Giardia lamblia*, as well as to viruses. The removal of protozoa, however, is not a difficult task – even in the cyst form the hydraulic diameter of protozoa is approximately double that of typical bacteria [221]. Indeed, the 4.3 LRV of *C. parvum* with 0.2 μm ceramic membranes [222] and complete removal of both *C. parvum* and *G. lamblia* with submerged 60 nm flat-sheet ceramic membranes [223] were reported in two separate studies. Viruses (that on average have a hydraulic diameter 100 times smaller than that of bacteria) were also tested. Current regulations require reduction of 4 LRV in concentration of viruses and mainly satisfactory results were reported. Clasen and Menon [224] reported more than 4 LRV of MS2 bacteriophage, a well-known surrogate for enteric viruses [225,226]. Ciora and Liu [227] reported more than 3-log removal of MS2 in large-scale ceramic membrane field tests. A 7.0 LRV of bacteriophage Qβ was reported in a combined application of ceramic membranes with flocculation [228]. Currently, the accepted paradigm is that ceramic membranes are providing the microbiological defence at the level required by health authorities. Ceramic membranes are fully competitive with polymer MF and UF membranes, and with granular filters. All low-pressure filtration options are only partially successful in retention of numerous other impurities including dissolved organic matter, suspended solids and salts. For example, the reported retention levels of total organic carbon (TOC) are between 40 and 80% [229,230], and turbidity retention is between 95 and 99%.

The expected population growth by 2030 is 25%, from the current 7 billion to 9 billion people. The expected water demand growth is 53%, more than double, from 4500 billion m^3 today (or 4500 km^3) to 6900 billion m^3 [231]. That is not because people are so thirsty – the usual drinking water demand of 1–1.5 litres per person per day is small compared with the agricultural boost that accounts for 70% of human usage of freshwater. Agriculture water demand will increase to 4500 billion m^3 by 2030. For example, global demand for meat is expected to increase by 50% by 2025, and double by 2050. Farm fish production is at a tremendous rise and the expectations are that by 2030 two-thirds of global food fish will be produced by fish farming. The aggregate agricultural production (all crop and livestock products) is expected to increase by 70% [232].

India (projected water demand of 1195 billion m^3 in 2030), sub-Saharan Africa (820 billion m^3) and China (420 billion m^3) will be the top three water-demanding regions in 2030. Water treatment systems in these regions are either non-existent or at the initial development stage. The developed world will have to provide solutions to the water treatment problems. And that is exactly where ceramic membranes can make a difference.

Water quality demands in many developing countries closely match those of the United Nations Health Organization. In a variety of different parameters, the most important are microbial pathogens. Note that their required retention level is lower than the standard in developed countries. For example, the US EPA Long Term 2 Enhanced Surface Water Treatment Rule (LT2 rule) requires a

6-log removal of bacteria, a 4-log retention of viruses, a 3-log retention of *G. lamblia* and a 2-log retention of *C. parvum.* This is higher than 2-log retention of *E. coli* and no reduction of viruses required by ABNT NBR 14908 and ABNT NBR 15176 standards in Brazil [233]. Even WQA ORD0901 suggested for developing countries requires 3-log retention for bacteria and viruses and no retention of cysts [234]. Ceramic membranes can easily match these requirements. In addition, the mechanical stability of ceramic membranes permits filtering at high fluxes, thus saving on the required total membrane area. The backwash can be performed with high velocities and using high air pressure to eject the backwash concentrate. Ceramics are intrinsically hydrophilic, an advantage in terms of required transmembrane pressure and removal of dissolved organics. Their chemical stability allows chemical cleaning with many different cleaning agents. This means that installation operators can use chemicals that are available locally, rather than the expensive cleaning solutions that are needed to preserve and avoid possible damage in the case of polymer membranes. Thermal stability allows running filtration experiments regardless of the feed water temperature and even performing membrane cleaning with boiling water [235]. The sustainability of ceramic membrane is in 'zero emission' as the spent modules will be used as ceramic products but not wasted [236].

Considering these advantages and the technical developments in membrane manufacturing and installation, several major water treatment companies and equipment suppliers have been showing increasing interest in ceramic membranes. That said, we feel that this interest is not for replacing current installations of polymer membranes, or in competition in developed countries. The interest is in on-the-shelf technologies available for a day to come when new installations will be needed.

Currently, there are several membrane manufacturers that offer ceramic membranes suitable for direct water treatment, albeit only one company has a proven record in installations and maintenance of ceramic membrane drinking water plants. That is Metawater Co. (Tokyo, Japan). As of now, the company has more than 100 installations in water treatment plants with a total daily flux of 486 400 m^3. The company started the industrial production of its modules in 1985 but until recently was active only in the Japanese water market. The biggest was the installation at Kawai Water Purification Plant (Yokohama Waterworks Bureau) with a daily capacity of 171 070 m^3. This all changed with a first contract signed in 2009 for drinking water treatment at the base of Rueter–Hess Reservoir at Parker Water and Sanitation District (Colorado, USA). The new water plant is capable of producing up to 37 850 m^3/day using 560 ceramic membranes. In all these installations, the company uses the third generation of their unique monolith membrane elements that comprise 2000 membrane filtration cells of 2.5 mm diameter [236]. Figure 4.22 depicts the Metawater ceramic membrane structure.

Several water treatment plants in Europe use Metawater membranes. The largest is at Andijk III (the Netherlands), a 120 000 m^3/day ceramic membrane plant with a CapEx of €60 million. Here Metawater membranes are incorporated

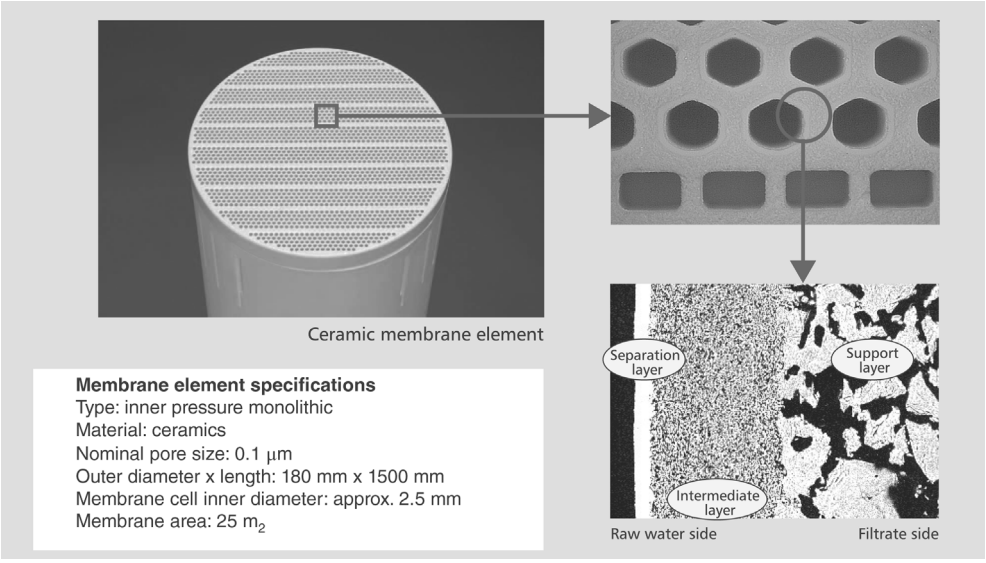


Figure 4.22 Ceramic membrane module structure. (Courtesy of Metawater Japan, Inc.)

in CeraMac® vessels developed by PWN Technologies [237] (Velserbroek, the Netherlands). The company claims that its special design that bundles 192 elements in a single vessel offers a considerable reduction in the investment cost due to less stainless steel required in construction and a smaller footprint. A similar set-up of Metawater membranes in CeraMac® vessels is currently tested at South West Water (southern England) for the treatment of 140 m^3 of surface water per day.

In addition to the above, there are several large water treatment companies and membrane manufacturers that have an available line of suitable membranes. Veolia Water that offers a line of microfiltration 'CeraMem' membranes made of silicon carbide (SiC) with pore sizes of 5, 50 and 200 nm, titania with pore sizes of 0.01 and 0.1 µm, α-alumina with pore sizes of 0.1 and 0.2 µm, and mixed oxide with a pore size of 0.5 µm is one example [238]. The membranes are capable of working at temperatures above 150 °C and TMPs of 10 bar. Kubota Corporation (Osaka, Japan) offers Kubota FILCERA® tank-submerged ceramic membrane filtration systems with a proven installation record in wastewater membrane bioreactors (MBRs). TAMI Industries (Nyons, France) offers CéRAM membranes with hydraulic diameters of 1.6, 2.5, 3.5, 4.6, 5.5 and 6 mm suitable for water treatment applications.

4.4.3
Low-Cost Ceramic Filters

Water problems appear mostly in countries that lie close to equator. Here the water shortage is accompanied by a high pollution of existing water sources and

is further aggravated by the consequences of a low personal income. According to some predictions, by 2030 one-third of the population concentrated in developing countries will live in basins with a water deficit larger than 50% [239]. Asia is another naturally water-stressed region where 60% of the world's population has an access to 28–30% of its freshwater. A full list of water-related conflicts that accounts for more than 300 events was published by the Pacific Institute [240]. Readers interested in more information can access the *Water Conflict Chronology*, an open-access web resource. Most of these conflicts are currently resolved by water-sharing agreements, and some even led to cooperation of conflicting sides in other areas.

Ceramic membranes can be used in two different ways to reduce the tension and even partially release water stress. Application of ceramic membranes can turn almost every water source into safe drinkable water. The problem is that the situation in the suffering countries is such that people suffer from hunger before they consider whether their water is drinkable. Half of the people in the developing world have health problems related to inadequate water and sanitation [241]. The few installations sponsored by the World Bank of Development will never match the population growth [242]. Another solution is to develop low-cost filters to filter the water at household level. That approach is currently gaining popularity as an immediate solution for suffering poor that takes nothing but a bit of time and effort. Out of 37 available options, low-cost ceramic filters are within the 5 best treatment options with a proven record in reducing turbidity and bacteria by more than 99% [243].

A number of studies performed in the last decade showed various degrees of retention of pathogenic microorganisms by low-cost filters. Dies [244] found more than 98% retention of *E. coli* by Katadyn filter, white clay LCF and Hong Phuc LCF. Sagara [245] reported 4.6 LRV of *G. lamblia* with Nepalese LCF. Lantagne [246] reported 4.3 LRV of *C. parvum* and more than 98% retention of *E. coli* with white clay LCF. Roberts [247], Duke *et al.* [248] and Hwang [249] reported a 94–99.9% retention of total coliforms and 88% removal of *E. coli* with white clay Nepalese LCF. Coulbert [250] found 99.8% retention of *E. coli* with LCF. McAllister [251] found 99% retention of bacteria and 20% retention of viruses with the filter designed by Potters for Peace (PFP), a Nicaragua-based non-government organization (NGO) that makes low-cost filters from clay by hydraulic pressing. Van Halem *et al.* [252] reported 3–6.8 LRV of *E. coli* and 3.3–4.9 LRV of *Clostridium* spores with ceramic silver-impregnated pot filters. Baumgartner *et al.* [253] found more than 99.8% retention of *E. coli* and 99.4% reduction in total coliforms. Oyanedel-Craver and Smith reported 97.8% retention of *E. coli* and less than 90% retention of viruses [254]. Brown and Sobsey reported 2.1–2.9 LRV of *E. coli* and 1–2 LRV of bacteriophage MS2 [243]. Simonis and Basson [219] were able to retain 5.5 logs of *E. coli*, 4.2 logs of *E. faecalis* and 3.6 logs of *B. cereus* using a low-cost filter made of lithium aluminosilicates. van der Laan et al. found LRVs of 2.1 for *E. coli* and 2.3 for total coliforms [255]. The average *E. coli* retention level found in 15 independent laboratory and field studies is therefore 2 LRV. True, this is low compared with the US EPA 6 LRV

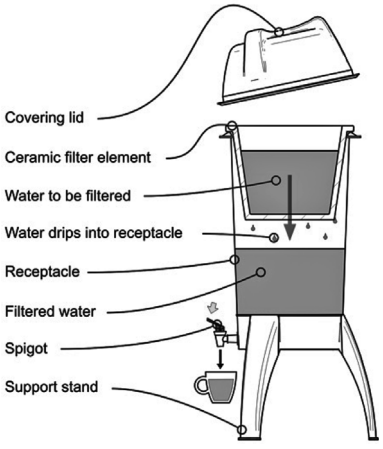


Figure 4.23 Cartoon of a low-cost ceramic filter system for home use where clean drinking water is hard to come by. The original work of Martin Bolton was found at http://opensourceecology.org/wiki/Vhembe_Water_Filter, accessed on December 5, 2015.

standard, but it sufficiently reduces the immediate microbial threat from drinking water.

Low-cost ceramic membranes made from a mix of locally available combustibles can be an interim answer to immediate microbial threats in rural communities in developing countries. The industrial manufacturing requires high degree of purity of raw materials such as α-alumina, γ-alumina, zirconia, titania and silica, to avoid cracking and channelling at sintering. These industrial membranes will always exhibit superior performance to those made at home. But the industrial membranes are expensive and their installation requires trained personnel. Low-cost membranes are available and may give the immediate answer to the most urgent microbial threats. A massive production of low-cost ceramic membranes started at the end of 1990s in Nicaragua by Potters for Peace, a NGO that supports potters in Latin America. The PFP idea is to develop a low-cost ceramic filter from available materials and train locals to produce it (see Figure 4.23). For the last 20 years, the concept has been accepted in the entire Latin America and parts of Africa and the Middle East [256]. There are 35 factories in 18 countries worldwide now that produce low-cost filters [257]. More than 4 million people use them [255].

During that period, the ceramic filters were made of apatite powder [258], fly ash [259], natural clay [260,261], dolomite [262] and kaolin [263]. Apparently, kaolin is the inexpensive raw material that can ensure a stable repeatable formation of low-cost filters [264]. The initial slurry is therefore made of kaolin with addition of quartz and other chemicals such as calcium carbonate, sodium carbonate, boric acid and sodium metasilicate [265]. An alternative process might use a mix of local terracotta clay and sawdust or other combustibles, such as rice husk readily available almost everywhere in the world. The filters are typically made by pressing to a final form of pot [266].

The formed filter is sintered at about 860 °C and tested for the flow rate. Filters that meet the flow requirements of 1.5–2.5 l/h are coated with colloidal silver when available. The silver is considered to be a disinfectant although a recent study suggests that silver does not play a dominant role in inactivation of microorganisms [255]. The life expectancy of a low-cost filter is 2–3 years if properly maintained. The typical cost per filter is only $15–25, and that investment (considering countries with daily income below $1.25) is returned by way of fewer sick days and lower medical expenses. Replacement clay filters will cost $4–6. A study in Cambodia showed that the use of low-cost filters decreases the frequency of diarrheal diseases by 54% [267]. Those membrane features found during initial trials built the current definition of low-cost ceramic membranes. Currently, low-cost filters have to be accessible (manufactured in the community), ensure 2 LRV of *E. coli*, have a flow rate between 1 and 3 l/h, have a life expectancy between 1 and 2 years [268].

Despite this bright forecast future for low-cost filters, they do have one major disadvantage: none of them can reduce the concentration of viruses. A multibarrier approach, including also the addition of free chlorine, is one possible (albeit more complex) solution to the water pollution problem in developing countries. The chlorine can be distributed as a formulated compound, in a tablet or powder form. One such example is *PuR* and *WaterGuard* tablets distributed by PACE (Program for Accessible Health, Communication and Education) in Uganda [269].

4.4.4 Treating Additional Pollutants

The invention and fast progress of new analytical tools and their implementation in water analysis increased our ability for detecting compounds in water tremendously. Suddenly it turns out that water contains not just humic and fulvic acids that are a bunch of organic molecules, proteins and polysaccharides [270]. These include pharmaceuticals and personal care products (PPCPs), endocrine disruptive compounds (EDCs) and halogenated organics. Many of them cannot be treated by current water and wastewater treatment systems, and have a proven negative effect on human health. A few of these molecules, such as bisphenol A, belong to the 'aristocratic club' shown in Figure 4.24.

The list of PPCPs alone contains more than 1000 compounds, and it is growing. A separate list of EDCs – chemical agents that interfere with the functioning of natural hormones in human body – includes steroid hormones, alkylphenols, phthalates and phytoestrogens. That group contains up to 400 compounds although it somewhat overlaps with PPCPs. Halogenated organics such as carbon tetrachloride, dichloroethane, dichloroethylene, bromodichloromethane and bromoform are carcinogenic. They are present in the water due to the chlorination applied ultimately to drinking water before its distribution to final users. Whether these molecules actually affect the human health and the biota is still a

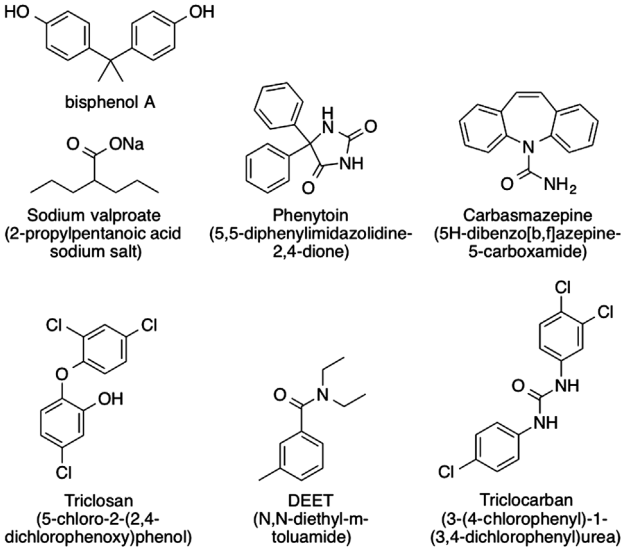


Figure 4.24 Molecular structures of some of the most notorious chemical contaminants in water.

moot point, but there is already enormous societal pressure to limit their presence in drinking water.

Currently, there are no complete technological options for dealing with the light organics fraction pollutants. One of the options that is gaining popularity is a combination of membrane treatment with the so-called *advanced oxidation process* (AOP). The membrane physically retains particles, and then the AOP chemically decomposes the low-MW pollutants. This decomposition is done by releasing hydroxyl ($OH^{\bullet}$) radicals [271]. Hydroxyl radicals are highly reactive (and therefore unselective) oxidizing agents that can cause the decomposition of many organic compounds including PPCPs and EDCs. However, these radicals also attack and decompose the polymer membranes, creating an opportunity for ceramic membranes, which are impervious to radical oxidation. This combined solution is relatively new, and is not yet applied in industrial installations. Nevertheless, the application potential of combining the advantages of ceramic membrane with AOP is high, and we will discuss more on it in the next sections.

4.4.5
Membrane Distillation

Distillation is one of the most known and widely implemented separation techniques. In this process, a liquid from a mixture or from a suspension is selectively evaporated and condensed. The selective evaporation becomes possible due to differences in the volatilities of mixture's compounds. There are two phase-changing steps in the process, and these are performed in different

reactors when the vapour is transferred from an evaporator to a condenser. As a result, a liquid is removed from the evaporator and 'reappears' in the condenser. A complete disappearance/appearance cycle yields practically pure liquid, whereas partial distillation results in a pure liquid and increased concentration of compounds in the liquid mixture.

Industrial distillation is typically performed in large, vertical cylindrical vessels known as distillation towers or distillation columns. The energy costs and capital input required for industrial distillation are typically very large, often accounting for over 60% of the CapEx of a chemical plant and over 50% of its energy demands. Yet practically every chemical plant uses distillation towers [272]. Many attempts have been made to alter the conventional distillation and decrease its high energy demands. One of the successful alterations is called *membrane distillation* (MD) – a process where the evaporator and the condenser are divided by a membrane. Membrane distillation is more energy-efficient than conventional distillation, as it requires only partial vaporization of the transferred liquid. A lyophobic porous membrane is prone to penetration of a liquid unless the transmembrane pressure is higher than the membrane liquid entry pressure. The latter is the minimum hydrostatic pressure to be applied on the feed liquid to overcome hydrophobic forces of the membrane [273]. The liquid transport through the membrane can be summarized into three consecutive steps [274]:

1) Formation of a vapour gap at the hot feed solution–membrane interface.
2) Transport of the vapour through membrane pores.
3) Condensation of vapour at the cold site of the membrane.

Note that no capillary condensation takes place inside the pores. Only vapour is transported through the membrane [275]. This vapour is then condensed to a pure liquid over a cold surface on the permeate side.

There are four different types of membrane distillation. These differ in the manner in which the vapours are condensed on the permeate side. The system where the permeated vapour is condensed over a 'cold trap' inside the module after crossing an air gap is called *air gap membrane distillation* (AGMD). Similarly, a system where the cooling solution is in a direct contact with the permeating side of the membrane is called *direct contact membrane distillation* (DCMD). In *vacuum membrane distillation* (VMD), the vapour is carried by vacuum out of the system and collected outside of the module. Finally, in *sweeping gas membrane distillation* (SGMD), a carrier gas sweeps vapour out of the system for a further condensation by cooling. The driving force in different configurations varies. In VMD, the driving force through the membrane is the vapour pressure on the permeate side. In SGMD, the vapour is carried through the membrane by the sweeping gas, while in AGMD and DCMD the vapour passes through due to a partial vapour pressure difference on both sides of a membrane. Figure 4.25 depicts the four types of membrane distillation. A detailed discussion of the pros and cons of each configuration is published elsewhere [273].

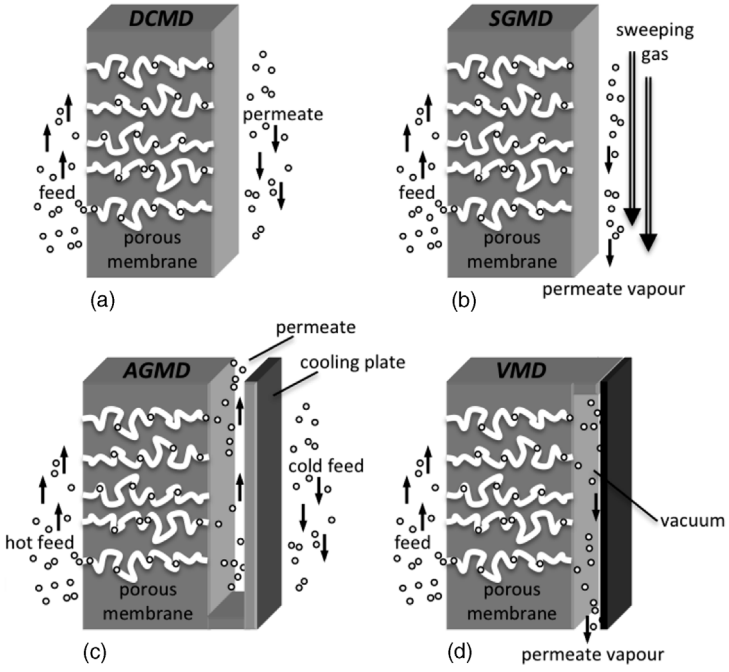


Figure 4.25 Membrane distillation configurations: DCMD (a), SGMD (b), AGMD (c) and VMD (d). The four types of membrane distillation set-ups differ in the way in which the vapours are condensed on the permeate side.

Despite the differences in the driving force, all four schemes have one thing in common: The higher liquid temperature in the evaporator results in more vapour that passes through a membrane at a higher flux. There is therefore a significant interest in performing distillation at a high temperature gap between feed and permeate, usually by increasing the feed temperature towards 100 °C. Membrane distillation was tried already some 50 years ago, but with little commercial success. The boom in reverse-osmosis desalination as an energy-saving alternative kept membrane distillation on the sideline for many years. However, today there is a renewed interest in membrane distillation as a green alternative to reverse-osmosis desalination. It turns out that distillation, unlike RO desalination, can be partially powered by solar energy, waste heat, geothermal energy or other alternative energy sources. Today, the two dominant seawater desalination technologies are RO and multistage flash distillation (MSF). Together, these two account for approximately 90% of the market share for desalination worldwide. MSF (which has a market share of about 25%) is much more energy-intensive, requiring 25–40 kWh/m^3 water produced. Conversely, RO consumes only 1.5–7 kWh/m^3 water produced. The predicted energy consumption for membrane distillation is 22–67 kWh/m^3 [276]. At first glance, this places it way behind RO and can at best be comparable to MSF. But that snap

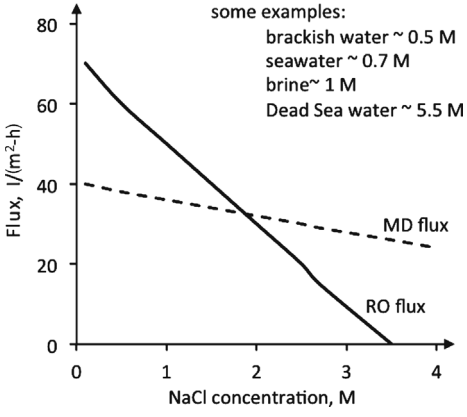


Figure 4.26 Flux as a function of salt concentration for hypothetical RO and MD modules (the effects of salt precipitation are ignored in both cases). (Concept drawn after Ref. [277].)

judgment changes when we look at Figure 4.26, which illustrates how MD treats brine and solutions with increased salt concentrations.

Looking at Figure 4.26, we see that the transmembrane flux through RO membranes drops towards zero when the molar concentration of NaCl in the feed approaches 3 M. But this concentration (and even higher concentrations) of NaCl has no influence on the flux in the case of MD. Although the figure shows empirical data, it highlights an important conceptual difference. The RO method can work well under limited salt concentrations due to concentration polarization effect and increased TMP. The RO desalination is also considered an operation with high OpEx due to the need to maintain high operational TMP. This high TMP is needed to overrule osmotic pressure that increases with salt concentration. Conversely, MD has no such limitations and can (theoretically) result in a brine that is 100% salt. This feature is extremely useful and advantageous in desalination of brine and treatment of highly concentrated aqueous solutions in industry. In addition, MD does not produce waste and therefore its OpEx is free of brine disposal costs. It can be performed in a single stage, with 60 °C on the feed side and 20 °C on the permeate side, because it is not necessary to heat the process liquids above their boiling temperatures. The gap between temperatures on the feed and permeate can be as low as 20 °C [273]. Indeed, some applications, such as stripping of volatile compounds from aqueous solutions, can be run even without heating the feed side at all. Such cases are known as *isothermal membrane distillation*.

The possible implementations are not limited to seawater and brackish water desalination, but also include MBR wastewater treatment [278], cold purification of fruit juices by osmotic distillation, rectification of bioethanol and purification of shale gas and shale oil [279]. MD can be applied in treatment of nuclear waste and radioactive water that require a very high rejection rate of certain components [273]. All these applications utilize one core process – purification or

separation of water. The need to repel water by membrane pores requires hydrophobic membranes, and this demand is opposite to the usual need for hydrophilic membranes. There are some hydrophobic polymers such as polytetrafluoroethylene (PTFE), polypropylene (PP) and polyvinylidene fluoride (PVDF) that are currently used in low-temperature MD, but these polymer membranes have limited thermal and chemical stability. In addition, polymer membranes have large pore size distribution that might result in various scenarios from low flux to pore wetting. An acceptable pore size range for MD application is between 100 nm and 1 μm [280].

Recent reports expand on the interest to modify ceramic membranes in order to increase their hydrophobicity. Modifications in the form of chemisorption result in the formation of hydrophobic surfaces, such as the chemisorption of alcohol to γ-alumina membranes that results in the formation of alkoxide surface groups that are stable up to 200 °C [281]. Chemisorption is a desirable modification that helps avoid weakly bound surface layers that can potentially be removed by scouring or other physical means [282]. Leger *et al.* modified alumina membranes using trichlorooctadecylsilane and polydimethylsiloxane, and found that the modified membranes are thermally stable up to 300 °C [283,284]. Other modifications included grafting via soaking of organochlorosilanes on mesoporous γ-alumina [285], of fluoroalkylsilanes on zirconia membranes [286], of fluorodecyltriethoxysilane on zirconia, alumina and aluminosilicate [287], of fluoroalkylsilanes on alumina hollow fibres [288] and of perfluoroalkylsilanes on tubular and planar TiO_2 ceramic membranes [288]. The first desalination experiments with hydrophobic ceramic membranes were performed in 2004 [289]. Since then, several hydrophobic ceramic membranes were successfully applied for MD water desalination. Reported salt rejections were above 95% yet fluxes are quite low [287,290,291]. With a temperature gap of 90 °C, the reported fluxes were 6.5 and 6.7 LMH in both VMD [289] and AGMD [292] configurations. A flux through 200 nm alumina Anodisc™ membranes (Whatman, UK) in DCMD configuration was even lower and varied between 2 and 3 LMH [282].

A recent promising strategy is to provide drinking water using solar-powered membrane distillation systems in rural areas of countries with extremely high water stress. Examples include Namibia, Canary Islands and Mexico. Two prototypes of compact solar-powered desalination units have been tested. The first is designed to produce 100–120 l/day from seawater or brackish water. The required thermal energy is supplied by a 6.5 m^2 solar thermal collector field, and the electrical energy is supplied by a 75 W PV module [293]. The system is designed to serve areas with undeveloped infrastructure. The second is a two-loop system with a daily capacity of 2000 l. That system already required collector area of 225 m^2, although the trials are to use 100% solar power or to combine it with waste heat. In both cases, no additional source of electricity is needed. The systems are being developed and marketed by the Solar Spring GmbH, a spin-off company of the Fraunhofer Institute for Solar Energy Systems.

4.4.6 Pervaporation

Pervaporation (a combination of permeation and evaporation) helps to remove water to receive pure organics, or organics to purify water. It is best applied when the feed contains mainly retentate and small concentration of the permeate. If the feed is rich in permeate, a number of membrane stages may be needed. Even when one stage is sufficient, the feed may be heated before membrane filtration [294]. The feed usually contains mainly organic liquid and water is considered here the impurity. In that case, the selective transport of the impurity through the membrane minimizes OpEx due to removal of unwanted water out of the site. That type of separation is called dehydration. When the feed contains almost equal amounts of organic liquid and water such as water–pyridine with 41.3% water, pervaporation is applied for separation into permeate water-rich and retentate pyridine-rich streams that are further separated by distillation [295]. The selective separation of water prescribes the use of hydrophilic membranes that will selectively take up water molecules and repel organics. The previous limited use of hydrophilic ceramic membranes in membrane distillation becomes an advantage here.

Although pervaporation may look very similar to membrane distillation, there is a basic difference between the two. In membrane distillation, the vapour itself diffuses through the membrane. Conversely, in pervaporation the liquid diffuses through a membrane and then evaporates (see the schematic in Figure 4.27). During the pervaporation process, a liquid in contact with the membrane pore on the feed side travels through the pores to the permeate side and evaporates as a vapour at the permeate side of the membrane. This vaporization is due to a low vapour pressure on the permeate side. The low partial pressure is achieved

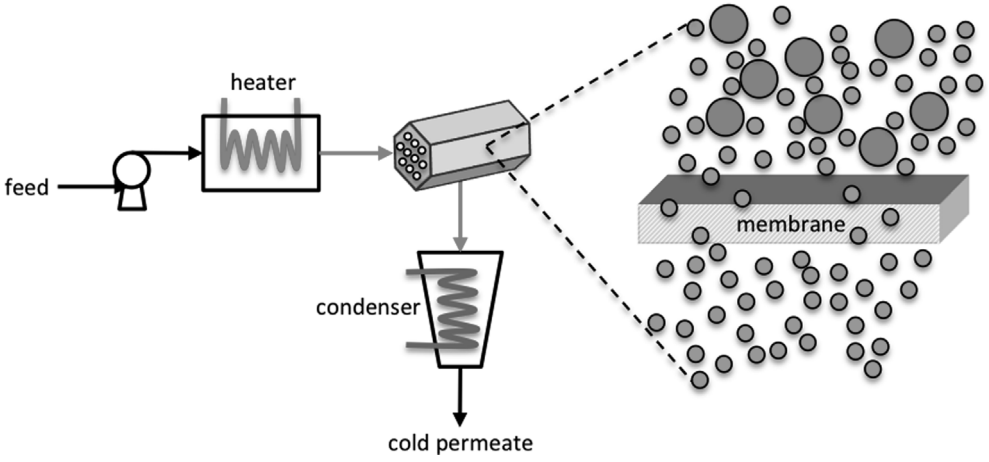


Figure 4.27 The key principles of pervaporation.

by employing a carrier gas or by using a vacuum pump [296]. Vaporization might occur near the membrane inside the membrane support. In that case, the membrane operates in liquid- and vapour-phase zones.

Whereas in membrane distillation the advocates of ceramic membranes struggle to find how to turn ceramics into applicable membrane material, in pervaporation the ceramics are the state of the art. Indeed, in many cases of pervaporation ceramic membranes are the only feasible separation material. That is not only due to the intrinsic hydrophilicity of ceramic material, but also a function of the membrane pore size. This is crucial for selective separation of water and organics when both molecules are approximately 1 nm in size [296]. Membrane supports with very large pores make the formation of selective top layer difficult. In addition to membrane hydrophilicity, the size selectivity at that stage helps to receive a selective dissolution of water molecules in membrane pores and therefore the chemical potential gradient for the mass transfer. At the second stage, the dissolved species diffuse along the membrane pores. Different species will have different affinity to the membrane material, and usually also different molecular weights, resulting in different diffusivity coefficients. An additional differentiation occurs at that stage. At the third stage, the diffused species evaporate at the permeate side of the membrane. This stage is usually the fastest, so the pervaporation rate is limited by former sorption and diffusion steps [297]. The process is much more complex than a simple vaporization and results in permeate whose composition is significantly different from that expected in membrane distillation. In that three-stage solution-diffusion process, the intrinsic hydrophilicity and sharp pore size distribution make ceramics (especially zeolites and silica) very popular membrane materials.

The concentration on separation of water/organic mixtures is not the only application of pervaporation. It was an easy start into the pervaporation field that can be subdivided into aqueous and non-aqueous applications. The aqueous applications include dehydration – removal of water from organic solvents such as chlorinated hydrocarbons and alcohols (ethanol, butanol, *i*-propanol) – and removal of volatile organic compounds from water. The separation of non-aqueous mixtures includes polar/non-polar separations of methanol/toluene, ethanol/hexane and methanol/methyl *t*-butyl ether (MTBE), aromatic/aliphatic separations of cyclohexane/benzene and hexane/toluene, and separation of isomers such as *o*-xylene, *m*-xylene, *p*-xylene, styrene and ethylbenzene [296]. Pervaporation can be a very selective option for separating azeotropic mixtures or species with close boiling points. These mixtures are very common in the chemical and petrochemical industries and are separated by azeotropic distillation, extractive distillation or adsorption over molecular sieves [297] or over MOFs [151]. A careful choice of pervaporation membranes promotes the single-stage efficient selective separation approach. One of the most successful commercial applications of pervaporation is the dehydration of ethanol with NaA zeolite membranes that according to Lurgi saves over 50% of the energy compared with conventional distillation [298]. As a low-heat option, pervaporation is used in food processing and cosmetics, especially in the recovery of

heat-sensitive compounds such as flavours and fragrances [299,300] as well as fermentation products [301,302]. Since pervaporation is a modular membrane process, it can easily be coupled with other separation processes such as distillation [303] or chemical processes such as esterification [295].

Pervaporation can therefore be considered as the energy-saving variation of membrane distillation, especially for extracting minor compounds from liquid feed streams. The term itself was first coined by Kober in 1917 [304]. Pervaporation can be employed almost in any liquid–liquid separation process. Among the most popular processes are industrial dehydration of alcohol and chlorinated hydrocarbon from water [305,306] and separation of organic–organic mixtures [307,308]. Today, there are a number of commercial pervaporation plants that run processes for recovering solvents, removing organics from wastewater and even the dealcoholization of wines. The largest ethanol dehydration plant worldwide (in Betheniville, France) has a capacity of 150 000 l/day, or roughly 35 ktpa [272]. That application was initially developed with polymeric membranes. However, these were soon abandoned due to their lack of chemical resistance to organic solvents. Ceramic tubular membranes made of microporous silica and zeolites with their excellent chemical resistance as well as high thermal and mechanical stability were more suitable [308].

The main advantages of zeolites in pervaporation applications are their extremely high separation selectivity and high permeate fluxes. Both features are attributed to hydrophilic interactions of zeolites with water and the narrow (about 0.4 nm) uniform pores that enable molecular sieving between water and organic solvents [309]. These higher fluxes can be partially explained by the absence of swelling (which occurs with polymer membranes). The water flux, estimated by the difference in weight of water in the feed and in the condensed permeate per unit of membrane surface per unit time, can exceed 10 kg/(m^2 h). This is two orders of magnitude higher than that of organic polymer membranes used for dewatering. Recently, the Hitachi Zosen Corp. reported a 50 kg/(m^2 h) water flux through a new A-type zeolite membrane with water permselectivity of more than 1000 and ethanol/water mixture of 90/10 (w/w) [310]. A separation factor of more than 10 000 was reported in the dehydration of ethanol at a Mitsui Engineering & Shipbuilding (MES) factory in Japan. The factory produces 530 l/h of dehydrated alcohol with water content of 0.2%. Impressively, the feed for that process contains 10% water. The pervaporation is performed with 20–30 μm thick NaA zeolite membranes coated on tubular ceramic supports [311]. This is a highly hydrophilic zeolite due to its low Si/Al ratio, with 0.41 nm pores. The pore width is larger than the kinetic diameter of water but smaller than many alcohols. The same MES company has built six large-volume pervaporation plants for dehydration of biomass ethanol in Europe [312]. Each module is composed of 550 zeolite NaA membrane elements that can produce 5000 l of dehydrated ethanol per day. The German company Fraunhofer IKTS installed a 120 m^2 demonstration plant for bioethanol drying [313]. Another five plants were built by the German consortium GFT Membrane Systems GmbH Homburg/Saar [314]. There are several companies that currently offer pervaporation membranes for

the industrial market. In addition to MES, zeolite A membranes are offered by Mitsubishi and Inocermic. Other companies that currently manufacture zeolite membranes are GFT Membrane Systems GmbH (Germany), UOP (United States), Buss-SMS-Canzler GmbH (Germany), HITK (Germany), Tekhinservis (Ukraine), Kühni (Switzerland) and Hitachi Zosen (Japan). Silica pervaporation membranes are offered by Pervatech and Sulzer Chemtech.

The highest efficiency is obtained when there is a perfect match between the zeolite membrane and the mixture. A separation in the same mixture with another membrane is much less efficient. Table 4.10 details permeation and selectivity of zeolite and silica membranes in separation of water/organic and organic/organic mixtures.

Table 4.10 Performance of NaA and NaY zeolites in separation of water/organic and organic/organic mixtures.[a)]

Zeolite	Feed	Temperature (°C)	α	Flux (kg/(m^2 h))	Reference
NaA	Methanol/	50	2100	0.57	Xu *et al.* [315]
	water	105	5700	3.50	
	Ethanol/water	75	10 000	2.15	
	2-Propanol/	105	30 000	4.53	
	water	75	10 000	1.76	
	Acetone/water	50	5600	0.91	
	Dioxane/water	60	9300	1.87	
		105	8900	7.80	
NaA	Ethanol/water	95	>5000	2.35	Kondo *et al.* [316]
Mitsui A/Mitsui T	Ethanol/water	70	18 000	1.12	Sommer and
	Ethanol/water	70	1000	0.91	Melin [317]
ECN silica	Ethanol/water	70	350	1.6	van Veen *et al.* [318]
NaY	DMF/water	60	8700	0.95	Xu *et al.* [315]
	Ethanol/water	75	130	1.59	
	Methanol/	60	3800	0.93	
	benzene	60	5300	1.70	
	Methanol/	105	6400	2.13	
	MTBE	150	600	2.59	
	Ethanol/	60	930	0.22	
	benzene	60	1000	0.27	
	Ethanol/	50	1200	0.21	
	cyclohexane				
	Ethanol/ETBE				
	Benzene/*n*-	65	7	0.02	Startin and
	hexane	105	29	0.05	Elliot [319]
	Benzene/	150	18	0.21	
	cyclohexane	105	45	0.007	
		150	41	0.01	

a) Data from Ref. [320] unless otherwise noted.

The NaA zeolite membranes were found to be very effective in water/ethanol separation, while NaY zeolites showed excellent performance in the separation of organic binary mixtures. However, NaA membranes are unstable at high temperature or in the presence of organic acids. Increasing the Si/Al ratio of the zeolite can enhance its thermal and acid stability, but it also increases hydrophobicity. Zeolite membranes with medium Si/Al ratio such as T, CHA, mordenite and ZSM-5 are more appropriate for dewatering of organic acids. In general, the separation of lipophilic mixtures is less successful due to the hydrophilic character of these zeolites. Organoselective zeolite membranes successfully separated the MeOH/MTBE mixture [321,322]. The zeolite membranes were more selective, but gave lower fluxes compared with the polymer membranes. The scope of ceramic membranes available for pervaporation is constantly increasing. Today, more than 20 zeolite structures are used, including mordenite, ZSM5, silicalite-1 and SAPO-34 [308].

Silica membranes are less selective than zeolite membranes but in certain applications they can have higher permeate flux. For example, the membrane area needed for dewatering of ethanol with silica membranes is 10 times lower than the area needed for dewatering with polymer membranes [318]. However, full-scale implementations of silica membranes are rare, due to the higher cost of the membranes and suboptimal module design [323]. One interesting development in this field is the invention of hybrid silica, or HybSi [285,324–327]. Invented jointly at the University of Amsterdam, University of Twente, Pervatech and ECN, HybSi has been commercialized through the ECN and showed excellent results in dehydration experiments with a membrane that exhibits high hydrothermal and chemical stability. The potential of HybSi membranes for separating organic mixtures is yet unexplored.

Another field of application that is gaining interest is the recovery of valuable products from fermentation broths and their downstream purification. Biofuel such as bioethanol is one example. The dehydration of acetic acid is another. Acetic acid (CH_3COOH) is produced as a precursor to cellulose acetate and polyvinyl acetate by either methanol carbonylation or oxidative fermentation. The carbonylation occurs in three steps:

$$CH_3OH + HI \rightarrow CH_3I + H_2O \tag{4.16}$$

$$CH_3I + CO \rightarrow CH_3COI \tag{4.17}$$

$$CH_3COI + H_2O \rightarrow CH_3COOH + HI \tag{4.18}$$

The oxidative fermentation is performed in one step by acetic acid bacteria *Acetobacter* from a variety of alcohol-rich foodstuffs. This bacteria basically catalyses the aerobic oxidation of ethanol to acetic acid:

$$C_2H_5OH + O_2 \rightarrow CH_3COOH + H_2O \tag{4.19}$$

Both of these pathways give stoichiometric amounts of water that must be removed. Traditionally, the dehydration was performed by distillation [328]. But that process is far from perfect due to high CapEx associated with the large

number of trays needed in the distillation column to perform the separation [329]. Additional drawbacks of distillation in this case are low separation efficiency, because the feed typically contains 15–40% impurities. Pervaporation is considered a valuable alternative. Polymer membranes are less suitable for this application as they possess limited solvent, thermal and mechanical stability [322]. The latter is important since carbonylation is performed at both elevated temperature (~190 °C) and pressure (~28 bar) [330]. Polymeric membranes also suffer from swelling, which can change the membrane structure and properties significantly [329].

Zeolite membranes are seen as the future of pervaporation. Despite technical difficulties and high investment risk, many chemical plants are considering switching to pervaporation. The estimated reduction in the energy demand compared with conventional distillation exceeds 70% [310]. Among already available and proven zeolites, the market offers type A and type T NaA zeolites, manufactured by Mitsui Engineering & Shipbuilding Co. The membranes are available on the European market under a cooperation agreement with Sulzer Chemtech and are recommended for dehydration of alcohols. Another ceramic membrane manufacturer, Pervatech (Rijssen, the Netherlands), offers a variety of silica membrane modules based on single-channel and four-channel ceramic elements of 0.25–1.2 m length and 0.005–1.9 m^2 membrane surface. The core applications of this company's membranes are in dehydration processes: solvent drying, breaking of azeotropic mixtures and enhancing chemical condensation reactions in aggressive environments. Another manufacturer of NaA zeolites, Inocermic GmbH (Hermsdorf, Germany), intends its membranes for dewatering processes such as production of bioethanol. Core Inopor NF ceramic membranes are thermally stable up to 200 °C, stable at pH 2–12 at temperatures higher than 40 °C and stable at any pH at temperatures below 20 °C. The membrane support layer is built of available α-alumina and coated with TiO_2 of cut-off ranges of 350 and 750 Da, and SiO_2 of 600 Da. The water content in retentate organic solutions can be as low as 0.1% in feed solutions with 90% ethanol. Water fluxes at 100–120 °C pervaporation are 7–12 kg/(m^2 h), with a water/ethanol separation factor above 1000 [331]. This company reported that their standard four-channel 1.2 m modules are used in a number of industrial bioethanol pervaporation plants with 30 000, 60 000, 80 000, 100 000 and 200 000 l/day capacity. The plants are built in cooperation with GFT Membrane Systems GmbH [332].

A recent estimate of Sulzer Chemtech, a leading supplier company of pervaporation plants and equipment, reckons that there are more than 250 pervaporation plants worldwide [333]. Nearly 90% of these plants are used for dehydration of ethanol or isopropanol.

The average pervaporation process is 30–40% cheaper on operating costs (OpEx) compared with azeotropic distillation on the same scale. Sulzer Chemtech showed that in an ethanol plant incorporating a pervaporation unit between the two first distillation towers increased the production capacity by 40% [334]. The costs in a parallel installation (also operated by Sulzer Chemtech) were reduced dramatically: CapEx by 28% and OpEx by 40% [303]. Another industrial

example is the dehydration of isopropanol. By volume it is second only to ethanol as a pervaporation process. A cost estimate shows a production capacity increase of 35% and an annual energy savings of €960 000 [333].

4.5 Cleaning of Wastewater with Ceramic Membranes

Proper water supply and wastewater removal is the key for a better future. This was true at the time of the Roman Empire and it is still very true today. According to the World Resources Institute [335], there are already 37 countries in the world that face 'extremely high' levels of water stress. This term means that more than 80% of available water is used annually and the depleting water resources put the entire region under a high-risk level of water scarcity.

Dealing with water stress means either increasing available water sources or decreasing water demands. The water supply is increased by desalination of sea and brackish water, and by reuse of treated wastewater. Decreased water demand is an interim solution for countries with decreasing population or when the water demand is larger than available water resources by no more than 10%. Water demands are decreased by water saving, saltwater agriculture on coastlines, hydroponics, aquaponics, increasing vegetarianism and decreasing water leakage in pipes. Additional methods include drip irrigation [336,337], use of rainwater, watershed management, seawater greenhouse and precision agriculture.

Wastewater treatment therefore can both increase available water resources and decrease water demands. Wastewaters flowing back to adsorbing water bodies are the future water sources. Untreated wastewaters bring many of waterborne diseases back to the water intake point and severely worsen feed water quality. About 80% of diseases in the developing world are water-related, and most are due to inadequate sanitation. At least 1.8 million children under 5 years of age die every year due to consumption of unsafe water.

4.5.1 Membrane Bioreactors

Membrane bioreactors are a combination of biological treatment with membrane separation that comes to replace the conventional wastewater treatment [338,339]. Some 30–40 years ago, the treatment became a necessity and a number of technologies had been developed. Total organic matter in wastewater is measured by TOC or by two indirect methods that are on the market for a long time. Those are biological oxygen demand (BOD) and chemical oxygen demand (COD) that measure the concentration of oxygen consumed biologically or chemically to oxidize the organic matter in wastewater. These technologies addressed municipal streams, the largest pollutant by volume. A biological treatment is also very widespread in industries that produce wastewater with high organic content. The high efficiency of biological treatment is in almost

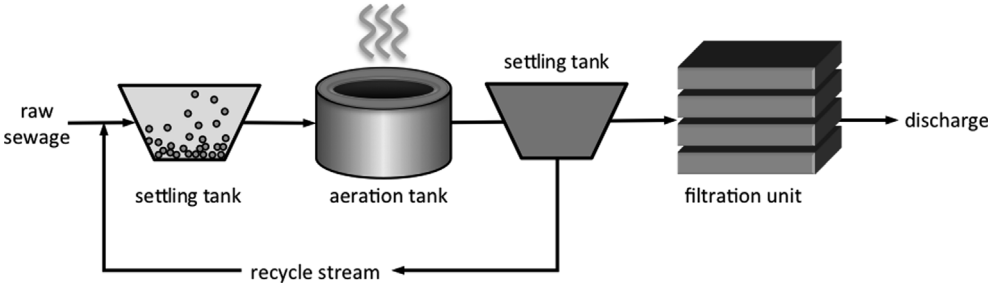


Figure 4.28 A conventional wastewater treatment scheme by activated sludge.

complete mineralization of large organic molecules, that is their conversion into CO_2, H_2O and inorganic nitrogen products. Essentially, the biological treatment is the biodegradation of biodegradable organic matter within wastewater by a commune of microorganisms that are kept within a bioreactor. The microorganisms can be aerobic (oxygen-dependent) or anaerobic (oxygen-independent). Figure 4.28 presents a conventional municipal wastewater treatment scheme.

The treatment contains the stages of pretreatment or screening of gross solids, primary treatment or sedimentation of settleable solids, secondary treatment or bioreactor, and tertiary treatment. The tertiary treatment aims at preventing the pollution of receiving water bodies and was initially performed by disinfection. Current tertiary treatments include slow and rapid sand filtrations, membrane filtration (MF, UF or NF), ozonation, chlorination and UV radiation. The continuous functioning of a bioreactor requires a constant biomass that is assured by its separation from secondary effluents. In fixed film processes, the separation is fairly easy, as biofilm grows on filter media and stays attached to it. In activated sludge processes, bacteria are suspended within the media and are separated from effluents by sedimentation of bacterial flocs and gentle decantation. In the latter process, the bacteria should grow up to a size that allows their precipitation. Hence, the bacteria must be retained in the bioreactor for a certain solid retention time. The solid retention time is usually several days and that affects the dimensions of bioreactor. Using MBRs eliminates the need for retention time. The separation is performed by membranes with pore sizes less than 0.1 μm, significantly smaller than the smallest bacteria within the reactor. The MBR thus effectively produces clarified effluent that contains no microorganisms, reduces the size of the bioreactor and increases its efficiency. A separate class of MBRs is a replacement of trickling filters where membrane serves as a growing medium for anaerobic bacteria. The anaerobic degradation of complex organics to methane and carbon dioxide inside anaerobic MBRs (anMBRs) offers a number of advantages over aerobic MBRs. Anaerobic treatment generates less waste sludge. Nutritional requirements are low. A biogas is produced [340]. However, the biomass growth rate is relatively low, the CapEx of anMBR is higher than that in an aerobic MBR, the operation is more complex and anMBR is not effective in removal of residual levels of soluble and colloidal organic content [341].

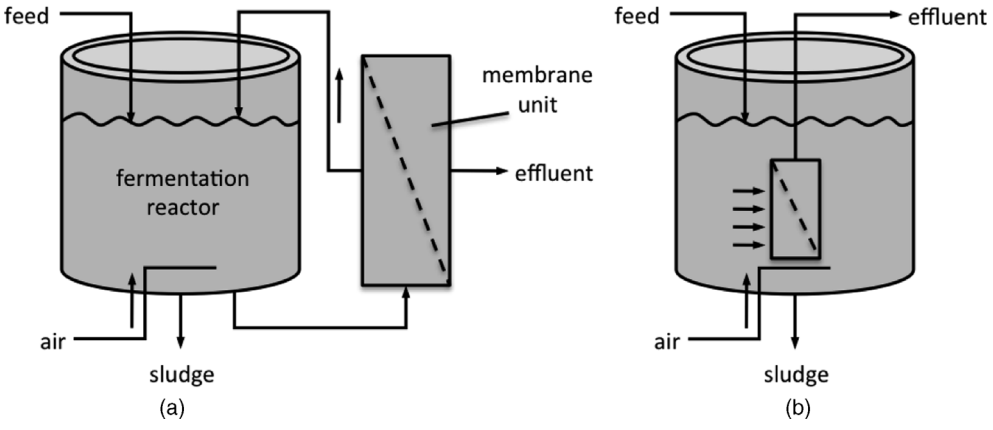


Figure 4.29 Pressure (a) and vacuum (b) MBR configurations.

Depending on the membrane location, two MBR configurations exist. The first is when the membrane is immersed within the aerated reactor and the clarified effluent is soaked out by a vacuum pump. The submerged MBRs use hollow-fibre and flat-sheet membrane modules. The second is when the membrane is placed outside the bioreactor and the separated biomass is returned to the bioreactor by external circulation. That external or side stream process enjoys the possibility to apply pressure, thus intensifying the process. That application is often performed with tubular membranes. In either arrangement, membranes are mounted in cassettes or modules. Figure 4.29 presents schematically both vacuum and pressure MBRs.

The external circulation is a better process in terms of process intensification, membrane flow and control over biomass recycling to/from the bioreactor. It suffers, however, from high energy demand and therefore high OpEx. The immersed MBRs were developed to reduce the MBR cost. They currently lead the MBR technology, particularly in municipal wastewater treatment. To minimize the fouling, immersed membranes are under constant cleaning performed with air bubbles directed parallel to the membrane surface. The aeration serves as shear, reducing the thickness of fouling layer and facilitating the oxygen transport to bioreactor's bacteria.

The first MBR was developed commercially by Dorr-Oliver in the late 1960s. This MBR used flat-sheet UF membranes and operated with excessive 3.5 bar pressure to pump mixed liquor into a membrane unit. The use of high-pressure pumps and associated OpEx, high cost of membranes and low economic value of the produced effluents made the invention less attractive [341]. First-generation MBRs were mainly used in niche applications such as ships, isolated trailer parks or ski resorts [342]. Launched in 1985 by the Japanese Ministry of International Trade and Industry (MITI), the 6-year research and development program Aqua-Renaissance '90 prompted the development of energy-saving and smaller footprint MF MBR by the agricultural machinery company Kubota (Osaka, Japan).

Submerging the membranes in bioreactor and using vacuum pressure to exert the effluents resulted in low OpEx and was the real breakthrough for MBRs. Following successful pilot demonstrations at Hiroshima in 1990 and at Sakai-Rinkai in 1992, Kubota started MBR plant installations. By the end of 1996, Kubota already had 60 plant installations with total installed capacity of 5.5 MLD [343]. At the same time, the company started to market their MBRs outside of Japan. Kingston Seymour operated by Wessex Water in the United Kingdom was the first Kubota installation outside of Japan [342]. Kubota used chlorinated polyethylene (PE) flat sheets. In parallel, another Japanese company, Mitsubishi Rayon Engineering (now Mitsubishi Rayon Company), used PE fibres. Immersed hollow-fibre MBR was the technology developed also in the United States by Zenon, although the company used PVDF membranes. Zenon introduced its first HF ZeeWeed® ZW145 module (145 ft^2) in 1993. Similarly, flat-sheet technology uses a series of membrane panels sealed back to back and separated by a spacer. The panels are inserted into cassette modules as layers in a sandwich with active layers facing the feed. The space between the sandwich layers is 6–7 mm, enough for creating a feed channel. The advantages of flat-sheet modules are cost efficiency in small- and medium-scale applications due to relatively low manufacturing cost compared with hollow fibres, despite the low packing density [344]. The packing density of hollow-fibre MBRs is 2.5–3.0 higher compared with flat-sheet modules [341]. The higher packing density in hollow-fibre modules prescribes smaller feed channels. Indeed, the average feed channel in hollow-fibre modules is 2–3 mm. The advantages of hollow fibres are in both footprint and air use that can be optimized to improve the cleaning efficiency. The disadvantages are in higher chances of clogging and biofouling [345]. Flat-sheet and hollow-fibre MBRs are the leading configurations on the market. Companies that specialize in MBRs can be classified into those producing hollow-fibre modules and those with flat-sheet modules. Along with Zenon (now GE), hollow-fibre MBRs are produced by Asahi Kasei (Microza), Koch Membrane Systems, Litree Purifying Technology, Mitsubishi Rayon Engineering and Siemens Water (MemPulse™). Flat-sheet MBRs are offered by Kubota (EK/ES), Microdyn-Nadir (BioCel®), Toray (Membray®), Weise Water Systems (MicroClear®), A3 (Max-Flow), Alfa Laval (Hollow Sheet) and Huber (VRM®, Biomem). These MBRs are typically PVDF, PE, PES and PP polymer membranes.

The MBR market is considered one of the fastest growing segments in the membrane sector. It reached a size of $488 million in 2013 from $217 million in 2005 and $296 million in 2008. This corresponds to compound annual growth rate (CAGR) of 10.5% [346]. A more optimistic prognosis released by LiqTech International CEO Finn Helmer expects an approximately 20% CAGR raise per year and the total MBR market to exceed $3 billion in 2018 [347]. This boom is driven by legislation in Northern Europe, the United States and Canada, as well as by water stress in China, India, Australia and the Middle East.

Ceramic MBR modules started from niche applications where polymer membranes either failed or provided insufficient results. Those are applications that require high effluent quality or depend on ceramic membrane robustness [348].

Another core application of ceramic MBRs is the treatment of harsh industrial wastewater or streams with high organic loads. Examples include leachates, oily wastewater and biorefractory compounds. Small or decentralized MBR installations are designed for minimum intervention and fewer qualified trained personnel on site. Ceramic MBRs are resistant to extreme pH values. Tubular ceramic modules have large diameters and can handle highly viscous liquids or liquids with high concentration of mixed liquor suspended solids (MLSS) up to 30 g/l [349]. Thus, ceramic MBRs are not constrained to low fluxes when the MLSS concentration is low (unlike submerged polymer membranes). That, plus the absence of decanters needed to separate effluents and biomass, decreases the footprint of ceramic MBRs. Implementation of ceramic MBRs in general and pressure ceramic MBRs in particular can therefore be done in installation with space constraints. The same pressure ceramic MBR can be implemented to upgrade the existing wastewater treatment plant (WWTP). A conventional WWTP built several years ago most likely includes primary and secondary treatments. The tertiary treatment by disinfection fits the previous requirements to the quality of released effluents. New and more stringent regulations require the upgrade of the tertiary treatment by an implementation of combined physical and chemical treatments. Ceramic membrane filtration is a good tertiary treatment option. It can either convert conventional activated sludge (CAS) into an external MBR with the recirculation of biomass back to the membrane reactor or serve as an advanced filtration. Typically, the latter application is performed with narrow UF pore sizes between 2 and 5 nm. A comparison between CAS and an external ceramic MBR showed that removal efficiencies for soluble components in MBR are higher. For example, COD removal in the MBR was 99.0% versus 94.5% in CAS. Higher 99.2% versus 98.9% and 96.6% versus 88.5% removals of ammonium and total phosphorous in MBR versus CAS were also reported [350].

Several companies offer ceramic membranes based on a technological platform developed with polymer MBRs. Kubota offers a tank-submerged Kubota FILCERA® aluminium oxide membrane filtration system with a nominal pore size of 0.1 µm. TAMI Industries (Cedex, France) offers its tubular ceramic membrane elements INSIDE CéRAM™ also for MBRs. Pall Corporation (Port Washington, NY) offers its Pall Membralox IC asymmetric multichannel ceramic elements with a 4 mm channel diameter. The membranes are composed of a porous alumina support with a 12 µm pore size and a filtering layer (alumina, zirconia, titania). These membranes were used by Société d'Impression d'Hem (Lille, France) to treat their highly coloured wastewaters with 10–15 g/l COD in a Pall Membralox Ceramic Membrane Bio-Reactor. The system consisted of four filtration loops in parallel, corresponding to a total filtration surface area of 432 m^2, and treating up to 58 m^3 of effluent per hour. Continuous monitoring pointed to more than 99% BOD reduction and the recycling of 50% of the treated effluent for use as washing water for the printing machines. Similarly, Meidensha Corporation (Tokyo, Japan) offers 0.5 m^2 flat-sheet ceramic elements made of alumina with a pore size of 0.1 µm for industrial and domestic

wastewater treatment. The plate has internal permeate channels, thus creating a panel in a single piece. The company has recently installed Singapore's first ceramic membrane bioreactor plant coupled with an upflow anaerobic sludge blanket to treat and recycle industrial wastewater at Jurong Water Reclamation Plant. A successful run of the treatment plant can open a new way to ceramic MBR with low OpEx due to low air scouring rates and fewer chemical cleanings. The plant's daily treatment capacity is 4550 m^3. LiqTech International (Ballerup, Denmark) offers silicon carbide (SiC) flat-sheet membranes for MBR operating in outside-in principle. Likuid Nanotek (San Sebastián, Spain) has a number of industrial installations of ceramic MBRs. The Coosur plant at Jaen in Spain processes an average daily influent flow of 100 m^3. Here, the wastewater is treated by a ceramic MBR with six vertically aligned Likuid Nanotek modules. The total membrane area is 54.6 m^2, the initial COD is 4500 mg/l and the COD removal efficiency is more than 98%. This project is an upgrade of an existing biological treatment reactor with external membrane installation and the possibility for reusing treated effluents. Lyonnaise des Eaux used a ceramic MBR in treatment of wastewater of dairy and cosmetic industries. The implementation of ceramic MBR allowed the reuse of 400 m^3/day out of 500 m^3/day. The COD of MBR effluents was below 50 ppm and of CAS effluents 90 ppm. The difference in BOD was even higher – less than 5 ppm in MBR effluents and 30 ppm in CAS effluents. The energy requirements of MBR are, however, higher than those in CAS: 8 kWh/m^3 versus 5 kWh/m^3 [351].

Another important application of ceramic MBRs is in the treatment of wastewater from agricultural and agri-industry sources [352]. Manure and wastewater are treated by a combination of anaerobic digestion and aerobic MBR producing water for direct reuse or safe discharge. Ceramic MBRs are also used for treating the wastewater generated by food processing industries such as slaughterhouses, and dairy, eggs and potato processing [320].

4.5.2 Oil–Water Separation

4.5.2.1 Applications in Oil Recovery

Oil–water separation is one of the important industrial applications that can be viewed as a procedure to treat the wastewater and stay with clean effluents, or as a method to recover the oil for future use. In both cases, the problem is that the emulsion oil in water is very hard to separate. Oil extraction is the process used to extract oil from oil-containing rock formations. The initial phase or *primarily oil recovery* process uses natural mechanisms such as natural water displacement, natural gas expansion or gravity drainage to move the oil towards the wells for pumping. All this results in a recovery of 10–30% of original oil. That is usually not enough and a *secondary oil recovery* process is applied. This is done by flooding. Water is injected into the reservoir to displace (sweep) oil towards the well. The flooding can enhance oil recovery by additional 5–15% [353]. The *tertiary* oil recovery or *enhanced oil recovery* process also

recovers oil with water using either chemical or thermal enhancement. A chemical enhanced oil recovery involves flooding with a solution of polymers, surfactants and other additives in water. A thermal enhancement uses heat or gas to lower the viscosity of heavy oil fractions and sweep the oil towards the well. Thermal enhanced oil recovery is performed by steam flooding or fire flooding. The fire flooding is based on the formation of a flame front that generates heat, steam and CO_2. The CO_2 and other gases such as natural gas, nitrogen and flue gas can also be injected into the process. This gas injection can be alternated with water floods [354]. The recovery can be increased by 5–20%.

Although very few people associate oil extraction with massive use of water, in fact it is one of the most water-demanding operations. Actually, water is present initially with the oil within the reservoirs (formation water) as a layer above the oil. When the extraction starts, this water migrates and mixes with the oil, forming an emulsion. Drilling, secondary and tertiary oil recoveries, fracturing and completion all use large quantities of water to extract oil. As the oil recovery technology improves and new oil sources become available, the quantity of water used in petrochemical industry rises. Estimates in 2012 discuss volumes of 9–14 billion m^3 of oily wastewater generated globally [355]. As we already discussed, the use of fossil fuels and especially oil will continue to increase both in absolute numbers and in percentage in the coming decades and therefore the production of oily wastewater is expected to grow [353]. An additional factor that will increase the generation of oily wastewater volume is the depletion of ageing oil reservoirs that requires more water per oil barrel. The primary recovery requires a water to oil ratio (WOR) of just 0.2. However, the secondary recovery has already an average WOR of 8.6. The tertiary recovery might require a WOR of up to 13. Average WOR values were between 3 and 6 just a decade ago. They are now around 8, and by all forecasts are expected to rise. Another factor that will push the WOR up is the production of oil from unconventional sources such as horizontal wells in shales and tight formations (sandstones and limestones). In the United States alone, the onshore oil production increased from 12% in 2008 to 35% in 2012, and it is projected to increase to almost 50% by 2019 [356]. The low permeability of these formations requires large volumes of water at high pressure to produce either oil or gas.

Oil production therefore requires large quantities of water and incurs massive volumes of oily wastewater. The quality of this wastewater depends on the water source, and the degree of treatment is prescribed by the intended use of the wastewater. The process water can be released back to the source, injected into reservoirs or set off for a future use in agriculture (irrigation). Currently, 96% of the water produced in onshore wells is injected into oil-producing and non-producing reservoirs [357]. The remaining 4% is treated and released to the environment affecting drinking water and groundwater resources, endangering human health, polluting the atmosphere, affecting crop production, killing plants and aquatic life, contaminating soils and destroying natural landscapes [358]. Production water usually spends relatively long periods of time in reservoirs in contact with oil and minerals. Its quality is therefore influenced by the composition of the

surrounding minerals and varies by source and location. Typically, oily wastewater contains several groups of pollutants:

- Minerals – clays, silica, Ca, Fe and S mineral precipitates, dissolved solids such as NaCl and $MgCl_2$.
- Organics – dissolved and suspended hydrocarbons – benzene, toluene, ethylbenzene and xylene commonly referred as BTEX, naphthalenes, naphthenic acids, phenols, organic acids such as formic and propionic acids, and polycyclic aromatic hydrocarbons [359].
- Heavy and naturally occurring radioactive materials (NORMs), for example radium isotopes.
- Additives used in tertiary oil recovery – alkalines, surfactants, polymers.
- Dissolved gases – CO_2, O_2, H_2S.

The oil in oily wastewater can form a separate bulky fraction called *floated oil* or *dispersed oil*, or form an oil/water emulsion. In the latter case, the water represents the bulky media. The oil form in water depends on oil-to-water ratio. Oil is classified floated or dispersed if it contains >90% of the bulk. Similarly, oil is considered dispersed if its content in water is less than 0.5% [360]. The treatment of oily wastewater includes several stages. At the primary treatment stage, the floated oil is separated from water mechanically by separators and hydrocyclones. The primary treatment can be sufficient for the separation of the bulk mass of oil, so the water can only be slightly treated and send back to the subsurface. However, after few cycles the water purity deteriorates and water should be disposed subject to secondary treatment. The secondary treatment separates emulsified oil droplets from water, so the water can be refilled back to the subsoil. Finally, the tertiary polishing treatment stage removes dispersed oil, fine particles, dissolved organics, dissolved solids, radioactive materials and heavy metals. After the tertiary treatment, the water can be disposed to receiving water bodies or to a municipal wastewater collection system.

The core of the separation process is therefore the secondary treatment of emulsified oil droplets. It provides the water that can be either reused or processed further for agricultural irrigation or aquifer recharge. The removal of a large portion of floated oil typically does not guarantee the effluent quality sufficient for discharge or reuse. An efficient separation also provides additional oil and reduces a volume of oil in offshore transportation systems. Several studies have been conducted to develop suitable technologies for the separation of oil–water emulsions. The most popular treatment options, together with their pros and cons, are summarized in Table 4.11. These options are equally applicable in onshore and offshore oil extraction. In general, the offshore platforms have neither space nor time for biological processes such as MBRs, bioslurry and biopile/compositing. As a result, only intense physical–chemical separations are applicable. Most of these technologies are, however, only partially successful in oil–water separation.

Current regulations for allowable oil and grease content in produced water are strict and demanding. The Australian offshore oil and grease limitation for

Table 4.11 Oil–water separation technologies.[a)]

Method	Advantages	Disadvantages
Multimedia filtration	Efficient retention of solid particles and oil droplets larger than 10 μm	Not effective in retention of small oil droplets and dissolved contaminants
Solvent extraction	Efficient, fast	High cost, not sustainable, no heavy metals removal
Centrifugation	Easy, robust, sustainable, no additives	High energy demand, minimal droplet size is 2 μm
Induced gas flotation (no flocculants)	Easy to apply, energy-efficient process	Removes oil droplets larger than 25 μm, WOR extremely high
UV irradiation	No waste stream, fast and effective, no chemicals	Expensive equipment, fouling of UV lamps, unable to treat heavy metals
Chemical precipitation followed by gravity settling	Easy to process, efficient removal of heavy metals, flexible	High cost, high energy demand, low efficiency for dissolved components, secondary purification for chemicals/water is needed
Adsorption	Short treatment process, suitable for cold regions, compact packed bed modules, cheap, efficient	High retention time, following treatment required, heavy metals not removed
Air stripping	Very fast, efficient, no chemicals, proven technology	Creates a new waste stream, costly, impractical for small areas, heavy metals not removed
Pyrolysis	Large treatment capacity, fast and effective	High CapEx and OpEx
Incineration	Rapid, complete removal of hydrocarbons in oily sludge	High CapEx, separate process to remove ash is required, applicable to high oil concentrations
Oxidation	Rapid and simple, complete decomposition of hydrocarbons	Large amount of chemicals, high cost, disposal of toxic waste
Biological treatment	Less cost and large treatment capacity	Very slow process, large mass of sludge produced, high footstep
UF membrane treatment	Highly efficient, cost-effective, no added chemicals, small footprint, low CapEx and OpEx	Low retention of heavy metals and dissolved organics

a) Modified from Ref. [361].

the discharge of process water is 30 ppm [362]. The EPA regulations prescribe the daily maximum limit of 42 ppm for oil and grease and a monthly average limit of 29 ppm [359]. In China, the monthly average oil and grease concentration is just 10 ppm [363,364]. In Northeast Atlantic including Canada, the limitation on the discharge of dispersed oil is 40 ppm [365]. Many of the above processes cannot comply with these limits, generally leaving the treatment for membrane applications. The typical advantages are low CapEx, small footprint,

steady permeate quality, lower energy consumption, and possibility of continuous operation [366]. Ceramic membranes are preferable over polymer membranes due to their higher mechanical and chemical stability and overall lower life cycle cost [367,368]. An additional advantage of ceramic membranes is the higher permeability of $1.3 \pm 0.1\,l/(m^2\,Pa\,h)$ versus $0.87 \pm 0.08\,l/(m^2\,Pa\,h)$ for polymer membranes. The calculated membrane resistance showed that $2.2 \times 10^5\,m^{-1}$ resistance of ceramic membranes is lower than $2.3 \times 10^6\,m^{-1}$ resistance of polymer ones. The separation is usually performed in cross-flow mode due to the high degree of fouling. The reported results suggest that a successful combination of a membrane and flow regime results in the retention of more than 99% of emulsified oil. These retention levels were reported in laboratory experiments with 50 nm pore size α-Al_2O_3 ceramic MF membranes [369]. The TOC removal efficiency was above 92.4% in all experiments. The highest flux was found at highest cross-flow velocity of 1.68 m/s and highest TMP of 0.3 MPa. A retention of up to 99% in treatment of produced water with Al_2O_3, TiO_2/Al_2O_3 and TiO_2 MF, UF and NF membranes was reported by Ebrahimi *et al.* [370]. In another study, a highly concentrated oil–water emulsion was treated with a 300 kDa TiO_2 UF membrane [371]. The oil removal efficiency was 99.5%. Recent studies showed that zirconia membranes exhibit better performance and more stable flux than MF α-Al_2O_3 ceramic membranes made of other materials due to the high hydrophilicity of ZrO_2 [372]. The use of hydrophilic membranes is preferable since oil is easily wetted on hydrophobic surfaces and induces fouling. In other experiments, the emulsions were treated with zeolite-modified membranes [373].

There are several ways to minimize the degree of fouling in membrane applications. One is to pretreat the feed neutralizing the possibility of a contact between the membrane and the foulant. This can be realized by addition of surfactant and thereby binding or dissolving the contaminant molecules into micelles. The formation of micelles prior to the membrane separation step, or micellar-enhanced ultrafiltration (MEUF), was successfully implemented to reject more than 95% of the soluble organics and more than 98% of surfactant itself [374]. Another solution is working in cross-flow mode to minimize the concentration polarization effect. However, a high cross-flow velocity might break the oil droplets, resulting in a transfer of oil to the permeate, while a low velocity does not produce the high shear stress required to reduce fouling layers.

Table 4.12 provides a partial list of membrane manufacturers that develop membranes specifically for oil–water separation.

A preliminary economic assessment showed that under the optimal cross-flow velocity of 2 m/s and 95% water recovery rate the CapEx and OpEx for treatment of produced water with Likuid Nanotek membranes are $\$0.23/m^3$ and $\$3.21/m^3$, respectively. An installation of a full plant capable of treating $1000\,m^3/h$ requires a capital investment of $7.33 million [375].

4.5.2.2 Applications in Bilge Water Treatment

The bilge is the lowest compartment on a ship, below the waterline, where the two sides meet at the keel. Water not drained off the side of the deck drains

Table 4.12 A list of membrane manufacturers that have membranes for oil–water separation.

Manufacturer	Product line	Filtration range	Support material	Membrane material
Pall	Membralox®, Schumasiv®	5 nm to 0.2 µm	Al_2O_3	Al_2O_3 (MF), ZrO_2 and TiO_2 (UF)
Corning	CerCor®	5 nm to 0.2 µm	Mullite ($3Al_2O_3{\cdot}2SiO_2$)	ZrO_2 (MF) and TiO_2 (UF)
TAMI	INSIDE CéRAM®	0.02–1.4 µm	ATZ	ZrO_2 (MF) and TiO_2 (UF)
Atech	Atech	0.01–1.2 µm	Al_2O_3	Al_2O_3 (MF), ZrO_2 and TiO_2 (UF)
Orelis	Kerasep™	5 kDa to 0.8 µm	Al_2O_3	ZrO_2 and TiO_2
LiqTech	CoMem		Silicon carbide	
Likuid Nanotek		0.1 mm	ZrO_2	

down through the ship to bilge and is pumped off the ship after a treatment. The bilge water contains up to 50% of oil, seawater, urine, detergents and solvents. It cannot be discharged as is, and requires a treatment before the disposal. Recent regulations differ from country to country, and require less than 15 ppm oil in bilge discharge within 12 nautical miles of shore and 100 ppm outside the limit in the United States [376], 5 ppm in European countries and Canada [377] and 15 ppm in other countries subject to the International Convention for the Prevention of Pollution from Ships and the International Maritime Organization [378]. Bilge water can be treated by bioremediation, gravity plate separator, absorption and UF membrane treatment. Bioremediation using a combination of microorganisms can decompose almost any organic contaminant. The operation, however, is very time consuming and requires a large footprint. Although there are several reports on the implementation of ceramic MBRs for treatment of bilge water [379,380], the common practice is using separators. A gravity plate separator uses oleophilic plates to coalesce oil in water and transfer the oil to a waste oil tank. The separation efficiency seldom reaches the required limit for discharge combined with a secondary stage. A typical complementary treatment is performed with absorption columns that are bulky and expensive. Ceramic membranes are considered a valuable replacement of such absorption columns as they can successfully treat bilge water producing an effluent with less than 10 ppm oil. In one example, γ-Al_2O_3 membranes with 70% porosity and fluxes between 50 and 100 l/(m^2 h) were used [381]. The separation, however, suffers from severe fouling and requires the feed pretreatment. A pretreatment with $FeCl_3$ enhanced the performance of Membralox 0.2, 0.5 and 0.8 µm membranes to the average permeate fluxes between 140 and 340 l/(m^2 h) while keeping the oil concentration in the permeate below 6 ppm [382]. Somewhat lower fluxes

between 800 and 1200 l/(m^2 h) with 0.8 μm membranes were reported by Zaidi *et al.* [383].

4.6 Ceramic Membranes in Food Applications

During last 30 years, ceramic membranes grew from a niche application into a key technology in food and especially beverage processes. The main success was in the dairy industry (e.g. milk, whey and brine). Other successful applications were in beverages (fruit juice, wine and beer) and food additives sectors (gelatin, pectin and alginates) [384]. Currently, worldwide market for membrane technology in the food industry is about €800–850 million. This is the second largest industrial membrane market after water and wastewater treatment including desalination [385]. The most common solutions use pressure-driven membranes including MF, UF, NF and RO. Among these, UF has a 35% share, while MF membranes and systems account for additional 33% [385].

The usual content of the feed contains a large portion of the separable compound. Juice pulp can comprise 3–4% of the feed; casein and whey proteins are also on average between 3 and 5% of the total volume. Yeast cells are less common, yet can still reach as much as 1%. Soon after the separation begins, the membrane becomes significantly fouled with compounds that can either occupy places on the membrane surface and within membrane pores or simply remain close to the membrane surface. The transmembrane flux falls, and the membrane urgently needs a cleaning. A standard cleaning by hydraulic backwash (reverse flow from the permeate to the feed side of the membrane) is usually insufficient. The membrane has to be cleaned chemically or thermally. In gentle applications such as separation of whey from milk, the cleaning is done with hot water, steam or heat sterilization [386]. That cleaning deteriorates proteins weakening their contact with the membrane surface. The proteins are then removed by hydraulic backwash [387]. The cleaning is always a step back in membrane applications as it takes time and money and does not return any revenue. A typical cleaning takes between 2 and 4 h and is performed daily. That is as much as 15% of the total membrane production time. Food companies naturally try to reduce that time by performing rapid and efficient cleaning. In chemical cleaning that means high concentrations of aggressive solutions such as up to 3% caustic soda, up to 2% nitric acid and sodium hypochlorite for sanitation [388,389]. Phosphoric and hydrofluoric acids should, however, be avoided if polymer membranes are used. Typical cleaning in food industry is performed with diluted acid, alkaline and enzymatic solutions [387]. Steam sterilization is performed at high temperatures that are, however, limited by thermal stability of some module elements such as gaskets.

In the following subsections, we will look at several examples of successful applications of ceramic membranes in the food industry and outline the bright

future of membrane-based separations of dairy products, beer, wine, juice and food additives.

4.6.1 The Dairy Industry

There are more than 6 billion consumers of milk and milk products. Over 750 million people live within dairy farming households [390]. Annual milk consumption growth rate is between 7 and 8% [390]. In 2011, worldwide dairy farms produced 730 million ton of milk from 260 million dairy cows [391]. Already in 2013 world total milk consumption was 782 million ton [392]. Figure 4.30 depicts the worldwide trend of milk consumption in the last 40 years [393].

Interestingly, despite the clear consumption growth rate the average milk consumption per year per capita remained at the same level of 100 l per capita per year for over 40 years now, or one glass of milk per day [393]. Possible reasons for that are the growing consumption in developing countries combined with a decrease in consumption in developed countries [394]. In any case, more dairy plants mean more equipment, including membranes. The market forecast for the membranes in dairy industry predicts a 5-year CAGR of 10.0%.

The collected raw milk is transported from farms to dairy plants for further processing. The main processes include *pasteurization* (heat treatment to ensure the safety of milk for human consumption [395]), *homogenization* for an even distribution of fat in the milk, *separation* into cream and skim milk for the production of butter, cheese and skim milk, and *dehydration* for the production of hard cheeses and milk powders for prolonged storage.

The separation of cream from raw milk is performed at the beginning of milk processing at the dairy plant by centrifugation. This yields two streams. The milk

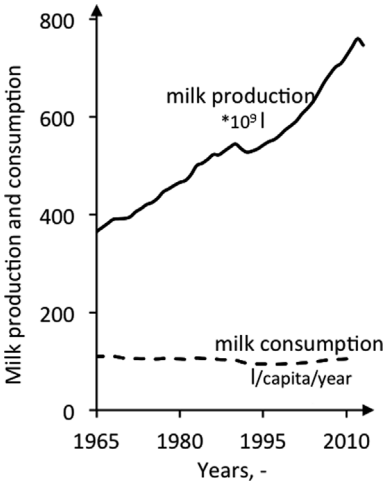


Figure 4.30 Worldwide milk production (in billions of litres) and average milk consumption per capita.

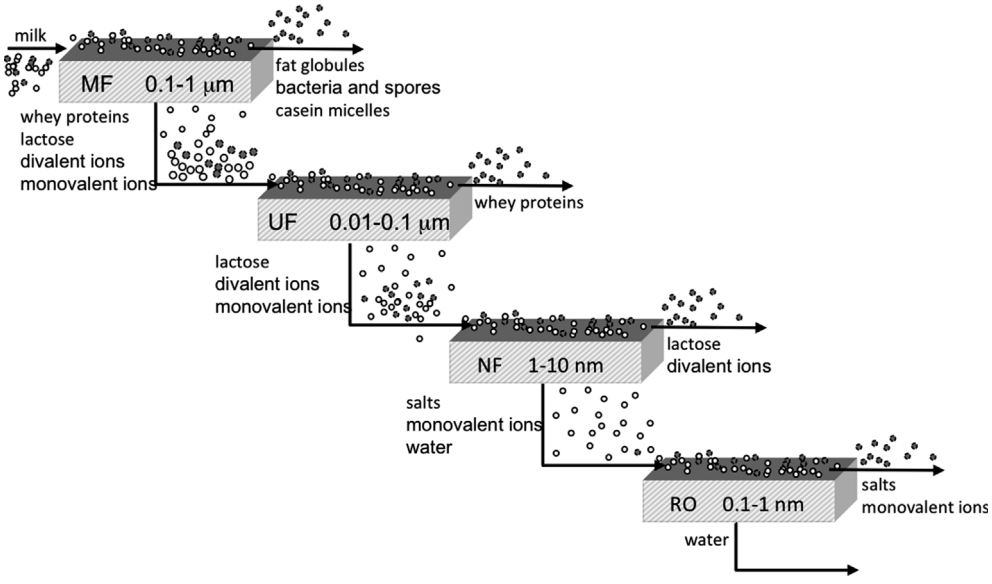


Figure 4.31 The essentials of ceramic membrane separation of raw milk.

stream contains the so-called skim milk, with less than 0.05% fat. The cream is used to make butter and to add flavour and texture to cheese. The second stream contains the cream, which is also sold separately in several grades such as half and half (10.5–18% fat), light cream (18–30% fat), light whipping cream (30–36% fat) and heavy cream (36% fat or more).

In principle, the separation of cream from milk can be done with MF membranes, although that application is not very popular. Traditionally, cream is separated by centrifuging. Membrane applications are more popular in the separation of casein from whey proteins, and the removal of pathogenic bacteria from skim milk and from brine in hard cheese making.

That said, the MF separation of cream from milk is a fairly straightforward process (see the flow diagram in Figure 4.31) [385,389]. Cow milk contains typically 88% water, 5% lactose (milk sugar), 3.5–5% protein and 3–5% fat. The rest is composed of minerals and enzymes. Membranes can separate between somatic cells (6–15 μm), fat globules (0.2–15 μm), bacteria (0.2–6 μm), casein micelles (0.03–0.3 μm) and whey proteins (0.003–0.006 μm) [389].

The use of filtered milk eliminates the need for preservatives such as polyphosphates to protect cheeses against superficial mould growth [396], propionic acids, nitrates and antibiotics such as nisin and natamycin. This operation can be performed with ceramic membranes comprising a multichannel geometry and a highly permeable support. The disadvantage of filtered milk is that not all bacteria are pathogenic. The absence of some bacteria and ferments in the membrane-processed milk might require an adjustment of the entire procedure [385]. Hence, the implementation of membranes instead of centrifugal cream separator

is not popular. The most successful implementation of ceramic membranes is in cheese production (see details below). Several studies, however, tried separating large (>2 μm) fat globules [397,398]. Apparently, the tactile properties of large and small fat globules differ, and yogurt and Cheddar cheese made with smaller fat globules are considered superior to the same products made with unspecified fat globules. In addition, the natural membrane that surrounds a milk fat globule has an additional value [399] as an emulsifying agent and a potential ingredient in functional foods [400].

4.6.1.1 Cheese Production

The first cheeses were produced during the agricultural revolution some 6000 years ago, most probably by accident. Fresh milk left overnight contained lactic acid bacteria that cause lactose fermentation. The pH decreased and the milk coagulated [401]. A parallel story says that an unknown rider on his way home filled his saddlebag with fresh milk. The saddlebag was made from a stomach of an animal and contained rennin, a coagulant enzyme. The riding, the sun and the enzyme resulted in a separation of milk into solid lumps of cheese and a pale liquid, the whey. Cheesemaking took off when farmers started adding salt to it, increasing its shelf life. Cheese was already on the menu at the time of the Roman Empire. Around 1860, industrial cheese production took an important step forward, thanks to the mass production of rennet – coagulant enzymes. Since then, cheese has become an everyday food. Today, worldwide cheese production is nearly 15 Mtpa, accounting for about a third of raw milk usage. Figure 4.32 depicts worldwide trends of cheese consumption in the last 40 years [393]. Altogether we consume more and more cheese every year.

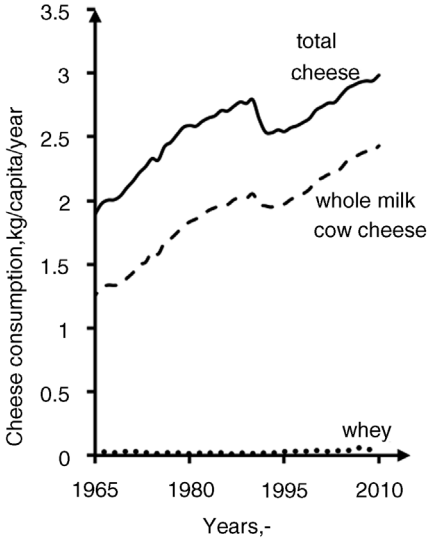


Figure 4.32 Trends in worldwide cheese consumption.

> Greece and France are two leading countries in annual cheese consumption per capita, with 27.3 and 24 kg, respectively. While in Greece three-quarters of this is feta, France has an enormous variety. As Charles De Gaulle once said: 'Comment voulez-vous gouverner un pays qui a deux cent quarante-six variétés de fromage?' (How can you govern a country which has 246 varieties of cheese?)

Ceramic membranes are employed in two stages of the cheese production: ripening and curd coagulation. At these stages, the casein (which accounts for about 78% of the protein in milk) is separated from the whey protein. Yellow cheese is produced from casein while white cheese is produced from whey proteins such as α-lactalbumin and β-lactoglobulin. Caseins are insoluble in milk and form multimolecular, large spherical structures called *casein micelles* [402]. These micelles contain enzymes, water and salts (mainly calcium and phosphorous). The separation process is known as curdling: the milk is first heated, then acidified and then coagulated by adding rennet (a complex of enzymes produced in stomachs of calves). The coagulated casein, or curd, settles down, separating from the upper liquid (the whey). Curds (also called 'farmer cheese' or 'strained yogurt') can be eaten after the separation. Alternatively, they can be pressed, shaped and aged to create 'hard cheeses' such as mozzarella and Cheddar.

Cheesemaking is a highly traditional and conservative industry. Gorgonzola has been made in the Po River Valley since 897. French monks produced Roquefort since 1070. Cheddar was produced in England since 1500, and Gouda in the Netherlands since 1697. Yet the application of MF and UF ceramic membranes opens up new opportunities. Why not to pre-concentrate the raw cheese milk and thus increase the percentage of proteins? In the following paragraphs, we will present and discuss three levels of pre-concentration. All three are based on membrane separation that results in permeate containing mainly whey proteins and a retentate that consists of native caseins. Such a separation is possible due to the different sizes of milk proteins (see Table 4.13).

The first level of pre-concentration is performed with ceramic membranes with pore diameters of 0.2 μm. Changes in process parameters such as pore size

Table 4.13 The sizes of different proteins in milk.[a)]

Protein	Size (nm)
Casein micelles	30–300
β-Lactoglobulin	3–6
α-Lactalbumin	3–6
Bovine serum albumin	3–6
Immunoglobulin	5–10
Lactoferrin	9

a) Based on Refs [403,404].

and pH can result in a standardized desired ratio of casein to total protein. Standardized cheese milk is concentrated by a factor of 1.2–2. The protein content in the milk increases up to 4.5–5% of the total volume. This simplifies and improves the efficiency of the subsequent coagulation process. The membrane pre-concentration of cheese milk is used in Cheddar, mozzarella, Edam and cottage cheese processing [405].

The second level of pre-concentration is performed with diafiltration (DF) and results in a product that consists of more than 90% of purified casein [405]. Here DF is a dilution of concentrate, usually with water, and continuous filtration until a satisfactory concentration of casein is achieved. Standardized cheese milk is concentrated by the factor of 2–6 and casein content in the cheese milk increases up to 6–20%. Conventional cheesemaking equipment cannot be used and a special process needs to be developed. Some sorts of Cheddar, feta, Gouda and blue cheese are prepared that way.

The third level of pre-concentration gives whey proteins in permeate and is called liquid pre-cheese concentration (LPC). The whey proteins are further concentrated by ceramic UF membranes with pore sizes of 0.14 µm and serve as the main source of white cheeses such as Camembert, mascarpone and ricotta. Figure 4.33 shows the membrane-driven pathways that lead to each cheese variety.

There are several advantages in using ceramic membranes instead of traditional methods of cheesemaking [385]. The pre-concentration of casein intensifies the process and reduces operational costs (smaller footprint and less energy). At the MCR level, using ceramic membranes reduces or minimizes the coagulation step, so that less rennet is required. This also decreases the wastewater flux and simplifies its treatment. Furthermore, it increases the nutritional value of the

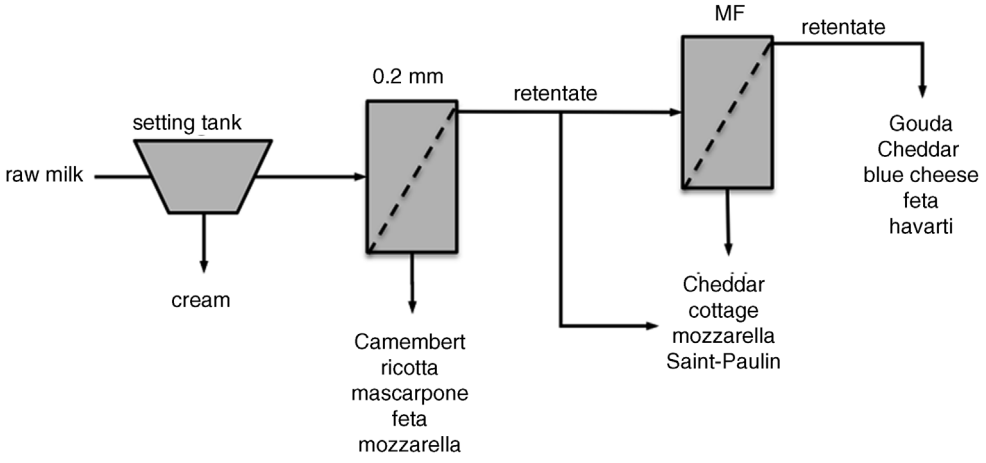


Figure 4.33 Simplified block diagram showing the membrane unit operations in cheese variety production.

cheese, as whey proteins are incorporated in it. However, intensification and implementation of UF membranes might have a negative impact on the ripening of semi-hard and hard cheeses. Whey proteins in the UF retentate reduce proteolysis during ripening and cause problems with the cheese texture [406]. UF is therefore viewed as a complementary, but not as the optimal process solution in production of semi-hard and hard cheeses [407,408].

4.6.1.2 Whey Separation

Whey is one of the important by-products of hard cheese manufacturing. It is the liquid that remains after the milk has been curdled and strained. Although we call it a by-product (because the process focuses on making cheese), there is actually much more whey than cheese: starting from 10 kg of raw cheese milk will typically give 1 kg of cheese and 9 kg of whey [401]. Until the 1950s, whey was considered a waste and fed to pigs. Additional whey disposal options were sewage disposal and spray on fields as a fertilizer. Since 1950s, and especially starting 1980s, whey proteins are a valuable product and a main source of whey cheeses such as ricotta and brown cheese *Brunost*. They are also used as a nutritional supplement for infants and sportsmen. Whey is also the main source of lactose, a disaccharide sugar that has a formula of $C_{12}H_{22}O_{11}$. Lactose is used in processed foods such as baked goods (breads, crackers, pastry), meats and beverages. It is extracted from the whey permeate evaporated to 60–65% solids and crystallized while cooling. Lactose can also be precipitated from whey using ethanol.

> Genetic research found that the gene for lactose persistence has evolved between 5000 and 10 000 years ago in European populations [409]. The advantage of lactose persistence is that when people migrate to colder clime their bodies are less exposed to sun and produce less vitamin D. Vitamin D is important in calcium absorption and people short of the vitamin are short of calcium. Lactose persistent people accept calcium directly from animal milk, have strong bones, healthier blood systems, can move to longer distances, and faster and better heal from injuries.

The problem is that whey itself is mainly water (93.5%). The rest is lactose (4.5–5.5%) and whey proteins (1–2%). The initial task is therefore separating the proteins from water and lactose. This was originally done by ion exchange and affinity chromatography. Despite the high selectivity, these methods are very expensive and were never applied industrially. An additional method called selective precipitation was accomplished by changes in pH, salt and temperature. None of the precipitations was applied on the commercial scale because of the high processing costs and difficulties with disposal of large volumes of undesired by-products [402].

Ceramic separation of whey with UF membranes was tested in 1960s, and was established as an industrial process in the 1970s. The permeate stream contains water enriched in lactose, while the retentate stream contains between 35 and

85% proteins by weight. In addition to their nutritional value, individual proteins have their own unique nutritional, functional and biological advantages. For example, α-lactalbumin has high tryptophan content and can be used in infant formula. Bovine serum albumin (BSA) is commonly used in immunodiagnostic procedures, clinical chemistry reagents and cell culture media [410]. Bovine immunoglobulin (Ig) is an immunological protein source to protect human bodies against diseases. The Ig is also added to infant formulae. Whey proteins also can be used in gelling, emulsifying and foaming agents, and are therefore added to sweets, beverages and even processed meats [385].

The reduced amount of skim milk with the application of UF compared with the traditional processes decreases bulk volumes. Less equipment, better quality control and improved cheese yield are other advantages of UF membranes. One potentially revolutionary application is the separation of proteins from the water prior to curdling. This process can in theory produce cheese without whey avoiding the curdling and whey removal steps. It might, however, affect the taste of the cheese and interrupt the ripening stage. Even now the whey separation by UF membranes is so successful that about two-thirds of the membrane area installed in the dairy industry is used for the treatment of whey and about one-third for milk [411]. Lipnizki [385] called the whey separation by UF the complementary process of cheesemaking.

4.6.1.3 Brine Disinfection

Apart from the use of UF membranes in preventing microbial contamination and the separation of whey from curds, there is an additional stage where membranes are employed. There is an increasing concern that the brine solution can be contaminated by pathogenic bacteria. Ceramic membranes are often employed to prevent this contamination. Interestingly, the salting itself was invented to prevent bacterial contamination by applying an osmotic shock, but probably the constant quest for less salty-flavoured types of cheese reduced the salt concentration in brine. Another possibility is the development of halotolerant (salt-resistant) bacteria. The implementation of ceramic membranes is a one-step solution to the contamination problem that is economically affordable, environmentally friendly and robust. The membrane can have large pores just to retain the bacteria and spores, so the applied TMP is quite low. Accordingly, the same brine can be reused several times with no need for a disposal. The obtained cheese quality is superior to the quality of cheese obtained after the traditional processes of heat treatment and kieselguhr filtration.

4.6.1.4 Pathogen Removal

Another application of ceramic membranes is in the removal of microorganisms from skim milk in the production of microbiologically safe raw milk. Raw milk always contains microorganisms due to contamination at several points along the dairy processes. The main culprits are the animal's udder, the milking machine and two tanks – the raw milk collection tank and the transportation tank. The reported list of pathogenic bacteria includes *C. jejuni*, Shiga

toxin-producing *E. coli* (STEC), *L. monocytogenes*, *Brucella*, *Mycobacterium* and *Salmonella* [412,413]. Many of these bacteria are characterized by low infectious doses, typically 1–100 colony-forming units (cfu), high pathogenicity in humans and serious acute illnesses including cholera, polio, anthrax, scarlet fever, bovine tuberculosis and botulism [414]. Between 1908 and 1918, the percentage of London's milk supply contaminated with tubercle bacillus ranged from 7.4 to 11.6% [409]. In several regions of the world, between 20 and 75% of raw milk was infected by brucellosis. Despite these facts, several groups of population consistently consume raw milk. Those are dairy producers, farm employees and their families, raw milk fans and consumers of several types of raw milk cheese (Brie, Camembert, Reblochon and Epoisses). These cheeses are aged less than 60 days and can contain potentially harmful bacteria. Cheeses older than 60 days (Cheddar, Colby, Parmigiano, and provolone) are considered safe to consume as the acids and salts inactivate the bacteria.

Raw milk with no preservatives is good for only a day or two. Even pasteurization does not guarantee its microbiological safety. Often, pasteurization does not inactivate all microorganisms, thus leading to the development of persistent pathogenic microorganisms in biofilms, eventual contamination of dairy products and food-borne diseases. The minimal high-temperature short-time (HTST) pasteurization is a procedure of heating milk to 72 °C for 15 s [415]. To extend shelf life, dairies pasteurize at higher temperatures up to 79 °C and times up to 30 s [416]. Although this guarantees a shelf life between 17 and 21 days, it does not extend it. The percentages of microbiologically safe pasteurized milk samples were 61, 45 and 28% at 7, 10 and 14 days of storage at 6 °C, respectively [417,418]. Another technological advantage that keeps the pasteurized milk safe is the stoppered milk bottle. Glass shortage during World War I led to optimization and use of milk cartons, which along with plastic jugs are the main distribution containers used today [409].

Current shelf-life extension strategies include ultra-pasteurization (UP), ultra-high-temperature (UHT) pasteurization, and microfiltration. Ultra-pasteurized milk is heated to 138 °C for at least 2 s, and generally has a shelf life of several weeks under refrigerated conditions. Same heating conditions are applied to receive the UHT pasteurized milk; however, the milk is aseptically packaged to avoid recontamination [417]. Children aged 6–11 years like HTST milk more than UP or UHT milk simply because the high-temperature pasteurization changes the milk taste [419]. An alternative approach for ensuring the microbiological safety of milk is *not* to heat it. Ceramic membranes can physically retain bacteria without changing the milk temperature. This process is called *cold pasteurization*. It comprises several stages, as depicted in Figure 4.34.

The cold pasteurization begins with a centrifugal removal of cream from raw whole milk by a commercial continuous cream separator. Then, the remaining skim milk is microfiltered with 1.4 μm ceramic membranes. The filtration is often performed at less than 0.5 bar and very high cross-flow velocities of 6–8 m/s [420,421]. Common permeate fluxes are between 500 and 800 LMH. This operational cycle can be as long as 10 h [389]. The first-stage MF retentate

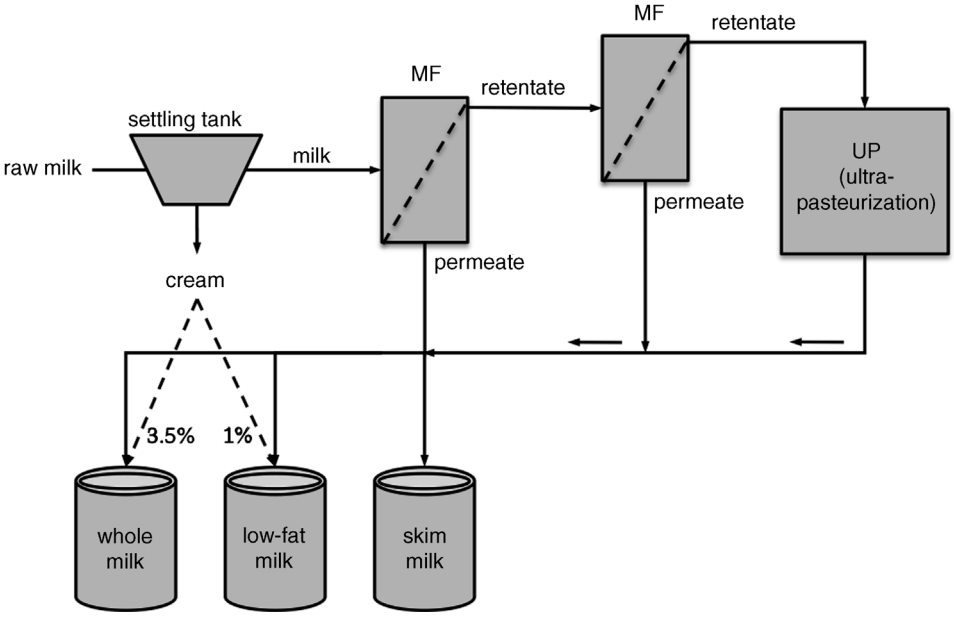


Figure 4.34 A scheme of two-stage microfiltration of raw milk. Here the applied membranes are typically 1.4 μm ceramic MF.

is approximately 5% of the volume of the skim milk, and it is further concentrated at the second path. The volume of the second-stage MF retentate is 0.5% of the feed volume of skim milk. This second-stage MF retentate undergoes UP treatment at 130 °C for 4 s, after which it is combined with the MF permeate [385]. The UP treatment of a small portion does not influence organoleptic and chemical properties of the entire milk bulk. A portion of previously separated cream is added back to the skim milk, and the entire suspension receives a minimum HTST treatment. Average reductions in bacteria counts in skim milk vary between 90% (1-log reduction) and 99.98% (3.8-log reduction) although not all pathogen bacteria and spores are removed [422]. For that reason, the UF treatment of raw milk cannot be considered as a complete replacement of pasteurization. A combination of UF and heat treatment by UP and HTST provides the best results in terms of increasing the shelf life of raw milk. Still, it does not guarantee the microbiological milk quality after the expiration date. Shelf life increased up to 42 days, and the milk taste was superior to heat-treated milk [422]. The nutritional value of membrane-pasteurized milk is higher as no thermal decomposition of compounds occurs.

The ceramic membranes used in this process are made of alumina support with titania or zirconia filtration layers. Membrane cleaning is performed with RO water heated to 80 °C, 0.3% (v/v) HNO_3 and a caustic solution (1.5% (v/v) Ultrasil 25, Ecolab) [416]. Due to a significant fouling, the MF is performed at high cross-flow velocity and constant TMP. In the original concept, the

constant TMP was achieved by recirculating some of the permeate concurrently with the feed. In that way, the same pressure gradient between the feed and permeate sides of the membrane is maintained. That approach was developed by Alfa Laval and marketed by Tetra Pak International SA (Pully, Switzerland) under the name Tetra Alcross Bactocatch [423]. Today, the constant TMP is achieved by using ceramic membranes with a longitudinal permeability gradient built into the support structure without modification of the filtration layer. One approach realized by TAMI Industries (France) in Isoflux® membranes is to reduce the thickness of the support layer, thus reducing the membrane resistance along the membrane. The other approach realized by Pall Exekia (France) in Membralox® GP membranes [424] is to increase the porosity of the support layer along the membrane surface, thus gradually reducing the membrane resistance.

4.6.2 Mineral Water and Juice

With pure water sources largely unavailable and a varied quality of tap water, people are consuming more and more mineral water. In fact, mineral water is currently the fastest growing segment of the beverage industry. The forecast CAGR is 9.3%, with the entire market increasing from $757 million to $1.18 billion. The 5-year sales of membrane modules during the forecast period will be almost US$5 billion. Mineral water is often not purified at all or purified as little as possible. Apart from economic reasons, the low degree of purification is needed to keep all microelements reducing only the risk of microbial contamination. The leading application in mineral water purification is ozonation, but it is an imperfect process. Ozone is a very powerful but not a selective oxidizer of microorganisms and therefore initiates a number of chain reactions that might completely change the water's taste. Another popular disinfectant, UV irradiation, does effectively neutralize microorganisms. However, the neutralized microorganisms are still present in the treated water and might reactivate themselves in sunlight, regaining their pathogenic ability. Thus, both disinfectant strategies are not optimal and mineral water companies are currently trying to combine chemical disinfection with physical retention of impurities.

The latter application is exclusively performed by membrane filtration using a range of porous filters such as MF, UF and NF. The filters are needed to keep all microelements intact removing selectively the impurities and confirming the microbiological safety of mineral water. That application is performed with both polymer and ceramic membranes. Ceramic membrane manufacturers, however, are much less active in this market segment than polymer ones. Their approach is to let the mineral water companies to come and ask for the membranes whilst polymer membranes are offered in a variety of sizes and fluxes. The leading membrane manufacturers are not in that segment yet although a quick search reveals that systems for mineral drinking water purification are already offered by companies such as Bansal Sweet Water Technology (Maharashtra, India),

ZhangJiaGang City YuFeng Beverage Machinery Co. (China) and Pentair Südmo (Riesbürg, Germany).

4.6.2.1 Orange Juice

Orange juice is the best known and the most popular raw food drink. Just 40 years ago, every person on Earth had one glass of orange juice per year. Now we drink three glasses. However, the increase is mainly in consumption of orange and apple juices. The average consumption of tomato, grape, lemon, pineapple, plum, tangerine and mango juices remained stable and lower than the consumption of orange and apple juices [393]. Today, in nearly every convenience store in every country you will find a pack of orange juice produced by one of the world's leading companies such as Tropicana and Simply Orange or by local producers. The highest consumption of orange juice per capita is in EU countries such as Germany, Finland, Norway, Spain, the Netherlands and the United States. This boosting consumption of orange juice can be attributed to a combination of its health effects, a continuous worldwide advertising and the optimization of harvesting technology.

The industrial harvesting of oranges is performed by either a relatively small number of very large companies (Brazil, USA) or a large number of medium-sized and small companies (Israel, Italy, Morocco). Practically everyone uses the same technology. Freshly harvested, healthy and intact fruits are delivered to a processing plant, washed, sorted according to their size and processed [425]. The extraction results in three intermediate products – juice/pulp that accounts for 45–55 vol.%, the peel which is 45–55 vol.% and the essential oil which is only 0.2–0.5 vol.%. The extracted orange juice has approximately 11°Brix and 20–25% pulp [425] (Brix is a term that refers to the dissolved solid content of the juice, mainly indicating the concentration of sugars such as glucose, fructose and sucrose).

The raw orange juice is opaque due to the presence of polysaccharides, proteins, pulp, cells and fibres that make up to 10–12% of the raw suspension. The first stage in the juice clarification (see the flow diagram in Figure 4.35) [426] is the degradation of pectin, a polysaccharide that binds the proteins and pulp into a stable suspension. [427]. The lower viscosity at the end of this step permits a more efficient mechanical separation or filtration of destabilized large settleable particles that consist of proteins, pulp, rags, cells and fibres. The mechanical separation is performed with decanters, finishers or centrifuges. At that stage, the pulp content is about 1% and the juice turbidity is around 5 NTU. Although that turbidity level is acceptable by wholesale consumers, orange juice is often further filtered through either diatomic earth or membrane filters. Diatomaceous filtration uses a filtration element in a form of paper or cloth to gradually build a cake layer that is used as the filtration media. Membrane technology uses cross-flow mode and UF membranes. Juice concentrate is received from this pre-clarified juice by evaporation. Approximately 10–12 ton of juice is needed to obtain 1 ton of concentrated orange juice with 65°Brix. Orange juice is sold as pulped or pulp-free or clear juice.

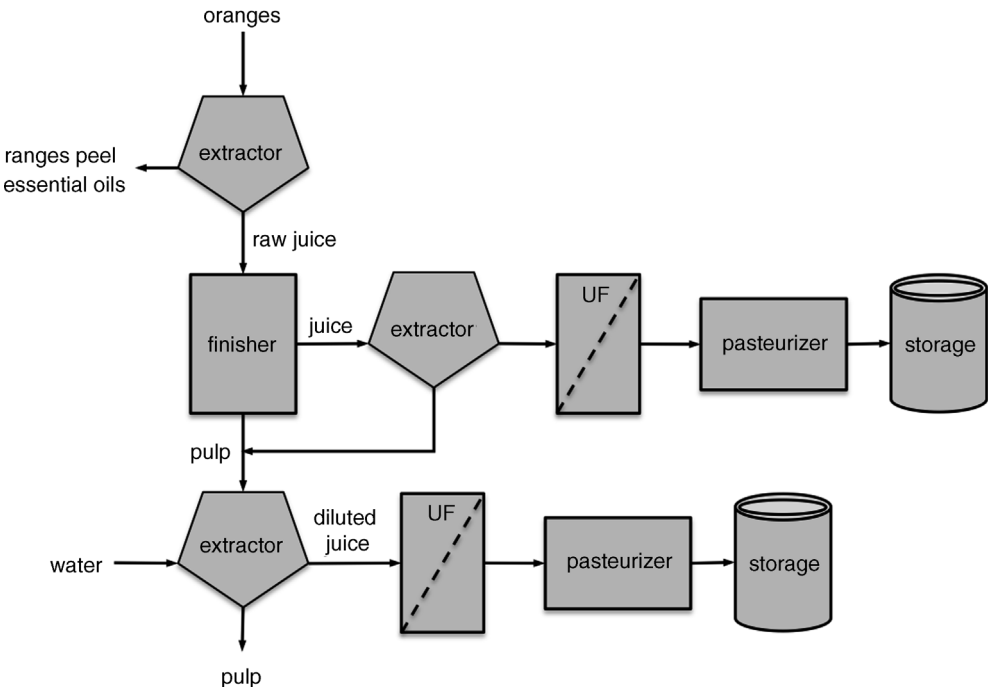


Figure 4.35 Two-stage orange juice recovery (Italian method).

Orange juice is membrane-treated at the final clarification stage just before bottling and marketing. The main purpose of the treatment is to produce juice of a superior quality free of any particles that might affect its transparency when chilled. That operation is typically performed with MF and UF membranes. In addition, that operation can help to disinfect the juice, so the final product will contain no microorganisms that can deteriorate the juice quality. That feature of membrane treatment is still under debate and often juice manufacturers use pasteurization to ensure the microbiological quality of their products. Typical thermal pasteurization is performed for 1 min at 90 °C [428]. The reported negative impacts of thermal pasteurization include loss of fresh flavour [429], degradation of ascorbic acid and loss of colour [430]. To avoid the negative impact of thermal pasteurization and to provide premium quality juices obtained from fruits and not from concentrate, the current tendency is to use non-thermal preservation techniques. The most popular techniques use ultraviolet (UV) light irradiation [431], high hydrostatic pressure [432], pulsed electric field (PEF) [433], ultrasound [434] and high-pressure carbon dioxide [435]. However, industrial implementation of these technologies remains limited [436]. Conversely, membrane filtration is a proven technology that is already implemented in orange juice clarification and as such can intensify the juice finishing and reduce the OpEx of the final process. The additional advantages of membrane filtration over traditional clarifications include shorter processing times, higher

juice yields, no need for disposal of spent filter material, a better and more reliable juice quality and reduced usage of enzymes [437].

Membrane filtration of orange juice is performed with either polymer or ceramic MF and UF membranes. The large pore size used in the separation indicates that currently the quality of treated juice is considered superior to a quality obtained after any other separation. Accordingly, the manufacturer does not have to worry about the juice quality, but rather reduce the CapEx by using membranes with large pores. The higher transmembrane flux reduces the required total membrane surface. A significant fouling found in dead-end filtration of orange juice resulted in the implementation of cross-flow filtration mode. Clear juice that passes through the membrane is collected in the clear juice tank, while the cloudy juice or retentate is redirected into the filtration circuit. The implementation of a cross-flow reduces the degree of fouling due to the shear stress imparted by the stream on the near-membrane film. Typical ceramic membranes used in the orange juice clarification have pore size between 20 and 200 nm. Typical flux is 50 l/(m^2 h), and the operation is performed at 1.5 bar with an average cross-flow velocity of 4.4 m/s. Despite that cross-flow membrane filtration in juice production started just 20 years ago, it is now considered the industrial standard in the field. Membrane filtration has successfully replaced traditional rotary vacuum-drum filters, diatomaceous earth and sheet filters.

4.6.2.2 Apple Juice

Apples have been cultivated since the Roman Empire in Asia and Europe, and have since become extremely popular. Over 80 million ton of apples were harvested worldwide in 2013 [393], most of them in China, the United States, Turkey and Italy. Apples are eaten raw or used for preparing apple juice and ciders. Unlike citrus fruits that are gently squeezed for juice, apples are washed, cut and ground into a mash, and then pressed. The resulting expelled juice (the cider) flows into collecting tanks. If this cider is further treated by enzyme degradation, clarified with decanters, finishers and centrifuges, filtered with either diatomaceous earth or membranes, and (optionally) pasteurized, it is called apple juice. Figure 4.36 depicts main stages of apple juice production.

The history of cider goes back a long way. Already in the Old Testament texts we find 'Shekhar' – an alcoholic drink that makes the drinker tipsy yet happy. This Shekhar (from the Greek σικερα meaning 'strong drink' and *shikaru* in Babylonian) was later transformed into cider in English or sidre in French. We are therefore probably discussing the oldest juice ever made – unclarified apple juice. Around the fifteenth century, brewers began using a mixture of sour, sweet and acid apples out of a variety of 7500 cultivars. The resulting ciders with different colours and flavours were the beginning of the variety of ciders we know today. Cider is no longer a 'Shekhar' but a healthy drink, especially when it contains no added flavourings, sugar or preservatives.

The chemical composition of cider reminds somewhat of milk although the relative concentrations of key compounds differ. Cider is 86–88% water, and contains carbohydrates, fat and proteins. But unlike milk, most of the carbohydrates

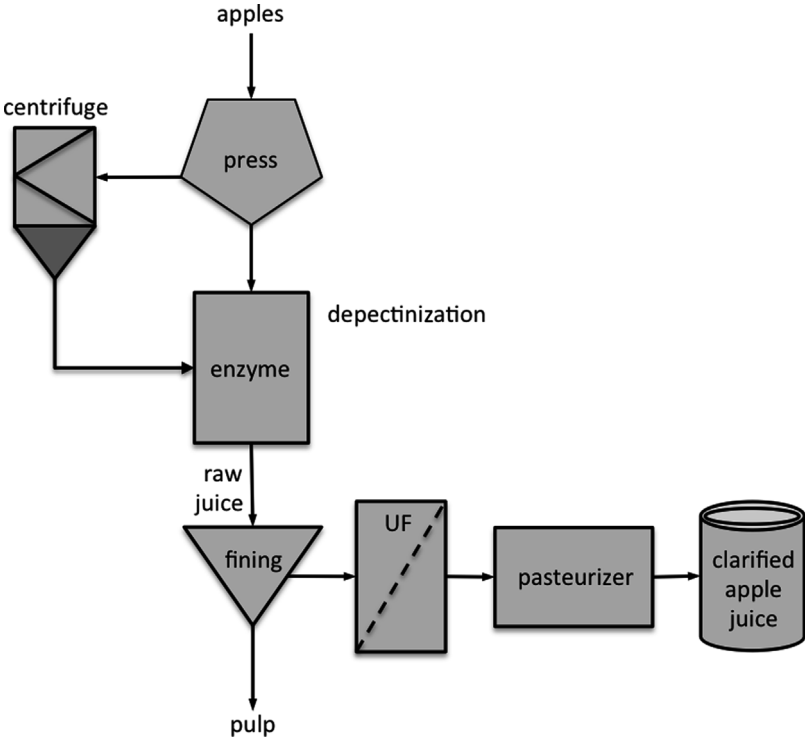


Figure 4.36 A complete process of apple juice making.

are natural sugars: 4.5–8.5% fructose, 1.5–4.5% sucrose and 1.2–2% glucose. Fat and proteins account for only 0.25% each. Apple juice also contains 0.5% fibres and minor concentrations of ascorbic acid (vitamin C), malic acid and citric acid. Ciders are often contaminated with various bacteria, yeasts and moulds that come from the apple surface and from contamination along the juicing process. The records, however, describe three outbreaks of human illnesses resulted from drinking of unpasteurized apple juice. A 1974 outbreak of nearly 200 illnesses caused by *Salmonella typhimurium* was traced to cider made in New Jersey. A 1980 outbreak in Canada was traced to unpasteurized cider with *E. coli* 0157:H7 bacteria. A 1991 outbreak in Massachusetts was prevented by the distribution of messages against unpasteurized cider [438]. Even without the pathogens, the shelf life of cold unpasteurized cider is only 12–14 days.

A typical preparation of apple juice starts from crushing and pressing of harvested and washed apples. The raw juice obtained after pressing is very turbid, viscous and dark. It contains a significant colloidal fraction stabilized in suspension by polysaccharides such as pectin, starch and gums [439].

The soluble colloids are removed by filtration. Historically, this was done using a mesh filtration by a simple revolving drum covered with a stainless mesh cloth. It was replaced by a granular filtration through a bentonite or diatomaceous

earth (kieselguhr) that until 20 years ago was considered a state of the art in apple juice purification. Until now the juice filtered through a granular filter meets the required turbidity standards and keeps the juice taste. The OpEx of granular filtration, however, is high. It is estimated between €60 000 and €100 000 per annum for small- and medium-sized fruit juice producers [440]. The replacement of spent filters can be associated with dust inhalation and can potentially result in lung diseases. The disposal of spent filter material requires special arrangement due to potential pollution and might be costly. For instance, the disposal of spent filter material in Germany costs €600 per ton. Granular filters might leave slight aftertaste in the juice [439]. Enzymes cannot be recovered and might serve as an additional pollution problem.

There are three primary areas where apple juice can be membrane-treated [437]. These are clarification of cloudy juices with MF and UF, production of juice concentrate with RO and deacidification with ED or NF. The last one is mainly applied in citrus juices. We will describe here only the first application – clarification. Membrane filtration is primarily used to intensify the apple juice processing. It is much faster than granular filtration and does not require the sedimentation step. Membrane filtration also does not require the enzymatic pectin degradation although studies show that a light enzymatic treatment reduces membrane fouling and viscosity and increases transmembrane flux. Alvarez *et al.* [441] showed that a pectinase treatment of apple juice tripled the permeate flux through a 15 kDa ZrO_2 membrane (Orelis, France). The increase from 50 to 150 LMH was observed at 50 °C with 400 kPa TMP and 3.7 m/s cross-flow velocity. A large increase in the permeate flux of mosambi juice through 0.285 μm ceramic membrane pretreated by pectinase was reported by Nandi *et al.* [442]. The use of tight membranes also minimizes the importance of pasteurization, thus avoiding the use of chemical preservatives such as 0.1% (v/v) potassium sorbate or sodium benzoate. de Bruijn *et al.* [443] reported that the apple juice filtered with 15 and 50 kDa ZrO_2 tubular membranes (Orelis, France) had a shelf life of at least 5 months. The juice was stored in glass containers at 16 °C in the dark. No significant changes in mosambi juice quality after a treatment with 0.285 μm ceramic membrane were observed during 30-day storage in a refrigerator [442]. The use of membrane technology improves the juice quality with respect to colour, clarity and taste, reduces the process OpEx, increases the juice recovery up to 98–99%, reduces the processing time and reduces enzyme consumption down to 25% of traditional quantities. In cross-flow membrane filtration, pectinase is added to the feed tank and recycles within the loop during the operation similar to the MBR recovery of activated sludge. The improved juice quality is due to the reliable and consistent removal of haze-forming components including suspended solids, colloidal particles, proteins and polyphenols. Typical turbidity levels of less than 1 NTU are much lower than the 5 NTU limit required by wholesale customers. The increased juice recovery comes from the elimination of granular media and fining agents that can absorb juice. A nominal 1% increase in recovery of a plant processing 350 000 l/day increases the revenue by $150 000 per season [437]. The conventional filtration

process results in 80–94% juice yield. Sedimentation and diatomaceous earth filtration may take up to 36 h when the average cross-flow filtration time is between 2 and 4 h. In general, shorter production times also help in keeping the essential juice ingredients intact, preventing their heat degradation. Membrane processes can also concentrate in the retentate potentially valuable ingredients such as pectin and enzymes. All these advantages resulted in a significant profit in a transition from a traditional clarification to membrane clarification of apple juice. An example published by Cheryan [437] reported that a transition from diatomaceous earth to UF membrane in Cadbury-Schweppes' processing over 500 000 l apple juice per day saved $350 000 annually. The difference was due to the elimination of more than 350 000 kg/year of diatomaceous earth and a 4% increase in yield. In another application, installing a tubular UF system resulted in savings of $50 000/year. The savings were due to absence of granular filter materials, 50% less enzyme usage, a 5% increase in juice yield and much shorter processing times.

All that said, membrane filtration is considered a new approach and juice manufacturers constantly compare the final quality of the juice after the membrane system with that obtained after pressure and granular filtration. Membrane filtration outperforms other clarifications. The point is that regulations require juice quality that can also be achieved by other methods and even when the juice manufacturers are interested in implementation of membrane technology, they are still subject to general standards. The manufacturers are interested in robust membrane technologies that guarantee high flux. The quality of clarified juice is not the problem. The general trend is therefore to use MF ceramic and UF polymer membranes with fluxes up to 300 LMH. There are also reports on membrane filtration of undepectinized juice with a flow of 35 LMH [444]. Typical membrane pores are 0.1–0.2 μm although the best juice quality is obtained with membranes with MWCO values below 50 kDa [445,446]. Larger pores are associated with higher fluxes. A flux of 300 LMH was obtained with filtration of depectinized apple juice through 0.2 μm ceramic membranes.

Opting for membrane filtration with tight membrane pores, however, incurs significant fouling. The most influential fouling mechanisms are cake formation and pore blocking depending on the membrane pore width [447,448]. There are several ways for reducing this fouling. The juice clarification is performed with UF and MF membranes that not only minimize the fouling but also improve the recovery of valuable compounds such as vitamin C, phenols and antioxidants. Similarly, cross-flow filtration enhances the shear stress and reduces the cake thickness. Pretreatment by decanters, finishers and centrifuges reduces the solid content in the feed, while cleaning in place (CIP) with caustic and free chlorine releases the foulants from the membrane surface.

Industrial applications of membrane filtration of apple juice are still few in number. Koch membrane systems reported the use of their SUPER-G tubular membrane modules at Peterson Farms (Shelby, Michigan). The modules employ 0.1 mm PVDF membranes used to clarify between 170 and 230 m^3 of apple juice daily. Centrifuging is used as a pretreatment and the CIP is performed with

caustic and caustic plus chlorine cycles [449]. The final juice turbidity is below 1 NTU (note that wholesale customers require 5 NTU or less) and the yield of filtered juice is between 98 and 99%.

In recent years, several fruit juice installations have incorporated ceramic membranes. The higher cost has been justified by the higher flux, much longer lifetime and better resistance to aggressive processing and cleaning conditions. Additional advantages include backflushing to unblock feed channels and backpulsing during operation [450]. Compared with the conventional clarification process, UF eliminates the use of diatomaceous earth, thereby reducing production costs and waste treatment problems [451].

The pretreatment using enzymes aims at hydrolysing mainly soluble polysaccharides responsible for high viscosity [452]. Using UF membranes allows enzyme recovery and reuse, thus reducing the total enzyme consumption by two-thirds [451]. The used ceramic tubular modules are, however, of relatively low compactness and incur high replacement cost. This step is often run in batch mode and diafiltration water has to be added at the final stage to maximize the process yield. The shelf life of UF clarified juices increases 6–10 times.

Despite the clear advantages of membrane processes, they are still in close competition with classical filtration technologies such as rotary vacuum-drum filters, diatomaceous earth and sheet filters. Those in favour of classical filtration argue that the flux through the membranes is low and that a large surface area is required. They also maintain that membrane filtration removes some of the precious colour from the juice. Therefore, large ceramic membrane manufacturers do not develop special equipment but rather offer their already developed membranes. Pall (New York, USA) offers Pall Membralox IC ceramic elements, multichannel membranes composed of a porous alumina support and a filtering layer (alumina, zirconia, titania). The membranes are available in MF segments (0.2 and 0.8 α-alumina) and UF segments (20, 50, 100 nm zirconia). GEA Westfalia reported that over the last 20 years it supplied more than 1000 lines of ceramic membranes with a pore size of 20–200 nm in the fruit juice industry [453]. Filtrox reported a full-scale installation of 191 m^2 MF ceramic membrane at Aston Cider (UK) to clarify apple cider.

4.6.3
Fermented Food Industry

Fermented beverages such as beer, wine and vinegar all require clarification for separating the fermenting agents from the product. The conventional technology today is filtration with diatomic earth (DE) also known as kieselguhr. The particles are precoated on a mesh screen and serve as a filter. DE filtration can not only remove large ferments but also improve the taste of the final liquid. Additional advantages of kieselguhr are its low price, high availability, excellent filtration results, high throughput per square filter area and good adjustability/flexibility. Kieselguhr, however, is not perfect. It can contain cristobalite, a suspected (but as yet unproven) lung carcinogen [454]. Inhalation of kieselguhr dust

during processing is a problem. The disposal of kieselguhr sludge (wet filter after use) costs roughly €0.17/kg in countries where landfill disposal is not possible [455]. Another problem is that washing kieselguhr filters requires large quantities of washing water, manpower and energy.

Starting in the 1970s, ceramic membranes were tested as an alternative filtration technology. The first full-scale installations went operational in 1980. Since then, ceramic membranes established themselves as a proven technology for clarification of fermented liquids [385]. Today, such installations of ceramic membranes still face severe fouling problems, in addition to several less critical issues that are beverage-specific. Filtrox, a Swiss company oriented on beer market, estimates that there are 2–3 installations of ceramic membranes for every 20 installations using kieselguhr. In the following subsections, we discuss the clarification of beer, wine and vinegar, addressing the pros and cons of both technologies and discussing the state of the art in ceramic membrane separation of fermented liquids.

4.6.3.1 Beer and Ceramic Membranes

Beer brewing is another interesting market segment where ceramic membranes can play a significant role in various steps. To understand this role, we must first learn a little more about brewing (most readers are probably just as interested in the beer as in the membranes anyway). Beer was probably one of the first drinks ever brewed. Shortly after the transition from travelling hunter-gatherer tribes to agricultural settlers, the settlements were faced with severe microbiological pollution of water sources. Six thousand years ahead of any FDA approval procedures, people found out empirically that boiling water prevents diseases. Boiling and cooling of water gives clean water, which quenches thirst but is not that exciting (tea and coffee were introduced much later). Boiling and cooling water *with additives* produces more interesting drinks. Beer was (and is) made from crushed grains called *malt* that were cooked in water [409,456]. Barley is often used for this purpose, although it contains only a trace amount of free sugar and a lot of starch [457]. The Sumerians are considered the first beer brewers, around 3000 BC. If the Sumerians avoided fermentation, they probably made *wort* – a thick sweet liquid of crushed grains boiled in water several times and cooled afterwards. What really makes the beer an alcoholic beverage is the addition of yeast – a single-cell fungus that converts the sugars in the wort into ethanol and CO_2. If a brewer is patient enough to wait for 7–10 days, the fermentable sugars are converted and the beer is ready. Brewers began adding hop blossoms to the wort from around the ninth century onwards to extend their beer's shelf life. These are removed later, at the *green beer clarification* step, because any hops, yeast cells or bacteria that remain in the so-called green beer can significantly alter its taste.

Raw beer contains four key ingredients – water, malt, yeast and hops. Three of them (malt, yeast and hops) have severe implications on microbiological, flavour and colloidal stability of the final beer. Microbiological stability deteriorates due to the presence of active yeast cells and bacteria. Uncontrolled bacterial growth

affects the taste of the beer and shortens its shelf life. The maximum allowed concentration of yeast cells is 5 cells per 100 ml. This is one stage where membranes come in handy: levels as low as 2 cells per 100 ml are possible using membrane filtration. Flavour stability is altered by flavour compounds in the beer and by the presence of dissolved oxygen (DO) [458]. The latter is formed in the wort that contains complex sugars and still active yeast cells, and leads to oxidative processes that alter the taste of the final beer. The retention of yeast cells solves the DO problem in most cases.

Colloids are formed in previously transparent yellowish or brownish beer at low temperatures due to the presence of proline-rich proteins coagulated by polyphenols. A 1 : 1 ratio of polyphenol-binding sites in the proteins to binding ends of the polyphenol molecules gives the maximal concentrations [459]. Polypeptides originate from barley and polyphenols from hops. The colloidal stability of the protein suspension deteriorates and white flocs (that scatter visible light) become visible in the beer [460]. Besides these, many colloidal particles are invisible to the naked eye yet still scatter the light, giving the beer a turbid appearance. Due to the colour, flocs give to the beer a cloudy appearance (so-called *chill haze*). This chill haze can also be of a biological origin due to any remaining yeast cells. Approximately 200 000 cells/ml are common in green beer decanted after primary fermentation or maturation. These cells cause a haze that persists even at room temperature, and is known as *permanent haze*. Typically, colloidal haze fully disappears at temperatures above +10 °C [461]. The formed flocs are slightly heavier than the beer and in time (after several weeks) they settle down at the bottom of the barrel. All that time, the temperature of the suspension should be practically 0 °C. That was recommended in small breweries and practiced historically. Besides gravity separation (which typically takes a long time), most brewers today use filter presses or pressure vessel filters. The filters are commonly precoated with DE (kieselguhr), perlite, cellulose or activated carbon. Kieselguhr filtration has been used to clarify beer for more than 50 years, and is still the leading technology today.

Ceramic membranes are considered a good alternative to kieselguhr filtration and are employed at several separation processes – hot wort separation, cold wort separation, wort clarification, green beer separation, rough beer clarification, yeast recovery, and malt and hope extraction [462,463]. Breweries use raw water and produce wastewater. Both processes need to comply with local and international standards. Moreover, brewers are typically proud of the special taste of their beer, which is partially linked to the water quality and its source. The additional advantage of preventing bacterial contamination during MF or UF using ceramic membranes matches perfectly the need for keeping the taste and flavour ingredients, while removing any potential microbiological hazards. Similarly, breweries can pretreat their wastewater with ceramic membranes, which results in retention of particles and allows the release of brewery wastewater into municipal collectors.

Previous attempts to use polymer membranes were unsuccessful due to several reasons. Besides the need for excellent mechanical stability, a membrane

used in beer brewing must withstand large temperature changes, ranging from 0 °C during filtration up to 80 °C during cleaning. Practical experience discovered that application of polymer membranes results in unpredictable and inconstant fluxes. Despite the higher investment in equipment, ceramic membranes are the only viable membrane choice for the beer industry, and this message has been received by all major ceramic manufacturers. In the last 20 years, the manufacturers adjusted their line of available membranes with products that are specifically adapted for beer brewers' needs. Examples include Cerinox® BF (Bucher Filtrox Systems AG, St. Gallen, Switzerland), Clearamic (GEA Westfalia Separator), CéRAM (TAMI Industries), Membralox (GE Water) and Atech Innovations. Some of these membranes are already used in full-scale installations. For example, Bucher Filtrox reported two full-scale installations of Bucher Filtrox Systems: one in Fürstenberg, Germany with a total area of 26 m^2 and the other in Boituva, Brazil with 239 m^2 [464]. Both breweries use vertically mounted microfiltration ceramic membrane units for separating the yeast cells during the process. When the yeast slurry concentration reaches a final value of 18–20% dry matter, water is added to increase the total amount of beer recovered (so-called diafiltration) [465]. Another example is the Keraflux beer recovery system produced by Pall Corporation [466].

Ceramic-based separations can be used in four different stages of the beer-making process: wort separation before fermentation, clarification of green beer, filtration of bottoms of fermentation tanks and sterilization of rough beer before packaging. Figure 4.37 details the main stages at a brewery and shows how ceramic membranes are used for the sterilization of rough beer before packaging.

Ceramic separation of malt and hop from the wort is performed with open tubular microfiltration membranes with pore sizes of 40–60 μm. Microfiltration is a good compromise between the need for retaining large particles and transmitting soluble macromolecules. The MF membranes are capable of removing up to 95% of total suspended solids (TSS) in the first stage of the operation and the additional 5% in the second stage. An alternative procedure is using a decanter followed by 1.3 μm MF membranes [384].

At the end of beer fermentation or maturation, the bottom of a fermentation vessel contains a sludge of yeast cells and beer. The sludge volume is between 1.5 and 2% of the fermentation tank volume, and the beer in the sludge can be recovered and blended with the main stream of green beer. That operation is performed with 0.4–0.5 μm MF ceramic membranes and might be prolonged by using DF water to increase the amount of recovered extract. The DF water is added to the fermentation tank before the filtration and dilutes the yeast concentration to continue the MF. That is a sustainable application that results in two valuable streams. The liquid stream joins the green beer (although sometimes the quality of the beer recovered from tank bottoms is different from the main green beer stream). Eagles and Wakeman [467] found a higher concentration of some yeast metabolites (ethyl acetate, butyl alcohol and amyl alcohol) in the permeate of 0.45 μm MF alumina membranes. That is because the fermentation tank bottoms have relatively large amounts of yeast, proteins and polyphenols [455].

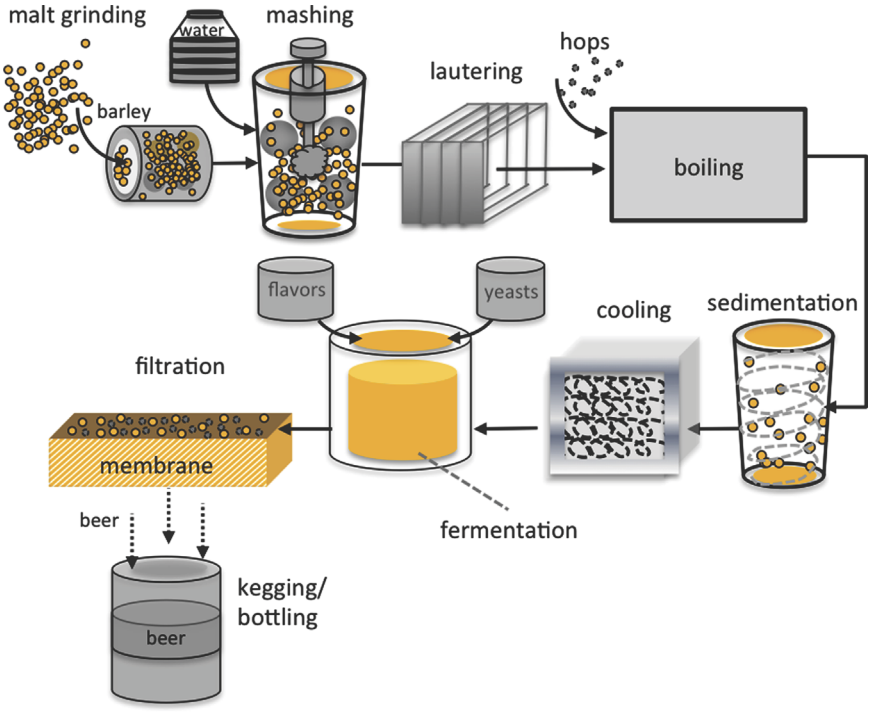


Figure 4.37 A scheme of traditional beer making with ceramic membrane used for sterilization of rough beer.

In practice, the sludge filtration should be performed as soon as possible to minimize the detrimental effects of consolidating yeast slurry. The remaining sludge, is then recycled back to the fermentation reactor.

Clarification of rough beer is usually done using ceramic membranes with pore sizes between 0.2 and 0.8 µm. The industry standard today is 0.5 µm. Pores smaller than 0.2 µm might retain important components that affect the beer's character: bitterness, fullness and foam formation [467]. Pores larger than 0.8 µm might not separate proteins properly. The filtration of green beer is performed by ceramic membrane modules that are combined into a filtration loop. The feed is then circulated in the loop and separates into a permeate stream of clarified beer and a retentate stream of green beer that is recycled back to the feed tank. This feed is pumped into the loop in either a continuous or batch mode.

Separating the proteins from the green beer is a difficult task. A typical membrane application is to retain hydrophobic proteins and transfer the hydrophilic proteins. Hydrophobic proteins are more suspected of fouling and thus often unwanted. Hydrophilic proteins are readily soluble in water, participate less in fouling and are hardly retained by most membranes. Protein separation from green beer must achieve the opposite: retain the hydrophilic proteins and transfer hydrophobic ones. The hydrophilic proteins are the ones that cause the

unwanted chill haze at low temperatures, while hydrophobic proteins give the beer its essential foam properties. Unfortunately, the hydrophobic proteins in the beer are only slightly bigger than hydrophilic ones [468]. UF ceramic membrane separation is always at risk of over-transmission of haze proteins and under-transmission of foam proteins [458]. The separation is further complicated by a continuous fouling that changes the hydrophilicity of the ceramic membrane surface [324] due to selective adsorption of hydrophilic proteins and polyphenols. Other major foulants are yeast cells (different strains of *Saccharomyces cerevisiae*) that form a cake layer over the membrane surface, as well as arabinoxylans, β-glucans and polysaccharides [458]. Reversible fouling is removed by short-time backflushes, while irreversible fouling is removed by chemical cleaning. Typical cleaning of ceramic membranes is quite harsh and might include high temperatures of 85 °C and aggressive chemicals such as sodium hypochlorite or hydrogen peroxide. The advantage of this approach is that the cleaning step is relatively inexpensive and short (it takes only about 45 min). An expensive enzymatic cleaning is thus avoided.

Finally, ceramic membranes are employed instead of heat pasteurization as the final step before bottling. When the wort is boiled, the beer loses water, so after maturation the rough beer contains too little water and too much alcohol. In general, breweries use 5–6 litres of water per litre of beer. A blend of rough beer and water is either sterilized in dead-end mode with 0.4–0.7 μm membranes or pasteurized. Breweries use either flash pasteurization at 71–74 °C for 15–30 s on a plate heat exchanger or tunnel pasteurization at 60 °C for 10 min with tunnel pasteurizers [465]. Pasteurization is said to alter the flavour of the final product, reducing the beer's 'freshness'. This is why sterile filtration has been used as an alternative to pasteurization for many years. Ceramic filters are installed between the bright beer tank and the filling machine. The resulting beer is free from beer-spoiling bacteria and tastes fresh and natural (as it has not been heat-treated). Since the quality of membrane-sterilized beer is considered superior to pasteurized beer, while the costs for membrane sterilization are comparable to the costs of pasteurization, ceramic membranes are widely applied here [384]. In some applications, the alcohol content of the beer can be reduced by a factor of 8–10 with thin-film composite RO membranes in a spiral-wound configuration. Whether such a reduction is really a good idea or not is an excellent topic of pub debate.

Implementing ceramic membranes in beer brewing brings with it a number of advantages over conventional technologies. Ceramic membranes can replace the granular media, avoiding the handling and disposal problems associated with it [469]. Beer losses are reduced [470], the beer quality improves and the operational costs are lowered. Ceramic membranes can remove malt and hops from the wort while it is still hot. They are completely inert and food compatible. Typical membrane fluxes are much higher compared with kieselguhr filtration, and therefore the footprint used for membrane clarification is much smaller. Membrane separation at the end of the pipe exchanges or at least minimizes heat pasteurization. The separation process, however, is still not perfect. This is

because the chemical composition of different beers varies, and might contain more than 1000 compounds. A typical barley beer is 90% water, 4% ethanol, 1% proteins and 5% of other volatile and non-volatile organic compounds. The latter group includes aliphatic carbonyl compounds, alcohols, monocarboxylic acids and their esters, nitrogen- and sulfur-containing compounds, hydrocarbons, terpene derivatives, heterocyclics and aromatics, unfermented sugars, dibasic and tribasic carboxylic acids, colouring substances, tannic and polyphenolic substances [471]. Many of these compounds can cause a severe fouling of ceramic membranes. The fouling starts with internal pore blocking, followed by an external surface fouling. The composition of the fouling layer is dominated by proteins associated with polyphenols and β-glucans [472]. Other carbohydrates are also embedded into the fouling bed, making it extremely complex and difficult to handle. Recent studies proved that yeast cells play no role in membrane fouling [473]. Obtaining and maintaining a reasonable flux remains the most urgent technological problem that needs to be resolved before a full-scale implementation of ceramic membranes can be considered. Although the fouling affects all applications of ceramic membranes in food industry, it is more pronounced in beer brewing compared with milk, wine or juice clarification. As a result, full-scale installations of ceramic membranes in the beer industry lag behind installations in other beverage sectors. Another major drawback is variations in the turbidity, protein and aroma retention in beers cleaned with the same membrane [474]. Uncertain flux and varying quality, severe fouling and absence of full-scale installations are the reasons that nearly 99% of all brewers still do their beer clarification using kieselguhr [475].

The simplicity of procedure, the variety of tastes (different grains and even different water sources can give the beer a different taste) and alcoholic content made the beer a very popular drink already thousands of years ago. Up to 40% of the grains harvested in Sumeria were used for beer brewing [476]. In many places, beer became the national drink. Figure 4.38 shows the distribution of top beer breweries per country [393].

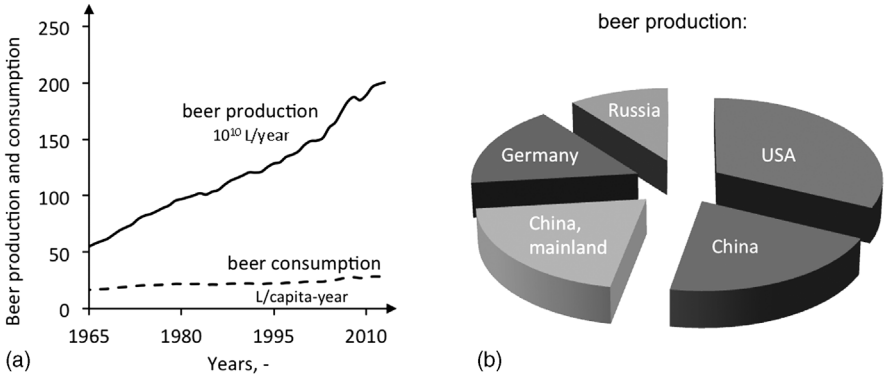


Figure 4.38 Worldwide beer production (in tens of billions of litres) and average beer consumption in litres per capita per year (a), and top 5 beer producers in 2013 in the world (b).

In general, beer brewers have no time to worry. They just have to produce more beer. Our average beer consumption has doubled in the past four decades. The average consumption of barley beer 40 years ago was 15 l per capita per year. In 2013, we consumed more than 28 l per capita. Interestingly, countries that top the list of beer producers are not the countries that consume most of the beer per capita. The one exception is Germany with 106 l per year per capita. Among most beer-drinking countries are Czech Republic with 150 l per year per capita and Austria with 108 l per year per capita.

Although ceramic membranes are progressing slowly in the brewery sector, the number of installations is rising steadily. Today, 4% of all the beer produced in the world is filtered with membranes. The CapEx and OpEx for kieselguhr and ceramic membrane filtrations are comparable. An average price for cold sterilization with ceramic filter is €0.26 per hectolitre of beer, compared with €0.20 per hectolitre for flash pasteurization. Membrane yeast separation costs €0.44 per hectolitre while dead-end kieselguhr filtration costs €0.43 per hectolitre [455]. Ceramic membranes suit ambitious sustainability goals to reduce water, energy and solid waste footprints. The average solid waste weight is 0.8 kg per hectolitre, and kieselguhr disposal represents 50% of it. The production of kieselguhr is an energy-demanding process and the use of ceramic membranes reduces the CO_2 footprint by about 40% [477].

4.6.3.2 Winemaking and Ceramic Membranes

Winemaking is a very old industry, probably as old as ceramics. The first wines of which we have written records were produced around 6000 BCE in Iran [409,478]. The word spread, and at the time of the Greek and Roman Empires wine became very popular worldwide. It is still very popular in southern Europe as a part of a meal but it has been partially replaced by a glass of beer in northern Europe. The annual worldwide wine consumption is around 4 l per capita, although this has been decreasing in recent years [393]. Two-thirds of all wine is produced in Europe, mainly in France, Italy and Spain. Despite what many aficionados would have us believe, winemaking is really a simple and straightforward process, where basically all one needs is good grapes. After harvesting, the grapes are crushed and pressed to initiate a contact between the sugars in the juice and yeasts on grape skin. The fermented juice, called *must*, is then separated from the yeasts by centrifugation, kieselguhr dead-end filtration or ceramic membranes, and *voilà*, the wine is ready. Depending on the region, the grapes might or might not contain enough sugar. The concentration of sugar in insufficiently mature grapes grown in cold weather is adjusted by simply adding sugar. A higher content of sugar in the must means more alcohol after fermentation. The fermentation is performed with or without the addition of yeast, depending on the wine type [384]. In several wine types, the liquid from a fermentation tank is passed to a second fermentation tank for maturation. Wines are roughly subdivided into still or table wines with 8.5–14% alcohol, sparkling wines from a secondary fermentation tank and fortified wines (containing more than 14% alcohol) [479].

Grape harvesting and winemaking are very traditional processes that pass from generation to generation. Any changes in the process are received with much scepticism, and debated and tested for years before full-scale implementation. That is why for a long time yeasts were separated by centrifuging. The wine flowed through the opening in the upper part of a fermentation tank, and the sludge that contained the yeast diluted in the wine was removed from the bottom. Two traditional problems are associated with this approach. The sludge (called the *wine lees*) contains useful yeasts that could be recovered, plus wine that could be simply sold. Instead, the entire volume that is as much as 13% of the fermentation reactor is thrown away, or at best used for producing food-grade spirits. The upper liquid contains a high concentration of yeast that passes with the wine to the oak barrels (or to stainless steel tanks) for maturation and aging. On many occasions, the actual taste of the most impressive aged wines is somewhat disappointing and vinegar-like. In addition, the wine is turbid and contains colloids such as polysaccharides, proteins, polymerized phenolic compounds and colloidal aggregates, and particles including yeasts, bacteria, cell debris, colloidal aggregates and potassium tartrate crystals [479]. The colloids and the particles make the wine turbid, and may create sediments that are regarded as a sign of wine deterioration. The initial turbidity of wines typically varies between 25 and 1000 NTU [480].

Kieselguhr (DE) filtration entered the wine industry at the beginning of the twentieth century, first as a polishing procedure and for the last 50 years as the main yeast separation process. The pros and cons of kieselguhr are detailed in the sections above. In addition, a high value of filtered wines led to a downwash approach specific for kieselguhr filters. In this process, the wine trapped inside the filter media is blown down by an inert gas such as CO_2 [481]. A new arrangement of filter media after the blowdown results either in a naked screen or in insufficient filter depth that affects the filter performance immediately after the filtration restarts. The Kieselguhr also absorbs wine in a range of 1.25 g of wine per each gram [482]. This causes large product losses to the winery. The general perception therefore is that kieselguhr filters are less suitable for wine clarification. Basically as the time passed and as more and more stringent regulation on the sludge land disposal were enforced, the use of kieselguhr became less advantageous and more problematic.

Ceramic membranes were first tried by the winemaking industry in the 1980s. A decade later, microfiltration using ceramic membranes was accepted as a valuable alternative to other separation methods. The cross-flow microfiltration (CFMF) technology was embraced by the wine industry because it offered a good compromise: On one hand, it answered the need for removing yeast, bacteria and macromolecules such as proteins and polysaccharides. On the other hand, it kept the taste and flavour ingredients in the final product, retaining the elusive 'personality' of good wines [483]. During cross-flow microfiltration, the crude wine flows parallel to the membrane surface and permeates through the membrane due to a pressure drop. The shear exerted by the feed is considerable, sweeping foulants away from the membrane surface and keeping the fouling layer relatively

thin. This method allows prolonged filtration runs, with up to 20 h between cleanings. A rough estimate, however, suggests that energy requirements for CFMF are three to five times higher than those for dead-end filtration.

The initial idea was to perform the wine clarification/filtration/sterilization in a single step. This turned out to be problematic. The energy requirements were high due to an intensive fouling, and the fluxes were low as UF membranes were used. Moreover, the separation of yeasts and bacteria at a single stage did not address nor solve the secondary microbiological contamination problem. Clarified wine is often kept in storage tanks and bottled and distributed when needed. To eliminate the risk of microbiological contamination, the wine is heat pasteurized before bottling. As a result, the UF treatment in the initial set-up was unnecessary and mainly increased the OpEx. An updated scheme uses a two-stage approach – the separation of yeasts by MF, followed by a cold sterilization by UF membranes. Ceramic membranes can handle 35–50% throughput and operate 18–20 h continuously between cleanings [320]. The resulting filtered wines have a turbidity below 1 NTU as required from brilliant wines. Here, *brilliant wine* is a term used for describing wine that is crystal clear, with no cloudiness or sediment. Washing and regeneration of ceramic membranes is performed at temperatures of 70–80 °C.

There are three stages during wine manufacturing where ceramic membranes can be implemented. These are clarification of wine after fermentation, side treatment of wine lees and cold sterilization. Figure 4.39 details the main stages of wine harvesting and the stages where ceramic membranes can be implemented.

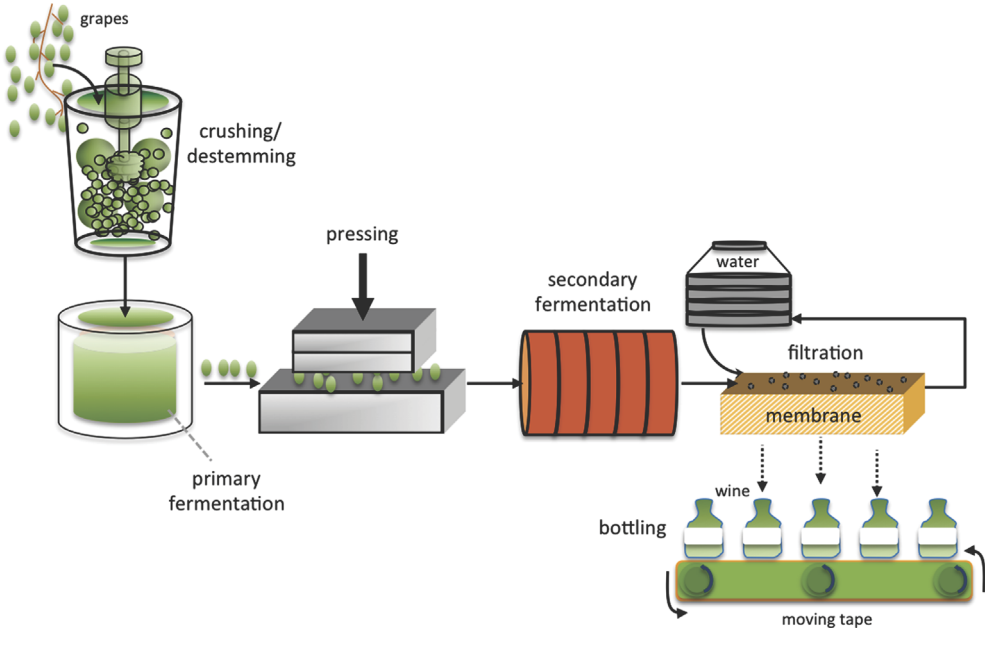


Figure 4.39 A general scheme of wine harvesting with ceramic membrane used for wine clarification and sterilization.

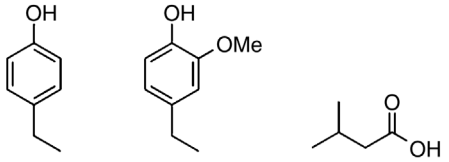
The production of sweet wine requires that fermentation stops before all of the sugar in the medium is converted into alcohol. While centrifugation keeps significant concentrations of yeasts and macromolecules in the wine, microfiltration is a hassle-free simple operation that removes all particles. The fouling here takes the form of a porous yeast cake on top of a membrane and does not affect the membrane flux significantly. A typical litre of wine contains 750–900 ml of water, 69–121 ml of ethanol, 5–20 g/l of glycerol, 3–20 g/l of organic acids, 0.5–5 g/l of amino acids and proteins, and 0.4–0.7 g/l of polysaccharides and phenolic compounds [479]. Polyphenols (especially tannins), polysaccharides (pectins and mannoproteins) and proteins are the main foulants. In addition, any external fouling with yeast (mainly *S. cerevisiae*), bacteria and cell debris might result in a cake formation [484]. Wine tannins cause a quick adsorption followed by pore adsorption and cake formation. Similarly, pectins contribute significantly to the formation of a gel layer [485]. Due to the relatively mild conditions needed for retaining a good wine's 'personality', the wine clarification process is often performed with polymer hollow fibres. These typically have pore diameters between 0.2 and 0.65 µm [384]. Ceramic membranes, which incur higher capital expenses, lag behind polymer membranes in this application. Several leading membrane manufacturers opened a line of polymer membrane-based clarification systems especially adjusted to the wine industry. Koch Membrane, for example, offers the WINEFILTER cross-flow systems operable with a variety of PVDF membranes. Pall Corporation offers the Oenoflow system equipped with hollow-fibre PVDF modules. The company has sold already more than 1000 Oenoflow systems to the wine industry [486]. Bucher Vaslin (Chalonnes-sur-Loire, France), a company that specializes on wine market and considered second only to Pall in the US membrane wine separation market, offers a number of filtration systems named FX2, FX3 and FX6 at prices ranging between $85 000 and $155 000. These processes clarify the raw wine using PS membranes with 3 mm inner diameter and a nominal pore size of 0.2 µm [482]. Such systems can produce a transmembrane flux range between 800 and 8000 l/h (LPH).

One step in the winemaking process where ceramic membranes show a clear advantage is during the *wine lees* filtration. Wine lees, a general term referring to the sediment at the bottom of fermentation tanks, consists of yeast, seeds and fining agents, plus substantial amounts of wine. Direct ceramic membrane filtration or a combination of microfiltration with decantation results in higher quality of wine that is returned to the main wine stream. Part of the recovered yeast is recycled back to the fermentation tank, while the wine that was filtered out of the lees is returned to the main line. Several membrane manufacturers offer wine lees filtration installations based on ceramic membranes. Pall offers the Membralox ceramic membrane elements in three configurations assembled in two industrial modules [487]. SIVA (France) offers an autonomous 'VINI-TIS' module that integrates ceramic membranes and a pump into a circulation loop that creates a tangential flow. GEA Westfalia Separator Group offers its Membraflow ceramic membrane elements with capillaries between 1.3 and 8 mm and

pore sizes from 5 nm all the way up to 1.4 μm [482]. The elements are arranged as hollow fibres or honeycombs and a single element might contain between 1 and 277 capillaries. This company also offers a flexible range of filter element lengths. TAMI Industries (France) offers the INSIDE CéRAM MF membranes. Della Toffola ceramic membranes were used in a number of successful installations in Italy and Australia: several leading Australian winemakers such as McGuigan-Simeon at Loxton, Master Winemakers in the Yarra Valley and Casella Estate repeatedly announced the use of Della Toffola membranes for wine clarification [488]. Eaton Corporation (Dublin, Ireland) developed a BECO LiquiControl2 instrument for determining wine filterability. In this process, which is very similar to a standard silt density index (SDI), a sample of wine is filtered through a 47 mm diameter, 0.45 or 0.65 μm pore size membrane under a preset constant operating pressure that typically ranges between 0 and 3 bar. The sample is considered filterable if a defined quantity of filtrate is obtained at the applied TMP.

Mature or aged wines are pasteurized before bottling and distribution. The wine is often held in short-term to medium-term bottling storage tanks and fed to the bottling line when desired. This storage can result in microbial contamination, as well as in excessive alcohol levels (if the raw wine was centrifuged). The reduction of alcohol level with distillation or with RO membranes might affect taste and odour of the final wine and is therefore less popular. In addition, the International Code of Oenological Practices limits the use of RO to reduce the initial volume of wine by up to 20% and to change the potential alcohol content by up to 2% [489]. The microbial quality of wine is assured by heat pasteurization or by cold pasteurization with dead-end UF membranes. A proper design of cold pasteurization should be that the permeate is drawn directly into bottling holding tank or surge tank. Typically, the best results are obtained with 0.1 μm membrane pore size for white wines and 0.2–0.4 μm pore size for red wines. The suggested pore sizes are based on the assumption that a previous clarification step is also performed with membranes with pore size between 0.2 and 1 μm. This allows the reduction of the membrane pore size at the cold pasteurization step for better results. If the previous separation is performed using centrifugation, the cold pasteurization will be performed with 0.45 μm membranes to ensure microbial stability.

Wineries that usually have good microbial quality of their wines might use membranes with 0.65, 0.8 and 1.0 μm to ensure the removal of yeast, while keeping the taste and odour compounds. That approach, however, is not recommended since improperly treated wines are at risk of developing a so-called *Bretty character*. This happens if the yeast bacterium *Brettanomyces bruxellensis* and its close relative, *Dekkera bruxulensis*, cause the formation of a number of compounds that affect the aroma of the wines. The three most important (and often detected and smelly) compounds in this respect are 4-ethylphenol, 4-ethylguaiacol and isovaleric acid (see Figure 4.40). All three can give the wine unpleasant smells, reminiscent of sweaty animals, cheese, smoked bacon, wet dogs or creosote. The 'Bretty' wine character is mainly acquired during



4-ethylphenol 4-ethylguaiacol isovaleric acid

Figure 4.40 Molecular structures of 4-ethylphenol, 4-ethylguaiacol and isovaleric acid – the three most notorious compounds responsible for *Bretty* wine character.

maturation of red wines in oak barrels and can result in decreased shelf life, withdrawal of wine for reprocessing or simply dismissal of an entire production series. That is why the cold pasteurization is increasingly important. Sometimes heat pasteurization is preceded by ceramic membranes with 1.0–1.2 μm pore size. That multi-barrier approach saves on energy expenses of both treatments, albeit it increases the CapEx. The cold pasteurization market is also almost entirely dominated by polymer membranes made of nylon, PVDF, PES and cellulose acetate. Millipore, Sartorius and Pall hold an estimated 80% of the total market share [481].

Although in general wine consumption has remained steady over the years, it is one of the fastest growing beverage markets in developed countries. The wine industry is the second only to bottled water growing market in the United States. The agreement in the recent years is that membrane treatment is better than kieselguhr (DE) filtration as it leaves all essential compounds that give the wine its unique taste and aroma. Cellar staff repeatedly report that membrane treatment presents a major advance in winemaking and wine production technology [481]. The fouling degree in wine clarification, moreover, is low. This means that ceramic membranes can compete with PES and PVDF ones. If wine lees treatment becomes a standard operation, which is likely, the market share of ceramic membranes in winemaking will grow further.

Exercises

4.1. The Brix of the raw apple juice is 11. Explain how this number will change if 25% of the feed will be retained by a ceramic membrane.

4.2. Silica, alumina and perovskites are all metal oxides, yet the first two are not suitable as dense electrolyte membranes for fuel cell applications. List three reasons why perovskite oxides are preferred over silica and alumina as electrolyte membranes for ion transport in fuel cells. Do you think that perovskite oxides can also be used as ceramic membranes in other applications such as beer and juice clarification? Explain your answer.

4.3. Examine the 'cat-in-a-cup' concept shown in Figure 4.15. Do you think that by using different types of ceramic materials this concept can also be adapted successfully to the filtering of organometallic complexes such as nickel triphenyl phosphite (which is used as a catalyst in the DuPont nylon process)? If so, which materials would you recommend for constructing these filters?

4.4. When properly applied, a catalytic membrane reactor can shift the equilibrium of a chemical process towards the desired products, even without changing the reaction temperature. This seems to be in conflict with the laws of thermodynamics, according to which K_{eq} is a function of temperature only. Explain the 'legal loophole' that allows the CMR to circumnavigate these laws.

4.5. List three market segments in the water industry where ceramic membranes have a significant growth potential, and explain what are the current barriers that must be overcome to realize the potential in each case.

4.6. Two filtration modes are shown in Figure 4.41.

a) Name both modes and mark two main parameters that characterize each mode.
b) Explain the difference in the application of each filtration mode in the processing of orange juice.
c) Recommend a filtration regime and outline the main parameters for a successful membrane filtration of orange juice.

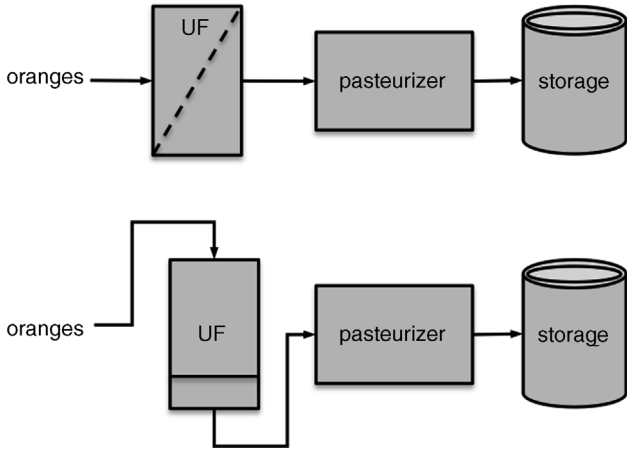


Figure 4.41 Orange juice filtration with ceramic membranes.

4.7. The fuel oxidation scheme shown in Figure 4.42 functions with limited efficiency.

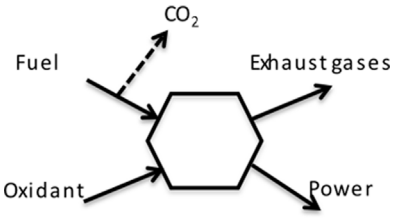


Figure 4.42 Fuel oxidation scheme.

a) Name possible reasons for the poor functioning of the system.
b) Compare the suggested oxidation scheme with other schemes.
c) Suggest ways to improve the efficiency of the scheme.

4.8. Figure 4.43 shows the scheme of a filtration cycle in whey protein separation.

a) Is this filtration system working properly? Explain your answer using the terms transmembrane flux and transmembrane pressure.
b) What could be the reason for the flux behaviour that you see? Detail the explanation by using terms such as foulant, protein, pressure drop, flux drop and reversibility.
c) Suggest at least one hydraulic/technological approach and at least one chemical approach for improving this filtration cycle.

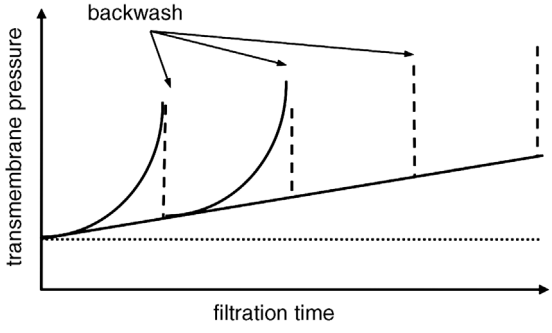


Figure 4.43 Whey protein separation scheme.

4.9. You found a bottle of beer in the freezer. It is hot outside and you would like to drink the beer. You wait until the beer thaws, open the bottle and pour the beer into a glass. Then you see that the beer in the glass is cloudy (not transparent).

a) Name and explain this phenomenon, suggesting at least two reasons why your beer is not transparent.

b) Suggest a way to single out a most probable reason for what you see.
c) How you can prove or disprove your assumption at home with no laboratory equipment?
d) If your assumption is correct, would you drink this beer now? Explain your answer.

4.10. You are travelling in Peru, away from urban hustles, and find a water source. The water, however, is turbid, and possibly contains not only minerals but also bacteria. Fortunately, you have with you a copy of *Ceramic Membranes* by Gitis and Rothenberg. You are in a mountain area and have also a spoon shovel, burning coal and some matches. There are 3 h left until sunset. You have no other water sources and there is no other water close by. Based on these data, outline five steps that will help you filter the water so that you can drink it and not get sick in the morning. You may assume that any viruses that may be in the water are not pathogenic.

4.11. You are a leading engineer in a company that is currently promoting the use of new fuel cells that have a potential to replace the conventional electricity supply from power stations. However, for some time you find yourself in uneasy situation when you hear the explanations provided by the company. Diagnose yourself and find at least three reasons why you feel the way you do. Are these deficiencies solvable? If they are, explain how. If they are not, explain why.

4.12. Burning hydrogen is better than using fossil fuels. The efficiency of an engine is higher and there are no pollution issues. Still, powering an internal combustion engine with hydrogen is not considered an optimal solution when you have pure hydrogen available. Explain the reasons for this and suggest an optimal (or at least, better) way for obtaining energy from pure hydrogen.

4.13. Hydraulic cleaning is better than chemical cleaning of polymer membranes. Ceramic membranes can be cleaned hydraulically and chemically with no preference between two methods. Why? What are the additional treatments applicable in ceramic membrane cleaning?

4.14. Ceramic membrane filtration is currently one of the leading applications in the food industry. List at least three reasons why ceramic membranes can successfully compete with polymer membranes, centrifuges and kieselguhr filtration. What are the next necessary steps that will help spread ceramic membranes even further?

4.15. Explain the differences between an inert membrane reactor and a catalytic membrane reactor, and give an example of a chemical process where each type of reactor is used.

4.16. You are a top manager in the food company that considers improving the shelf life of its products using an additional separation process. You have

an opportunity to apply coagulation, flocculation, sedimentation, granular filtration, membrane filtration, centrifugation, aeration and adsorption.

a) Name three leading applications you would consider to be most applicable for the company needs. Learn about the theory of reasoned action also known as the Fishbein–Ajzen model. Apply the model to explain your preferences and the final choice of the separation process.
b) Draw a technical scheme that will include the separation process you suggest.

References

1 Bredesen, R. (2006) Inorganic membranes. Proceedings of the 9th International Conference on Inorganic Membranes, Selskapet for Industriell og Teknisk Forskning, Lillehammer, Norway.
2 Mathur, S. and Ray, S.S. (2011) Ceramic engineering and science proceedings, in *Nanostructured Materials and Nanotechnology*, John Wiley & Sons, Inc., Hoboken, NJ.
3 Christian, G. and Adam, S. (2015) Ceramic membranes technology: current applications and future development, in *Handbook of Membrane Separations: Chemical, Pharmaceutical, Food and Biotechnological Applications*, CRC Press, Boca Raton, FL, pp. 215–258.
4 Aguado, S., Nicolas, C.-H., Moizan-Basle, V., Nieto, C., Amrouche, H., Bats, N. *et al.* (2011) Facile synthesis of an ultramicroporous MOF tubular membrane with selectivity towards CO_2. *New Journal of Chemistry*, **35** (1), 41–44.
5 Hwang, S.T. and Kammermeyer, K. (1975) *Membranes in Separations* (ed. K. Kammermeyer), John Wiley & Sons, Inc., New York.
6 Lu, G.Q., da Costa, J.C.D., Diniz, J.C., Duke, M., Giessler, S., Socolow, R. *et al.* (2007) Inorganic membranes for hydrogen production and purification: a critical review and perspective. *Journal of Colloid and Interface Science*, **314** (2), 589–603.
7 Freeman, B. and Yampolskii, Y. (2010) *Membrane Gas Separation*, John Wiley & Sons, Ltd, Chichester.
8 Scott, K. (1998) *Handbook of Industrial Membranes* (ed. K. Scott), Elsevier, Amsterdam, pp. 3–185.
9 Robeson, L.M. (1991) Correlation of separation factor versus permeability for polymeric membranes. *Journal of Membrane Science*, **62** (2), 165–185.
10 Li, K. (2007) *Ceramic Membranes for Separation and Reaction*, John Wiley & Sons, Ltd, Chichester.
11 Pandey, P. and Chauhan, R.S. (2001) Membranes for gas separation. *Progress in Polymer Science*, **26** (6), 853–893.
12 Keizer, K., Uhlhorn, R.J.R. and Burggraaf, T.J. (1995) Gas separation using inorganic membranes, in *Membrane Separation Technology. Principles and Applications* (eds D.N. Richard and S.A. Stern), Elsevier, Amsterdam, pp. 553–588.
13 van Veen, H.M., Bracht, M., Hamoen, E. and Alderliesten, P. (1996) Feasibility of the application of porous inorganic gas separation membranes in some large-scale chemical processes, in *Fundamentals of Inorganic Membrane Science and Technology* (eds A.J. Burggraaf and L. Cot), Elsevier, Amsterdam, pp. 641–680.
14 Barker, T., Bashmakov, I., Bernstein, L., Bogner, J., Bosch, P. and Dave, R. (2007) Climate Change 2007: The Physical Science Basis. Intergovernmental Panel on Climate Change, Cambridge, UK.
15 Lomborg, B. (2001) *The Skeptical Environmentalist: Measuring the Real State of the World*, Cambridge University Press, Cambridge.

16 Keeling, C.D., Piper, S.C., Bacastow, R.W., Wahlen, M., Whorf, T.P., Heimann, M. *et al.* (2005) Atmospheric CO_2 and $^{13}CO_2$ exchange with the terrestrial biosphere and oceans from 1978 to 2000: observations and carbon cycle implications, in *A History of Atmospheric CO and Its Effects on Plants, Animals, and Ecosystems* (eds J.R. Ehleringer, T.E. Cerling and M.D. Dearing), Springer, New York.

17 US Energy Information Administration (2014) International Energy Outlook 2014.

18 International Energy Agency (2014) CO_2 Emissions from Fuel Combustion Highlights.

19 He, X., Yu, Q. and Hägg, M.-B. (2013) CO_2 capture, in *Encyclopedia of Membrane Science and Technology*, John Wiley & Sons, Inc., Hoboken, NJ.

20 Dhaval, B., Anthony, Y.K. and Surinder, S. (2015) Membranes in power generation: a review of current uses and emerging applications, in *Handbook of Membrane Separations*, CRC Press, Boca Raton, FL, pp. 485–504.

21 Haszeldine, R.S. (2009) Carbon capture and storage: how green can black be? *Supramolecular Science*, **325** (5948), 1647–1652.

22 Institute, E.P.R. (2008) Program on Technology Innovation: Post-combustion CO_2 Capture Technology Development. Electric Power Research Institute, Palo Alto, CA.

23 D'Alessandro, D.M., Smit, B. and Long, J.R. (2010) Carbon dioxide capture: prospects for new materials. *Angewandte Chemie, International Edition*, **49** (35), 6058–6082.

24 Doctor, R., Palmer, A., Coleman, D., Davison, J., Hendriks, C., Kaarstad, O. *et al.* (2005) IPCC Special Report on Carbon Dioxide Capture and Storage. Intergovernmental Panel on Climate Change, Cambridge, UK.

25 Draper, E.L. and Leer, S.F. (2000) Research and Development Needs for the Sequestration of Carbon Dioxide as Part of a Carbon Management Strategy. National Coal Council.

26 Scholes, C.A., Smith, K.H., Kentish, S.E. and Stevens, G.W. (2010) CO_2 capture from pre-combustion processes – strategies for membrane gas separation. *International Journal of Greenhouse Gas Control*, **4** (5), 739–755.

27 Favre, E., Bounaceur, R. and Roizard, D. (2009) A hybrid process combining oxygen enriched air combustion and membrane separation for post-combustion carbon dioxide capture. *Separation and Purification Technology*, **68** (1), 30–36.

28 Merkel, T.C., Lin, H., Wei, X. and Baker, R. (2010) Power plant post-combustion carbon dioxide capture: an opportunity for membranes. *Journal of Membrane Science*, **359** (1–2), 126–139.

29 Ward, W.J. and Robb, W.L. (1967) Carbon dioxide–oxygen separation – facilitated transport of carbon dioxide across a liquid film. *Supramolecular Science*, **156** (3781), 1481–1484.

30 Hanioka, S., Maruyama, T., Sotani, T., Teramoto, M., Matsuyama, H., Nakashima, K. *et al.* (2008) CO_2 separation facilitated by task-specific ionic liquids using a supported liquid membrane. *Journal of Membrane Science*, **314** (1–2), 1–4.

31 Favre, E. (2011) Membrane processes and postcombustion carbon dioxide capture: challenges and prospects. *Chemical Engineering Science*, **171** (3), 782–793.

32 Favre, E., Roizard, D., Bounaceur, R. and Koros, W.J. (2009) CO_2/N_2 reverse selective gas separation membranes: technological opportunities and scientific challenges. *Industrial & Engineering Chemistry Research*, **48** (7), 3700–3701.

33 Rao, A.B. and Rubin, E.S. (2002) A technical, economic, and environmental assessment of amine-based CO_2 capture technology for power plant greenhouse gas control. *Environmental Science & Technology*, **36** (20), 4467–4475.

34 Anderson, M., Wang, H.B. and Lin, Y.S. (2012) Inorganic membranes for carbon dioxide and nitrogen separation. *Reviews in Chemical Engineering*, **28** (2–3), 101–121.

35 Kanniche, M., Gros-Bonnivard, R., Jaud, P., Valle-Marcos, J., Amann, J.M. and

Bouallou, C. (2010) Pre-combustion, post-combustion and oxy-combustion in thermal power plant for CO_2 capture. *Applied Thermal Engineering*, **30** (1), 53–62.

36 Yang, H., Xu, Z., Fan, M., Gupta, R.B., Slimane, R.B., Bland, A.E. *et al.* (2008) Progress in carbon dioxide separation and capture: a review. *Journal of Environmental Sciences, China*, **20** (1), 14–27.

37 Ku, A.Y., Kulkarni, P., Shisler, R. and Wei, W. (2011) Membrane performance requirements for carbon dioxide capture using hydrogen-selective membranes in integrated gasification combined cycle (IGCC) power plants. *Journal of Membrane Science*, **367** (1–2), 233–239.

38 Li, J.R., Kuppler, R.J. and Zhou, H.C. (2009) Selective gas adsorption and separation in metal-organic frameworks. *Chemical Society Reviews*, **38** (5), 1477–1504.

39 Yun, S. and Oyama, S.T. (2011) Correlations in palladium membranes for hydrogen separation: a review. *Journal of Membrane Science*, **375** (1–2), 28–45.

40 Krishnan, G., Steele, D., O'Brien, K., Callahan, R., Berchtold, K. and Figueroa, J. (2009) Simulation of a process to capture CO_2 from IGCC syngas using a high temperature PBI membrane. *Greenhouse Gas Control Technologies 9*, **1** (1), 4079–4088.

41 Keizer, K., Uhlhorn, R.J.R., Vanvuren, R.J. and Burggraaf, A.J. (1988) Gas separation mechanisms in microporous modified gamma-Al_2O_3 membranes. *Journal of Membrane Science*, **39** (3), 285–300.

42 Uhlhorn, R.J.R., Keizer, K. and Burggraaf, A.J. (1989) Gas and surface diffusion in modified gamma-alumina systems. *Journal of Membrane Science*, **46** (2–3), 225–241.

43 Ma, Y.H., Becker, Y.L., Moser, W.R. and Dixon, A.G. (1991) Effect of catalyst impregnation on the transport properties of porous alumina membranes. Proceedings of Inorganic Membranes ICIM2-91 (eds A.J. Burggraaff, J. Charpin and L. Cot), Montpellier, France, pp. 337–346.

44 Cho, Y.K., Han, K.W. and Lee, K.H. (1995) Separation of CO_2 by modified gamma-Al_2O_3 membranes at high temperature. *Journal of Membrane Science*, **104** (3), 219–230.

45 Hyun, S.H., Jo, S.Y. and Kang, B.S. (1996) Surface modification of gamma-alumina membranes by silane coupling for CO_2 separation. *Journal of Membrane Science*, **120** (2), 197–206.

46 Othman, M.R. and Kim, J. (2008) Permeation characteristics of H_2, N_2 and CO_2 in a binary mixture across mesoporous Al_2O_3 and Pd-Al_2O_3 asymmetric composites. *Microporous and Mesoporous Materials*, **112** (1–3), 403–410.

47 Scholes, C.A., Kentish, S.E. and Stevens, G.W. (2009) The effect of condensable minor components on the gas separation performance of polymeric membranes for carbon dioxide capture. *Greenhouse Gas Control Technologies 9*, **1** (1), 311–317.

48 Liu, Y., Ng, Z., Khan, E.A., Jeong, H.-K., Ching, C.-B. and Lai, Z. (2009) Synthesis of continuous MOF-5 membranes on porous alpha-alumina substrates. *Microporous and Mesoporous Materials*, **118** (1–3), 296–301.

49 Li, Y.-S., Liang, F.-Y., Bux, H., Feldhoff, A., Yang, W.-S. and Caro, J. (2010) Molecular sieve membrane: supported metal-organic framework with high hydrogen selectivity. *Angewandte Chemie, International Edition*, **49** (3), 548–551.

50 US Energy Information Administration (2014) International Energy Outlook 2014: World Petroleum and Other Liquid Fuels with Projections to 2040.

51 BP (2014) BP Statistical Review of World Energy.

52 Gupta, R.B. (2008) *Hydrogen Fuel: Production, Transport, and Storage*, CRC Press, Boca Raton, FL.

53 Ogden, J. (2010) Hydrogen as an Energy Carrier: Outlook for 2010, 2030 and 2050. The Pew Center on Global Climate Change and the National Commission on Energy Policy, Institute of Transportation Studies, University of California, Davis.

54 Wisniak, J. (2013) Thomas Graham. II. Contributions to diffusion of gases and

liquids, colloids, dialysis, and osmosis. *Para Quitarle El Polvo Educación Química*, **24** (2), 506–515.
55 Baker, R.W., Cussler, E.L., Eykamp, W., Koros, W.J., Riley, R.L. and Strathmann, H. (1991) *Membrane Separation Systems: Recent Developments and Future Directions*, William Andrew Publishing/ Noyes Publications.
56 Air Liquide (2015) Hydrogen membrane – refineries. Available at http://www.medal.airliquide.com/en/hydrogen-membrane-gas-separation/hydrogen-membrane-technology.html (updated 7 July 2015).
57 Uemiya, S. (1999) State-of-the-art of supported metal membranes for gas separation. *Separation and Purification Methods*, **28** (1), 51–85.
58 Basu, S., Khan, A.L., Cano-Odena, A., Liu, C.Q. and Vankelecom, I.F.J. (2010) Membrane-based technologies for biogas separations. *Chemical Society Reviews*, **39** (2), 750–768.
59 Vanveen, H.M., Tol, J., Engelen, C.W.R. and Veringa, H.J. (1991) High-temperature gas separation with alumina membranes. Proceedings of Inorganic Membranes: ICIM2-91 (eds A.J. Burggraaff, J. Charpin and L. Cot), Montpellier, France, pp. 593–597.
60 Uhlhorn, R.J.R., Keizer, K. and Burggraaf, A.J. (1992) Gas transport and separation with ceramic membranes. 2. Synthesis and separation properties of microporous membranes. *Journal of Membrane Science*, **66** (2–3), 271–287.
61 Kitao, S. and Asaeda, M. (1991) Gas separation performance of thin porous silica membrane prepared by sol–gel and CVD methods. Proceedings of Inorganic Membranes: ICIM2-91 (eds A.J. Burggraaff, J. Charpin and L. Cot), Montpellier, France, pp. 267–272.
62 Jia, M.D., Peinemann, K.V. and Behling, R.D. (1993) Ceramic zeolite composite membranes – preparation, characterization and gas permeation. *Journal of Membrane Science*, **82** (1–2), 15–26.
63 Sea, B. and Lee, K.H. (2001) Modification of mesoporous gamma-alumina with silica and application for hydrogen separation at elevated temperature. *Journal of Industrial and Engineering Chemistry*, **7** (6), 417–423.
64 Burggraaf, A.J. and Cot, L. (1996) *Fundamentals of Inorganic Membrane Science and Technology*, Elsevier, Amsterdam.
65 Bose, A.C. (2010) *Inorganic Membranes for Energy and Environmental Applications*, Springer, New York.
66 Tsuru, T., Yamaguchi, K., Yoshioka, T. and Asaeda, M. (2004) Methane steam reforming by microporous catalytic membrane reactors. *AIChE Journal*, **50** (11), 2794–2805.
67 US DOE (2007) Zeolite membrane reactor for water-gas-shift reaction for hydrogen production. US DOE Hydrogen Annual Merit Review Meeting.
68 Ashok, D. (2008) *Hydrogen Separation and Purification*, CRC Press, Boca Raton, FL, pp. 283–324.
69 Guan, J., Dorris, S.E., Balachandran, U. and Liu, M. (1997) Transport properties of $BaCe_{0.95}Y_{0.05}O_3$-alpha mixed conductors for hydrogen separation. *Solid State Ionics*, **100** (1–2), 45–52.
70 Schwartz, M., Gade, S., Schaller, R. and Berland, B. (2002) Novel composite membranes for hydrogen separation in gasification processes in Vision 21 plants. 19th Annual International Pittsburgh Coal Conference, Pittsburgh, PA.
71 Ellgas, S. (2008) *Simulation of a Hydrogen Internal Combustion Engine with Cryogenic Mixture Formation*, Cuvillier Verlag, Göttingen.
72 Lane, R. (2014) Tesla founder Elon Musk says hydrogen R&D only to make automakers seem 'constructive'. Available at http://ecomento.com/2014/01/16/tesla-founder-elon-musk-says-hydrogen-rd-make-automakers-seem-constructive/ (updated 7 July 2015).
73 Silbey, R.J., Alberty, R.A. and Bawendi, M.G. (2004) *Physical Chemistry*, 4th edn, John Wiley & Sons, Inc., Hoboken, NJ.
74 Li, X. (2007) Thermodynamic performance of fuel cells and comparison with heat engines. *Advances in Fuel Cells*, **1**, 1–46.

75 Wright, S.E. (2003) Comparison of the theoretical performance potential of fuel cells and heat engines. *Renewable Energy*, **29**, 179–195.

76 Hemmes, K. (2004) Fuel cells. *Modern Aspects of Electrochemistry*, **37**, 131–251.

77 Behling, N.H. (2013) *Fuel Cells. Current Technology Challenges and Future Research Needs* (ed. N.H. Behling), Elsevier, Amsterdam, pp. 7–36.

78 Luna-Sandoval, G., Urriolagoitia, G., Hernández, L.H., Urriolagoitia, G. and Jiménez, E. (2011) Hydrogen fuel cell design and manufacturing process used for public transportation in Mexico City. World Congress on Engineering, London, UK.

79 Mond, L., Langer, C. and Quincke, F. (1990) Action of carbon monoxide on nickel (reprinted from J Chem Soc, vol 57, 749–753, 1890). *Journal of Organometallic Chemistry*, **383** (1–3), 1–5.

80 Wee, J.H. (2007) Applications of proton exchange membrane fuel cell systems. *Renewable & Sustainable Energy Reviews*, **11** (8), 1720–1738.

81 Alcaide, F., Cabot, P.L. and Brillas, E. (2006) Fuel cells for chemicals and energy cogeneration. *Journal of Power Sources*, **153** (1), 47–60.

82 Minh, N.Q. (1993) Ceramic fuel cells. *Journal of the American Ceramic Society*, **76** (3), 563–588.

83 Carrette, L., Friedrich, K.A. and Stimming, U. (2000) Fuel cells: principles, types, fuels, and applications. *ChemPhysChem*, **1** (4), 162–193.

84 Varcoe, J.R. and Slade, R.C.T. (2005) Prospects for alkaline anion-exchange membranes in low temperature fuel cells. *Fuel Cells*, **5** (2), 187–200.

85 Services, E.G.T. (2004) *Fuel Cell Handbook*, 7th edn, US Department of Energy Office of Fossil Energy, National Energy Technology Laboratory.

86 Grot, W. (2011) *Fluorinated Ionomers*, 2nd edn (ed. W. Grot), Elsevier, Amsterdam, pp. 5–10.

87 Geng, D.S., Hu, Y.H., Li, Y.L., Li, R.Y. and Sun, X.L. (2012) One-pot solvothermal synthesis of doped graphene with the designed nitrogen type used as a Pt support for fuel cells. *Electrochemistry Communications*, **22**, 65–68.

88 O'Hayre, R., Cha, S.W., Colella, W. and Prinz, F.B. (2009) *Fuel Cell Fundamentals*, John Wiley & Sons, Inc., Hoboken, NJ.

89 Kim, Y.B. (2011) Nanoscale surface engineering for ceramic fuel cells. Ph.D. thesis, Stanford University.

90 Kreuer, K.D. (2003) Proton-conducting oxides. *Annual Review of Materials Research*, **33**, 333–359.

91 de Grotthuss, C.J.T. (1806) Sur la décomposition de l'eau et des corps qu'elle tient en dissolution à l'aide de l'électricité galvanique. *Annali di Chimica*, **58**, 54–73.

92 Kreuer, K.D., Paddison, S.J., Spohr, E. and Schuster, M. (2004) Transport in proton conductors for fuel-cell applications: simulations, elementary reactions, and phenomenology. *Chemical Reviews*, **104** (10), 4637–4678.

93 Kreuer, K.D., Schonherr, E. and Maier, J. (1994) Proton and oxygen diffusion in $BACEO_3$ based compounds – a combined thermal gravimetric analysis and conductivity study. *Solid State Ionics*, **70**, 278–284.

94 Xu, F. and Mu, S. (2014) Nanoceramic oxide hybrid electrolyte membranes for proton exchange membrane fuel cells. *Journal of Nanoscience and Nanotechnology*, **14** (2), 1169–1180.

95 Iwahara, H., Yajima, T., Hibino, T., Ozaki, K. and Suzuki, H. (1993) Protonic conduction in calcium, strontium and barium zirconates. *Solid State Ionics*, **61** (1–3), 65–69.

96 Lin, Y.S., Ran, R., Guo, Y., Zhou, W., Cai, R., Wang, J. *et al.* (2010) Proton-conducting fuel cells operating on hydrogen, ammonia and hydrazine at intermediate temperatures. *International Journal of Hydrogen Energy*, **35** (7), 2637–2642.

97 Ruiz-Trejo, E. and Irvine, J.T.S. (2012) Ceramic proton conducting membranes for the electrochemical production of syngas. *Solid State Ionics*, **216**, 36–40.

98 Ricote, S., Bonanos, N., Manerbino, A. and Coors, W.G. (2012) Conductivity

study of dense $BaCe_xZr_{(0.9-x)}Y_{0.1}O_{(3-\delta)}$ prepared by solid state reactive sintering at 1500 °C. *International Journal of Hydrogen Energy*, **37** (9), 7954–7961.

99 McAree, G. (2015) Ballard customer demonstrates world's first hydrogen fuel cell tram. Available at http://www.ballard.com/about-ballard/newsroom/news-releases/news04071501.aspx (updated 10 July 2015).

100 Badwal, S.P.S., Giddey, S., Munnings, C. and Kulkarni, A. (2014) Review of progress in high temperature solid oxide fuel cells. *Journal of the Australian Ceramic Society*, **50**, 23–37.

101 Metcalfe, I.S. (2003) Fuel cells, advanced reactors and smart catalysis: the exploitation of ceramic ion-conducting membranes. *Chemical Engineering & Technology*, **26**, 857–862.

102 Badwal, S.P.S. and Ciacchi, F.T. (2000) Oxygen-ion conducting electrolyte materials for solid oxide fuel cells. *Ionics*, **6** (1–2), 1–21.

103 Badwal, S.P.S. (1992) Zirconia-based solid electrolytes: microstructure, stability and ionic conductivity. *Solid State Ionics*, **52** (1–3), 23–32.

104 Nernst, W. (1899) On the electrolytic conduction of solid bodies at high temperatures. *Zeitschrift für Elektrochemie*, **6**, 41.

105 Wachsman, E.D. and Lee, K.T. (2011) Lowering the temperature of solid oxide fuel cells. *Science*, **334**, 935–939.

106 Shim, J.H., Kang, S., Cha, S.-W., Lee, W., Kim, Y.B., Park, J.S. *et al.* (2013) Atomic layer deposition of thin-film ceramic electrolytes for high-performance fuel cells. *Journal of Materials Chemistry A*, **1**, 12695–12705.

107 Nomura, K., Mizutani, Y., Kawai, M., Nakamura, Y. and Yamamoto, O. (2000) Aging and Raman scattering study of scandia and yttria doped zirconia. *Solid State Ionics*, **132** (3–4), 235–239.

108 Pornprasertsuk, R., Ramanarayanan, P., Musgrave, C.B. and Prinz, F.B. (2005) Predicting ionic conductivity of solid oxide fuel cell electrolyte from first principles. *Journal of Applied Physics*, **98**, 103513.

109 Lo Faro, M. and Aricò, A.S. (2014) Ceramic membranes for intermediate temperature solid oxide fuel cells (SOFCs): state of the art and perspectives. *Woodhead Publishing Series in Energy*, **13**, 237–265.

110 Bloom Energy (2015) Solid oxide fuel cells. Available at http://www.bloomenergy.com/fuel-cell/solid-oxide/ (updated 7 July 2015).

111 Lee, K.T. and Wachsman, E.D. (2014) Role of nanostructures on SOFC performance at reduced temperatures. *MRS Bulletin*, **39**, 783–791.

112 Jung, D.W., Lee, K.T. and Wachsman, E.D. (2014) Terbium and tungsten co-doped bismuth oxide electrolytes for low temperature solid oxide fuel cells. *Journal of the Korean Ceramic Society*, **51**, 260–264.

113 Lee, K.T., Gore, C.M. and Wachsman, E.D. (2012) Feasibility of low temperature solid oxide fuel cells operating on reformed hydrocarbon fuels. *Journal of Materials Chemistry*, **22**, 22405–22408.

114 Lee, K.T., Yoon, H.S. and Wachsman, E.D. (2012) The evolution of low temperature solid oxide fuel cells. *Journal of Materials Science*, **27**, 2063–2078.

115 Beckers, J. and Rothenberg, G. (2010) Sustainable selective oxidations using ceria-based materials. *Green Chemistry*, **12** (6), 939–948.

116 Beckers, J. and Rothenberg, G. (2008) Redox properties of doped and supported copper-ceria catalysts. *Dalton Transactions*, (46), 6573–6578.

117 Rothenberg, G., de Graaf, E.A. and Bliek, A. (2003) Solvent-free synthesis of rechargeable solid oxygen reservoirs for clean. *Hydrogen Oxidation*, **42**, 3366–3368.

118 Zhu, B. (1999) Intermediate temperature proton conducting salt-oxide composites. *Solid State Ionics*, **125** (1), 397–405.

119 Zhu, B., Albinsson, I., Mellander, B.-E. and Meng, G. (1999) Intermediate-temperature proton-conducting fuel cells – present experience and future opportunities. *Solid State Ionics*, **125** (1–4), 439–446.

120 Beckers, J., van der Zande, L.M. and Rothenberg, G. (2006) Clean diesel power

via microwave susceptible oxidation catalysts. *ChemPhysChem*, **7**, 747–755.

121 Kan, W.H., Roushanafshar, M., Vincent, A., Fuerstenhaupt, T., Parvez, M., Luo, J. *et al.* (2013) Effect of substitution of B-sites by Mn, Fe and Co in double perovskite-type $Ba_3CaNb_2O_9$ on structure and electrical properties. *RSC Advances*, **3**, 23824–23832.

122 Munoz-Garcia, A.B., Ritzmann, A.M., Pavone, M., Keith, J.A. and Carter, E.A. (2014) Oxygen transport in perovskite-type solid oxide fuel cell materials: insights from quantum mechanics. *Accounts of Chemical Research*, **47**, 3340–3348.

123 Zhang, C. and Bristowe, P.D. (2013) First principles calculations of oxygen vacancy formation in barium-strontium-cobalt-ferrite. *RSC Advances*, **3**, 12267–12274.

124 Beckers, J., Clerc, F., Blank, J.H. and Rothenberg, G. (2008) Selective hydrogen oxidation catalysts via genetic algorithms. *Advanced Synthesis and Catalysis*, **350** (14–15), 2237–2249.

125 van der Zande, L.M., Zhang-Steenwinkel, Y., Rothenberg, G. and Bliek, A. (2004) Microwave regeneration of diesel soot filters. *NATO Science Series II: Mathematics, Physics and Chemistry*, **173**, 247–251.

126 Kato, H., Iguchi, F. and Yugami, H. (2014) Compatibility and performance of $La_{0.675}Sr_{0.325}Sc_{0.99}Al_{0.01}O_3$ perovskite-type oxide as an electrolyte material for SOFCs. *Journal of Applied Electrochemistry*, **82**, 845–850.

127 Ras, E.-J. and Rothenberg, G. (2014) Heterogeneous catalyst discovery using 21st century tools: a tutorial. *RSC Advances*, **4**, 5963–5974.

128 Roy, R. (1954) Multiple ion substitution in the perovskite lattice. *Journal of the American Ceramic Society*, **37** (12), 581–588.

129 Suzuki, T., Hasan, Z., Funahashi, Y., Yamaguchi, T., Fujishiro, Y. and Awano, M. (2009) Impact of anode microstructure on solid oxide fuel cells. *Science*, **325**, 852–855.

130 Hou, S.-E., Alonso, J.A., Rajasekhara, S., Martinez-Lope, M.J., Fernandez-Diaz, M.T. and Goodenough, J.B. (2010) Defective Ni perovskites as cathode materials in intermediate-temperature solid-oxide fuel cells: a structure–properties correlation. *Chemistry of Materials*, **22**, 1071–1079.

131 Huang, Y.-H., Liang, G., Croft, M., Lehtimaki, M., Karppinen, M. and Goodenough, J.B. (2009) Double-perovskite anode materials Sr_2MMoO_6 (M = Co, Ni) for solid oxide fuel cells. *Chemistry of Materials*, **21**, 2319–2326.

132 Lemes-Rachadel, P., Garcia, G.S., Machado, R.A.F., Hotza, D. and da Costa, J.C.D. (2014) Current developments of mixed conducting membranes on porous substrates. *Materials Research*, **17**, 242–249.

133 Chueh, W.C. and Haile, S.M. (2012) Electrochemistry of mixed oxygen ion and electron conducting electrodes in solid electrolyte cells. *Annual Review of Chemical and Biomolecular Engineering*, **3**, 313–341.

134 Imashuku, S., Wang, L., Mezghani, K., Habib, M.A. and Shao-Horn, Y. (2013) Oxygen permeation from oxygen ion-conducting membranes coated with porous metals or mixed ionic and electronic conducting oxides. *Journal of the Electrochemical Society*, **160**, E148–E153.

135 Sunarso, J., Baumann, S., Serra, J.M., Meulenberg, W.A., Liu, S., Lin, Y.S. *et al.* (2008) Mixed ionic–electronic conducting (MIEC) ceramic-based membranes for oxygen separation. *Journal of Membrane Science*, **320** (1–2), 13–41.

136 Basile, A. (2013) *Handbook of Membrane Reactors*, vols 1 and 2, Woodhead Publishing.

137 Caro, J. (2014) Catalytic membrane reactors – lab curiosity or key enabling technology. *Chemie Ingenieur Technik*, **86**, 1901–1905.

138 Diban, N., Aguayo, A.T., Bilbao, J., Urtiaga, A. and Ortiz, I. (2013) Membrane reactors for *in situ* water removal: a review of applications. *Industrial & Engineering Chemistry Research*, **52**, 10342–10354.

139 Fontananova, E. and Drioli, E. (2014) Membrane reactors: advanced systems for intensified chemical processes. *Chemie Ingenieur Technik*, **86**, 2039–2050.

140 Coronas, J. and Santamaría, J. (1999) Catalytic reactors based on porous ceramic membranes. *Catalysis Today*, **51**, 377–389.

141 Ramos, R., Menéndez, M. and Santamaría, J. (2000) Oxidative dehydrogenation of propane in an inert membrane reactor. *Catalysis Today*, **56**, 239–245.

142 Gomez-Quero, S., Tsoufis, T., Rudolf, P., Makkee, M., Kapteijn, F. and Rothenberg, G. (2013) Kinetics of propane dehydrogenation over Pt-Sn/Al_2O_3. *Catalysis Science & Technology*, **3** (4), 962–971.

143 Beckers, J. and Rothenberg, G. (2009) Lead-containing solid "oxygen reservoirs" for selective hydrogen combustion. *Green Chemistry*, **11** (10), 1550–1554.

144 Ramachandra, A.M., Lu, Y., Ma, Y.H., Moser, W.R. and Dixon, A.G. (1996) Oxidative coupling of methane in porous Vycor membrane reactors. *Journal of Membrane Science*, **116** (2), 253–264.

145 Capannelli, G., Carosini, E., Cavani, F., Monticelli, O. and Trifiro, F. (1996) Comparison of the catalytic performance of V_2O_5/γ-Al_2O_3 in the oxydehydrogenation of propane to propylene in different reactor configurations: (i) packed-bed reactor, (ii) monolith-like reactor and (iii) catalytic membrane reactor. *Chemical Engineering Science*, **51** (10), 1817–1826.

146 O'Neill, C. and Wolf, E.E. (2010) Partial oxidation of propane to acrolein in a dual bed inert membrane reactor. *Catalysis Today*, **156**, 124–131.

147 Ge, S.H., Liu, C.H. and Wang, L.J. (2001) Oxidative dehydrogenation of butane using inert membrane reactor with a nonuniform permeation pattern. *Chemical Engineering Journal*, **84**, 497–502.

148 Caro, J. and Noack, M. (2008) Zeolite membranes – recent developments and progress. *Microporous and Mesoporous Materials*, **115**, 215–233.

149 Caro, J., Noack, M. and Kölsch, P. (2005) Zeolite membranes: from the laboratory scale to technical applications. *Adsorption*, **11** (3–4), 215–227.

150 Kuhn, J., Yajima, K., Tomita, T., Gross, J. and Kapteijn, F. (2008) Dehydration performance of a hydrophobic DD3R zeolite membrane. *Journal of Membrane Science*, **321**, 344–349.

151 Plessius, R., Kromhout, R., Datos Ramos, A.L., Ferbinteanu, M., Mittelmeijer-Hazeleger, M.C., Krishna, R. *et al.* (2014) Highly selective water adsorption in a lanthanum metal-organic framework. *Chemistry – A European Journal*, **20** (26), 7922–7925.

152 van den Bergh, J., Gücüyener, C., Gascon, J. and Kapteijn, F. (2011) Isobutane dehydrogenation in a DD3R zeolite membrane reactor. *Chemical Engineering Journal*, **166** (1), 368–377.

153 Gaikwad, A.V., Boffa, V., ten Elshof, J.E. and Rothenberg, G. (2008) Cat-in-a-cup: facile separation of large homogeneous catalysts. *Angewandte Chemie, International Edition*, **47** (29), 5407–5410.

154 Dijkstra, H.P., van Klink, G.P.M. and van Koten, G. (2002) The use of ultra- and nanofiltration techniques in homogeneous catalyst recycling. *Accounts of Chemical Research*, **35**, 798–810.

155 van den Bergh, J., Nishiyama, N. and Kapteijn, F. (2010) Zeolite membranes in catalysis: what is new and how bright is the future, in *Novel Concepts in Catalysis and Chemical Reactors*, Wiley-Blackwell, pp. 211–237.

156 Julbe, A., Farrusseng, D. and Guizard, C. (2001) Porous ceramic membranes for catalytic reactors – overview and new ideas. *Journal of Membrane Science*, **181** (1), 3–20.

157 Zaspalis, V.T., Van Praag, W., Keizer, K., Van Ommen, J.G., Ross, J.R.H. and Burggraaf, A.J. (1991) Reactions of methanol over catalytically active alumina membranes. *Applied Catalysis*, **74**, 205–222.

158 Harold, M.P., Lee, C., Burggraaf, A.J., Keizer, K., Zaspalis, V.T. and de Lange,

R.S.A. (1994) Catalysis with inorganic membranes. *MRS Bulletin*, **19**, 34–39.

159 He, J., Yoneyama, Y., Xu, B., Nishiyama, N. and Tsubaki, N. (2005) Designing a capsule catalyst and its application for direct synthesis of middle isoparaffins. *Langmuir*, **21** (5), 1699–1702.

160 Nishiyama, N., Ichioka, K., Park, D.-H., Egashira, Y., Ueyama, K., Gora, L. *et al.* (2004) Reactant-selective hydrogenation over composite silicalite-1-coated Pt/TiO_2 particles. *Industrial & Engineering Chemistry Research*, **43** (5), 1211–1215.

161 Wichner, N.M., Beckers, J., Rothenberg, G. and Koller, H. (2010) Preventing sintering of Au and Ag nanoparticles in silica-based hybrid gels using phenyl spacer groups. *Journal of Materials Chemistry*, **20** (19), 3840–3847.

162 Šefčík, J. and Rankin, S.E. (2003) Monte Carlo simulations of size and structure of gel precursors in silica polycondensation. *Journal of Physical Chemistry B*, **107** (1), 52–60.

163 Brinker, C.J. and Scherer, G. (1990) *Sol–Gel Science: The Physics and Chemistry of Sol–Gel Processing*, Academic Press, San Diego, CA.

164 Paul, G., Steuernagel, S. and Koller, H. (2007) Non-covalent interactions of a drug molecule encapsulated in a hybrid silica gel. *Chemical Communications*, (48), 5194–5196.

165 Ramos-Fernandez, E.V., Geels, N.J., Shiju, N.R. and Rothenberg, G. (2014) Titania-catalysed oxidative dehydrogenation of ethyl lactate: effective yet selective free-radical oxidation. *Green Chemistry*, **16** (6), 3358–3363.

166 Peureux, J., Torres, M., Mozzanega, H., Giroir-Fendler, A. and Dalmon, J.A. (1995) Nitrobenzene liquid-phase hydrogenation in a membrane reactor. *Catalysis Today*, **25** (3–4), 409–415.

167 Gunji, T., Saravanan, G., Tanabe, T., Tsuda, T., Miyauchi, M., Kobayashi, G. *et al.* (2014) Long-term, stable, and improved oxygen-reduction performance of titania-supported PtPb nanoparticles. *Catalysis Science & Technology*, **4**, 1436–1445.

168 Liu, M., Zhao, Z.-P., Chen, K.-C. and Liu, W.-F. (2015) New chiral catalytic membrane reactor created by immobilizing salen-Mn(III) onto APTES modified ceramic membrane and its performances in epoxidation of styrene. *Catalysis Communications*, **64**, 70–74.

169 Davies, S.H., Baumann, M.J., Byun, S., Corneal, L.M., Tarabara, V.V. and Masten, S.J. (2010) Fabrication of catalytic ceramic membranes for water filtration. *Water Science and Technology: Water Supply*, **10**, 81–86.

170 Zhao, H., Draelants, D.J. and Baron, G.V. (2000) Preparation and characterisation of nickel-modified ceramic filters. *Catalysis Today*, **56** (1–3), 229–237.

171 Hou, J., Dong, G., Xiao, B., Malassigne, C. and Chen, V. (2015) Preparation of titania based biocatalytic nanoparticles and membranes for CO_2 conversion. *Journal of Materials Chemistry A*, **3**, 3332–3342.

172 Zhu, Y., Zhang, H. and Zhang, X. (2014) Study on catalytic ozone oxidation with nano-TiO_2 modified membrane for treatment of municipal wastewater. *Asian Journal of Chemistry*, **26**, 3871–3874.

173 Bernardo, P., Algieri, C., Barbieri, G. and Drioli, E. (2006) CO Selox reaction using Y-type zeolite catalytic membranes. *Korean Membrane Journal*, **8**, 13–20.

174 Bernal, M.P., Coronas, J., Menendez, M. and Santamaria, J. (2002) Coupling of reaction and separation at the microscopic level: esterification processes in a H-ZSM-5 membrane reactor. *Chemical Engineering Science*, **57**, 1557–1562.

175 Alfonso, M.J., Menendez, M. and Santamaria, J. (2002) Oxidative dehydrogenation of butane on V/MgO catalytic membranes. *Chemical Engineering Journal*, **90**, 131–138.

176 Barbieri, G., Violante, V., Di Maio, F.P., Criscuoli, A. and Drioli, E. (1997) Methane steam reforming analysis in a palladium-based catalytic membrane reactor. *Industrial & Engineering Chemistry Research*, **36**, 3369–3374.

177 Beckers, J., Drost, R., van Zandvoort, I., Collignon, P.F. and Rothenberg, G. (2008) Selective hydrogen oxidation in the presence of C_3 hydrocarbons using

perovskite oxygen reservoirs. *ChemPhysChem*, **9** (7), 1062–1068.

178 Blank, J.H., Beckers, J., Collignon, P.F., Clerc, F. and Rothenberg, G.A. (2007) "Green route" to propene through selective hydrogen oxidation. *Chemistry – A European Journal*, **13**, 5121–5128.

179 Sato, T., Kumagai, A. and Itoh, N. (2010) A catalytic ZSM-5 membrane sandwiched with silicalite-1 layers for highly selective toluene disproportionation. *Separation and Purification Technology*, **73**, 32–37.

180 Julbe, A., Rouessac, V., Durand, J. and Ayral, A. (2008) New approaches in the design of ceramic and hybrid membranes. *Journal of Membrane Science*, **316**, 176–185.

181 Wu, J.C.S., Sabol, H., Smith, G.W., Flowers, D.L. and Liu, P.K.T. (1994) Characterization of hydrogen-permselective microporous ceramic membranes. *Journal of Membrane Science*, **96** (3), 275–287.

182 Okubo, T. and Inoue, H. (1989) Single gas permeation through porous glass modified with tetraethoxysilane. *AIChE Journal*, **35**, 845–848.

183 Baccile, N., Babonneau, F., Thomas, B. and Coradin, T. (2009) Introducing ecodesign in silica sol–gel materials. *Journal of Materials Chemistry*, **19**, 8537–8559.

184 Mathur, S. (2004) Molecular chemical concepts for the synthesis of nanocrystalline ceramics. *NATO Science Series II*, **169**, 425–442.

185 Riedel, R., Horvath-Bordon, E., Nahar-Borchert, S. and Kroke, E. (2003) Molecular chemical concepts for the synthesis of novel ceramics. *Key Engineering Materials*, **247**, 121–128.

186 Agoudjil, N., Lamrani, N. and Larbot, A. (2014) Silica porous membranes synthesis and characterization. *Desalination and Water Treatment*, **1**, 1–8.

187 Cheraitia, A., Ayral, A., Julbe, A., Rouessac, V. and Satha, H. (2010) Synthesis and characterization of microporous silica–alumina membranes. *Journal of Porous Materials*, **17**, 259–263.

188 Wang, C., Hu, X., Yu, J., Wei, L. and Huang, Y. (2014) Intermediate gel coating on macroporous Al_2O_3 substrate for fabrication of thin carbon membranes. *Ceramics International*, **40**, 10367–10373.

189 Lafarga, D., Santamaríía, J. and Menéndez, M. (1994) Methane oxidative coupling using porous ceramic membrane reactors. I. Reactor development. *Chemical Engineering Science*, **49** (12), 2005–2013.

190 Pina, M.P., Menéndez, M. and Santamaría, J. (1996) The Knudsen-diffusion catalytic membrane reactor: an efficient contactor for the combustion of volatile organic compounds. *Applied Catalysis B: Environmental*, **11** (1), L19–L27.

191 Julbe, A., Guizard, C., Larbot, A., Cot, L. and Giroir-Fendler, A. (1993) The sol–gel approach to prepare candidate microporous inorganic membranes for membrane reactors. *Journal of Membrane Science*, **77**, 137.

192 Zhao, H.B., Pflanz, K., Gu, J.H., Li, A.W., Stroh, N., Brunner, H. *et al.* (1998) Preparation of palladium composite membranes by modified electroless plating procedure. *Journal of Membrane Science*, **142** (2), 147–157.

193 Zhang, X., Xiong, G. and Yang, W. (2008) A modified electroless plating technique for thin dense palladium composite membranes with enhanced stability. *Journal of Membrane Science*, **314** (1–2), 226–237.

194 Farrusseng, D., Julbe, A. and Guizard, C. (2001) Evaluation of porous ceramic membranes as O_2 distributors for the partial oxidation of alkanes in inert membrane reactors. *Separation and Purification Technology*, **25** (1–3), 137–149.

195 Lafarga, D., Lafuente, A., Menéndez, M. and Santamaría, J. (1998) Thermal stability of γ-Al_2O_3/α-Al_2O_3 mesoporous membranes. *Journal of Membrane Science*, **147** (2), 173–185.

196 Coronas, J. and Santamaria, J. (1999) Separations using zeolite membranes. *Separation and Purification Methods*, **28**, 127–177.

197 Yu, M., Noble, R.D. and Falconer, J.L. (2011) Zeolite membranes: microstructure characterization and permeation mechanisms. *Accounts of Chemical Research*, **44**, 1196–1206.

198 Jana, S., Purkait, M.K. and Mohanty, K. (2012) Preparation and applications of zeolite membranes: a review, in *Membrane Technologies and Applications*, CRC Press, Boca Raton, FL, pp. 57–76.

199 Bakker, W.J.W., Kapteijn, F., Poppe, J. and Moulijn, J.A. (1996) Permeation characteristics of a metal-supported silicalite-1 zeolite membrane. *Journal of Membrane Science*, **117** (1–2), 57–78.

200 Okamoto, K.-I., Kita, H. and Horii, K. (2001) Zeolite NaA membrane: preparation, single-gas permeation, and pervaporation and vapor permeation of water/organic liquid mixtures. *Industrial & Engineering Chemistry Research*, **40** (1), 163–175.

201 Li, S., Falconer, J.L. and Noble, R.D. (2004) SAPO-34 membranes for CO_2/CH_4 separation. *Journal of Membrane Science*, **241** (1), 121–135.

202 Farrusseng, D., Julbe, A., Lopez, M. and Guizard, C. (2000) Investigation of sol–gel methods for the synthesis of VPO membrane materials adapted to the partial oxidation of *n*-butane. *Catalysis Today*, **56** (1–3), 211–220.

203 Armor, J.N. (1995) Membrane catalysis: where is it now, what needs to be done? *Catalysis Today*, **25** (3–4), 199–207.

204 Coronas, J., Menendez, M. and Santamaria, J. (1994) Development of ceramic membrane reactors with a non-uniform permeation pattern. Application to methane oxidative coupling. *Chemical Engineering Science*, **49**, 4749–4757.

205 Julbe, A., Farrusseng, D., Cot, D. and Guizard, C. (2001) The chemical valve membrane: a new concept for an auto-regulation of O_2 distribution in membrane reactors. *Catalysis Today*, **67**, 139–149.

206 Lai, S.M., Martin-Aranda, R. and Yeung, K.L. (2003) Knoevenagel condensation reaction in a membrane microreactor. *Chemical Communications*, (2), 218–219.

207 Lai, S.M., Ng, C.P., Martin-Aranda, R. and Yeung, K.L. (2003) Knoevenagel condensation reaction in zeolite membrane microreactor. *Microporous and Mesoporous Materials*, **66** (2–3), 239–252.

208 Zhang, X., Man Lai, E.S., Martin-Aranda, R. and Yeung, K.L. (2004) An investigation of Knoevenagel condensation reaction in microreactors using a new zeolite catalyst. *Applied Catalysis A: General*, **261** (1), 109–118.

209 Wan, Y.S.S., Yeung, K.L. and Gavriilidis, A. (2005) TS-1 oxidation of aniline to azoxybenzene in a microstructured reactor. *Applied Catalysis A: General*, **281** (1–2), 285–293.

210 Au, L.T.Y., Chau, J.L.H., Ariso, C.T. and Yeung, K.L. (2001) Preparation of supported Sil-1, TS-1 and VS-1 membranes: effects of Ti and V metal ions on the membrane synthesis and permeation properties. *Journal of Membrane Science*, **183** (2), 269–291.

211 Bouwmeester, H.J.M. (2003) Dense ceramic membranes for methane conversion. *Catalysis Today*, **82** (1–4), 141–150.

212 Balachandran, U., Dusek, J.T., Maiya, P.S., Ma, B., Mieville, R.L., Kleefisch, M.S. *et al.* (1997) Ceramic membrane reactor for converting methane to syngas. *Catalysis Today*, **36** (3), 265–272.

213 Luo, H.X., Wei, Y.Y., Jiang, H.Q., Yuan, W.H., Lv, Y.X., Caro, J. *et al.* (2010) Performance of a ceramic membrane reactor with high oxygen flux Ta-containing perovskite for the partial oxidation of methane to syngas. *Journal of Membrane Science*, **350** (1–2), 154–160.

214 Hamakawa, S., Sato, K., Inoue, T., Nishioka, M., Kobayashi, K. and Mizukami, F. (2006) Design of one-component ceramic membrane-reactor for natural gas conversion. *Catalysis Today*, **117** (1–3), 297–303.

215 Hamlin, C. (2000) Water, in *The Cambridge World History of Food*, Cambridge University Press.

216 Corso, P.S., Kramer, M.H., Blair, K.A., Addiss, D.G., Davis, J.P. and Haddix, A.C. (2003) Cost of illness in the 1993

waterborne *Cryptosporidium* outbreak, Milwaukee, Wisconsin. *Emerging Infectious Diseases*, **9** (4), 426–431.

217 Muhammad, N., Sinha, R., Krishnan, E.R. and Patterson, C.L. (2009) Ceramic filter for small system drinking water treatment: evaluation of membrane pore size and importance of integrity monitoring. *Journal of Environmental Engineering (ASCE)*, **135** (11), 1181–1191.

218 Bodzek, M. and Konieczny, K. (1998) Comparison of various membrane types and module configurations in the treatment of natural water by means of low-pressure membrane methods. *Separation and Purification Technology*, **14** (1–3), 69–78.

219 Simonis, J.J. and Basson, A.K. (2011) Evaluation of a low-cost ceramic micro-porous filter for elimination of common disease microorganisms. *Physics and Chemistry of the Earth*, **36** (14–15), 1129–1134.

220 Kaniganti, C.M., Emani, S., Thorat, P. and Uppaluri, R. (2014) Microfiltration of synthetic bacteria solution using low cost ceramic membranes. *Separation Science and Technology*, **50** (1), 121–135.

221 Gitis, V., Freger, V., Haugth, R.C. and Clark, R.M. (2005) Removal of *Cryptosporidium parvum* oocysts by rapid sand filtration with ballasted flocculation-filtration and intermediate downwashes. *Acta Hydrochimica et Hydrobiologica*, **33** (4), 355–364.

222 Drozd, C. and Schwartzbrod, J. (1997) Removal of *Cryptosporidium* from river water by crossflow microfiltration: a pilot-scale study. *Water Science and Technology*, **35** (11–12), 391–395.

223 Fan, X.J., Tao, Y., Wang, L.Y., Zhang, X.H., Lei, Y., Wang, Z. *et al.* (2014) Performance of an integrated process combining ozonation with ceramic membrane ultra-filtration for advanced treatment of drinking water. *Desalination*, **335** (1), 47–54.

224 Clasen, T. and Menon, S. (2007) Microbiological performance of common water treatment devices for household use in India. *International Journal of Environmental Health Research*, **17** (2), 83–93.

225 Gitis, V., Haught, R.C., Clark, R.M., Gun, J. and Lev, O. (2006) Nanoscale probes for the evaluation of the integrity of ultrafiltration membranes. *Journal of Membrane Science*, **276** (1–2), 199–207.

226 Duek, A., Arkhangelsky, E., Krush, R., Brenner, A. and Gitis, V. (2012) New and conventional pore size tests in virus-removing membranes. *Water Research*, **46** (8), 2505–2514.

227 Ciora, R.J., Jr. and Liu, P.K.T. (2003) Ceramic membranes for environmental related applications. *Fluid–Particle Separation Journal*, **15** (1), 51–60.

228 Matsushita, T., Matsui, Y., Shirasaki, N. and Kato, Y. (2005) Effect of membrane pore size, coagulation time, and coagulant dose on virus removal by a coagulation–ceramic microfiltration hybrid system. *Desalination*, **178** (1–3), 21–26.

229 Lerch, A., Panglisch, S., Buchta, P., Tomita, Y., Yonekawa, H., Hattori, K. *et al.* (2005) Direct river water treatment using coagulation/ceramic membrane microfiltration. *Desalination*, **179** (1–3), 41–50.

230 Chiu, T.Y. (2011) Effect of ageing on the microfiltration performance of ceramic membranes. *Separation and Purification Technology*, **83**, 106–113.

231 2030 Water Resources Group (2009) Charting Our Water Future: Economic Frameworks to Inform Decision-Making.

232 Alexandratos, N. and Bruinsma, J. (2012) World agriculture towards 2030/2050: the 2012 revision. ESA Working Paper No. 12-03, Food and Agriculture Organization of the United Nations, Rome, Italy.

233 Moorman, L. (2012) Brazilian requirements for POU/POE products. *Water Conditioning & Purification*, **7** (7), 1–2.

234 Andrew, R. (2012) An overview of global standards, protocols and guidelines for POU and POE microbial reduction claims. *Water Conditioning & Purification*, **54** (10), 1–2.

235 Loi-Brugger, A., Panglisch, S., Buchta, P., Hattori, K., Yonekawa, H., Tomita, Y.

et al. (2006) Ceramic membranes for direct river water treatment applying coagulation and microfiltration. 5th World Water Congress: Drinking Water Quality and Treatment, vol. **6**, no. 4, pp. 89–98.
236 Kato, T. (2010) Using of membrane processed for water treatment in the world. Voda Zlín 2010, pp. 41–46.
237 PWN Technologies (2015) Andijk III – PWN, the Netherlands. Available at www.pwntechnologies.nl/ (updated 7 July 2015).
238 Veolia (2015) CeraMem ceramic membranes. Available at http://technomaps.veoliawatertechnologies.com/ceramem/ (updated 7 July 2015).
239 United Nations Educational, Scientific and Cultural Organization (2014) The United Nations World Water Development Report. United Nations Educational, Scientific and Cultural Organization, Paris, France.
240 Pacific Institute (2015) Water Conflict.
241 Brown, J., Proum, S. and Sobsey, M.D. (2009) Sustained use of a household-scale water filtration device in rural Cambodia. *Journal of Water and Health*, **7** (3), 404–412.
242 UNICEF (2014) *Progress on Sanitation and Drinking Water – 2014 Update*. WHO Press.
243 Brown, J. and Sobsey, M.D. (2010) Microbiological effectiveness of locally produced ceramic filters for drinking water treatment in Cambodia. *Journal of Water and Health*, **8** (1), 1–10.
244 Dies, R.W. (2003) Development of a Ceramic Water Filter for Nepal. Department of Civil and Environmental Engineering, Massachusetts Institute of Technology, Cambridge, MA.
245 Sagara, J. (2000) Study of Filtration for Point-of-Use Drinking Treatment in Nepal. Department of Civil Engineering and Environment, Massachusetts Institute of Technology, Cambridge, MA.
246 Lantagne, D. (2001) Investigation of the Potters for Peace Colloidal Silver Impregnated Ceramic Filter. Report 1: Intrinsic Effectiveness. Jubilee House Community/USAID.
247 Roberts, M. (2004) Field test of a silver-impregnated ceramic filter. 30th WEDC International Conference, Vientiane, Laos.
248 Duke, W.F., Nordin, R. and Mazumder, A. (2006) Comparative Analysis of the Filtron and Biosand Water Filters. Potters Without Borders, pp. 1–6.
249 Hwang, S.K. (2003) Point-of-Use Arsenic Removal for Drinking Water in Nepal Using Coagulation and Filtration. Department of Civil and Environment Engineering, Massachusetts Institute of Technology, Cambridge, MA.
250 Coulbert, B. (2005) An Evaluation of Household Drinking Water Treatment Systems in Peru: the Table Filter and the Safe Water System. Department of Civil and Environmental Engineering, Massachusetts Institute of Technology, Cambridge, MA.
251 McAllister, S. (2005) Analysis and Comparison of Sustainable Water Filters. Department of Mechanical Engineering, University of Wisconsin.
252 Van Halem, D., Heijman, S.G.J., Soppe, A.I.A., Van Dijk, J.C. and Amy, G.L. (2007) Ceramic silver-impregnated pot filters for household drinking water treatment in developing countries: material characterization and performance study. *Water Science and Technology: Water Supply*, **7**, 9–17.
253 Baumgartner, J., Murcott, S. and Ezzati, M. (2007) Reconsidering 'appropriate technology': the effects of operating conditions on the bacterial removal performance of two household drinking-water filter systems. *Environmental Research Letters*, **2** (2), 024003.
254 Oyanedel-Craver, V.A. and Smith, J.A. (2008) Sustainable colloidal-silver-impregnated ceramic filter for point-of-use water treatment. *Environmental Science & Technology*, **42** (3), 927–933.
255 van der Laan, H., van Halem, D., Smeets, P.W.M.H., Soppe, A.I.A., Kroesbergen, J., Wubbels, G. *et al.* (2014) Bacteria and virus removal effectiveness of ceramic pot filters with different silver applications in a long term experiment. *Water Research*, **51**, 47–54.

256 Potters for Peace (2015) Ceramic Water Filter Project. Available at http://pottersforpeace.com/ceramic-water-filter-project/ (updated 1 June 2015).

257 Rayner, J., Skinner, B. and Lantagne, D. (2013) Current practices in manufacturing locally-made ceramic pot filters for water treatment in developing countries. *Journal of Water, Sanitation and Hygiene for Development*, **3** (2), 252–261.

258 Masmoudi, S., Larbot, A., El Feki, H. and Ben Amar, R. (2007) Elaboration and characterisation of apatite based mineral supports for microfiltration and ultrafiltration membranes. *Ceramics International*, **33** (3), 337–344.

259 Saffaj, N., Younssi, S.A., Albizane, A., Messouadi, A., Bouhria, M., Persin, M. *et al.* (2004) Preparation and characterization of ultrafiltration membranes for toxic removal from wastewater. *Desalination*, **168** (1–3), 259–263.

260 Saffaj, N., Persin, M., Younssi, S.A., Albizane, A., Bouhria, M., Loukili, H. *et al.* (2005) Removal of salts and dyes by low $ZnAl_2O_4$–TiO_2 ultrafiltration membrane deposited on support made from raw clay. *Separation and Purification Technology*, **47** (1–2), 36–42.

261 Saffaj, N., Persin, M., Younsi, S.A., Albizane, A., Cretin, M. and Larbot, A. (2006) Elaboration and characterization of microfiltration and ultrafiltration membranes deposited on raw support prepared from natural Moroccan clay: application to filtration of solution containing dyes and salts. *Applied Clay Science*, **31** (1–2), 110–119.

262 Almandoz, M.C., Marchese, J., Prádanos, P., Palacio, L. and Hernández, A. (2004) Preparation and characterization of non-supported microfiltration membranes from aluminosilicates. *Journal of Membrane Science*, **241** (1), 95–103.

263 Bouzerara, F., Harabi, A., Achour, S. and Larbot, A. (2006) Porous ceramic supports for membranes prepared from kaolin and doloma mixtures. *Journal of the European Ceramic Society*, **26** (9), 1663–1671.

264 Potdar, A., Shukla, A. and Kumar, A. (2002) Effect of gas phase modification of analcime zeolite composite membrane on separation of surfactant by ultrafiltration. *Journal of Membrane Science*, **210** (2), 209–225.

265 Nandi, B.K., Uppaluri, R. and Purkait, M.K. (2008) Preparation and characterization of low cost ceramic membranes for micro-filtration applications. *Applied Clay Science*, **42** (1–2), 102–110.

266 Simonis, J.J. and Basson, A.K. (2012) Manufacturing a low-cost ceramic water filter and filter system for the elimination of common pathogenic bacteria. *Physics and Chemistry of the Earth*, **50–52** (0), 269–276.

267 Henry, M., Maley, S. and Mehta, K. (2013) Designing a low-cost ceramic water filter press. *International Journal for Service Learning in Engineering*, **8** (1), 62–77.

268 van Halem, D., van der Laan, H., Heijman, S.G.J., van Dijk, J.C. and Amy, G.L. (2009) Assessing the sustainability of the silver-impregnated ceramic pot filter for low-cost household drinking water treatment. *Physics and Chemistry of the Earth*, **34** (1–2), 36–42.

269 Programme for Accessible Health Communication and Education (2015) Water Guard. Available at www.pace.org.ug/ (updated 10 July 2015).

270 Gitis, V., Lerch, A. and Gimbel, R. (2005) Retention of humic acid by ultrafiltration with polyaluminium coagulant. *Journal of Water Supply Research and Technology – AQUA*, **54** (4), 213–223.

271 Timchak, E. and Gitis, V. (2012) A combined degradation of dyes and inactivation of viruses by UV and UV/H_2O_2. *Chemical Engineering Science*, **192** (0), 164–170.

272 Vishwas, G.P. and Sangita, P. (2008) Pervaporation, in *Handbook of Membrane Separations*, CRC Press, Boca Raton, FL, pp. 107–138.

273 Drioli, E., Ali, A. and Macedonio, F. (2015) Membrane distillation: recent developments and perspectives. *Desalination*, **356**, 56–84.

274 Onsekizoglu, P. (2012) *Membrane Distillation: Principle, Advances, Limitations and Future Prospects in Food Industry* (ed. S. Zereshki), InTech.

275 Smolders, K. and Franken, A.C.M. (1989) Terminology for membrane distillation. *Desalination*, **72** (3), 249–262.

276 Al-Obaidani, S., Curcio, E., Macedonio, F., Di Profio, G., Ai-Hinai, H. and Drioli, E. (2008) Potential of membrane distillation in seawater desalination: thermal efficiency, sensitivity study and cost estimation. *Journal of Membrane Science*, **323** (1), 85–98.

277 Hendren, Z.D. (2011) Novel Ceramic Membranes for Membrane Distillation: Surface Modification, Performance Comparison with PTFE Membranes, and Treatment of Municipal Wastewater. Department of Civil and Environmental Engineering, Duke University.

278 Xie, M., Nghiem, L.D., Price, W.E. and Elimelech, M. (2013) A forward osmosis-membrane distillation hybrid process for direct sewer mining: system performance and limitations. *Environmental Science & Technology*, **47** (23), 13486–13493.

279 Macedonio, F., Ali, A., Poerio, T., El-Sayed, E., Drioli, E. and Abdel-Jawad, M. (2014) Direct contact membrane distillation for treatment of oilfield produced water. *Separation and Purification Technology*, **126**, 69–81.

280 Alkhudhiri, A., Darwish, N. and Hilal, N. (2012) Membrane distillation: a comprehensive review. *Desalination*, **287**, 2–18.

281 Dafinov, A., Garcia-Valls, R. and Font, J. (2002) Modification of ceramic membranes by alcohol adsorption. *Journal of Membrane Science*, **196** (1), 69–77.

282 Hendren, Z.D., Brant, J. and Wiesner, M.R. (2009) Surface modification of nanostructured ceramic membranes for direct contact membrane distillation. *Journal of Membrane Science*, **331** (1–2), 1–10.

283 Leger, C., Lira, H.L. and Paterson, R. (1996) Preparation and properties of surface modified ceramic membranes. Part III. Gas permeation of 5 nm alumina membranes modified by trichloro-octadecylsilane. *Journal of Membrane Science*, **120** (2), 187–195.

284 Leger, C., De Lira, H.L. and Paterson, R. (1996) Preparation and properties of surface modified ceramic membranes. Part II. Gas and liquid permeabilities of 5 nm alumina membranes modified by a monolayer of bound polydimethylsiloxane (PDMS) silicone oil. *Journal of Membrane Science*, **120** (1), 135–146.

285 Sah, A., Castricum, H.L., Bliek, A., Blank, D.H.A. and Ten Elshof, J.E. (2004) Hydrophobic modification of γ-alumina membranes with organochlorosilanes. *Journal of Membrane Science*, **243** (1–2), 125–132.

286 Picard, C., Larbot, A., Tronel-Peyroz, E. and Berjoan, R. (2004) Characterisation of hydrophilic ceramic membranes modified by fluoroalkylsilanes into hydrophobic membranes. *Solid State Sciences*, **6** (6), 605–612.

287 Gazagnes, L., Cerneaux, S., Persin, M., Prouzet, E. and Larbot, A. (2007) Desalination of sodium chloride solutions and seawater with hydrophobic ceramic membranes. *Desalination*, **217** (1–3), 260–266.

288 Fang, H., Gao, J.F., Wang, H.T. and Chen, C.S. (2012) Hydrophobic porous alumina hollow fiber for water desalination via membrane distillation process. *Journal of Membrane Science*, **403–404**, 41–46.

289 Larbot, A., Gazagnes, L., Krajewski, S., Bukowska, M. and Kujawski, W. (2004) Water desalination using ceramic membrane distillation. *Desalination*, **168** (1–3), 367–372.

290 Cerneaux, S., Struzyńska, I., Kujawski, W.M., Persin, M. and Larbot, A. (2009) Comparison of various membrane distillation methods for desalination using hydrophobic ceramic membranes. *Journal of Membrane Science*, **337** (1–2), 55–60.

291 Zhang, J.W., Fang, H., Wang, J.W., Hao, L.Y., Xu, X. and Chen, C.S. (2014) Preparation and characterization of silicon nitride hollow fiber membranes for seawater desalination. *Journal of Membrane Science*, **450**, 197–206.

292 Krajewski, S.R., Kujawski, W., Bukowska, M., Picard, C. and Larbot, A. (2006) Application of fluoroalkylsilanes (FAS) grafted ceramic membranes in membrane distillation process of NaCl solutions. *Journal of Membrane Science*, **281** (1–2), 253–259.

293 The Fraunhofer Institute for Solar Energy Systems ISE (2015) Power from the Sun.

294 Seader, J.D., Henley, E.J. and Roper, D.K. (2011) Chemical and biochemical operations, in *Separation Process Principles*, John Wiley & Sons, Inc., Hoboken, NJ.

295 Néel, J. (1995) Pervaporation, in *Membrane Separations Technology: Principles and Applications* (eds D.N. Richard and S.A. Stern), Elsevier, Amsterdam, pp. 143–211.

296 Mulder, M. (1996) *Basic Principles of Membrane Technology*, Kluwer Academic Publishers, Dordrecht.

297 Jonquières, A., Arnal-Herault, C. and Babin, J. (2013) Pervaporation, in *Encyclopedia of Membrane Science and Technology*, John Wiley & Sons, Inc., Hoboken, NJ.

298 Sander, U. and Soukup, P. (1988) Design and operation of a pervaporation plant for ethanol dehydration. *Journal of Membrane Science*, **36**, 463–475.

299 Karlsson, H.O.E. and Tragardh, G. (1993) Pervaporation of dilute organic–water mixtures – a literature review on modeling studies and applications to aroma compound recovery. *Journal of Membrane Science*, **76** (2–3), 121–146.

300 Pereira, C.C., Ribeiro, C.P., Nobrega, R. and Borges, C.P. (2006) Pervaporative recovery of volatile aroma compounds from fruit juices. *Journal of Membrane Science*, **274** (1–2), 1–23.

301 Vane, L.M. (2005) A review of pervaporation for product recovery from biomass fermentation processes. *Journal of Chemical Technology and Biotechnology*, **80** (6), 603–629.

302 Huang, H.J., Ramaswamy, S., Tschirner, U.W. and Ramarao, B.V. (2008) A review of separation technologies in current and future biorefineries. *Separation and Purification Technology*, **62** (1), 1–21.

303 Tusel, G.F. and Bruschke, H.E.A. (1985) Use of pervaporation systems in the chemical industry. *Desalination*, **53** (1–3), 327–338.

304 Kober, P.A. (1917) Pervaporation, perstillation and percrystallization. *Journal of the American Chemical Society*, **39** (5), 944–948.

305 Aminabhavi, T.M., Khinnavar, R.S., Harogoppad, S.B., Aithal, U.S., Nguyen, Q.T. and Hansen, K.C. (1994) Pervaporation separation of organic–aqueous and organic–organic binary mixtures. *Journal of Macromolecular Science – Reviews in Macromolecular Chemistry and Physics*, **C34** (2), 139–204.

306 Verweij, H. (2003) Ceramic membranes: morphology and transport. *Journal of Materials Science*, **38** (23), 4677–4695.

307 Yoshida, W. and Cohen, Y. (2003) Ceramic-supported polymer membranes for pervaporation of binary organic/organic mixtures. *Journal of Membrane Science*, **213** (1–2), 145–157.

308 Bowen, T.C., Noble, R.D. and Falconer, J.L. (2004) Fundamentals and applications of pervaporation through zeolite membranes. *Journal of Membrane Science*, **245** (1–2), 1–33.

309 van den Berg, A.W.C., Gora, L., Jansen, J.C., Makkee, M. and Maschmeyer, T. (2003) Zeolite A membranes synthesized on a UV-irradiated TiO_2 coated metal support: the high pervaporation performance. *Journal of Membrane Science*, **224** (1–2), 29–37.

310 Matsukata, M., Sawamura, K., Sekine, Y. and Kikuchi, E. (2011) Review on prospects for energy saving in distillation process with microporous membranes, in *Inorganic, Polymeric and Composite Membranes: Structure, Function and Other Correlations* (eds S.T. Oyama and M.S.-W. Susan), Elsevier, Amsterdam, pp. 175–193.

311 Morigami, Y., Kondo, M., Abe, J., Kita, H. and Okamoto, K. (2001) The first large-scale pervaporation plant using tubular-type module with zeolite NaA membrane. *Separation and Purification Technology*, **25** (1–3), 251–260.

312 Yamamura, T., Kondo, M., Abe, J., Kita, H. and Okamoto, K. (2004) The vapor

permeation module using zeolite NaA membrane for producing absolute ethanol from biomass ethanol. Proceedings of the 8th International Conference on Inorganic Membranes, Cincinnati, OH, pp. 599–603.

313 Weyd, M. (2015) Research Field: Environmental and Process Engineering. Available at http://www.ikts.fraunhofer.de/en/research_fields/Environmental_EngineeringandBioenergy/Biomass_Technologies/membran_process_techmodeling.html (updated 10 July 2015).

314 Huang, A., Wang, N. and Caro, J. (2012) Synthesis of multi-layer zeolite LTA membranes with enhanced gas separation performance by using 3-aminopropyltriethoxysilane as interlayer. *Microporous and Mesoporous Materials*, **164**, 294–301.

315 Xu, X.C., Yang, W.S., Liu, J., Lin, L.W., Stroh, N. and Brunner, H. (2004) Synthesis of NaA zeolite membrane on a ceramic hollow fiber. *Journal of Membrane Science*, **229** (1–2), 81–85.

316 Kondo, M., Komori, M., Kita, H. and Okamoto, K. (1997) Tubular-type pervaporation module with zeolite NaA membrane. *Journal of Membrane Science*, **133** (1), 133–141.

317 Sommer, S. and Melin, T. (2005) Performance evaluation of microporous inorganic membranes in the dehydration of industrial solvents. *Chemical Engineering and Processing*, **44** (10), 1138–1156.

318 van Veen, H.M., van Delft, Y.C., Engelen, C.W.R. and Pex, P. (2001) Dewatering of organics by pervaporation with silica membranes. *Separation and Purification Technology*, **22–23** (1–3), 361–366.

319 Startin, A. and Elliott, G. (2001) Treating industrial hot gases with ceramic filters. *Filtration & Separation*, **38** (9), 38–40.

320 Pierre, A. and Christian, G. (2008) Current status and prospects for ceramic membrane applications, in *Handbook of Membrane Separations*, CRC Press, Boca Raton, FL, pp. 139–179.

321 Kita, H. (2006) Gas and vapor separation membranes based on carbon membranes, in *Materials Science of Membranes for Gas and Vapor Separation*, John Wiley & Sons, Inc., Hoboken, NJ, pp. 337–354.

322 Wee, S.L., Tye, C.T. and Bhatia, S. (2008) Membrane separation process – pervaporation through zeolite membrane. *Separation and Purification Technology*, **63** (3), 500–516.

323 Schleger, M., Sommer, S. and Melin, T. (2004) Module arrangement for solvent dehydration with silica membranes. *Desalination*, **163** (1–3), 281–286.

324 Castricum, H.L., Paradis, G.G., Mittelmeijer-Hazeleger, M.C., Bras, W., Eeckhaut, G., Vente, J.F. *et al.* (2014) Tuning the nanopore structure and separation behavior of hybrid organosilica membranes. *Microporous and Mesoporous Materials*, **185**, 224–234.

325 Castricum, H.L., Sah, A., Mittelmeijer-Hazeleger, M.C., Huiskes, C. and ten Elshof, J.E. (2007) Microporous structure and enhanced hydrophobicity in methylated SiO_2 for molecular separation. *Journal of Materials Chemistry*, **17** (15), 1509–1517.

326 Castricum, H.L., Sah, A., Mittelmeijer-Hazeleger, M.C. and ten Elshof, J.E. (2005) Hydrophobisation of mesoporous gamma-Al_2O_3 with organochlorosilanes – efficiency and structure. *Microporous and Mesoporous Materials*, **83** (1–3), 1–9.

327 Kreiter, R., Rietkerk, M.D.A., Castricum, H.L., van Veen, H.M., ten Elshof, J.E. and Vente, J.F. (2011) Evaluation of hybrid silica sols for stable microporous membranes using high-throughput screening. *Journal of Sol-Gel Science and Technology*, **57** (3), 245–252.

328 Chien, I.L., Zeng, K.L., Chao, H.Y. and Liu, J.H. (2004) Design and control of acetic acid dehydration system via heterogeneous azeotropic distillation. *Chemical Engineering Science*, **59** (21), 4547–4567.

329 Jullok, N., Darvishmanesh, S., Luis, P. and Van der Bruggen, B. (2011) The potential of pervaporation for separation of acetic acid and water mixtures using polyphenylsulfone membranes. *Chemical Engineering Science*, **175**, 306–315.

330 Jones, J.H. (2000) The Cativa™ process for the manufacture of acetic acid. *Platinum Metals Review*, **44** (3), 94–105.

331 Richter, H., Voigt, I. and Kuehnert, J.T. (2006) Dewatering of ethanol by pervaporation and vapour permeation with industrial scale NaA-membranes. *Desalination*, **199** (1–3), 92–93.

332 Caro, J. and Noack, M. (2010) Zeolite membranes – status and prospective, in *Advances in Nanoporous Materials* (ed E. Stefan), Elsevier, Amsterdam, pp. 1–96.

333 Maus, E.M. (2012) Dense polymeric membranes fundamentals & applications: packaging, barriers & industrial applications. XXIX European Membrane Society Summer School on Membranes, Université de Lorraine, Nancy.

334 Nunes, S.P. and Peinemann, K.V. (2006) *Membrane Technology: In the Chemical Industry*, John Wiley & Sons, Inc., Hoboken, NJ.

335 World Resources Institute (2015) Measuring, mapping and understanding water risks around the globe. Available at http://www.wri.org/our-work/project/aqueduct (updated 10 July 2015).

336 Shalhevet, J. (1994) Using water of marginal quality for crop production: major issues. *Agricultural Water Management*, **25** (3), 233–269.

337 Shani, U. and Dudley, L.M. (2001) Field studies of crop response to water and salt stress. *Soil Science Society of America Journal*, **65** (5), 1522–1528.

338 Judd, S. and Jefferson, B. (2003) *Membranes for Industrial Wastewater Recovery and Re-Use*, Elsevier, Amsterdam.

339 Schrader, G.A., Zwijnenburg, A. and Wessling, M. (2005) The effect of WWTP effluent zeta-potential on direct nanofiltration performance. *Journal of Membrane Science*, **266** (1–2), 80–93.

340 Skouteris, G., Hermosilla, D., Lopez, P., Negro, C. and Blanco, A. (2012) Anaerobic membrane bioreactors for wastewater treatment: a review. *Chemical Engineering Science*, **198**, 138–148.

341 Basile, A. and Gallucci, F. (2010) *Membranes for Membrane Reactors: Preparation, Optimization and Selection*, John Wiley & Sons, Inc., Chichester.

342 Judd, S. (2011) *The MBR Book: Principles and Applications of Membrane Bioreactors for Water and Wastewater Treatment*, Elsevier, Amsterdam.

343 Pearce, G. (2014) Commercial technologies and selected case studies, in *Membrane Biological Reactors: Theory, Modeling, Design, Management and Applications to Wastewater Reuse* (eds F.I. Hai, K. Yamamoto and C.H. Lee), IWA Publishing, London, pp. 401–445.

344 Hai, F.I., Yamamoto, K. and Lee, C.H. (2014) *Membrane Biological Reactors: Theory, Modeling, Design, Management and Applications to Wastewater Reuse*, IWA Publishing, London.

345 Stefanski, M., Kennedy, S. and Judd, S. (2011) The determination and origin of fibre clogging in membrane bioreactors. *Journal of Membrane Science*, **375** (1–2), 198–203.

346 Hanft, S. (2008) Membrane Bioreactors in the Changing World Water Market. Report C-240, Business Communications Company.

347 LiqTech International (2013) LiqTech launches SiC flat-sheet membrane discs. *Membrane Technology* **2013** (5), 3–4.

348 Xing, C.H., Tardieu, E., Qian, Y. and Wen, X.H. (2000) Ultrafiltration membrane bioreactor for urban wastewater reclamation. *Journal of Membrane Science*, **177** (1–2), 73–82.

349 Meabe, E., Lopetegui, J., Ollo, J. and Lardies, S. (2013) Ceramic Membrane Bioreactor: Potential Applications and Challenges for the Future. Likuid Nanotek.

350 Cicek, N., Franco, J.P., Suidan, M.T., Urbain, V. and Manem, J. (1999) Characterization and comparison of a membrane bioreactor and a conventional activated-sludge system in the treatment of wastewater containing high-molecular-weight compounds. *Water Environment Research*, **71** (1), 64–70.

351 Wang, L.K., Pereira, N.C. and Hung, Y.T. (2009) Advanced physicochemical treatment processes, in *Handbook of Environmental Engineering*, Humana Press, New York.

352 Cicek, N. (2003) A review of membrane bioreactors and their potential

application in the treatment of agricultural wastewater. *Canadian Biosystems Engineering*, **45**, 6.37–6.49.
353 Hailemariam, L.M., Johnson, A., Roy, A., Olanrewaju, K. and Reyntjens, K. (2013) Membranes for produced water treatment, in *Encyclopedia of Membrane Science and Technology*, John Wiley & Sons, Inc., Hoboken, NJ.
354 Babadagli, T. (2007) Development of mature oil fields – a review. *Journal of Petroleum Science and Engineering*, **57** (3–4), 221–246.
355 Duraisamy, R.T., Beni, A.H. and Henni, A. (2013) State of the art treatment of produced water, in *Water Treatment*, InTech.
356 Scanlon, B.R., Reedy, R.C. and Nicot, J.P. (2014) Comparison of water use for hydraulic fracturing for unconventional oil and gas versus conventional oil. *Environmental Science & Technology*, **48** (20), 12386–12393.
357 Clark, C. and Veil, J. (2009) Produced Water Volumes and Management Practices in the United States. Environmental Science Division, Argonne National Laboratory, US Department of Energy, Office of Fossil Energy, National Energy Technology Laboratory.
358 Hu, G., Li, J., Zeng, G. (2013) Recent development in the treatment of oily sludge from petroleum industry: A review. *Journal of Hazardous Materials*, **261**, 470–490.
359 Ahmadun, F.R., Pendashteh, A., Abdullah, L.C., Biak, D.R.A., Madaeni, S.S. and Abidin, Z.Z. (2009) Review of technologies for oil and gas produced water treatment. *Journal of Hazardous Materials*, **170** (2–3), 530–551.
360 Johnston, C.S. and Morris, R.J. (1980) *Oily Water Discharges: Regulatory, Technical and Scientific Considerations*, Elsevier, Amsterdam.
361 Padaki, M., Murali, R.S., Abdullah, M.S., Misdan, N., Moslehyani, A., Kassim, M.A. *et al.* (2015) Membrane technology enhancement in oil–water separation. A review. *Desalination*, **357**, 197–207.
362 Neff, J.M. (2002) Effect of contaminants from oil well produced water, in *Bioaccumulation in Marine Organisms*, Elsevier, Amsterdam.
363 Baker, R.W. (2010) Research needs in the membrane separation industry: looking back, looking forward. *Journal of Membrane Science*, **362** (1–2), 134–136.
364 Bensadok, K., Belkacem, M. and Nezzal, G. (2007) Treatment of cutting oil/water emulsion by coupling coagulation and dissolved air flotation. *Desalination*, **206** (1–3), 440–448.
365 Tellez, G.T., Nirmalakhandan, N. and Gardea-Torresdey, J.L. (2002) Performance evaluation of an activated sludge system for removing petroleum hydrocarbons from oilfield produced water. *Advances in Environmental Research*, **6** (4), 455–470.
366 Zhang, W., Zhu, Y., Liu, X., Wang, D., Li, J., Jiang, L. *et al.* (2014) Salt-induced fabrication of superhydrophilic and underwater superoleophobic PAA-*g*-PVDF membranes for effective separation of oil-in-water emulsions. *Angewandte Chemie, International Edition*, **53** (3), 856–860.
367 Gourgouillon, D., Schrive, L., Sarrade, S. and Rios, G.M. (2000) An environmentally friendly process for the regeneration of used oils. *Environmental Science & Technology*, **34** (16), 3469–3473.
368 Chen, X., Hong, L., Xu, Y. and Ong, Z.W. (2012) Ceramic pore channels with inducted carbon nanotubes for removing oil from water. *ACS Applied Materials & Interfaces*, **4** (4), 1909–1918.
369 Hua, F.L., Tsang, Y.F., Wang, Y.J., Chan, S.Y., Chua, H. and Sin, S.N. (2007) Performance study of ceramic microfiltration membrane for oily wastewater treatment. *Chemical Engineering Science*, **128** (2–3), 169–175.
370 Ebrahimi, M., Willershausen, D., Ashaghi, K.S., Engel, L., Placido, L., Mund, P. *et al.* (2010) Investigations on the use of different ceramic membranes for efficient oil-field produced water treatment. *Desalination*, **250** (3), 991–996.
371 Falahati, H. and Tremblay, A.Y. (2011) Flux dependent oil permeation in the

ultrafiltration of highly concentrated and unstable oil-in-water emulsions. *Journal of Membrane Science*, **371** (1–2), 239–247.

372 Zhou, J., Chang, Q., Wang, Y., Wang, J. and Meng, G. (2010) Separation of stable oil–water emulsion by the hydrophilic nano-sized ZrO_2 modified Al_2O_3 microfiltration membrane. *Separation and Purification Technology*, **75** (3), 243–248.

373 Cui, J., Zhang, X., Liu, H., Liu, S. and Yeung, K.L. (2008) Preparation and application of zeolite/ceramic microfiltration membranes for treatment of oil contaminated water. *Journal of Membrane Science*, **325** (1), 420–426.

374 Deriszadeh, A., Husein, M.M. and Harding, T.G. (2010) Produced water treatment by micellar-enhanced ultrafiltration. *Environmental Science & Technology*, **44** (5), 1767–1772.

375 Weschenfelder, S.E., Mello, A.C.C., Borges, C.P. and Campos, J.C. (2015) Oilfield produced water treatment by ceramic membranes: preliminary process cost estimation. *Desalination*, **360** (0), 81–86.

376 US EPA (1999) Phase one final rule and technical development document of uniform national discharge standards: surface vessel bilgewater/oil water separator: nature of discharge. Available at http://water.epa.gov/lawsregs/lawsguidance/cwa/vessel/unds/upload/2007_07_10_oceans_regulatory_unds_TDDdocuments_appAsurface.pdf (updated 10 July 2015).

377 Ghidossi, R., Veyret, D., Scotto, J.L., Jalabert, T. and Moulin, P. (2009) Ferry oily wastewater treatment. *Separation and Purification Technology*, **64** (3), 296–303.

378 Gard, A.S. (2013) Prevention of pollution of oil. Available at http://www.gard.no/ikbViewer/Content/72338/pollution (updated 10 July 2015).

379 Sun, C., Leiknes, T., Weitzenbock, J. and Thorstensen, B. (2010) Development of an integrated shipboard wastewater treatment system using biofilm-MBR. *Separation and Purification Technology*, **75** (1), 22–31.

380 Nguyen, T.D., Kim, K.R., Han, S.J., Cho, H.Y., Kim, J.W., Park, S.M. *et al.* (2010) Pretreatment of rice straw with ammonia and ionic liquid for lignocellulose conversion to fermentable sugars. *Bioresource Technology*, **101** (19), 7432–7438.

381 Benito, J.M., Sanchez, M.J., Pena, P. and Rodriguez, M.A. (2007) Development of a new high porosity ceramic membrane for the treatment of bilge water. *Desalination*, **214** (1–3), 91–101.

382 Mueller, J., Cen, Y. and Davis, R.H. (1997) Crossflow microfiltration of oily water. *Journal of Membrane Science*, **129** (2), 221–235.

383 Zaidi, A., Simms, K. and Kok, S. (1992) The use of micro/ultrafiltration for the removal of oil and suspended solids from oil-field brines. *Water Science and Technology*, **25** (10), 163–176.

384 Lipnizki, F. and Dupuy, A. (2013) Food industry applications, in *Encyclopedia of Membrane Science and Technology*, John Wiley & Sons, Inc., Hoboken, NJ.

385 Lipnizki, F. (2010) Cross-flow membrane applications in the food industry, in *Membrane Technology: Membranes for Food Applications*, Wiley-VCH Verlag GmbH, Weinheim, pp. 1–24.

386 Carvalho, A.F. and Maubois, J.L. (2009) Applications of membrane technologies in the dairy industry, in *Engineering Aspects of Milk and Dairy Products*, CRC Press, Boca Raton, FL, pp. 33–56.

387 Naim, R., Levitsky, I. and Gitis, V. (2012) Surfactant cleaning of UF membranes fouled by proteins. *Separation and Purification Technology*, **94**, 39–43.

388 Kuzmenko, D., Arkhangelsky, E., Belfer, S., Freger, V. and Gitis, V. (2005) Chemical cleaning of UF membranes fouled by BSA. *Desalination*, **179** (1–3), 323–333.

389 Saboya, L.V. and Maubois, J.L. (2000) Current developments of microfiltration technology in the dairy industry. *Lait*, **80** (6), 541–553.

390 Hemme, T. and Otte, J. (2010) Status and Prospects for Smallholder Milk Production: A Global Perspective. Food

and Agriculture Organization of the United Nations.
391 Food and Agriculture Organization of the United Nations (2012) Food Outlook – Global Market Analysis.
392 Madaan, N., Haufe, R., Shiju, N.R. and Rothenberg, G. (2014) Oxidative dehydrogenation of *n*-butane: activity and kinetics over VO_x/Al_2O_3 catalysts. *Topics in Catalysis*, **57**, 1400–1406.
393 Food and Agriculture Organization of the United Nations Statistics Division (2015) Production of Commodity in Selected Country.
394 United States Department of Agriculture Economic Research Service (2015) Food Availability (Per Capita) Data System. Available at http://www.ers.usda.gov/data-products/food-availability-(per-capita)-data-system/.aspx (updated 10 July 2015).
395 Langer, A.J., Ayers, T., Grass, J., Lynch, M., Angulo, F.J. and Mahon, B.E. (2012) Nonpasteurized dairy products, disease outbreaks, and state laws – United States, 1993–2006. *Emerging Infectious Diseases*, **18** (3), 385–391.
396 Suarez, V.B., Tremmel, G.J., Rivera, M., Reinheimer, J.A. and Meinardi, C.A. (2012) Polyphosphates as inhibitors of surface mould growth on hard cheese during ripening. *International Journal of Dairy Technology*, **65** (3), 410–415.
397 Goudedranche, H., Fauquant, J. and Maubois, J.L. (2000) Fractionation of globular milk fat by membrane microfiltration. *Lait*, **80** (1), 93–98.
398 Michalski, M.C., Leconte, N., Briard-Bion, V., Fauquant, J., Maubois, J.L. and Goudedranche, H. (2006) Microfiltration of raw whole milk to select fractions with different fat globule size distributions: process optimization and analysis. *Journal of Dairy Science*, **89** (10), 3778–3790.
399 Dewettinck, K., Rombaut, R., Thienpont, N., Le, T.T., Messens, K. and van Camp, J. (2008) Nutritional and technological aspects of milk fat globule membrane material. *International Dairy Journal*, **18** (5), 436–457.
400 Brans, G., Schroen, C., van der Sman, R.G.M. and Boom, R.M. (2004) Membrane fractionation of milk: state of the art and challenges. *Journal of Membrane Science*, **243** (1–2), 263–272.
401 Fox, P.F. and McSweeney, P.L.H. (1998) *Dairy Chemistry and Biochemistry*, Blackie Academic & Professional, London.
402 Zydney, A.L. (1998) Protein separations using membrane filtration: new opportunities for whey fractionation. *International Dairy Journal*, **8** (3), 243–250.
403 Dewit, J.N. (1981) Structure and functional behavior of whey proteins. *Netherlands Milk and Dairy Journal*, **35** (1), 47–64.
404 Vivekanand, V., Kentish, S.E., O'Connor, A.J., Barber, A.R. and Stevens, G.W. (2004) Microfiltration offers environmentally friendly fractionation of milk proteins. *Australian Journal of Dairy Technology*, **59** (2), 186–188.
405 Rosenberg, M. (1995) Current and future applications for membrane processes in the dairy industry. *Trends in Food Science & Technology*, **6** (1), 12–19.
406 Horton, B.S. (1997) Whatever happened to the ultrafiltration of milk? *Australian Journal of Dairy Technology*, **52** (1), 47–49.
407 Bastian, E.D., Hansen, K.G. and Brown, R.J. (1993) Inhibition of plasmin by beta-lactoglobulin using casein and a synthetic substrate. *Journal of Dairy Science*, **76** (11), 3354–3361.
408 Harper, J., Iyer, M., Knighton, D. and Lelievre, J. (1989) Effects of whey proteins on the proteolysis of Cheddar cheese slurries (a model for the maturation of cheeses made from ultrafiltered milk). *Journal of Dairy Science*, **72** (2), 333–341.
409 Wolf, A., Bray, G.A. and Popkin, B.M. (2008) A short history of beverages and how our body treats them. *Obesity Reviews*, **9** (2), 151–164.
410 Levitsky, I., Dahan, Y., Arkhangelsky, E. and Gitis, V. (2014) Retention of modified BSA by ultrafiltration membranes. *Journal of Chemical Technology and Biotechnology*, **91**, 1–10.
411 Saxena, A., Tripathi, B.P., Kumar, M. and Shahi, V.K. (2009) Membrane-based

techniques for the separation and purification of proteins: an overview. *Advances in Colloid and Interface Science*, **145** (1–2), 1–22.

412 Oliver, S.P., Jayarao, B.M. and Almeida, R.A. (2005) Foodborne pathogens in milk and the dairy farm environment: food safety and public health implications. *Foodborne Pathogens and Disease*, **2** (2), 115–129.

413 Jayarao, B.M. and Henning, D.R. (2001) Prevalence of foodborne pathogens in bulk tank milk. *Journal of Dairy Science*, **84** (10), 2157–2162.

414 Paton, J.C. and Paton, A.W. (1998) Pathogenesis and diagnosis of Shiga toxin-producing *Escherichia coli* infections. *Clinical Microbiology Reviews*, **11** (3), 450–472.

415 Food and Drug Administration (2011) Grade A Pasteurized Milk Ordinance (PMO). US Department of Health and Human Services, Public Health Service, Washington, DC.

416 Caplan, Z. and Barbano, D.M. (2013) Shelf life of pasteurized microfiltered milk containing 2% fat. *Journal of Dairy Science*, **96** (12), 8035–8046.

417 Boor, K.J. (2001) ADSA Foundation Scholar Award – fluid dairy product quality and safety: looking to the future. *Journal of Dairy Science*, **84** (1), 1–11.

418 PennState College of Agricultural Sciences (2010) Making, Handling and Marketing Safe, High-Quality Apple Cider.

419 Chapman, K.W. and Boor, K.J. (2001) Acceptance of 2% ultra-pasteurized milk by consumers, 6 to 11 years old. *Journal of Dairy Science*, **84** (4), 951–954.

420 Guerra, A., Jonsson, G., Rasmussen, A., Nielsen, E.W. and Edelsten, D. (1997) Low cross-flow velocity microfiltration of skim milk for removal of bacterial spores. *International Dairy Journal*, **7** (12), 849–861.

421 Baruah, G.L., Nayak, A. and Belfort, G. (2006) Scale-up from laboratory microfiltration to a ceramic pilot plant: design and performance. *Journal of Membrane Science*, **274** (1–2), 56–63.

422 Elwell, M.W. and Barbano, D.M. (2006) Use of microfiltration to improve fluid milk quality. *Journal of Dairy Science*, **89**, E20–E30.

423 Sandblom, R.M. (1978) Filtering process. US Patent 4105547 (to Alfa-Laval AB, Sweden).

424 Pall Corporation (2015) Membralox® GP membranes. Available at http://www.pall.com/main/food-and-beverage/ (updated 10 July 2015).

425 GEA Mechanical Equipment (2015) Separators, Decanters and Process Lines from GEA Westfalia Separator for Citrus Processing. Available at http://us.westfalia-separator.com/fileadmin/GEA_WS_US/Documents/Brochures/Beverage/GEA_WS_Citrus-Brochure.pdf (updated 10 July 2015).

426 Capannelli, G., Bottino, A., Munari, S., Ballarino, G., Mirzaian, H., Rispoli, G. *et al.* (1992) Ultrafiltration of fresh orange and lemon juices. *Food Science and Technology (Lebensmittel-Wissenschaft & Technologie)*, **25** (6), 518–522.

427 Braddock, R.J. (1981) Pectinase treatment of raw orange juice and subsequent quality changes in 60-degrees Brix concentrate. *Proceedings of the Florida State Horticultural Society*, **94**, 270–273.

428 Eagerman, B.A. and Rouse, A.H. (1976) Heat inactivation temperature–time relationships for pectinesterase inactivation in citrus juices. *Journal of Food Science*, **41** (6), 1396–1397.

429 Braddock, R.J. (1999) *Handbook of Citrus By-Products and Processing Technology*, Wiley-Interscience, New York.

430 Arreola, A.G., Balaban, M.O., Marshall, M.R., Peplow, A.J., Wei, C.I. and Cornell, J.A. (1991) Supercritical carbon dioxide effects on some quality attributes of single strength orange juice. *Journal of Food Science*, **56** (4), 1030–1033.

431 Guerrero-Beltrán, J.A. and Barbosa-Cánovas, G.V. (2004) Review. Advantages and limitations on processing foods by UV light. *Food Science and Technology International*, **10** (3), 137–147.

432 Timmermans, R.A.H., Mastwijk, H.C., Knol, J.J., Quataert, M.C.J., Vervoort, L., Van der Plancken, I. *et al.* (2011) Comparing equivalent thermal, high

pressure and pulsed electric field processes for mild pasteurization of orange juice. Part I. Impact on overall quality attributes. *Innovative Food Science & Emerging Technologies*, **12** (3), 235–243.

433 Vervoort, L., Van der Plancken, I., Grauwet, T., Timmermans, R.A.H., Mastwijk, H.C., Matser, A.M. *et al.* (2011) Comparing equivalent thermal, high pressure and pulsed electric field processes for mild pasteurization of orange juice. Part II. Impact on specific chemical and biochemical quality parameters. *Innovative Food Science & Emerging Technologies*, **12** (4), 466–477.

434 Valero, M., Recrosio, N., Saura, D., Munoz, N., Marti, N. and Lizama, V. (2007) Effects of ultrasonic treatments in orange juice processing. *Journal of Food Engineering*, **80** (2), 509–516.

435 Garcia-Gonzalez, L., Geeraerd, A.H., Spilimbergo, S., Elst, K., Van Ginneken, L., Debevere, J. *et al.* (2007) High pressure carbon dioxide inactivation of microorganisms in foods: the past, the present and the future. *International Journal of Food Microbiology*, **117** (1), 1–28.

436 Dahdouh, L., Wisniewski, C., Kapitan-Gnimdu, A., Servent, A., Dornier, M. and Delalonde, M. (2015) Identification of relevant physicochemical characteristics for predicting fruit juices filterability. *Separation and Purification Technology*, **141** (0), 59–67.

437 Cheryan, M. (1998) *Ultrafiltration and Microfiltration Handbook*, Taylor & Francis/Routledge, Lancaster.

438 PennState College of Agricultural Sciences (2010) Making, Handling and Marketing Safe, High-Quality Apple Cider. Available at extension.psu.edu/publications (updated 5 February 2015).

439 Alvarez, S., Riera, F.A., Alvarez, R., Coca, J., Cuperus, F.P., Bouwer, S.T. *et al.* (2000) A new integrated membrane process for producing clarified apple juice and apple juice aroma concentrate. *Journal of Food Engineering*, **46** (2), 109–125.

440 The Danish Environmental Protection Agency (2000) Cross-Flow Filtration of Fruit Juice.

441 Alvarez, S., Alvarez, R., Riera, F.A. and Coca, J. (1998) Influence of depectinization on apple juice ultrafiltration. *Colloids and Surfaces A: Physicochemical and Engineering Aspects*, **138** (2–3), 377–382.

442 Nandi, B.K., Das, B., Uppaluri, R. and Purkait, M.K. (2009) Microfiltration of mosambi juice using low cost ceramic membrane. *Journal of Food Engineering*, **95** (4), 597–605.

443 de Bruijn, J.P.F., Venegas, A., Martinez, J.A. and Borquez, R. (2003) Ultrafiltration performance of Carbosep membranes for the clarification of apple juice. *Food Science and Technology (Lebensmittel-Wissenschaft & Technologie)*, **36** (4), 397–406.

444 Alvarez, V., Andres, L.J., Riera, F.A. and Alvarez, R. (1996) Microfiltration of apple juice using inorganic membranes: process optimization and juice stability. *Canadian Journal of Chemical Engineering*, **74** (1), 156–162.

445 Youn, K.S., Hong, J.H., Bae, D.H., Kim, S.J. and Kim, S.D. (2004) Effective clarifying process of reconstituted apple juice using membrane filtration with filter-aid pretreatment. *Journal of Membrane Science*, **228** (2), 179–186.

446 Rai, P., Majumdar, G.C., Das Gupta, S. and De, S. (2007) Effect of various pretreatment methods on permeate flux and quality during ultrafiltration of mosambi juice. *Journal of Food Engineering*, **78** (2), 561–568.

447 de Barros, S.T.D., Andrade, C.M.G., Mendes, E.S. and Peres, L. (2003) Study of fouling mechanism in pineapple juice clarification by ultrafiltration. *Journal of Membrane Science*, **215** (1–2), 213–224.

448 Yazdanshenas, M., Tabatabaee-Nezhad, S.A.R., Soltanieh, M., Roostaazad, R. and Khoshfetrat, A.B. (2010) Contribution of fouling and gel polarization during ultrafiltration of raw apple juice at industrial scale. *Desalination*, **258** (1–3), 194–200.

449 Koch Membrane System (2015) A Clear Solution for Peterson Farms' Juice Making Operation. Available at http://www.kochmembrane.com/PDFs/Case-

Studies/KMS_Peterson_Farms_Case_Study.aspx (updated 6 April 2015).
450 Padillazakour, O. and McLellan, M.R. (1993) Optimization and modeling of apple juice cross-flow microfiltration with a ceramic membrane. *Journal of Food Science*, **58** (2), 369–374.
451 Vladisavljevic, G.T., Vukosavljevic, P. and Bukvic, B. (2003) Permeate flux and fouling resistance in ultrafiltration of depectinized apple juice using ceramic membranes. *Journal of Food Engineering*, **60** (3), 241–247.
452 de Oliveira, R.C., Doce, R.C. and de Barros, S.T.D. (2012) Clarification of passion fruit juice by microfiltration: analyses of operating parameters, study of membrane fouling and juice quality. *Journal of Food Engineering*, **111** (2), 432–439.
453 GEA Mechanical Equipment (2015) Systems and Processes from GEA Westfalia Separator for the Fruit-Processing and Juice-Making Industries. Available at http://us.westfalia-separator.com/fileadmin/GEA_WS_US/Documents/Brochures/Beverage/GEA_WS_Juice-Brochure.pdf (updated 4 March 2015).
454 Knirsch, M., Penschke, A. and Meyer-Pittroff, R. (1999) Disposal situation for brewery waste in Germany – results of a survey. *Brauwelt International*, **4**, 477–481.
455 Fillaudeau, L., Blanpain-Avet, P. and Daufin, G. (2006) Water, wastewater and waste management in brewing industries. *Journal of Cleaner Production*, **14** (5), 463–471.
456 Toussaint-Samat, M. (2008) *A History of Food*, Wiley-Blackwell, Hoboken, NJ.
457 Cantrell, P.A. (2000) Beer and ale, in *The Cambridge World History of Food* (eds K. Kiple and K. Ornelas), Cambridge University Press.
458 Gan, Q., Howell, J.A., Field, R.W., England, R., Bird, M.R., O'Shaughnessy, C.L. *et al.* (2001) Beer clarification by microfiltration – product quality control and fractionation of particles and macromolecules. *Journal of Membrane Science*, **194** (2), 185–196.
459 Siebert, K.J. and Lynn, P.Y. (1997) Mechanisms of adsorbent action in beverage stabilization. *Journal of Agricultural and Food Chemistry*, **45** (11), 4275–4280.
460 Lopez, M. and Edens, L. (2005) Effective prevention of chill-haze in beer using an acid proline-specific endoprotease from *Aspergillus niger*. *Journal of Agricultural and Food Chemistry*, **53** (20), 7944–7949.
461 Siebert, K.J., Carrasco, A. and Lynn, P.Y. (1996) Formation of protein–polyphenol haze in beverages. *Journal of Agricultural and Food Chemistry*, **44** (8), 1997–2005.
462 Bamforth, C.W. (2006) *New Brewing Technologies: Setting the Scene* (ed. C.W. Bamforth) Woodhead Publishing, pp. 1–9.
463 Ambrosi, A., Cardozo, N.S.M. and Tessaro, I.C. (2014) Membrane separation processes for the beer industry: a review and state of the art. *Food and Bioprocess Technology*, **7** (4), 921–936.
464 Leeder, G., Weigand, T. and Zuber, J. (2011) Kieselguhr vs. Cross-Flow Filtration; Economical & Ecological Aspects. Available at https://www.vlb-berlin.org/sites/default/files/Seite/Bangkok%20Conference%202011%20-%20Downloads/thu04-filtrox.pdf (updated 3 December 2014).
465 Moraru, C.I. and Schrader, E.U. (2008) Applications of membrane separation in the brewing industry, in *Handbook of Membrane Separations*, CRC Press, Boca Raton, FL, pp. 553–579.
466 Pall Corporation (2015) Breweries Using Pall's Keraflux® Tangential Flow Filtration (TFF) Technology Increase Yield and Reduce Waste Streams.
467 Eagles, W.P. and Wakeman, R.J. (2002) Interactions between dissolved material and the fouling layer during microfiltration of a model beer solution. *Journal of Membrane Science*, **206** (1–2), 253–264.
468 Burrell, K.J. and Reed, R.J.R. (1994) Cross-flow microfiltration of beer – laboratory scale studies on the effect of pore size. *Filtration & Separation*, **31** (4), 399–405.
469 Lea, A.G.H. and Piggott, J.R. (1995) *Fermented Beverage Production*,

Blackie Academic and Professional, Glasgow.
470 Le, M.S. (1987) Recovery of beer from tank bottoms with membranes. *Journal of Chemical Technology and Biotechnology*, **37** (1), 59–66.
471 International Agency for Research on Cancer (1988) IARC Monographs on the Evaluation of Carcinogenic Risks to Humans/Chemical Composition of Alcoholic Beverages, Additives and Contaminants. World Health Organization
472 Taylor, M., Faraday, D.B.F., O'Shaughnessy, C.L., Underwood, B.O. and Reed, R.J.R. (2001) Quantitative determination of fouling layer composition in the microfiltration of beer. *Separation and Purification Technology*, **22–23** (1–3), 133–142.
473 Gan, Q. (2001) Beer clarification by cross-flow microfiltration – effect of surface hydrodynamics and reversed membrane morphology. *Chemical Engineering and Processing: Process Intensification*, **40** (5), 413–419.
474 Reed, R.J.R. (1989) Advances in filtration. *The Brewer*, **75**, 965–970.
475 Cimini, A. and Moresi, M. (2014) Beer clarification using ceramic tubular membranes. *Food and Bioprocess Technology*, **7** (9), 2694–2710.
476 Tannahill, R. (1989) *Food in History*, Broadway Books, New York.
477 van 't Oever, R. (2014) Beer and Wine Membranes: Replace Diatomaceous Earth (Kieselguhr) for Yeast Removal and Other Applications. Available at http://www.membraneforum.com/images/presentations/RonaldVantOever_BeerWineFiltration.pdf (updated 23 February 2015).
478 Kiple, K.F. and Ornelas, K.C. (2000) *The Cambridge World History of Food*, Cambridge University Press.
479 El Rayess, Y., Albasi, C., Bacchin, P., Taillandier, P., Raynal, J., Mietton-Peuchot, M. *et al.* (2011) Cross-flow microfiltration applied to oenology: a review. *Journal of Membrane Science*, **382** (1–2), 1–19.
480 Grainger, K. (2013) Wine, in *Membrane Processing: Dairy and Beverage Applications*, Blackwell Publishing, Oxford, pp. 316–333.
481 Starbard, N. (2009) *Beverage Industry Microfiltration*, Wiley-Blackwell, Ames, IA.
482 Lyko, H. (2014) Separation technology in winemaking. *F&S Filtration and Separation International Edition*, (14), 22–25.
483 Gergely, S., Bekassy-Molnar, E. and Vatai, G. (2003) The use of multiobjective optimization to improve wine filtration. *Journal of Food Engineering*, **58** (4), 311–316.
484 Ulbricht, M., Ansorge, W., Danielzik, I., Koenig, M. and Schuster, O. (2009) Fouling in microfiltration of wine: the influence of the membrane polymer on adsorption of polyphenols and polysaccharides. *Separation and Purification Technology*, **68** (3), 335–342.
485 El Rayess, Y., Albasi, C., Bacchin, P., Taillandier, P., Mietton-Peuchot, M. and Devatine, A. (2012) Analysis of membrane fouling during cross-flow microfiltration of wine. *Innovative Food Science & Emerging Technologies*, **16**, 398–408.
486 Pall Corporation (2015) Pall Corp. Celebrates Sale of 1,000th Oenoflow™ Filtration System to the Wine Industry. Available at news.pall.com/article_display.cfm?article_id=4717 (updated 13 February 2015).
487 Pall Corporation (2015) Membralox® Ceramic Membrane Products. Available at http://www.pall.com/main/food-and-beverage/product.page?id=41052 (updated 2 December 2014).
488 Wilson, T. (2005) Australian wineries investing in 'New World' of ceramics. *Australian and New Zealand Grapegrower and Winemaker*, **495**, 97.
489 International Organisation of Vine and Wine (2005) International Code of Oenological Practices.

5
Economics

5.1
Introduction

This chapter is about the economics of practical applications of ceramic membranes. To put it simply, commercial applications are ultimately all about economic benefit. Sometimes this is dressed up as a societal or even psychological advantage, but all commercial transactions are ultimately driven by economics. There is even an interesting debate on whether taxation on charity contributions should be justified by the fact that the giver of charity actually benefits psychologically from the act of giving [1].

In our experience, academic colleagues will readily agree that economic considerations are important for practical application of scientific research. But in practice, most of us do not emphasize economics in our research. We often maintain that scientific research, and especially the so-called *basic research*, is (and should remain) curiosity-driven rather than money-driven. But this is changing for both companies and governments. Few companies today have 'central research' departments where basic research is done. And even government funding is moving towards paradigms such as 'science and society' and 'science for industry'. Thus, scientists are expected by society to help in solving actual and practical problems.

In the case of ceramic membranes, economics plays a key role. Everyone agrees that ceramic membranes have benefits: They are more robust than polymeric ones, more stable at high temperatures, and less prone to fouling. But all these technical benefits are offset against an economic disadvantage: Ceramic membranes are more expensive than polymeric ones, especially when considering the initial capital investment. In this chapter, we will try to qualify and quantify these statements, illustrating the numbers with simple graphics (inspired by David MacKay's approach in his excellent book discussing the pros and cons of sustainable energy [2]).

If we compare with the engineering concepts and equations derived in Chapter 2, the mathematics involved in quantifying economic parameters is simple. The problem is that each case is governed by many factors, and it is hard to judge which ones are the important ones. Moreover, even when considering two

Ceramic Membranes: New Opportunities and Practical Applications, First Edition. Vitaly Gitis and Gadi Rothenberg.
© 2016 Wiley-VCH Verlag GmbH & Co. KGaA. Published 2016 by Wiley-VCH Verlag GmbH & Co. KGaA.

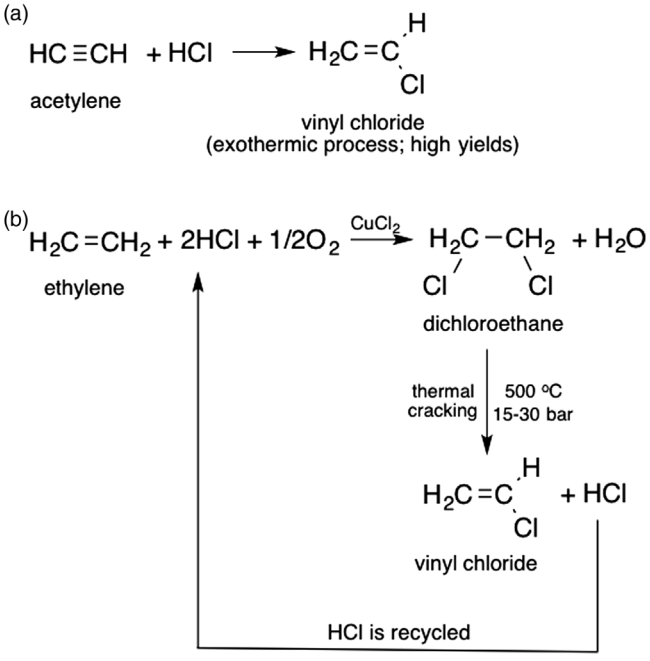


Figure 5.1 Two routes used today for the industrial production of vinyl chloride monomer (VCM). (a) Addition of HCl to acetylene. (b) Oxychlorination of ethylene.

identical technical cases in two different countries, the location itself may change the importance of the deciding factors. This holds true for many industrial sectors. For example, the synthesis of vinyl chloride monomer (VCM) (the building block for polyvinyl chloride (PVC)) can be done starting either from acetylene or from ethylene (Figure 5.1). The acetylene route was common before ethylene became widely available, thanks to the ubiquity of polyethylene [3]. Today, most plants in Europe use the ethylene route, which is cheaper (in Europe) for three reasons: the availability of low-cost ethylene, the relatively high prices of acetylene, and the hazard associated with using the latter. But VCM producers in China still use the (improved) acetylene route [4,5], because the large reserves of coal there make acetylene production cheaper (coal has very little hydrogen compared to crude oil or natural gas, so making something like acetylene, C_2H_2, makes sense). The final product is exactly the same, and in both cases, the economic factors tip the scales, but in opposite directions.

Considering that many readers (and both authors) are not economists, we will start by giving a very short general introduction to project and product evaluation. This introduction will outline methods and models used for comparing the value of processes and products, as well as the degree of complexity used in each estimation step. Following this, we will examine the market parameters for ceramic membranes, using data based on discussions and interviews of several membrane-producing and membrane-using companies. Then, we will look at three

manufacturing case studies: design and manufacturing of ceramic membranes in Germany, Denmark, and Japan, and compare the economic factors that lie behind each of these industrial successes. Finally, we will examine two application case studies: pretreatment using gamma-alumina membrane filters of petrochemical wastewater in Mahshahr, Iran, and CO_2 capture using zeolite membranes of flue gases in Rhône-Alpes, France. The chapter concludes with quantitative and qualitative exercises, including a special project exercise for advanced students.

5.2
A Layman Scientist's Guide to Project Appraisal: SWOT, PEST and LCA

One of the main problems with evaluating new projects and products is that it involves making good *judgemental* decisions. People (and especially scientists) are good at making *quantitative* decisions. When values are given in numbers, or when objects belong to the same class, we can easily compare them. Even in cases where the objects are different, we can still compare them quite easily, as long as the comparison does not involve too many factors. Simple examples include purchasing equipment or services for a specific task, or increasing/decreasing stock, or going on holiday. In each case, you can calculate the alternative cost, and make an informed decision.

The problem starts when the decision involves unknown factors, and especially when entering a new field, because new factors are likely to arise. Many economic scenarios fall into the latter category, where decisions must be made based on judgement (also known as intuition or 'gut feeling') rather than based on a quantitative comparison. The process of making intuitive decisions in itself is a thriving subject of research, and certainly out of the scope of this book. Readers wishing to delve deeper into the subject should see the excellent overview by Hayashi [6]. But to put it simply, there are two factors that can help people make good judgemental decisions: relevant experience and objective data. Here, we will discuss very briefly the first, and give a short overview of the tools for obtaining and organizing the second.

The fact that experienced managers make better judgemental decisions than newcomers to the field is undisputed [6,7]. As a rule of thumb, it takes 5–10 years of experience before people develop a good 'gut feeling' in a given field (this is also one reason why many advertisements for managers specify 'a relevant education plus seven years of relevant experience' as requirements). Interestingly, intuition is apparently field specific (so, for example, someone who did a great job as an army general is not always the best choice for managing a large company in the private sector). All studies show that when it comes to making good judgemental decisions, there is no substitute for relevant experience.

But even experienced managers can make decisions based on only good data, and these data should be presented and discussed objectively, because one of the problems with intuitive decisions is that people make them very quickly, and are usually loath to change them afterwards [8,9]. There are several useful methods

and models for presenting project data clearly and simply. Here, we will outline three common methods that can help you view both internal and external factors: SWOT analysis, PEST analysis and life cycle assessment (LCA). All three methods are aimed at presenting the available data in such a way that will help you make good judgemental decisions.

5.2.1 SWOT Analysis

The SWOT – strengths, weaknesses, opportunities and threats – analysis is a simple and generally effective tool for evaluating projects and businesses.. Typically, these are arranged in a 2×2 matrix (also called the *SWOT matrix*, see Figure 5.2). The SWOT analysis is useful because it is simple, and yet shows the relation between internal factors (strengths and weaknesses) and external ones (opportunities and threats). Ideally, you can (and should) use the SWOT analysis to check whether your objectives are realistic. In its simplest form, SWOT does not give quantitative answers, and so it should be combined with an alternative cost/relative size analysis (see below).

The internal factors are listed as strengths or weaknesses. The strengths are the advantages of the project. These could be related to supplier contracts, intellectual property rights (IPR), market position and manufacturing capacity, goodwill from key stakeholders or geographic location. Similarly, the weaknesses are the internal disadvantages: equipment limitations, absence of skilled personnel, insufficient market access, soon-to-expire IP or lack of capital.

The threats and opportunities are external factors, reflecting the situation in the environment around the project, business unit or organization. Typical threats can be the number of competitors and the likely entry of new competitors, the introduction of substitute products, a growing bargaining power of suppliers or customers, adverse demographic changes or a shift in the market owing to a change in government regulations. Likewise, the opportunities can include

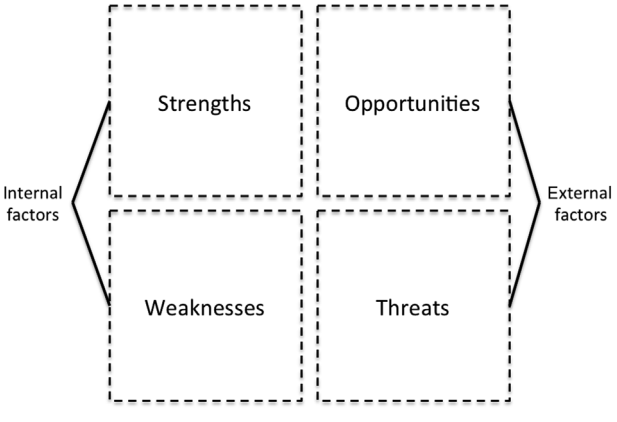


Figure 5.2 The 2×2 matrix summarizing the SWOT parameters.

possibilities to enter new markets, new customer focus on local suppliers, introduction of complementary products or services, possibilities for mergers or valorization of old IP in new market segments.

5.2.1.1 Identifying, Matching and Converting

Once you identify the different SWOTs, the matrix can help you in improving your position. Since the strengths and weaknesses are internal, dealing with them is usually within the scope of the organization. The threats and opportunities are external, so the organization must react to them. This can be done by matching the strengths to opportunities (e.g. entering an emerging market segment by capitalizing on a patent that was originally filed to protect the organization in another market). Similarly, you can try and convert the negative aspects (weaknesses and threats) to positive ones (strengths and opportunities). For example, if you recognize the threat of a competitor in a related market segment, you can convert this into an opportunity by sharing the market through a merger or joint venture, or by agreeing to consolidate your efforts in one of the two market segments.

Once the SWOT analysis has been performed, you can use it to validate the feasibility of your objectives. Presenting the positive and negative aspects next to each other decreases the chance of ignoring those factors that go against the decision-makers' 'gut feeling'. In 2001, Kitts *et al.* showed that given enough data, the simple SWOT matrix can also be expanded into the so-called three-dimensional 'fitness landscape'. This allows viewing the business or project's situation in the past and making predictions about its future. It also gives information about the rate of change in the environment (seen as deformations on the surface) and about the uncertainty of the predictions [10]. The last 10 years have seen an explosion of data-collecting algorithms (so-called 'big data' collections) and more and better data; more companies are applying such tools in their decision-making process.

5.2.2 PEST Analysis

A project, business unit or organization usually has a reasonable (if sometimes biased) overview of its own strengths and weaknesses. Listing and analysing the external factors is more challenging, especially since these can vary greatly between different environments. The analysis of political, economic, social and technological (PEST) parameters is one method for collecting these external factors and evaluating their influence. Similar to the SWOT analysis described above, the PEST analysis can give insight into how these external factors influence your project or organization. Depending on the type of project or business, some analysts also add environmental factors. However, in the case of ceramic membranes, the environmental factors are important enough to merit their own analysis method (life cycle assessment, see below).

Figure 5.3 shows a typical PEST analysis table, listing the different factors by category. The political factors can include new and upcoming regulations such

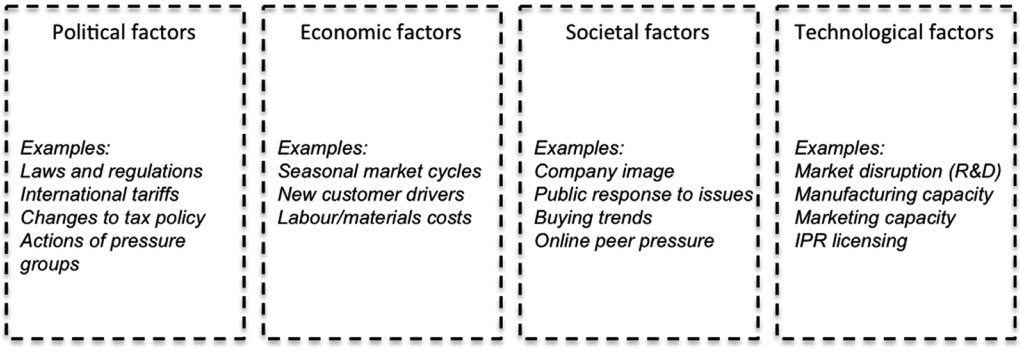


Figure 5.3 A typical PEST analysis table.

as REACH, changing international tariffs and tax policy and the formation and action of lobbying and pressure groups. Similarly, the economic factors can include market seasonal cycles, new drivers for customers and end users. The social factors will reflect the brand and company image, industry trends, buying patterns and public responses to end-of-life questions such as waste disposal. Finally, the technological part should cover R&D activities, emerging technologies, manufacturing and marketing capacity and IP protection and licensing. Some of these parameters will overlap with those presented in the SWOT matrix, but the advantage of combining the two evaluation methods is that this may give additional insight into how to match positive factors and/or convert negative ones.

Many of these factors are closely related, so that changing two different PEST factors can have far-reaching results. Consider the example of the opening of the telecommunications market in Britain (a change in regulations) combined with the falling cost of long-distance communications (an improvement in technology). This combination of factors allowed many UK firms to move their 'back office' services to India, thus benefiting from cheap labour costs. Interestingly, this move also fuelled a surge in ICT businesses in India, adding to the already booming hi-technology hubs in places like Bangalore. In some cases, the original British or American companies had added so many Indian employees that they had to adapt their human resources policies accordingly. (If a company's headquarters are based in London but 90% of its employees are in Bangalore, is it a British company or an Indian one?)

5.2.3 Life Cycle Assessment

In the past decade, more and more analysts include environmental factors in their assessments. The drive for this comes both top-down (new government regulations) and bottom-up (societal pressure). Some projects are more sensitive to environmental factors than others, but ceramic membranes definitely deserve

attention from this respect. One tool that helps us evaluate the environmental impact of a product or process is the life cycle assessment. The main advantage of LCA is that it gives an overall view. This includes raw materials extraction and acquisition, chemical reactions, processing, manufacturing, packaging, transportation, distribution, consumer use and end-of-life management [11]. A typical LCA has four main stages: (i) defining the assessment scope and boundaries; (ii) quantifying energy and materials flows (inventory analysis); (iii) impact analysis, determining the effects on the environment and human health; and (iv) improvement analysis, which can include methods such as green chemistry and green engineering, and environmental design [12]. Figure 5.4 shows the four stages in life cycle assessment. Note that LCA is by no means limited to ceramic membranes. It is applied in many diverse areas, from assessing roof types [13] to groundwater remediation technologies [14]. This short outline is based on our discussion of the application of LCA to the chemical industry sectors, which is published elsewhere [15].

The first step in LCA is *defining the scope* and goal of the study [16]. In this stage, functional units are defined. This allows you to compare products based on the functions they fulfil, rather than by their amount. For example, a milk bottle that is collected, cleaned and reused 20 times, fulfils the same *function* as 20 disposable milk cartons. Defining the study scope and goal within your sphere of influence is useful; because then you can actually carry out the recommendations once the assessment is completed (the sphere of influence is equivalent to the space of internal factors under your control in the SWOT analysis).

The second step is *making an inventory* of all the environmental interventions, such as emissions to air and water during production, use of utilities such as electricity and water and the acquisition of raw materials. This is done using mass and energy balances. The interventions are then clustered by type, and totalled for all the processes. Such inventory tables can contain over 100 entries, for example the total emission of lead, SO_2 or hydrocarbon particulates.

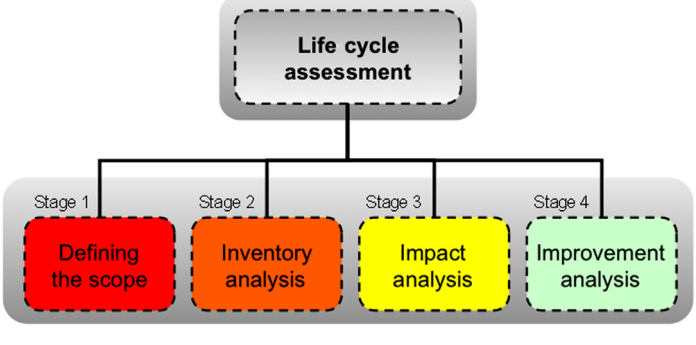


Figure 5.4 The four stages in life cycle assessment.

The third step is an *impact analysis*. First, impact categories are classified. These usually pertain to common environmental threats, such as global warming, acid rain or ozone depletion. The environmental interventions from step 2 are then translated into scores in each impact category. These scores are used for calculating an overall environmental impact profile for the original product or process. This is often the most problematic step, because quantifying the environmental impact of a process or a product is complex and debatable.

Finally, the results are interpreted and an *improvement analysis* tries to pinpoint the process elements that can be changed, by using a different technology or a different design. This is where we apply the tools of research and development, and the so-called green engineering.

The quantification of different effects and the ranking of these by their relative size (or by size of influence) is a key point. There are many cases where discussions seem to revolve around relatively small factors that have small effects on the economic outcome. In such cases, a simple back-of-the-envelope calculation can show quickly if a certain factor is worth including in the analysis or not.

5.3 Economic Considerations in the Manufacturing and Application of Ceramic Membranes

In this section, we will try to find out the factors that govern the economic success in the manufacturing and application of ceramic membranes. The data for this chapter were collected from two sources: case studies published in professional literature, and in-depth interviews of key industrial players. As you can expect, visiting the manufacturing companies teaches volumes that cannot be learned from published papers. Many of the decisions that these membrane manufacturing companies make are judgemental ones, and we tried to understand the strategy and the objectives involved. For this reason, we chose to bring the case stories below with as much details as possible, following our talks with the people on the work floor and with the management, so that you, the reader, can hopefully experience the same effect.

In each of the case studies below, we have incorporated some of the analysis tools from the previous section. Sometimes one method is more appropriate, and sometimes another method gives more information. It is up to you to make the conclusions based on the data presented.

5.3.1 Case Study 1: Atech Innovations GmbH (Germany)

The German company *Atech Innovations* is located close to the city of Duisburg, in the western part of the Ruhr Area (*Ruhrgebiet*) in North Rhine-Westphalia. Its building is typical of the industry in this region: a modern, grey, squarish structure, projecting good solid values. Coming in, we were met by one of

Atech's founders, Dr. Giovanni Catania, and one of the senior sales managers, Erik Kossin. Everything about the building and its inhabitants, from the utilitarian offices to the walk-in calcination ovens, gives a feeling of simplicity and efficiency. Atech is one of those German companies that *The Economist* writes about when it talks about the quality of the German *mittelstand* [17]. A small-medium enterprise (SME, defined as a company with fewer than 250 employees), it employs about 50 people, and makes basically one product: ceramic membrane modules.

In the late 1980s, the company *Aran Holdings* was working in the waste business (solid and liquid) and wanted to enter a new market, for water purification via ultrafiltration. Setting up Atech innovations, they bought a licence for a French patent for making silicon carbide (SiC) membranes, building wastewater treatment systems for the German market. However, this led to a conflict between the company and some of its clients, who were original equipment manufacturers (OEMs; companies that manufacture pieces of equipment and sell it to other companies that then sell it under their brand name). Clearly, the company could not manufacture and sell both the ceramic membranes and the complete installations for water purification. At that point, Atech innovations decided to focus on making and selling ceramic membranes only.

However, the people working at Atech remained throughout this transition from membranes and systems production to membranes-only. And this was a crucial point, since these engineers have a thorough knowledge of membrane systems and their applications. This gives Atech a technical edge over other producers of ceramic membranes: Their engineers know how to make membranes, but are also well versed with the day-to-day issues that their clients face. This means that the service that Atech gives is better, because its engineers understand well the systems used by their clients.

Subsequently, Atech decided to move away from SiC membranes and focus on alpha-alumina, for chemical reasons. The SiC membranes were not robust, and this created problems. These membranes were fine as long as the client used them exactly to specifications. The problem was that you could never guess what the client would do, and Atech realized that they must make more robust membranes that can withstand harsher conditions (e.g. washing with basic solutions).

For the clients, there was not much difference. The colour was different, white instead of black, but the diameters were the same and the performance was better. Still, introducing the alpha-alumina membranes into the market took time. The new membranes were made with a layered structure, either completely from alpha-alumina or with some separation layers made from titania.

Today, Atech's business accounts for about 20% of the ceramic membranes market, working with one OEM in India, one in South Africa, three in the United States, and three to four in China. The membranes are used for microfiltration and ultrafiltration. The company's know-how is its biggest asset. Much of this know-how is preserved as trade secrets, rather than in patents. The combined know-how in the manufacturing of ceramic membranes and the understanding of the design and operation of complete systems is the key to success.

This is especially important when facing the harsh competition and fast development in the Far East. According to Catania, the main source for ceramic membranes in China is the University of Nanjing. Graduates from this university open new companies for making ceramic membranes at the rate of three to four companies per year! These companies produce very cheaply – a typical ceramic membrane module costs only €20–30, compared to about €300 for an Atech module.

The difference is that these competitors know about ceramic membranes, but not about markets, applications, and technical issues and problems. Moreover, according to Catania, the competitors use binders, which means that they can sinter their membranes at lower temperatures and save on production costs. The drawback is that the binder makes for a less efficient and less robust membrane. Atech's binder-free production technology (again, a trade secret) gives them the edge on the competition – a higher mechanical strength and a narrower pore distribution.

Currently, Atech's technology and knowledge preserves its market and clients. Clients do buy cheaper modules (the exchange website AliBaba lists over 100 Chinese companies selling ceramic membranes) to try them out, but they always return to Atech. Apparently, with ceramic membranes, you get what you pay for. But Catania is concerned about the rate of advancement of innovation in China. It is only a matter of time, he says, before the new companies improve their technology to a level where competition would be tougher, but simultaneously that would also mean that their costs would increase. Interestingly, Atech employs a full-time Chinese engineer, who invests much time reading the published literature on ceramic membranes in China, much of which is available only in Mandarin.

Moving with Catania and Kossin to the membrane production area, we see that the equipment is simple and manual: injection tubes, immersion baths, stirrers and ovens (the largest oven fits on average 450 membrane pipes, each 1.5 m long). Catania confirms that the investment costs are low. Making good ceramic membranes does not need expensive machinery or clean rooms. The costs are mainly for personnel – Atech has highly qualified personnel (the company is based on chemical engineers and mechanical engineers) and these are costly. The workers on the floor are men in their 40s and 50s. They work unhurriedly, methodically. Each membrane is turned, cut by hand, cleaned and examined for faults; quality control is strict. The smallest fault, and the entire module is set aside and numbered, so that its source can be traced. Perhaps it is the extrusion step; perhaps the grain size was not optimal. Each case is studied and discussed, so that such faults are minimized.

The main trade secrets are in the extrusion and the sintering steps. Here, the fact that Atech uses only alpha-alumina and no binder gives an advantage of strength, so that they can produce modules that are 1.5 m in length – exceptionally long and yet straight. Not using a binder is simple (excluding an ingredient is easier than including it) but that does not mean that it is easy to get it right. The fact that Atech is basing its technology on trade secrets is a little



Figure 5.5 SWOT analysis of the product and process situation of Atech Innovations GmbH.

problematic, since someone else could in principle file patents on these (see our SWOT analysis in Figure 5.5), although Atech could still claim the right to operate. However, Catania feels that it would be difficult to patent the production of membranes, since most of the technology is well known. Moreover, it would be very hard for a company to prove patent infringement in ceramic membrane production, since the end product does not necessarily show the actual production steps.

According to Catania, there is not sufficient demand for ceramic membranes for automating the production. There have been investments and companies who started with high automation levels, but even though they produced many membranes (10 times as much as Atech), they had no market success. The membranes were not good enough, and they could not follow-up on marketing the product and servicing clients. It is a chicken-and-egg problem: on one hand, demand must increase for justifying making large numbers of membrane modules that would justify the cost of automation. On the other hand, prices must go down enough to justify an increased demand.

At this time, however, Atech is doing well. The apt definition of the mittelstand model, 'highly focused, achieving unprecedented efficiencies by designing a business model with a razor-thin focus and learning to do the one thing really well' seems to fit perfectly here [18]. Atech moved to ceramic membrane manufacturing 25 years ago. In the next 20 years, the company will most likely still be here, making high-quality ceramic membranes.

5.3.2
Case Study 2: LiqTech A/S (Denmark)

The Danish company LiqTech A/S (a contraction of *Liquid Technologies*) was established in 1999 with the vision of producing ceramic membranes for liquid

filtration. Its initial focus area was the dairy industry, using SiC membranes with an oxide coating that were introduced to the market in 2000. At the same time, LiqTech started manufacturing diesel particulate filters, which today still remain an important business area for the company. In the following years, the SiC-based coatings for the membrane substrates were further developed and commercialized by a daughter company, CoMeTas A/S, which introduced the first 100% based SiC membranes to the market in 2004. CoMeTas grew quickly, and was merged with the mother company in 2011, forming today's *LiqTech International A/S*.

We interviewed Dr. Daniel Sereth Larsen, LiqTech's product manager for membranes. Asked how he views the entry of LiqTech products into the membranes market, and the competition with the current polymer-based membranes, Larsen replied that naturally they are aware that ceramic membranes still only account for a relatively small amount of the total membrane market. However, they see that the market acceptance and adoption of ceramic membranes is growing. There are several cases where polymeric hollow fibre membranes experience fibre breakage or were destroyed by high temperatures or upstream upset. This has shifted some focus towards the more reliable CM technology. Indeed, much of LiqTech's competition is with other CM producers, such as Atech (see above), Metawater (see the next case study), Veolia, Tami, Pall, Orelis, Atech, Inopor, Jiuwu and StarSep. According to Larsen, LiqTech products offer a higher flux and better durability compared with alumina-based membranes.

The main competition advantage against polymeric membranes is in applications where these fail due to high temperatures, oil in the feed (which blocks polymeric membranes) or an aggressive (chemical) environment which leads to very short lifetimes. In the long term, LiqTech is eyeing the success of MetaWater in Japan that has developed efficient CMs for drinking water applications. The company's focus today is on applications that require robust membrane technology and where fouling and scaling is present and must be controlled. They also focus on oily water feeds (from the oil/gas industries, refineries and fracking). LiqTech's hydrophilic membranes perform well in oil–water separation.

Regarding the company's market share, Larsen says that quantifying this is difficult, because some ceramic membrane manufacturers also supply systems, so it is not clear how much of their turnover is actual CMs. Independent analyses put LiqTech's share at 10–20% of the market, while their own analysis is a more modest 10–15%. Larsen expects the total ceramic membrane market to grow significantly in the future and LiqTech's share is projected to reach 25% within the coming decade, simply because they see customers shifting from alumina-based CMs towards SiC-based ones.

Just like Atech, LiqTech recognizes that technical expertise is one of the most important factors for success. To quote Larsen: 'Most customers expect that we know everything about how to operate the membranes in different application before they have the confidence in our technology.' Yet unlike Atech, which has decided to keep the knowledge but step out of the systems market and focus all

its energy on making CMs for other people's modules, LiqTech has also developed its own piloting equipment. It now also offers, in addition to the single-membrane components, a 'full service' sales process from laboratory trial to field trial and finally to detailed engineering design of full-scale units.

Larsen agrees that market penetration is slow, especially since the market is flooded with cheap polymeric membranes produced in Asia. One reason for the slow acceptance is the common perception in the market that ceramic membranes are very expensive compared to polymeric ones. It is true that the cost per square metre is higher, but if you look at the higher flux, lower energy consumption and longer lifetime, the total cost of ownership (TCO) is lower for ceramics on the long term. The company sees the biggest potential is in markets related to the oil and gas industry and industrial wastewater (e.g. removing heavy metals at power plants and mines). Here CMs have a distinct advantage: In some cases, LiqTech has replaced polymeric membranes, and the driving factor was that the polymers had to be changed two to three times per year, compared to up to once a decade for CMs.

According to Larsen, the advantages of ceramic membranes are especially long lifetime, higher flux and smaller footprint. Furthermore, SiC membranes offer extreme durability with respect to chemical and temperature resistances compared to polymeric membranes and even alumina-based CMs. This means that SiC membranes can be used in applications that have been too difficult for existing membranes, as well as improve the performance of existing systems. Moreover, SiC has increased fouling resistance compared to other common membrane materials resulting in longer lifetime of the membrane and less chemical cleaning requirements. The membranes can also be regenerated in an oxidation furnace, so that if for some reason you get serious organic fouling, you can (in principle) simply burn it away. The main limitations are cost related, especially where people are focused on capital expenses (CapEx) only.

Practically, the key costs today are the firing of the membranes in the high-temperature furnaces. However, the growing adoption of ceramic membranes seen on the market also means that LiqTech (and other manufacturers) can benefit from economies of scale, and this drives cost down to a level where they can compete with polymeric membranes (price/performance ratio). Competing against polymeric membranes in applications such as drinking water is very price sensitive (note, however, that Metawater is doing this, as we will see in the next case study, and LiqTech of course knows this and is trying to follow). Automation in the factory is low key, and Larsen views it as uneconomical unless one 'standard membrane' would be used in (almost) all applications.

Another limitation is the lack of knowledge and experience with cross-flow filtration and ceramic membranes on the market. LiqTech is approached by many system integrators which are highly interested in its technology, but without the process knowledge it simply takes time before they are capable of building their own systems. Thus, much training is needed and forms a crucial part of the supplier–customer relationship. Interestingly, this is one aspect where European companies are still ahead of their Chinese competitors, which currently



Figure 5.6 SWOT analysis of the product and process situation of LiqTech International A/S.

gives companies like LiqTech and Atech an advantage, but maybe not for long (see our SWOT analysis in Figure 5.6).

The fact that LiqTech also develops membrane housings and systems help it in tackling the known deficiencies of CMs: mechanical brittleness and low compatibility with module materials. The company has invested a lot of resources and time into developing housing solutions for protecting their CMs. The membranes are brittle, and thus must be protected against vibrations, transported safely and mounted carefully. According to Larsen, the most critical point is actually during assembly of the membrane and housing where improper handling can cause chip damages. In the beginning, these problems were frequent due to the lack of experience, but with the right equipment such as protection covers, mounting manuals and presence of LiqTech technicians on-site, most problems are now avoided.

5.3.3
Case Study 3: Metawater Co. (Japan)

The Japanese company Metawater was officially formed in April 2008 in a consolidation between Fuji Electric Water Environmental Systems and NGK Water Environment Systems. Fuji brought into this merger expertise in electric technology, while NGK contributed know-how on machinery and equipment technology. The background R&D of Metawater dates further back to 1988, with the start of R&D at NGK on ceramic membrane filtration systems for drinking water treatment plants (DWTPs). Development followed with demonstration projects in 1991 and commercial installations in 1996 (30 mm modules) and 2001 (180 mm modules). In 2006, the company opened its first large ceramic membrane DWTP, treating 38 900 m^3 of water per day. Two years later, Metawater was awarded the largest membrane DWTP contract in Japan, an installation

handling over 170 000 m^3 of water per day (to get an idea of the size, that is enough water to fill 68 Olympic-sized swimming pools every day). Today, Metawater is one of the total service providers that focuses on drinking water purification and reclamation (see Figure 5.7). This area received particular boost in Japan, where drinking water treatment came with a requirement of epidemiological safety improvement, fostering technology to remove turbidity and resolve waterborne infection by protozoa. The company's main business is in Japan, but it is also expanding to other markets and other market segments. Currently, their R&D unit includes a basic technology development department and an advanced technology development department, and the company focuses its R&D on drinking water applications as well as on wastewater applications.

We talked to Dr. Chiho Kojima, Metawater's departmental chief of International Sales & Marketing, part of the International Business Division. As we can expect, based on the two previous case studies and on the fundamental aspects treated in the previous chapters, Metawater chose ceramic membranes to overcome the inherent weaknesses of polymer membranes. Any cleaning process requiring corrosive chemicals, high pressures or high temperatures is ultimately more suitable for CMs. Thus, Metawater sees its competitors more as other CM manufacturers. However, producing CMs on a large commercial scale is difficult, and requires large investments. This means that not all manufacturers can compete commercially on a large scale, even if they have the knowledge and skill needed to produce high-quality membranes.



Figure 5.7 Photo of a municipal drinking water treatment plant (DWTP) unit in Ehime, Japan. (Courtesy of Metawater Co., Ltd., Japan.)

According to Kojima, the market share of Metawater's ceramic membrane filtration systems (MF/UF membrane filtration of municipal DWTPs) in Japan was about 40% in 2013. Generally (and similar to the situation at LiqTech) the company sees a gradual market increase, mainly because the CapEx investment cost in CM systems is higher than needed for polymer-based membranes. However, if customers calculate the operating expenses (OpEx) for 20 years and consider 'invisible' costs, such as 'time', the market share will increase considerably. Thus, the key to expansion of the CM market is getting customers to think in terms of operating costs and long-term scenarios, rather than just looking at short-term capital expenses.

The membranes manufactured by Metawater have several advantages. These include long lifetimes (no membrane was replaced since the first one was installed 16 years ago), little or no breakage, high resistance against chemicals and low energy requirements (in dead-end filtration, the typical power consumption is $<0.1\,kWh/m^3$). The main limitation, according to Kojima, is the pore size. The CMs are intended for microfiltration, with a nominal pore size of 0.1 μm. In some cases, applying coagulants enables the removal of particles smaller than 0.1 μm. In general, these membranes cannot remove ionized materials and dissolved species.

Metawater is expanding its technology to new markets, and sees opportunities for CMs in three main areas: oil and gas applications including fracking flow back, offshore applications and enhanced oil recovery (EOR), mining applications with high TSS/TOC and tertiary treatment for water reuse.

5.3.4
Case Study 4: Pretreatment of Petrochemical Wastewater in Mahshahr, Iran

Notwithstanding the large research efforts towards a biomass-based economy [19,20], petrochemicals are and will remain the largest chemical industry segment by volume, at least in the twenty-first century. These large-scale processes have their problems. Hydrocracking, for example, which is a key step in the making of jet fuel, diesel, naphtha and LPG, suffers from coking. Small carbon particles form in hydrocracking reactors, causing heat loss and corrosion and contaminating wastewater [21]. The latter is a serious problem, since very large amounts of water are involved. Currently, this contaminated wastewater is typically cleaned using coalescing filtration units [22]. The filters are usually made of woven fabrics sandwiched between perforated supports. But the coke particles also clog these filters, lowering their efficiency. Thus, reducing the effluent coke loading remains an important challenge [23,24].

One effective alternative for pretreating such effluents is membrane filtration. Although either organic or ceramic membranes can be used, this is an application where the superior thermal, chemical and mechanical stability [5–7] of ceramic membranes offer important advantages. Here, we follow the techno-economic studies published by Salehi *et al.* [25], augmenting those by interviewing with the scientists involved. We chose this for a case study because the

authors used actual industrial data for assessing the feasibility of implementing a ceramic membrane pretreatment unit for coke elimination. These data were obtained in collaboration with the Marun Petrochemical Co. (Mahshahr, Iran). Established in 1995, the company operates one of the largest olefin plants in the world, with an annual production capacity of 11 MMT polyethylene and a total production site of over 100 ha (140 soccer fields).

Salehi *et al.* assessed the financial viability of the project based upon the following parameters: projected flow diagram, the total estimated investment, the economic potential and payback time and the saving and profitability. For the design, they considered both 7- and 19-channel modules, made by a local manufacturer (Iran Membrane Co.). The technical specifications of these membranes are shown in Table 5.1. Their experimental results showed that a single pass of the feed through the membranes sufficed for eliminating the coke. From this, the number of membrane units was calculated using Eq. (5.1):

$$n_{\max} = \frac{F}{Q_{\min} A} = \frac{F}{F_{\mathrm{m}}} \tag{5.1}$$

where F and F_{m} are the feed flow rate and the permeated water flow rate in m^3/h, respectively, $Q_{\min}$ is the minimum permeated water flux in $m^3/(h\ m^2)$, and A is the membrane active surface area in m^2. Accordingly, the maximum numbers of 7- and 19-channel modules were 3700 and 1850, respectively. In practice, the estimated numbers of modules were set as 2500 and 1250, also including safety limits.

Next, the housings for each type of module were considered. Typically, this choice is based again on local availability – There is no special need to design and manufacture new types of housing. In this case, 37- and 99-capacity

Table 5.1 Technical specifications of the ceramic membranes used in this study.[a,b)]

Number of channels		Single channel	7-Channel	19-Channel
Dimensions	Outer diameter (mm)	10	25	30
	Channel diameter (mm)	6	6	4
	Thickness (mm)	1.5–2		
	Length (m)	1		
	Specific area (m^2/m)	0.03	0.12	0.24
Parameters	Porosity of support (%)	>35		
	Average pore size (μm)	0.05, 0.1, 0.2, 0.5		
	Breaking strength (MPa)	>50		
	Distilled water flux (l/(m^2 h)	>500		
Material		Al_2O_3		

a) Data provided courtesy of Prof. E. Salehi, including data provided by the membrane manufacturer (Iran Membrane Co.), reproduced with permission.
b) Operating conditions: 800 °C max; pH 0–14.

Table 5.2 Configuration alternatives for the ceramic membrane modules and housings.[a)]

Configuration	7-Channel membrane	19-Channel membrane
37-Capacity housing		
Number of modules	2500	1250
Number of housings	68	34
Cost	$361 000	$197 550
99-Capacity housing		
Number of modules	2500	n/a
Number of housings	26	n/a
Cost	$321 000	n/a
91-Capacity housing		
Number of modules	n/a	1250
Number of housings	n/a	14
Cost	n/a	$172 550

a) Data provided courtesy of Prof. E. Salehi, including data provided by the membrane manufacturer (Iran Membrane Co.), reproduced with permission.
n/a = not available.

housings were available for the 7-channel modules, and 37- and 91-capacity housings for the 19-channel modules (Table 5.2). With these, a simplified process flow diagram could be made (Figure 5.8), and the costs can be calculated. The total capital investment for the ceramic membrane unit includes fixed capital expenses (CapEx) and operating expenses [13,14]. The CapEx comprises both

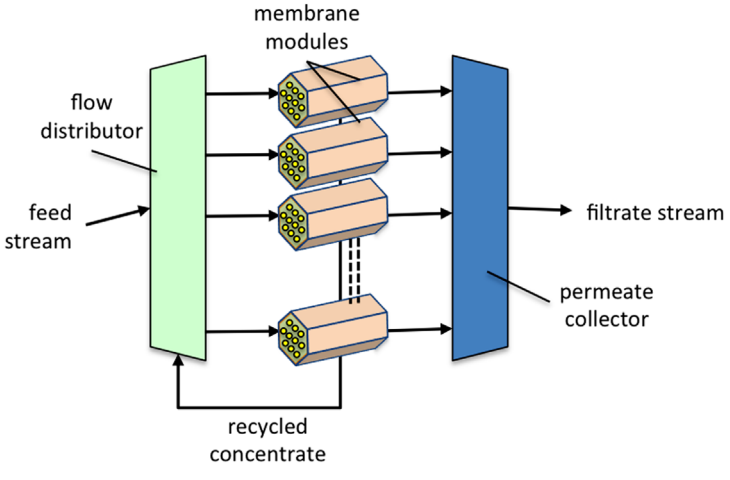


Figure 5.8 A simplified process flow diagram for the ceramic membrane unit in the Mahshahr study.

direct and indirect costs. These are calculated based on the main investment (i.e. the cost of the ceramic membrane unit given in Table 5.2). Any change in the cost of the CMU will thus directly affect the CapEx of the project. Similarly, the OpEx include labour costs, equipment maintenance and depreciation and energy consumption.

In practice, operating the CMU would also involve cleaning (backwashing), choosing the cleaning agent and method and so on. At this stage, however, these are included in the general operating costs under maintenance. A fully itemized costs list and discussion of the model used for estimating each item's costs is published elsewhere [25]. The total CapEx and OpEx for the project, based on the most economical housing configuration (19-channel ceramic membranes with 91-capacity housings), were \$445 945 and \$89 399/year, respectively.

Based on this, the authors could calculate the costs and estimate the benefits from installing and operating the CMUs (Table 5.2). The calculation was based on the company site at Mahshahr, which uses 28 filter coalescing units for its wastewater treatment. Currently (without using ceramic membranes pretreatment), the filters are replaced every 2 weeks, at a cost of \$300 per filter. This means 672 filter replacement per year, at a total cost of \$201 000. Using ceramic membranes increases the filter lifetime, giving a direct saving of 560 filter purchases per annum, or \$168 000. On top of that comes an additional profit created by the fact that clean, filtrated water is not available on-site. This filtrated water can be used to produce dilution steam water (DSW) which is then used in the thermal cracking process. The DSW helps in reducing the hydrogen partial pressure and shifting the equilibrium the ethylene side. Based on 330 operation days per year and an effluent stream of 70 ton/h (average) to 220 ton/h (max), the filtrate production capacity would be about 650 ktpa. Considering that the average price of the filtrated water is about 0.15 \$/ton, the minimum gain from using this additional clean water will be around \$97 500 per annum. Adding this to the savings in filter purchases gives \$168 000 + \$97 500 = \$265 500 of annual profit.

The payback period (PBP) is a simple parameter for assessing the utility of a project. It is simply the number of years needed for the projected profits from the business or venture to pay back the capital investment. This is calculated by dividing the CapEx by the annual profits, shown in Eq. (5.2). Substituting the data for this ceramic membrane unit gives a PBP of 2 years. Thus, all things considered, the installation of ceramic membrane units is well justified economically in this case:

$$\mathrm{PBP} = \frac{\mathrm{CapEx}}{P_{\mathrm{annual}}} \tag{5.2}$$

5.3.5
Case Study 5: Techno-Economic Analysis of CO_2 Capture from Flue Gases (France)

In the previous case study, we examined the economic feasibility of using alumina ultrafiltration membranes for removing coke particles from process wastewater

streams. This case study addresses a problem that differs from both the technical and the economical perspectives: the capture of CO_2 from flue gases. Wastewater in chemical plants is a local problem, but a CO_2 emission is a global one. In fact, CO_2 emission is arguably the most infamous environmental issue that our society faces today. Although the causal connection between CO_2 levels and global warming remains a moot point [26], the increase in anthropogenic CO_2 levels is undisputed [27,28]. If we ignore it, we may have to face the consequences.

Thanks to this public awareness, and because people are also generally loath to change their habits (i.e. stop driving), CO_2 capture, transport and long-term storage is a 'hot topic'. Of these three steps, CO_2 capture is by far the most expensive, accounting for 50–90% of the overall chain cost (and depending strongly on the emission source). In principle, capturing CO_2 coming from fossil fuel combustion can be done at various stages in the combustion chain. The most popular of these is post-combustion capture (i.e. end-of-pipe CO_2 recovery). From the engineering point of view, this is also the most challenging option, because the post-combustion effluent is dilute (containing <12% v/v CO_2), wet (3–10% v/v water) and low pressure (1–3 bar). Nevertheless, it is the most popular because it is the most compatible with retrofitting. Interestingly, this is simply an economic effect: Power plants are hugely expensive installations (a 1 GW coal-powered power plant costs about $1 billion), and complex retrofitting of one entails large investments and therefore large risks, which no one wants to take. Post-combustion CO_2 capture, although difficult, can at least be fitted literally as an 'end-of-pipe' solution.

The state-of-the-art technology for capturing CO_2 uses absorption by various ethanolamines, typically in packed towers or membrane contactors. After absorption, the CO_2 is released by heating and/or reducing the pressure above the solution and then recycling the ethanolamine solution back to the reactor. This technology, however, is very energy intensive [29]. Membrane technology is an interesting alternative, and ceramic membranes in particular are attractive for such an application, since high stability and robustness is a strong advantage here.

In 2012, Pera-Titus and co-workers published a detailed techno-economical assessment of the use of MFI-type zeolite membranes for CO_2 capture from flue gases [30]. The research was done in collaboration with the Séché Environmental group and membrane producer Pall. It covered a laboratory set-up and analysis, as well as an economical assessment of possible large-scale implementation. This case study is based on their publications and on discussions with Dr. Pera-Titus.

Zeolite membranes are interesting for flue gas separation because they can separate compounds by combining molecular sieving, selective adsorption and differences in surface diffusion rates [31,32]. Many laboratory-scale studies using zeolite membranes have been done, but there are no large-scale applications as yet. The main reason for this is the difficult manufacturing process of large-surface defect-free zeolite membranes. These require very thin supported layers that are prone to cracking. These engineering challenges, however, are likely to

be met as the demand for such membranes grows. The authors used nanocomposite MFI-type membranes that are relatively easy to synthesize [33] and show high CO_2 permeability even in the presence of water vapour.

Based on the results of the laboratory-scale tests, the authors then proposed a set-up for capturing the CO_2 emitted from post-NO_x reduction exhaust of the TREDI incineration plant operating in Rhône-Alpes (about 1900 ktpa). This gas is made up of 75 : 15 : 10 $N_2 : H_2O : CO_2$, flowing at atmospheric pressure at 150 °C. They suggested first removing the water down to 10 vol% and cooling down to 100 °C, followed by a cascade system of three MFI membrane units that would in total capture at least 85 mol% of the CO_2. Figure 5.9 shows a simplified flow sheet of the membrane cascade system, containing three sequential membrane units. The module parameters were calculated using commercial 19-channel Membralox® modules (Pall-Exekia EP1960) as supports, and coating those with an MFI zeolite layer.

We can immediately see that the scale of the proposed operation here is two orders of magnitude larger than the coke pretreatment case. To remove 85% of the CO_2 (equivalent to 146 ktpa), the three membrane units require $310\,000 + 47\,000 + 6700 = 363\,700$ modules. This means a very large capital investment in equipment (as we saw before, equipment costs account for the main part of the CapEx in membrane projects). Since MFI modules are not available as off-the-shelf products, the authors based their calculations on the cost of the Membralox modules, adding another 10% for the cost of growing the MFI layer. The main equipment cost for the membrane cascade system was estimated as $84 million. Based on this, and after adding the costs for compressors,

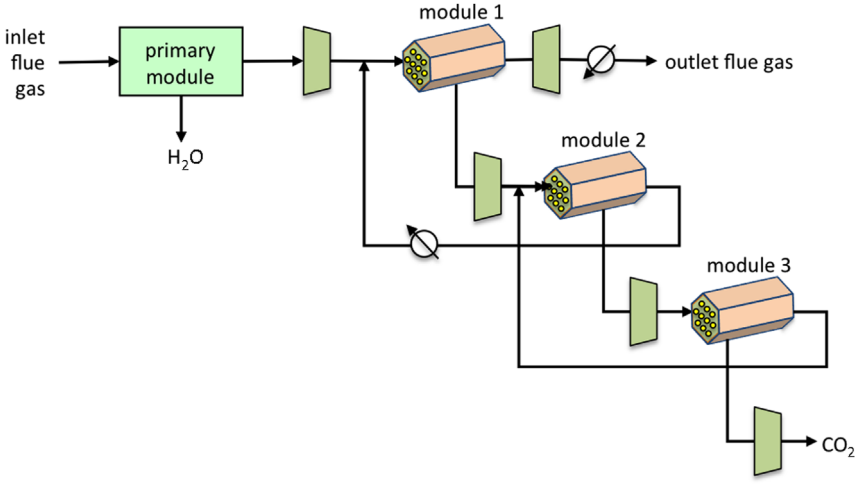


Figure 5.9 A simplified flow sheet of the proposed membrane cascade system, showing the three sequential membrane units. Parameters based on Membralox EP1960 modules (Pall-Exekia Corp.) were used for the calculations.

heat exchangers and condensers, the total CapEx including installation was estimated as $278 million.

The annual OpEx of the plant that would capture 146 ktpa CO_2 was estimated as $50 million (5-ha-based plant with an annual energy consumption of about 10 MW). Note that about 35% of these costs are due to membrane replacement (20% of the membrane surface per year) and another 7% for power consumption. These costs would translate into $330 per ton CO_2 captured. This cost is very high compared with the IPCC estimate for CO_2 removal using mature technologies such as ethanolamine absorption ($35–70 per ton CO_2 captured) or even new technologies ($150–180 per ton). But these are only estimates, and there is a paucity of actual data. Both the OpEx and the CapEx depend strongly on the price and the performance of the MFI ceramic membranes (if the production cost of the membranes would be halved, the CapEx would be reduced by 40%). Because these are not yet available as tested products, the uncertainty in the estimation is high. This high uncertainty and the paucity of data make a direct cost/benefit comparison difficult.

Interestingly, although cost-wise it would seem that the membrane solution is way too expensive in this case, social and political factors are likely to play an important role. People need power plants, and economic growth benefits from cheap and available electricity, but not at any price. Social and political pressure can be considerable here. For example, the growth economy in China relies heavily on energy from coal-fired power plants, but anyone who has spent time in the last winters in Beijing or in Shanghai can attest to the high air pollution levels – as much as 250 counts on average days (the 'healthy' limit is under 50). This is already causing economic repercussions – trained people are moving away from the polluted areas if they get an opportunity. Moreover, companies, and especially multinationals, have a harder time convincing employees with young children to accept expat positions in such places. The problem is recognized by the government, which is now setting up long-term plans for reducing pollution.

Figure 5.10 shows a PEST analysis table that lists the various factors that play a role in CO_2 capture. Because of the size of the power plants, the decisions regarding the capture of CO_2 (and pollutants) affect society on a local and national level.

5.4 Discussion

The above case studies can teach us several things. The companies and projects we examined are each in a different country, and they deal with different applications. Yet they all share several common aspects (Figure 5.11). These stem from three main factors: the market size for ceramic membrane applications, the specific demands of these applications and the detailed know-how that is required to produce good ceramic membranes. The first two factors are external,

Political factors	Economic factors	Societal factors	Technological factors
CO_2 removal high on governmental wish list, as CO_2 is perceived as a cause of climate change *Current policy has rules on removing pollution and reducing waste* *Long-term policy should be that of preventing waste at the source, which means using renewable energy (e.g. solar power) that does not emit any CO_2*	*The costs of large-scale membrane units are estimates only, as these products are at the initial point of their manufacturing cycle* *Since separation using membranes is a physical process (unlike using ethanolamines) as long as the mebranes are robust enough, the economic returns on the process should be high*	*People are more likely to approve a less-polluting power plant close to their homes, although some options,such as nuclear power plants, suffer form a problematic public image*	*The zeolite MFI membranes are not yet industrial products. This means that risky steps are needed to make them, with unknown technical challenges* *There is no large-scale set-up yet, so quantifying the benefits is difficult* *This early stage also has technological opportunities, for example changing the support from alumina to mullite, $(Al_2O_3)_3(SiO_2)_2$ can reduce unit costs*

Figure 5.10 PEST analysis table outlining the case of CO_2 capture from power plants.

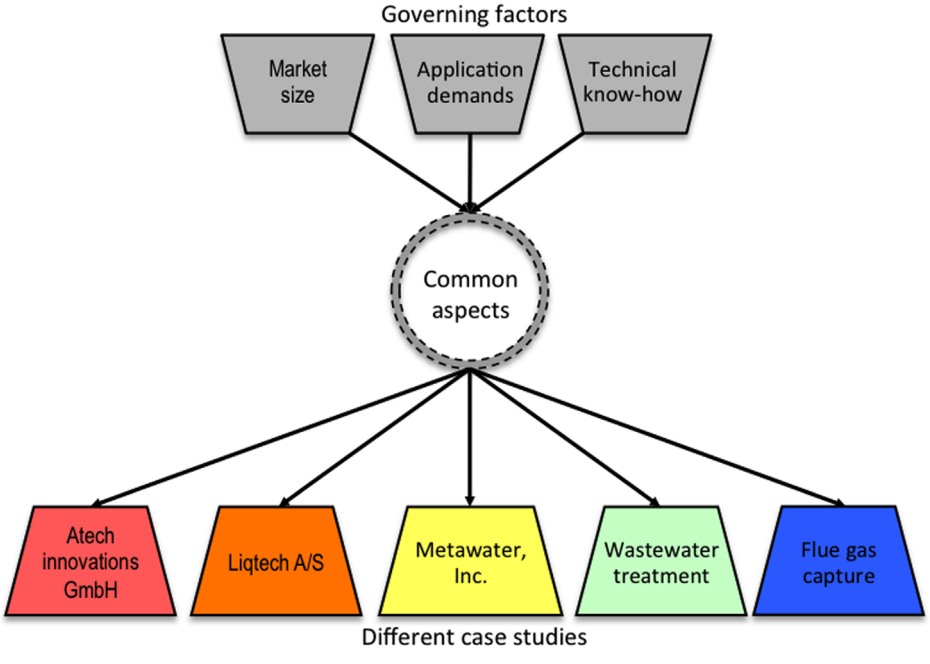


Figure 5.11 The five case studies presented above share aspects arising from three common governing factors: market size, specific application demands and detailed technical know-how.

and belong to the 'opportunities/threats' section of the SWOT analysis. The third factor is internal, forming part of the 'strengths/weaknesses' side. Here, we will explain the influence of these three factors on the ceramic membrane market.

5.4.1 Market Size and the Adversity to Change

First and foremost, we see that the demand for ceramic membranes is small compared to polymer ones. This is not surprising – polymer membranes are already long established in the market. They are cheaper and perform reasonably well in most applications. In addition, in most cases, regardless of the final application, the membrane unit itself is hidden from the eyes of the user. It is a 'black box', often performing a function that addresses a sideline concern of the business unit. Therefore, as long as polymeric membranes do what they are supposed to do, users have no interest in replacing them or switching to other technical solutions. In many cases, even if studies show that a business unit could save substantial amounts of money by switching to another technical solution (in our case, by switching from polymer membranes to ceramic ones), the impetus for doing this is low. This is because such switching involves two things that company managers dislike: *capital investment* and *risk*. Keeping to a known technology may not be the best economic solution in the long term, but switching is *always* costly in the short term. The manager can easily chalk up a SWOT analysis and explain to anyone proposing new technologies how the threats outweigh the opportunities.

This adversity for change is boosted by something that has nothing to do with the hard numbers of the economics *per se*, but rather with an interesting aspect of corporate culture. To put it simply, the membrane separation unit and process is often only a sideline activity of a company. True, in some cases (e.g. for a company that sells water purification systems), the membrane unit stands at the heart of the technology. But very often the separation and cleaning unit is considered only as a 'necessary evil' that is imposed on the company by outside regulators. For long-established companies, it could be that these waste cleaning units were only recently introduced, because before that there was not so much control over what waste the company threw away as part of its process wastewater. The company acknowledges that these units are essential (because without them the company will not get approval for its production process) but they do not produce anything – they only cost money. In such cases, the resources allocated to the wastewater-treating teams are usually lower, and even the people managing these teams have less say in policy and budgetary meetings, because they are not considered as 'part of a revenue-generating business unit'.

Another factor that comes into play in many real-life company situations is the business relationship with current suppliers. Switching to ceramic membranes often means changing suppliers. If a company and its managers have a long-

term business relationship with a certain supplier, changing can be difficult. This is especially true if the membrane unit operations that the company now uses are not seen as a 'core business' (see above) but are still supplied by the same supplier that supplies also the core business units.

These factors are difficult to quantify in an economic analysis. They are best filed under 'goodwill' or 'personal feelings', and rarely appear in the business units' reports. Yet they carry much weight in practice. After years of discussions with chemical companies, we can say that these qualitative factors account for a sizeable fraction of business decisions.

5.4.2 Specific Product Demands Dictated by Application

The small market segment taken by ceramic membranes is made more complex by the fact that market demand is focused on specific applications. These, in turn, depend on specific material capabilities. Ceramic membranes offer unique advantages, especially robustness at high temperatures and under extreme conditions (organic solvents, pH, high/low pressures). These advantages, however, differ with type of membrane produced. Therefore, we see that some companies offer solutions for water treatment, while others offer solutions for wastewater or water/oil suspensions. The focus on different niches in the market stems from each company's technological expertise, and it is also closely linked to the type of membranes each company produces. Alumina membranes are suitable for some applications; SiC membranes are suitable for others; zeolite or cerianite membranes are suitable for yet other applications. This certainly applies to the smaller producers covered in our case studies (we also contacted bigger producers of ceramic membranes, namely Pall and Tami, but Pall did not respond at all to our enquiries, and Tami declined to participate on grounds of confidentiality). Each company, of course, highlights the advantages of their type of membranes for these specific applications. And because the applications demand differ, all the claims can be simultaneously correct.

This one-to-one relationship between type of membrane and market niche is both a curse and a blessing from the economic point of view. On one hand, the fact that solutions are provided on a case-by-case basis hinders the development of standardized modules. The equipment and membrane units used for separating fats and proteins from milk are not the same as those used for separating the pulp out of fresh-squeezed orange juice. If standard modules could be made available off-the-shelf, manufacturing costs would go down, because more modules would be produced. Membrane-producing companies would feel safer producing more and keeping larger numbers in stock, because the standard solution and set-ups would mean that they would sell this stock sooner or later. Automated production, which is always a sore point for small markets (because it requires a large capital investment), would then be easier to justify. Moreover, standardization of off-the-shelf solution would lower the risk of switching to ceramic membranes for larger companies. These typically run larger scale

applications, and need more assurance that modules for their membrane set-ups will be available. Standard modules built to specification would mean that even if one supplier would go bust, another could easily take its place.

On the other hand, the fact that the market is based on a tailored solution for each problem gives companies the chance to specialize and secure and keep a market niche for long term. This is especially true for SMEs that can then focus on product and service quality, thereby gleaning more profit from individual client projects. If ceramic membranes were to be completely standardized, the larger players (and probably web-outsourcing platforms such as *Alibaba*) would dominate the field.

5.4.3 Detailed Technical Know-How

The third factor is not related to market demands, but rather to the intricate process of producing the membranes themselves. On the face of it, making ceramic membranes seems easy – you choose a precursor, make a slurry, form an intermediate 'green body' and then dry and calcine it, obtaining the final product. In reality, the process is anything but simple. As we learned in Chapters 2 and 3, small changes in preparation parameters have diverse effects on the porosity, mechanical strength and overall performance of the final membrane. In fact, the production process of ceramic membranes is so sensitive to changes that any 'cutting of corners', any stepping away from the recipe or slackness in quality control will often result in a vastly inferior product. Tellingly, the people at both Atech Innovations and LiqTech name the adherence to the recipe and attention to details in quality control as their main advantages over current cheaper competitors India and especially China (but this situation is changing as production and quality control standards are improving there as well). The development of an optimized recipe is very time-consuming and knowledge intensive. Each company has a limited number of such recipes (sometimes only one or two) and sticks to these. Developing and refining in-house expertise for a few processes is good, but it also means that companies face a larger barrier when they wish to enter new market segments. Such processes also require highly trained staff, and this in turn increases production cost because of higher salaries. However, it seems to us that there is no way of avoiding these costs if you want to make high-quality membranes, at least not until automation and standardization reform (and enlarge) the market.

This focus on a small number of recipes is further complicated by the fact that the recipes themselves are most often kept as 'trade secrets' rather than patents. Obtaining a patent for a specific membrane production recipe is difficult, because the actual changes that make all the difference in the optimized recipe are actually minor, and could easily be considered by a patent examiner as 'within the capability of a person skilled in the art'. Moreover, even if a company obtains a patent, it only receives the right to sue another company for infringing that patent – and proving that someone has copied your recipe is very difficult if

not impossible. Patents can be useful in cases where a clear distinction can be made on the product and/or on the technology. For example, if a company finds that using star-shaped modules improves performance considerably compared to the conventional cylinders, it would be easy to check whether competitors changed the shapes of their modules. But in most cases, membrane-producing companies simply prefer keeping their recipes secret, even if it means that competitors can try and copy them.

5.5 Outlook

What will the future bring for ceramic membranes? Will they remain as niche products or will they grow and eventually take over from polymeric membranes? And how will the recent and foreseen global changes affect the ceramic membranes market? In this section, we will try and answer these questions based on the case studies and general indicators discussed above.

5.5.1 Persistent Market Entry Barriers

From the discussions with the companies, it looks like the barriers for market entry for ceramic membranes are still too high for them to compete in traditional applications with polymeric membranes. Cost-cutting by clients, plus the fact that polymeric membranes are perfectly good for some applications, means that there is little incentive for today's clients to switch. The companies making ceramic membranes are well aware of this. However, the fact that the membrane unit is often seen as a 'black box' performing a specific function is also an advantage for the newcomers once a client decides to try out the new technology. This is because replacing one black box with another is simpler and less taxing than changing a key part of the production process. The flip side of this coin is that customer loyalty becomes lower – if a competitor offers a better-performing product in the future, the client may switch.

5.5.2 Global Changes and New Opportunities

At the moment, it looks like ceramic membranes will remain a niche market. However, this may change if new regulations and/or new technology will come forward where their advantages are really important, for example where extreme working conditions (high temperature, solvents, pH, biofilms) are needed. Two large-scale opportunities for ceramic membranes in the coming decade are water purification (providing drinking water via decontamination and desalination) and air purification (especially scrubbing out nanosized particulates). Let us examine these two cases more closely.

Providing people with drinking water is something most of us take for granted as one of the government's tasks. With the exception of people living in arid areas, most of us don't think twice about it. Water comes from the tap. But clean water is becoming a concern in many places as population grows and, more importantly, countries become more industrialized. Happily, there is no shortage of water – 70% of the Earth is literally covered with it. Desalination of sea water and recycling of wastewater for agricultural and household use will probably become a major application area for ceramic membranes in the coming decade, as already perceived by companies like Metawater and Tami. Looking at the world market shares, there are two major markets: in the United States and in China. The former is well developed, with polymeric (and some ceramic) membrane applications. The latter is rather closed, and interesting because decisions are typically made centrally and acted upon quickly. However, considering the growing number of China-based ceramic membrane manufacturers, plus the understandable preference of the government for promoting local firms, it is likely that once regulations are set in place, the bulk of the technology will be produced locally. Still, the size of the Chinese market would mean that if a company makes ceramic membranes for water purification applications successfully there, it would advance standardization and automation, with the associated implications (see above).

The issue of air pollution, especially smog and its varieties, has been on-and-off the news and the public agenda in the last decades. More often than not, companies see air pollution as something that (with a little help from the wind) can easily become somebody else's problem. Los Angeles and Mexico City are (in)famous for their smog and haze. But anyone who has been to Beijing, Shanghai, Guangzo or Delhi recently will immediately tell you that air pollution, and especially particulate emissions, cannot be ignored any longer. The problem is especially acute in northern China, because coal-fired power stations are used for heating, and there is often no alternative.

Ceramic membranes can be effective filters for such particulates. These would apply to diesel-type engines as well as to heavy-oil ones, cleaning out their emissions. They would also apply to power stations, where the advantages of robustness and stability at high temperatures could tilt the table in favour of ceramic membranes. The filters would clog up, of course, but they can be regenerated in various ways, and there are several companies who are in the soot-filter and particulate-filter regenerating business. There are also new technologies for soot-filter regeneration. To give one example, as we showed a few years ago [34,35], the regeneration of ceramic diesel soot filters can be done efficiently by coating the filter with a specific perovskite layer that functions as a microwave-sensitive soot oxidation catalyst (see Figure 5.12). Then, by using induction microwave, one can heat the coating layer specifically, creating a 'hot catalyst' on a relatively 'cold' ceramic support, and thus burning away the soot particles efficiently.

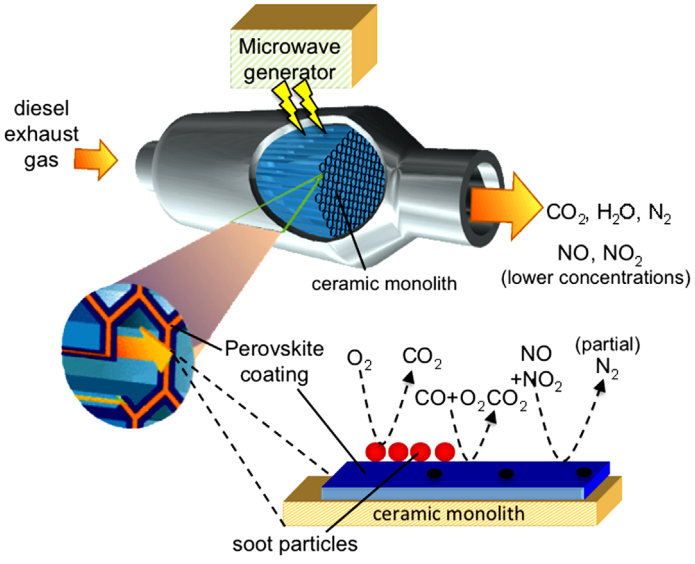


Figure 5.12 Schematic representation of a ceramic diesel soot filter that is coated by a specific perovskite oxide layer that is both sensitive to induction microwave and catalytically active in the selective oxidation of soot particles to CO_2.

Although the principle is sound, the practical application of such a multilayer system is a good example of the complexity of multiparameter optimization: Besides having the appropriate ceramic monolith structure of the filter itself, the perovskite coating must fulfil at least four conditions. Three of these are chemical: It must be highly susceptible to microwave induction, it must be insensitive to sulfur poisoning and it should provide a clean catalytic burning profile of the soot to CO_2, rather than CO. The fourth constraint is economical: The coating (and indeed the overall soot filter) must be cheap enough for implementing in regular diesel and heavy-oil engines. This economical constraint has an interesting political twist, as the price of many perovskites, which contain rare earth cations such as gadolinium, samarium and neodymium, is controlled by the Chinese government [36] (practically all of the world's supply of rare earths today comes from China). Politics aside, however, the concept works.

Yet politics, or at least government policy, is crucial in this case. The technology is there – but the regulations are not. Getting rid of air pollution is everybody's problem, in practice everyone treats it as somebody else's problem, and therefore changes will be made only when government regulations change. Ultimately, the economic drivers against pollution are the same ones that drive company profit – convincing high-quality workers and managers to move to polluted cities is getting more and more difficult. In more than one way, this example reflects the factors that will decide when and how large the market for ceramic membranes will become.

Exercises

5.1. Steel production is a huge industrial sector, employing more than two million people worldwide. While steel can be easily recycled (over 97% of the steel is recycled; the steel for the spoon you used at dinner could have well been made 150 years ago) mankind needs ever more of it. In 2014 our world produced a staggering 1.7 billion tons of steel. A typical steel mill uses thousands of cubic metres of water as coolant, most of which circulates in the plant and never leaves. However, about 10% of this water has to be replaced every hour, which tallies up to a sizeable amount. The water is cleaned using different methods, including flocculation, sedimentation and filtration.

You are in charge of a water-cleaning unit in a local steel mill, which has 1500 m^3 water circulating as coolant, and of which 10% must be refreshed and disposed of every hour. Up to now, this cleaning has been done in flocculation basins. However, new regulations have come in, and you must now also remove organic/inorganic particulate contaminants that are roughly 100 nm in size. Your assignment is to evaluate the economic feasibility of using ceramic membranes for this purpose, given the following assumptions:

- At this stage, management only needs a rough figure for the CapEx to get an idea of how much they will need to invest in the new unit. You can ignore the costs related to installation, permits and the operating expenses for maintenance, backwashing and cleaning of the membrane units.
- Your laboratory experiments show that a single pass of the wastewater through the membrane is sufficient for reducing the particulates in the effluent to acceptable levels.
- Both 7- and 19-channel alumina membrane modules are available commercially, with the technical specifications given in Table 5.1. The cost of these modules is $170 and $300 each, respectively.

a) Draw a schematic set-up for the cleaning using ceramic membrane units and calculate how many modules you would need of each type to purify the leftover coolant water.

b) Consider the alternative cleaning method using flocculation and filtration. The cost of flocculation with aluminium sulfate (alum) is 3.2 cents/m^3, and with ferric chloride it is 2.8 cents/m^3 of treated wastewater. The filtration cost is 12.4 cents/m^3 of treated wastewater. What are the pros and cons of both methods? Which method is more economical? Explain your answer.

5.2. (*Intended for a group of students*) Air pollution from particulate matter is one of the big problems associated with coal-fired power plants. Current brown coal plants emit about 3200 g particulates/GJ (mostly fly ash), while oil and gas power plants emit only 16 and <1 g/GJ, respectively [37].

Consider a situation in the near future, where the Chinese government, for example, announces that all new coal-fired power stations in China must be equipped with filters that can scrub out particulate matter down to below 20 g/GJ.

a) Using the data for the modules given in Table 5.1, and considering that a typical coal-fired power station generates about 400 m^3 of flue gas per GJ, estimate the number of 19-channel modules needed for scrubbing out the particulate matter from the effluents from a 500-MW power station. Assume first that a single pass through the module is sufficient. Then, try and estimate the effects of recycling streams and the need for periodic cleaning of the membrane units.
b) Search on the Internet and estimate the current market size for ceramic membranes compared to polymer membranes. Assuming that only ceramic membranes can be used for the power station application above, how many of these power stations would be needed before the market demand for CMs worldwide would double?
c) Compile a PEST analysis table for the case of scrubbing out particulates from power station flue gases. Assume that the capital investment in the system depreciates over 10 years. If each 19-channel module costs $300, and all other factors are equal, what would be the increase in the price of energy (in $/J) you would need to repay the investment in the equipment within 10 years? Within 20 years?

References

1 Reich, R. (2013) Philanthropy and caring for the needs of strangers. *Social Research: An International Quarterly*, **80**, 517–538.
2 Mackay, D.J.C. (2009) *Sustainable Energy: Without the Hot Air*, UIT Cambridge, Cambridge.
3 Tyrell, J.A. (2014) *Fundamentals of Industrial Chemistry*, John Wiley & Sons, Inc., Hoboken.
4 Yan, B., Lu, W. and Cheng, Y. (2012) China goes green: cleaner production of chemicals. *Green Processing and Synthesis*, **1**, 33–47.
5 Zhang, J., Liu, N., Li, W. and Dai, B. (2011) Progress on cleaner production of vinyl chloride monomers over non-mercury catalysts. *Frontiers of Chemical Science and Engineering*, **5**, 514–520.
6 Hayashi, A.M. (2001) When to trust your gut. *Harvard Business Review*, **79**, 59–65.
7 Eisenhardt, K.M. (1989) Making fast decisions in high-velocity environments. *The Academy of Management Journal*, **32**, 543–576.
8 Kahneman, D. (2013) *Thinking, Fast and Slow*, Farrar, Straus and Giroux, New York, 512 pp.
9 Kihlstrom, J.F. (1987) The cognitive unconscious. *Science*, **237**, 1445–1452.
10 Kitts, B., Edvinsson, L. and Beding, T. (2001) Intellectual capital: from intangible assets to fitness landscapes. *Expert Systems with Applications*, **20** (1), 35–50.
11 Lankey, R.L. and Anastas, P.T. (2002) Life-cycle approaches for assessing green chemistry technologies. *Industrial & Engineering Chemistry Research*, **41** (18), 4498–4502.
12 McDonough, W., Braungart, M., Anastas, P.T. and Zimmerman, J.B. (2003) Applying the principle of green engineering to cradle-to-cradle design. *Environmental*

Science & Technology, **37** (23), 434A–441A.
13 Saiz, S., Kennedy, C., Bass, B. and Pressnail, K. (2006) Comparative life cycle assessment of standard and green roofs. *Environmental Science & Technology*, **40** (13), 4312–4316.
14 Bayer, P. and Finkel, M. (2006) Life cycle assessment of active and passive groundwater remediation technologies. *Journal of Contaminant Hydrology*, **83** (3–4), 171–199.
15 Rothenberg, G. (2008) *Catalysis: Concepts and Green Applications*, Wiley-VCH Verlag GmbH, Weinheim.
16 Tukker, A. (2002) Life-cycle assessment and the precautionary principle. *Environmental Science & Technology*, **36** (3), 70A–75A.
17 The Economist (2014) Schumpeter: German lessons.
18 Girotra, K. and Netessine, S. (2013) Extreme focus and the success of Germany's mittelstand 2013. Available at http://blogs.hbr.org/2013/02/good-old-focused-strategy/ (updated 7-10-2014).
19 Strassberger, Z., Tanase, S. and Rothenberg, G. (2014) The pros and cons of lignin valorisation in an integrated biorefinery. *RSC Advances*, **4**, 25310–25318.
20 Kiss, A.A., Dimian, A.C. and Rothenberg, G. (2006) Solid acid catalysts for biodiesel production: towards sustainable energy. *Advanced Synthesis & Catalysis*, **348**, 75–81.
21 Bernardo, P., Criscuoli, A., Clarizia, G., Barbieri, G., Drioli, E., Fleres, G. *et al.* (2004) Applications of membrane unit operations in ethylene process. *Clean Technologies and Environmental Policy*, **6** (2), 78–95.
22 Cai, H., Krzywicki, A. and Oballa, M.C. (2002) Coke formation in steam crackers for ethylene production. *Chemical Engineering and Processing: Process Intensification*, **41** (3), 199–214.
23 Cheryan, M. and Rajagopalan, N. (1998) Membrane processing of oily streams: wastewater treatment and waste reduction. *Journal of Membrane Science*, **151** (1), 13–28.
24 Strathmann, H. (1976) Membrane separation processes in advanced wastewater treatment. *Pure and Applied Chemistry*, **46**, 213–220.
25 Salehi, E., Madaeni, S.S., Shamsabadi, A.A. and Laki, S. (2014) Applicability of ceramic membrane filters in pretreatment of coke-contaminated petrochemical wastewater: economic feasibility study. *Ceramics International*, **40** (3), 4805–4810.
26 Lomborg, B. (2001) *The Skeptical Environmentalist: Measuring the Real State of the World*, Cambridge University Press, Cambridge.
27 Neftel, A., Moor, E., Oeschger, H. and Stauffer, B. (1985) Evidence from polar ice cores for the increase in atmospheric CO_2 in the past two centuries. *Nature*, **315** (6014), 45–47.
28 Keeling, C.D., Bacastow, R.B., Bainbridge, A.E., Ekdahl, C.A., Guenther, P.R., Waterman, L.S. *et al.* (1976) Atmospheric carbon dioxide variations at Mauna Loa Observatory, *Hawaii. Tellus*, **28** (6), 538–551.
29 Aaron, D. and Tsouris, C. (2005) Separation of CO_2 from flue gas: a review. *Separation Science and Technology*, **40** (1–3), 321–348.
30 Sublet, J., Pera-Titus, M., Guilhaume, N., Farrusseng, D., Schrive, L., Chanaud, P. *et al.* (2012) Technico-economical assessment of MFI-type zeolite membranes for CO_2 capture from postcombustion flue gases. *AIChE Journal*, **58**, 3183–3194.
31 Coronas, J. and Santamaria, J. (1999) Separations using zeolite membranes. *Separation and Purification Methods*, **28**, 127–177.
32 Caro, J. and Noack, M. (2008) Zeolite membranes: recent developments and progress. *Microporous and Mesoporous Materials*, **115**, 215–233.
33 Miachon, S., Landrivon, E., Aouine, M., Sun, Y., Kumakiri, I., Li, Y. *et al.* (2006) Nanocomposite MFI-alumina membranes via pore-plugging synthesis: preparation and morphological characterisation. *Journal of Membrane Science*, **281**, 228–238.

34 Beckers, J., van der Zande, L.M. and Rothenberg, G. (2006) Clean diesel power via microwave susceptible oxidation catalysts. *ChemPhysChem*, **7**, 747–755.
35 van der Zande, L.M., Zhang-Steenwinkel, Y., Rothenberg, G. and Bliek, A. (2004) Microwave regeneration of diesel soot filters. *NATO Science Series II: Mathematics, Physics and Chemistry*, **173**, 247–251.
36 Ma, D. (2012) China digs it. Foreign Affairs. Available at http://www.foreignaffairs.com/print/134853 (accessed 1-3-2015).
37 EEA (2008) Air Pollution from Electricity-Generating Large Combustion Plants. European Environment Agency, Copenhagen.

Index

a

absorption, 2, 59, 70, 183, 186, 188, 219, 303, 374, 376
activation energy, 61, 102, 103, 107, 133, 242
adsorption, 2, 31, 72, 73, 122, 128, 129, 131, 135, 160, 170, 201, 221, 232, 234, 250, 261, 281, 319, 324, 330
advanced oxidation process (AOP), 275
air gap membrane distillation (AGMD), 276, 277, 279
alumina, (Al_2O_3), 16, 26, 27, 34, 51, 53, 57, 66, 155, 204, 218, 236
aluminium, 26, 27
aluminophosphates (AlPO), 70
anaerobic MBRs (anMBRs), 287
atmospheric pressure chemical vapour deposition (APCVD), 58, 62, 64
atomic force microscopy (AFM), 150, 178–181
attenuated total reflection Fourier transform infrared spectroscopy (ATR-FTIR), 187

b

Bacillus cereus, 268
backscattered radiation, 182–185
barium cerate ($BaCeO_3$), 237
barium perovskite oxides, 243
barium zirconate, 243
bending test, 192, 195
bend stress, 195
best management practices (BMPs), 267
bilge water, 296
biological oxygen demand (BOD), 286, 290, 291
bovine serum albumin (BSA), 304
brackish water, 267, 278, 279
Brownian motion, 103
Brunauer–Emmett–Teller (BET) method, 160
bubble point test, 156, 157

c

calcination, 189, 257, 363
calcium oxide, 2
Campylobacter jejuni, 268, 304
capillary condensation, 91, 125, 131–133, 138
capital expenses (CapEx), 217, 367, 372
Carman–Kozeny equation, 116, 154
Carnot cycle, 239
caseins, 301, 302
catalytic membrane reactor (CMR), 250, 254–259
catalytic membranes, 256, 258
cathode reactions, in acidic environment, 239
$CaTiO_3$ crystal structure, 237
caustic agents, 21
cellulose acetate (CA), 10
centreless grinding, 54
CeramiCell®, 237
ceramic filters, 2, 3, 266, 271–274, 319
ceramic fuel cells, 246
ceramic MBRs. *see* ceramic membranes reactors
ceramic membranes
– advantages, 22, 23, 25
– intermediate/top layers, 54–58
– limitations, 25
– reactors 250
– Robeson diagram, 24
– tailor-made, 23
– technical specifications of, 371
– *vs.* polymer membranes, 22–25
ceramics
– layman's definition, 2
– slurry content, 39
Chapman–Enskog theory, 100
chemical contaminants, 275
chemical oxygen demand (COD), 286, 290, 291
chemical vapour deposition (CVD), 1, 28, 55–66, 70, 236, 261

Ceramic Membranes: New Opportunities and Practical Applications, First Edition. Vitaly Gitis and Gadi Rothenberg.
© 2016 Wiley-VCH Verlag GmbH & Co. KGaA. Published 2016 by Wiley-VCH Verlag GmbH & Co. KGaA.

chemical vapour infiltration (CVI), 261
chemisorption, 65, 111, 279
citric acid, 21
cleaning, 20–22
cleaning-in-place (CIP), 22, 23, 313
cleaning-out-of-place (COP), 22
coarsening, 48
colloids, 66
compact tension method, 195
composite membranes, 260
compressive strain, 192
concentration polarization model, 118–120
confocal microscopy, 173
confocal Raman spectroscopy, 189
confocal scanning laser microscopy (CSLM), 150, 173
contact angles, 150, 157, 158, 160, 162, 196, 197
continuous stirred-tank reactors (CSTRs), 250, 251
convection, 95
convective mass transfer, 91, 111–113
conventional activated sludge (CAS), 290
counter-diffusion, geometry, 65
Cr_2O_3/Al_2O_3 catalyst, 253
cross-flow microfiltration (CFMF) technology, 322
cryogenic distillation, 221
Cryptosporidium parvum, 168, 266
crystallization, 2, 31, 70, 71, 73
CsNaX zeolite catalyst, 263
CSR Qingdao Sifang Company (CSR Sifang), 244
cubic boron nitride (CBN), 54

d

Dalton's law, 93
Darcy equation, 116, 191
DD3R zeolite membrane, 253
Debye length, 201
deflocculants, 36
deformations, 193, 194
dehydration, 34, 252, 253, 280–282, 284–286, 298
Della Toffola membranes, for wine clarification, 325
dense electrolyte membranes, 246
dense membranes, 11, 193
deprotonation, 199
dextrans, 171
diatomic earth (DE), 314
dibutyl-*o*-phthalates, 38
dielectric permittivity, 198
differential scanning calorimeter (DSC), 163
diffusion, 8, 46, 48, 61, 65, 95, 98, 101, 103, 115, 124, 221, 261
– Ashby, 47
– coefficients, 99, 102
– in gases, 91, 99–103
– lattice, 47
– in liquids, 103–105
– mass fluxes, 95, 96
– rate, 44
– in solids, 105–107
– solution-diffusion theory, 234
– turbulent, 95
– velocity, 95
dilution steam water (DSW), 373
dip coating, 56
dipole–electric dipole, 189
direct contact membrane distillation (DCMD), 276
dispersed oil, 293
dissolved oxygen (DO), 316
distillation, 2, 23, 221, 250, 275, 276. *see also* membrane distillation (MD)
Donnan potential, 200
drilling, 292
drinking water treatment plants (DWTPs), 368, 369
dry gel conversion method, 72
dry membrane, 157, 161, 178
dynamic viscosity, 103, 114, 116, 117, 154, 198

e

economic considerations, in manufacturing/applications, 355
– Atech Innovations GmbH (Germany), 362–365
– LiqTech A/S (Denmark), 365–368
– Metawater Co. (Japan), 368–370
– petrochemical wastewater, pretreatment of, 370–373
– Techno-Economic Analysis of CO_2 capture from flue gases (France), 373–376
elastic deformation, 194
electrical double layer (EDL), 198
electrochemical impedance spectroscopy (EIS), 199
electron energy loss spectroscopy (EELS), 182
electronic conductivity, 139, 140, 237, 249
electroosmotic flow, 198
electrostatic repulsion, 67, 201
elongation tests, 194
endocrine disruptive compounds (EDCs), 274
energy demand, 2

energy-dispersive X-ray spectroscopy (EDS/EDX), 150
see activation energy, 102
Enterococcus faecalis, 268
EPA regulations, 294
Escherichia coli, 268
ethanol, 281, 282
ethylbenzene, 281
ethyl-2-cyano-3-phenylacrylate, 263
ethylenediamine, 72
ethylenediamine tetra acetic acid (EDTA), 22
ethylene glycol, 72
4-ethylguaiacol, 326
4-ethylphenol, 326

f

fast Fourier Transform (FFT), 181
feasibility, 152, 371, 373, 384
feed spacer, 16
fermentation, 282, 284, 300, 315–318, 321–324
Fickian diffusion, 128
Fick's law, 96–99, 110
filtration, 71, 91, 168, 198
Fischer–Tropsch process, 256, 264
flat-sheet technology, 289
flue gases, 227, 357, 373
fluoroalkylsilanes, 279
fluorodecyltriethoxysilane, 279
fluxes, 115, 117, 118, 124–125
– through non-porous membranes, 138–142
fossil fuels, 3
fouling, 18–20, 21, 123, 181, 187
Fourier transform infrared spectroscopy (FTIR), 150, 187
Fourier transform Raman spectroscopy (FT-Raman), 188, 189
free energy, 156
friction coefficient, 103
fuel cells, 3, 55, 239–245

g

gas adsorption–desorption, 150, 160, 161
gas–liquid permporometry, 150, 161, 162
gas permeability, 136
– test, 154, 155
gas separation, 3, 10, 14, 221–232
gel formation, 19
German company Fraunhofer IKTS, 282
Gibbs–Thomson equation, 163
grain size, 51
green body, 34, 36
green cast, 36
grinding, 53, 54
Grotthuss mechanism, 242
groundwater resources, 292

h

Hagen–Poiseuille equation, 116, 154
H_2–CO_2 membranes, 230
heat transfer, 92
Helmholtz–Smoluchowski approximation, 198
Herring's scaling law, 48
high-pressure membranes, 150
high-resolution techniques, 174
hold-up volume, 17
homogenization, 298
honeycomb configuration, 17
hopping model, 130
hybrid membranes, 68
hydraulic residence time, 170
hydrodynamic hindrance, 104
hydrodynamic model, 103, 130
hydrogen, 3, 155–156, 232–239
hydrolysis, 21, 58, 64, 67
hydrophilicity, 70, 150, 156, 157, 196, 197, 253
hydrophobicity, 20, 157, 196, 197, 279, 284
hydrothermal treatment, 55
hydroxyethyl cellulose, 45
hysteresis, 161

i

ideal gas equation, 93
ideal initial slurry, 173
impedance spectroscopy, 198
inert membrane reactor (IMR), 250, 254, 261
infrared spectroscopy, 186
inherently catalytic membranes, 258
inside-out mode, 17
integrity tests, 170
intellectual property rights (IPR), 358
interfacial tension, 196
internal grinding, 54
'inverse spectroscopy' instruments, 186
ion-transfer mechanism, 139
iso-propyl propanoate, 253
isothermal membrane distillation, 278
isothermal-stage sintering, 51
isotropic, 12
– membrane, 1, 3
isovaleric acid, 325, 326

j

jet fuel, 370
juice–pulp suspension, 95

k

Keeling curve, 225
Kerasep® membrane module, 17
Kieselguhr (DE) filtration, 314, 322, 326
Kirkendall effect, 107
Knoevenagel condensation, 263
Knudsen diffusion, 91, 101, 125–127, 132, 137, 154, 231, 236, 261
Knudsen number, 101
Knudsen transport mechanism, 258
Kozeny theory, 117
Kröger–Vink notation, 242

l

lactose, 303
lanthanum strontium magnesium gallate (LSGM), 246
lapping, 53
Lennard-Jones potential, 100
life cycle assessment (LCA), 358, 360–362
linearity, 152
liquid–liquid displacement (LLD), 150, 158
liquid pre-cheese concentration (LPC), 302
liquid separation/purification, 265–297
– fermented food industry, 314, 315–326
– in food applications, 297–308, 310, 314
liquid–vapour interfaces, 132
lithium aluminosilicates, 272
lithium dodecylsulfates, 171
log removal values (LRVs), 268

m

macropores, 11
magnesium oxide (MgO), 38
malt, 315, 317
market size, 376–383
mass-average velocity, 94, 95
mass balance equation, 107, 119
mass diffusivity, 99, 113
mass flux, 94, 95
mass fraction, 92, 93
mass transfer, 91, 92
Maxwell's equilibrium formulae, 100
mechanical strength tests, 192–195
MEDAL commercial polymeric membrane module, 234
Membralox® GP membranes, 17, 121
membrane–air interface, 44
membranes
– morphology of, 11–15, 49, 259
– reactors, 250, 251, 264, 265
– separation (*see* membrane separation, basics of)
– thickness (*see* thickness)
membrane distillation (MD), 276
membrane electrode assembly (MEA), 240
membrane separation, basics of, 4–10, 94
mercury intrusion porosimetry (MIP), 159
mercury porosimetry, 150, 159, 160
mesopores, 11, 137, 152, 162, 165
metal alkoxide, 66
metal-organic frameworks (MOFs), 227
metal oxides, 197
methanol/methyl t-butyl ether (MTBE), 281
methyl cellulose, 45
MEUF. *see* micellar-enhanced ultrafiltration (MEUF)
MF. *see* microfiltration (MF)
micellar-enhanced ultrafiltration (MEUF), 295
micelles, 22, 295, 299, 301
Michelson interferometer, 186
microcracks, 51
microfiltration (MF), 9, 10, 150, 305
micropores, 11, 28, 130, 131, 133, 152, 219, 236, 261
micro-Raman spectrometer, 188
microreactors, 263
microscopy methods, 150, 172
mixed ionic-electronic conducting membranes (MIECs), 249
mixed liquor suspended solids (MLSS), 290
mixed matrix membranes (MMMs), 73
molecular sieving, 67, 91, 125, 133–135
molten carbonate fuel cells (MCFCs), 240, 243
monoethanolamine (MEA), 228
multistage flash distillation (MSF), 277

n

NaA/NaY zeolites, 283–285
nanofiltration (NF), 1, 9
naphtha, 370
neutralizing water-soluble contaminants, 266
Ni-based alloys, 241
Ni–Gd-doped ceria (GDC), 247
nitridation, 64
nuclear magnetic resonance (NMR), 150, 164, 165
nuclear magnetic resonance cryoporometry (NMRC), 163
nuclear reaction analysis (NRA), 181
nucleation, 72

o

offshore transportation systems, 293
Ohm's law, 101
oil–water separation, 291, 294, 296

operating expenses (OpEx), 218, 234, 286, 370
original equipment manufacturers (OEMs), 363
Ostwald ripening, 49
oxidative dehydrogenation, 251
oxygen, 249
– flux, 155
– partial pressure, 155
– permeation tests, 155
o-xylene, 281

p
PACE (Program for Accessible Health, Communication and Education), 274
packing densities, 35
palladium membranes, 235
parallel diffusion, 101, 102
parallel transport model, 134–137
partial densities, 92, 95
partial pressure, 155
particle-induced X-ray emission (PIXE), 181
particle–liquid separation, 9
passive barrier, 1
pasteurization, 298, 305, 306
– high-temperature short-time (HTST), 305
– ultrahigh-temperature (UHT), 305
– ultra-pasteurization (UP), 305
payback period (PBP), 373
PCFC membranes, 242, 243
peel strength test, 195
permeability, 136, 141, 153
– coefficients, 154
– tests, 153
pervaporation, 70, 280, 282
pharmaceuticals and personal care products (PPCPs), 274
phase separation/leaching method, 236
phenyltriethoxysilane, 257
physical parameters, membrane characterization, 150, 189, 197–201
physical vapour deposition (PVD), 55
physico-chemical parameters, 129
physisorption, 160
plasma-enhanced chemical vapour deposition (PECVD), 58
plastic deformations, 47, 194
plasticizers, 38
plate-and-frame modules, 15
plug-flow reactors (PFRs), 250, 252, 262
Poiseuille flow, 154
polarization model, 119
polishing, 53
political, economic, social and technological (PEST), 358–360
polyacrylonitrile (PAN), 10
polyamide (PA), 10
poly(butyl methacrylate) (PBMA), 38
polycrystalline diamond (PCD), 54
polydiallyldimethylammonium (PDDA) chloride, 71
polydimethylsiloxane (PDMS), 187, 221
polyelectrolytes, 198
polyethersulfone (PES), 10
polyethylene (PE), 289
polyethylene glycols (PEGs), 38, 171
polymeric MF/UF membranes, 10
polymer swelling, 188
poly(propylene carbonate) (PPC), 38
polypropylene (PP) hydrophobic polymers, 278
polysulfone (PS), 10
polytetrafluoroethylene (PTFE) hydrophobic polymers, 278
polyvinyl acetate (PVAc), 38, 45
polyvinyl alcohol, 45
polyvinyl butyral (PVB), 38
polyvinyl chloride (PVC), 356
polyvinylidene fluoride (PVDF), 10
– hydrophobic polymers, 278
pore blocking model, 123–125
pore charge, 198, 200
pore resistances, 138
pore size, 11–14, 26, 32, 38, 52, 56, 57, 73, 101, 102, 129–135, 150–159, 171, 200, 201
– diameter, 157, 236, 255, 301
– distribution, 11, 101, 150, 152, 153, 157, 158, 170, 174, 236
– length, 116, 138, 154
– shape and connectivity, 19, 149, 164, 178, 190, 191
– tests, groups of, 152
Potters for Peace (PFP), 272, 273
pouring grains, 35
powdered activated carbon (PAC) particles, 170
power spectral density (PSD), 181
pre-combustion technology, 229
pressure swing adsorption (PSA), 221
pristine membrane, 152
project appraisal, 357
protonation, 199
proton conducting fuel cells (PCFCs), 242, 243
proton conducting membranes, 236
proton exchange membrane (PEM), 240
proton exchange membrane fuel cell (PEMFC), 240–245

pugging, 39, 40
pulsed electric field (PEF), 309

r
racks, 15
Raman shifts, 189
Raman spectroscopy, 150, 188
random walk model, 130
redox-tunable membrane, 263
reduction, 63, 74, 285, 290, 306, 319, 325, 375
Renkin diffusion, 104
resistance-in-series model, 122, 123, 134, 138
reverse osmosis, 9, 23, 277, 278
Reynolds numbers, 103, 114
rheology, 37
ring diffusion mechanism, 107
roughness factor, 196
Rutherford backscattering spectrometry (RBS), 150, 185

s
Saccharomyces cerevisiae, 319
Salmonella typhimurium, 311
salt gradient, 200
scanning electron microscopy (SEM), 150, 174–176
Schmidt number, 113, 121
Scotch tape test, 195
sedimentation, 313
semipermeable active, 1
sensitivity, 168
shear stresses, 192
Shiga toxin-producing *E. coli* (STEC), 305
Si/Al ratio, 70
SiC membranes, 284, 363, 379
sieving, 55
silicalites, 70, 256
silicoaluminophosphates (SAPO), 70
silicon alkoxide, 67
silicon carbide (SiC), 271, 291, 363
silver catalyst nanoparticles, 257
sintering, 12, 46, 47, 50, 51, 189, 190, 195
skids, 15
slipcasting, 41
slurry mixing techniques, 40
SOFCs. *see* solid oxide fuel cells (SOFCs)
sol–gel-coated ceramic membranes, 69
sol-gel technology, 1, 55, 66–69, 257, 261
solid–liquid thermoporometry, 150, 162–164
solid oxide fuel cells (SOFCs), 155, 236, 245, 247
solid–vapour interface, 48
solute rejection tests, 165–169
solute–solute attachment, 19
solute transport tests, 150
solvent evaporation, 37
solvothermal synthesis, 261
soot-filter regeneration, 382
specific conductivity, 198
spiking tests, 169–171
spiral-wound modules, 16
Sr_1Fe_1-$CO_{0.5}O_x$ tubular membrane reactor, 264
stacks of tubular alumina membranes, 16
steady-state conditions, 140
steam-assisted crystallization, 73
steric hindrance, 67, 68, 104
sterilization, 23, 297, 317–319, 321, 323
Stokes' relation, 103
streaming potential, 150, 198, 199
stress–strain and stress-compression diagrams, 193, 194
strontium cerate ($SrCeO_3$), 237
styrene, 281
sulfonated tetrafluoroethylene PFSA-class fluoropolymer copolymer, 241
sulfur-containing compounds, 320
Sumerians, 320
supermicropores, 11
surface charge, 199
surface diffusion, 46, 91, 125, 128–131
– of hydrogen, 137
surface-enhanced Raman spectroscopy (SERS), 188
surface grinding, 54
surface tension, 38, 157, 160, 196
surface wettability, evaluation of, 196
surfactants, 22, 198
sweeping gas membrane distillation (SGMD), 276
SWOT (strengths, weaknesses, opportunities and threats) analysis, 358, 359

t
tangential potential, 199
tape casting, 41, 42
Teflon, 69, 254
temperature-independent pre-exponential term, 102
tensile/compressive strengths, 193
tensile strengths, 194
tensile stress, 192
tetraethoxysilane (TEOS), 63, 66
tetramethoxysilane (TMOS), 63, 66
tetrapropylammonium bromide (TPABr), 72
tetrapropylammonium hydroxide (TPAOH), 72

theoretical flow-pressure curve, 156
thermally decomposed tetraethoxysilane (TEOS), 64
thermal stability, 32, 73, 241
thermodynamic equilibrium, 250
thermogravimetric analysis (TGA), 44
thermolysis, 45
thickness, 13, 41, 57, 59, 115, 140, 154, 201
thin-layer membrane, 260
three-point bending test, 195
TiO_2 ceramic membranes, 279
titania, 33
toluene, 260
tortuosity, 191
total cost of ownership (TCO), 367
total diffusion coefficient, 101, 102
total gas permeation rate, 154
total organic carbon (TOC), 269, 295
total suspended solids (TSS), 317
trains, modules assembled in, 15
transmembrane flux, 91, 170, 198, 278, 297
transmembrane pores, 152
transmembrane pressure (TMP), 6, 7, 154, 157
transmembrane streaming potentials, set-up for, 199
transmembrane potentials, measurements, 199
transmission electron microscopy (TEM), 150, 176–178
triethylamine, 72
TS-1 nanoparticles, 264
tubular and plate-and-frame modules, 17, 18, 95
tubular porous membrane reactor, 262
turbulent diffusion, 95
turbulent flow, 114

u

ultrafiltration (UF), 1, 9, 10, 55, 150, 295, 363
ultramicropores, 11
uranium isotopes, 3

v

vacuum membrane distillation (VMD), 276
validity, 154
vibrational spectroscopy, 185–189
VINI-TIS module, 324
vinyl chloride monomer (VCM), 356
volatile organic compounds (VOCs), 44

w

Wagner equation, 141
water conflict chronology, 272
water electrolysis, 239
WaterGuard tablets, 274
water quality, 269
water softening, 70
water to oil ratio (WOR), 292
water treatment, 271, 286
– plants, 269, 270, 286, 290
wet membrane, 157
wettability, 37, 196
Wilke–Chang equation, 104
wine, 321, 325
– and ceramic membranes, 321–326
– clarification, 55, 322, 323, 326
– consumption, 326
– deterioration, 322
– filtration installations, 324
– filtration/sterilization, 323
– lees, 322
– tannins, 324
wort, 315

x

X-ray diffraction (XRD), 150, 184, 259
X-ray photoelectron spectroscopy (XPS), 150, 172

y

Young modulus, 193, 195
– equation modification of, 196
yttrium oxide (Y_2O_3), 38

z

zeolites, 55, 70, 198, 282
– coating, 69–73
– membranes, 31, 32, 174, 252, 261, 285, 374
– modifications, 1
– structures, 70
– ZSM-5 membrane, 252, 253, 264
zero emission cycle, 230
zeta potential, 198
zirconia, 29, 33
– membranes, 30